frontiers | Research Topics

Traditional medicines and natural products for liver diseases: Pharmacology, and toxicology in the context of drug discovery and herbal medicine use, volume I

Edited by
Guangyue Su, Yi Wu, Peng-Fei Wu, Yanyu Huang and Yuzhi Zhou

Published in
Frontiers in Pharmacology

ISSN 1664-8714
ISBN 978-2-8325-3493-9
DOI 10.3389/978-2-8325-3493-9

About Frontiers

Frontiers is more than just an open access publisher of scholarly articles: it is a pioneering approach to the world of academia, radically improving the way scholarly research is managed. The grand vision of Frontiers is a world where all people have an equal opportunity to seek, share and generate knowledge. Frontiers provides immediate and permanent online open access to all its publications, but this alone is not enough to realize our grand goals.

Frontiers journal series

The Frontiers journal series is a multi-tier and interdisciplinary set of open-access, online journals, promising a paradigm shift from the current review, selection and dissemination processes in academic publishing. All Frontiers journals are driven by researchers for researchers; therefore, they constitute a service to the scholarly community. At the same time, the *Frontiers journal series* operates on a revolutionary invention, the tiered publishing system, initially addressing specific communities of scholars, and gradually climbing up to broader public understanding, thus serving the interests of the lay society, too.

Dedication to quality

Each Frontiers article is a landmark of the highest quality, thanks to genuinely collaborative interactions between authors and review editors, who include some of the world's best academicians. Research must be certified by peers before entering a stream of knowledge that may eventually reach the public - and shape society; therefore, Frontiers only applies the most rigorous and unbiased reviews. Frontiers revolutionizes research publishing by freely delivering the most outstanding research, evaluated with no bias from both the academic and social point of view. By applying the most advanced information technologies, Frontiers is catapulting scholarly publishing into a new generation.

What are Frontiers Research Topics?

Frontiers Research Topics are very popular trademarks of the *Frontiers journals series*: they are collections of at least ten articles, all centered on a particular subject. With their unique mix of varied contributions from Original Research to Review Articles, Frontiers Research Topics unify the most influential researchers, the latest key findings and historical advances in a hot research area.

Find out more on how to host your own Frontiers Research Topic or contribute to one as an author by contacting the Frontiers editorial office: frontiersin.org/about/contact

Traditional medicines and natural products for liver diseases: Pharmacology, and toxicology in the context of drug discovery and herbal medicine use - volume I

Topic editors

Guangyue Su — Shenyang Pharmaceutical University, China
Yi Wu — Nanjing Agricultural University, China
Peng-Fei Wu — Huazhong University of Science and Technology, China
Yanyu Huang — University of California, Davis, United States
Yuzhi Zhou — Shanxi University, China

Citation

Su, G., Wu, Y., Wu, P.-F., Huang, Y., Zhou, Y., eds. (2023). *Traditional medicines and natural products for liver diseases: Pharmacology, and toxicology in the context of drug discovery and herbal medicine use - volume I*. Lausanne: Frontiers Media SA. doi: 10.3389/978-2-8325-3493-9

Table of contents

05 LC–MS-based lipidomic analysis of liver tissue sample from spontaneously hypertensive rats treated with extract hawthorn fruits
Luping Sun, Bingqing Chi, Mingfeng Xia, Zhen Ma, Hongbin Zhang, Haiqiang Jiang, Fang Zhang and Zhenhua Tian

16 Better detoxifying effect of ripe forsythiae fructus over green forsythiae fructus and the potential mechanisms involving bile acids metabolism and gut microbiota
Tao Wang, Xu-Jiong Li, Ling-Hao Qin, Xue Liang, Huan-Huan Xue, Jing Guo, Shi-Fei Li and Li-Wei Zhang

34 Targeted bile acid profiles reveal the liver injury amelioration of Da-Chai-Hu decoction against ANIT- and BDL-induced cholestasis
YueHua Zhou, YunZhong Zhou, YiFei Li, Wei Sun, ZhaoLong Wang, Long Chen, Ye He, XiaoLong Niu, Jialiang Chen and Guangtao Yao

52 Detoxification technology and mechanism of processing with *Angelicae sinensis* radix in reducing the hepatotoxicity induced by rhizoma *Dioscoreae bulbiferae in vivo*
Lingling Song, Junming Wang, Mingzhu Gong, Yueyue Zhang, Yamin Li, Xiaohui Wu, Lingyu Qin and Yaqian Duan

69 Potential hepatoprotective effects of *Cistanche deserticola Y.C. Ma*: Integrated phytochemical analysis using UPLC-Q-TOF-MS/MS, target network analysis, and experimental assessment
Haichao Wang, Yaying Li, Yifei Bian, Xue Li, Yubei Wang, Ke Wu, Chuanguo Liu, Yuhong Liu and Xiaoming Wang

90 Tandem mass tag-based proteomics analysis reveals the multitarget mechanisms of *Phyllanthus emblica* against liver fibrosis
Puyang Gong, Kehuan Yin, Xiaomin Luo, Jian Gu, Rui Tan, Yan Wu and Dapeng Li

105 Caffeine in liver diseases: Pharmacology and toxicology
Liang Shan, Fengling Wang, Dandan Zhai, Xiangyun Meng, Jianjun Liu and Xiongwen Lv

118 *Astragalus* saponins and its main constituents ameliorate ductular reaction and liver fibrosis in a mouse model of DDC-induced cholestatic liver disease
Linzhang Zhang, Yonghong Hu, Shenglan Qi, Congcong Zhang, Qun Zhou, Dingqi Zhang, Yongping Mu, Hua Zhang, Gaofeng Chen, Ping Liu, Jiamei Chen and Wei Liu

133 Ameliorative effect of *Berberidis radix* polysaccharide selenium nanoparticles against carbon tetrachloride induced oxidative stress and inflammation
Fei Gao, Huimin Liu, Hao Han, Xin Wang, Lihua Qu, Congmin Liu, Xuemei Tian and Ranran Hou

149 Hepatoprotective effect of botanical drug formula on high-fat diet-induced non-alcoholic fatty liver disease by inhibiting lipogenesis and promoting anti-oxidation
De-Shan Ning, Yu-Ju Chen, Chien-Ju Lin, Ching-Chiung Wang, Hong-Wei Zhao, Kun-Teng Wang, Ming-Chung Lee, Lemmuel L. Tayo, Wan-Chun Chiu, Chiu-Li Yeh and Chia-Jung Lee

164 Aqueous extract of Artemisia capillaris improves non-alcoholic fatty liver and obesity in mice induced by high-fat diet
Meng Liang, Mohan Huo, Yi Guo, Yuyi Zhang, Xiao Xiao, Jianwen Xv, Lixue Fang, Tianqi Li, Huan Wang, Siyu Dong, Xiaowen Jiang and Wenhui Yu

180 *Ganoderma lucidum*: Current advancements of characteristic components and experimental progress in anti-liver fibrosis
Haoyuan Peng, Lei Zhong, Lin Cheng, Lu Chen, Rongsheng Tong, Jianyou Shi and Lan Bai

193 The IDI1/SREBP2 axis drives intrahepatic cholestasis and is a treatment target of San-Huang-Cai-Zhu formula identified by sequencing and experiments
Junbin Yan, Yunmeng Nie, Zheng Chen, Jiaming Yao, Shuo Zhang and Zhiyun Chen

207 Mechanisms of Yajieshaba in the treatment of liver fibrosis through the Keap1-Nrf2 signaling pathway
Yuanmei Bai, Haimei Wu, Lijie Zheng, Yuhuan Xie, Feifan Liu, Yan Wan, Qiongchao Li and Peixin Guo

225 Aqueous extract of *Amydrium sinense (Engl.) H. Li* alleviates hepatic fibrosis by suppressing hepatic stellate cell activation through inhibiting Stat3 signaling
Jingyan Li, Bingmin Wu, Lishan Zeng, Ying Lin, Qiuhe Chen, Haixia Wang, Lin An, Jiajun Zhang, Siyan Chen, Junying Huang, Ruoting Zhan and Guifang Zhang

frontiers | Frontiers in Pharmacology

TYPE Original Research
PUBLISHED 09 August 2022
DOI 10.3389/fphar.2022.963280

OPEN ACCESS

EDITED BY
Yi Wu,
Nanjing Agricultural University, China

REVIEWED BY
Xue Xiao,
Guangdong Pharmaceutical University, China
Jiayu Zhang,
Binzhou Medical University, China

*CORRESPONDENCE
Haiqiang Jiang,
jhq12723@163.com
Fang Zhang,
zfang_819@163.com
Zhenhua Tian,
tianzhenhuatina@163.com

SPECIALTY SECTION
This article was submitted to Ethnopharmacology, a section of the journal Frontiers in Pharmacology

RECEIVED 07 June 2022
ACCEPTED 05 July 2022
PUBLISHED 09 August 2022

CITATION
Sun L, Chi B, Xia M, Ma Z, Zhang H, Jiang H, Zhang F and Tian Z (2022), LC–MS-based lipidomic analysis of liver tissue sample from spontaneously hypertensive rats treated with extract hawthorn fruits.
Front. Pharmacol. 13:963280.
doi: 10.3389/fphar.2022.963280

LC–MS-based lipidomic analysis of liver tissue sample from spontaneously hypertensive rats treated with extract hawthorn fruits

Luping Sun[1], Bingqing Chi[1], Mingfeng Xia[2], Zhen Ma[2], Hongbin Zhang[1], Haiqiang Jiang[2]*, Fang Zhang[1]* and Zhenhua Tian[3]*

[1]College of Pharmacy, Shandong University of Traditional Chinese Medicine, Jinan, China, [2]Innovative Institute of Chinese Medicine and Pharmacy, Shandong University of Traditional Chinese Medicine, Jinan, China, [3]Experimental Center, Shandong University of Traditional Chinese Medicine, Jinan, China

At present, many experiments provide support for the cardiovascular protective effect of hawthorn (*Crataegus oxyacantha*) flower, leaf and fruit extracts. The aim of this study was to investigate the intervention mechanism of hawthorn fruit extract on spontaneously hypertensive rats (SHR) and its effect on their lipid metabolic pattern. After SHR was intervened by hawthorn extract (1.08 g/kg/d) for 6 weeks, the blood pressure and liver histopathology of rats were evaluated. An UHPLC-Q Extractive metabolomics approach was used to collect information on rat liver lipid metabolites, combined with multivariate data analysis to identify significantly different substances and potential biomarkers through mass spectrometry and database searches. Histomorphology of the liver was partially restored in the hawthorn-treated group. Hawthorn extract interferes with sphingolipid metabolism, glycerophospholipid metabolism and glycerolipids metabolism, improving partially disturbed metabolic pathways. This study showed that hawthorn could partially restore liver histomorphology and has anti-hypertensive effect by regulating lipid metabolism.

KEYWORDS

hawthorn, spontaneously hypertensive, untargeted metabolomics, lipidomics, liver tissue

Introduction

Cardiovascular and cerebrovascular diseases (CVDs) caused by disorders of the heart and blood vessels, are the most morbid, disabling and mortal diseases by far in China, which include coronary heart disease (heart attack), cerebrovascular disease (stroke), elevated blood pressure (hypertension), etc., (Rastogi et al., 2016). Hypertension is one of the main risk factors for CVDs and can increase the risk of heart, brain, kidney and other diseases (Verma et al., 2021). Hypertension is defined as persistent systolic blood pressure (SBP) (≥140 mmHg) and diastolic BP (DBP) (≥90 mmHg), which is mainly of two types:

Primary or essential hypertension (90%–95%) and Secondary hypertension (5%–10%) (Cloud et al., 2019). Furthermore, it is the major cause of premature death worldwide, and its complex pathogenesis is the focus of CVDs research. The most direct and effective treatment for hypertension is to reduce blood pressure through various means (Mills et al., 2020). In recent decades, angiotensin converting enzyme inhibitors (ACE inhibitors), angiotensin receptors blockers (ARBs), direct vasodilators, calcium channel blockers, ganglion blockers, and thiazide type of diuretics are the main clinical drugs in the treatment of hypertension (Goit and Yang, 2019). At present, the clinical treatment focuses on the combined use of a variety of antihypertensive drugs. Nebivolo/valsartan combination is effective and well-tolerated to obtain excellent antihypertensive effect (Wang and Sander, 2021). However, it has been reported that the risk of adverse reactions of antihypertensive drugs in subjects is high, such as stroke, coronary heart disease and cardiovascular diseases (Gronewold et al., 2019).

Most herbs from different regions have multiple anti-cardiovascular effects (Rastogi et al., 2016). Hawthorn (*Crataegus oxyacantha*) is the ripe fruit of a plant in the Rosaceae family and is used worldwide as a food and medicine. In particular, a large number of experimental studies have proved that hawthorn has the effects of anti-hypertension, protecting vascular endothelial function, anti-arrhythmia, regulating lipid metabolism, lowering blood lipids, inhibiting platelet function, decreasing oxidative stress, and reducing inflammatory response (Chang et al., 2005; Zhao et al., 2017). The hawthorn flower and leaf extract possess antioxidant effect and blood-thinning properties (Rababa'h et al., 2020). The rich polyphenolic components of hawthorn peel and pulp could differentially modulate dyslipidemia, inflammation, oxidative stress, and alleviate liver injury in mice, which is the main reason for its excellent antioxidant and free radical scavenging abilities (Han et al., 2016; Zhao et al., 2017). The mediated cardiogenic, vasodilatory and antioxidant effects of flavonoid bioactive compounds in hawthorn extracts making them beneficial in the prevention of pulmonary hypertension syndrome and heart disease (Ahmadipour et al., 2020). Flavonoids and oligomeric proanthocyanidins play a major role in the protection and treatment of various CDVs (Rigelsky and Sweet, 2002).

Hypertension is a clinical syndrome characterized by varying degrees of lipid metabolism disorder (Xie, et al., 2019). Chinese medicine considers hypertension be-longing to dizziness, headache, stroke, liver wind. It occurs the pathogenesis induces wind, fire, phlegm, empty, stasis. These five aspects extremely are closest with the liver relations (Wang et al., 2014). Liver is an essential organ of lipid metabolism (Trefts et al., 2017) and serves as the main site of carbohydrate and lipid biosynthesis in the body (Jones, 2016). Lipids are important small biomolecules and could maintain lipid metabolic homeostasis. Moreover, it is an essential element of the mammalian life form (Nguyen et al., 2008a). Overexpression of lipids can lead to excessive accumulation of fat in hepatocytes, increase triglycerides and low-density lipoprotein cholesterol levels, decrease high-density lipoprotein cholesterol levels and insulin resistance, eventually leading to elevated blood lipids and aggravating the occurrence and progress of spontaneous hypertension (Nguyen et al., 2008b). Thus, lipid disorders can indeed aggravate the occurrence and progress of spontaneous hypertension. Lipidomics analysis can reveal changes in lipid metabolism and related regulatory mechanisms in response to internal and external stimuli (Duan and Xie, 2020). Lipidomics may be an useful tool for identifying biomarkers of visceral fat and liver fat content (Boone et al., 2019). Liquid chromatography-mass spectrometry (LC-MS) has been widely used for lipidomics analysis of various samples with the advantage of high sensitivity and high resolution to determine more metabolic phenotypes of polar metabolites by untargeted and targeted analysis (Gika et al., 2019; Guo et al., 2021).

In this study, we investigated the effects of hawthorn fruit extract on the metabolism of spontaneously hypertensive rats using untargeted LC-MS liposome analysis. This study provides new insights into the mechanism of hawthorn treatment in spontaneously hypertensive rats.

Materials and methods

Chemicals and reagents

HPLC-grade methanol, acetonitrile, formic acid water, and 2-propanol were purchased from Tedia Co., Inc. (Fairfield, OH, United States). All aqueous solutions were prepared using ultrapure Milli-Q water (EMD Millipore, Billerica, MA, United States).

Preparation of the extract of hawthorn fruit

Hawthorn fruit (No. 20121602) were purchased from Shandong Shunshengtang Prepared Slices of Chinese Crude Drugs Co., Ltd. (Heze, Shandong, China), which were subjected to chemical analysis according to the Chinese Pharmacopoeia and identified as satisfactory. Ultrasonic extraction was performed with hawthorn-70% ethanol (1:9, m/v) for 1 h, and repeated for 2 times. After filtration, the extract was concentrated by decompression and dried. When administered in animal experiments, 3.0 g/ml extract was prepared by dissolving the extract in physiological saline. Hawthorn extract solution were stored at 4°C until used in the animal study.

Animal experiment

12 Wistar-Kyoto rats (WKYs, aged 12 weeks) and 36 male Spontaneously Hypertensive Rats (SHRs, aged 8 weeks), each weighing 190 ± 10 g, were procured from the Vital River Laboratory Animal Technology Co., Ltd. (Beijing, China, Permit No. SCXK Lu 20170022). All experimental procedures were performed in accordance with the guidelines of the guidelines of the National Research Council of China and were approved by the Animal Ethics Committee of the Affiliated Hospital of Shandong University of Traditional Chinese Medicine (SDUTCM20210721002).

The 12 WKYs were defined as the control group (C), and the 24 SHRs were randomly divided into model group (M, n = 12) and hawthorn treated group (S, n = 12). All rats were kept under controlled environmental conditions (temperature of approximately 23°C ± 3°C, humidity of 55% ± 15% and a 12 h light/dark cycle). All rats were acclimatized to the laboratory 1 week before the experiments. They were allowed free access to food and water throughout the study. Drug administration in rats calculated by human dose (9–12 g/d) in the Chinese Pharmacopoeia and the dose of hawthorn extract in group S was 1.08 g/kg/d (Xu et al., 2002; Chen, 2006). The Groups of C and M were intragastric with equal amount of normal saline. All animals were intragastric once daily for 6 weeks.

Detection of systolic blood pressure and diastolic BP

Both of SBP and DBP were measured for each rat in each group before the experiment and every week (1–6 weeks respectively) conducted by the noninvasive blood pressure apparatus (Dotop Biotech Co., Ltd., BP-2000).

Collection and preparation of samples

At the end of the experiment, all animals were fasted for 12 h, the rats were anesthetized with sodium pentobarbital, and blood was collected from the abdominal aorta. At the same time, the fresh tissue of the right lobe of the liver was rapidly removed and the surface blood was washed with pre-cooled normal saline. Part of the liver sample was immersed in 4% paraformaldehyde and fixed for subsequent detection, and the remaining part was placed in a centrifuge tube and stored in a—80°C refrigerator for lipid analysis.

Quality control (QC) samples were used to rule out the possibility that significant differences in liver lipid metabolites analyzed by LC-MS were primarily caused by instrument drift, and thus to measure instrument stability. QC samples were obtained by taking 20 μL of each liver tissue homogenate and processing the mixture in the same manner as the other samples. 5 consecutive QC samples were performed to equilibrate the system before the actual liver tissue samples were tested, and then a QC sample was inserted into every 5 samples (Yang et al., 2020). The obtained QC sample data matrix was subjected to principal component analysis (PCA) to further monitor the system stability.

ELISA kit test

100 mg of liver tissue stored at −80°C was added with 900 μL precooled isopropyl alcohol for rapid homogenization, centrifuged at 4°C for 12,000 r/min for 15 min, and then NO (Cat.#m1058803-2) and TNF-α (Cat.#m1002859-2) levels in liver samples were determined by ELISA (Shanghai Enzyme-linked Biotechnology Co., Ltd., Shanghai, China) according to manufacturer's instructions. The concentrations of NO and TNF-α in liver samples were calculated according to the calibration curve.

Hematoxylin and eosin staining and oil red staining

The same part of the liver tissues were fixed with 10% formalin and embedded in paraffin blocks, which were further sectioned at 5 μm and stained hematoxylin and eosin (H&E). 10% formalin-fixed fresh liver tissue was embedded with OCT embedding gel and sectioned for 5 μm using a freeze sectioning machine, then, stained with oil red O and hematoxylin. Finally, the sections were then photographed with Axiophot 2 upright microscope (Axio Imager. A2).

UHPLC-Q extractive analysis

Liver tissue (100 mg) and water (900 μL) were homogenized for 1 min, then centrifuged at 12,000 rpm for 15 min at 4°C to remove water-soluble impurities. Then, the supernatant was discarded and dichloro-methanol (2:1, v/v) was added to the lower tissue pellet and vortexed for 5 min. After centrifugation at 12,000 rpm for 15 min at 4°C, the bottom layer was carefully aspirated and dried with high-purity nitrogen. Finally, it was resolved with 100 μL isopropanol-acetonitrile-water (2:1:1, v/v/v), collected using a 0.22 μm microporous membrane and filtered with 3 μL into a column for UHPLC-Q Extractive analysis (Furse et al., 2020).

The data analysis was performed using a UHPLC-Q Extractive (Thermo Fisher Scientific) equipped with a Aegla-Hlao C_{18} column (2.1 mm × 100 mm, 2.7 μm). The mobile phases were 0.05% formic acid in acetonitrile-water (4:6, v/v) solution (A) and 0.05% formic acid in acetonitrile-isopropanol (1:9, v/v) solution (B), the gradient program is as follows: 0–3 min, 2%–45% B; 3–10 min, 45%–65% B; 10–25 min, 65%–85% B; 25–25.2 min, 2% B. The injection volume was 3 μL, and the flow rate was 0.3 ml/min. The column was maintained at 45°C.

An electrospray ionization ion (ESI) source was used for mass detection in positive and negative mode, and the drying gas temperature and drying gas flow rate were set to 350°C and 10 ml/min, respectively. The capillary voltage was set at 3,500 V, the atomization gas pressure was set at 35 psi, the fragmentation voltage was 140 V and the skimmer voltage was 60 V. Data were collected in centroid mode from 100 to 1,000 m/z. Normalized Collision Energy (NCE) was 30, 50, and 70 eV.

Data processing and multivariate analysis

Peak alignment and extraction were performed using R (R Project V3.2.2, The University of Auckland, New Zealand) (Zhang et al., 2016), and the original data were converted and normalized. The processed normalized data were imported into SIMCA-P (V14.1, MKS Data Analytics Solutions Umea, Sweden) for multivariate analysis, including principal component analysis (PCA) and partial least squares discriminant analysis (PLS-DA) for pattern recognition. The purpose of PCA is to eliminate outlier samples by similarity between the groups, and the aims of PLS-DA is to identify the significantly changed metabolites of plasma samples in different groups (Dong et al., 2020). According to a score plot of PLS-DA, we selected the variable importance prediction (VIP) of the projected first principal component greater than 1 to screen the differential metabolites for further analysis (Yang et al., 2017). Then, the VIP >1 data of SHR group and normal group were imported into Mass Profiler Professional (V12.6.1, Agilent Technologies, United States) software for *t*-test. Values with *p* values less than 0.05 and fold changes greater than 2 were retained as potential biomarkers (Tian et al., 2020).

The Human Metabolomics Database online (HMDB, www.hmdb.ca) was used for metabolite identification. According to the relevant literature (Alseekh et al., 2021), the accurate molecular weight and tandem mass spectrometry results, the mass spectrometry information in the library was matched, and the types of differential metabolites were further identified. At the same time, the analysis of compounds was also carried out with reference to the Kyoto encyclopedia of genes and genomes (KEGG, www.kegg.com) (Guma et al., 2016). Other bioinformatics tools for path mapping and network visualization, including MetaboAnalyst 5.0 (dev.metaboanalyst.ca), are also used in this study. Finally, the metabolic pathways were drawn.

Statistical analysis

Data from ELISA assays were processed with SPSS 26.0 (SPSS Inc., United States) statistical software. Data were expressed as mean ± standard deviation (SD) for processing independent sample *t*-test and one-way analysis of variance (ANOVA). $p < 0.05$ indicated that the difference was statistically significant.

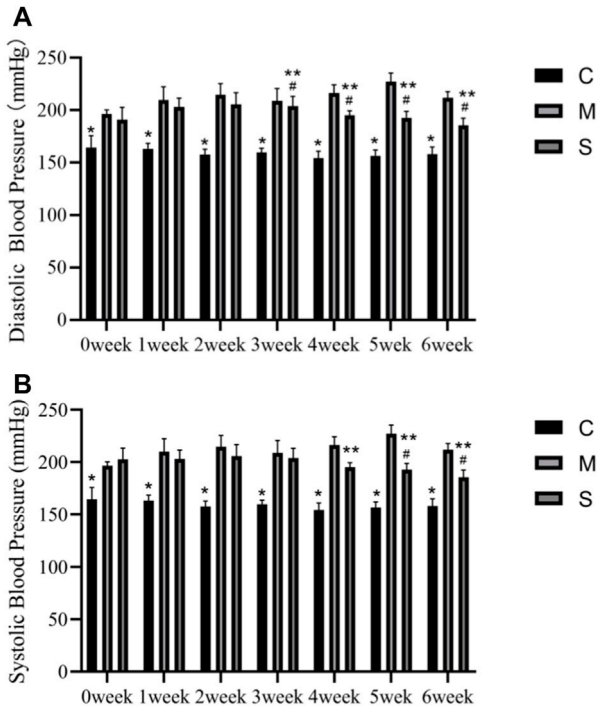

FIGURE 1
(A) Diastolic blood pressure in the normal control (C), SHR model (M) and hawthorn treated (S) rats. **(B)** Systolic blood pressure in the normal control (C), SHR model (M) and hawthorn treated (S) rats. $^{*}p < 0.05$ vs. model group, $^{\#}p < 0.05$ vs. 0 weeks, $^{\#\#}p < 0.05$ vs. SHR.

Results

Hawthorn extract reduces blood pressure in spontaneously hypertensive rats

Figure 1 shows the comparative results of diastolic and systolic blood pressure in normal control (C), SHR model (M) and hawthorn treated (S) rats during 6 weeks. SBP and DBP were significantly higher in both group M and group S without pharmacological intervention (0 weeks) than in group C. Compared with the M group, the S group showed a significant decrease in SBP at 4, 5, and 6 weeks ($p < 0.05$) and a decrease in DBP from the 3rd week ($p < 0.05$). Compared to the pre-intervention S group (0 weeks), the SBP decreased at 5 and 6 weeks ($p < 0.05$) and DBP decreased significantly at 3, 4, 5, and 6 weeks ($p < 0.05$) (Figure 1).

Hawthorn extract promotes NO and inhibites TNF-α production

NO and TNF-α indexes were measured in rat liver tissue homogenates by ELISA. Compared with the normal control group (C), NO was significantly decreased in the model group

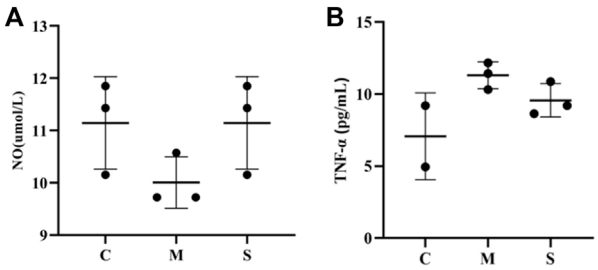

FIGURE 2
(A) The NO level in liver tissues of in normal group (C), model group (M) and hawthorn group (S). **(B)**The TNF-α levels in liver tissues of in normal group (C), model group (M) and hawthorn group (S).

(M), while TNF-α levels were significantly increased ($p < 0.01$). After administration of the treatment, NO levels in the S group were improved and significantly increased ($p < 0.01$), while the decrease in TNF-α levels was not significant (Figure 2). It proved that hawthorn could achieve therapeutic effects by elevating NO and decreasing TNF-α.

Hawthorn extract improves liver histological abnormality

At the end of the 6th week of the experiment, the liver tissue of the healthy control (C) group was clear, and no histological abnormality was found in the liver section, while in the SHR model (M) group, liver cells showed obvious fatty change and small necrotic area (Figure 3). Compared with the M group, the steatosis of the hepatic cells in the S groups was reduced, and the fat content of the hepatic cells was significantly reduced.

The oil red O staining showed that a large number of red lipid droplets appeared in the hepatocytes of SHR in group M compared with group C, and the area of oil red staining was significantly increased, indicating that their intracellular lipid content was significantly higher than that of group C. In contrast, the number of red intracellular lipid droplets was significantly reduced in the S group treated with hawthorn compared to the M group, implying a significant reduction in lipid content (Figure 3). The staining results proved that hawthorn can significantly improve liver pathology, reduce the degeneration of SHR hepatocytes, and lower the lipid content in the liver, making it a practical and effective drug for improving cardiovascular disease (Dong et al., 2020).

Multivariate data analysis and pattern recognition

Representative total ion chromatograms of the liver samples from the QC groups in the positive (A) and negative (B) ESI mode was shown in Supplementary Figure S1 and UHPLC-Q Extractive analysis Total ion Chromatograms (TIC) of liver tissue samples from each experimental group were shown (Figure 4; Supplementary Figures S2, S3). To confirm the good stability and

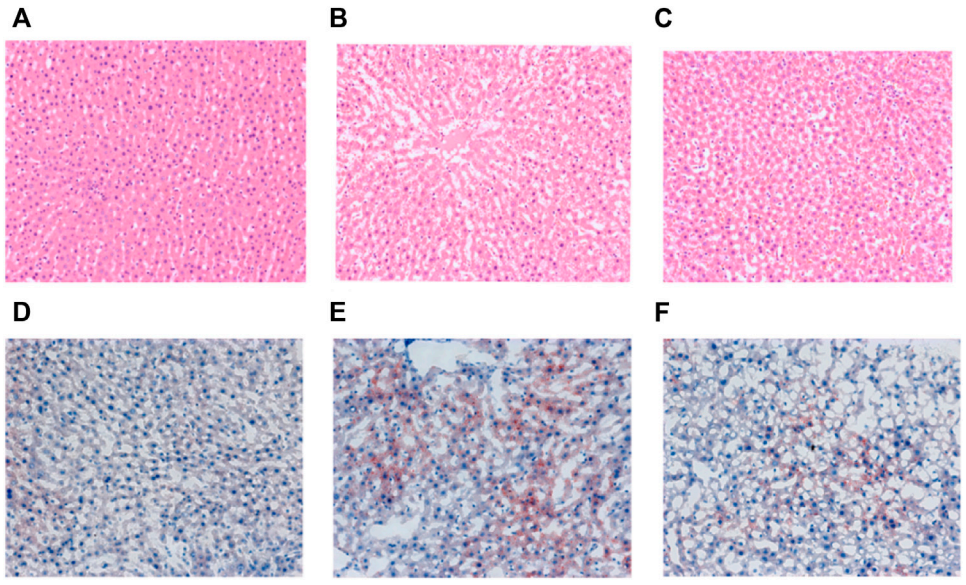

FIGURE 3
Representative H&E staining (magnification, × 200) of liver sections from the C **(A)**, M **(B)** and S **(C)** groups and oil red staining (magnification, × 200) of liver sections from the C **(D)**, M **(E)** and S **(F)** groups at the end of 6th week.

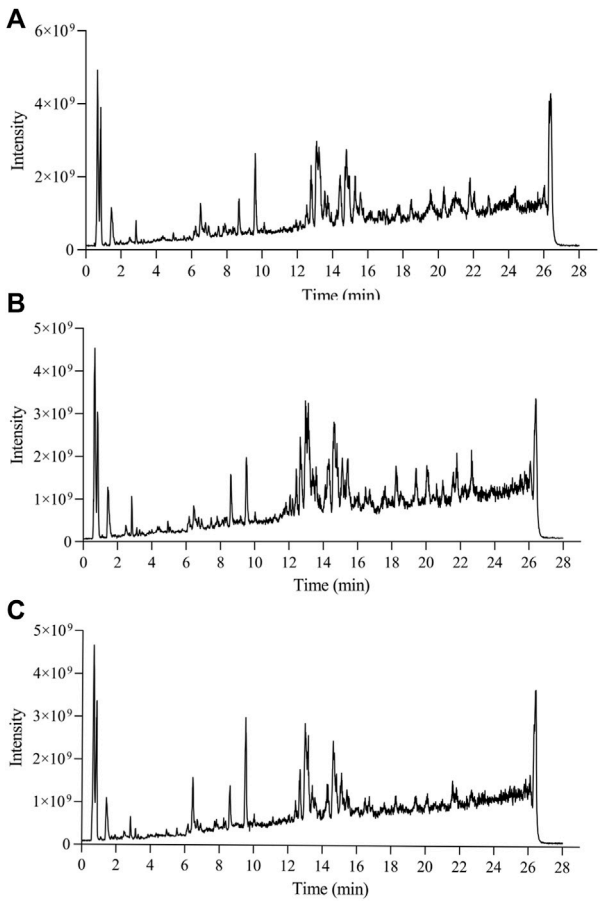

FIGURE 4
Total ion chromatograms of WKY **(A)**, SHR **(B)** Hawthorn treated **(C)** in positive ion mode obtained from UPLC-QE-MS analysis.

applicability of the metabolomics platform, we extracted the retention time and peak area of each of the five representative ions in QC samples in positive and negative ion mode using the analytical method in the literature, and calculated the RSD value <5% for the corresponding intensity of each ion (Supplementary Tables S1, S2), indicating that the instrument was in good condition, data quality was reliable. To further perform method validation to obtain the deviation variation of QC samples, the stability of QC was evaluated by principal component analysis, and the results showed that the 12 QC samples in both positive and negative ion mode were within the region of 2SD and 95% confidence interval (Supplementary Figure S4).

Principal component analysis (PCA) is an unsupervised pattern recognition method in multivariate statistical analysis, which can obtain classification information between different samples and clearly show the two-dimensional spatial distribution relationships between different groups, and the results are shown as score plots. In this study, the PCA model was used to assess the metabolomic differences between the 3 groups and all 3 groups were significantly separated in both positive and negative modes, as shown in Figures 5A,B). The results showing the PCA score plots for lipids in positive and negative ionization mode. The positive mode ($R^2X = 0.872$, $Q^2 = 0.785$) and the negative mode ($R^2X = 0.745$, $Q^2 = 0.661$) indicate that the developed PCA model has good predictive and explanatory power. The QC samples were found to be significantly clustered and concentrated within the 95% confidence interval in the PCA score scatter plot, providing the necessary conditions for a large-scale metabolomics study.

To further elucidate the differences in lipid metabolism patterns among the groups, this experiment used partial least squares discriminant analysis (PLS-DA), a more mature supervised projection method, to analyze the data of each group and obtain PLS-DA scatter plots (Figures 5C,D), from which it can be seen that the three groups of samples appeared clearly spatially classified without crossover or overlap, and the PLS-DA models of R^2X, R^2Y, and Q^2 are within the specified ranges of 0.626, 0.998, 0.98 (positive mode) and 0.814, 0.996, 0.966 (negative mode), respectively, implying that the experimentally established model is valid. The study established the alignment test as an internal validation method to demonstrate the validity of the OPLS-DA model. The 200 permutation tests for the positive ion model ($R^2 = 0.354$, $Q^2 = -0.359$) and the negative ion model ($R^2 = 0.47$, $Q^2 = -0.447$) (Figures 5E,F) showed that the intercept of Q^2 on the vertical axis was seen to be negative. All the established OPLS-DA models are sreliable and robust with no over-fitting and the model validation is valid.

Analysis and identification of potential biomarkers and lipid metabolic pathways in hypertension

The variable importance prediction (VIP) values generated by the PLS-DA model were used to filter variance variables. The larger the VIP value of a variable, the greater its contribution to the group. Potential endogenous components with VIP >1 were screened and further independent samples *t*-test and fold change (FC) analysis were performed to select variables with $p < 0.05$ and FC > 2. In conclusion, we considered variables that satisfied both VIP >1, $p < 0.05$ and FC > 2 as potential biomarkers. Based on the above conditions, 31 differential variables were identified as potential biomarkers, including 13 in the positive ion mode and 18 in the negative ion mode, and the differences and trends of these biomarkers were summarized in Table 1.

We constructed a clustering heatmap using MetaboAnalyst 5.0 (dev.metaboanalyst.ca), which is able to characterize the relative content of each component to analyze the identified lipid data (Figure 6). The heatmap shows the differences in the content of the identified lipids, with dark blue indicating lower levels and dark red indicating higher levels. Based on the information in the graph, it can be observed that the color change in the hawthorn treatment group (S) has converged to the level of the normal group (C). For example, the

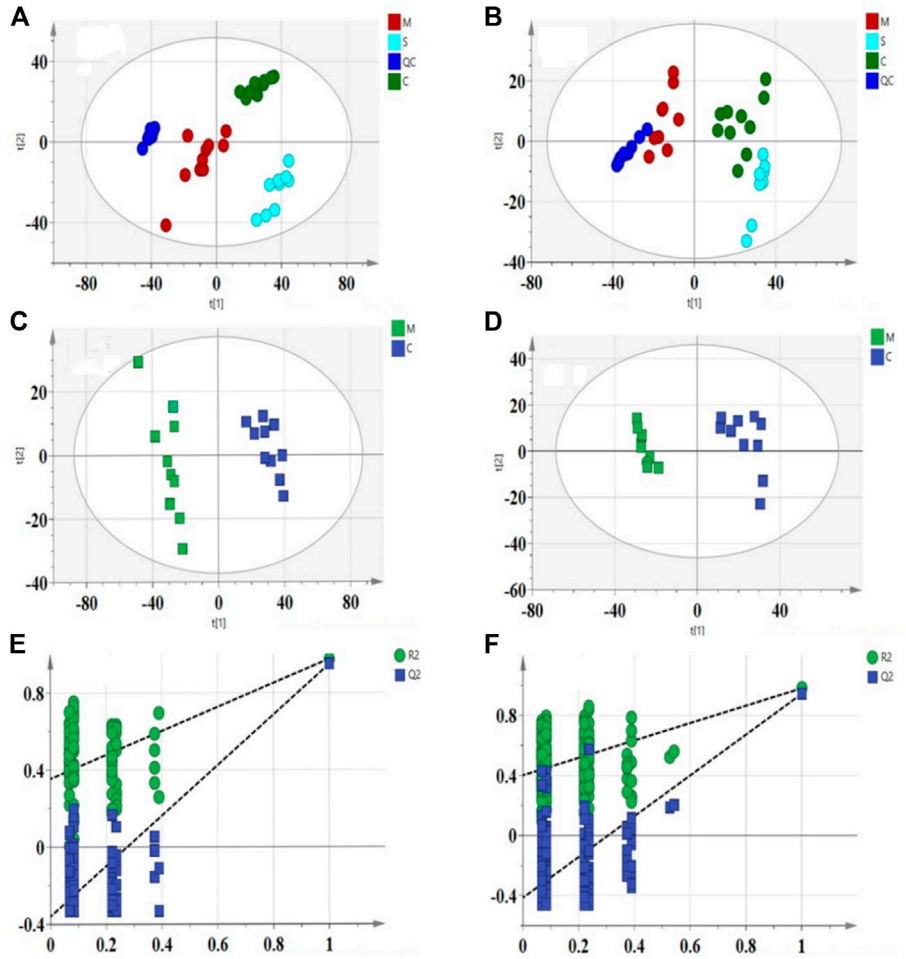

FIGURE 5
PCA score scatter plots for liver samples from 3 groups in the positive **(A)**: $R^2X = 0.872$, $Q^2 = 0.785$) and negative **(B)**: $R^2X = 0.745$, $Q^2 = 0.661$) ESI mode. OPLS-DA score scatter plots for C and M groups in the positive **(C)**: $R^2X = 0.626$, $R^2Y = 0.998$, $Q^2 = 0.98$) and negative **(D)**: $R^2X = 0.814$, $R^2Y = 0.9958$, $Q^2 = 0.966$) ESI mode. Permutation test of lipid species OPLS-DA model in positive mode **(E)**: $R^2 = 0.354$, $Q^2 = -0.359$) and negative mode **(F)**: $R^2 = 0.47$, $Q^2 = -0.447$).

levels of ceramides (Cer, 18:1/26:0), p-glycoprotein (PGP, 20:1/18:2; 18:1/22:5), phosphatidic acid (PA, 18:0/18:1; 24:0), phosphatidylcholine (PC, 18:4; 14:0; 18:3), phosphatidylethanolamine (PE, 16:0/18:3; 18:3/16:0), phosphatidylserine (PS, 20:3/20:3; 20:2/18:1; 20:3/16:0; 18:1/18:0; 22:6/22:2), diglycerides (DG, 22:6/20:3/0:0; 38:5) and triglycerides (TG, 14:0/20:4/20:4) were significantly higher in the model group than in the control group, but the metabolite levels returned to the control group after treatment with hawthorn, which indicates that the metabolite levels were regulated and the abnormalities of lipid metabolism were improved to varying degrees with the intervention of hawthorn, suggesting that hawthorn has a regulatory effect on lipid disorders in the liver of SHR.

Then, to explore the signaling pathways that may be affected by hawthorn, we performed metabolic pathway analysis of the identified lipid differential metabolites. Figure 7 showed that sphingolipid metabolism and glycerophospholipid metabolism. The results showed that 3 metabolic pathways: sphingolipid metabolism, glycerophospholipid metabolism and glycerolipids metabolism were all disturbed, implying that these metabolic pathways were significantly associated with the effect of hawthorn in treating SHR.

Discussion

The effect of hawthorn extract on SHR was studied. Under experimental conditions, the regulation effect of hawthorn on improving lipid metabolism is moderate and positive. 3 metabolic pathways were identified by lipidomics. Thus, hawthorn can regulate liver lipidomics through sheath lipid metabolism, glycerin phospholipid metabolism and glycerin metabolism, thereby regulating lipid content and exerting its therapeutic effect on hypertension. A total of 31 lipid types closely related to

TABLE 1 Identification of ions and their alteration trend in positive and negative mode.

No	tR (min)	m/z	Formula	Identification	Fragments	Change trend[#]		Pathway
						Control[#]	Hawthorn[#]	
1	6.56	691.5278	C45H70O5	DG (22:6/20:3/0:0)	M + H	↓	↓	Glycerolipids
2	6.72	697.4424	C41H65O8P	PA (18:4/20:4)	M-H20-H	↑	↑	Glycerophospholipids
3	9.52	678.6843	C44H87NO3	Cer(18:1/26:0)	M + H	↓	↓	Sphingolipids
4	11.81	937.5278	C49H81N2O11 PS	PC(18:4)	M + H	↓	↓	Glycerophospholipids
5	11.89	863.5125	C44H82O13P2	PGP (20:1/18:2)	M + H-H2O	↓	↓	Glycerophospholipids
6	12.21	889.5266	C45H81N2O11 PS	PC(14:0)	M + H	↓	↓	NC
7	12.35	699.5023	C39H73O9P	PA (18:0/18:1)	M + H-H2O	↓	↓	NC
8	12.36	698.4993	C39H72NO7P	PE (16:0/18:3)	M + H	↓	↓	Glycerophospholipids
9	12.49	728.5277	C40H76NO9P	PE (18:3/16:0)	M + H-H2O	↓	↓	Glycerophospholipids
10	12.83	939.5446	C49H83N2O11 PS	PC(18:3)	M + H	↓	↓	NC
11	12.99	816.5313	C46H78NO10P	PS(20:3/20:3)	M-H20-H	↓	↓	Glycerophospholipids
12	13.19	794.5302	C44H80NO10P	PS(20:2/18:1)	M-H20-H	↓	↓	Glycerophospholipids
13	13.57	784.5012	C42H76NO10P	PS(20:3/16:0)	M-H	↓	↓	Glycerophospholipids
14	14.13	770.5297	C42H80NO10P	PS(18:1/18:0)	M-H20-H	↓	↓	Glycerophospholipids
15	14.31	868.5643	C50H82NO10P	PS(22:6/22:2)	M-H20-H	↓	↓	Glycerophospholipids
16	14.36	794.5477	C44H80NO10P	PS(20:3/18:0)	M-H20-H	↑	↑	Glycerophospholipids
17	14.78	859.5980	C47H87O11P	PA (24:0)	M + H	↓	↓	NC
18	15.91	808.5985	C46H84NO8P	PE-NMe(22:4/18:0)	M-H	↑	↑	Glycerophospholipids
19	16.05	676.4808	C36H72NO8P	PE (16:0/15:0)	M-H	↑	↑	Glycerophospholipids
20	16.09	902.6041	C46H80O13P2	PGP (22:6/18:0)	M-H	↑	↑	Glycerophospholipids
21	17.61	849.6478	C57H88O6	TG (20:5/14:1/20:5)	M-H20-H	↑	↑	Glycerolipids
22	17.68	823.6308	C55H86O6	TG (14:1/20:5/18:4)	M-H20-H	↑	↑	Glycerolipids
23	18.25	735.5132	C39H75O10P	PA (18:1/18:0)	M + H	↓	↓	NC
24	18.34	629.5506	C41H76O5	DG (18:1/0:0/20:1)	M-H20-H	↑	↑	Glycerolipids
25	18.58	836.6542	C49H94NO8P	PE-NMe2 (18:1/24:1)	M-H20-H	↑	↑	Glycerophospholipids
26	19.46	927.6815	C63H94O6	TG (18:4/22:5/20:5)	M-H20-H	↑	↑	Glycerolipids
27	19.47	853.6671	C57H92O6	TG (14:0/20:5/20:4)	M-H20-H	↑	↑	Glycerolipids
28	20.06	873.7097	C57H94O6	TG (14:0/20:4/20:4)	M-H	↓	↓	Glycerolipids
29	22.84	839.5599	C47H83O10P	PA (i-24:0)	M + H	↑	↑	NC
30	23.99	625.5183	C41H70O5	DG (38:5)	M + H-H2O	↓	↓	Glycerolipids
31	24.29	901.5058	C46H80O13P2	PGP (18:1/22:5)	M-H	↓	↓	Glycerophospholipids

Model[#]: Trends of the model group compared with the control group of metabolites. Hawthorn[#]: Trends of the treatment group compared with the model group of metabolites. NC: not classified.

hypertension were identified in this study, mainly produced in the plasma of hepatocytes, including fatty acids, glycerolipids (including TG, DG), and glycerophospholipids (including PC, PE, PS, and PA) (Alves-Bezerra and Cohen, 2017). Hepatocytes are the major hepatic parenchymal cells that control hepatic biochemical and metabolic functions and play a key role in lipid metabolism (Gong et al., 2017). These lipid overexpressions can result in excessive accumulation of fat in hepatocytes, and ultimately lead to elevated blood lipids, which are the main risk factors for hypertension (Graessler et al., 2009).

Glycerophospholipids and sphingolipids are common in all tissues, and sphingolipids are the most important polar lipids in biology (Castro-Gómez et al., 2015). Based on the nature of their polar groups, glycerophospholipids are broadly classified as PC, PE, PS, phosphatidylinositol (PI), PA and cardiolipin (CL) (Castro-Gómez et al., 2015; Wang et al., 2020). PC and PE are the two most abundant phospholipids in all mammalian cell membranes (Wang et al., 2020). It has been shown that inhibition of PC synthesis impairs the secretion of very low density lipoproteins (LDL) and that abnormal changes in PC or PE levels in various tissues lead to metabolic disorders and are associated with disease progression, such as hypertension, atherosclerosis, insulin resistance and obesity (van der Veen et al., 2017). PE could use different substrates and enzymes to synthesize PS through two metabolic pathways. In the presence of the same ER enzyme, the reaction is reversible, and PS can in turn regenerate PE and serine (Castro-Gómez et al., 2015).

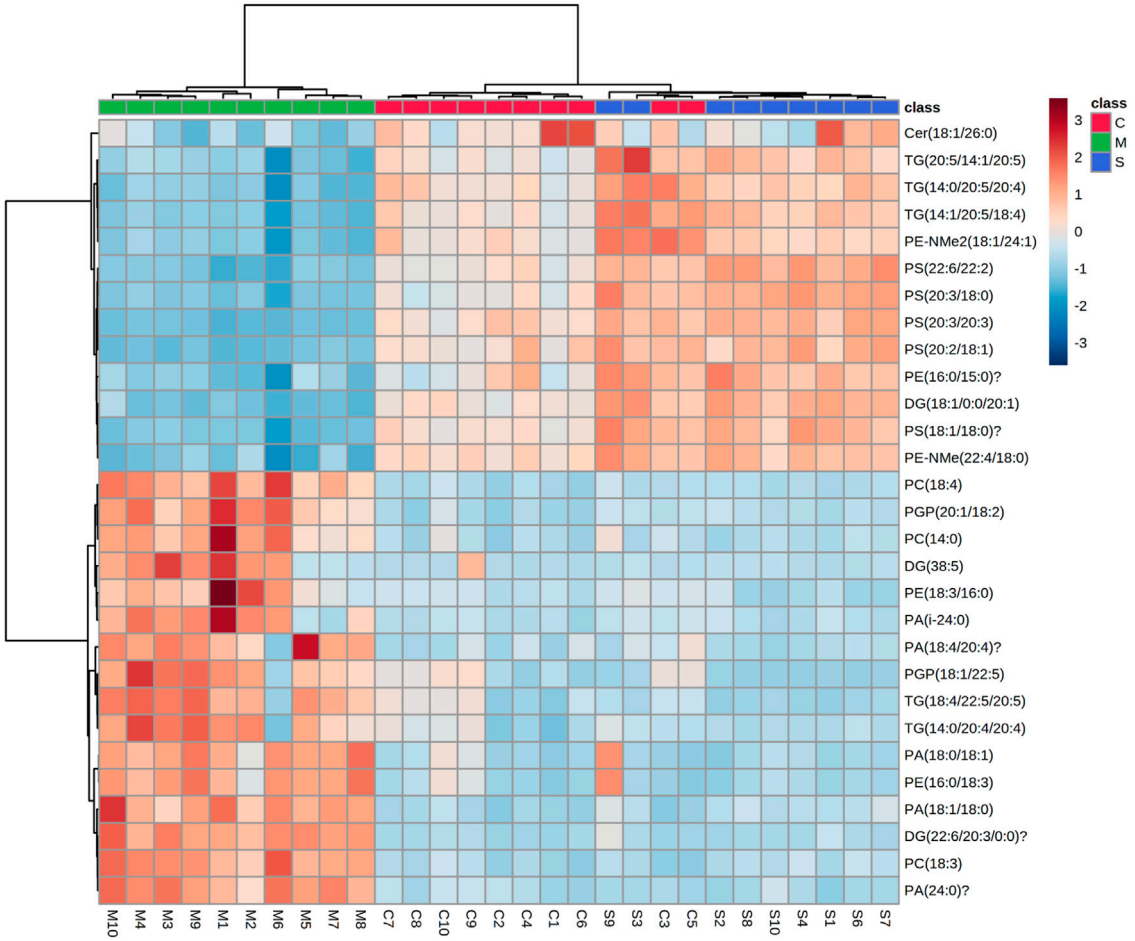

FIGURE 6
Heat map of the 31 differential lipid metabolites between the control (C1-C10) group, model (M1-M10) group and S (S1-S4 and S6-S10) group. Rows: samples; columns: metabolites. Dark red plots indicated upregulated metabolites and dark blue plots indicated downregulated metabolites in rats.

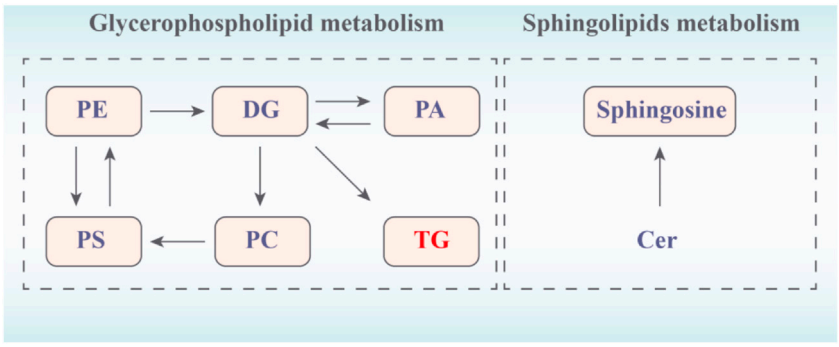

FIGURE 7
Network of changes in potential biomarkers of SHR regulated by hawthorn (red: upregulated, blue: downregulated).

Sphingolipids consist of PC or PE, and mainly include Cer, sphingomyelin (SM), and glycosphingolipids (GSLs), which are involved in various indispensable metabolic, neural and intracellular signaling processes (Castro-Gómez et al., 2005; Wang et al., 2020). Sphingolipids are broken down by sphingomyelinase to produce Cer and PC which accelerate the formation of DG by phosphatidylcholine. DG is the final product of the lipid signaling pathway, and plays a role in regulating protein kinase C activity and calcium release with second messenger inositol 1,4,5-triphosphate (Au et al., 2017). TG could be lipolyzed to large amounts of free fatty acids (FFA). FFA contribute to the development of hypertension by causing a sustained accumulation of DG and TG in the liver and muscle, leading to endothelial diastolic dysfunction, inactivating NO oxidation and activating some serine/threonine kinases (Kulkarni et al., 2013), which may induce hypertension lipotoxicity (Kulkarni et al., 2013; Hu et al., 2010). In fact, compared with WKY, the results of this study showed that increased Cer (18:1/26:0), PC (18:4; 14:0; 18:3) and PE (16:0/18:3; 18:3/16:0) in SHR accelerated the release of PS (20:3/20:3; 20:2/18:1; 20:3/16:0; 18:1/18:0; 22:6/22:2), DG (22:6/20:3/0:0; 38:5), resulting in increased TG (14:0/20:4/20:4). However, these changes were apparently reversed after hawthorn treatment. Therefore, hawthorn can play a therapeutic role in hypertension by regulating Cer, PC, PE, PS, DG and TG. It is worth noting that compared with WKY, the NO content in SHR was significantly reduced, indicating that hypertension was accompanied by endothelial dysfunction. However, after the intervention of hawthorn, the NO content was higher than that of SHR, which indicated that hawthorn had a certain improvement effect on endothelial dysfunction and played a role in the treatment of hypertension.

In summary, this study revealed the overall changes in the hawthorn extract treatment of hypertension by lipidomics technology, a total of 31 biomarkers and 3 pathways were identigfied. The results showed that after hawthorn treatment, the blood pressure level, liver lipid accumulation and lipid metabolism disorder in SHR were positively alleviated. Additionally, the vascular endothelial damage was improved and inflammatory factors inhibited in liver. In general, hawthorn could antagonize hypertension by regulating specific lipid molecules through lipidomics.

Data availability statement

The original contributions presented in the study are included in the article/Supplementary Material, further inquiries can be directed to the corresponding authors.

Ethics statement

The animal study was reviewed and approved by The Animal Ethics Committee of the Affiliated Hospital of Shandong University of Traditional Chinese Medicine.

Author contributions

LS: Conceptualization, data curation, formal analysis, software, investigation, formal analysis, writing—original draft. BC: Data curation, visualization. ZM: Data curation, visualization, investigation, software. HZ: Software, investigation. MX: Visualization, software. Validation. HJ: Conceptualization, project administration, funding acquisition. FZ: Methodology, writing-review and editing. ZT: Methodology, writing-review and editing.

Funding

This research was supported by the Science and technology development plan of Shandong Administration of traditional Chinese Medicine (2019–0021) and approved by the Youth and innovation talent introduction and education plan of colleges and universities in Shandong Province in 2021: Active natural products research and development team.

Acknowledgments

We thank LS, BC, MX, ZM, HZ, HJ, FZ, and ZT for their participation and contributions to this study.

Conflict of interest

The authors declare that the research was conducted in the absence of any commercial or financial relationships that could be construed as a potential conflict of interest.

Publisher's note

Supplementary material

The Supplementary Material for this article can be found online at: https://www.frontiersin.org/articles/10.3389/fphar.2022.963280/full#supplementary-material

References

Ahmadipour, B., Kalantar, M., Schreurs, N. M., Raza, S. H. A., Khan, R., and Khan, S. (2020). Flavonoid bioactive compounds of hawthorn extract can promote growth, regulate electrocardiogram waves, and improve cardiac parameters of pulmonary hypertensive chickens. *Poult. Sci.* 99 (2), 974–980. doi:10.1016/j.psj.2019.10.022

Alseekh, S., Aharoni, A., Brotman, Y., Contrepois, K., D'Auria, J., Ewald, J., et al. (2021). Mass spectrometry-based metabolomics: A guide for annotation, quantification and best reporting practices. *Nat. Methods* 18 (7), 747–756. doi:10.1038/s41592-021-01197-1

Alves-Bezerra, M., and Cohen, D. E. (2017). Triglyceride metabolism in the liver. *Compr. Physiol.* 8 (1), 1–8. doi:10.1002/cphy.c170012

Au, A., Cheng, K. K., and Wei, L. K. (2017). Metabolomics, lipidomics and pharmacometabolomics of human hypertension. *Adv. Exp. Med. Biol.* 956, 599–613. doi:10.1007/5584_2016_79

Boone, S., Mook-Kanamori, D., Rosendaal, F., den Heijer, M., Lamb, H., de Roos, A., et al. (2019). Metabolomics: A search for biomarkers of visceral fat and liver fat content. *Metabolomics* 15 (10), 139. doi:10.1007/s11306-019-1599-x

Castro-Gómez, P., Garcia-Serrano, A., Visioli, F., and Fontecha, J. (2015). Relevance of dietary glycerophospholipids and sphingolipids to human health. *Prostagl. Leukot. Essent. Fat. Acids* 101, 41–51. doi:10.1016/j.plefa.2015.07.004

Chang, W. T., Dao, J., and Shao, Z. H. (2005). Hawthorn: Potential roles in cardiovascular disease. *Am. J. Chin. Med.* 33 (1), 1–10. doi:10.1142/S0192415X05002606

Chen, Q. (2006). *Chinese medicine Pharmacology research methodology*. Beijing: People's Medical Publishing House.

Cloud, A. M. E., Vilcins, D., and McEwen, B. J. (2019). The effect of hawthorn (*crataegus spp.*) on blood pressure: A systematic review. *Adv. Integr. Med.* 7, 167–175. doi:10.1016/j.aimed.2019.09.002

Dong, H., Zhang, S., Du, W., Cong, H., and Zhang, L. (2020). Pharmacodynamics and metabonomics study of tianma gouteng decoction for treatment of spontaneously hypertensive rats with liver-yang hyperactivity syndrome. *J. Ethnopharmacol.* 253, 112661. doi:10.1016/j.jep.2020.112661

Duan, J. J., and Xie, P. (2020). The potential for metabolomics in the study and treatment of major depressive disorder and related conditions. *Expert Rev. Proteomics* 17 (4), 309–322. doi:10.1080/14789450.2020.1772059

Furse, S., Watkins, A. J., and Koulman, A. (2020). Extraction of lipids from liquid biological samples for high-throughput lipidomics. *Molecules* 25 (14), 3192. doi:10.3390/molecules25143192

Gika, H., Virgiliou, C., Theodoridis, G., Plumb, R. S., and Wilson, I. D. (2019). Untargeted LC/MS-Based metabolic phenotyping (Metabonomics/Metabolomics): The state of the art. *J. Chromatogr. B Anal. Technol. Biomed. Life Sci.* 1117, 136–147. doi:10.1016/j.jchromb.2019.04.009

Goit, L. N., and Yang, S. (2019). Treatment of hypertension: A review. *Yangtze Med.* 3 (2), 101–123. doi:10.4236/ym.2019.32011

Gong, Z., Tas, E., Yakar, S., and Muzumdar, R. (2017). Hepatic lipid metabolism and non-alcoholic fatty liver disease in aging. *Mol. Cell. Endocrinol.* 455, 115–130. doi:10.1016/j.mce.2016.12.022

Graessler, J., Schwudke, D., Schwarz, P. E., Herzog, R., Shevchenko, A., Bornstein, S. R., et al. (2009). Top-down lipidomics reveals ether lipid deficiency in blood plasma of hypertensive patients. *PLoS One* 4 (7), e6261. doi:10.1371/journal.pone.0006261

Gronewold, J., Kropp, R., Lehmann, N., Stang, A., Mahabadi, A. A., and Kälsch, H. (2019). Cardiovascular risk and atherosclerosis progression in hypertensive persons treated to blood pressure targets. *Hypertens. 1979* 74 (6), 1436–1447. doi:10.1161/HYPERTENSIONAHA.119.13827

Guma, M., Tiziani, S., and Firestein, G. S. (2016). Metabolomics in rheumatic diseases: Desperately seeking biomarkers. *Nat. Rev. Rheumatol.* 12 (5), 269–281. doi:10.1038/nrrheum.2016.1

Guo, Y., Liao, J. H., Liang, Z. L., Balasubramanian, B., and Liu, W. C. (2021). Hepatic lipid metabolomics in response to Heat stress in local broiler chickens breed (huaixiang chickens). *Vet. Med. Sci.* 7 (4), 1369–1378. doi:10.1002/vms3.462

Han, X., Li, W., Huang, D., and Yang, X. (2016). Polyphenols from hawthorn peels and fleshes differently mitigate dyslipidemia, inflammation and oxidative stress in association with modulation of liver injury in high fructose diet-fed mice. *Chem. Biol. Interact.* 257, 132–140. doi:10.1016/j.cbi.2016.08.002

Hu, C., Hoene, M., Zhao, X., Häring, H. U., Schleicher, E., Lehmann, R., et al. (2010). Lipidomics analysis reveals efficient storage of hepatic triacylglycerides enriched in unsaturated fatty acids after one bout of exercise in mice. *PloS one* 5 (10), e13318. doi:10.1371/journal.pone.0013318

Jones, J. G. (2016). Hepatic glucose and lipid metabolism. *Diabetologia* 59 (6), 1098–1103. doi:10.1007/s00125-016-3940-5

Kulkarni, H., Meikle, P. J., Mamtani, M., Weir, J. M., Barlow, C. K., Jowett, J. B., et al. (2013). Plasma lipidomic profile signature of hypertension in Mexican American families: Specific role of diacylglycerols. *Hypertension* 62 (3), 621–626. doi:10.1161/HYPERTENSIONAHA.113.01396

Mills, K. T., Stefanescu, A., and He, J. (2020). The global epidemiology of hypertension. *Nat. Rev. Nephrol.* 16 (4), 223–237. doi:10.1038/s41581-019-0244-2

Nguyen, N. T., Magno, C. P., Lane, K. T., Hinojosa, M. W., and Lane, J. S. (2008b). Association of hypertension, diabetes, dyslipidemia, and metabolic syndrome with obesity: Findings from the national health and nutrition examination survey, 1999 to 2004. *J. Am. Coll. Surg.* 207 (6), 928–934. doi:10.1016/j.jamcollsurg.2008.08.022

Nguyen, P., Leray, V., Diez, M., Serisier, S., Le Bloc'h, J., Siliart, B., et al. (2008a). Liver lipid metabolism. *J. Anim. Physiol. Anim. Nutr.* 92 (3), 272–283. doi:10.1111/j.1439-0396.2007.00752.x

Rababa'h, A. M., Al Yacoub, O. N., El-Elimat, T., Rabab'ah, M., Altarabsheh, S., Deo, S., et al. (2020). The effect of hawthorn flower and leaf extract (*crataegus spp.*) on cardiac hemostasis and oxidative parameters in sprague dawley rats. *Heliyon* 6 (8), e04617. doi:10.1016/j.heliyon.2020.e04617

Rastogi, S., Pandey, M. M., and Rawat, A. K. (2016). Traditional herbs: A remedy for cardiovascular disorders. *Phytomedicine* 23 (11), 1082–1089. doi:10.1016/j.phymed.2015.10.012

Rigelsky, J. M., and Sweet, B. V. (2002). Hawthorn: Pharmacology and therapeutic uses. *Am. J. Health. Syst. Pharm.* 59 (5), 417–422. doi:10.1093/ajhp/59.5.417

Tian, Z., Zhang, S., Wang, H., Chen, Z., Sun, M., Sun, L., et al. (2020). Intervention of uncaria and its components on liver lipid metabolism in spontaneously hypertensive rats. *Front. Pharmacol.* 11, 910. doi:10.3389/fphar.2020.00910

Trefts, E., Gannon, M., and Wasserman, D. H. (2017). The liver. *Curr. Biol.* 27 (21), R1147–R1151. doi:10.1016/j.cub.2017.09.019

van der Veen, J. N., Kennelly, J. P., Wan, S., Vance, J. E., Vance, D. E., Jacobs, R. L., et al. (2017). The critical role of phosphatidylcholine and phosphatidylethanolamine metabolism in health and disease. *Biochim. Biophys. Acta. Biomembr.* 1859 (9), 1558–1572. doi:10.1016/j.bbamem.2017.04.006

Verma, T., Sinha, M., Bansal, N., Yadav, S. R., Shah, K., Chauhan, N. S., et al. (2021). Plants used as antihypertensive. *Nat. Prod. Bioprospect.* 11 (2), 155–184. doi:10.1007/s13659-020-00281-x

Wang, J., Xiong, X., and Liu, W. (2014). Traditional Chinese medicine syndromes for essential hypertension: A literature analysis of 13, 272 patients. *Evid. Based. Complement. Altern. Med.* 418206. doi:10.1155/2014/418206

Wang, R., Li, B., Lam, S. M., and Shui, G. (2020). Integration of lipidomics and metabolomics for in-depth understanding of cellular mechanism and disease progression. *J. Genet. Genomics* 47 (2), 69–83. doi:10.1016/j.jgg.2019.11.009

Wang, S. J., and Sander, G. E. (2021). Nebivolol/valsartan combination for the treatment of hypertension: A review. *Future Cardiol.* 17 (4), 573–583. doi:10.2217/fca-2020-0079

Xie, J., Jiang, H. Q., Li, Y. L., Nie, L., Zhou, H. L., Yang, W. Q., et al. (2019). Study on the intervention effects of pinggan prescription on spontaneously hypertensive rats based on metabonomic and pharmacodynamic methods. *Chin. J. Integr. Med.* 25 (5), 348–353. doi:10.1007/s11655-015-2126-1

Xu, S. Y., Bian, R. L., and Chen, X. (2002). *Experimental methodology of Pharmacology*. Beijing: People's Medical Publishing House.

Yang, W., Deng, Y., Zhou, H., Jiang, H., Li, Y., Chu, Y., et al. (2017). Metabolic characteristics of rhizoma coptidis intervention in spontaneously hypertensive rats: Insights gained from metabolomics analysis of serum. *Mol. Med. Rep.* 16 (4), 4301–4308. doi:10.3892/mmr.2017.7119

Yang, B., Xuan, S., Ruan, Q., Jiang, S. Q., Cui, H., Zhu, L. P., et al. (2020). UPLC/Q-TOF-MS/MS-Based metabolomics revealed the lipid-lowering effect of ilicis rotundae cortex on high-fat diet induced hyperlipidemia rats. *J. Ethnopharmacol.* 256, 112784. doi:10.1016/j.jep.2020.112784

Zhang, A., Sun, H., Yan, G., Wang, P., and Wang, X. (2016). Mass spectrometry-based metabolomics: Applications to biomarker and metabolic pathway research. *Biomed. Chromatogr.* 30 (1), 7–12. doi:10.1002/bmc.3453

Zhao, C. N., Meng, X., Li, Y., Li, S., Liu, Q., Tang, G. Yi., et al. (2017). Fruits for prevention and treatment of cardiovascular diseases. *Nutrients* 9 (6), 598. doi:10.3390/nu9060598

frontiers | Frontiers in Pharmacology

TYPE Original Research
PUBLISHED 12 August 2022
DOI 10.3389/fphar.2022.987695

OPEN ACCESS

EDITED BY
Guangyue Su,
Shenyang Pharmaceutical University, China

REVIEWED BY
Rongrui Wei,
Jiangxi University of Traditional Chinese Medicine, China
Shenghao Xu,
Qingdao University of Science and Technology, China

*CORRESPONDENCE
Xu-Jiong Li,
qazw3000@126.com
Li-Wei Zhang,
lwzhang@sxu.edu.cn

SPECIALTY SECTION
This article was submitted to Ethnopharmacology, a section of the journal Frontiers in Pharmacology

RECEIVED 06 July 2022
ACCEPTED 19 July 2022
PUBLISHED 12 August 2022

CITATION
Wang T, Li X-J, Qin L-H, Liang X, Xue H-H, Guo J, Li S-F and Zhang L-W (2022), Better detoxifying effect of ripe forsythiae fructus over green forsythiae fructus and the potential mechanisms involving bile acids metabolism and gut microbiota.
Front. Pharmacol. 13:987695.
doi: 10.3389/fphar.2022.987695

Better detoxifying effect of ripe forsythiae fructus over green forsythiae fructus and the potential mechanisms involving bile acids metabolism and gut microbiota

Tao Wang[1,2], Xu-Jiong Li[3]*, Ling-Hao Qin[4], Xue Liang[1], Huan-Huan Xue[1], Jing Guo[1], Shi-Fei Li[1] and Li-Wei Zhang[1]*

[1]Institute of Molecule Science, Modern Research Center for Traditional Chinese Medicine, Key Laboratory of Chemical Biology and Molecular Engineering of Ministry of Education, Shanxi University, Taiyuan, China, [2]Department of Pharmacy, Changzhi Medical College, Changzhi, China, [3]Department of Physiology, Changzhi Medical College, Changzhi, China, [4]School of Pharmacy, Guangdong Pharmaceutical University, Guangzhou, China

Forsythiae Fructus (FF), the fruit of *Forsythia suspensa* (Thunb.) Vahl. (Lianqiao), is one of the most fundamental herbs in Traditional Chinese Medicines (TCM), mainly due to its heat-clearing and detoxifying effects. There are two types of FF, the greenish fruits that start to ripen (GF) and the yellow fruits that are fully ripe (RF), called "Qingqiao" and "Laoqiao" referred to the Chinese Pharmacopoeia, respectively. It undergoes a complex series of changes during the maturation of FF. However, the clinical uses and preparation of phytopharmaceuticals of FF have not been distinguished to date. Moreover, there is limited information on the study of the difference in pharmacological activity between RF and GF. In this study, a rat model of bile duct ligation (BDL)-induced cholestasis was used to compare the differences in their effects. RF was found to have better results than GF in addressing toxic bile acids (BAs) accumulation and related pathological conditions caused by BDL. The underlying mechanism may be related to the interventions of gut microbiota. The results of the present study suggest that the better detoxifying effect of RF than GF may be indirectly exerted through the regulation of gut microbiota and thus the improvement of BAs metabolism.

KEYWORDS

forsythiae fructus, bile duct ligation, detoxifying, bile acids, gut microbiota

Introduction

Forsythia suspensa (Thumb.) Vahl. (Family Oleaceae) is widely distributed in China, Korea, Japan, and many European nations (Li et al., 2014). The dried fruit of the plant, Forsythiae Fructus (FF), named "Lianqiao" in Chinese, is one of the most recognized traditional Chinese medicines (TCM) due to its removal effects of heat and toxins (Bao et al., 2016). It has been used for anti-inflammatory, antioxidant, antiendotoxin, antimicrobial and antiviral purposes (Lu et al., 2010; Li and Peng, 2013; Kuo et al., 2014; Lee et al., 2016; Law et al., 2017). FF is listed as an official drug in Chinese, Korean, and Japanese Pharmacopoeias (Nishibe, 2002). In addition, FF has been studied and developed as a dietary supplement for food and feed considering its nutritional properties (Lu et al., 2010; Jeong et al., 2021).

According to the maturity level, FF could be classified into green Forsythiae Fructus (GF, called "Qingqiao" in Chinese) and ripe Forsythiae Fructus (RF, called "Laoqiao" in Chinese). Both of them are official sources of FF (Nishibe, 2002; Qu et al., 2008; Xia et al., 2009). F. suspensa undergoes a complex series of physical and biochemical changes during the ripening process from GF to RF. There must be differences between GF and RF in chemical constituents and biological activities. Studies showed that the contents of some representative constituents, such as forsythoside A, phillyrin, and rutin, were significantly higher in GF than in RF (Bai et al., 2015). In fact, GF is more frequently selected as a raw material for the production of herbal preparations containing FF in China. As a result, GF is often over-harvested, which in turn reduces the supply of RF. However, RF was preferred for traditional Chinese formula and export market (Qu et al., 2017). Thus, how to choose between RF and GF is still an open question, and the clinical applications of the two have not been distinguished to date. Consequently, evaluating the differences between RF and GF is both necessary and urgent (Wang et al., 2018).

In our previous investigations, eight constituents were found to be different between RF and GF. Furthermore, the antioxidant activity of GF was higher than that of RF (Jia et al., 2015). However, *in vivo* experiments on the comparison of the two have not been conducted. As a continuing program aimed at discovering the distinction between RF and GF, an animal model suitable for the comparative evaluation is urgently needed.

Obstruction of the biliary flow into the duodenum, accumulation of bile salts in the liver cells and biliary tract are known as cholestasis. As a result of cholestasis, some pathological changes occur in the organism. Some of the predominant ones at early stage include increased bile salt concentrations in plasma and hepatocyte, and decreased bile acids (BAs) in intestinal lumen (Sarac et al., 2015). The former causes pruritus, hepatocellular toxic injury and progressive hepatic fibrogenesis. While, the latter leads to bacterial proliferation, disruption of intestinal integrity, bacterial translocation and endotoxemia (Erenoğlu et al., 2011; Haque and Barritt Iv, 2016). These pathophysiological disturbances associated with cholestatic liver disease were discovered in both humans and experimental animals. A well-established experimental animal model of extrahepatic cholestasis is bile duct ligation (BDL) in rodents (Gujral et al., 2003; Pavlidis and Pavlidis, 2018). Inflammation, oxidative stress, elevated endotoxin levels and intestinal dysbacteriosis are important features of BDL model (Hong et al., 2007; Wiest et al., 2017; Tan et al., 2018). As a traditional herbal medicine, FF has effects of antifebrile, detoxification, detumescence, liver protection and cholagogue (Nishibe, 2002; Wang et al., 2018). Modern pharmacological researches also indicated that the extracts or the components of FF possessed anti-inflammatory, anti-oxidant, anti-bacterial, anti-endotoxin, and hepatobiliary protective activities (Lu et al., 2010; Kuo et al., 2014; Bao et al., 2016; Lee et al., 2016; Wang et al., 2016; Zhao et al., 2017; Qin et al., 2020). Given the many correspondences between the pathological features of the BDL model and the pharmacological effects of FF, we attempted to apply this model to the comparative evaluation of RF and GF.

In our preliminary experiments, RF and GF showed different trends in their effects on BDL animals. In view of this, more in-depth research needs to be carried out. The purpose of this study was to evaluate the similarities and differences of therapeutic effects between RF and GF, as well as the underlying mechanism. The study was designed as shown in Figure 1. We hope the results could provide references for the correct selection and reasonable application of FF.

Materials and methods

Preparation of herbal extracts

RF and GF samples were collected from Changzhi, Shanxi province of China, which is considered the main producing area of FF. The samples were authenticated by L-WZ of Shanxi University. All voucher specimens were deposited in the Institute of Molecular Science, Shanxi University, Taiyuan, China. All samples were ground to a fine powder and sieved with a bolt (20 meshes). RF and GF power (100 g) were respectively refluxed with 1,000 ml distilled water for 1 h, 2 times. The twice-extracted decoctions were combined and concentrated to generate suspensions of RF and GF (1.0 g/ml, which were relative to the quantity of the dried herbal powder).

Animal treatment

Male Sprague-Dawley rats (180–200 g, 5–6 weeks-of-age, SPF) were purchased from Si Pei Fu biotech Ltd. (Beijing, China). Animals were provided chow and water *ad libitum*, and maintained in a 12 h light/dark cycle for 1 week prior to

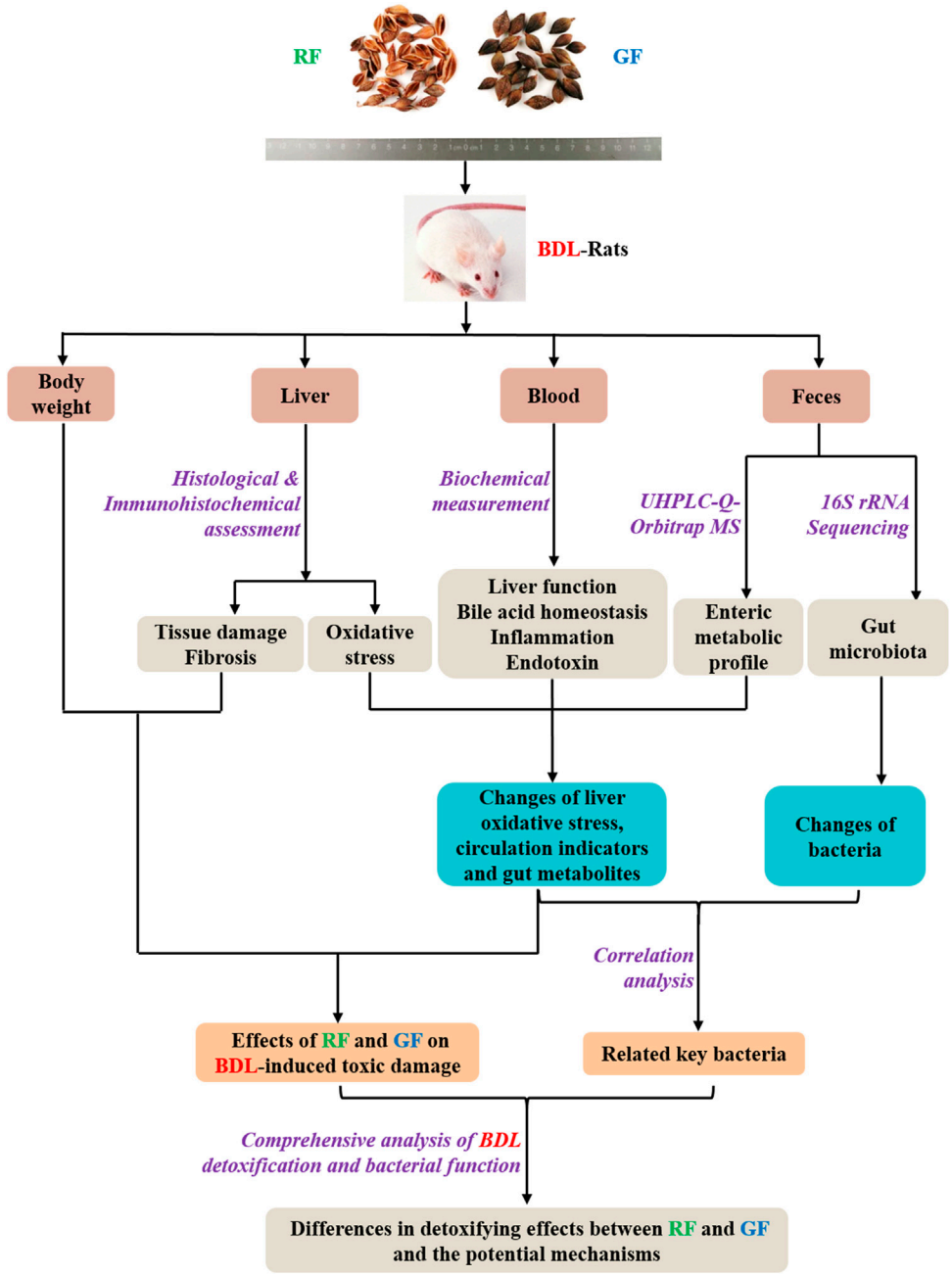

FIGURE 1
Research scheme for investigating the differences in detoxifying effects between RF and GF and the potential mechanisms.

experimentation. All rats were cared carefully under a protocol that was in accordance with institutional guidelines for animal research and was approved by the Ethics Committee of Changzhi Medical College (NO. DW2021048). Efforts were made to minimize animal suffering and reduce the number of animals used in experimental groups.

A total of 24 rats were randomly divided into four groups with 6 animals in each: group of Sham operation (Sham Group), group of bile duct ligation (BDL Group), group of bile duct ligation treated with RF (BDL_RF Group) and group of bile duct ligation treated with GF (BDL_GF Group). Under ketamine anesthesia (100 mg/kg, intramuscular), the rats in BDL, BDL_RF, and BDL_GF groups underwent common bile duct

ligation (BDL) as described in our previous research (Li et al., 2017). Briefly, the common bile duct was doubly ligated by 3/0 silk thread. Then, the abdominal layers were closed one by one after common bile duct was cut in the middle of the double ligation thread. Common bile duct was left without ligation in rats of the Sham group, and the remaining operations were the same as in the other groups. One day after BDL surgery, BDL_RF and BDL_GF groups were administrated (i.g.) 1.35 ml/kg (calculated according to the recommended dose of Chinese Pharmacopoeia) RF and GF extraction solution for 3 weeks respectively. Sham and BDL groups were i.g. administrated 1.35 ml/kg physiological saline. The body weight of each animal was assessed every day.

Three weeks after surgery, fecal and blood samples were collected from each rat. The feces were collected and transferred to sterilized airtight vials and weighted within 30 min, then immediately snap frozen with liquid nitrogen and stored in −80°C until use. Blood was centrifuged at 3,000 rpm for 10 min at 4°C to obtain the serum and stored at −20°C for further testing. Liver tissues were harvested, rinsed in cold isotonic saline and either fixed with 4% paraformaldehyde or immediately frozen in liquid nitrogen for further analysis.

Histological assessment of liver

Liver samples of rats were fixed in 10% formalin solution. Following dehydration in a gradient ascending ethanol, the liver tissues were cleared in xylene and embedded in paraffin. Then, the tissues were cut into 5 μm sections and prepared for HE and Masson staining. The obtained histological slides were examined under a light microscope (Olympus CH20, Olympus, Japan).

Immunohistochemical and oxidative stress assessment of liver

For immunohistochemical analysis, liver sections (4-μm thick) were prepared from paraffin-embedded specimens, using routine methods. Endogenous peroxidase was inactivated by treating sections with 3% H_2O_2 at room temperature for 15 min. After blocking with goat serum for 1 h, anti-Nrf2 antibody (1: 200, ab31163, Abcam, United States) was added for incubation at 4°C overnight. The slides were then incubated with a secondary antibody for 1 h at room temperature and visualized using DAB reagent. Yellow and brown staining in the nucleus and cytoplasm were considered positive. For measurement of oxidative stress indicators, accurately weighed liver tissue was rapidly homogenized with cold saline, centrifuged, and the supernatant was taken as the liver homogenate to be tested. The levels of SOD and MDA in livers were measured using MDA and SOD assay kits (Nanjing Jiancheng, China).

Biochemical measurement of serum

Commercial ELISA kits (Shanghai MlBio, China) of ALP, ALT, AST,γ-GT, IL-1β, IL-6, TNF-α and ET were used to determine the serum levels of these biochemical indicators according to the manufacturer's instructions. TBA, TBIL and DBIL levels were measured using commercial colorimetric assay kits (Abcam, United States) in accordance with the instructions.

Enteric metabolomics analysis

Fecal samples were immersed in 0.1% formic acid acetonitrile 3 times their total weight, and then vortexed for 1 min and ultrasonic-extracted for 10 min. The extracts were centrifuged at 12,000 rpm for 10 min at 4°C. The supernatant was filtered by 0.22 μm ultrafiltration membrane for LC-MS analysis. In addition, to investigate the stability of instruments and analytical methods, QC sample was prepared through combining 50 μL of each analyzed sample, and analyzed per 4 samples during the whole analysis process.

The metabolomics profiling was accomplished using a UHPLC Q-Exactive Orbitrap mass spectrometer (Thermo Fisher, United States) equipped with a heated electrospray ionization (HESI) probe. Acquisition mode, positive and negative ion switching; scan mode, full scan/dd-MS2; m/z acquisition range, 100–1,500; positive electrode spray voltage, 3.5 kV; negative electrode spray voltage, 2.5 kV; capillary temperature, 320°C; probe heater temperature, 300°C; sheath gas flow rate, 35 arb; auxiliary gas flow rate, 10 arb; resolution setting, MS full scan 35,000 FWHM and MS/MS 17500 FWHM; NCE settings, 20, 40, 60 eV.

Chromatography separations were performed on a Waters ACQUITY UPLC HSS T3 column (2.1 × 100 mm, 1.7 μm, Waters, United States). Mobile phase A, 0.1% formic acid water; mobile phase B, acetonitrile; flow rate, 0.2 ml min-1; injection volume, 5 μL; column temperature, 45°C. The mobile phase gradient was as follows: 0–2 min, 2% B; 2–3 min, 2–40% B; 3–5 min, 40–43% B; 5–11 min, 43%–50% B; 11–18 min, 50–70% B; 18–23 min, 70–98% B; 23–24 min, 98% B; 24–24.5 min, 98–2% B; 24.5–27 min, 2% B.

The LC–MS raw data were exported using an Xcalibur workstation (Thermo Fisher, United States), and then imported to Compound Discoverer 3.1 (Thermo Fisher, United States) to obtain the aligned peak data. The parameters were set as follows: quality range, 100–1,500; mass tolerance, 5 ppm; retention time tolerance, 0.2 min; SNR threshold, 3. All integrated spectra were normalized to their total areas to eliminate the concentration differences. Then, metabolite peaks were introduced into Simca-P 13.0 software (Umetric, Sweden) for PCA and OPLS-DA. The quality of OPLS-DA model was validated by computing the cross-validation (double cross validation) parameter Q^2. The value of Q^2 close

to 1 indicated an excellent predictability of the model. S-plots constructed using OPLS-DA were applied to select the potential variables for differentiation. VIP values presented the impact of each metabolite in the OPLS-DA model. Metabolite peaks were then assigned by molecular weights, MS/MS, and elemental compositions, and interpreted with available biochemical databases, such as HMDB (http://www.hmdb.ca/), KEGG (https://www.kegg.jp/), METLIN (http://metlin.scripps.edu/) and Chemspider (http://www.chemspider.com/).

Microbiota analysis

Fecal genomic DNA was extracted and purified using Fast DNA SPIN extraction kits (MP Biomedicals, United States). Agarose gel electrophoresis was performed to assess the quality of the extracted DNA. The V3-V4 region of bacterial 16S rRNA gene was amplified. AMPure XP Beads (Beckman Coulter, United States) was used to purify amplicons, followed by quantification using Quant-iT PicoGreen dsDNA Assay Kit (Invitrogen, United States). Purified amplicons were mixed in equal amounts, and 2 × 300-bp pair-end sequencing was conducted on Illumina MiSeq platform. QIIME (version 1.80) was employed to process the raw data. High-quality sequences were clustered into operational taxonomic units (OTUs) at 97% sequence identity. The sequence with the highest abundance in each OTU was selected as the representative sequence for that OTU. Taxonomic classification was carried out by comparing OUT representative sequences with template sequences from Greengenes databases. The abundance matrix after removal of rare OTUs with abundances below 0.001% was used for subsequent comparative analysis between groups and visualization. Alpha diversity and taxa summaries were created through QIIME with sequencing depth and maximum rarefaction depth. The sequencing datasets are deposited in NCBI (https://www.ncbi.nlm.nih.gov/sra/PRJNA837391). The microbial community analysis was performed by Shanghai Personal Biotechnology Co., Ltd. (Shanghai, China).

Statistical analysis

All the bar plots in this study were generated with Prism 8.0 software (GraphPad, United States). Statistical differences between groups were analyzed by one-way analysis of variance (ANOVA) followed by Tukey's multiple comparisons test. Differences of microbial data between multiple samples were assessed by Mann–Whitney *U*-test. Results are presented as mean ± SEM. $p < 0.05$ was considered statistically significant. Correlations were performed by one-tailed Spearman's analysis with 95% confidence interval and heatmaps were constructed using the GENESCLOUD online platform of Personal Biotechnology (https://www.genescloud.cn/).

Results

Compared with GF, RF has a stronger effect on preventing the disease progress of bile duct ligation-rats

After 21 days, the Sham group gained an average of 71 g of body weight, while the BDL group lost 3 g of body weight. The body weight changes of rats in BDL_RF and BDL_GF groups showed significant differences ($p < 0.05$, Figure 2A). The BDL_RF group gained 40 g of body weight, while the BDL_GF group lost 23 g of body weight. Haematoxylin-eosin (HE) staining results (Figure 2B) showed that the Sham group had intact hepatic lobules with a central vein surrounded by radially arranged hepatocyte cords. Disorganized hepatic cords and inflammatory cell infiltration were found in the BDL group, and liver lobules were segmented, leading to the formation of pseudo-lobules. Cellular infiltration and liver injury were significantly reduced in the BDL_RF group. However, there was a slight remission of liver injury in the BDL_GF group compared to the BDL group. Liver fibrosis and collagen depositions in liver tissues were determined by Masson staining (Figure 2B). The Sham group showed normal liver lobular with central veins. The BDL group showed extensive collagen deposition and fibrosis. The fibrotic process was reversed in the BDL_RF group. Fibrosis remained severe in the BDL_GF group, although there appeared to be some improvement compared to the BDL group. All these results suggest that RF exerted a better disease-modifying effect on BDL rats compared to GF.

RF better alleviates bile duct ligation-induced hepatic oxidative stress than GF

Immunohistochemical staining for NF-E2-related factor 2 (Nrf2) of rat livers were shown in Figure 3A. Significantly increased Nrf2-positive areas in BDL and BDL_GF group did not counteract persistent liver damage. BDL_RF group showed both enhanced nuclear localization of Nrf2 and improvement of liver injury. As shown in Figure 3B, the levels of liver superoxide dismutase (SOD) were significantly decreased in BDL group compared to the Sham group. The SOD levels were elevated in both BDL_RF ($p < 0.05$) and BDL_GF ($p < 0.05$) groups compared to the BDL group. Compared with the BDL group, the hepatic malondialdehyde (MDA) levels were attenuated in BDL_RF ($p < 0.05$) group. The MDA levels of BDL_GF group also decreased, but the difference was not significant ($p > 0.05$) compared to the BDL group. The findings indicate that RF better alleviated the oxidative stress damage to the liver of BDL rats.

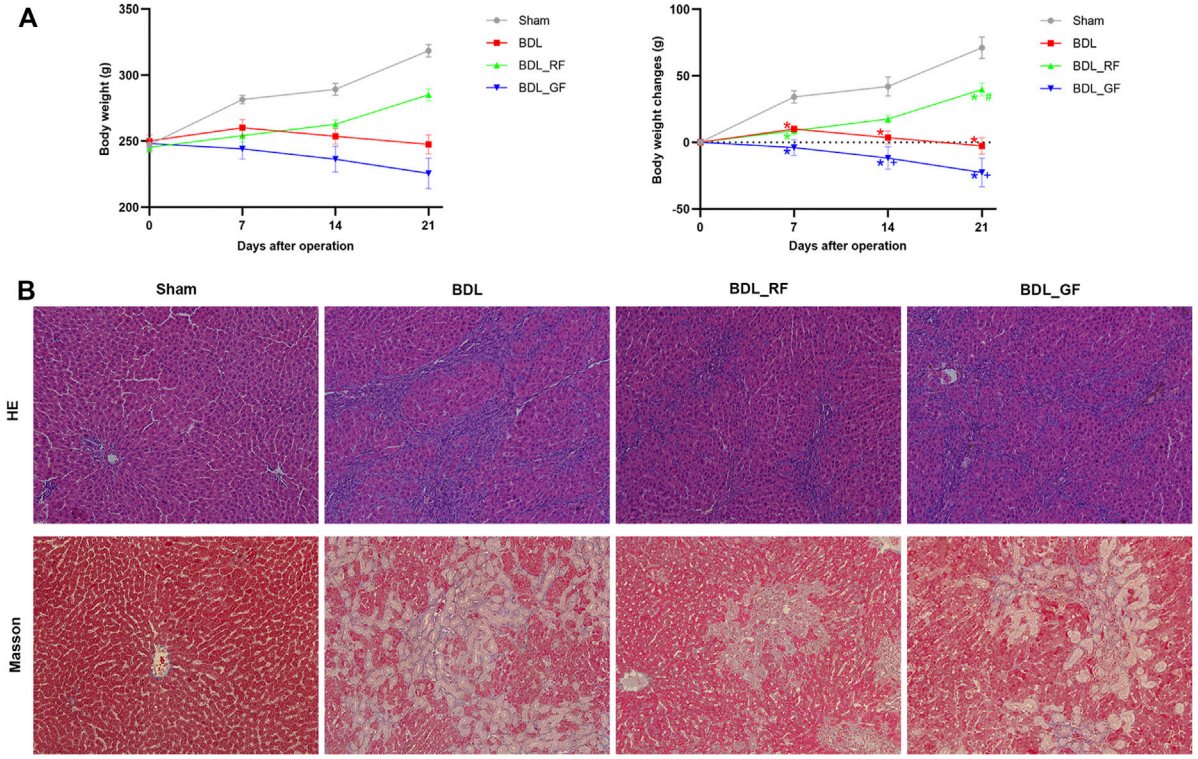

FIGURE 2
Effects of RF and GF on body weight and liver injury of BDL-rats. **(A)** Body weight changes; (*: $p < 0.05$, compared with the Sham group; #: $p < 0.05$, compared with the BDL group; +: $p < 0.05$, compared with the BDL_RF group, $n = 6$). **(B)** Representative histopathological findings of liver tissues stained with haematoxylin-eosin (HE) (×200 magnification) and Masson (×200 magnification).

RF better prevents bile duct ligation-induced deterioration of serum biochemical indicators than GF

The biochemical analysis results are presented in Figure 4. Serum levels of 11 indicators were significantly higher in the BDL group compared to the Sham group ($p < 0.05$). RF administration significantly reduced serum levels of alanine aminotransferase (ALT), γ-glutamyl transpeptidase (γ-GT), total bile acid (TBA), interleukin-1β (IL-1β), interleukin-6 (IL-6) and endotoxin (ET) compared to the BDL group ($p < 0.05$). Compared with the BDL group, GF had no significant effect ($p > 0.05$) on serum levels of TBA, IL-6 and tumor necrosis factor-α (TNF-α), and aggravated the deterioration of the other 8 indicators ($p < 0.05$). Almost all indicators (10 out of 11) in the BDL_GF group are higher than those in the BDL_RF group ($p < 0.05$), except for TNF-α ($p > 0.05$). These results show that RF had an ameliorating effect on the biochemical changes induced by BDL, while GF had no effect or made the situation worse.

RF better ameliorates bile duct ligation-induced enteric metabolic disorder, especially the decrease in bile acids metabolism, compared to GF

The intestinal metabolic differences among groups were characterized using the established UHPLC-Q-Orbitrap MS untargeted metabolomics approach. Quality control (QC) samples were analyzed for the validation of repeatability and stability of analytical methods and instrument. The base peak intensity (BPI) chromatograms were shown in Supplementary Figures S1A,B. All QC samples were within twice standard deviation (SD) in the score map (Supplementary Figure S1C), 92.37% of which variables possessed a relative standard deviation (RSD) less than 30% (Supplementary Figure S1D). The overall intestinal metabolic profile could be visualized in the principal component analysis (PCA) plot (Figure 5A). The tightly clustered QC samples also reflected the stability of the analytical system and high quality of obtained data. Compared with the Sham group, the BDL group showed obvious disorders in enteric metabolism. The

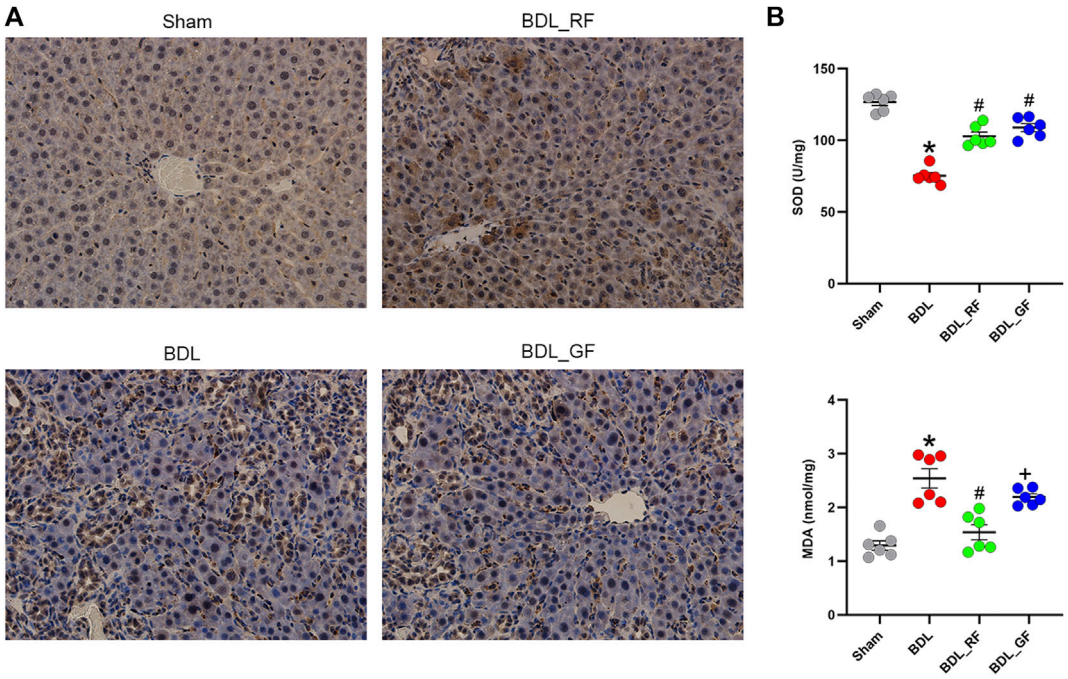

FIGURE 3
Effects of RF and GF on liver oxidative stress of BDL-rats. **(A)** Representative immunohistochemical staining for NF-E2-related factor 2 (Nrf2) (×400 magnification) of liver tissues. **(B)** Superoxide dismutase (SOD) and malondialdehyde (MDA) levels of liver tissues. (*: $p < 0.05$, compared with the Sham group; #: $p < 0.05$, compared with the BDL group; +: $p < 0.05$, compared with the BDL_RF group, $n = 6$).

BDL_RF group was close to the Sham group. In contrast, the BDL_GF and BDL groups were roughly clustered together.

The orthogonal partial least squares discriminant analysis (OPLS-DA) score plot (Figure 5B) showed two separated clusters between Sham and BDL groups, indicating that BDL led to changes in the enteric endogenous metabolism in rats. After cross-validation, the value of $Q^2 = 0.91$ demonstrated this model was robust and not over-fitted (Figure 5C). Metabolites were screened and identified based on S-plot (Figure 5D) and Variable importance on projection (VIP) values (Supplementary Table S1). Metabolites with the value of VIP >5 were defined as the most significant metabolite markers. In particular, totally six bile acid metabolites were discovered, and their identities were temporarily explored by matching retention time (RT), accurate molecular mass (MW), fragment ions with reference substances and the metabolites found in on-line databases. To be specific, the molecular formula of ion at m/z 407.2802 (RT 8.70) was calculated as $C_{24}H_{39}O_5$ with mass accuracy less than 5 ppm, which corresponded to the deprotonated molecular ions $[M-H]^-$ of β-Muricholic acid (β-MCA). Ion (RT 8.70) at m/z 453.2862 had 46 Da more than that of $[M-H]^-$ of β-MCA, which could be the ion $[M + HCOO]^-$ of β-MCA. The ions at m/z 391.2853 (RT 10.54) and m/z 437.2911 (RT 10.54) were assigned as $[M-H]^-$ and $[M + HCOO]^-$ of Ursodeoxycholic acid (UDCA). The ions at m/z 407.2803 (RT 8.15), m/z 453.2863 (RT 8.15), and m/z 815.5684 (RT 8.15), could be respectively $[M-H]^-$, $[M + HCOO]^-$, and $[2M-H]^-$ of ω-Muricholic acid (ω-MCA). Similarly, the ions at m/z 391.2858 (RT 10.56), m/z 437.2912 (RT 10.56), and m/z 783.5783 (RT 10.56), could be respectively $[M-H]^-$, $[M + HCOO]^-$, and $[2M-H]^-$ of Hyodeoxycholic acid (HDCA). Ions at RT 8.77 and RT 15.02 were identified to be an isomer of Cholic acid (CA isomer) and Deoxycholic acid (DCA). Their related parameters are listed in Supplementary Table S1. Furthermore, the box plots of relative contents of the six fecal BAs were demonstrated in Figure 5E. Compared with the Sham group, the relative intensities of six fecal BAs, including three primary BAs (β-MCA, CA isomer, UDCA) and three secondary BAs (ω-MCA, DCA, HDCA) in the BDL group, were significantly decreased ($p < 0.05$). All six BAs were significantly increased in the BDL_RF group compared with the BDL group ($p < 0.05$). However, there was no significant difference between BDL_GF group and BDL group.

For the overall profile of the gut microbiota, RF and GF have both similar and different effects on bile duct ligation-rats

The Chao1 and abundance-based coverage estimator (ACE) mainly reflect the richness of species. While the Shannon and Simpson index, mainly reflect the diversity of species. As shown

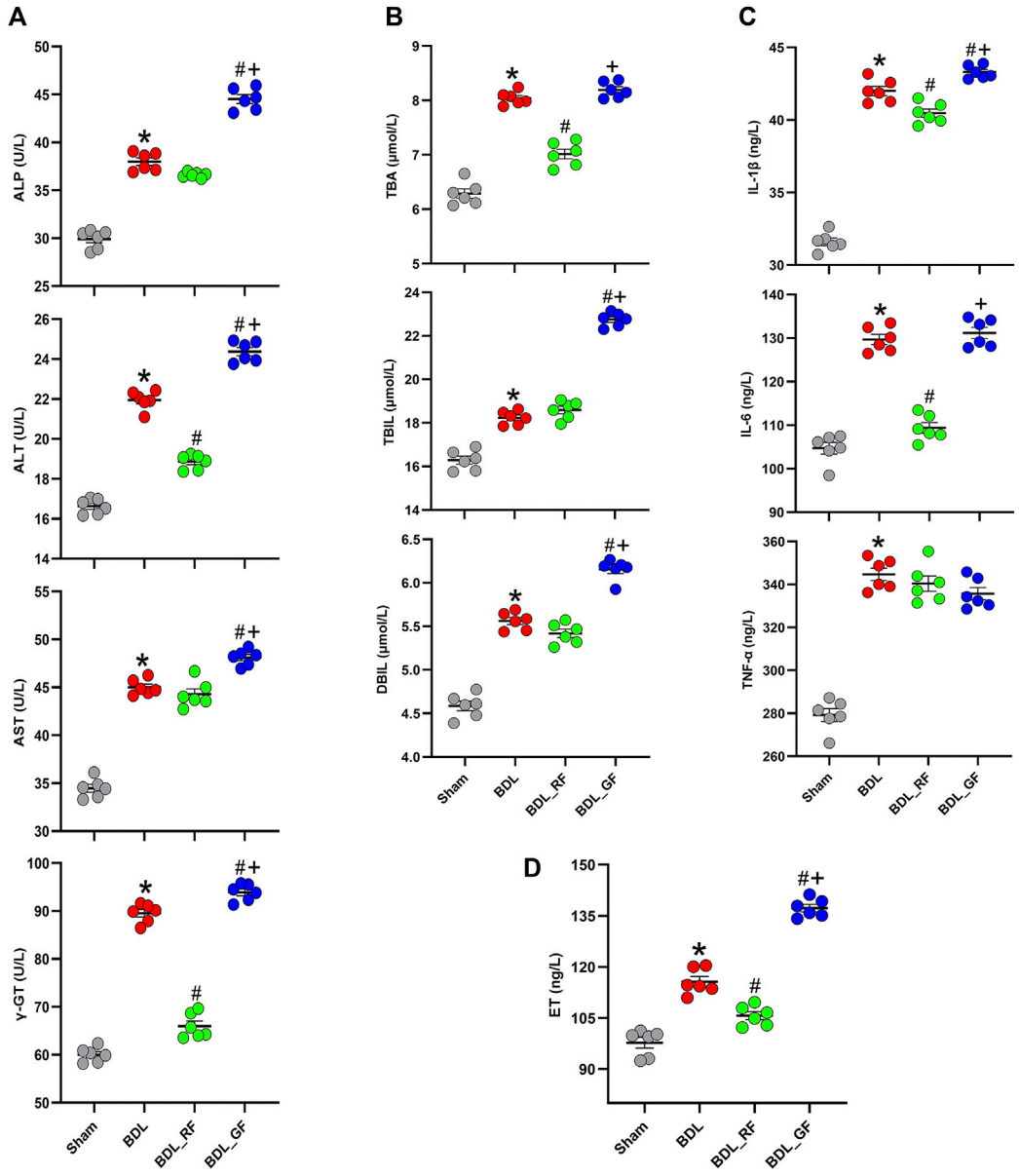

FIGURE 4
Effects of RF and GF on serum biochemical indicators of BDL-rats. **(A)** Serum levels of alkaline phosphatase (ALP), alanine aminotransferase (ALT), aspartate aminotransferase (AST), and γ-glutamyl transpeptidase (γ-GT). **(B)** Serum levels of total bile acid (TBA), total bilirubin (TBIL), and direct bilirubin (DBIL). **(C)** Serum levels of interleukin-1β (IL-1β), interleukin-6 (IL-6), and tumor necrosis factor-α (TNF-α). **(D)** Serum levels of endotoxin (ET). (*: $p < 0.05$, compared with the Sham group; #: $p < 0.05$, compared with the BDL group; +: $p < 0.05$, compared with the BDL_RF group, $n = 6$).

in Figure 6A, the Chao1 and ACE, as well as the Shannon and Simpson index, decreased in the BDL group. The four indices were even lower in the BDL_GF group than in the BDL group. The four indices in the BDL_RF group showed recovery tendency. However, none of these differences were significant ($p > 0.05$). The Simpson index was higher in the RF group than in the GF group ($p < 0.05$). As shown in Figure 6B, at the phylum level, the four groups differed in their major microbiota composition. There were some similarities between BDL_RF and BDL_GF groups, such as higher abundance of Firmicutes and lower abundance of Actinobacteria. The abundance of Proteobacteria was lower in the BDL_RF group and higher in the BDL_GF group. In addition, BDL decreased the abundance of the Bacteroidetes. RF treatment upregulated its abundance, and GF treatment made it even lower. These in turn reflect the different effects of RF and GF on the intestinal bacteria of BDL rats. As shown in Figure 6C, at the family and genus level, the four groups differed in the composition of the major species. The results in this section mainly reflect the different trends in the overall profile of gut

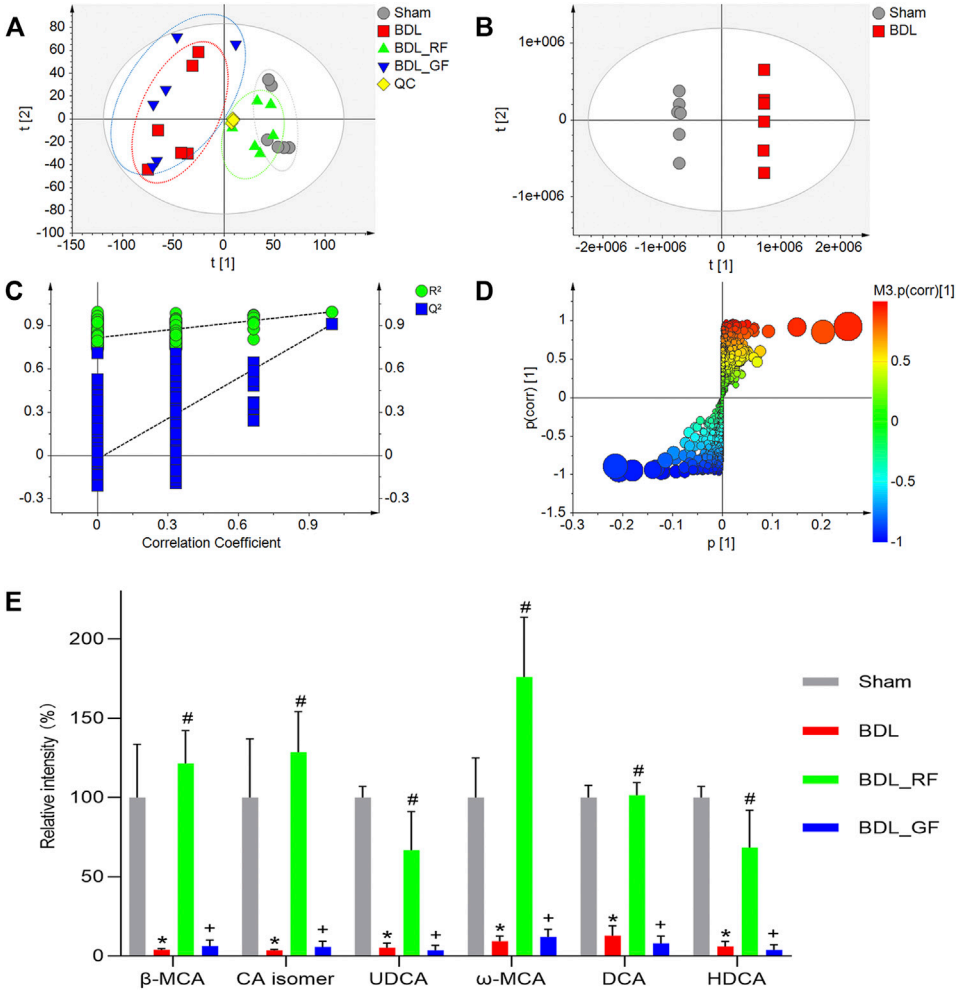

FIGURE 5
Effects of RF and GF on enteric metabolism of BDL-rats. **(A)** Principal component analysis (PCA) score plot of four groups. **(B)** Orthogonal partial least squares discriminant analysis (OPLS-DA) score plot of the Sham and BDL groups. **(C)** Cross-validation of the constructed model. **(D)** OPLS-DA S-plot of the Sham and BDL groups. The size of each point was shown according to its value of Variable importance on projection (VIP). **(E)** Relative contents variations of bile acid metabolites. (*: $p < 0.05$, compared with the Sham group; #: $p < 0.05$, compared with the BDL group; +: $p < 0.05$, compared with the BDL_RF group, $n = 6$).

microbiota between groups. The effect of BDL on important bacteria and the interventional role of RF and GF, as well as the relationship of these bacteria with BAs metabolism and disease progression will be focused on in the next section.

RF has superior effects than GF on the regulation of bacteria potentially associated with bile acids metabolism and disease progression in bile duct ligation-rats

After correlation analysis and between-group difference analysis based on the results of the correlation analysis, a total of six families and seven genera were screened for close association with BAs metabolism and disease progression (Figures 7A–D). As shown in Figure 7A, for instance, the relative abundance of Lachnospiraceae was positively correlated with the levels of six enteric BAs and the hepatic antioxidant index SOD, and negatively correlated with three serum BA-related indicators, two serum inflammatory indexes, ET, and the hepatic oxidative stress index MDA. This implies that the increase of Lachnospiraceae may predict some recovery of BAs metabolism and improvement in the condition of BDL-rats. Meanwhile, the relative abundance of Lachnospiraceae was significantly different among the four groups. Compared with the Sham group, BDL obviously reduced the abundance of Lachnospiraceae. The abundance of

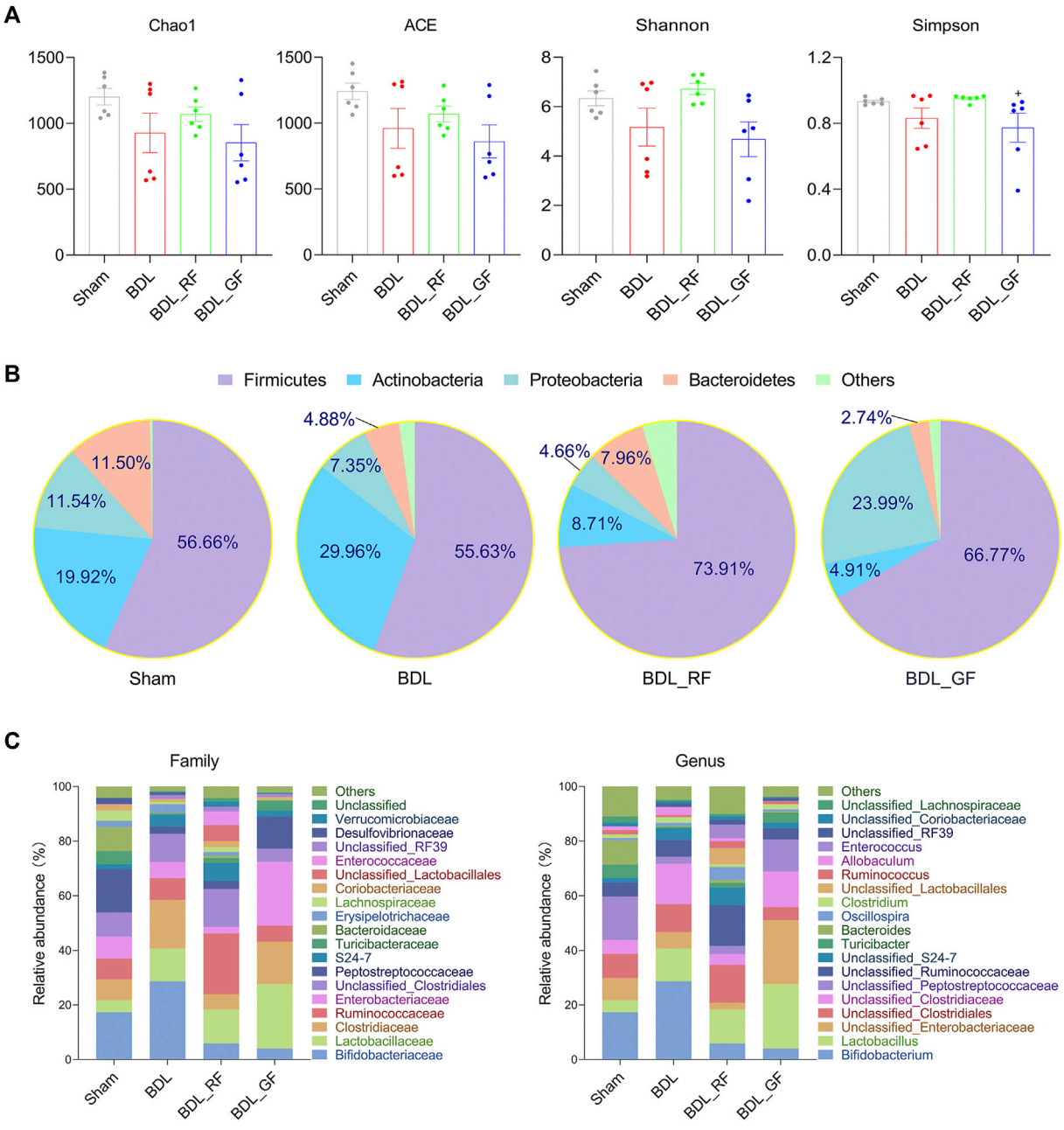

FIGURE 6
Comparison of gut microbiota profile between the four groups. **(A)** The Chao1 and abundance-based coverage estimator (ACE), as well as the Shannon and Simpson index. (+: $p < 0.05$, GF_BDL compared with the RF_BDL group, $n = 6$). **(B)** Phylum level microbiota composition. Data are the means, mainly showing the top 5 species in relative abundance. **(C)** Family and genus level microbiota composition. Data are the means, mainly showing the top 20 species in relative abundance.

Lachnospiraceae was higher in RF_BDL group ($p < 0.05$) but lower in GF_BDL group ($p > 0.05$), compared to the BDL group. The relative abundance of Lachnospiraceae in RF_BDL group was significantly higher than that in GF_BDL group ($p < 0.05$, Figure 7B). Similarly, the relative abundance of *Enterococcaceae*, *Micrococcaceae*, *Christensenellaceae*, and *Eubacteriaceae* that decreased in the BDL group were significantly higher in RF_BDL group ($p < 0.05$) than in GF_BDL group (Figure 7B). In contrast, BDL increased the relative abundance of Unclassified_Clostridia, compared to the Sham group. The relative abundance of Unclassified Clostridia was lower in RF_BDL group ($p < 0.05$) but higher in GF_BDL

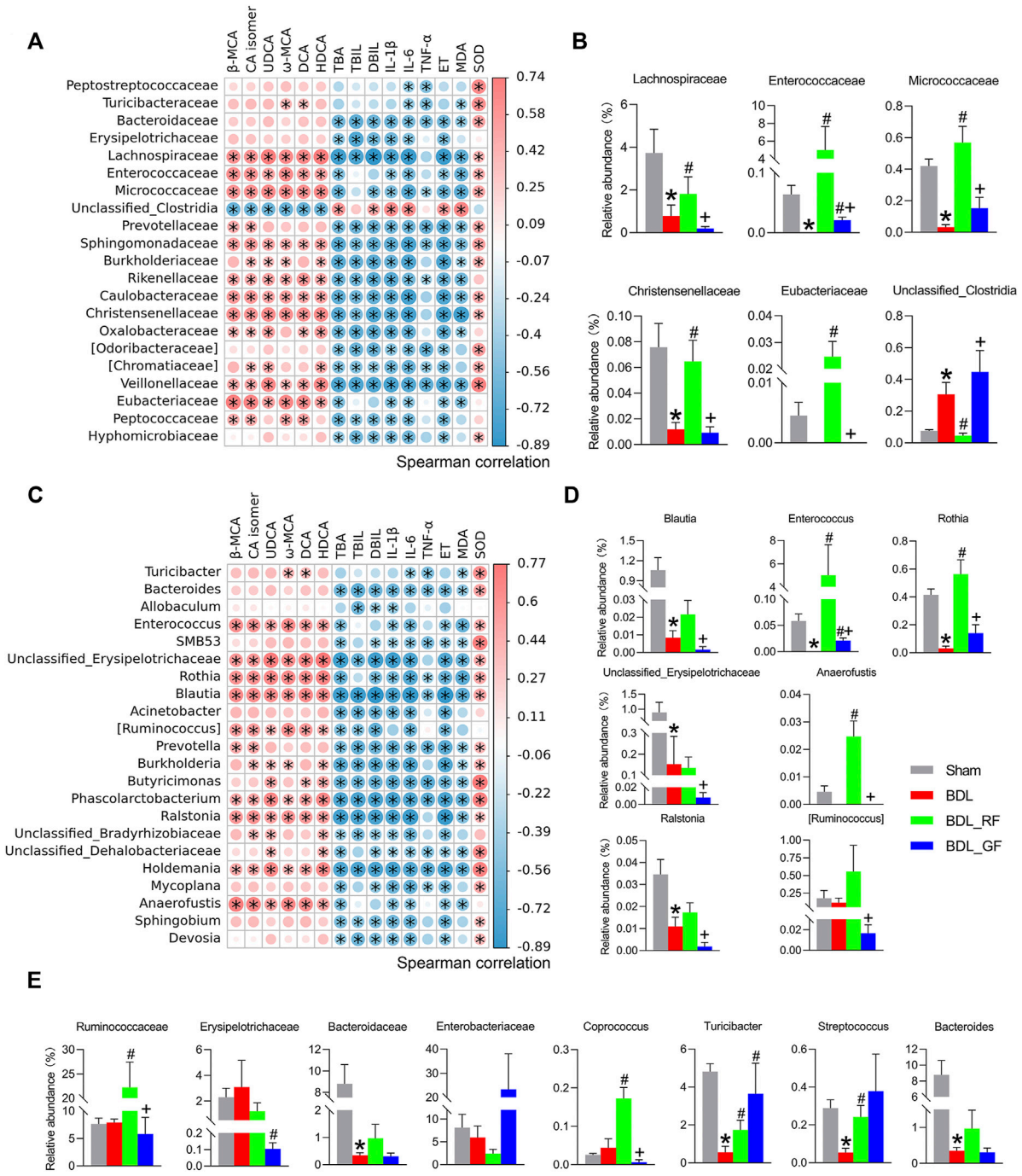

FIGURE 7
Bacteria potentially associated with bile acids metabolism and disease progression. **(A,C)** Heatmaps of Spearman correlations between bacteria and enteric bile acids, serum biochemical indicators, and liver oxidative stress at the family and genus levels. The heatmap was created based on data on bacterial abundance and enteric bile acids, serum biochemical indicators, and liver oxidative stress levels. A Spearman correlation coefficient close to 1 (>0.6) indicates a strong positive correlation, while a Spearman correlation coefficient close to −1 (<−0.6) indicates a strong negative correlation. (*: $p < 0.05$, $n = 6$). **(B,D)** Bacteria with intergroup differences in relative abundance among those screened by Spearman correlation analysis at the family and genus levels. **(E)** Intergroup differences in the relative abundance of other important bacteria at the family and genus levels. (*: $p < 0.05$, compared with the Sham group; #: $p < 0.05$, compared with the BDL group; +: $p < 0.05$, compared with the BDL_RF group, $n = 6$).

group ($p > 0.05$), compared to the BDL group (Figure 7B). The relative abundance of Unclassified_Clostridia in RF_BDL group was significantly lower than that in GF_BDL group ($p < 0.05$, Figure 7B). At the genus level, the relative abundance of *Blautia*, *Enterococcus*, *Rothia*, Unclassified_*Erysipelotrichaceae*, *Anaerofustis*, *Ralstonia*, and [*Ruminococcus*] that declined in the BDL group were significantly higher in RF_BDL group ($p < 0.05$) than in GF_BDL group (Figure 7D). In addition, intergroup comparisons of eight other important bacteria (*Ruminococcaceae*, *Erysipelotrichaceae*, *Bacteroidaceae*, *Enterobacteriaceae*, *Coprococcus*, *Turicibacter*, *Streptococcus*, and *Bacteroides*) are also presented in Figure 7E. These results indicate that RF better restored bacteria that potentially involved in BAs metabolism and disease progression in BDL-rats compared to GF.

Discussion

In this study, a BDL model was used to evaluate two different harvesting periods of FF (RF & GF). The results showed that BDL caused a series of pathological, biochemical, enteric metabolic and gut microbiota changes in rats, and that RF was superior to GF in reversing these changes. We speculate that these changes should be interrelated, and that BAs and gut microbiota may be important and critical links between them. The differences in the effects of RF and GF on BDL rats and the mechanisms responsible for such differences are discussed as follows.

BDL causes hepatic and intestinal impairment and loss of appetite in experimental animals. In the present study, RF restored the normal trend of weight gain in BDL rats, which was in contrast to the continuous weight loss caused by GF. The repair of liver tissue and attenuation of cellular infiltration by RF in BDL rats were observed. RF also alleviated collagen deposition and fibrosis in the liver caused by BDL. The effect of RF in restoring body weight in BDL rats may be partly related to its improvement in liver physiological function.

Impaired hepatic bile flow induced by BDL can lead to excessive accumulation of toxic BAs in hepatocytes, causing hepatic cholestasis and liver injury. Nrf2 is a regulator of hepatic detoxification and antioxidant mechanisms. Therefore, the activation of Nrf2 is considered to be useful for prevention or treatment of cholestatic liver injury (Shin et al., 2013). The activated Nrf2 in BDL group confirmed the spontaneous response to oxidative stress. The beneficial antioxidant effects of FF through activation of Nrf2 have been recently found in animal models of inflammatory liver injury (Zhao et al., 2017) and melanoma (Bao et al., 2016). In this study, RF and GF elevated the levels of SOD, one of the Nrf2 targets in liver. However, RF and GF have different effects on nuclear localization of Nrf2, MDA, and liver injury. Nrf2 half-life is around 13–20 min. In oxidative stress and in the presence of antioxidant molecules, the half-life of Nrf2 is duplicated (Dinkova-Kostova et al., 2001). Thus, we speculate that RF may have more antioxidant components entering the circulation and liver than GF, resulting in a longer half-life and enhanced nuclear localization of Nrf2, which in turn exerts better antioxidant and hepatoprotective effects. Additional experiments are warranted.

The increase in serum transaminases and TBA, TBIL, DBIL caused by BDL seems to reflect the toxic effects of regurgitated BAs to the liver. For these indicators of liver function and bile acid circulation, RF provided some improvement, while GF made the situation worse. The significant difference in the effect of RF and GF on these indicators suggests that they do not behave consistently in response to hepatocellular injury (reflected by ALT and AST), biliary epithelial cell injury (reflected by ALP and γ-GT) and bile acid imbalance (reflected by TBA, TBIL and DBIL) caused by BDL. The liver, located at the gateway of the portal blood flow draining the gastrointestinal tract, is strategically and uniquely positioned as the final barrier to prevent gut bacteria and bacterial products, such as ET, from entering the systemic blood stream. Therefore, the increase in serum ET caused by BDL indicates not only a deficiency of the hepatic barrier function, but also implies a disturbance of the gut microbiota. Similar to the aforementioned indicators, RF reduced ET levels, while GF exacerbates the ET elevation. It has been reported that IL-6 is the best marker of tissue inflammation and injury (Hu et al., 2020). Due to ET stimulation, Kupffer cells secrete a large number of active mediators, including cytokines such as IL-1β, IL-6, TNF-α, and reactive oxygen species (ROS). This also results in elevated hepatic function markers, eventually triggering the liver damage (Sato et al., 2016; Xie et al., 2019; Zou et al., 2020). In this study, serum IL-1β and IL-6 were increased in BDL rats and were reduced by RF. However, GF failed to bring down these cytokines. Overall, in our study, cholestasis caused by BDL left the rats in a worse condition, as evidenced by lower body weight, structural damage to liver tissue and impaired liver function. For these pathological changes, the beneficial effects of RF, rather than GF, may be generated by reducing ET, hepatic oxidative stress and systemic inflammation.

As a result of BDL, the natural flux of BAs from the liver to the gut is impaired, causing not only an accumulation of toxic BAs in the liver, but also a deficiency of BAs in the intestine (Alaish et al., 2013). Therefore, on the one hand, bacterial overgrowth and increased intestinal permeability occur in BDL due to the decreased antibacterial and intestinal protective function of BAs (De Minicis et al., 2014). This promotes the translocation of bacteria and bacterial products, such as ET, from the permeable gut into the liver via the porta circulation, exacerbating hepatic inflammation and fibrosis (Konturek et al., 2018). On the flip side, BAs and other enteric metabolites are also modified and transformed by intestinal bacteria. Thus, the interaction between these metabolites and gut microbiota links the intestine closely to the liver and plays a key role in the cholestatic disease process

(Schnabl, 2013). Changes in enteric metabolites and intestinal bacteria caused by BDL, as well as the effects of RF and GF administration were designed in the study. Metabolomics analysis showed that RF ameliorated the overall metabolic disorder caused by BDL in rats. However, GF had no significant effect. In particular, BDL induced a significant decrease in the level of major enteric BAs. This indicates that BDL intercepts the bile flow secreted from the liver to the intestine. In other words, reduced levels of bile acid-related metabolites may also be primarily involved in shaping the enteric metabolic profile in the pathological state of BDL-induced cholestasis. To some extent, fecal BAs reflect both the level of intestinal BAs and the amount of BAs excreted through the stool. In rodents, β-MCA is the main primary BA, while ω-MCA and HDCA account for the most in secondary BAs (de Aguiar Vallim et al., 2013; Li and Chiang, 2015; Lin et al., 2020). In terms of the BA pool, elevated enteric BAs (β-MCA, CA isomer, UDCA, ω-MCA, DCA, HDCA) after RF intervention in BDL rats could promote the excretion of BAs by fecal loss. It would also reasonably be expected to result in a relaxation of circulating toxic BAs accumulation. From the perspective of the intestine itself, increased levels of enteric bile acids will play a beneficial role in protecting resident bacteria, inhibiting opportunistic pathogenic bacteria, and restoring the gut microecology.

The metabolism of primary and secondary BAs in the gut is regulated by the enzymes of specific bacteria. This creates an interactive relationship between BAs and intestinal bacteria. It is worth exploring whether the alteration of BAs by BDL is accompanied by an alteration of intestinal bacteria. It is also intriguing whether the restorative effect of RF on BA disorders is associated with its effect on intestinal bacteria. Of course, it is especially crucial to clarify how the improvement of BAs metabolism and the regulation of gut microbiota contribute to the recovery of the pathological condition caused by BDL. Unlike GF, RF showed a tendency to elevate the reduction in flora richness and diversity caused by BDL. At the phylum level, GF elevated the average abundance of Proteobacteria, which contains many pathogens. While, RF and GF increased and decreased the average abundance of Bacteroidetes, which is closely related to BAs metabolism, respectively. At the family and genus level, the present study also showed that RF and GF interventions had different effects on the altered flora composition due to BDL. However, these results only reflect different trends in the overall profile of the microbiota.

To investigate whether the effects of BDL, RF and GF on gut microbiota were associated with BAs metabolism and disease progression, Spearman's correlation analysis and between-group difference analysis were successively performed. The results indicated that Lachnospiraceae, for instance, was related to increased levels of major fecal BAs and decreased levels of three serum bile acid-related indicators. Dysregulation of BAs metabolism is a key hallmark of cholestatic disease. A shrinking enteric BA leads to increases in microbes with potent pro-inflammatory molecules coupled with harmful metabolites such as ET, which in turn add to the burden of liver damage (Ridlon et al., 2013). The recovery of BAs metabolism means, to some extent, the improvement of cholestasis. In the present study, we also observed that Lachnospiraceae was associated with an increase in hepatic antioxidant marker and a decrease in hepatic oxidative stress level, two serum inflammatory markers and ET level. This implies that the increase of Lachnospiraceae may predict enhancement of BAs metabolism and remission in the condition of BDL rats. Thus, Lachnospiraceae may be a beneficial family for the improvement of BDL-induced cholestatic disease. BA formation is mediated exclusively by gut microbiota via deconjugation (the first step of BAs metabolism, removal of glycine or taurine from conjugated BAs to obtain primary BAs), dehydroxylation (the second step of BAs metabolism, removal of a hydroxyl group from primary BAs to produce secondary BAs) and other reactions. The dehydroxylation appears restricted to a limited number of intestinal anaerobes in the order of Clostridiales, including Lachnospiraceae, Ruminococcaceae and Blautia (Ridlon et al., 2006; Ridlon et al., 2013). Lachnospiraceae and Blautia are also ranked among the bacterial strains hold bile salt hydrolase (BSH) genes, catalyzing the deconjugation transformation (Song et al., 2019). These findings suggest the usefulness of Lachnospiraceae for the critical two-step conversion of intestinal BAs. Therefore, our results indicate that promoting the production of intestinal BAs and excretion of fecal BAs by upregulating the abundance of bacteria such as Lachnospiraceae may be one of the mechanisms by which RF alleviated cholestasis in BDL rats. It is worth noting that Lachnospiraceae and Ruminococcaceae are also butyrate producing bacteria. Butyrate, as a representative short-chain fatty acid (SCFA), has various protective effects on the innate and adaptive immune systems, increasing anti-bacterial peptides and suppressing inflammatory cytokine (Qin et al., 2014; Fukui, 2017). In short, these RF-boosted bacteria, which promote BAs metabolism and maintain intestinal health, can be defined as "good" bacteria for BDL-induced cholestasis.

The other four families obtained from the screening, *Enterococcaceae*, *Micrococcaceae*, *Christensenellaceae*, and *Eubacteriaceae*, were affected by BDL, RF, and GF in a similar way to *Lachnospiraceae*. Among them, *Enterococcaceae* is a family rich in strains with BSH activity (Song et al., 2019). *Micrococcaceae* (Shao et al., 2020) and *Eubacteriaceae* (Nagano and Yano, 2020) are SCFAs producing bacteria. *Christensenellaceae*, a family that is highly heritable and shows compelling associations with host health, appeared to be depleted in conditions associated with inflammation (Waters and Ley, 2019). Unclassified_*Clostridia* is the only possible "bad" family in the screened species. Its relative abundance was elevated by BDL and GF and pulled down by RF. In a previous study, an increase of *Clostridium* was found in mice at day 7 after BDL. They

postulated that increased abundance of *Clostridium* may contribute to the overall progression of liver disease by promoting Lipopolysaccharide (LPS) induced liver injury and inflammation (Cabrera-Rubio et al., 2019). Since no definite family or genus has been obtained, further work on bacterial identification and functional exploration is needed. At the genus level, *Blautia*, *Enterococcus* and *Rothia*, belong to the first three families screened at the family level, *Lachnospiraceae*, *Enterococcaceae* and *Micrococcaceae*, respectively. These genera and the families to which they belong are essentially similar in function and intergroup variation trends. The role of *Blautia* has been previously described (Ridlon et al., 2006; Ridlon et al., 2013; Song et al., 2019), while the latter two are both overwhelmingly dominant species in their respective families. Consistent with these three bacteria, the relative abundances of the other four genera obtained from the screening, i.e., Unclassified_*Erysipelotrichaceae*, *Anaerofustis*, *Ralstonia* and [*Ruminococcus*], were all significantly higher in the RF group than in the GF group. A study of Crohn's disease found *Erysipelotrichaceae* among the predominant taxa within the secondary BA-dominant assemblages (Connors et al., 2020). *Anaerofustis*, a fibrolytic bacteria, could be involved in the fermentation of carbohydrates and glucose metabolism. A study of inflammatory bowel disease (IBD) identified an enrichment of *Anaerofustis* in the control group (Masoodi et al., 2020). The decreased body weight in the BDL and GF groups in our study may be related to the depletion of such digestive bacteria in the pathological state. *Ralstonia* is the best studied genus with respect to polyhydroxyalkanoates (PHAs) accumulation (Pötter et al., 2002). PHAs, the polymers of β-hydroxy SCFAs, can be degraded in the gastrointestinal tract of mammals and result in SCFAs release. Therefore, PHAs could beneficially affect the host–microbe interaction in the gut in a way similar to SCFAs (Defoirdt et al., 2009). *Ruminococcus* species with BSH, oxidation and epimerization activities are extensively involved in BAs metabolism and have beneficial effects in promoting host intestinal homeostasis (Chen et al., 2018; Jia et al., 2018; Connors et al., 2020; Vega-Magaña et al., 2020). The different effects of RF and GF on these bacteria imply that, in addition to BA-metabolizing bacteria, the improvement of RF in BDL rats is also related to its ability to promote the growth of other beneficial and protective bacteria in the intestine.

There are species that did not stand out in the two-step screening. One of the reasons could be their discrete data. However, considering their important functions found in previous studies and their close relationship with the bacteria obtained from the screening in this study, their intergroup differences were also analyzed and shown. *Ruminococcaceae* and *Coprococcus*, similar to *Lachnospiraceae*, are both BA-dehydroxylating and SCFAs producing bacteria (Ridlon et al., 2013; Qin et al., 2014; Fukui, 2017; Connors et al., 2020). The positive relationship of *Erysipelotrichaceae* with secondary BAs has been described (Connors et al., 2020). Studies have also found a positive correlation between Turicibacter and both secondary and primary BAs (Chen et al., 2018; Kemis et al., 2019). In addition, several minor secondary BAs were positively associated with BSH producing genera *Streptococcus* (Ridlon et al., 2013; Chen et al., 2018; Huang et al., 2019; Connors et al., 2020). *Bacteroidaceae* and *Enterobacteriaceae* are two representative families with high relative abundance. The prevalence of BSH activity in *Bacteroidaceae* species reflects the wide distribution of BSH genes in gut microbiota. This is quite different from the narrow distribution of bacteria that catalyze the production of secondary BAs. In other words, for the conversion of conjugated BAs to primary BAs, these BSH producers are interchangeable with each other (Ridlon et al., 2006; Song et al., 2019). As demonstrated in Figure 7, even RF failed to have a remedy for the decline in Bacteroidaceae (including its major genus *Bacteroides*) caused by BDL. In contrast, *Enterococcaceae* (including its major genus *Enterococcus*), which also has a large number of BSH strains, improved substantially after RF administration and surpassed the Sham group. Almost all strains in *Bacteroides* and *Enterococcus* contain BSH protein sequences (Song et al., 2019). When considered in terms of BAs metabolic homeostasis, we speculated that this could be an alternative compensatory measure taken by the organism through intestinal bacteria under bile restriction stress. In pathological conditions, this potential defense mechanism requires pharmacological intervention to be amplified and realized. It remains unknown what the other consequences of the RF-induced increase in the alternative bacteria will be, other than our concern about the restoration of BAs metabolism. The roles and exact mechanisms involved are fascinating. *Enterobacteriaceae*, on the other hand, contains a large number of conditional pathogenic and pro-inflammatory members. Previous studies have shown that gut microbiome changes or dysbiosis in patients with chronic liver disease are often accompanied by a decrease in BA-dehydroxylating bacteria and an increase in pathogenic Gram-negative bacteria, particularly *Enterobacteriaceae* (Shao et al., 2021). In a study on hepatic encephalopathy, a positive correlation was found between *Enterobacteriaceae*, endotoxemia inflammation and oxidative stress indicators (Ridlon et al., 2013). The expansion of *Enterobacteriaceae* is hypothesized to initiate or exacerbate the overactive immune response and the ensuing tissue damage characteristic of disease (Connors et al., 2020). In the current study, *Enterobacteriaceae*, referred to as LPS releasing and ET producing bacteria, tended to be enriched in the GF group. This trend is consistent with the previously mentioned case of Proteobacteria to which it belongs. These "bad" bacteria may worsen the vicious cycle characterized by gut dysbiosis, metabolic imbalance and organ injuries, resulting in a poor prognosis of GF administration.

The above results of BDL modeling, FF intervention, difference comparisons, and stepwise screening in our study indicate that the dynamic interactions between intestinal BAs

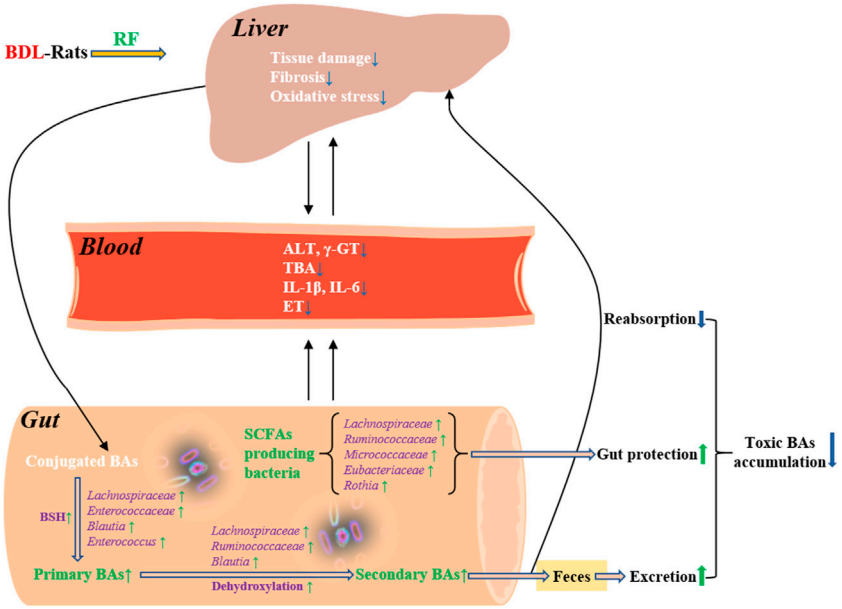

FIGURE 8
Detoxifying effects of RF on BDL-rats and the potential mechanisms involving bile acids metabolism and gut microbiota.

metabolism and gut microbiota were closely associated with disease changes. A picture is now starting to emerge regarding the liver-BA-microbiome-gut axis in BDL-induced cholestatic disease. BDL caused a decrease in both intestinal primary and secondary BA levels, accompanied by depletion of the associated BA-metabolizing bacteria. These changes are firstly a consequence of the disease and secondly act as irritants to further aggravate the severity of the disease. In addition, protective SCFAs producing bacteria and destructive ET producing bacteria may also be involved in disease progression. Some of the bacteria obtained from screening that appear to be very beneficial for disease recovery combine two types of functions: intestinal BAs metabolism and gut protection. The restorative effect of RF may be due precisely to the capture of these so-called key bacteria, which accelerate BAs metabolism and enhance intestinal protection by adjusting these core bacteria to detoxify and alleviate the disease. We focused specifically on two groups of BA-metabolizing bacteria: secondary BA producing bacteria and primary BA producing bacteria. The former group of bacteria, which has a narrow distribution and thus a relatively more important role, is at greater risk of depletion after being affected by disease. This type of bacteria was better recovered by RF. For the latter group of bacteria, which is widely distributed, RF responded mainly through alternative bacteria. GF did not show similar effects and had a tendency to encourage the reproduction of certain conditionally pathogenic bacteria.

Cholestasis is a pathologic condition characterized by impairment or cessation of the bile flow with consequent liver damage. Accumulation of toxic BAs is central to the pathogenesis of cholestatic disease. Therefore, reducing BAs overload is a therapeutic goal for the management of cholestasis. This goal could be achieved by strategies such as inhibition of BAs reabsorption from intestine. Recent studies suggest that gut microbiota play an important role in the pathophysiology of cholestatic disease and targeting microbiota may offer novel treatment options for this disease (Liu et al., 2020). In the present study, administration of RF increased the abundance of primary BA producing bacteria and secondary BA producing bacteria of BDL-rats. Their deconjugating and dehydroxylating effects accelerated fecal excretion of BAs, because deconjugated and dehydroxylated BAs are less hydrophilic and therefore are less likely to be reabsorbed. To some extent, more fecal BAs excretion relieved the body from toxic BAs accumulation. The putative detoxifying effects and potential mechanisms of RF on BDL-rats are illustrated in Figure 8.

As a well-known herb for clearing heat and detoxifying, the heat-clearing effects of FF have been studied extensively. These studies seem to show that GF has a stronger heat-clearing effect than RF (Nishibe, 2002; Dong et al., 2017; Wang et al., 2018). FF is the main ingredient of Forsythiae honeysuckle (Lian-Hua-Qing-Wen) prescription recommended in the TCM treatment protocol of COVID-19 in China (Liang et al., 2021). The better heat-clearing ability of GF (mainly based on the anti-inflammatory

properties) might explain the more frequent uses of GF in these TCM prescriptions (Nishibe, 2002; Dong et al., 2017; Wang et al., 2018). However, in this study, the detoxifying effect on BDL-induced accumulation of toxic BAs appeared to be better in RF than in GF. We assume that the direct and strong anti-inflammatory and anti-pathogenic effects of GF may be suitable for clearing heat against Fei (roughly lung and respiratory tract, Upper Jiao as referred to in TCM theory) infections. Nevertheless, severe heat-clearing effect of GF may cause deficiency and coldness of the Pi (roughly corresponds to the spleen) and Wei (roughly corresponds to the stomach), when used in middle and lower Jiao and result in poor prognosis. In this study, the weakness of the body such as loss of appetite, indigestion, disruption of normal enterohepatic circulation, and imbalance of gut microbiota caused by BDL may amplify the bitter, cold, and violent characteristics of GF. This could become a disadvantage of GF and be detrimental to treatment. While the indirect and gentle gut microbiota regulating and detoxifying effects of RF are more useful for the conveyance and dispersion treatment of hepatobiliary diseases. Corresponding in-depth experiments need to be designed and conducted in the future.

In fact, the use of FF for hepatobiliary diseases is also available in ancient TCM books. Zhang Zhong-Jing's herbal prescriptions are considered to be the classic and are still used as the guidelines for TCM clinical work nowadays. In Shang-Han Lun (Treatise on Exogenous Febrile Diseases, written around 210 AD in the Han Dynasty), he recorded the treatment of jaundice with Ma-Huang Lian-Qiao Chi-Xiao-Dou Tang (Ephedra Forsythiae Adzuki-bean decoction) (Xiong, 2000). However, since ancient times, it has not been conclusive whether GF or RF should be used for this prescription. Our research suggests that RF may be a good choice. In terms of TCM theory, RF is also closer to the medicinal properties and odor of Forsythiae root as chosen in the original Shang-Han Lun. This seems to be a remote echo and mutual corroboration of ancient TCM experience and modern pharmacological experiments.

The intestinal tract is the primary site of interaction between bile acid metabolites and bacteria. The interaction between the two profoundly affects the host, and the physio-pathological state of the host in turn affects the intestinal environment. This triangular relationship is very interesting in hepatobiliary diseases, reflecting the fact that the disease progression is not a single, static but a multiple and dynamic process. The host, flora, as well as their co-metabolites, are equally indispensable. This holistic concept is similar to the view of TCM, according to which treatment with herbs or combinations of herbs does not act on a single target, but on a multi-actor collection. The elements of this collection are always interacting and dynamically changing in a multi-dimensional space-time.

Conclusion

In the face of BDL-induced cholestasis, RF and GF showed different effects. BAs and gut microbiota may be the main players in this process and are essential for improvement of the condition, but should not be the whole picture. The causes and progression of cholestasis are complex. In addition to toxic BAs, pathologically elevated and accumulated other endogenous substances may also cause toxic damage to the organism. In-depth studies to more comprehensively assess the detoxifying effects of FF (RF and GF) and explore the intrinsic mechanisms will open up new perspectives for the medicinal research of FF.

At the end, we are aware of the limitations of the present study. Firstly, the pathological manifestations of the animals were related to the duration of the BDL model. A long period of time may result in more deaths in the model groups of animals, whereas if not enough time has elapsed, changes in the flora have not yet occurred significantly. We chose 3 weeks based on our pre-experimental experience, therefore, the time factor cannot be ignored when comparing with other relevant BDL studies. Second of all, the administration of FF in this study was converted from the recommended oral dose in humans, and the high, medium and low doses were not designed for the time being. Finally, this paper focuses on the possibility that FF (RF) may alleviate cholestasis by modulating the gut microbiota to alter the BA profile to reduce its reabsorption and increase its excretion. It is important to note that the BA profile is influenced by *de novo* BA synthesis and the feedback regulatory pathway. The complex interactions that occur between nuclear receptors, G protein-coupled receptors and BA molecules in the pathway (de Aguiar Vallim et al., 2013; Liu et al., 2020; Shao et al., 2021) are not addressed at this time. Whether FF acts directly or indirectly on these enzymes of BA synthesis, receptors, and relevant transporters is a work in progress and is expected to follow.

To our knowledge, there are few studies comparing the *in vivo* detoxifying effects of the two types of FF, of which those involving the gut microbiota have not been reported. Such comparative studies are urgently needed and have strong theoretical and practical implications. We hope this is a promising exploration and a good start.

Data availability statement

The datasets presented in this study can be found in online repositories. The names of the repository/repositories and accession number(s) can be found below: https://www.ncbi.nlm.nih.gov/, PRJNA837391.

Ethics statement

The animal study was reviewed and approved by the Ethics Committee of Changzhi Medical College.

Author contributions

TW executed the experiments and drafted the manuscript. X-JL executed the experiments and wrote a small part of the manuscript. L-HQ and XL contributed to the data analysis and figures preparation. H-HX, JG, and S-FL assisted with experiments and data collection. X-JL and L-WZ conceived and designed the experiments. L-WZ was responsible for the overall direction of the project and for the edits to the manuscript.

Funding

This research was funded by Shanxi Provincial Key Research and Development Project (201603D3114015) and Natural Science Foundation of Shanxi Province (201801D121362).

Conflict of interest

The authors declare that the research was conducted in the absence of any commercial or financial relationships that could be construed as a potential conflict of interest.

Publisher's note

All claims expressed in this article are solely those of the authors and do not necessarily represent those of their affiliated organizations, or those of the publisher, the editors and the reviewers. Any product that may be evaluated in this article, or claim that may be made by its manufacturer, is not guaranteed or endorsed by the publisher.

Supplementary material

The Supplementary Material for this article can be found online at: https://www.frontiersin.org/articles/10.3389/fphar.2022.987695/full#supplementary-material

References

Alaish, S. M., Smith, A. D., Timmons, J., Greenspon, J., Eyvazzadeh, D., Murphy, E., et al. (2013). Gut microbiota, tight junction protein expression, intestinal resistance, bacterial translocation and mortality following cholestasis depend on the genetic background of the host. *Gut Microbes* 4 (4), 292–305. doi:10.4161/gmic.24706

Bai, Y., Li, J., Liu, W., Jiao, X. C., He, J., Liu, J., et al. (2015). Pharmacokinetic of 5 components after oral administration of Fructus Forsythiae by HPLC-MS/MS and the effects of harvest time and administration times. *J. Chromatogr. B Anal. Technol. Biomed. Life Sci.* 993, 36–46. doi:10.1016/j.jchromb.2015.04.041

Bao, J. L., Ding, R. B., Zou, L. D., Zhang, C., Wang, K., Liu, F., et al. (2016). Forsythiae fructus inhibits B16 melanoma growth involving MAPKs/Nrf2/HO-1 mediated anti-oxidation and anti-inflammation. *Am. J. Chin. Med.* 44 (5), 1043–1061. doi:10.1142/S0192415X16500580

Cabrera-Rubio, R., Patterson, A. M., Cotter, P. D., and Beraza, N. (2019). Cholestasis induced by bile duct ligation promotes changes in the intestinal microbiome in mice. *Sci. Rep.* 9 (1), 12324–12410. doi:10.1038/s41598-019-48784-z

Chen, T. L., You, Y. J., Xie, G. X., Zheng, X. J., Zhao, A. H., Liu, J. J., et al. (2018). Strategy for an association study of the intestinal microbiome and brain metabolome across the lifespan of rats. *Anal. Chem.* 90 (4), 2475–2483. doi:10.1021/acs.analchem.7b02859

Connors, J., Dunn, K. A., Allott, J., Bandsma, R., Rashid, M., Otley, A. R., et al. (2020). The relationship between fecal bile acids and microbiome community structure in pediatric Crohn's disease. *ISME J.* 14 (3), 702–713. doi:10.1038/s41396-019-0560-3

de Aguiar Vallim, T. Q., Tarling, E. J., and Edwards, P. A. (2013). Pleiotropic roles of bile acids in metabolism. *Cell Metab.* 17 (5), 657–669. doi:10.1016/j.cmet.2013.03.013

De Minicis, S., Rychlicki, C., Agostinelli, L., Saccomanno, S., Candelaresi, C., Trozzi, L., et al. (2014). Dysbiosis contributes to fibrogenesis in the course of chronic liver injury in mice. *Hepatology* 59 (5), 1738–1749. doi:10.1002/hep.26695

Defoirdt, T., Boon, N., Sorgeloos, P., Verstraete, W., and Bossier, P. (2009). Short-chain fatty acids and poly-β-hydroxyalkanoates:(New) Biocontrol agents for a sustainable animal production. *Biotechnol. Adv.* 27 (6), 680–685. doi:10.1016/j.biotechadv.2009.04.026

Dinkova-Kostova, A. T., Massiah, M. A., Bozak, R. E., Hicks, R. J., and Talalay, P. (2001). Potency of Michael reaction acceptors as inducers of enzymes that protect against carcinogenesis depends on their reactivity with sulfhydryl groups. *Proc. Natl. Acad. Sci. U. S. A.* 98 (6), 3404–3409. doi:10.1073/pnas.051632198

Dong, Z. L., Lu, X. Y., Tong, X. L., Dong, Y. Q., Tang, L., and Liu, M. H. (2017). Forsythiae fructus: a review on its phytochemistry, quality control, pharmacology and pharmacokinetics. *Molecules* 22 (9), 1466. doi:10.3390/molecules22091466

Erenoğlu, C., Kanter, M., Aksu, B., Sağıroğlu, T., Ayvaz, S., Aktaş, C., et al. (2011). Protective effect of curcumin on liver damage induced by biliary obstruction in rats. *Balk. Med. J.* 2011 (4), 352–357. doi:10.5174/tutfd.2010.04312.1

Fukui, H. (2017). Gut microbiome-based therapeutics in liver cirrhosis: basic consideration for the next step. *J. Clin. Transl. Hepatol.* 5 (3), 249–260. doi:10.14218/JCTH.2017.00008

Gujral, J. S., Farhood, A., Bajt, M. L., and Jaeschke, H. (2003). Neutrophils aggravate acute liver injury during obstructive cholestasis in bile duct-ligated mice. *Hepatology* 38 (2), 355–363. doi:10.1053/jhep.2003.50341

Haque, T. R., and Barritt Iv, A. S. (2016). Intestinal microbiota in liver disease. *Best. Pract. Res. Clin. Gastroenterol.* 30 (1), 133–142. doi:10.1016/j.bpg.2016.02.004

Hong, J. Y., Sato, E. F., Hiramoto, K., Nishikawa, M., and Inoue, M. (2007). Mechanism of liver injury during obstructive jaundice: role of nitric oxide, splenic cytokines, and intestinal flora. *J. Clin. Biochem. Nutr.* 40 (3), 184–193. doi:10.3164/jcbn.40.184

Hu, Z. H., Kong, Y. Y., Ren, J. J., Huang, T. J., Wang, Y. Q., and Liu, L. X. (2020). Kidney and lung tissue modifications after BDL-induced liver injury in mice are associated with increased expression of IGFBPrP1 and activation of the NF-κB inflammation pathway. *Int. J. Clin. Exp. Pathol.* 13 (2), 192–202.

Huang, F. J., Zheng, X. J., Ma, X. H., Jiang, R. Q., Zhou, W. Y., Zhou, S. P., et al. (2019). Theabrownin from Pu-erh tea attenuates hypercholesterolemia via modulation of gut microbiota and bile acid metabolism. *Nat. Commun.* 10 (1), 4971–5017. doi:10.1038/s41467-019-12896-x

Jeong, Y. H., Hwang, Y., Kim, T. I., Oh, Y., and Ma, J. Y. (2021). Forsythia fruit prevents fulminant hepatitis in mice and ameliorates inflammation in murine macrophages. *Nutrients* 13 (8), 2901. doi:10.3390/nu13082901

Jia, J. P., Zhang, F. S., Li, Z. Y., Qin, X. M., and Zhang, L. W. (2015). Comparison of fruits of Forsythia suspensa at two different maturation stages by NMR-based metabolomics. *Molecules* 20 (6), 10065–10081. doi:10.3390/molecules200610065

Jia, W., Xie, G. X., and Jia, W. P. (2018). Bile acid–microbiota crosstalk in gastrointestinal inflammation and carcinogenesis. *Nat. Rev. Gastroenterol. Hepatol.* 15 (2), 111–128. doi:10.1038/nrgastro.2017.119

Kemis, J. H., Linke, V., Barrett, K. L., Boehm, F. J., Traeger, L. L., Keller, M. P., et al. (2019). Genetic determinants of gut microbiota composition and bile acid profiles in mice. *PLoS Genet.* 15 (8), e1008073. doi:10.1371/journal.pgen.1008073

Konturek, P. C., Harsch, I. A., Konturek, K., Schink, M., Konturek, T., Neurath, M. F., et al. (2018). Gut–liver axis: how do gut bacteria influence the liver? *Med. Sci.* 6 (3), 79. doi:10.3390/medsci6030079

Kuo, P. C., Chen, G. F., Yang, M. L., Lin, Y. H., and Peng, C. C. (2014). Chemical constituents from the fruits of Forsythia suspensa and their antimicrobial activity. *Biomed. Res. Int.* 2014, 304830. doi:10.1155/2014/304830

Law, A. H., Yang, C. L., Lau, A. S., and Chan, G. C. (2017). Antiviral effect of forsythoside a from Forsythia suspensa (Thunb.) Vahl fruit against influenza A virus through reduction of viral M1 protein. *J. Ethnopharmacol.* 209, 236–247. doi:10.1016/j.jep.2017.07.015

Lee, S. E., Lim, C. Y., Kim, H. W., and Cho, S. (2016). A study of the anti-inflammatory effects of the ethyl acetate fraction of the methanol extract of forsythiae fructus. *Afr. J. Tradit. Complement. Altern. Med.* 13 (5), 102–113. doi:10.21010/ajtcam.v13i5.14

Li, T. G., and Chiang, J. Y. (2015). Bile acids as metabolic regulators. *Curr. Opin. Gastroenterol.* 31 (2), 159–165. doi:10.1097/MOG.0000000000000156

Li, T., and Peng, T. (2013). Traditional Chinese herbal medicine as a source of molecules with antiviral activity. *Antivir. Res.* 97 (1), 1–9. doi:10.1016/j.antiviral.2012.10.006

Li, C., Dai, Y., Duan, Y. H., Liu, M. L., and Yao, X. S. (2014). A new lignan glycoside from Forsythia suspensa. *Chin. J. Nat. Med.* 12 (9), 697–699. doi:10.1016/S1875-5364(14)60107-2

Li, X. J., Chen, Y. X., Chang, Y. L., Li, S. F., Zhao, Z. F., and Zhang, H. Y. (2017). CXCR2 is involved in pulmonary intravascular macrophage accumulation and angiogenesis in a rat model of hepatopulmonary syndrome. *Clin. Sci.* 131 (2), 159–168. doi:10.1042/CS20160593

Liang, C. Y., Hui, N., Liu, Y. Z., Qiao, G. P., Li, J., Tian, L., et al. (2021). Insights into forsythia honeysuckle (lianhuaqingwen) capsules: a Chinese herbal medicine repurposed for COVID-19 pandemic. *Phytomed. Plus.* 1 (2), 100027. doi:10.1016/j.phyplu.2021.100027

Lin, M., Chen, X., Wang, Z., Wang, D. M., and Zhang, J. L. (2020). Global profiling and identification of bile acids by multi-dimensional data mining to reveal a way of eliminating abnormal bile acids. *Anal. Chim. Acta* 1132, 74–82. doi:10.1016/j.aca.2020.07.067

Liu, Y. H., Chen, K. F., Li, F. Y., Gu, Z. L., Liu, Q., He, L. Q., et al. (2020). Probiotic Lactobacillus rhamnosus GG prevents liver fibrosis through inhibiting hepatic bile acid synthesis and enhancing bile acid excretion in mice. *Hepatology* 71 (6), 2050–2066. doi:10.1002/hep.30975

Lu, T., Piao, X. L., Zhang, Q., Wang, D., Piao, X. S., and Kim, S. W. (2010). Protective effects of Forsythia suspensa extract against oxidative stress induced by diquat in rats. *Food Chem. Toxicol.* 48 (2), 764–770. doi:10.1016/j.fct.2009.12.018

Masoodi, I., Alshanqeeti, A. S., Alyamani, E. J., Allehibi, A. A., Alqutub, A. N., Alsayari, K. N., et al. (2020). Microbial dysbiosis in irritable bowel syndrome: a single-center metagenomic study in Saudi Arabia. *JGH Open* 4 (4), 649–655. doi:10.1002/jgh3.12313

Nagano, T., and Yano, H. (2020). Effect of dietary cellulose nanofiber and exercise on obesity and gut microbiota in mice fed a high-fat-diet. *Biosci. Biotechnol. Biochem.* 84 (3), 613–620. doi:10.1080/09168451.2019.1690975

Nishibe, S. (2002). The plant origins of herbal medicines and their quality evaluation. *Yakugaku Zasshi* 122 (6), 363–379. doi:10.1248/yakushi.122.363

Pavlidis, E. T., and Pavlidis, T. E. (2018). Pathophysiological consequences of obstructive jaundice and perioperative management. *Hepatobiliary Pancreat. Dis. Int.* 17 (1), 17–21. doi:10.1016/j.hbpd.2018.01.008

Pötter, M., Madkour, M. H., Mayer, F., and Steinbüchel, A. (2002). Regulation of phasin expression and polyhydroxyalkanoate (PHA) granule formation in Ralstonia eutropha H16. *Microbiology* 148 (8), 2413–2426. doi:10.1099/00221287-148-8-2413

Qin, N., Yang, F. L., Li, A., Prifti, E., Chen, Y. F., Shao, L., et al. (2014). Alterations of the human gut microbiome in liver cirrhosis. *Nature* 513 (7516), 59–64. doi:10.1038/nature13568

Qin, H., Zhang, L. L., Xiong, X. L., Jiang, Z. X., Xiao, C. P., Zhang, L. L., et al. (2020). Li-Dan-He-Ji improves infantile cholestasis hepatopathy through inhibiting calcium-sensing receptor-mediated hepatocyte apoptosis. *Front. Pharmacol.* 11, 156. doi:10.3389/fphar.2020.00156

Qu, H. H., Li, B. X., Li, X., Tu, G. Z., Lü, J., and Sun, W. J. (2008). Qualitative and quantitative analyses of three bioactive compounds in different parts of Forsythia suspensa by high-performance liquid chromatography-electrospray ionization-mass spectrometry. *Microchem. J.* 89 (2), 159–164. doi:10.1016/j.microc.2008.02.002

Qu, J. L., Yan, X. J., Li, C. Y., Wen, J., Lu, C. N., Ren, J. G., et al. (2017). Comparative evaluation of raw and ripe fruits of Forsythia suspensa by HPLC–ESI-MS/MS analysis and anti-microbial assay. *J. Chromatogr. Sci.* 55 (4), 451–458. doi:10.1093/chromsci/bmw203

Ridlon, J. M., Kang, D. J., and Hylemon, P. B. (2006). Bile salt biotransformations by human intestinal bacteria. *J. Lipid Res.* 47 (2), 241–259. doi:10.1194/jlr.R500013-JLR200

Ridlon, J. M., Alves, J. M., Hylemon, P. B., and Bajaj, J. S. (2013). Cirrhosis, bile acids and gut microbiota: unraveling a complex relationship. *Gut microbes* 4 (5), 382–387. doi:10.4161/gmic.25723

Sarac, F., Salman, T., Gun, F., Celik, A., Gurler, N., Abbasoglu, S. D., et al. (2015). Effect of probiotic supplementation on bacterial translocation in common bile duct obstruction. *Pediatr. Surg. Int.* 31 (2), 155–161. doi:10.1007/s00383-014-3643-2

Sato, K., Hall, C., Glaser, S., Francis, H., Meng, F., and Alpini, G. (2016). Pathogenesis of Kupffer cells in cholestatic liver injury. *Am. J. Pathol.* 186 (9), 2238–2247. doi:10.1016/j.ajpath.2016.06.003

Schnabl, B. (2013). Linking intestinal homeostasis and liver disease. *Curr. Opin. Gastroenterol.* 29 (3), 264–270. doi:10.1097/MOG.0b013e32835ff948

Shao, H. Q., Zhang, C. Y., Wang, C. H., and Tan, Z. J. (2020). Intestinal mucosal bacterial diversity of antibiotic-associated diarrhea (AAD) mice treated with Debaryomyces hansenii and Qiweibaizhu powder. *3 Biotech.* 10 (9), 392–411. doi:10.1007/s13205-020-02383-2

Shao, J. W., Ge, T. T., Chen, S. Z., Wang, G., Yang, Q., Huang, C. H., et al. (2021). Role of bile acids in liver diseases mediated by the gut microbiome. *World J. Gastroenterol.* 27 (22), 3010–3021. doi:10.3748/wjg.v27.i22.3010

Shin, S. M., Yang, J. H., and Ki, S. H. (2013). Role of the Nrf2-ARE pathway in liver diseases. *Oxid. Med. Cell. Longev.* 2013, 763257. doi:10.1155/2013/763257

Song, Z. W., Cai, Y. Y., Lao, X. Z., Wang, X., Lin, X. X., Cui, Y. Y., et al. (2019). Taxonomic profiling and populational patterns of bacterial bile salt hydrolase (BSH) genes based on worldwide human gut microbiome. *Microbiome* 7 (1), 9–16. doi:10.1186/s40168-019-0628-3

Tan, M. A., Kang, J. H., She, S. F., Cao, M., Li, Q., Wu, H. B., et al. (2018). Effects of yinzhihuang injection on oxidative stress and FXR gene expression in cholestatic hepatitis rats. *J. Guangzhou Univ. Tradit. Chin. Med.* 35 (3), 466–470. doi:10.13359/j.cnki.gzxbtcm.2018.03.019

Vega-Magaña, N., Galiana, A., Jave-Suárez, L. F., Garcia-Benavides, L., Del Toro-Arreola, S., Andrade-Villanueva, J. F., et al. (2020). Microbiome alterations are related to an imbalance of immune response and bacterial translocation in BDL-rats. *Iran. J. Basic Med. Sci.* 23 (2), 178–185. doi:10.22038/IJBMS.2019.36487.8753

Wang, Y., Zhao, H. F., Lin, C. X., Ren, J., and Zhang, S. Z. (2016). Forsythiaside A exhibits anti-inflammatory effects in LPS-stimulated BV2 microglia cells through activation of Nrf2/HO-1 signaling pathway. *Neurochem. Res.* 41 (4), 659–665. doi:10.1007/s11064-015-1731-x

Wang, Z. Y., Xia, Q., Liu, X., Liu, W. X., Huang, W. Z., Mei, X., et al. (2018). Phytochemistry, pharmacology, quality control and future research of forsythia suspensa (thunb.) Vahl: A review. *J. Ethnopharmacol.* 210, 318–339. doi:10.1016/j.jep.2017.08.040

Waters, J. L., and Ley, R. E. (2019). The human gut bacteria Christensenellaceae are widespread, heritable, and associated with health. *BMC Biol.* 17 (1), 83–11. doi:10.1186/s12915-019-0699-4

Wiest, R., Albillos, A., Trauner, M., Bajaj, J. S., and Jalan, R. (2017). Targeting the gut-liver axis in liver disease. *J. Hepatol.* 67 (5), 1084–1103. doi:10.1016/j.jhep.2017.05.007

Xia, Y. G., Yang, B. Y., Wang, Q. H., Liang, J., Wei, Y. H., Yu, H. D., et al. (2009). Quantitative analysis and chromatographic fingerprinting for the quality evaluation of Forsythia suspensa extract by HPLC coupled with photodiode array detector. *J. Sep. Sci.* 32 (23-24), 4113–4125. doi:10.1002/jssc.200900488

Xie, Y. Y., Guo, C. Y., Liu, Y., Shi, L. Y., and Yu, J. S. (2019). Dexmedetomidine activates the PI3K/Akt pathway to inhibit hepatocyte apoptosis in rats with obstructive jaundice. *Exp. Ther. Med.* 18 (6), 4461–4466. doi:10.3892/etm.2019.8085

Xiong, M. Q. (2000). *Advanced serial books of traditional Chinese medicine: Treatise on exogenous febrile disease*. Beijing: People's Medical Publishing House, 522–530.

Zhao, P. F., Piao, X. S., Pan, L., Zeng, Z. K., Li, Q. Y., Xu, X., et al. (2017). Forsythia suspensa extract attenuates lipopolysaccharide-induced inflammatory liver injury in rats via promoting antioxidant defense mechanisms. *Anim. Sci. J.* 88 (6), 873–881. doi:10.1111/asj.12717

Zou, Y. T., Li, S. Y., Xu, B. L., Guo, H. Y., Zhang, S. C., and Cai, Y. (2020). Inhibition of Proprotein Convertase Subtilisin/Kexin type 9 ameliorates liver fibrosis via mitigation of intestinal Endotoxemia. *Inflammation* 43 (1), 251–263. doi:10.1007/s10753-019-01114-x

frontiers | Frontiers in Pharmacology

TYPE Original Research
PUBLISHED 19 August 2022
DOI 10.3389/fphar.2022.959074

OPEN ACCESS

EDITED BY
Peng-Fei Wu,
Huazhong University of Science and Technology, China

REVIEWED BY
Yao Yufeng,
Guangzhou University of Chinese Medicine, China
Fan Yang,
University of Pennsylvania, United States

*CORRESPONDENCE
Guangtao Yao,
yaoguangtao1969@126.com

SPECIALTY SECTION
This article was submitted to Ethnopharmacology, a section of the journal Frontiers in Pharmacology

RECEIVED 01 June 2022
ACCEPTED 18 July 2022
PUBLISHED 19 August 2022

CITATION
Zhou Y, Zhou Y, Li Y, Sun W, Wang Z, Chen L, He Y, Niu X, Chen J and Yao G (2022), Targeted bile acid profiles reveal the liver injury amelioration of Da-Chai-Hu decoction against ANIT- and BDL-induced cholestasis.
Front. Pharmacol. 13:959074.
doi: 10.3389/fphar.2022.959074

Targeted bile acid profiles reveal the liver injury amelioration of Da-Chai-Hu decoction against ANIT- and BDL-induced cholestasis

YueHua Zhou[1], YunZhong Zhou[2], YiFei Li[1], Wei Sun[3], ZhaoLong Wang[2], Long Chen[4], Ye He[2], XiaoLong Niu[1], Jialiang Chen[1] and Guangtao Yao[1,3]*

[1]Shanghai Innovation Center of TCM Health Service, Shanghai University of Traditional Chinese Medicine, Shanghai, China, [2]Institute of Pharmaceutical Preparation Research, Jinghua Pharmaceutical Group Co., Ltd., Jiangsu, China, [3]Center for Drug Safety Evaluation and Research, Innovation Research Institute of Traditional Chinese Medicine, Shanghai University of Traditional Chinese Medicine, Shanghai, China, [4]Experimental Center for Science and Technology, Shanghai University of Traditional Chinese Medicine, Shanghai, China

Multiple types of liver diseases, particularly cholestatic liver diseases (CSLDs) and biliary diseases, can disturb bile acid (BA) secretion; however, BA accumulation is currently seen as an important incentive of various types of liver diseases' progression. Da-Chai-Hu decoction (DCHD) has long been used for treating cholestatic liver diseases; however, the exact mechanisms remain unclear. Currently, our study indicates that the liver damage and cholestasis status of the α-naphthylisothiocyanate (ANIT)-induced intrahepatic cholestasis and bile duct ligation (BDL)-induced extrahepatic cholestasis, following DCHD treatment, were improved; the changes of BA metabolism post-DCHD treatment were investigated by targeted metabolomics profiling by UPLC-MS/MS. DCHD treatment severely downregulated serum biochemical levels and relieved inflammation and the corresponding pathological changes including necrosis, inflammatory infiltration, ductular proliferation, and periductal fibrosis in liver tissue. The experimental results suggested that DCHD treatment altered the size, composition, and distribution of the BAs pool, led the BAs pool of the serum and liver to sharply shrink, especially TCA and TMCA, and enhanced BA secretion into the gallbladder and the excretion of BAs by the urinary and fecal pathway; the levels of BAs synthesized by the alternative pathway were increased in the liver, and the conjugation of BAs and the pathway of BA synthesis were actually affected. In conclusion, DCHD ameliorated ANIT- and BDL-induced cholestatic liver injury by reversing the disorder of BAs profile.

KEYWORDS

Da-Chai-Hu decoction, intrahepatic cholestasis, extrahepatic cholestasis, targeted metabolomics, bile acid profiles

Introduction

Cholestasis is a clinical syndrome caused by disturbances of bile secretion, intake, and flow, which cause an accumulation of bile constituents in the liver and serum (van Golen et al., 2018). Cholestasis is not only a common pathological state of many liver diseases but also a key cause of aggravating the liver disease process (Expert Committee of expert consensus on the diagnosis and treatment of cholestatic liver disease, 2015). Various causes may contribute to this condition, including noxious compounds, viral hepatitis, obstruction of the bile duct, genetic abnormality, and disturbance of the intestinal microbiota (Mariotti et al., 2018). A result of this process can be the retention of BAs, accompanied by hepatocyte damage or cholangiocyte injury, inflammation, and apoptosis. In the absence of timely treatment, cholestasis can advance to hepatic failure, fibrosis, cirrhosis, and even hepatic carcinoma (Boyer, 2007). Therefore, reducing hepatic BA overload is a primary goal for treating or blocking the development of the disease. Based on different cholestatic sites, different types can be distinguished, such as the bile duct function in intrahepatic cholestasis patients is basically normal, and the lesions are mainly manifested as lobular bile ducts and are above the bile ducts or hepatocellular lesions (Bacon et al., 2006; Burt et al., 2012). However, extrahepatic cholestasis is usually accompanied by bile duct dysfunction, and the lesions are mainly located in the septal bile ducts and below the bile duct lesions or obstruction (Bacon et al., 2006; Ofliver, 2009). Different types of cholestatic liver disease exist, such as primary biliary cholangitis (PBC), primary sclerosing cholangitis (PSC), intrahepatic cholestasis of pregnancy (ICP), and drug-induced liver injury (DILI). Most patients with cholestatic disease are characterized by intrahepatic cholestasis, but some patients have both intrahepatic and extrahepatic cholestasis (Bacon et al., 2006; European Association for the Study of the Liver, 2009). PBC and PSC are two commonly recognized types of cholestatic liver disease and have a prevalence ranging from 2 to 40 per 100,000 inhabitants and 0 to 16 per 100,000 inhabitants; the former belongs to the category of intrahepatic cholestasis; however, the latter is a mixture of intrahepatic and extrahepatic cholestasis (Boonstra et al., 2012; Nguyen et al., 2014). The development of new drugs to treat cholestasis is greatly hampered by the complications of its etiology and mechanism of injury so that there are few effective therapeutic approaches for cholestasis at present (Chinese Society of Hepatology, Chinese Medical Association; Chinese Society of Gastroenterology, Chinese Medical Association; Chinese Society of Infectious Diseases, Chinese Medical Association, 2016). In clinics, only ursodeoxycholic acid (UDCA) and obeticholic acid (OCA) are approved by the FDA for use in treating cholestasis. UDCA is the most commonly used agent to treat cholestasis, but 40% of patients exhibited tolerance for monotherapy of UDCA (Chascsa et al., 2017). Thus, OCA has gained clinical approval for a new supplementary agent for patients who were unresponsive to UDCA treatment (Samur et al., 2017). However, there are still a range of unmet therapeutic needs.

Currently, there has been an important need to develop novel safe and effective drugs for the treatment of cholestasis; traditional herbal medicines including Chinese materia medica formulae are a potential source of cholestatic treatment drugs. Da-Chai-Hu decoction (DCHD) has been used for treating digestive system diseases for more than 1,000 years in China as classical traditional Chinese materia medica formulae (Qian et al., 2016). Several studies have reported that DCHD exhibits beneficial effects on protecting the liver, cholagogic action, anti-inflammation, and regulating glucose and lipid metabolism (Kuo et al., 2019; Song et al., 2019; Wang et al., 2022). DCHD has been widely used in the clinical treatment of the digestive system diseases including cholecystitis, cholelithiasis, pancreatitis, and gastric and duodenal ulcers (Xue, 2017; Wang and Cui, 2021). It has been shown to exhibit beneficial effects on cholestatic liver damage, significantly reduce the serum levels of ALP, TBA, and TBIL, and alleviate the degree of liver fibrosis and damage (Ohta et al., 1995; Li et al., 2008; Pang et al., 2008). Furthermore, it has been demonstrated that DCHD could decrease the level of FXR mRNA expression in liver tissue and increase TBA levels in the gallbladder (Lu et al., 2015; Wang et al., 2022). A recent study indicated that DCHD inhibited liver inflammation and bile accumulation by activating PPARα, thus preventing acute intrahepatic cholestasis (Xu et al., 2022). However, it remains unclear how DCHD can improve the disorder of BA metabolism and the subsequent pathological changes in the treatment of cholestasis. Recently, studies have highlighted that the functions of BAs not only stimulated the circulatory flow of bile to promote lipid absorption but also acted as signaling molecules to regulate the BA synthesis and the homeostasis of glucose, lipid, and energy metabolism (Arab et al., 2017). A variety of enzymatic reactions and the action of intestinal flora led to a wide variety of BAs; differences in biological properties of BAs including their choleretic effect, solubilization action, and activation of BA receptors are determined by structural differences (Carey, 1984; Cabrera et al., 2019; Fiorucci et al., 2021). Interestingly, BAs and their derivatives are currently the main therapeutic drugs for the treatment of liver metabolic diseases, such as TUDCA and NorUDCA, which are the derivatives of UDCA; OCA is the new semisynthetic BA derivative of CDCA. There is a delicate balance between the therapeutic and damaging effects of BAs; therefore, the size and composition alteration of the BAs pool may reflect the impaired state of BA synthesis due to liver injury, obstruction of bile ducts, or inflammation (Chiang and Ferrell, 2020). Thus, it is conceivable that the work exploring DCHD in the treatment of cholestasis through the direction of BA metabolism has beneficial effects.

The main goal of this study was to examine the hepatoprotective effect of DCHD against acute cholestatic

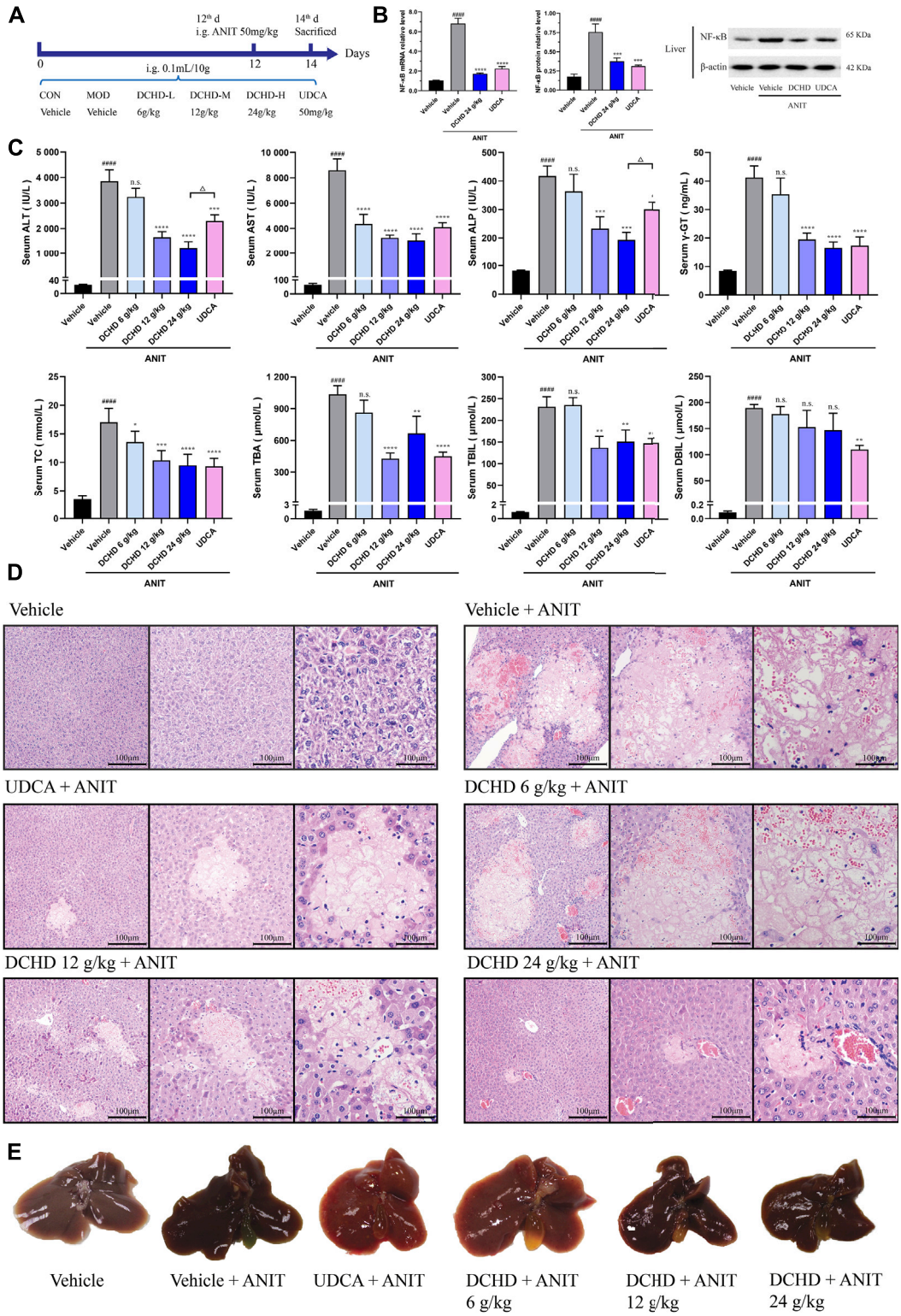

FIGURE 1
DCHD treatment alleviated cholestatic liver damage and the cholestasis status of the ANIT-induced intrahepatic cholestatic model mice. **(A)** Experimental design demonstrating DCHD treatment of ANIT-induced intrahepatic cholestatic mice. **(B)** Effects of DCHD treatment on hepatic inflammatory cytokine mRNA and protein expression levels in ANIT-induced intrahepatic cholestatic mice. **(C)** Changes of serum biochemical levels in the ANIT-induced intrahepatic cholestatic mice after DCHD treatment. **(D)** Representative images of H&E staining of liver sections in ANIT mice. **(E)** Representative liver and gallbladder pictures. Data are presented as mean ± SEM ($n = 8$). $^{\#}p < 0.05$, $^{\#\#}p < 0.01$, $^{\#\#\#}p < 0.001$, and $^{\#\#\#\#}p < 0.0001$, vs. the vehicle group; $^{*}p < 0.05$, $^{**}p < 0.01$, $^{***}p < 0.001$, and $^{****}p < 0.0001$, vs. the ANIT group; $^{\triangle}p < 0.05$, $^{\triangle\triangle}p < 0.01$, $^{\triangle\triangle\triangle}p < 0.001$, and $^{\triangle\triangle\triangle\triangle}p < 0.0001$, vs. the UDCA group.

liver damage and to better understand these mechanisms. For this purpose, we established an intrahepatic cholestatic mouse model using ANIT-induced cholestasis and an extrahepatic cholestasis mouse model using BDL-induced liver injury and then researched the conventional serological biochemical and histological changes. The changes of BA metabolism post-DCHD treatment were investigated by targeted metabolomics profiling.

Materials and methods

Reagents

The DCHD fluid extract (lot number: 43201101) was provided by Jinghua Pharmaceutical Group Co., Ltd. (Jiangsu, China). The quality control of DCHD in accordance with the Chinese State Food and Drug Administration national standard (YBZ00102008) and the quality control report of DCHD used in this study are shown in the Supplementary Material. According to the national standard, eight traditional Chinese herbs comprise 12 g Bupleuri Radix (Apiaceae; *Bupleurum falcatum* L), 9 g Scutellariae Radix (Lamiaceae; *Scutellaria baicalensis* Georgi), 9 g Paeoniae Radix Alba (Pall Paeoniaceae; *Paeonia lactiflora*), 9 g Pinelliae Rhizoma [Araceae; *Pinellia ternata* (Thunb.) Makino], 9 g Aurantii Fructus Immaturus (Rutaceae; *Citrus* × *aurantium* L), 6 g Rhei Radix et Rhizome (Polygonaceae; *Rheum palmatum* L), 15 g Zingiberis Rhizoma Recens (Zingiberaceae; *Zingiber officinale* Roscoe), and 12 g Jujubae Fructus (Rhamnaceae; *Ziziphus jujuba* Mill) and were processed in accordance with the standardized production process. DCHD contained paeoniflorin, aloe-emodin, rhein, emodin, chrysophanol, physcion, naringin, hesperidin, neohesperidin, and baicalin, analyzed by HPLC-DAD (Hu Y. et al., 2013; Hu Y. F. et al., 2013; Mao et al., 2017).

ANIT was acquired from Sigma-Aldrich (N4525, Sigma-Aldrich, United States). Ursodeoxycholic acid (UDCA) was acquired from Losan Pharma GmbH (H20150398); the γ-glutamyl transpeptidase ELISA assay kit was obtained from Signalway Antibody (EK3281, SAB, USA). ALT, AST, ALP, TBA, TBIL, and DBIL assay kits were purchased from Shino-Test Corporation (Japan). The total listing of reagents and antibodies used in this study is spelled out in Supplementary Material.

Animal experiments

All animal protocols were approved by the Use of Live Animals for Teaching and Research Committee of the Shanghai University of Traditional Chinese Medicine (Registration number: PZSHUTCM201120009). Male C57BL/6 J mice (6–8 weeks of age, 20 ± 2 g) were purchased from Vital River Laboratories (Zhejiang, China, Animal License: No. SCXK (Zhejiang) 2019-0001). Mice were raised in the SPF-level breeding room at 22°C with the light/dark cycle (12 h light/12 h dark), provided free access to normal chow diet and sterile water.

To determine the protective function of DCHD against the ANIT-induced intrahepatic cholestasis, mice were randomly divided into six groups. (A) The ANIT model group (vehicle + ANIT, n = 8), where the mice were fed with ANIT olive oil solution; (B) the control group (vehicle, n = 8), where the mice were orally administered with the same volume of olive oil; (C) the high/medium/low dose of DCHD-treated group (DCHD 24 g/kg + ANIT, DCHD 12 g/kg + ANIT, and DCHD 6 g/kg + ANIT; n = 8), where the mice were given the same volume of DCHD, and the DCHD dose in this experiment refers to the crude drug dose; and (D) the UDCA-treated group (UDCA 50 mg/kg + ANIT, n = 8), where the mice were given the same volume of UDCA. The experimental flow is shown in Figure 1A; the animals were pretreated with vehicle, DCHD, and UDCA everyday by gavage administration for 12 days prior to ANIT induction. After ANIT processing, mice were gavaged with DCHD, UDCA, or vehicle control for another 3 days. The fecal matter and urine were collected using metabolic cages before the animals were euthanized.

To determine the protective function of DCHD against the BDL-induced extrahepatic cholestasis, mice were randomly divided into six groups. (A) The BDL model group (vehicle + BDL, n = 8), where the mice were orally administered with vehicle control; (B) the Sham group (SHAM, n = 8), where the mice were given the same volume of vehicle; (C) the high/medium/low dose of DCHD-treated group (DCHD 48 g/kg + BDL, DCHD 24 g/kg + BDL, and DCHD 12 g/kg + BDL; n = 8), where the mice were given the same volume of DCHD; and (D) the UDCA-treated group (UDCA 50 mg/kg + BDL, n = 8), where the mice were given the same volume of UDCA. The experimental flow is shown in Figure 2A; the animals were pretreated with vehicle, DCHD, and UDCA everyday by gavage for 14 days prior to BDL surgery. Following the BDL surgery, mice were gavaged with DCHD, UDCA, or vehicle control for another 6 days. The fecal matter and urine were collected using metabolic cages before the animals were euthanized.

In both the experiments, the blood collected from the abdominal aorta, the tissues, the fecal matter, and urine were collected and stored at −80°C or fixed in 4% formalin solution and processed for hematoxylin and eosin (H&E) staining for biochemical assay, pathological analysis, and BAs profile analysis.

Biochemical analyses

Serum biochemical levels including ALT, AST, ALP, TC, TBA, TBIL, and DBIL were quantified using an automated clinical chemistry analyzer (7080, Hitachi, Japan). γ-glutamyl transpeptidase (γ-GT) levels were measured by using enzyme-linked immunoassay kits.

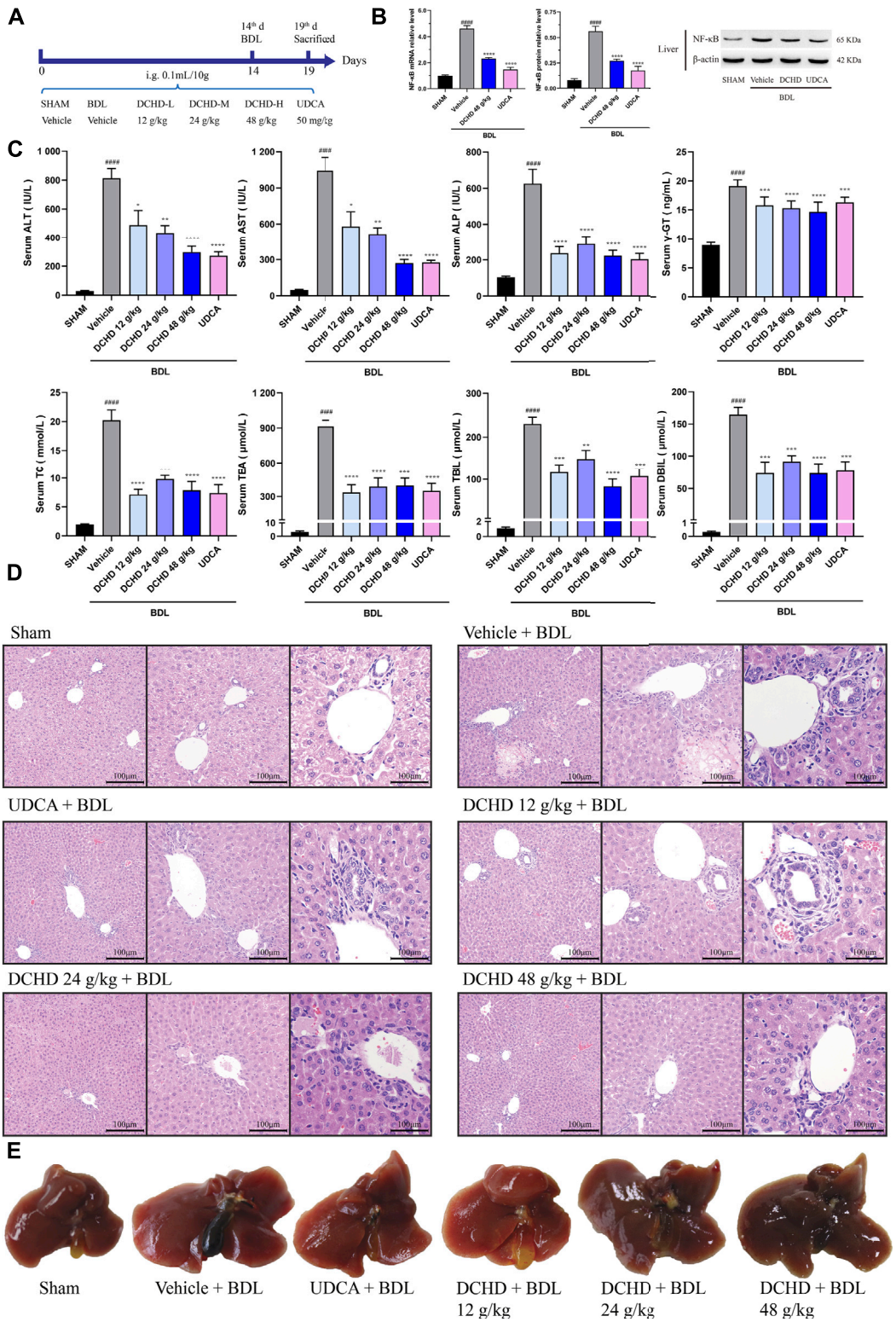

FIGURE 2
DCHD treatment alleviated cholestatic liver damage and cholestasis status of the BDL-induced extrahepatic cholestatic model mice. **(A)** Experimental design demonstrating DCHD treatment of BDL-induced extrahepatic cholestatic mice. **(B)** Effects of DCHD treatment on hepatic inflammatory cytokines mRNA and protein expression levels in BDL-induced intrahepatic cholestatic mice. **(C)** Changes of serum biochemical levels in the BDL-induced extrahepatic cholestatic mice after DCHD treatment. **(D)** Representative images of H&E staining of liver sections in BDL mice. **(E)** Representative liver and gallbladder pictures. Data are presented as mean ± SEM ($n = 8$). $^{\#}p < 0.05$, $^{\#\#}p < 0.01$, $^{\#\#\#}p < 0.001$, and $^{\#\#\#\#}p < 0.0001$, vs. the sham group; $^{*}p < 0.05$, $^{**}p < 0.01$, $^{***}p < 0.001$, and $^{****}p < 0.0001$, vs. the BDL group; $^{\triangle}p < 0.05$, $^{\triangle\triangle}p < 0.01$, $^{\triangle\triangle\triangle}p < 0.001$, and $^{\triangle\triangle\triangle\triangle}p < 0.0001$, vs. the UDCA group.

Pathological analysis

The pathological analysis of the fixed livers tissues was performed by H&E staining, which included hepatocyte degeneration, inflammation, necrosis, ductular proliferation, and fibrosis. According to the semi-quantitative scoring system (Cullen et al., 2016; Schafer et al., 2018; van Golen et al., 2018), hepatic and biliary injuries were scored as follows: grade 0, within normal limits; grade 1, minimal; grade 2, mild; grade 3, moderate; and grade 4, marked. The extent of necrosis and inflammation was scored (hepatocyte necrosis and inflammatory cell infiltration area 0: absent, 1: <25%, 2: 25–50%, 3: 50–75%, and 4: 75–100%). The extent of biliary hyperplasia and fibrosis was scored (increased bile duct profiles around the portal and fibroblast circumferential proliferation around bile duct area 0: absent, 1: <25%, 2: 25–50%, 3: 50–75%, and 4: 75–100%).

Bile acid profile analysis

The liver, gallbladder, fecal, and urine samples were collected from the mice for total BA measurement. The serum, liver, and gallbladder samples were collected from the mice for total BA profiling, as described. Briefly, standard and internal standard (IS) solutions were prepared in methanol (IS composition: 1 ml each of 480 ng mycophenolic acid; standard solution composition: 0.1 μM each of CA, CDCA, DCA, LCA, UDCA, HDCA, GCA, TCA, GDCA, TDCA, GCDCA, TCDCA, GUDCA, TUDCA, THDCA, TLCA, GLCA, and GHDCA).

The serum and bile samples were diluted with the dilution vehicle. The mouse liver tissue (1 g in 9 ml of PBS) was used for preparation of the liver tissue homogenate; after vortexing for 1 min, the samples were centrifuged at 5,000 rpm for 15 min at 4°C. Next, 50 μL of serum, liver, and bile sample dilute solutions was added to 150 μL of a mixed solution consisting of IS and methanol solutions (v/v = 2:1), which was vortexed and followed by centrifugation at 12,000 rpm for 10 min at 4°C. Finally, 5 μL of the supernatant was detected by UPLC-MS/MS (ACQUITY UPLC: Waters, MA, USA, Quadrupole 5,500: Applied Biosystems, CA, USA) with an ACQUITY BEH C18 column (1.7 μm, 100 mm × 2.1 mm) (Waters, Milford, MA) and analyzed by Analyst software 1.6.3 platform, integration, and BA quantification, according to previous reports (Yang et al., 2008; Li Y. F. et al., 2017).

Quantitative real-time PCR

According to the manufacturer's instructions, TRIzol reagent was used to isolate total RNA from liver samples. Total RNA was used for reverse transcription to cDNA using the PrimeScript RT reagent Kit. GAPDH were used as internal controls, and primers for the experiment are listed in Supplementary Tables S2, S3 Real-time PCR was performed by using the SYBR green reaction mixture in the ABI-StepOnePlus Sequence Detection System (Applied Biosystems).

Western blotting

Total protein was isolated using the RIPA lysis buffer containing the protease inhibitor cocktail from liver tissues. The determination of the total protein concentration was accomplished by using the BCA protein assay kit. Equal amounts of protein samples were separated by 12% SDS-PAGE in a Bio-Rad Mini-PROTEAN system, and the separated proteins were transferred to polyvinylidene fluoride membranes. The membranes were incubated overnight with specific primary antibodies (FXR, BSEP, and NF-κB-p65). After washing and incubation with the secondary antibody, the protein bands were detected by using ECL Western blotting reagents and quantified by optical densitometry and corrected by the values obtained from the β-actin.

Multivariate data analysis

Analyst Software 1.6.3 was used to analyze and process the mass spectrometric data, calculate the standard curve of each component of BAs, and then calculate the content of each bile acid component of each test sample according to the standard curve. Relative quantification of α-MCA, β-MCA, and TMCA was performed, according to the concentrations of CA and TCA. Then, the bile acid component concentration data were imported into the MetaboAnalyst 5.0 (https://www.metaboanalyst.ca/MetaboAnalyst/ModuleView.xhtml) database for normalization using the internal standard and analyzed by partial least squares discriminant analysis (PLS-DA) and hierarchical clustering heatmap analysis.

Statistical analysis

All experimental values were calculated for mean ± SEM. All statistical analyses were performed by SPSS 25.0 and GraphPad Prism 8.0. The normality and homogeneity of variance were tested by using the one-sample Kolmogorov–Smirnov test. The statistical significance of the differences was determined by one-way ANOVA, followed by the least significant difference (LSD) test when equal variance was assumed or Dunnett's *post hoc* test when equal variance was not assumed, and $p < 0.05$ was considered as significant.

Results

DCHD treatment ameliorated ANIT-induced intrahepatic and BDL-induced extrahepatic cholestatic liver injuries

In this study, the data indicated that cholestasis and obvious liver damage were observed after ANIT and BDL induction. The serum biochemical levels including ALT, AST, ALP, TC, TBA, TBIL, and DBIL levels were significantly elevated (Figures 1C, 2C). Clinically, ALT and AST levels reflect the damage status of hepatocytes, and the elevated levels of ALP and γ-GT are used as the criteria for judging cholestatic liver disease (Chinese Society of Hepatology, Chinese Medical Association; Chinese Society of Gastroenterology, Chinese Medical Association; Chinese Society of Infectious Diseases, Chinese Medical Association, 2016; Wei, 2016). The serum ALP level can be used as an important indicator for judging disease severity and disease prognosis in specific patients with liver diseases such as PBC and PSC (Shen and Lu, 2016). The level of the γ-GT activity can reflect the degree of hepatobiliary pathology when intrahepatic and extrahepatic bile ducts were blocked (Luo et al., 2014). In addition, the body weight was significantly decreased, and the organ coefficient was significantly increased (Supplementary Figure S2). The H&E staining of liver confirmed the serum biochemical data, and liver histological changes induced by ANIT treatment and BDL surgery were obvious (Figures 1D,E, 2D,E, Supplementary Figure S3). Hepatocyte degeneration, necrosis, inflammatory infiltration, ductular proliferation, and onion skinning periductal fibrosis around the portal area and central vein were observed (Bedossa et al., 2012; Yang et al., 2018; Gijbels et al., 2021). Our observations showed that the ANIT treatment model focused on hepatocyte necrosis, while the BDL surgery model focused on ductular proliferation and periductal fibrosis (Figures 1D, 2D; Supplementary Figure S3). Since inflammation is also another important manifestation of cholestatic liver injury (Li M. et al., 2017), the expression level of NF-κB mRNA and protein was detected (Figure 1B; Figure 2B). Our results demonstrated that the increased expression level of NF-κB induced by ANIT treatment and BDL surgery was obvious (Figures 1B, 2B).

DCHD treated at doses of 12 g/kg and 24 g/kg could ameliorate ANIT-induced cholestatic liver injury; DCHD treated at doses of 12 g/kg, 24 g/kg, and 48 g/kg could ameliorate BDL-induced cholestatic liver injury. Therefore, our results show that the liver damage and cholestasis status of the intrahepatic and extrahepatic cholestasis models, following DCHD treatment, were improved. Moreover, the 12 g/kg and 24 g/kg DCHD treatment could decrease ALT, AST, ALP, γ-GT, TC, TBA, and TBIL levels in the ANIT-induced intrahepatic cholestasis model; the 24 g/kg DCHD-treated group produced a greater lessened effect on ALT and ALP levels than the UDCA-treated group (Figure 1C). When the 12 g/kg, 24 g/kg, and 48 g/kg DCHD treatment could decrease ALT, AST, ALP, γ-GT, TC, TBA, TBIL, and DBIL levels in the BDL-induced extrahepatic cholestasis model, the depressed effect of DCHD on ALT and AST levels positively correlated with the administration dose (Figure 2C). Additional proof of the liver damage state amelioration, following DCHD therapy, was supplied by H&E staining and the detected results of NF-κB (Figures 1B, D, 2B, D).

DCHD ameliorated the disordered BA homeostasis in intrahepatic and extrahepatic cholestatic mice

Since the BA metabolism disorder has a crucial impact on liver damage induced by cholestatic liver disease, we explored the role of DCHD therapy on BA metabolism in the ANIT and BDL models. The total BA levels of the serum, liver, and urine were significantly increased, and the total BA levels of gallbladder and fecal matter were significantly reduced in the ANIT and BDL models (Figures 3A, 4A). After treatment with DCHD, this situation was reversed except that the increase in the TBA level of urine continued to be enhanced (Figures 3A, 4A). DCHD treatment removed the accumulation of BAs by enhancing BA excretion of the urinary and fecal pathway.

To explore the effects of DCHD on BA metabolism in intrahepatic and extrahepatic cholestasis models *in vivo*, we measured the contents of the 21 types of BAs in the serum, liver, and gallbladder from mice that were given either DCHD or other treatment in this study. The content data on BAs were determined based on PLS-DA and hierarchical clustering heatmap analysis in both intrahepatic and extrahepatic cholestasis models. The BAs profile of DCHD groups was well separated with the vehicle and ANIT group from serum and liver tissues (Figure 3B), and the hierarchical clustering heatmaps of BA composition were different in serum, liver, and gallbladder tissues (Figure 3C). The BAs profile and the hierarchical clustering heatmaps of BA composition of DCHD groups were well separated with the sham and BDL groups from serum and liver tissues (Figures 4B,C), indicating the BA metabolite differences among these groups. The results show that the BA metabolites significantly changed upon ANIT or BDL injury and in response to DCHD treatment. The findings reveal that BA metabolites altered considerably after ANIT or BDL damage, as well as in response to DCHD therapy.

To elucidate the distinction further, we investigated the BAs pool size, distribution, and composition including hydrophilic and hydrophobic, primary and secondary, 12-OH (CA and its derivatives) and non-12-OH (CDCA and its derivatives), conjugated and unconjugated, and taurine-conjugated and glycine-conjugated BAs. After ANIT treatment and BDL surgery, the BAs pool size and composition of the serum, liver, and gallbladder from mice significantly changed (Figures

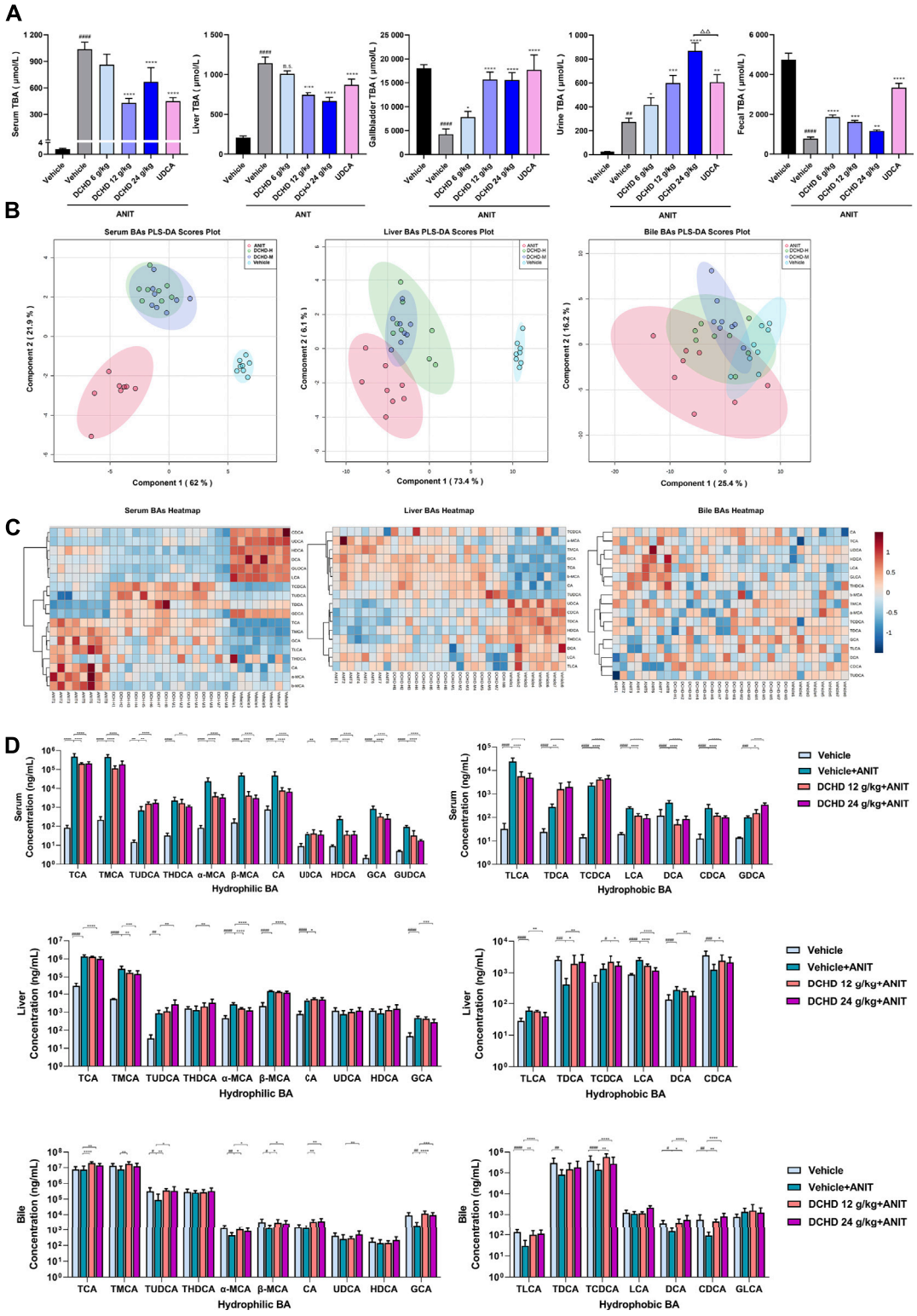

FIGURE 3
Changes of total bile acid (TBA) and bile acid (BA) profiles in the ANIT-induced intrahepatic cholestatic model mice after DCHD treatment. **(A)** Effects of DCHD treatment on TBA in ANIT-induced intrahepatic cholestatic mice. **(B–C)** Multivariate analysis model (PLS-DA) and hierarchical clustering heatmaps based on the bile acid profile of the serum, liver, and bile. **(D)** Changes of the individual bile acid level in the serum, liver and gallbladder in the ANIT-induced intrahepatic cholestatic model mice after DCHD treatment. Data are presented as mean ± SEM (n = 8). $^{\#}p < 0.05$, $^{\#\#}p < 0.01$, $^{\#\#\#}p < 0.001$, and $^{\#\#\#\#}p < 0.0001$, vs. the vehicle group; $^{*}p < 0.05$, $^{**}p < 0.01$, $^{***}p < 0.001$, and $^{****}p < 0.0001$, vs. the ANIT group; $^{\triangle}p < 0.05$, $^{\triangle\triangle}p < 0.01$, $^{\triangle\triangle\triangle}p < 0.001$, and $^{\triangle\triangle\triangle\triangle}p < 0.0001$, vs. the UDCA group.

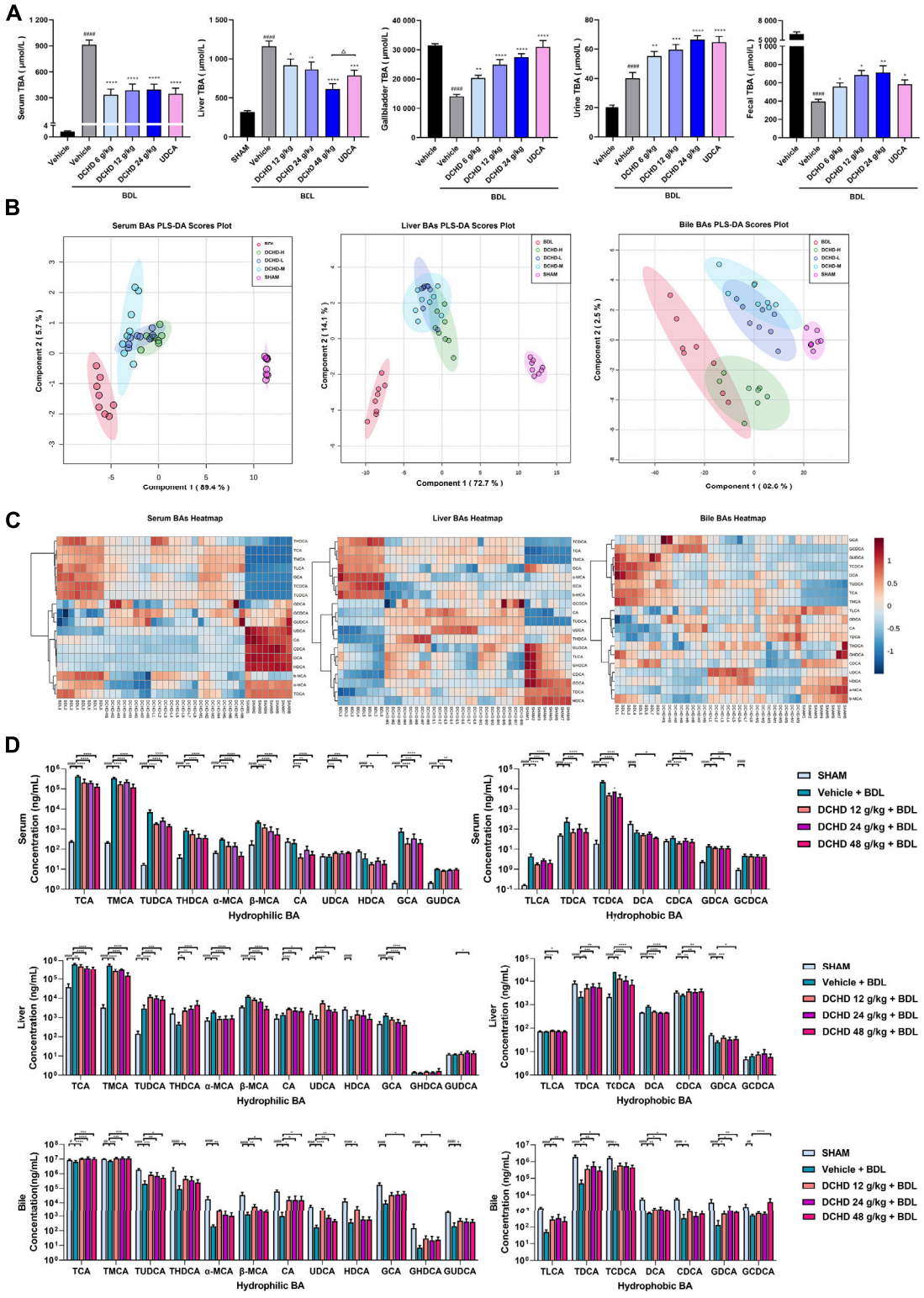

FIGURE 4
Changes of total bile acid (TBA) and bile acid (BAs) profiles in the BDL-induced extrahepatic cholestatic model mice after DCHD treatment. **(A)** Effects of DCHD treatment on TBA in BDL-induced extrahepatic cholestatic mice. **(B–C)** Multivariate analysis model (PLS-DA) and hierarchical clustering heatmaps based on the bile acid profile of the serum, liver, and bile. **(D)** Changes of the individual bile acid level in the serum, liver, and gallbladder in the BDL-induced extrahepatic cholestatic model mice after DCHD treatment. Data are presented as mean ± SEM (n = 8). $^{\#}p < 0.05$, $^{\#\#}p < 0.01$, $^{\#\#\#}p < 0.001$, and $^{\#\#\#\#}p < 0.0001$, vs. the sham group; $^{*}p < 0.05$, $^{**}p < 0.01$, $^{***}p < 0.001$, and $^{****}p < 0.0001$, vs. the BDL group; $^{\triangle}p < 0.05$, $^{\triangle\triangle}p < 0.01$, $^{\triangle\triangle\triangle}p < 0.001$, and $^{\triangle\triangle\triangle\triangle}p < 0.0001$, vs. the UDCA group.

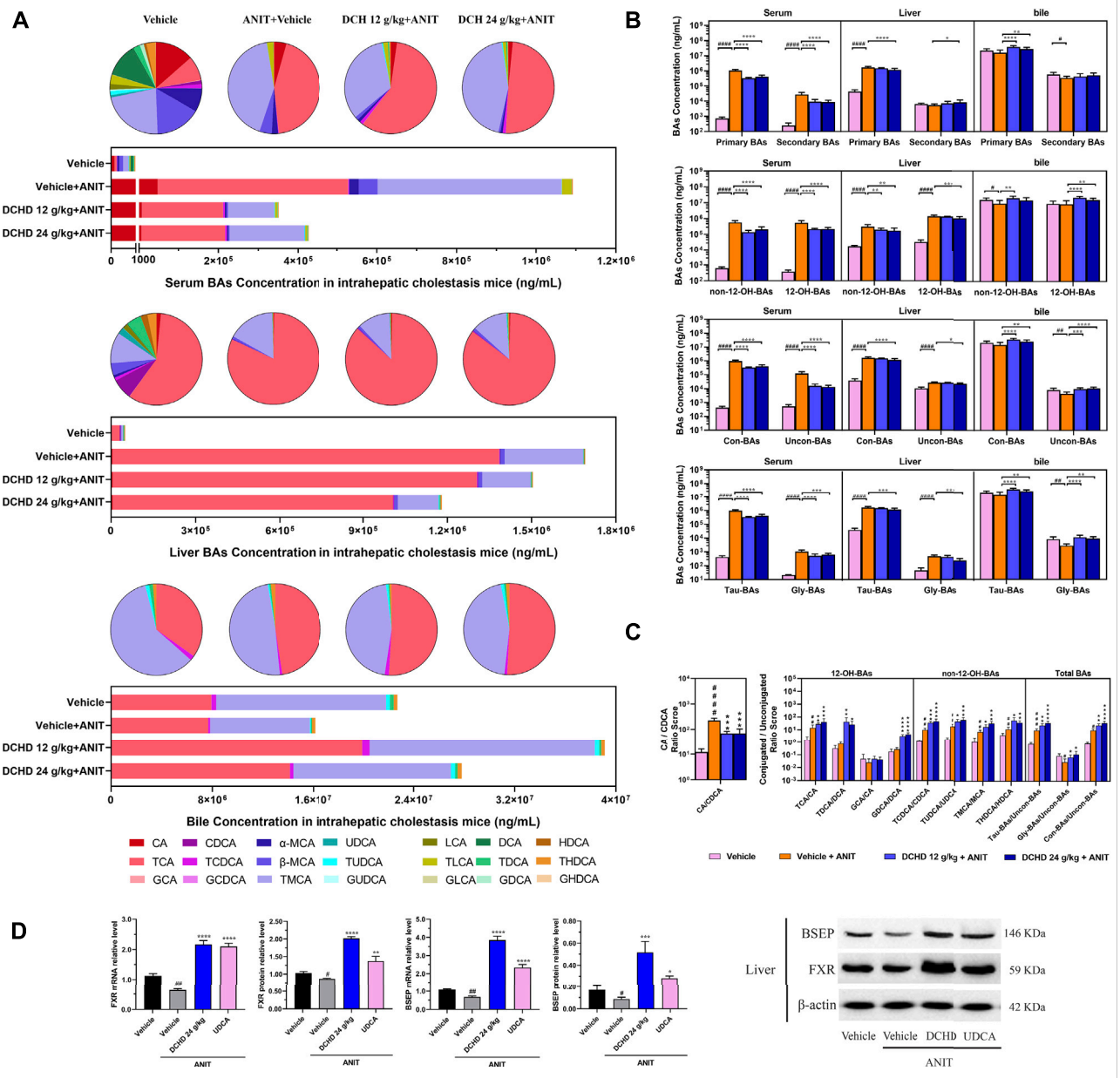

FIGURE 5
Effects of DCHD treatment on bile acid metabolism in ANIT-induced intrahepatic cholestatic mice. **(A)** Changes of BA composition in ANIT-induced intrahepatic cholestatic mice's serum, liver, and gallbladder BAs pool upon DCHD treatment. The circle graphs show the mean percentage of the individual bile acids in the BAs pool. The bar graphs show the amount and distribution of the individual BAs. **(B)** Changes of different types of bile acid levels including primary BAs and secondary BAs, 12-OH-BAs (derived from the classical pathway) and non-12-OH-BAs (derived from the alternative pathway), Con-BAs (conjugated BAs) and Uncon-BAs (unconjugated BAs), and Tau-BAs (taurine-conjugated BAs) and Gly-BAs (glycine-conjugated BAs). **(C)** Bar graphs are the ratios of the CA/CDCA and the conjugated/unconjugated BAs in the mouse serum. **(D)** Effects of DCHD treatment on hepatic nuclear receptors, transporter mRNAs, and protein expression levels in ANIT-induced intrahepatic cholestatic mice. Data are presented as mean ± SEM ($n = 8$). $^{\#}p < 0.05$, $^{\#\#}p < 0.01$, $^{\#\#\#}p < 0.001$, and $^{\#\#\#\#}p < 0.0001$, vs. the vehicle group; $^{*}p < 0.05$, $^{**}p < 0.01$, $^{***}p < 0.001$, and $^{****}p < 0.0001$, vs. the ANIT group; $^{\triangle}p < 0.05$, $^{\triangle\triangle}p < 0.01$, $^{\triangle\triangle\triangle}p < 0.001$, and $^{\triangle\triangle\triangle\triangle}p < 0.0001$, vs. the UDCA group.

3D, 4D, 5A, 6A). The BAs pool size of the serum and liver was sharply increased, and the BAs pool size of the gallbladder was sharply decreased after ANIT treatment and BDL surgery, while the BAs pool mainly composed of TCA and TMCA was formed in the serum, liver, and gallbladder (Figures 3A, 4A, 5A, 6A). The primary and secondary, 12-OH and non-12-OH, conjugated and unconjugated, and taurine-conjugated and glycine-conjugated BA levels of the serum increased significantly (Figures 5B, 6B).

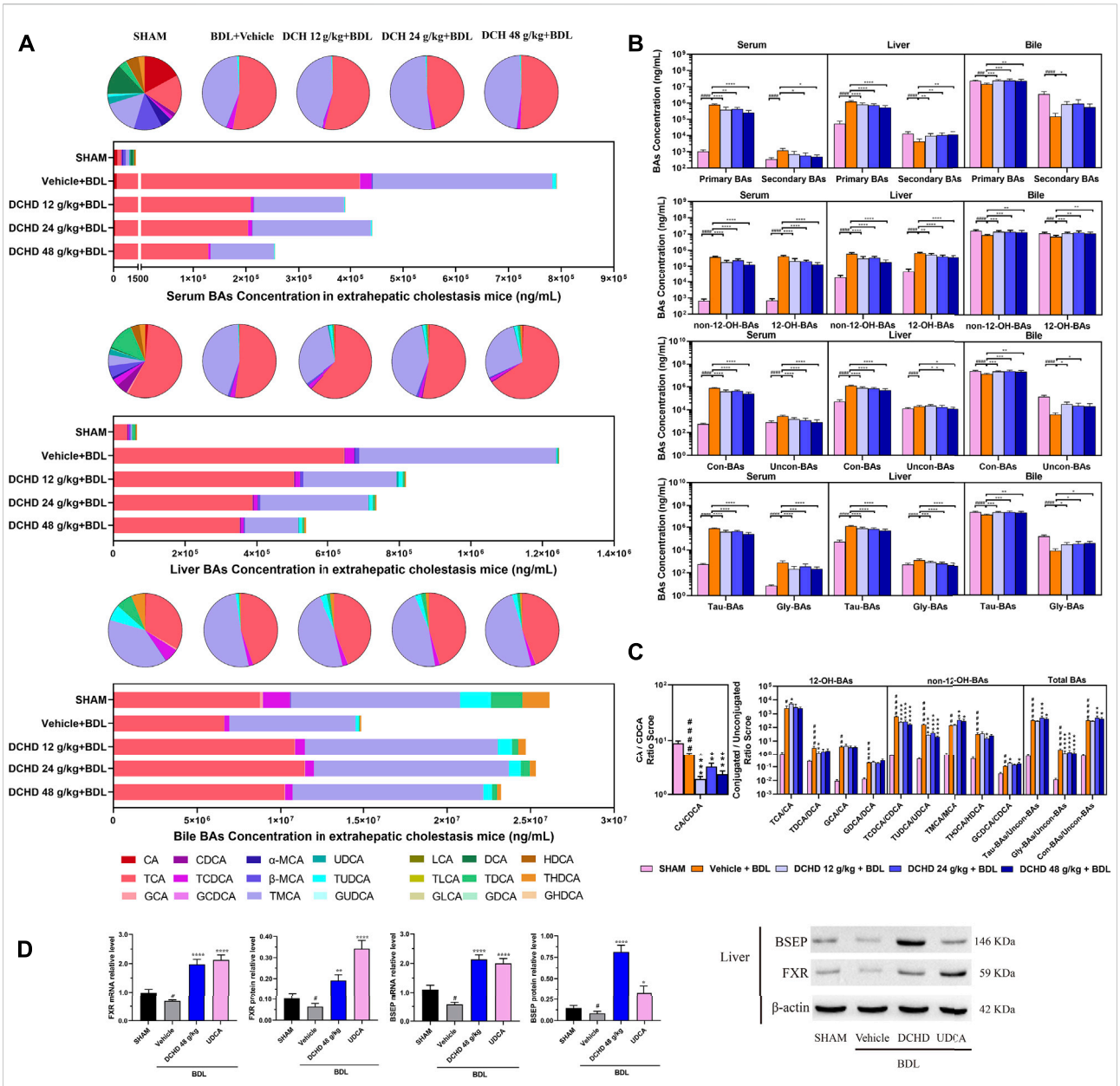

FIGURE 6
Effects of DCHD treatment on bile acid metabolism in BDL-induced extrahepatic cholestatic mice. **(A)** Changes of BA composition in BDL-induced extrahepatic cholestatic mice's serum, liver, and gallbladder BAs pool upon DCHD treatment. The circle graphs show the mean percentage of the individual bile acids in the BAs pool. The bar graphs show the amount and distribution of the individual BAs. **(B)** Changes of different types of bile acid levels including primary BAs and secondary BAs, 12-OH-BAs (derived from the classical pathway) and non-12-OH-BAs (derived from the alternative pathway), Con-BAs (Conjugated BAs) and Uncon-BAs (Unconjugated BAs), and Tau-BAs (taurine-conjugated BAs) and Gly-BAs (glycine-conjugated BAs). **(C)** Bar graphs are the ratios of the CA/CDCA and the conjugated/unconjugated BAs in the mouse serum. **(D)** Effects of DCHD treatment on hepatic nuclear receptors, transporter mRNAs, and protein expression levels in BDL-induced extrahepatic cholestatic mice. Data are presented as mean ± SEM ($n = 8$). $^{\#}p < 0.05$, $^{\#\#}p < 0.01$, $^{\#\#\#}p < 0.001$, and $^{\#\#\#\#}p < 0.0001$, vs. the sham group; $^{*}p < 0.05$, $^{**}p < 0.01$, $^{***}p < 0.001$, and $^{****}p < 0.0001$, vs. the BDL group; $^{\triangle}p < 0.05$, $^{\triangle\triangle}p < 0.01$, $^{\triangle\triangle\triangle}p < 0.001$, and $^{\triangle\triangle\triangle\triangle}p < 0.0001$, vs. the UDCA group.

Except for secondary BAs, the changes of other types of bile acids in the liver were consistent with those of the serum, and the change of gallbladder BAs is opposite to that of serum. The ANIT group following treatment with DCHD (12 g/kg and 24 g/kg) and the BDL group following treatment with DCHD (12 g/kg, 24 g/kg, and 48 g/kg); the BAs pool size of the serum and liver was sharply decreased, and the BAs pool size of the gallbladder was sharply increased (Figures 3A, 4A, 5A, 6A).

The BAs pool mainly composed of TCA and TMCA still formed in the serum, liver, and gallbladder; the TCA and TMCA levels of the serum and liver were decreased significantly, and the gallbladder TCA and TMCA levels were increased significantly. The levels of BAs synthesized by an alternative pathway including CDCA, TUDCA, and THDCA in the liver were increased significantly, and the DCA level was decreased significantly (Figures 3D, 4D, 5A, 6A). The transformations in primary and secondary, 12-OH and non-12-OH, conjugated and unconjugated, and taurine-conjugated and glycine-conjugated BA levels of the serum, liver, and gallbladder were reversed after DCHD treatment (Figures 5B, 6B). The ratios of each conjugated/unconjugated BA and total conjugated/total unconjugated BAs are shown in Figure 2E. An increase in ratios of total conjugated/total unconjugated BAs and taurine-conjugated/unconjugated BAs was observed in the serum of cholestatic mice after administration with ANIT and BDL surgery; the ratios were further elevated after DCHD intervention (Figures 5C, 6C).

Activation of FXR was shown to provide liver protection in BDL-induced or ANIT-induced cholestatic models (de Aguiar Vallim et al., 2013). BSEP is positively regulated by FXR, and the increased expression of FXR could promote the expression of this protein and accelerate the efflux of BAs from the liver to the capillary bile ducts (Alrefai and Gill, 2007). Consequently, we evaluated the BA nuclear receptor FXR and the transporter BSEP at both the mRNA and protein levels. Hepatic FXR and BSEP mRNA expressions and protein levels were lower in the ANIT and BDL groups. On the contrary, hepatic FXR and BSEP were upregulated by DCHD treatment, either in mRNA or protein expression (Figures 5D, 6D). In summary, these results indicate that BA synthesis was inhibited, and BA efflux was facilitated in the liver after DCHD treatment.

Difference of the BA spectrum between intrahepatic and extrahepatic cholestatic mice treated with Da-Chai-Hu decoction

In addition to differences in liver tissue damage, the BAs profile also differed between intrahepatic and extrahepatic cholestatic mice. Although the BAs pool of the liver was dominated by TCA and TMCA, the proportions of TCA and TMCA in intrahepatic cholestatic mouse liver tissues reached 81.59% and 16.53%, and the proportions of TCA and TMCA in extrahepatic cholestatic mouse liver tissues reached 51.71% and 44.13% (Figures 5A, 6A, Supplementary). In addition, the CA, α-MCA, β-MCA, and TLCA levels of the serum and the β-MCA levels of the liver from the ANIT model increased significantly and accounted for a significant proportion of their respective BAs pool (Figure 5A). However, the LCA levels of the serum and liver were undetectable; the TCDCA and TUDCA levels of the serum and the TCDCA and β-MCA levels of the liver from the BDL model increased significantly and accounted for a significant proportion of their respective BAs pool (Figure 6A). The HDCA and DCA levels of the serum in the intrahepatic cholestatic mice were significantly increased, while the HDCA and DCA levels of the serum in the extrahepatic cholestatic mice were significantly decreased (Figures 3D, 4D). The changes of TUDCA, TDCA, TUDCA/UDCA, and TCDCA/CDCA levels in intrahepatic and extrahepatic cholestatic model mice were opposite after DCHD intervention (Figures 5C, 6C). The CA levels of the serum and liver in the intrahepatic cholestatic mice were significantly increased, while the CA levels of the serum and liver in the extrahepatic cholestatic mice did not show significant changes, and the CDCA level was significantly increased in the serum of both cholestatic model groups' mice and significantly decreased in the liver of both cholestatic model groups' mice (Figures 3D, 4D). The BA ratios could reflect changes of enzymatic processes in BA metabolism; the CA: CDCA ratio was selected to test if a possible shift in BA synthesis from the classical to the alternative BA pathway occurs in the liver (MahmoudianDehkordi et al., 2019). In comparison to the vehicle group, the CA: CDCA ratio of the ANIT group mice was significantly increased, while that of the BDL group mice demonstrated much lower levels than that of the sham group, suggesting that the BA synthesis in the ANIT-induced intrahepatic cholestatic model mice was still synthesized by the classical pathway, while that of BDL-induced extrahepatic cholestatic model mice shifted to the alternative pathway (Figures 5C, 6C). The CA: CDCA ratio of intrahepatic and extrahepatic cholestatic model mice after DCHD intervention was significantly decreased, suggesting that DCHD intervention induced the conversion of the BA synthesis pathway from the classical pathway to the alternative pathway in intrahepatic cholestatic model mice, while in extrahepatic cholestasis model, it further shifts toward alternative pathways (Figures 5C, 6C).

Discussion

Da-Chai-Hu decoction (DCHD), a classical formula from the *Treatise on Febrile Disease*, is used in the treatment of digestive system diseases such as pancreatitis, cholecystitis, cholelithiasis, and gastric and duodenal ulcers. Previous studies have demonstrated DCHD has a good liver protective effect; the mechanism of DCHD on the protective effect against liver injury caused by cholestasis is still obscure. In this investigation, our results revealed that DCHD has a therapeutic effect on liver injury and cholestasis induced by ANIT and BDL. It was notable that the size, composition, and distribution of the BAs pool were altered with DCHD treatment. DCHD treatment led the BAs pool of the serum and liver shrink and enhanced BA secretion into the gallbladder and excretion of the urinary and fecal pathway. TCA and TMCA, which are more prone to cause inflammation than others, were reduced (Zhang

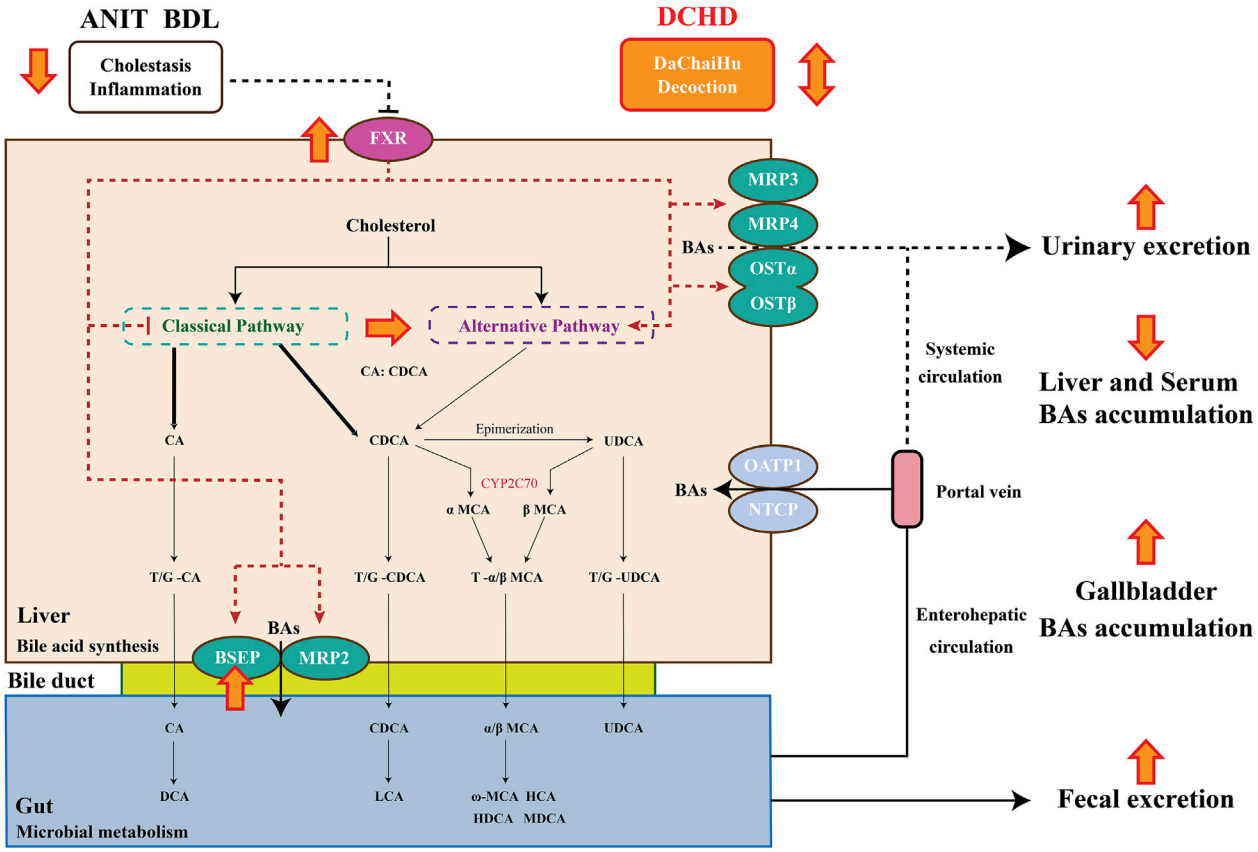

FIGURE 7
Bile acid synthesis and metabolism and the protective mechanism of Da-Chai-Hu decoction ameliorate acute cholestatic-induced liver injury through reversing the bile acid metabolism disorder.

et al., 2011). TUDCA was increased in the liver, and the pathway of BA synthesis was actually affected. However, these changes were likely to inhibit BA synthesis and enhance BA efflux by affecting the FXR signaling pathway, thereby affecting BAs profile changes.

To mimic cholestatic liver damage to examine the mechanism of the cholestatic liver disorder and monitor the effectiveness of innovative treatments, a large number of animal cholestatic models have been developed including surgery, chemical, viral infections, and gene-knockout–induced cholestasis in the last 20 years. α-naphthyl-isothiocyanate (ANIT) and bile duct ligation (BDL) are two frequent and valuable modeling methods but with different mechanisms. ANIT has generally been accepted as prototypic hepatotoxicants for provided acute or chronic cholestatic liver injury model (Desmet et al., 1968). *In vivo*, ANIT undergoes hepatocyte metabolism and forms ANIT-GSH complexes that temporarily lose their toxicity after conjugation with GSH, secreted into bile, whereby free ANIT toxicity recovers and exerts toxic effects on the bile duct epithelial cells (Orsler et al., 1999; Joshi et al., 2017; Yang et al., 2017). Persistent exposure to ANIT causes significant damage and necrosis to the bile ducts and hepatocytes, even periportal inflammation and cholestasis; however, the extrahepatic bile ducts are not damaged; thus, the ANIT-induced model resembles more of the intrahepatic cholestatic liver disease in humans (Mariotti et al., 2018; Gijbels et al., 2021). BDL has generally been accepted as the most widely used model mimicking extrahepatic cholestasis induced by bile duct obstruction. BDL surgery induces strong proliferation of cholangiocytes, resulting in cholestasis, ductular proliferation, and onion skinning periductal fibrosis (Mariotti et al., 2018; Gijbels et al., 2021). In this research, the ALT and AST levels of the ANIT-induced intrahepatic cholestasis model were significantly higher than those of the BDL-induced extrahepatic cholestasis model. Biochemical levels and pathological observations suggest that the ANIT treatment model focused on hepatocyte necrosis, and the BDL surgery model focused on ductular proliferation and periductal fibrosis, which was in agreement with the previous experiment. The relatively high mortality rates are an

unavoidable problem; thus, the BDL procedure and the administered dose of DCHD were adjusted as described (Weerachayaphorn et al., 2014; Dong et al., 2021).

The BA secretion can be disrupted by multiple types of liver diseases, especially cholestatic liver diseases and biliary diseases; however, hepatic buildup of BAs is currently thought to be a driving force of various types of liver diseases worsening (Boyer, 2007; Fickert and Wagner, 2017). Consequently, reducing the hepatic BA overload is a primary goal for the cholestatic liver disease therapy. Previous evidence has shown that DCHD treatment reduced the level of BAs in the serum at the same time and effectively promoted the excretion of stones in the biliary tract (Ohta et al., 1995; Li et al., 2008; Pang et al., 2008). Our finding that the levels of TBA of the serum and liver reduced, and the level of gallbladder reduction was consistent with studies recently published. The inconsistency in the results for the TBA level in urine and in feces after ANIT and BDL treatment brought our attention to the adaptive reaction to cholestasis that inhibits renal reabsorption of BAs and enhanced renal excretion of BAs in order to minimize hepatic injury (Soroka et al., 2010; de Aguiar Vallim et al., 2013). It was previously reported that BAs can be released into the blood circulation system through hepatocyte basolateral BA transporter and the cholehepatic shunt pathway (Xia et al., 2006) and then eliminate overload bile acids by renal excretion and adapt to cholestasis induced by bile duct obstruction (Soroka et al., 2010; Li and Chiang, 2014; Li et al., 2018). Our work demonstrates that DCHD administration led to enhancement of BA renal and fecal excretion and minimized hepatic injury, which may be related to the enhanced release of BAs into the circulatory system by DCHD *via* the hepatocyte basolateral BA transporter and eliminate overload bile acids through renal excretion while reducing BA reabsorption in the ileum and colon.

The differences in the BA structure account for differences in their biological properties, so we investigated the effect of DCHD therapy on BA metabolism in the ANIT and BDL models. In the present investigation, we found that the BAs pool size of the serum and liver, especially the TCA and TMCA levels of the serum and liver, was sharply decreased, and the TUDCA and THDCA levels of the liver were increased significantly. This is a critical finding as previous studies reported that taurine-conjugated BAs in mice are more sensitive to the cholestatic state than the other types of bile acid components, and the TCA and TMCA levels of cholestatic model animals increased sharply (Yang et al., 2008; Zhang et al., 2011; Wang et al., 2020; Thibaut et al., 2021). Compared with the direct toxic effects of hydrophobic BAs, the inflammatory injury caused by the massive accumulation of BA components such as TCA, TMCA, and MCA is more obvious (Murphy et al., 2005; Zhang et al., 2011). Evidence shows that the DCHD inhibited expressions of hepatic TNF-α and IL-6 and improved the inflammatory state of the liver (Chang and Wang, 2015). In this study, DCHD treatment led to the diminution of hepatocyte degeneration, necrosis, or inflammatory infiltration, and the lower expression levels of NF-κB mRNA and protein in the liver of ANIT- and BDL-induced mice. The improvement of liver inflammation by DCHD may be interrelated to the inhibition of the inflammatory response pathway and the reduction of TCA and TMCA accumulation. In addition, it was previously reported that DCHD treated cholecystitis and pancreatitis *via* inhibition of breaking a continuous cascade of inflammatory mediators (Lu et al., 2015; Fan, 2019; Wang et al., 2022). Apart from inhibiting the inflammatory response in the digestive system such as the liver, gallbladder, and pancreas, the DCHD also has an improving effect on inflammation in the lung tissue and circulatory system (Yang, 2017; Zhang et al., 2020). TUDCA is a taurine-binding derivative of UDCA, and the bound sulfonic acid group enhances the polarity and hydrophilicity of the molecule which more effectively promotes the hydrophilic transformation of bile pools and protects hepatocytes and cholangiocytes (Invernizzi et al., 1999; Chiang, 2009). At the same time, UDCA can reduce the saturation index of cholesterol in bile and intestinal cholesterol absorption and effectively prevent gallstone deposition (Hardison and Grundy, 1984; Setchell et al., 1996; Dorvash et al., 2018). In the experiment, it could be observed that the level of secondary BAs in the liver of cholestatic mice increases after administration of DCHD, and the increase of such bile acid levels was mainly caused by the increase in HDCA and THDCA levels in the liver. HDCA and THDCA belong to HCA species. Relevant studies have verified that HCA species were correlated with clinical blood glucose markers and played a key role in maintaining glucose homeostasis (Jia et al., 2021; Zheng et al., 2021).

The BA synthesis occurs mainly in the liver *via* two distinct pathways, the classical or neutral pathway, which predominantly produces CA and CDCA. It accounts for about 75% of BA production in the main pathway in the normal condition; the alternative or acidic pathway predominantly produces CDCA (Duane and Javitt, 1999; Schwarz et al., 2001). Cholesterol-7α-hydroxylase (CYP7A1) is the rate-limiting enzyme for BA synthesis, while sterol-12α-hydroxylase (CYP8B1) decides the ratio of CA to CDCA by promoting CA synthesis (Vlahcevic et al., 1991; Chiang, 2017). When the body is in certain pathological states, the activities of CYP7A1 and CYP8B1 in the liver are down-regulated, which regulates the balance of BA metabolism by stimulating the alternative pathway to produce CDCA (Axelson and Sjövall, 1990; Jia et al., 2021). Several research studies have previously been published which demonstrated that the non-12-OH BAs of cholesterol-7α-hydroxylase-deficient or transgenic expression mice increased significantly, which were derived from the alternative pathway, although the BAs pools of the former were significantly decreased, while those of the latter were significantly increased

(Li et al., 2010; Ferrell et al., 2016). Targeted disruption of the sterol 12α-hydroxylase gene results in CDCA and MCA synthesized by the alternative pathway was significantly increased, and the CA synthesized by the classical pathway was almost eliminated (Kaur et al., 2015). Recent research studies have emphasized the key role of the non-12-OH-BAs synthesized by the alternative pathway in regulation of lipid, cholesterol, and energy homeostasis (Jia et al., 2021). If the BAs synthesized by the alternative pathway are inhibited, the proportion of 12-OH-BAs synthesized by the classical pathway will increase, which will further lead to a decrease in the liver's ability to respond to hepatic lipid homeostasis and the inflammatory state, and the degree of liver fibrosis was significantly associated with 12-OH-BAs (Jia et al., 2018; Jia et al., 2021; Xie et al., 2021). Along this line, we calculated the ratio of CA to CDCA because the ratio of CA to CDCA was selected to test if a possible shift in BA synthesis from the classical to the alternative BA pathway occurs in the liver (Chen et al., 2019; MahmoudianDehkordi et al., 2019; Weingartner et al., 2021). In the present investigation, we found that the BA synthesis in the ANIT-induced intrahepatic cholestatic model was still dominated by the classical pathway; however, the BA synthesis pathway in the BDL-induced extrahepatic cholestatic model shifted to the alternative pathway, and the proportion of TCA and TMCA in the two types of model mouse's liver supported this conclusion. The difference in BA synthesis in both the ANIT-induced intrahepatic cholestatic model and BDL-induced extrahepatic cholestatic model may be due to the different mechanisms of model formation; as mentioned earlier, ANIT causes significant damage and necrosis to the hepatocytes and bile ducts, while BDL causes strong proliferation of cholangiocytes and periductal fibrosis in the early stages of surgery (Mariotti et al., 2018; Gijbels et al., 2021). DCHD treatment promoted the conversion of the bile synthesis pathway from the classical pathway to the alternative pathway in the intrahepatic cholestasis model and further strengthens the transition to the alternative pathway in the extrahepatic cholestatic model.

FXR is a very important part of the precise regulation system of BAs; as an important BA receptor, it is distributed in a variety of tissues. Among them, the expression level of FXR is the highest in the liver and intestine. In these two types of tissues, FXR receptors are deeply involved to regulate BA synthesis and transport to ensure optimal bile pool size and maintain BA metabolic homeostasis (Mencarelli and Fiorucci, 2010; Sonne, 2021). FXR activation was found to inhibit BA synthesis and prevent liver damage caused by excessive BA synthesis. At the same time, FXR activation inhibited hepatic NTCP and intestinal ASBP to reduce hepatic uptake of BAs and intestinal reabsorption of BAs, enhanced expression of hepatic BA transporters such as BSEP, MRP3, and OSTα/β, promoted the BA efflux, and decreased hepatic BA accumulation (Trauner et al., 2017; Stofan and Guo, 2020). Activation of FXR was shown to provide liver protection in BDL-induced or ANIT-induced cholestatic models (de Aguiar Vallim et al., 2013). Our work result was consistent with these findings; treatment with DCHD and the expressions of FXR and BSEP in the cholestatic mouse liver were activated in mice, and hepatic BA accumulation decreased. The activation of FXR in the liver tissue was more inclined to regulate CYP8B1, followed by the inhibition of CYP7A1, so it mainly inhibited the synthesis of CA (Kim et al., 2007; Kong et al., 2012). The CA was an important determinant of intestinal cholesterol absorption, and intestinal cholesterol absorption was suppressed, induced by reducing CA synthesis (Murphy et al., 2005). Of note, serum CA and TC levels in mice with intrahepatic and extrahepatic cholestasis significantly decreased after DCHD intervention. Study results show that DCHD has the potential to treat obesity and non-alcoholic fatty liver disease (Han et al., 2020). Upon DCHD treatment, the triglyceride content in hepatocytes was significantly reduced, and the fat deposition in the liver was reduced (Nakayama et al., 2007; Wang et al., 2021). Studies have pointed out that the *Scutellaria baicalensis* extract is the key component of DCHD to reduce serum total cholesterol levels and inhibit lipase and lipid absorption (Matsuo et al., 2018). Thus, whether DCHD reduces the supply of BA synthesis raw materials by inhibiting intestinal cholesterol absorption deserves further investigation.

Conclusion

In conclusion, our current study reports that the liver damage and cholestasis status of the intrahepatic and extrahepatic cholestasis, following DCHD treatment, were improved. The potential mechanism of DCHD on ameliorating cholestatic liver injury was revealed, which involved inhibition of BA synthesis and enhanced BA efflux *via* activation of the FXR signaling pathway, altered the size, composition and distribution of the BAs pool, and regulation of BA synthesis pathways, reducing overload BAs, especially TCA and TMCA in the liver, enhancement of BA fecal and urine elimination pathways, and reversed the imbalance of BA homeostasis (Figure 7). Overall, our findings provide reliable verification of the therapeutic action of DCHD on cholestatic liver injury and provide theoretical and experimental basis for the clinical application and new drug development of DCHD in the treatment of cholestatic liver disease.

Data availability statement

The original contributions presented in the study are included in the article/Supplementary Materials; further inquiries can be directed to the corresponding author.

Ethics statement

The animal study was reviewed and approved by the use of live animals for teaching and research committee of the Shanghai University of Traditional Chinese Medicine. Written informed consent was obtained from the owners for the participation of their animals in this study.

Author contributions

YHZ conceived, designed, and conducted most of the experiments, and wrote the manuscript. WS and XN supported several experiments. YH, YLZ, and ZW also contributed medicines and quality control data. GY, YL, and LC helped design the experiment and provided supervision. All authors interpreted and analyzed the data. All authors agreed to be accountable for all aspects of work ensuring integrity and accuracy.

Funding

This work was supported financially by the Scientific Research Project of Science and Technology Commission of Shanghai Municipality (Grant No. 22S21901300).

Acknowledgments

The authors are grateful to Jinghua Pharmaceutical Group Co., Ltd (Jiangsu, China) for provision of medicines and quality control data. They also thank the Center for Drug Safety Evaluation and Research in Shanghai University of Traditional Chinese Medicine for their assistance.

Conflict of interest

Authors YZZ, ZW, and YH were employed by the company Jinghua Pharmaceutical Group Co., Ltd.

The remaining authors declare that the research was conducted in the absence of any commercial or financial relationships that could be construed as a potential conflict of interest.

Publisher's note

All claims expressed in this article are solely those of the authors and do not necessarily represent those of their affiliated organizations, or those of the publisher, the editors, and the reviewers. Any product that may be evaluated in this article, or claim that may be made by its manufacturer, is not guaranteed or endorsed by the publisher.

Supplementary material

The Supplementary Material for this article can be found online at: https://www.frontiersin.org/articles/10.3389/fphar.2022.959074/full#supplementary-material

References

Arab, J. P., Karpen, S. J., Dawson, P. A., Arrese, M., and Trauner, M. (2017). Bile acids and nonalcoholic fatty liver disease: Molecular insights and therapeutic perspectives. *Hepatology* 65 (1), 350–362. doi:10.1002/hep.28709

Alrefai, W. A., and Gill, R. K. (2007). Bile acid transporters: Structure, function, regulation and pathophysiological implications. *Pharm. Res.* 24 (10), 1803–1823. doi:10.1007/s11095-007-9289-1

Axelson, M., and Sjövall, J. (1990). Potential bile acid precursors in plasma--possible indicators of biosynthetic pathways to cholic and chenodeoxycholic acids in man. *J. Steroid Biochem.* 36 (6), 631–640. doi:10.1016/0022-4731(90)90182-r

Bacon, B. R., O'Grady, J. G., Di Biscglie, A. M., and Lake, J. R. (2006). *Comprehensive clinical Hepatology*. Second Edition. Philadelphia: Mosby: Elsiver.

Bedossa, P., Poitou, C., Veyrie, N., Bouillot, J. L., Basdevant, A., Paradis, V., et al. (2012). Histopathological algorithm and scoring system for evaluation of liver lesions in morbidly obese patients. *Hepatology* 56 (5), 1751–1759. doi:10.1002/hep.25889

Boonstra, K., Beuer, U., and Ponsioen, C. Y. (2012). Epidemiology of primary sclerosing cholangitis and primary biliary cirrhosis: A systematic review. *J. Hepatol.* 56 (5), 1181–1188. doi:10.1016/j.jhep.2011.10.025

Boyer, J. L. (2007). New perspectives for the treatment of cholestasis: Lessons from basic science applied clinically. *J. Hepatol.* 46 (3), 365–371. doi:10.1016/j.jhep.2006.12.001

Burt, A. D., Portman, B. C., and Ferrell, L. D. (2012). *MacSween's pathology of the liver*. Sixth Edition. Philadelphia: Churchill Livingstone: Elsevier.

Cabrera, D., Arab, J. P., and Arrese, M. (2019). UDCA, NorUDCA, and TUDCA in liver diseases: A review of their mechanisms of action and clinical applications. *Handb. Exp. Pharmacol.* 256, 237–264. doi:10.1007/164_2019_241

Carey, M. C. (1984). Bile acids and bile salts: Ionization and solubility properties. *Hepatology* 4, 66S–71S. doi:10.1002/hep.1840040812

Chang, Y. C., and Wang, F. R. (2015). Dachaihu Decoction on high fat and high cholesterol in rats TNF-α, IL-6 expression level influence. *Chin. Pediatr. Integr. Traditional West. Med.* 7 (1), 17–19. doi:10.3969/j.issn.1674-3865.2015.01.007

Chascsa, D., Carey, E. J., and Lindor, K. D. (2017). Old and new treatments for primary biliary cholangitis. *Liver Int.* 37 (4), 490–499. doi:10.1111/liv.13294

Chen, J., Zheng, M., Liu, J., Luo, Y., Yang, W., Yang, J., et al. (2019). Ratio of conjugated chenodeoxycholic to muricholic acids is associated with severity of nonalcoholic steatohepatitis. *Obes. (Silver Spring)* 27 (12), 2055–2066. doi:10.1002/oby.22627

Chiang, J. Y. (2017). Recent advances in understanding bile acid homeostasis. *F1000Res.* 6, 2029. doi:10.12688/f1000research.12449.1

Chiang, J. Y. (2009). Bile acids: Regulation of synthesis. *J. Lipid Res.* 5010, 1955–1966. doi:10.1194/jlr.R900010-JLR200

Chiang, J. Y. L., and Ferrell, J. M. (2020). Bile acid receptors FXR and TGR5 signaling in fatty liver diseases and therapy. *Am. J. Physiol. Gastrointest. Liver Physiol.* 318 (3), G554–G573. doi:10.1152/ajpgi.00223.2019

Chinese Society of Hepatology, Chinese Medical Association; Chinese Society of Gastroenterology, Chinese Medical Association; Chinese Society of Infectious Diseases, Chinese Medical Association (2016). Consensus on the diagnosis and

management of autoimmune hepatitis (2015). *J. Clin. Hepatology* 32 (1), 9–22. doi:10.3969/j.issn.1001-5256.2015.10.002

Cullen, J. M., Faiola, B., Melich, D. H., Peterson, R. A., Jordan, H. L., Kimbrough, C. L., et al. (2016). Acute alpha-naphthylisothiocyanate-induced liver toxicity in germfree and conventional male rats. *Toxicol. Pathol.* 44 (7), 987–997. doi:10.1177/0192623316662360

de Aguiar Vallim, T. Q., Tarling, E. J., and Edwards, P. A. (2013). Pleiotropic roles of bile acids in metabolism. *Cell. Metab.* 17 (5), 657–669. doi:10.1016/j.cmet.2013.03.013

Desmet, V. J., Krstulović, B., and Van Damme, B. (1968). Histochemical study of rat liver in alpha-naphthyl isothiocyanate (ANIT) induced cholestasis. *Am. J. Pathol.* 52 (2), 401–421.

Dong, X., Luo, Y., Lu, S., Ma, H., Zhang, W., Zhu, Y., et al. (2021). Ursodesoxycholic acid alleviates liver fibrosis via proregeneration by activation of the ID1-WNT2/HGF signaling pathway. *Clin. Transl. Med.* 11 (2), e296. doi:10.1002/ctm2.296

Dorvash, M. R., Khoshnood, M. J., Saber, H., Dehghanian, A., Mosaddeghi, P., and Firouzabadi, N. (2018). Metformin treatment prevents gallstone formation but mimics porcelain gallbladder in C57Bl/6 mice. *Eur. J. Pharmacol.* 833, 165–172. doi:10.1016/j.ejphar.2018.06.002

Duane, W. C., and Javitt, N. B. (1999). 27-hydroxycholesterol: Production rates in normal human subjects. *J. Lipid Res.* 40 (7), 1194–1199. doi:10.1016/s0022-2275(20)33481-7

European Association for the Study of the Liver (2009). EASL clinical practice guidelines: Management of cholestatic liver diseases. *J. Hepatol.* 51 (2), 237–267. doi:10.1016/j.jhep.2009.04.009

Expert Committee of expert consensus on the diagnosis and treatment of cholestatic liver disease (2015). Expert consensus on the diagnosis and treatment of cholestatic liver disease: An update in 2015. *J. Clin. Hepatobiliary Dis.* 31 (10), 1563–1574. doi:10.3969/j.issn.1001-5256.2015.10.002

Fan, K. L. (2019). *The protective mechanism of heme oxygenase-1 and Dachaihu decoction on the pancreas and lung of the rats with severe acute pancreatitis* (Shan Dong: Shan Dong University). [master's thesis].

Ferrell, J. M., Boehme, S., Li, F., and Chiang, J. Y. (2016). Cholesterol 7α-hydroxylase-deficient mice are protected from high-fat/high-cholesterol diet-induced metabolic disorders. *J. Lipid Res.* 57 (7), 1144–1154. doi:10.1194/jlr.M064709

Fickert, P., and Wagner, M. (2017). Biliary bile acids in hepatobiliary injury - what is the link? *J. Hepatol.* 67 (3), 619–631. doi:10.1016/j.jhep.2017.04.026

Fiorucci, S., Distrutti, E., Carino, A., Zampella, A., and Biagioli, M. (2021). Bile acids and their receptors in metabolic disorders. *Prog. Lipid Res.* 82, 101094. doi:10.1016/j.plipres.2021.101094

Gijbels, E., Pieters, A., De Muynck, K., Vinken, M., and Devisscher, L. (2021). Rodent models of cholestatic liver disease: A practical guide for translational research. *Liver Int.* 41 (4), 656–682. doi:10.1111/liv.14800

Han, K., Kwon, O., Park, H. J., Jung, S. Y., Yang, C., and Son, C. G. (2020). Effect of daesiho-tang on obesity with non-alcoholic fatty liver disease: A study protocol for a randomised, double-blind, placebo-controlled pilot trial. *Trials* 21 (1), 128. doi:10.1186/s13063-020-4068-y

Hardison, W. G., and Grundy, S. M. (1984). Effect of ursodeoxycholate and its taurine conjugate on bile acid synthesis and cholesterol absorption. *Gastroenterology* 87 (1), 130–135. doi:10.1016/0016-5085(84)90135-5

Hu, Y. F., Lu, T. L., Mao, C. Q., Wu, H., Gong, X. D., Zhou, Y. Z., et al. (2013). Quality standard for Dachaihu granules. *Chin. Tradit. Pat. Med.* 35 (1), 68–73.

Hu, Y., Lu, T., Mao, C., Wu, H., Zhang, X., Wang, J., et al. (2013). Simultaneous determination of 10 components in traditional Chinese medicine Dachaihu Granule by reversed-phase-high-performance liquid chromatographic-diode array detector. *Pharmacogn. Mag.* 9 (33), 33–38. doi:10.4103/0973-1296.108136

Invernizzi, P., Setchell, K. D., Crosignani, A., Battezzati, P. M., Larghi, A., O'Connell, N. C., et al. (1999). Differences in the metabolism and disposition of ursodeoxycholic acid and of its taurine-conjugated species in patients with primary biliary cirrhosis. *Hepatology* 29 (2), 320–327. doi:10.1002/hep.510290220

Jia, W., Wei, M., Rajani, C., and Zheng, X. (2021). Targeting the alternative bile acid synthetic pathway for metabolic diseases. *Protein Cell.* 12 (5), 411–425. doi:10.1007/s13238-020-00804-9

Jia, W., Xie, G., and Jia, W. (2018). Bile acid-microbiota crosstalk in gastrointestinal inflammation and carcinogenesis. *Nat. Rev. Gastroenterol. Hepatol.* 15 (2), 111–128. doi:10.1038/nrgastro.2017.119

Joshi, N., Ray, J. L., Kopec, A. K., and Luyendyk, J. P. (2017). Dose-dependent effects of alpha-naphthylisothiocyanate disconnect biliary fibrosis from hepatocellular necrosis. *J. Biochem. Mol. Toxicol.* 31 (1), 1–7. doi:10.1002/jbt.21834

Kaur, A., Patankar, J. V., de Haan, W., Ruddle, P., Wijesekara, N., Groen, A. K., et al. (2015). Loss of Cyp8b1 improves glucose homeostasis by increasing GLP-1. *Diabetes* 64 (4), 1168–1179. doi:10.2337/db14-0716

Kim, I., Ahn, S. H., Inagaki, T., Choi, M., Ito, S., Guo, G. L., et al. (2007). Differential regulation of bile acid homeostasis by the farnesoid X receptor in liver and intestine. *J. Lipid Res.* 48 (12), 2664–2672. doi:10.1194/jlr.M700330-JLR200

Kong, B., Wang, L., Chiang, J. Y., Zhang, Y., Klaassen, C. D., and Guo, G. L. (2012). Mechanism of tissue-specific farnesoid X receptor in suppressing the expression of genes in bile-acid synthesis in mice. *Hepatology* 56 (3), 1034–1043. doi:10.1002/hep.25740

Kuo, Y. T., Lin, C. C., Kuo, H. T., Hung, J. H., Liu, C. H., Jassey, A., et al. (2019). Identification of baicalin from Bofutsushosan and Daisaikoto as a potent inducer of glucose uptake and modulator of insulin signaling-associated pathways. *J. Food Drug Anal.* 27 (1), 240–248. doi:10.1016/j.jfda.2018.07.002

Li, J., Woolbright, B. L., Zhao, W., Wang, Y., Matye, D., Hagenbuch, B., et al. (2018). Sortilin 1 loss-of-function protects against cholestatic liver injury by attenuating hepatic bile acid accumulation in bile duct ligated mice. *Toxicol. Sci.* 161 (1), 34–47. doi:10.1093/toxsci/kfx078

Li, M., Cai, S. Y., and Boyer, J. L. (2017). Mechanisms of bile acid mediated inflammation in the liver. *Mol. Asp. Med.* 56, 45–53. doi:10.1016/j.mam.2017.06.001

Li, N., Bu, P., Zhu, P. S., and Long, A. H. (2008). Pharmacological effects of three traditional Chinese medicine prescriptions on cholestatic liver fibrosis model rats. *Jiangsu J. Traditional Chin. Med.* 11, 113–115. CNKI:SUN:JSZY.0.2008-11-075.

Li, T., and Chiang, J. Y. (2014). Bile acid signaling in metabolic disease and drug therapy. *Pharmacol. Rev.* 66 (4), 948–983. doi:10.1124/pr.113.008201

Li, T., Owsley, E., Matozel, M., Hsu, P., Novak, C. M., and Chiang, J. Y. (2010). Transgenic expression of cholesterol 7alpha-hydroxylase in the liver prevents high-fat diet-induced obesity and insulin resistance in mice. *Hepatology* 52 (2), 678–690. doi:10.1002/hep.23721

Li, Y. F., Wu, J. S., Li, Y. Y., Dai, Y., Zheng, M., Zeng, J. K., et al. (2017). Chicken bile powder protects against α-naphthylisothiocyanate-induced cholestatic liver injury in mice. *Oncotarget* 27 (8), 97137–97152. doi:10.18632/oncotarget.21385

Lu, J. F., Xu, H. Q., Zhang, Z. F., Wang, Z. L., Jiang, S. Y., and Du, P. (2015). Study on the protective effect of Dachaihu granule on experimental chronic cholecystitis in Guinea pigs. *Jiangsu Tradit. Chin. Med.* 47 (4), 73–74+77.

Luo, L., Schomaker, S., Houle, C., Aubrecht, J., and Colangelo, J. L. (2014). Evaluation of serum bile acid profiles as biomarkers of liver injury in rodents. *Toxicol. Sci.* 137 (1), 12–25. doi:10.1093/toxsci/kft221

MahmoudianDehkordi, S., Arnold, M., Nho, K., Ahmad, S., Jia, W., Xie, G., et al. (2019). Altered bile acid profile associates with cognitive impairment in Alzheimer's disease-An emerging role for gut microbiome. *Alzheimers Dement.* 15 (1), 76–92. doi:10.1016/j.jalz.2018.07.217

Mao, C., Zhou, Y., Ji, D., Tan, X., Tao, Y., Zang, W., et al. (2017). Chemical fingerprint of Dachaihu granule and its chemical correlation between raw herbs. *J. Chromatogr. Sci.* 55 (4), 405–410. doi:10.1093/chromsci/bmw194

Mariotti, V., Strazzabosco, M., Fabris, L., and Calvisi, D. F. (2018). Animal models of biliary injury and altered bile acid metabolism. *Biochim. Biophys. Acta. Mol. Basis Dis.* 1864, 1254–1261. doi:10.1016/j.bbadis.2017.06.027

Matsuo, Y., Matsumoto, K., Inaba, N., and Mimaki, Y. (2018). Daisaikoto inhibits pancreatic lipase activity and decreases serum triglyceride levels in mice. *Biol. Pharm. Bull.* 41 (9), 1485–1488. doi:10.1248/bpb.b18-00324

Mencarelli, A., and Fiorucci, S. (2010). FXR an emerging therapeutic target for the treatment of atherosclerosis. *J. Cell. Mol. Med.* 14 (1-2), 79–92. doi:10.1111/j.1582-4934.2009.00997.x

Murphy, C., Parini, P., Wang, J., Björkhem, I., Eggertsen, G., and Gåfvels, M. (2005). Cholic acid as key regulator of cholesterol synthesis, intestinal absorption and hepatic storage in mice. *Biochim. Biophys. Acta* 1735 (3), 167–175. doi:10.1016/j.bbalip.2005.06.001

Nakayama, T., Suzuki, S., Kudo, H., Sassa, S., Nomura, M., and Sakamoto, S. (2007). Effects of three Chinese herbal medicines on plasma and liver lipids in mice fed a high-fat diet. *J. Ethnopharmacol.* 109 (2), 236–240. doi:10.1016/j.jep.2006.07.041

Nguyen, K. D., Sundaram, V., and Ayoub, W. S. (2014). Atypical causes of cholestasis. *World J. Gastroenterol.* 20 (28), 9418–9426. doi:10.3748/wjg.v20.i28.9418

Ofliver, E. (2009). EASL clinical practice guidelines: Management of cholestatic liver diseases. *J. Hepatol.* 51 (2), 237–267. doi:10.1016/j.jhep.2009.04.009

Ohta, Y., Sasaki, E., Nishida, K., Kobayashi, T., Nagata, M., and Ishiguro, I. (1995). Preventive effect of dai-saiko-to (da-chai-hu-tang) extract on disrupted hepatic active oxygen metabolism in rats with carbon tetrachloride-induced liver injury. *Am. J. Chin. Med.* 23 (1), 53–64. doi:10.1142/S0192415X95000080

Orsler, D. J., Ahmed-Choudhury, J., Chipman, J. K., Hammond, T., and Coleman, R. (1999). ANIT-induced disruption of biliary function in rat hepatocyte couplets. *Toxicol. Sci.* 47 (2), 203–210. doi:10.1093/toxsci/47.2.203

Pang, Y. L., Chang, R., and Zhu, P. S. (2008). Effects of Dachaihu decoction on liver function in cholestasis rats. *Henan Tradit. Chin. Med.* 11, 46–47. doi:10.16367/j.issn.1003-5028.2008.11.048

Qian, W., Cai, X., Zhang, X., Wang, Y., Qian, Q., and Hasegawa, J. (2016). Effect of daisaikoto on expressions of SIRT1 and NF-kappaB of diabetic fatty liver rats induced by high-fat diet and streptozotocin. *Yonago Acta Med.* 59 (2), 149–158.

Samur, S., Klebanoff, M., Banken, R., Pratt, D. S., Chapman, R., Ollendorf, D. A., et al. (2017). Long-term clinical impact and cost-effectiveness of obeticholic acid for the treatment of primary biliary cholangitis. *Hepatology* 65 (3), 920–928. doi:10.1002/hep.28932

Schafer, K. A., Eighmy, J., Fikes, J. D., Halpern, W. G., Hukkanen, R. R., Long, G. G., et al. (2018). Use of severity grades to characterize histopathologic changes. *Toxicol. Pathol.* 46 (3), 256–265. doi:10.1177/0192623318761348

Schwarz, M., Russell, D. W., Dietschy, J. M., and Turley, S. D. (2001). Alternate pathways of bile acid synthesis in the cholesterol 7α-hydroxylase knockout mouse are not upregulated by either cholesterol or cholestyramine feeding. *J. Lipid Res.* 42 (10), 1594–1603. doi:10.1016/s0022-2275(20)32213-6

Setchell, K. D., Rodrigues, C. M., Podda, M., and Crosignani, A. (1996). Metabolism of orally administered tauroursodeoxycholic acid in patients with primary biliary cirrhosis. *Gut* 38 (3), 439–446. doi:10.1136/gut.38.3.439

Shen, F. f., and Lu, L. G. (2016). Liver alkaline phosphatase: A marker of cholestasis and biliary injury. *J. Clin. Hepatobiliary Dis.* 32 (5), 1026–1030. doi:10.3969/j.issn.1001-5256.2016.05.052

Song, X. X., Huang, J. F., Tian, M., Liu, Y., Jia, Y. N., and Zheng, C. (2019). Pharmacology and clinical application of Dachaihu decoction. *Acta Chin. Med. Pharmacol.* 47 (4), 112–116. doi:10.19664/j.cnki.1002-2392.190128

Sonne, D. P. (2021). Mechanisms in endocrinology: FXR signalling: A novel target in metabolic diseases. *Eur. J. Endocrinol.* 184 (5), R193–R205. doi:10.1530/EJE-20-1410

Soroka, C. J., Mennone, A., Hagey, L. R., Ballatori, N., and Boyer, J. L. (2010). Mouse organic solute transporter alpha deficiency enhances renal excretion of bile acids and attenuates cholestasis. *Hepatology* 51 (1), 181–190. doi:10.1002/hep.23265

Stofan, M., and Guo, G. L. (2020). Bile acids and FXR: Novel targets for liver diseases. *Front. Med.* 7, 544. doi:10.3389/fmed.2020.00544

Thibaut, M. M., Sboarina, M., Roumain, M., Pötgens, S. A., Neyrinck, A. M., Destrée, F., et al. (2021). Inflammation-induced cholestasis in cancer cachexia. *J. Cachexia Sarcopenia Muscle* 12 (1), 70–90. doi:10.1002/jcsm.12652

Trauner, M., Fuchs, C. D., Halilbasic, E., and Paumgartner, G. (2017). New therapeutic concepts in bile acid transport and signaling for management of cholestasis. *Hepatology* 65 (4), 1393–1404. doi:10.1002/hep.28991

van Golen, R. F., Olthof, P. B., de Haan, L. R., Coelen, R. J., Pechlivanis, A., de Keijzer, M. J., et al. (2018). The pathophysiology of human obstructive cholestasis is mimicked in cholestatic Gold Syrian hamsters. *Biochim. Biophys. Acta. Mol. Basis Dis.* 1864 (3), 942–951. doi:10.1016/j.bbadis.2017.11.022

Vlahcevic, Z. R., Heuman, D. M., and Hylemon, P. B. (1991). Regulation of bile acid synthesis. *Hepatology* 13 (3), 590–600. doi:10.1002/hep.1840130331

Wang, G. F., Li, Y. Y., Shi, R., Wang, T. M., Li, Y. F., Li, W. K., et al. (2020). Yinchenzhufu decoction protects against alpha-naphthylisothiocyanate-induced acute cholestatic liver injury in mice by ameliorating disordered bile acid homeostasis and inhibiting inflammatory responses. *J. Ethnopharmacol.* 254, 112672. doi:10.1016/j.jep.2020.112672

Wang, M. L., and Cui, W. C. (2021). Application of Dachaihu decoction in the treatment of digestive system diseases. *J. Liaoning Univ. Traditional Chin. Med.* 23 (1), 163–166. doi:10.13194/j.issn.1673-842x.2021.01.038

Wang, M., Zhou, L., Sun, Y., Chen, L., Wu, M. Y., Zhang, X. L., et al. (2021). Relevant analysis of Dachaihu decoction and its "formula elements" on the "intesine-liver axis" in the NAFLD model. *World Chin. Med.* 16 (3), 430–436. doi:10.3969/j.ism.1673-7202.2021.03.012

Wang, S. Y., Xie, Y. C., and Min, L. (2022). Effect of modified da chaihutang on FXR/FGF15/FGFR4 signaling pathway in mice with cholesterol gallstone differentiated into damp-heat syndrome. *Chin. J. Exp. Traditional Med. Formulae* 28 (3), 15–24. doi:10.13422/j.cnki.syfjx.20220201

Weerachayaphorn, J., Luo, Y., Mennone, A., Soroka, C. J., Harry, K., and Boyer, J. L. (2014). Deleterious effect of oltipraz on extrahepatic cholestasis in bile duct-ligated mice. *J. Hepatol.* 60 (1), 160–166. doi:10.1016/j.jhep.2013.08.015

Wei, S. H. (2016). Clinical value of combined laboratory test results of ALT, AST, ALP and γ-GT in the diagnosis of various hepatobiliary diseases. *Laboratory Med. Clin.* 13 (6), 848–849. doi:10.3969/J.ISSN.1672-9455.2016.06.053

Weingartner, M., Stücheli, S., Kratschmar, D. V., Birk, J., Klusonova, P., Chapman, K. E., et al. (2021). The ratio of ursodeoxycholyltaurine to 7-oxolithocholyltaurine serves as a biomarker of decreased 11β-hydroxysteroid dehydrogenase 1 activity in mouse. *Br. J. Pharmacol.* 178 (16), 3309–3326. doi:10.1111/bph.15367

Xia, X., Francis, H., Glaser, S., Alpini, G., and LeSage, G. (2006). Bile acid interactions with cholangiocytes. *World J. Gastroenterol.* 12 (22), 3553–3563. doi:10.3748/wjg.v12.i22.3553

Xie, G., Jiang, R., Wang, X., Liu, P., Zhao, A., Wu, Y., et al. (2021). Conjugated secondary 12α-hydroxylated bile acids promote liver fibrogenesis. *EBioMedicine* 66, 103290. doi:10.1016/j.ebiom.2021.103290

Xu, S., Qiao, X., Peng, P., Zhu, Z., Li, Y., Yu, M., et al. (2022). Da-Chai-Hu-Tang protects from acute intrahepatic cholestasis by inhibiting hepatic inflammation and bile accumulation via activation of PPARα. *Front. Pharmacol.* 13, 847483. doi:10.3389/fphar.2022.847483

Xue, J., Qian, P., Li, H., Yang, H., Liu, X., Zhang, Y., et al. (2017). Atonic elements combined or uncombined with epileptic spasms in infantile spasms. *Clin. Neurophysiol.* 24 (2), 220–226. doi:10.1016/j.clinph.2016.11.008

Yang, L., Xiong, A., He, Y., Wang, Z., Wang, C., Wang, Z., et al. (2008). Bile acids metabonomic study on the CCl4- and alpha-naphthylisothiocyanate-induced animal models: Quantitative analysis of 22 bile acids by ultraperformance liquid chromatography-mass spectrometry. *Chem. Res. Toxicol.* 21, 2280–2288. doi:10.1021/tx800225q

Yang, R., Zhao, Q., Hu, D. D., Xiao, X. R., Huang, J. F., and Li, F. (2018). Metabolomic analysis of cholestatic liver damage in mice. *Food Chem. Toxicol.* 120, 253–260. doi:10.1016/j.fct.2018.07.022

Yang, T., Mei, H., Xu, D., Zhou, W., Zhu, X., Sun, L., et al. (2017). Early indications of ANIT-induced cholestatic liver injury: Alteration of hepatocyte polarization and bile acid homeostasis. *Food Chem. Toxicol.* 110, 1–12. doi:10.1016/j.fct.2017.09.051

Yang, Y. (2017). Clinical effect evaluation of modified Dachaihu decoction in the treatment of uremia. *J. Clin. Med. Literature* 4 (98), 19370+19372. doi:10.16281/j.cnki.jocml.2017.98.087

Zhang, S. A., Zheng, A. H., and Liu, H. M. (2020). Effect of da-chai-hu decoction on the level of proinflammatory cytokine levels in peripheral blood of patients with sepsis. *Asia-Pacific Tradit. Med.* 16 (7), 150–152. doi:10.11954/ytctyy.202007051

Zhang, Y., Hong, J. Y., Rockwell, C. E., Copple, B. L., Jaeschke, H., and Klaassen, C. D. (2011). Effect of bile duct ligation on bile acid composition in mouse serum and liver. *Liver Int.* 32 (1), 58–69. doi:10.1111/j.1478-3231.2011.02662.x

Zheng, X., Chen, T., Jiang, R., Zhao, A., Wu, Q., Kuang, J., et al. (2021). Hyocholic acid species improve glucose homeostasis through a distinct TGR5 and FXR signaling mechanism. *Cell. Metab.* 33 (4), 791–803.e7. e797. doi:10.1016/j.cmet.2020.11.017

frontiers | Frontiers in Pharmacology

TYPE Original Research
PUBLISHED 28 September 2022
DOI 10.3389/fphar.2022.984858

OPEN ACCESS

EDITED BY
Yi Wu,
Nanjing Agricultural University, China

REVIEWED BY
Shaojie Yin,
Yangzhou University, China
Xue Mei,
Nanjing University of Chinese Medicine, China

*CORRESPONDENCE
Junming Wang,
mjw98_2010@163.com

SPECIALTY SECTION
This article was submitted to Ethnopharmacology, a section of the journal Frontiers in Pharmacology

RECEIVED 02 July 2022
ACCEPTED 08 August 2022
PUBLISHED 28 September 2022

CITATION
Song L, Wang J, Gong M, Zhang Y, Li Y, Wu X, Qin L and Duan Y (2022), Detoxification technology and mechanism of processing with Angelicae sinensis radix in reducing the hepatotoxicity induced by rhizoma Dioscoreae bulbiferae in vivo. *Front. Pharmacol.* 13:984858. doi: 10.3389/fphar.2022.984858

Detoxification technology and mechanism of processing with *Angelicae sinensis* radix in reducing the hepatotoxicity induced by rhizoma *Dioscoreae bulbiferae in vivo*

Lingling Song[1], Junming Wang[1,2]*, Mingzhu Gong[1], Yueyue Zhang[1], Yamin Li[1], Xiaohui Wu[1], Lingyu Qin[1] and Yaqian Duan[1]

[1]College of Pharmacy, Henan University of Chinese Medicine, Zhengzhou, China, [2]Co-construction Collaborative Innovation Center for Chinese Medicine and Respiratory Diseases by Henan and Education Ministry of P. R. China, Henan University of Chinese Medicine, Zhengzhou, China

Rhizoma Dioscoreae Bulbiferae (RDB) was effective on relieving cough and expectorant but accompanied by severe toxicity, especially in hepatotoxicity. A previous study found that processing with Angelicae Sinensis Radix (ASR) reduced RDB-induced hepatotoxicity. However, up to now, the optimized processing process of ASR-processed RDB has not been explored or optimized, and the detoxification mechanism is still unknown. This study evaluated the detoxification technology and possible mechanism of processing with ASR on RDB-induced hepatotoxicity. The optimized processing process of ASR-processed RDB was optimized by the content of diosbulbin B (DB), the levels of serum alanine aminotransferase (ALT), aspartate aminotransferase (AST), alkaline phosphatase (ALP), and histopathological analysis. The processing detoxification mechanism was evaluated by detecting the antioxidant levels of nuclear factor E2 related factor 2 (Nrf2) and its downstream heme oxygenase 1 (HO-1), quinone oxidoreductase 1 (NQO1), glutamylcysteine ligase catalytic subunit (GCLM), and the levels of downstream antioxidant factors of Nrf2. Besides, the antitussive and expectorant efficacy of RDB was also investigated. This work found that processing with ASR attenuated RDB-induced hepatotoxicity, which can be verified by reducing the levels of ALT, AST, and ALP, and reversing the pathological changes of liver histomorphology. And the optimized processing process of ASR-processed RDB is "processing at a mass ratio of

Abbreviations: ALP, Alkaline phosphatase; ALT, Alanine aminotransferase; ASR, Angelicae Sinensis Radix; AST, Aspartate aminotransferase; GCLM, Glutamatecysteine ligase; GPx, Glutathione peroxidase; GSH, Reduced glutathione; GST, Glutathione S-transferase; HO-1, Heme Oxygenase-1; HPLC, High performance liquid chromatography; MDA, Malondialdchydc; NQO1, Quinone oxidoreductase 1; Nrf2, Nuclear Factor-E2-related factor 2; RDB, Rhizoma Dioscoreae Bulbiferae; T-SOD, Total superoxide dismutase.

100:20 (RDB:ASR) and a temperature of 140°C for 10 min." Further results corroborated that the intervention of processed products of ASR-processed RDB remarkably upregulated the Nrf2/HO-1/NQO1/GCLM protein expression levels in liver, and conserved antitussive and expectorant efficacy of RDB. The above findings comprehensively indicated that the optimized processing process of ASR-processed RDB was "processing at a mass ratio of 100:20 (RDB:ASR) and a temperature of 140°C for 10 min," and the processing detoxification mechanism involved enhancing the level of Nrf2-mediated antioxidant defense in liver as a key target organ.

KEYWORDS

optimized processing process, rhizoma dioscoreae bulbiferae, angelicae sinensis radix, hepatotoxicity, Nrf2 signaling pathway

Highlights

Processing with ASR alleviated serum transaminase levels caused by RDB.
Processing with ASR inhibitd the reduction of Nrf2 level caused by RDB.
Processing with ASR inhibitd liver lipid peroxidation caused by RDB.
Processing with ASR enhanced antioxidant levels caused by RDB.

Introduction

Traditional Chinese medicine (TCM), the great treasure of the Chinese nation, plays an important value with its unique advantages (He et al., 2019; Luo et al., 2019; Jiang et al., 2020; Lin et al., 2020; Qiu et al., 2020; Wu et al., 2021). However, more recently, with the wide application of TCM, adverse reactions (like hepatotoxicity) have been attracted growing attention worldwide (Xie et al., 2020a; Liu et al., 2021; Zhang S. et al., 2021). Therefore, how to reduce the liver toxicity is the key link to ensure the safety of TCM (Chu et al., 2017; Zhou et al., 2018; Jin et al., 2019; Ruan et al., 2019; Deng et al., 2020; Zhang W. et al., 2021).

Rhizoma Dioscoreae Bulbiferae (RDB) was first recorded in the Song Dynasty "Kaibao Bencao" (Zhang et al., 2017), with a medicinal history of more than 1,000 years. Modern researches suggested that RDB has pharmacological effects such as anti-tumor (Wang et al., 2012; Cui et al., 2016), anti-inflammatory (Mbiantcha et al., 2011), antioxidant (Chaniad et al., 2020), regulating immune function (Cui et al., 2016), and is widely used in the treatment of hyperthyroidism (Jiang, 1978), colorectal carcinoma (Ahmad et al., 2018), and other diseases (Ghosh et al., 2012). However, it is often accompanied by strong liver toxicity in the process of medication, which has been confirmed in several clinical (Jiang, 1976; Jiang, 1981; Feng, 1989; Jin, 1996; Hua et al., 2011; Huang et al., 2013; Lu and Wu, 2014) and preclinical animal (Su et al., 2003; Ma et al., 2013; Sheng et al., 2014; Yang et al., 2016; Qu et al., 2019) studies. Since the hepatotoxicity induced by RDB severely limits the exertion and application of its outstanding curative effect, it is very urgent to carry out the detoxification research.

The "using Chinese botanical drugs to process other Chinese botanical drugs" method is the principle of processing the primary medicine by using a certain TCM as processing adjuvant in the processing technology, which could attenuate drug toxic reaction (Huang et al., 2011; Su et al., 2016; Shan et al., 2018; Jiang T. et al., 2021; Zhang K. et al., 2021; Zhang M. et al., 2021; Ota and Makino, 2022) or (and) increase the synergistic effect (Huang et al., 2011; Lu et al., 2018; Wang J. et al., 2019; Liao et al., 2021; Kong et al., 2022; Wang T. et al., 2022). Angelicae Sinensis Radix (ASR) is sweet in taste and warm in nature (Chen Q. et al., 2021), and has been proved to have a variety of pharmacological effects such as hepatoprotective (Hua et al., 2014), anti-oxidation (Nai et al., 2021), and its main pharmacological components have been proved to significantly reduce liver damage induced by carbon tetrachloride (Wang et al., 2020), ethanol (Wang et al., 1997), and concanavalin A (Wang et al., 2016). In addition, previous studies (Wu et al., 2020a; Wang C. et al., 2022) indicated that processing with ASR effectively reduced RDB-induced hepatotoxicity. However, so far, the optimized processing process of ASR-processed RDB has not been explored or optimized, and the detoxification mechanism is still unknown.

Given that, this study optimized the processing process of ASR-processed RDB through the detection of diosbulbin B (DB) content, serum biochemical indicators and liver histopathology, and explained its detoxification mechanism. Additionally, this study also discussed the antitussive and expectorant efficacy of RDB. This current research will contribute to provide support for the wide application of RDB, improve the safety and effectiveness of the medication.

Materials and methods

Plant materials

RDB (origin: Hubei) and ASR (origin: Gansu) were identified as the dried tubers of *Dioscorea bulbifera* L., the dried root of

TABLE 1 The L9 (3^4) orthogonal experimental design table of ASR-processed RDB.

Factors/levels group	A. RDB: ASR (g)	B. Processing temperature (°C)	C. Processing time (min)
$A_1B_1C_1$	100:5	120	10
$A_1B_2C_2$	100:5	140	15
$A_1B_3C_3$	100:5	160	20
$A_2B_1C_2$	100:10	120	15
$A_2B_2C_3$	100:10	140	20
$A_2B_3C_1$	100:10	160	10
$A_3B_1C_3$	100:20	120	20
$A_3B_2C_1$	100:20	140	10
$A_3B_3C_2$	100:20	160	15

TABLE 2 Determination of DB content in 95% ethanol extracts of RDB and processed products of ASR-processed RDB.

Group	DB (mg/g)	Relative rate of change (%)
RDB	1.227 ± 0.003	–
$A_1B_1C_1$	1.020 ± 0.011[2)]	16.9
$A_1B_2C_2$	1.001 ± 0.020[2)]	18.4
$A_1B_3C_3$	0.996 ± 0.006[2)]	18.8
$A_2B_1C_2$	1.021 ± 0.003[2)]	16.8
$A_2B_2C_3$	1.077 ± 0.078[1)]	12.2
$A_2B_3C_1$	0.998 ± 0.019[2)]	18.7
$A_3B_1C_3$	0.979 ± 0.013[2)]	20.2
$A_3B_2C_1$	0.958 ± 0.047[2)]	21.9
$A_3B_3C_2$	0.969 ± 0.009[2)]	21.0
QC	1.191 ± 0.003	2.9
QSC	1.168 ± 0.007	4.8

Angelica sinensis (Oliv.) Diels of the Apiaceae by Professor Chen Suiqing of School of Pharmacy, Henan University of Chinese medicine. The numbers of voucher specimens are in the order of RDB20180811, and ASR180601, respectively.

Reagents and antibodies

Alanine aminotransferase (ALT), aspartate aminotransferase (AST), alkaline phosphatase (ALP), malondialdehyde (MDA), total superoxide dismutase (T-SOD), glutathione (GSH), glutathione peroxidase (GPx), glutathione transferase (GST) were all produced by Nanjing Jiancheng Bioengineering Institute (Nanjing, China). Antibodies such as nuclear factor-E2-related factor 2 (Nrf2), heme oxygenase-1 (HO-1), quinone oxidoreductase 1 (NQO1), glutamate cysteine ligase (GCLM) were obtained from GeneTex Inc. (San Antonio, United States). β-actin, and HRP-conjugated Affinipure Goat Anti-Rabbit lgG (H + L) were produced by Proteintech Group, Inc. (Chicago, United States). Antibody Lamin B was supported by Bioworld (Bioworld Technology Co. Ltd., Minnesota, United States).

Reference standard of DB was produced by Shanghai Yuanye Biotechnology Co., Ltd., (Shanghai, China). All chemicals and solvents were of chromatographic grade.

Orthogonal experimental design of angelicae sinensis radix-processed rhizoma dioscoreae bulbiferae

The key factors in the processing process, such as the ratio of main drug (RDB) to adjuvant (ASR), processing temperature, and processing time, etc. were taken as the investigation factors. Under each factor, the three levels involved in the routine were taken as the inspection level, and the factor level table was designed according to the principle of orthogonal experimental design, as illustrated in Table 1.

Preparation of rhizoma dioscoreae bulbiferae and processed products of angelicae sinensis radix-processed rhizoma dioscoreae bulbiferae

Different mass fractions of ASR were weighed and decocted for 30 min with water (1:10, w/v) to obtain the filtrate. Then, the dregs were boiled in water (1:8, w/v) for 20 min. Then, the filtrates were combined and concentrated to the corresponding volume (approximately 30 ml of ASR decoction was used for every 200 g of RDB).

An appropriate amount of RDB (e.g., 200 g) was taken and added the corresponding ASR decoction, respectively, according to the process combination in Table 1, mixed well, moisten, placed the drugs into the pan, processing them with different

TABLE 3 Processing with ASR reversed the significantly elevated serum biochemical levels induced by RDB.

Group	ALT (U/L^{-1})	Relative rate of change (%)	AST (U/L^{-1})	Relative rate of change (%)	ALP (Kim's unit)	Relative rate of change (%)
Control	13.436 ± 1.890	–	67.833 ± 3.599	–	59.479 ± 0.546	–
RDB	52.638 ± 1.397[2)]	291.8	120.165 ± 5.185[2)]	77.1	145.686 ± 3.752[2)]	144.9
$A_1B_1C_1$	28.500 ± 2.905[4)]	45.9	95.692 ± 4.226	20.4	130.314 ± 1.168[3)]	10.6
$A_1B_2C_2$	26.069 ± 2.406[4)]	50.5	87.167 ± 5.326[4)]	27.5	124.380 ± 1.181[4)]	14.6
$A_1B_3C_3$	30.115 ± 2.858[4)]	42.8	90.965 ± 4.111[3)]	24.3	127.355 ± 3.125[4)]	12.6
$A_2B_1C_2$	29.712 ± 2.954[4)]	43.6	103.686 ± 5.709	13.7	127.223 ± 1.210[4)]	12.7
$A_2B_2C_3$	33.775 ± 2.384[4)]	35.8	98.823 ± 5.578	17.8	132.281 ± 1.929	9.2
$A_2B_3C_1$	30.558 ± 2.799[4)]	41.9	80.738 ± 5.266[4)]	32.8	123.702 ± 2.603[4)]	15.1
$A_3B_1C_3$	27.338 ± 2.922[4)]	48.1	81.566 ± 6.262[4)]	32.1	111.223 ± 1.533[4)]	23.7
$A_3B_2C_1$	20.391 ± 2.190[4)]	61.3	78.709 ± 6.921[4)]	34.5	131.884 ± 4.107	9.5
$A_3B_3C_2$	18.658 ± 1.703[4)]	64.6	84.602 ± 7.058[4)]	29.6	115.653 ± 1.998[4)]	20.6
QC	46.885 ± 3.108	10.9	110.278 ± 7.494	8.2	144.744 ± 3.807	0.6
QSC	41.749 ± 2.222	20.7	106.019 ± 3.503	11.8	137.752 ± 6.935	5.4
ASR	16.367 ± 1.600	68.9	72.983 ± 5.127	39.3	61.942 ± 1.342	57.5

TABLE 4 The results of serum T value of each group of mice of ASR-processed RDB.

Group	t_{ALT}	t_{AST}	t_{ALP}	Comprehensive score
$A_1B_1C_1$	6.161	3.600	3.521	13.282
$A_1B_2C_2$	9.227	4.182	4.978	18.387
$A_1B_3C_3$	7.364	5.663	3.478	16.505
$A_2B_1C_2$	6.145	1.888	4.763	12.796
$A_2B_2C_3$	5.331	2.192	3.691	11.214
$A_2B_3C_1$	7.662	5.705	4.037	17.404
$A_3B_1C_3$	7.499	4.869	9.699	22.067
$A_3B_2C_1$	17.215	7.174	1.902	26.291
$A_3B_3C_2$	14.286	4.165	5.792	24.243

temperatures for the corresponding time, taken out, and dried to obtain the samples of processed products of RDB.

Processing RDB product (QC): The processing method was referred to the general processing rule 0213 method of Chinese Pharmacopoeia (Pharmacopoeia of the People's Republic of China, 2020). In brief, an appropriate amounts of RDB (e.g., 200 g) were weighed and placed in a preheated wok, processing them gently until they turns slightly brown (about 10 min), taken out and dried to get the processing RDB product.

Processing RDB with water (QSC): An appropriate amount of RDB (e.g., 200 g) was taken and added water (e.g., 30 ml), mixed well, and moisten (about 60 min), put the drugs into a preheated wok, processing gently until they were slightly brown (about 10 min), taken out and dried to get them.

ASR adjuvant group (ASR): An appropriate amount of ASR (such as 10 g) was taken, and added water (1:10, w/v) to decoct for 30 min, filter, the dregs were decocted in water (1:8, w/v) for 20 min, combined and centrifuged to obtain the supernatant, and concentrated to the corresponding volume.

High-performance liquid chromatography analysis

Appropriate amounts of RDB and processed products of ASR-processed RDB (such as 10 g) were weighed and extracted with 95% ethanol for 2 times, 2 h/time, and filtered. Then, the filtrates were combined and concentrated under reduced pressure until there was no alcohol smell, and evaporated to dryness to obtain the extract, and the yield was 17.83%, 11.26%, 9.93%, 11.25%, 10.39%, 13.68%, 9.42%, 12.68%, 14.73%, 16.08%, 12.60%, and 10.65%, (the order was RDB, the nine processed products, QC, QSC) separately. A certain volume of extract (equivalent to 3 g of medicinal materials) was precisely weighed, added methanol to dissolve, and fixed volume to a 25 ml volumetric flask.

The HPLC method was as reported by the previous research, with slightly improved (Wu et al., 2020b). The system was Agilent 1,260 (Agilent Technologies, Inc., United States) and a C18 chromatographic column (250 mm × 4.60 mm, 5 μm, Agilent Technologies, Inc., United States) was selected. Acetonitrile-water (25:75) was used as the mobile phase. The flow rate was 1.0 ml/min^{-1}, the column temperature was 30°C, and the detection wavelength was 210 nm.

TABLE 5 Processing with ASR reversed the significantly down-regulated Nrf2/HO-1 pathway related proteins in liver caused by RDB.

Group	Nrf2/Lamin B	Relative rate of change (%)	HO-1/β-actin	Relative rate of change (%)
Control	1.000 ± 0.202	–	1.000 ± 0.109	–
RDB	0.200 ± 0.049[2)]	80.0	0.276 ± 0.066[2)]	72.4
$A_2B_2C_3$	0.337 ± 0.067	68.5	0.373 ± 0.091	35.1
$A_2B_3C_1$	0.760 ± 0.190[3)]	280.0	0.786 ± 0.018[4,5)]	184.8
$A_3B_2C_1$	0.961 ± 0.018[4,5)]	380.5	0.894 ± 0.018[4,6)]	223.9
QC	0.203 ± 0.042[7,10)]	1.5	0.280 ± 0.079[8,10)]	1.4
QSC	0.252 ± 0.081[10)]	26.0	0.292 ± 0.057[8,10)]	5.8

TABLE 6 Processing with ASR reversed the significantly down-regulated NQO1/GCLM pathway related proteins in liver caused by RDB.

Group	NQO1/β-actin	Relative rate of change (%)	GCLM/β-actin	Relative rate of change (%)
Control	1.000 ± 0.024	–	1.000 ± 0.054	–
RDB	0.163 ± 0.010[2)]	83.7	0.109 ± 0.050[2)]	89.1
$A_2B_2C_3$	0.248 ± 0.015	52.1	0.298 ± 0.064	173.4
$A_2B_3C_1$	0.321 ± 0.026[4)]	96.9	0.440 ± 0.106[3)]	303.7
$A_3B_2C_1$	0.420 ± 0.024[4,6,7)]	157.7	0.513 ± 0.084[4)]	370.6
QC	0.217 ± 0.013[7,10)]	33.1	0.186 ± 0.003[9)]	70.6
QSC	0.221 ± 0.007[7,10)]	35.6	0.167 ± 0.032[9)]	53.2

TABLE 7 Processing with ASR remarkably reversed hepatic lipid peroxidation and enhanced antioxidant levels in the liver of mice caused by RDB.

Group	MDA (μg/mg protein)	Relative rate of change (%)	T-SOD (U/mg protein)	Relative rate of change (%)
Control	1.890 ± 0.200	–	59.260 ± 2.977	–
RDB	3.819 ± 0.286[2)]	102.1	31.012 ± 2.535[2)]	47.7
$A_2B_2C_3$	3.117 ± 0.387	18.4	42.094 ± 2.341	35.7
$A_2B_3C_1$	2.547 ± 0.236[3)]	33.3	47.772 ± 4.402[4)]	54.0
$A_3B_2C_1$	2.307 ± 0.290[4)]	39.6	51.488 ± 3.736[4)]	66.0
QC	3.626 ± 0.326[9)]	5.1	33.849 ± 3.237[7,10)]	9.1
QSC	3.413 ± 0.305	10.6	35.329 ± 2.604[9)]	13.9

Animals

SPF-grade male ICR mice (weighing 18–22 g) were obtained from Shandong Experimental Animal Center (Shandong China), license NO. SYXK (Lu) 2020–0004. The mice were randomly given standard food and water, and kept under a specified environment, with a relative temperature of 21–23°C, the humidity of 60 %–65%, and a 12 h/12 h light/dark cycle, with lighting turned on at 7 a.m. every day. All the procedures were in strict accordance with the P.R. China's legislation on the use and care of laboratory animals and approved by the Experimental Animal Ethical Committee of Henan University of Chinese Medicine (approval number: DWLL201903531).

Experimental protocol

After 1 week of acclimating, 140 SPF-grade male mice were stochastically separated into the control group, RDB group, the above nine processed groups of ASR-processed RDB, QC, QSC,

TABLE 8 Processing with ASR remarkably enhanced levels of glutathione antioxidant enzymess in the liver of mice caused by RDB.

Group	GSH (μg/mg protein)	Relative rate of change (%)	GPx (U/mg protein)	Relative rate of change (%)	GST (U/mg protein)	Relative rate of change (%)
Control	10.642 ± 0.923	–	1704.978 ± 78.231	–	172.167 ± 10.390	–
RDB	5.205 ± 0.292[2)]	51.1	756.807 ± 32.897[2)]	55.6	43.012 ± 6.793[2)]	75.0
$A_2B_2C_3$	8.393 ± 0.632	61.2	999.935 ± 45.373[3)]	32.1	85.613 ± 14.386	99.0
$A_2B_3C_1$	9.025 ± 0.647[3)]	73.4	1,185.429 ± 55.245[4)]	56.6	99.866 ± 10.838[4)]	132.2
$A_3B_2C_1$	9.101 ± 1.047[3)]	74.9	1,310.261 ± 66.209[4,6)]	73.1	116.210 ± 11.710[4)]	170.2
QC	7.556 ± 1.358	45.2	815.303 ± 32.070[8,10)]	7.7	62.427 ± 6.457[9)]	45.1
QSC	7.910 ± 0.429	52.0	820.837 ± 49.627[8,10)]	8.5	77.906 ± 11.938	81.1

TABLE 9 Processing with ASR conserved the antitussive and expectorant efficacy of RDB.

Group	The number of coughs	The cough latency (s)	The cough relieving rates (%)	Phenol red concentration (μg/ml^{-1})	Relative rate of change (%)
Model	40.300 ± 2.468	15.060 ± 1.192	–	0.299 ± 0.039	–
RDB	28.800 ± 2.185[2)]	27.004 ± 2.610[1)]	28.5	0.574 ± 0.038[1)]	92.0
$A_2B_2C_3$	28.200 ± 2.004[2)]	28.736 ± 2.110[2)]	30.0	0.629 ± 0.085[2)]	110.4
$A_2B_3C_1$	27.600 ± 1.752[2)]	29.887 ± 1.887[2)]	31.5	0.641 ± 0.086[2)]	114.4
$A_3B_2C_1$	24.300 ± 2.150[2)]	33.109 ± 2.522[2)]	39.7	0.716 ± 0.067[2)]	139.5
QC	30.800 ± 1.245[1)]	27.529 ± 2.936[1)]	23.6	0.581 ± 0.025[1)]	94.3
QSC	30.200 ± 2.832[1)]	26.492 ± 3.104[1)]	25.1	0.586 ± 0.047[1)]	96.0
Keke Tablets	20.900 ± 2.025[2)]	40.515 ± 2.850[2,4)]	48.1	0.778 ± 0.063[2)]	160.2

and ASR group (n = 10) based on their body weight. The RDB and the above-processed products were administered by gavage at the dose of 1.7 g/kg^{-1} for 14 days on the basis of the previous research (Wu et al., 2020b), and the gavage volume was 20 ml/kg^{-1}. The ASR group was administered with a dose of 0.4 g/kg^{-1}, and the control group was given an equal volume of 0.5% CMC-Na solution. After the last administration for 60 min, blood was taken from all mice, and after standing for 2 h, centrifuged to collect the upper serum. Then, the mice were sacrificed immediately, and the liver tissues of each group were quickly taken out and stored in a −80°C refrigerator.

Determination of serum biochemical indexes in mice

The serum ALT, AST, and ALP levels were measured on the basis of the colorimetric method, Lai's method, and sodium phenylene phosphate colorimetry method in the instructions of their respective kits, and calculated according to their corresponding formulas.

Histopathological analysis

The left lobe of liver were fixed in 4% paraformaldehyde solution, embedded in conventional paraffin, and sliced at 4–5 μm. Sections were stained with hematoxylin-eosin (HE) for histopathological examination under microscope and photographed at 200 ×.

Western blot

Liver proteins were detected by Western blot analysis. The extracted proteins were electrophoresis and transferred to PVDF membranes. After blocking with 5% skimmed milk powder, added the corresponding primary antibodies (rabbit anti-Nrf2: 1:500, rabbit anti-HO-1: 1:1,000, rabbit anti-NQO1: 1:1,000, rabbit anti-GCLM: 1:1,000) incubated overnight at 4°C. The next day, the membranes were washed with TBST for 4 times, each time/10 min. Then, HRP-conjugated affinipure goat anti-rabbit lgG (H + L) (1:5,000) was incubated for 1 h, washed again, and imaged with Tanon image software (Tianneng Technology

Co., Ltd., Shanghai, China). The optical density (O.D.) of the immune contents was normalized to β-actin (total protein) or Lamin B (nuclear protein).

Detection of lipid peroxidation and antioxidant levels in liver

The absorbance of liver tissue homogenate was detected by the thiobarbituric acid method in the instructions of the kit, and the MDA level was calculated by dividing the corresponding protein content of each group. The absorbance was measured based on the hydroxylamine method in the instructions of the kit, and then divided by the corresponding protein content of each group to calculate the T-SOD level in liver tissue. The levels of GSH, CPx, and GST were obtained by measuring the absorbance of liver tissue homogenate on the basis of the visible light colorimetric method in the kit instructions, and then dividing by the corresponding protein content of each group.

Cough model induced by ammonia

80 SPF male ICR mice were separated into eight groups on the basis of their body weight ($n = 10$), the model group, RDB group, worst processing technology ($A_2B_2C_3$) group, intermediate processing technology ($A_2B_3C_1$) group, the optimized processing technology ($A_3B_2C_1$) group, QC, QSC group, and positive drug Keke tablet group. The RDB and processed products of ASR-processed RDB were intragastrically administered with the same dose of 1.7 g/kg^{-1}, and 1.4 g/kg^{-1} Keke tablets were given by gavage to the positive drug group based on the previous study (Wu et al., 2020b). All groups were given continuous intragastric administration for 14 days. The ammonia-induced cough model was carried out 60 min after the last administration. Briefly (Hu et al., 2021), the 500 ml beaker was placed on the desktop with 1/4 of the 10 cm × 10 cm qualitative filter paper, and 0.1 ml of concentrated ammonia water was injected into the filter paper with 1 ml syringe. After 30 s of natural volatilization, the filter paper was quickly extracted and put into the mice to be tested. The cough was judged by abdominal contraction, mouth opening, and cough sound of mice, and the cough incubation period of cough was the time from the beginning to the first cough in mice. The cough latency and the number of coughs in each group within 2 min were recorded, and the cough relieving rate was calculated. Cough relieving rate (%) = (the number of coughs in the concentrated ammonia water-induced cough group - the number of coughs in the administration group)/the number of coughs in the concentrated ammonia water-induced cough group × 100%.

Effects on phenol red excretion from trachea of mice

The experimental grouping and administration method were referred to the cough experiment induced by concentrated ammonia water. Referred to the previous method, with slight modifications (Jiang et al., 2014). After the last administration for 30 min, 0.1 ml/10 g of 5% phenol red saline solution was intraperitoneally injected. The trachea with the same length from the thyroid cartilage to the tracheal branch was taken and placed in a centrifuge tube containing 2 ml of saline (NaCl 0.9%), and added 0.1 ml of 0.5% sodium bicarbonate solution. Then, the centrifuge tubes with trachea were ultrasonically treated, soaked, and centrifuged to obtain supernatant. The absorbance value was detected at 546 nm and substituted into the phenol red standard curve to calculate the concentration of phenol red, that is, the phenol red excretion of mouse trachea. Taking the excretion of phenol red in the model group as 100%, the percentage of red excretion percentage of the other groups was compared with that in the model group.

Statistical analysis

Statistical Package for the Social Sciences (version 20.0) software was applied for data analysis. The data of each group were presented as mean ± standard error (S.E.M.). One-way analysis of variance was used, and then Tukey multiple comparison test was performed. $p < 0.05$ was considered statistically significant. The graphs were drawn with GraphPad Prism version 8.0.

Results

Validation of HPLC method

The HPLC method was verified based on linearity, precision, stability, and reproducibility. Linearity was verified by using the standard solutions of DB. Taking the concentration as abscissa (X), and the peak area value as ordinate (Y), the linear regression equation was obtained: Y = 38.395 X—2,228.2. Data displayed that the linearity of DB in the concentration range of 0.06–0.20 mg/ml was linear (correlation coefficient r = 0.9991). Furthermore, the precision was obtained by injecting 10 μl of a standard solution six times, recording the peak area, and calculated the RSD value. Results showed that the RSD value was 0.46%, suggesting that the instrument has good precision. Besides, stability was obtained by measuring samples at 0, 3, 6, 9, 12, and 24 h, and the repeatability was determined by measuring 6 times the same sample. The results demonstrated that the RSD value of DB peak area was 2.01%, and 2.32%, separately,

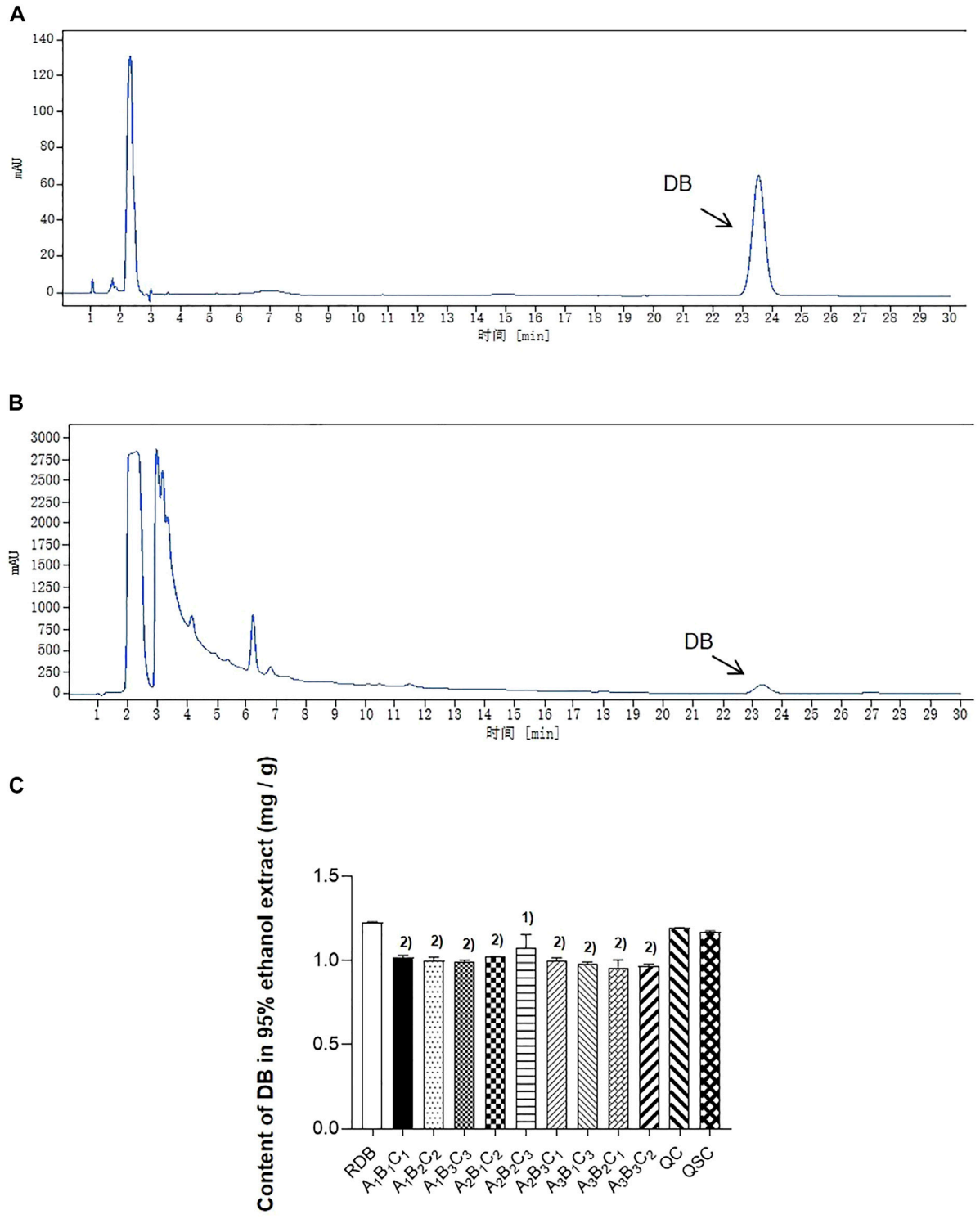

FIGURE 1
Processing with ASR alleviated the content of DB in RDB group. **(A)** The reference substance of DB in HPLC. **(B)** The sample of DB in HPLC. **(C)** The content of DB in RDB and other processed group. Data were expressed as mean ± S.E.M., with three samples in each group. 1) $p < 0.05$, 2) $p < 0.01$, compared with the RDB group.

indicating that the test solution stability in 24 h and the method repeatability were satisfactory.

Determination of diosbulbin B content in 95% ethanol extracts of rhizoma dioscoreae bulbiferae and processed products of angelicae sinensis radix-processed rhizoma dioscoreae bulbiferae

This study firstly evaluated whether processing with ASR could effectively reduce the RDB-caused hepatotoxicity via the detection of DB content in RDB and various processed products (Figure 1; Table 2). Results showed that the DB content in the processed products ($A_1B_1C_1$, $A_1B_2C_2$, $A_1B_3C_3$, $A_2B_1C_2$, $A_2B_2C_3$, $A_2B_3C_1$, $A_3B_1C_3$, $A_3B_2C_1$, and $A_3B_3C_2$) of ASR-processed RDB remarkably weakened ($p < 0.05$ or $p < 0.01$) when compared with the RDB group. Although DB content in QC and QSC products decreased somewhat, there was no discernible distinction ($p > 0.05$). In addition, based on the content of DB in RDB and processed products of ASR-processed RDB, the order from high to low was as follows: RDB product > QC product > QSC product > $A_2B_2C_3$ > $A_2B_1C_2$ > $A_1B_1C_1$ > $A_1B_2C_2$ > $A_2B_3C_1$ > $A_1B_3C_3$ > $A_3B_1C_3$ > $A_3B_3C_2$ > $A_3B_2C_1$. Among them, the content of DB in the RDB product was the highest, which was 1.227 mg/g, and the $A_3B_2C_1$ was the lowest, which was 0.958 mg/g.

Processing with angelicae sinensis radix reversed the significantly elevated serum biochemical levels and liver cell degeneration, cytoplasmic looseness induced by rhizoma dioscoreae bulbiferae

Then, this study investigated whether processing with ASR could effectively reduce the hepatotoxicity induced by RDB through the serum biochemical indicators sensitive to liver injury (Figure 2; Table 3). The results illustrated that the continuous administration of RDB remarkably elevated the levels of serum ALT, AST, and ALP by 291.8%, 77.1%, and 144.9%, respectively (all $p < 0.01$), indicating that the hepatotoxicity was induced in mice after continuous administration for 14 days. Among them, there was no obvious difference in the above-mentioned serum indexes in the ASR group ($p > 0.05$). Compared with the RDB group, the levels of serum ALT, AST, and ALP of mice decreased apparently after the intervention of five processed products, $A_1B_2C_2$, $A_1B_3C_3$, $A_2B_3C_1$, $A_3B_1C_3$, and $A_3B_3C_2$ ($p < 0.05$ or $p < 0.01$). In addition, the relative change rate of serum ALT index in $A_3B_3C_2$ group was the highest. In terms of the relative change rate of serum AST index, the change rate of $A_3B_2C_1$ group was the highest. In terms of the relative change rate of serum ALP index, the change rate of $A_3B_1C_3$ group was the highest.

According to the analysis of the results of the above indicators, the serum transaminase levels in each processed product of ASR-processed RDB were comprehensively evaluated and analyzed by a multi-index comprehensive method (Table 4), and found that the optimized processing process of ASR-processed RDB was "processing at a mass ratio of 100:20 (RDB:ASR) and a temperature of 140°C for 10 min." The attenuating effect of different processed products was as follows: $A_3B_2C_1$ > $A_3B_3C_2$ > $A_3B_1C_3$ > $A_1B_2C_2$ > $A_2B_3C_1$ > $A_1B_3C_3$ > $A_1B_1C_1$ > $A_2B_1C_2$ > $A_2B_2C_3$.

In addition, liver histopathology (Figure 3) showed that the RDB administration resulted in a large number of hepatocytes with cytoplasmic looseness and hepatocyte edema, inflammatory infiltration, and vascular congestion in the liver of mice. However, after the intervention of processed products of ASR-processed RDB ($A_1B_2C_2$, $A_3B_1C_3$, $A_3B_2C_1$, and $A_3B_3C_2$), the hepatotoxicity was significantly improved to varying degrees. Among them, other processed products, including the QC and QSC group, only improved the toxicity induced by RDB to a certain extent, and have not yet achieved a significant effect. The results of liver pathological were consistent with or basically consistent with the serum biochemical indexes.

Study on the detoxification mechanism of angelicae sinensis radix-Processed rhizoma dioscoreae bulbiferae under the best technology

In the early stage, we screened out the optimized processing process of ASR-processed RDB. Next, the worst detoxification technology group ($A_2B_2C_3$), the intermediate processing technology ($A_2B_3C_1$) group, the optimized processing ($A_3B_2C_1$) group, and QC, QSC group were selected to study the molecular mechanism.

Processing with angelicae sinensis radix reversed the significantly downregulated nrf2/heme oxygenase 1 pathway related proteins in liver caused by rhizoma dioscoreae bulbiferae

The current research explored the attenuating mechanism of ASR-processed RDB on the hepatotoxicity induced by RDB by detecting and analyzing the Nrf2/HO-1 pathway-related proteins in liver (Figure 4; Tables 5, 6). Results displayed that after continuous administration of RDB for 14 days, the protein expression levels of Nrf2/HO-1/NQO1/GCLM were remarkably down-regulated by 80.0%, 72.4%, 83.7%, and

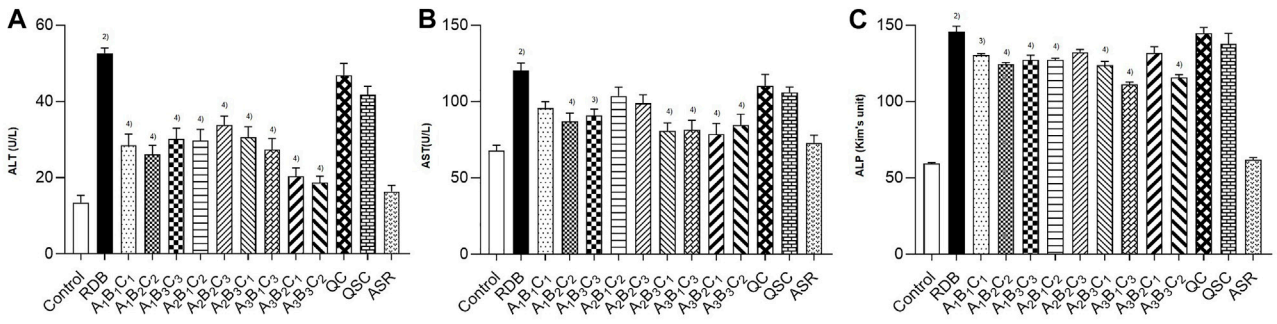

FIGURE 2
Processing with ASR inhibited the hepatotoxicity induced by RDB in mice. **(A)** Serum ALT levels. **(B)** Serum AST levels. **(C)** Serum ALP levels. Data were expressed as mean ± S.E.M., with 10 mice in each group. 1) $p < 0.05$, 2) $p < 0.01$, compared with the Control group, 3) $p < 0.05$, 4) $p < 0.01$, compared with the RDB group.

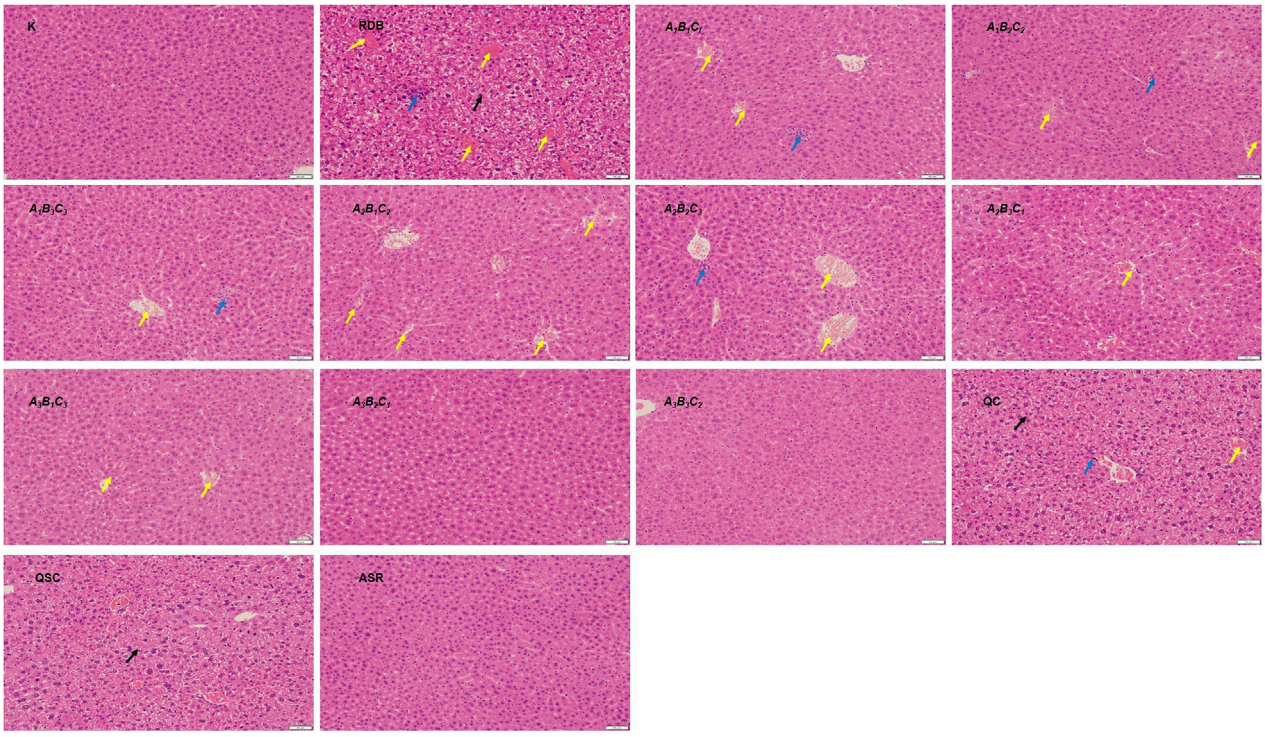

FIGURE 3
Processing with ASR improved the liver cell degeneration, cytoplasmic looseness, hepatocyte edema, inflammatory infiltration, and vascular congestion induced by RDB. HE staining (original magnifications, ×200) of liver tissues. (Black arrows indicated cytoplasmic looseness, blue arrows indicated inflammatory infiltration, and yellow arrows indicated vascular congestion).

89.1% ($p < 0.01$). After intervention with the $A_2B_3C_1$ and $A_3B_2C_1$ group, the Nrf2/HO-1/NQO1/GCLM expression protein levels were strikingly up-regulated by 280.0%, 184.8%, 96.9%, and 303.7%, respectively ($A_2B_3C_1$ group, $p < 0.05$ or $p < 0.01$), 380.5%, 223.9%, 157.7%, and 370.6% ($A_3B_2C_1$ group, $p < 0.01$). After the intervention of QC, QSC, and $A_2B_2C_3$ groups, although the above indicators showed an upward trend, there was no obvious distinction ($p > 0.05$). In addition, in terms of the relative change rate of Nrf2/HO-1/NQO1/GCLM, $A_3B_2C_1$ group had the highest rate of change.

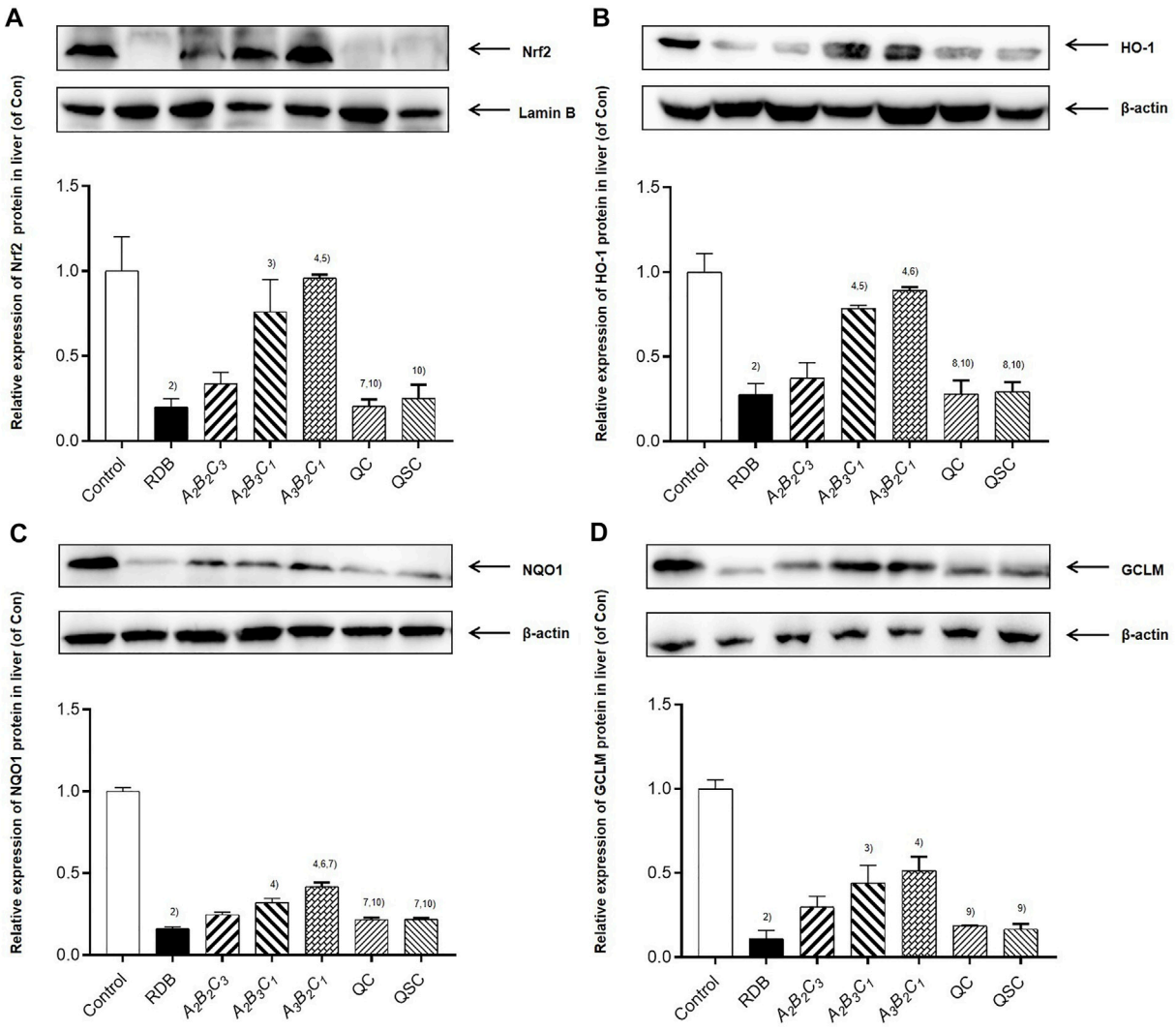

FIGURE 4
Processing with ASR reversed Nrf2-mediated antioxidant defense induced by RDB in mice. **(A)** Nrf2, **(B)** HO-1, **(C)** NQO1, **(D)** GCLM protein levels in liver determined by western blot. Data were expressed as mean ± S.E.M., with three mice in each group. 1) $p < 0.05$, 2) $p < 0.01$, compared with the Control group, 3) $p < 0.05$, 4) $p < 0.01$, compared with the RDB group, 5) $p < 0.05$, 6) $p < 0.01$, compared with the $A_2B_2C_3$ group, 7) $p < 0.05$, 8) $p < 0.01$, compared with the $A_2B_3C_1$ group, 9) $p < 0.05$, 10) $p < 0.01$, compared with the $A_3B_2C_1$ group, 11) $p < 0.05$, 12) $p < 0.01$, compared with the QC group.

Processing with angelicae sinensis radix remarkably reversed hepatic lipid peroxidation and enhanced antioxidant levels in the liver of mice caused by rhizoma dioscoreae bulbiferae

Next, the current research further evaluated the detoxification mechanism of ASR-processed RDB through the detection and analysis of lipid peroxidation and antioxidant levels in liver (Figure 5; Tables 7, 8). Data displayed that the MDA level was effectively augmented by 102.1% ($p < 0.01$) in liver, and the T-SOD, GSH, GPx, and GST levels were strikingly decreased by 47.7%, 51.1%, 55.6%, and 75.0% ($p < 0.01$), after 14 days of continuous administration of RDB. After the intervention of $A_2B_3C_1$ group and $A_3B_2C_1$ group, the MDA level was strikingly alleviated by 33.3% and 39.6% ($p < 0.05$ or $p < 0.01$), and the levels of T-SOD, GSH, GPx, and GST were significantly augmented by 54.0%, 73.4%, 56.6%, and 132.2% ($A_2B_3C_1$ group, $p < 0.05$ or $p < 0.01$), 66.0%, 74.9%, 73.1%, and 170.2% ($A_3B_2C_1$ group, $p < 0.05$ or $p < 0.01$), separately. However, the administration of $A_2B_2C_3$ group only remarkably increased the level of GPx in liver ($p < 0.05$). In addition, after the treatment with QC, QSC, and $A_2B_2C_3$ group, although the MDA level showed a decreasing

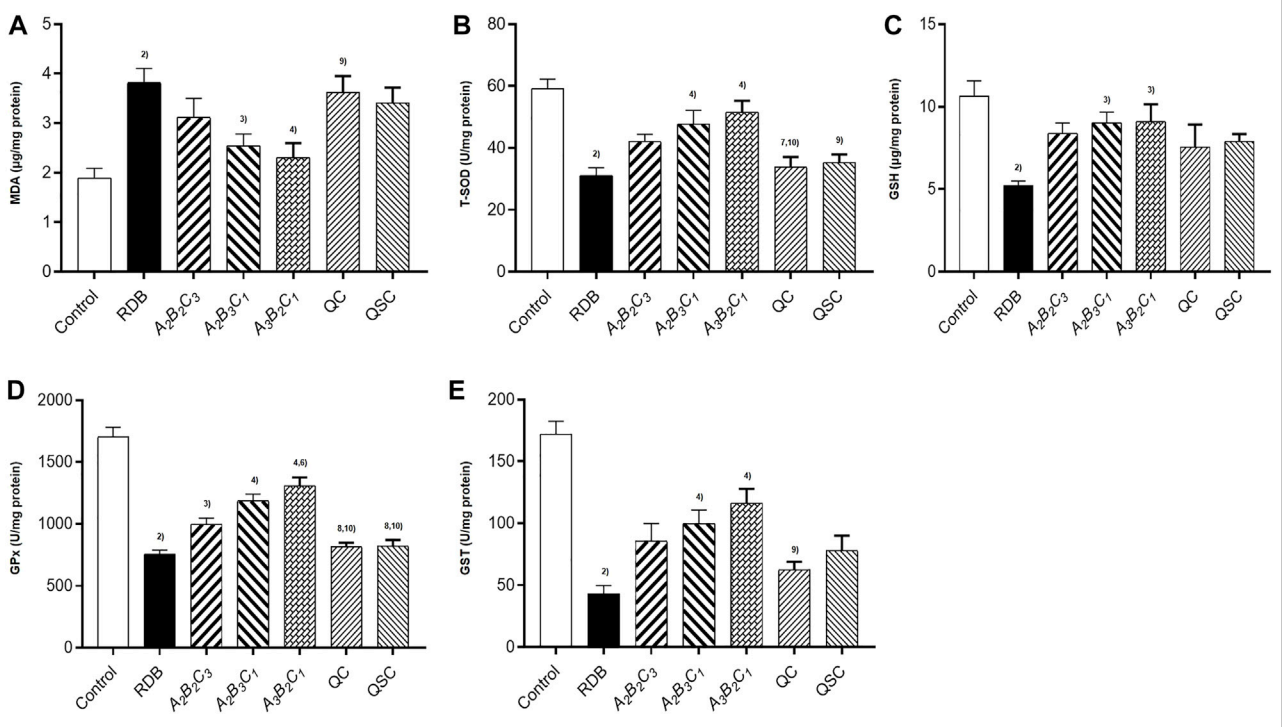

FIGURE 5
Processing with ASR ameliorated hepatic oxidative stress induced by RDB in mice. **(A)** Hepatic MDA levels. **(B)** Hepatic T-SOD activity. **(C)** Hepatic GSH levels. **(D)** Hepatic GPx activity. **(E)** Hepatic GST activity. Data were expressed as mean ± S.E.M., with 10 mice in each group. 1) $p < 0.05$, 2) $p < 0.01$, compared with the Control group, 3) $p < 0.05$, 4) $p < 0.01$, compared with the RDB group, 5) $p < 0.05$, 6) $p < 0.01$, compared with the $A_2B_2C_3$ group, 7) $p < 0.05$, 8) $p < 0.01$, compared with the $A_2B_3C_1$ group, 9) $p < 0.05$, 10) $p < 0.01$, compared with the $A_3B_2C_1$ group, 11) $p < 0.05$, 12) $p < 0.01$, compared with the QC group.

trend, the three indicators of T-SOD, GSH, and GST showed an increasing trend, there was no obvious difference ($p < 0.05$). Besides, for the relative change rates of MDA, T-SOD, GSH, GPx, and GST indicators mentioned above, $A_3B_2C_1$ group was the highest.

Processing with angelicae sinensis radix conserved the antitussive and expectorant efficacy of rhizoma dioscoreae bulbiferae

Finally, this study evaluated the efficacy of processing with ASR on the antitussive and expectorant effects of RDB through ammonia-induced cough model and the excretion of phenol red in the trachea (Figure 6; Table 9). Experimental data displayed that compared with the model group, after continuous administration of RDB and various processed products ($A_2B_2C_3$, $A_2B_3C_1$, $A_3B_2C_1$, QC, and QSC) of ASR-processed RDB, and the positive drug Keke Tablets, the cough latency and the amount of phenol red excretion in the trachea of mice were remarkably prolonged, and the number of coughs was effectively reduced ($p < 0.05$ or $p < 0.01$), and the cough relieving rates of processed products and Keke tablets were 28.5%, 30.0%, 31.5%, 39.7%, 23.6%, 25.1%, and 48.1%, respectively. The relative percentages of phenol red concentrations were 92.0%, 110.4%, 114.4%, 139.5%, 94.3%, 96.0%, and 160.2%, respectively. Compared with the RDB group, the cough latency of mice in the positive drug Keke tablet group was significantly prolonged ($p < 0.01$). In addition, there was no obvious distinction in cough latency, the number of coughs, or phenol red excretion between $A_3B_2C_1$ and Keke tablet group ($p > 0.05$).

Discussion

The detoxification technology of processing with ASR on RDB-induced hepatotoxicity was evaluated in the current research, and confirmed that the optimized processing process of ASR-processed RDB is "processing at a mass ratio of 100:20 (RDB:ASR) and a temperature of 140°C for 10 min," and the processing detoxification mechanism involved enhancing the level of Nrf2-mediated antioxidant defense.

As the main toxic component of RDB, if the DB content increased significantly, it often indicates toxicity is induced (Wang et al., 2012). Therefore, the DB content in processed

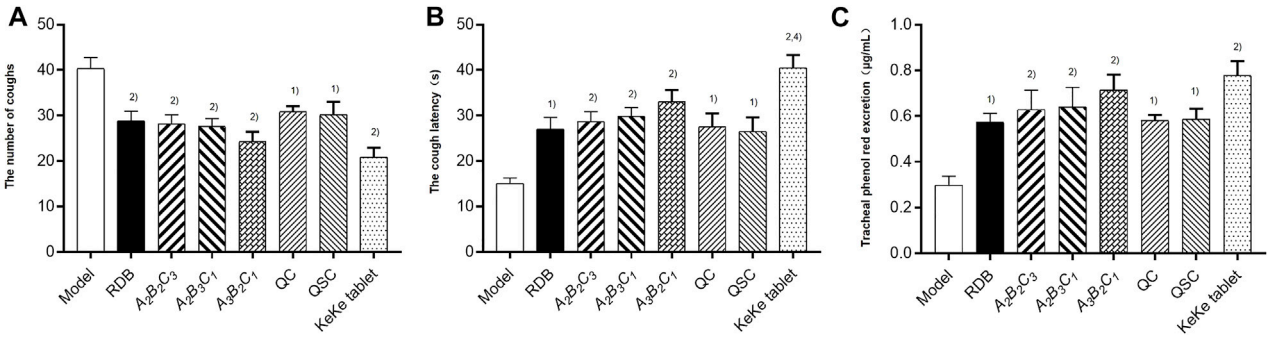

FIGURE 6
Processing with ASR conserved the antitussive and expectorant efficacy of RDB in mice. **(A)** The number of coughs. **(B)** The cough latency. **(C)** Tracheal phenol red excretion. Data were expressed as mean ± S.E.M., with 10 mice in each group. 1) $p < 0.05$, 2) $p < 0.01$, compared with the Model group, 3) $p < 0.05$, 4) $p < 0.01$, compared with the RDB group, 5) $p < 0.05$, 6) $p < 0.01$, compared with the $A_3B_2C_1$ group.

products of ASR-processed RDB was determined to preliminarily optimize the processing and detoxification technology. Results displayed that DB content in RDB and processed products of ASR-processed RDB all decreased to a certain extent, and the DB content in the processed products of $A_3B_2C_1$ decreased the most, which was 0.958 mg/g, with the reversal rate of 21.9%, suggested that processing with ASR reduced the toxicity induced by RDB, and the $A_3B_2C_1$ group had the best attenuating effect.

Under physiological conditions, there were only trace amounts of ALT and AST in the blood (Yuan et al., 2018; Guo et al., 2021). When hepatocytes were damaged, large amounts of ALT and AST will enter the blood, resulting in an obvious augment in serum ALT and AST levels (Salahshoor et al., 2018; Zhang et al., 2018; Wang L. et al., 2019; Kaya et al., 2021; Li H. et al., 2021). Therefore, serum ALT and AST indicators can be used to reflect the severity of liver damage (Gou et al., 2021; Jafaripour et al., 2021). In view of this, the research investigated the attenuating effect of processing with ASR on RDB-caused liver damage *via* measuring the serum ALT, AST, and ALP levels. Results found that RDB caused a noticeable increase in the levels of serum ALT, AST, and ALP by 291.8%, 77.1%, and 144.9%, respectively, indicating that the administration of RDB indeed induced liver toxicity, which was consistent or substantially consistent with some studies (Wang et al., 2010; Ma et al., 2014; Sheng et al., 2014). It was worth noting that the elevated serum ALT, AST, and ALP levels were remarkably reversed after administration of the five processed products ($A_1B_2C_2$, $A_1B_3C_3$, $A_2B_3C_1$, $A_3B_1C_3$, and $A_3B_3C_2$, respectively). The above results indicated that processing with ASR could inhibit the liver injury induced by RDB. However, for a single index of ALT, the optimized processing technology of ASR-processed RDB was $A_3B_3C_2$ group. For AST, $A_3B_2C_1$ group was the optimized detoxification technology. For ALP, $A_3B_1C_3$ group was the optimized detoxification technology. Subsequently, with the help of multi-index comprehensive evaluation and analysis method, the above three indicators were comprehensively evaluated and analyzed, and the optimized processing technology of ASR-processed RDB was selected as the eighth group, namely, "processing at a mass ratio of 100:20 (RDB:ASR) and a temperature of 140°C for 10 min." After that, in order to better judge the therapeutic effect of processing with ASR on liver injury induced by RDB, the pathological changes of liver tissues were observed by HE staining. Results showed that the processed products of ASR-processed RDB could significantly reduce cytoplasmic looseness and hepatocyte edema, inflammatory infiltration, and vascular congestion.

TCM believes that the main reason for the toxicity of RDB may be that it is bitter and cold, the strong attack and dispersion of RDB, the long-term medication for cancer treatment, the vulnerability and consumption of righteousness, and the syndrome of liver and kidney yin deficiency, phlegm and blood stasis (Fan et al., 2014). So why processing with ASR could effectively reduce the hepatotoxicity induced by RDB. It is preliminarily speculated that this may be related to its inherent composition, nature, flavor, and meridian tropism. ASR is sweet in taste, warm in nature, and returns to the meridians of liver, heart and spleen, which can not only support righteousness but also nourish Yin and blood. The material basis for reducing the toxicity of ASR-processed RDB may be related to its inherent "bitter and sweet phase" (Li et al., 2013).

Numerous studies have shown that oxidative stress occupied prominent values in the pathogenesis of hepatotoxicity (Guo et al., 2019; Lv et al., 2020; Temel et al., 2020; Jung et al., 2021; Lim et al., 2021). When the body's oxidation and anti-oxidation are out of balance, excess reactive oxygen species will be produced, resulting in a state of oxidative stress, lipid peroxidation of cell membranes, and abnormal organelle function (Bao et al., 2010;

Glade and Meguid, 2017; Hussein et al., 2020). As a core transcription factor of anti-oxidation, Nrf2 activation could mediate the expression of downstream antioxidant indicators (Liao et al., 2019; Chen et al., 2020). In addition, existing studies displayed that Nrf2 knockout mice are more likely to aggravate liver damage and induce oxidative stress response in liver than wild-type mice (Shi et al., 2018; Wei et al., 2018; Jin et al., 2019; Lyu et al., 2020), and the use of Nrf2 activator could alleviate the disease caused by oxidative stress (Kim et al., 2017; Kim et al., 2020). Moreover, most studies indicated that the expression level of Nrf2 in the liver was reflected by detecting the expression of Nrf2 in the nucleus (Lv et al., 2019; Wu et al., 2019; Wang et al., 2021; Zhou et al., 2021). As the final product of lipid peroxidation, the content of MDA could reflect the damage degree of lipid peroxidation (Jiang W. et al., 2021). T-SOD, GSH, and GPx are liver oxidation active enzymes, which could remove peroxides and free radicals, alleviate liver damage and protect hepatocytes (Li et al., 2018; Xie et al., 2020b; Li Z. et al., 2021; Yang et al., 2021), and were considered as important indicators reflecting hepatic oxidative damage (Park et al., 2019; Chen T. et al., 2021). Consequently, after confirming that processing with ASR could significantly improve the liver toxicity induced by RDB, the potential molecular mechanism of ASR-processed RDB to reduce its liver toxicity was evaluated by detecting and analyzing Nrf2 and its downstream-related molecules.

Similar to the results of previous studies (Wang et al., 2010; Ma et al., 2013), this study showed that the administration of RDB significantly downregulated the expression level of Nrf2 protein in liver, and decreased the expression of HO-1, NQO1, GCLM, T-SOD, GSH, and GPx, GST antioxidant signal molecules downstream of Nrf2, suggesting that RDB-induced hepatotoxicity involves weak antioxidant defense. Notably, data showed that the processed products of ASR-processed RDB effectively improved the abnormality of Nrf2 and its downstream molecules, manifesting that the detoxification mechanism of the processed products of ASR-processed RDB involved enhancing the Nrf2 signaling pathway. Other results also showed that the administration of RDB caused liver lipid peroxidation damage in mice, which was mainly manifested in the significant increase in MDA level, and similar to the study (Niu et al., 2014). Satisfyingly, the intervention of different processed products significantly reduced the MDA level, indicating that the inhibition of liver lipid peroxidation damage was also involved in its detoxification mechanism. However, it was worth noting that this study did not use target diagnostic agents (such as inhibitors and agonists) and gene knockout technology to explore the in-depth mechanism of processing with ASR to reduce liver toxicity induced by RDB, which was the limitation of the study and an important research direction in the future.

The above results showed that processing with ASR could effectively improve RDB-caused liver damage, so is it possible to reduce the hepatotoxicity, simultaneously, its curative effect is not reduced or even enhanced? Taking into account that RDB has good antitussive and expectorant efficacy, then, the present research mainly explored the antitussive and expectorant efficacy of RDB through the ammonia-induced cough model and the tracheal phenol red excretion experiment. The results showed that RDB and the products of ASR-processed RDB (processed products: $A_2B_2C_3$, $A_2B_3C_1$, and $A_3B_2C_1$), and the products of QC, QSC apparently augmented the cough latency and phenol red excretion of trachea in cough mice induced by ammonia to varying degrees, and reduced the number of coughs caused by ammonia, which suggested that the above-mentioned processed products have good efficacy in relieving cough and eliminating phlegm. However, compared with the two processed products of QC and QSC mentioned above, they did not remarkably improve the RDB-induced hepatotoxicity, which suggested that the two processed products of QC and QSC only have the preservation effect and did not have the effect of reducing toxicity. As for the processed products ($A_2B_2C_3$, $A_2B_3C_1$, and $A_3B_2C_1$), they not only conserved the antitussive and expectorant effect of RDB, but also improved the hepatotoxicity induced by RDB to a certain extent. In addition, from the results of serum transaminase level and the degree of pathological injury of liver tissue in mice, the $A_3B_2C_1$ group significantly reduced the levels of serum ALT, AST, and ALP and pathological injury of liver in mice, and the reversal rate of each index in $A_3B_2C_1$ group was the highest compared with other groups, which indicated that this group had the best detoxification effect, that was, the optimized processing technology group. From the results of antitussive and expectorant efficacy, the $A_3B_2C_1$ group significantly increased the cough latency and tracheal phenol red excretion, and reduced the number of coughs, and the reversal rate of each index in $A_3B_2C_1$ group was the highest compared with other groups, which indicated that this group had the best treatment effect, that was, the optimized processing technology group. To sum up, the optimized processing process of ASR-processed RDB was "processing at a mass ratio of 100:20 (RDB:ASR) and a temperature of 140°C for 10 min".

In conclusion, the current study confirmed that the optimized processing process of ASR-processed RDB was "processing at a mass ratio of 100:20 (RDB:ASR) and a temperature of 140°C for 10 min," and the processing detoxification mechanism involved enhancing the level of Nrf2-mediated antioxidant defense in liver. This study provided a certain experimental support for the promotion and application, and laid a preliminary foundation for the establishment of the detoxification system of RDB.

Data availability statement

The original contributions presented in the study are included in the article/supplementary material, further inquiries can be directed to the first author or the corresponding author.

Ethics statement

The experimental protocols were approved by the Experimental Animal Ethical Committee of Henan University of Chinese Medicine.

Author contributions

LS conceived the experimental design, completed the animal experiment, biochemical indexes, pathological results, western blotting, ELISA kits, designed diagrams, create and reviewed the manuscript. JW reviewed the manuscript and acquired funding. MG involved in the HPLC analysis. YZ, YL, and XW reviewed the manuscript. LQ and YD participated in the animal experiment and completed biochemical indexes.

Funding

This work was supported by the Key R and D and Promotion Special (Scientific Problem Tackling) Project of Henan Province (Grant Number. 182102310255).

Conflict of interest

The authors declare that the research was conducted in the absence of any commercial or financial relationships that could be construed as a potential conflict of interest.

Publisher's note

All claims expressed in this article are solely those of the authors and do not necessarily represent those of their affiliated organizations, or those of the publisher, the editors and the reviewers. Any product that may be evaluated in this article, or claim that may be made by its manufacturer, is not guaranteed or endorsed by the publisher.

References

Ahmad, H., Chan, C., Mohamad, J., and Abdul, K. (2018). Dioscorea bulbifera induced apoptosis through inhibition of ERK 1/2 and activation of JNK signaling pathways in HCT116 human colorectal carcinoma cells. *Biomed. Pharmacother.* 104, 806–816. doi:10.1016/j.biopha.2018.05.073

Bao, W., Li, K., Rong, S., Yao, P., Hao, L., Ying, C., et al. (2010). Curcumin alleviates ethanol-induced hepatocytes oxidative damage involving heme oxygenase-1 induction. *J. Ethnopharmacol.* 128 (2), 549–553. doi:10.1016/j.jep.2010.01.029

Chaniad, P., Tewtrakul, S., Sudsai, T., Langyanai, S., and Kaewdana, K. (2020). Anti-inflammatory, wound healing and antioxidant potential of compounds from *Dioscorea bulbifera* L. bulbils. *Plos One* 15 (12), e0243632. doi:10.1371/journal.pone.0243632

Chen, Q., Zhao, Y., Li, M., Zheng, P., Zhang, S., Li, H., et al. (2021). HPLC-MS and network pharmacology analysis to reveal quality markers of Huo-Xue-Jiang-Tang Yin, a Chinese herbal medicine for type 2 diabetes mellitus. *Evid. Based. Complement. Altern. Med.* 2021, 1072975. doi:10.1155/2021/1072975

Chen, T., Zou, L., Wang, D., Li, W., Yang, Y., Liu, X., et al. (2021). Metabolomics study of *Angelica sinensis* (Oliv.) Diels on the abnormal uterine bleeding rats by ultra-performance liquid chromatography-quadrupole-time-of-flight mass spectrometry analysis. *Food Sci. Nutr.* 9 (12), 6596–6609. doi:10.1002/fsn3.2605

Chen, Z., Zhao, Y., Song, C., Li, N., Liao, J., Luo, X., et al. (2020). SanWeiGanJiang San relieves liver injury via Nrf2/Bach1. *J. Ethnopharmacol.* 51, 112445. doi:10.1016/j.jep.2019.112445

Chu, H., Shi, Y., Jiang, S., Zhong, Q., Zhao, Y., Liu, Q., et al. (2017). Treatment effects of the traditional Chinese medicine Shenks in bleomycin-induced lung fibrosis through regulation of TGF-beta/Smad3 signaling and oxidative stress. *Sci. Rep.* 7 (1), 2252. doi:10.1038/s41598-017-02293-z

Cui, H., Li, T., Wang, L., Su, Y., and Xian, C. (2016). *Dioscorea bulbifera* polysaccharide and cyclophosphamide combination enhances anti-cervical cancer effect and attenuates immunosuppression and oxidative stress in mice. *Sci. Rep.* 5, 19185. doi:10.1038/srep19185

Deng, J., Jiang, W., Chenm, C., Leem, L., Li, P., Huang, W., et al. (2020). *Cordyceps cicadae* mycelia ameliorate cisplatin-induced acute kidney injury by suppressing the TLR4/NF-κB/MAPK and activating the HO-1/Nrf2 and Sirt-1/AMPK pathways in mice. *Oxid. Med. Cell. Longev.* 2020, 7912763. doi:10.1155/2020/7912763

Fan, J., Hua, B., Liu, J., and Huang, Z. (2014). Experimental study of Rhizoma Dioscoreae Bulbiferae concerted Radix Glycyrrhiza reducing renal toxicity in rats. *J. Med. Res.* 43 (9), 31–33.

Feng, J. (1989). A report of 2 cases of toxic hepatitis caused by Rhizoma Dioscoreae Bulbiferae. *Shandong Zhongyi Zazhi* 2, 30. CNKI:SUN:SDZY.0.1989-02-022.

Ghosh, S., Ahire, M., Patil, S., Jabgunde, A., Bhat, D., Joshi, B., et al. (2012). Antidiabetic activity of gnidia glauca and *Dioscorea bulbifera*: Potent amylase and glucosidase inhibitors. *Evid. Based. Complement. Altern. Med.* 2012, 929051. doi:10.1155/2012/929051

Glade, M., and Meguid, M. (2017). A Glance at . . . ethanol consumption, GSH suppression, and oxidative liver damage. ethanol consumption, GSH suppression, and oxidative liver damage. *Nutrition* 33, 199–203. doi:10.1016/j.nut.2016.07.003

Gou, S., He, M., Li, B., Zhu, N., and Ni, J. (2021). Hepatoprotective effect of total flavonoids from Glycyrrhiza uralensis Fisch in liver injury mice. *Nat. Prod. Res.* 35 (24), 6083–6087. doi:10.1080/14786419.2020.1824223

Guo, H., Sun, J., Li, D., Hu, Y., Yu, X., Hua, H., et al. (2019). Shikonin attenuates acetaminophen-induced acute liver injury via inhibition of oxidative stress and inflammation. *Biomed. Pharmacother.* 112, 108704. doi:10.1016/j.biopha.2019.108704

Guo, Z., Li, P., Wang, C., Kang, Q., Tu, C., Jiang, B., et al. (2021). Five constituents contributed to the Psoraleae Fructus-induced hepatotoxicity via mitochondrial dysfunction and apoptosis. *Front. Pharmacol.* 12, 682823. doi:10.3389/fphar.2021.682823

He, S., Zhang, X., Lu, S., Zhu, T., Sun, G., and Sun, X. (2019). A computational toxicology approach to screen the hepatotoxic ingredients in traditional Chinese medicines: Polygonum multiflorum thunb as a case study. *Biomolecules* 9 (10), 577. doi:10.3390/biom9100577

Hu, J., Jung, C., Ku, S., Jung, D., Bashir, K., Ku, S., et al. (2021). Anti-inflammatory, expectorant, and antitussive properties of Kyeongok-go in ICR mice. *Pharm. Biol.* 59 (1), 321–334. doi:10.1080/13880209.2021.1892155

Hua, B., Hu, J., Wang, R., Li, Y., Lin, J., Zheng, L., et al. (2011). Experimental research of Radix Glycyrrhiza on reducing hepatic toxicity induced by Rhizoma Dioscoreae Bulbiferae. *Shijie Zhongxiyi Jiehe Zazhi* 6 (1), 24–27. doi:10.13935/j.cnki.sjzx.2011.01.024

Hua, Y., Xue, W., Zhang, M., Wei, Y., and Ji, P. (2014). Metabonomics study on the hepatoprotective effect of polysaccharides from different preparations of Angelica sinensis. *J. Ethnopharmacol.* 151 (3), 1090–1099. doi:10.1016/j.jep.2013.12.011

Huang, C., Yang, R., Liu, S., Hsieh, P., and Lin-Shiau, S. (2011). Evidence for improved neuropharmacological efficacy and decreased neurotoxicity in mice with traditional processing of Rhizoma Arisaematis. *Am. J. Chin. Med.* 39 (5), 981–998. doi:10.1142/S0192415X11009354

Huang, Z., Hua, B., Chen, X., Shi, D., Chen, X., Wang, Y., et al. (2013). Analysis of liver injury in 78 cases caused by Rhizoma Dioscoreae Bulbiferae and related preparation. *Zhongguo Shiyan Fangjixue Zazhi* 19 (23), 295–297. doi:10.11653/syfj2013230295

Hussein, O., Hozayen, W., Bin-Jumah, M., Germoush, M., Abd, El., and Mahmoud, A. (2020). Chicoric acid prevents methotrexate hepatotoxicity via attenuation of oxidative stress and inflammation and up-regulation of PPARγ and Nrf2/HO-1 signaling. *Environ. Sci. Pollut. Res. Int.* 27 (17), 20725–20735. doi:10.1007/s11356-020-08557-y

Jafaripour, L., Naserzadeh, R., Alizamani, E., Javad, M., Moghadam, E., Nouryazdan, N., et al. (2021). Effects of rosmarinic acid on methotrexate-induced nephrotoxicity and hepatotoxicity in wistar rats. *Indian J. Nephrol.* 31 (3), 218–224. doi:10.4103/ijn.IJN_14_20

Jiang, D. (1976). A report of 2 cases of toxic hepatitis caused by Rhizoma Dioscoreae Bulbiferae. *Abstr. Xinyixue* 1, 30. CNKI:SUN:XYXX.0.1976-01-017.

Jiang, K., Song, Q., Wang, L., Xie, T., Wu, X., Wang, P., et al. (2014). Antitussive, expectorant and anti-inflammatory activities of different extracts from Exocarpium Citri grandis. *J. Ethnopharmacol.* 156, 97–101. doi:10.1016/j.jep.2014.08.030

Jiang, M., Zhao, S., Yang, S., Lin, X., He, X., Wei, X., et al. (2020). An "essential herbal medicine"-licorice: A review of phytochemicals and its effects in combination preparations. *J. Ethnopharmacol.* 249, 112439. doi:10.1016/j.jep.2019.112439

Jiang, S. (1978). *Dictionary of Chinese crude drugs*. Shanghai (China): Shanghai Scientific Technological Publisher.

Jiang, T., Liu, L., Zhang, M., Qiao, Z., Zhao, T., Su, J., et al. (2021). Metabolomics reveals the mechanisms for the pulmonary toxicity of *siegesbeckia orientalis* L. and the toxicity-reducing effect of processing. *Front. Pharmacol.* 12, 630319. doi:10.3389/fphar.2021.630319

Jiang, W., Deng, J., Huang, S., Wu, S., Chen, C., Liao, J., et al. (2021). Sanghuangporus sanghuang mycelium prevents paracetamol-induced hepatotoxicity through regulating the MAPK/NF-κB, Keap1/Nrf2/HO-1, TLR4/PI3K/Akt, and CaMKKβ/LKB1/AMPK pathways and suppressing oxidative stress and inflammation. *Antioxidants (Basel)* 10 (6), 897. doi:10.3390/antiox10060897

Jiang, Z. (1981). A report of 17 cases of drug-induced hepatitis caused by Rhizoma Dioscoreae Bulbiferae. *Zhongyi Zazhi* 2, 37–38. doi:10.13288/j.11-2166/r.1981.02.017

Jin, A. (1996). A case of abnormal liver function caused by Rhizoma Dioscoreae Bulbiferae. *Zhongguo Zhongyao Zazhi* 6, 57. CNKI:SUN:ZGZY.0.1996-06-025.

Jin, Y., Huang, Z., Li, L., Yang, Y., Wang, C., Wang, Z., et al. (2019). Quercetin attenuates toosendanin-induced hepatotoxicity through inducing the Nrf2/GCL/GSH antioxidant signaling pathway. *Acta Pharmacol. Sin.* 40 (1), 75–85. doi:10.1038/s41401-018-0024-8

Jung, Y., Lee, S., Chun, S., Kim, D., Jang, B., Han, M., et al. (2021). *In vitro* and *in vivo* protective effects of lentil *(Lens culinaris)* extract against oxidative stress-induced hepatotoxicity. *Molecules* 27 (1), 59. doi:10.3390/molecules27010059

Kaya, T., Erdem, G., Gül, M., Tektemur, A., Özcan, Y., Kavak, B., et al. (2021). The combination of N-acetylcysteine and cyclosporin A reduces acetaminophen-induced hepatotoxicity in mice. *Ultrastruct. Pathol.* 45 (1), 19–27. doi:10.1080/01913123.2020.1850964

Kim, J., Shin, S., Ko, Y., Miki, T., Bae, H., Kang, J., et al. (2017). HX-1171, a novel Nrf2 activator, induces NQO1 and HMOX1 expression. *J. Cell. Biochem.* 118 (10), 3372–3380. doi:10.1002/jcb.25993

Kim, S., Indu, V., Park, J., Lee, H., Park, A., Choi, J., et al. (2020). Nrf2 activator via interference of Nrf2-Keap1 interaction has antioxidant and anti-inflammatory properties in Parkinson's disease animal model. *Neuropharmacology* 167, 107989. doi:10.1016/j.neuropharm.2020.107989

Kong, S., Li, P., Verpoorte, R., Wang, J., Zhu, C., Dai, Y., et al. (2022). Synergistic mechanism for the bioactivity fortification of licorice by honey. *J. Ethnopharmacol.* 289, 115048. doi:10.1016/j.jep.2022.115048

Li, H., Zhai, B., Sun, J., Fan, Y., Zou, J., Cheng, J., et al. (2021). Antioxidant, anti-aging and organ protective effects of total saponins from aralia taibaiensis. *Drug Des. devel. Ther.* 15, 4025–4042. doi:10.2147/DDDT.S330222

Li, W., Jiang, N., Li, B., Wan, M., Chang, X., Liu, H., et al. (2018). Antioxidant activity of purified ulvan in hyperlipidemic mice. *Int. J. Biol. Macromol.* 113, 971–975. doi:10.1016/j.ijbiomac.2018.02.104

Li, Y., Tian, Y., Ou, W., Gan, L., Chen, B., and Li, Y. (2013). Study on the combination of rhizoma Dioscoreae Bulbiferae and Radix *Angelicae sinensis* with diosbulbin B and catechin as marker components. *J. Beijing Inst. Technol.* 33 (8), 866–870. doi:10.15918/j.tbit1001-0645.2013.08.015

Li, Z., Lyu, Y., Zhao, J., Li, D., Lin, Z., To, K., et al. (2021). Disease status-dependent drug-herb interactions: NASH lowered the risk of hepatotoxicity in rats coadministered with simvastatin and *Gardenia jasminoides*. *J. Ellis. Front. Pharmacol.* 12, 622040. doi:10.3389/fphar.2021.622040

Liao, W., Chen, Y., Zhu, Z., Chen, J., Gao, T., Limsila, B., et al. (2021). Vinegar-processed Curcuma phaeocaulis promotes anti-angiogenic activity and reduces toxicity in zebrafish and rat models. *Pharm. Biol.* 59 (1), 410–417. doi:10.1080/13880209.2021.1874427

Liao, Z., Zhang, J., Liu, B., Yan, T., Xu, F., Xiao, F., et al. (2019). Polysaccharide from Okra (*Abelmoschus esculentus* (L.) Moench) improves antioxidant capacity via PI3K/AKT pathways and Nrf2 translocation in a type 2 diabetes model. *Molecules* 24 (10), 1906. doi:10.3390/molecules24101906

Lim, J., Yun, D., Lee, J., Kwon, Y., Lee, Y., Lee, D., et al. (2021). Extract of triticum aestivum sprouts suppresses acetaminophen-induced hepatotoxicity in mice by inhibiting oxidative stress. *Molecules* 26 (21), 6336. doi:10.3390/molecules26216336

Lin, W., Wu, Y., Wang, J., Lin, H., Xu, X., He, G., et al. (2020). Network pharmacology study of the hepatoprotective effects of quercetin-containing Traditional Chinese Medicine, anoectochilus roxburghii, and validation of quercetin as an anti-liver injury agent in a mouse model of liver injury. *Med. Sci. Monit.* 26, e923533. doi:10.12659/MSM.923533

Liu, S., Xian, Z., Zhao, Y., Wang, L., Tian, J., Pan, C., et al. (2021). Quantitative determination and toxicity evaluation of aristolochic acid analogues in *Asarum* heterotropoides F. Schmidt (Xixin) and traditional Chinese patent medicines. *Front. Pharmacol.* 12, 761593. doi:10.3389/fphar.2021.761593

Lu, J., Liu, L., Zhu, X., Wu, L., Chen, Z., Xu, Z., et al. (2018). Evaluation of the absorption behavior of main component compounds of salt-fried herb ingredients in Qing'e pills by using Caco-2 Cell model. *Molecules* 23 (12), 3321. doi:10.3390/molecules23123321

Lu, X., and Wu, Q. (2014). Literature analysis of 33 cases of liver injury induced by the compound preparation of *Dioscorea bulbifera* L. *Sichuan Zhongyi* 32, 162–164.

Luo, S., Wen, R., Wang, Q., Zhao, Z., Nong, F., Fu, Y., et al. (2019). Rhubarb Peony Decoction ameliorates ulcerative colitis in mice by regulating gut microbiota to restoring Th17/Treg balance. *J. Ethnopharmacol.* 231, 39–49. doi:10.1016/j.jep.2018.08.033

Lv, H., Yang, H., Wang, Z., Feng, H., Deng, X., Cheng, G., et al. (2019). Nrf2 signaling and autophagy are complementary in protecting lipopolysaccharide/d-galactosamine-induced acute liver injury by licochalcone A. *Cell Death Dis.* 10 (4), 313. doi:10.1038/s41419-019-1543-z

Lv, H., Zhu, C., Wei, W., Lv, X., Yu, Q., Deng, X., et al. (2020). Enhanced Keap1-Nrf2/Trx-1 axis by daphnetin protects against oxidative stress-driven hepatotoxicity via inhibiting ASK1/JNK and Txnip/NLRP3 inflammasome activation. *Phytomedicine* 71, 153241. doi:10.1016/j.phymed.2020.153241

Lyu, H., Wang, H., Li, L., Zhu, J., Chen, F., Chen, Y., et al. (2020). Hepatocyte-specific deficiency of Nrf2 exacerbates carbon tetrachloride-induced liver fibrosis via aggravated hepatocyte injury and subsequent inflammatory and fibrogenic responses. *Free Radic. Biol. Med.* 150, 136–147. doi:10.1016/j.freeradbiomed.2020.02.015

Ma, Y., Ji, L., Wang, S., Shi, S., and Wang, Z. (2013). Protection of Grateloupia filicina polysaccharide against hepatotoxicity induced by *Dioscorea bulbifera* L. *Yao Xue Xue Bao* 48 (8), 1253–1258. doi:10.16438/j.0513-4870.2013.08.011

Ma, Y., Niu, C., Wang, J., Ji, L., and Wang, Z. (2014). Diosbulbin B-induced liver injury in mice and its mechanism. *Hum. Exp. Toxicol.* 33 (7), 729–736. doi:10.1177/0960327113506232

Mbiantcha, M., Kamanyi, A., Teponno, R., Tapondjou, A., Watcho, P., and Nguelefack, T. (2011). Analgesic and anti-inflammatory properties of extracts from the Bulbils of *Dioscorea bulbifera* L. var sativa (Dioscoreaceae) in mice and rats. *Evid. Based. Complement. Altern. Med.* 2011, 912935. doi:10.1155/2011/912935

Nai, J., Zhang, C., Shao, H., Li, B., Li, H., Gao, L., et al. (2021). Extraction, structure, pharmacological activities and drug carrier applications of Angelica sinensis polysaccharide. *Int. J. Biol. Macromol.* 183, 2337–2353. doi:10.1016/j.ijbiomac.2021.05.213

Niu, C., Wang, J., Ji, L., and Wang, Z. (2014). Protection of *Angelica sinensis* (Oliv) Diels against hepatotoxicity induced by *Dioscorea bulbifera* L. and its mechanism. *Biosci. Trends* 8 (5), 253–259. doi:10.5582/bst.2014.01076

Ota, M., and Makino, T. (2022). History and the immunostimulatory effects of heat-processed licorice root products with or without honey. *J. Ethnopharmacol.* 292, 115108. doi:10.1016/j.jep.2022.115108

Park, S., Fernando, I., Han, E., Kim, M., Jung, K., Kang, D., et al. (2019). *In vivo* hepatoprotective effects of a peptide fraction from krill protein hydrolysates against alcohol-induced oxidative damage. *Mar. Drugs* 17 (12), 690. doi:10.3390/md17120690

Pharmacopoeia of the People's Republic of China (2020). *Chinese Pharmacopoeia Commission, vol. IV*. Beijing: People's Medical Publishing House, 31.

Qiu, M., Xiao, F., Wang, T., Piao, S., Zhao, W., Shao, S., et al. (2020). Protective effect of Hedansanqi Tiaozhi Tang against non-alcoholic fatty liver disease *in vitro* and *in vivo* through activating Nrf2/HO-1 antioxidant signaling pathway. *Phytomedicine* 67, 153140. doi:10.1016/j.phymed.2019.153140

Qu, X., Zhai, J., Hu, T., Gao, H., Tao, L., Zhang, Y., et al. (2019). *Dioscorea bulbifera* L. delays the excretion of doxorubicin and aggravates doxorubicin-induced cardiotoxicity and nephrotoxicity by inhibiting the expression of P-glycoprotein in mice liver and kidney. *Xenobiotica.* 49 (9), 1116–1125. doi:10.1080/00498254.2018.1498560

Ruan, L., Li, M., Xing, Y., Hong, W., Chen, C., Chen, J., et al. (2019). Hepatotoxicity and hepatoprotection of Polygonum multiflorum Thund. as two sides of the same biological coin. *J. Ethnopharmacol.* 230, 81–94. doi:10.1016/j.jep.2018.10.032

Salahshoor, M., Roshankhah, S., Hosseni, P., and Jalili, C. (2018). Genistein improves liver damage in male mice exposed to morphine. *Chin. Med. J.* 131 (13), 1598–1604. doi:10.4103/0366-6999.235117

Shan, X., Yu, H., Wu, H., Wang, W., Zhang, Y., Cheng, Z., et al. (2018). Intestinal toxicity of different processed products of Crotonis Fructus and effect of processing on fatty oil and total protein. *Zhongguo zhongyao zazhi* 43 (23), 4652–4658. doi:10.19540/j.cnki.cjcmm.20181105.005

Sheng, Y., Ma, Y., Deng, Z., Wang, Z., and Ji, L. (2014). Cytokines as potential biomarkers of liver toxicity induced by *Dioscorea bulbifera* L. *Biosci. Trends* 8 (1), 32–37. doi:10.5582/bst.8.32

Shi, L., Hao, Z., Zhang, S., Wei, M., Lu, B., Wang, Z., et al. (2018). Baicalein and baicalin alleviate acetaminophen-induced liver injury by activating Nrf2 antioxidative pathway: The involvement of ERK1/2 and PKC. *Biochem. Pharmacol.* 150, 9–23. doi:10.1016/j.bcp.2018.01.026

Su, L., Zhu, J., Cheng, L., and Li, Y. (2003). Experimental pathological study of subacute intoxication by *Dioscorea bulbifera* L. *Fa yi xue za zhi* 19 (2), 81–83. doi:10.3969/j.issn.1004-5619.2003.02.006

Su, T., Tan, Y., Tsui, M., Yi, H., Fu, X., Li, T., et al. (2016). Metabolomics reveals the mechanisms for the cardiotoxicity of Pinelliae Rhizoma and the toxicity-reducing effect of processing. *Sci. Rep.* 6, 34692. doi:10.1038/srep34692

Temel, Y., Kucukler, S., Yıldırım, S., Caglayan, C., and Kandemir, F. (2020). Protective effect of chrysin on cyclophosphamide-induced hepatotoxicity and nephrotoxicity via the inhibition of oxidative stress, inflammation, and apoptosis. *Naunyn. Schmiedeb. Arch. Pharmacol.* 393 (3), 325–337. doi:10.1007/s00210-019-01741-z

Wang, C., Liang, F., Liu, X., Zhou, F., Lv, X., Hu, X., et al. (2022). The influence of different processing methods on the anti-gastric cancer effect and hepatotoxicity of *Dioscorea bulbifera* L. *J. Jining Med. Univ.* 45 (1), 1–5.

Wang, C., Liu, T., Tong, Y., Cui, R., Qu, K., Liu, C., et al. (2021). Ulinastatin protects against acetaminophen-induced liver injury by alleviating ferroptosis via the Sirt1/Nrf2/HO-1 pathway. *Am. J. Transl. Res.* 13 (6), 6031–6042.

Wang, H., Peng, R., Wang, R., and Kong, R. (1997). Antagonizing effect of sodium ferulate on the changes of hepatic antioxidative function induced by ethanol in mice. *Yao Xue Xue Bao* 32 (7), 511–514.

Wang, J., Ji, L., Branford-White, C., Wang, Z., Shen, K., Liu, H., et al. (2012). Antitumor activity of *Dioscorea bulbifera* L. rhizome *in vivo*. *Fitoterapia* 83 (2), 388–394. doi:10.1016/j.fitote.2011.12.001

Wang, J., Ji, L., Liu, H., and Wang, Z. (2010). Study of the hepatotoxicity induced by *Dioscorea bulbifera* L. rhizome in mice. *Biosci. Trends* 4 (2), 79–85.

Wang, J., Li, J., Cai, H., Chen, R., Zhang, Y., Zhang, L., et al. (2019). Nrf2 participates in mechanisms for reducing the toxicity and enhancing the antitumour effect of Radix *Tripterygium wilfordii* to S180-bearing mice by herbal-processing technology. *Pharm. Biol.* 57 (1), 437–448. doi:10.1080/13880209.2019.1634106

Wang, K., Song, Z., Wang, H., Li, Q., Cui, Z., and Zhang, Y. (2016). *Angelica sinensis* polysaccharide attenuates concanavalin A-induced liver injury in mice. *Int. Immunopharmacol.* 31, 140–148. doi:10.1016/j.intimp.2015.12.021

Wang, K., Wang, J., Song, M., Wang, H., Xia, N., and Zhang, Y. (2020). *Angelica sinensis* polysaccharide attenuates CCl4-induced liver fibrosis via the IL-22/STAT3 pathway. *Int. J. Biol. Macromol.* 162, 273–283. doi:10.1016/j.ijbiomac.2020.06.166

Wang, L., Wei, W., Xiao, Q., Yang, H., and Ci, X. (2019). Farrerol ameliorates APAP-induced hepatotoxicity via activation of Nrf2 and autophagy. *Int. J. Biol. Sci.* 15 (4), 788–799. doi:10.7150/ijbs.30677

Wang, T., Song, Y., Xu, H., Liu, Y., He, H., Zhou, M., et al. (2022). Study on the mechanism of reducing biofilm toxicity and increasing antioxidant activity in vinegar processing phytomedicines containing pentacyclic triterpenoid saponins. *J. Ethnopharmacol.* 290, 115112. doi:10.1016/j.jep.2022.115112

Wei, M., Zheng, Z., Shi, L., Jin, Y., and Ji, L. (2018). Natural polyphenol chlorogenic acid protects against acetaminophen-induced hepatotoxicity by activating ERK/Nrf2 antioxidative pathway. *Toxicol. Sci.* 162 (1), 99–112. doi:10.1093/toxsci/kfx230

Wu, C., Deng, J., Huang, W., Shieh, P., Chung, M., and Huang, G. (2019). Salvianolic acid C against acetaminophen-induced acute liver injury by attenuating inflammation, oxidative stress, and apoptosis through inhibition of the Keap1/Nrf2/HO-1 signaling. *Oxid. Med. Cell. Longev.* 2019, 9056845. doi:10.1155/2019/9056845

Wu, X., Hu, X., Zhang, Q., Liu, F., and Xiong, K. (2021). Regulatory role of Chinese herbal medicine in regulated neuronal death. *CNS Neurol. Disord. Drug Targets* 20 (3), 228–248. doi:10.2174/1871527319666200730165011

Wu, X., Wang, J., Liu, C., Zhang, S., Cui, Y., and Cao, C. (2020a). Experimental study on enhancing the antitussive efficacy and reducing the toxicity of *Dioscorea bulbifera* L. by the processing technology. *Chin. Pharm. J.* 55 (10), 817–823. doi:10.11669/cpj.2020.10.013

Wu, X., Wang, J., Song, L., Guan, Y., Zhang, Y., and Cui, Y. (2020b). Experimental study on processing and enhancing the anti-inflammatory, analgesic and expectorant efficacy of *Dioscorea bulbifera* L. *Shizhen Guoyi Guoyao* 31 (11), 2649–2652. doi:10.3969/j.issn.1008-0805.2020.11.025

Xie, L., Shen, M., Wen, P., Hong, Y., Liu, X., and Xie, J. (2020b). Preparation, characterization, antioxidant activity and protective effect against cellular oxidative stress of phosphorylated polysaccharide from Cyclocarya paliurus. *Food Chem. Toxicol.* 145, 111754. doi:10.1016/j.fct.2020.111754

Xie, L., Zhao, Y., Duan, J., Fan, S., Shu, L., Liu, H., et al. (2020a). Integrated proteomics and metabolomics reveal the mechanism of nephrotoxicity induced by Triptolide. *Chem. Res. Toxicol.* 33 (7), 1897–1906. doi:10.1021/acs.chemrestox.0c00091

Yang, F., Liang, Y., Xu, L., Ji, L., Yao, N., Liu, R., et al. (2016). Exploration in the cascade working mechanisms of liver injury induced by total saponins extracted from Rhizoma *Dioscorea bulbifera*. *Biomed. Pharmacother.* 83, 1048–1056. doi:10.1016/j.biopha.2016.08.017

Yang, S., Sun, J., Gu, D., Li, P., Yao, L., Shi, D., et al. (2021). Antioxidant activities of sulfated Codonopsis polysaccharides in acute oxidative stress. *J. Food Biochem.* 45 (12), e13974. doi:10.1111/jfbc.13974

Yuan, R., Tao, X., Liang, S., Pan, Y., He, L., Sun, J., et al. (2018). Protective effect of acidic polysaccharide from Schisandra chinensis on acute ethanol-induced liver injury through reducing CYP2E1-dependent oxidative stress. *Biomed. Pharmacother.* 99, 537–542. doi:10.1016/j.biopha.2018.01.079

Zhang, K., Liu, Y., Lin, X., Yang, J., and Wu, C. (2021). Assessment of reproductive toxicity and genotoxicity of Aconiti Lateralis Radix Praeparata and its processed products in male mice. *J. Ethnopharmacol.* 275, 114102. doi:10.1016/j.jep.2021.114102

Zhang, M., Gao, M., Wu, S., Zhou, L., Cao, L., Qiao, R., et al. (2021). Hepatotoxicity comparison of crude and licorice-processed Euodiae Fructus in rats with stomach excess-cold syndrome. *Front. Pharmacol.* 12, 756276. doi:10.3389/fphar.2021.756276

Zhang, M., Lin, L., Lin, H., Qu, C., Yan, L., and Ni, J. (2018). Interpretation the hepatotoxicity based on pharmacokinetics investigated through oral administrated different extraction parts of polygonum multiflorum on rats. *Front. Pharmacol.* 9, 505. doi:10.3389/fphar.2018.00505

Zhang, S., Li, C., Feng, T., Cao, S., Zhou, H., Li, L., et al. (2021). A metabolic profiling study of realgar-induced acute kidney injury in mice. *Front. Pharmacol.* 12, 706249. doi:10.3389/fphar.2021.706249

Zhang, W., Wang, M., Song, H., Gao, C., Wang, D., Hua, H., et al. (2021). CYP3A4 inducer aggravates big flower Evodiae Fructus-induced hepatotoxicity whereas limonin attenuates its hepatotoxicity. *J. Ethnopharmacol.* 264, 113277. doi:10.1016/j.jep.2020.113277

Zhang, Z., Lin, D., Li, W., Gao, H., Peng, Y., and Zheng, J. (2017). Sensitive bromine-based screening of potential toxic furanoids in *Dioscorea bulbifera* L. *J. Chromatogr. B Anal. Technol. Biomed. Life Sci.* 1057, 1–14. doi:10.1016/j.jchromb.2017.04.033

Zhou, L., Zhou, C., Feng, Z., Liu, Z., Zhu, H., and Zhou, X. (2018). Triptolide-induced hepatotoxicity can be alleviated when combined with Panax notoginseng saponins and Catapol. *J. Ethnopharmacol.* 214, 232–239. doi:10.1016/j.jep.2017.12.033

Zhou, Y., Tan, Z., Huang, H., Zeng, Y., Chen, S., Wei, J., et al. (2021). Baicalein pre-treatment alleviates hepatic ischemia/reperfusion injury in mice by regulating the Nrf2/ARE pathway. *Exp. Ther. Med.* 22 (6), 1380. doi:10.3892/etm.2021.10816

frontiers | Frontiers in Pharmacology

TYPE Original Research
PUBLISHED 12 October 2022
DOI 10.3389/fphar.2022.1018572

OPEN ACCESS

EDITED BY
Yanyu Huang,
University of California, Davis,
United States

REVIEWED BY
Ming Niu,
Fifth Medical Center of the PLA General Hospital, China
Chao-Zhan Lin,
Guangzhou University of Chinese Medicine, China
Aijun Wang,
University of California, Davis,
United States

*CORRESPONDENCE
Yuhong Liu,
yhliu@sdutcm.edu.cn
Xiaoming Wang,
lmlwxm123@163.com

†These authors have contributed equally to this work

SPECIALTY SECTION
This article was submitted to Ethnopharmacology, a section of the journal Frontiers in Pharmacology

RECEIVED 13 August 2022
ACCEPTED 27 September 2022
PUBLISHED 12 October 2022

CITATION
Wang H, Li Y, Bian Y, Li X, Wang Y, Wu K, Liu C, Liu Y and Wang X (2022), Potential hepatoprotective effects of *Cistanche deserticola Y.C. Ma*: Integrated phytochemical analysis using UPLC-Q-TOF-MS/MS, target network analysis, and experimental assessment. *Front. Pharmacol.* 13:1018572. doi: 10.3389/fphar.2022.1018572

Potential hepatoprotective effects of *Cistanche deserticola Y.C. Ma*: Integrated phytochemical analysis using UPLC-Q-TOF-MS/MS, target network analysis, and experimental assessment

Haichao Wang[1†], Yaying Li[2,3,4†], Yifei Bian[5], Xue Li[1], Yubei Wang[1], Ke Wu[5], Chuanguo Liu[2,3,4], Yuhong Liu[1*] and Xiaoming Wang[2,3,4*]

[1]College of Pharmaceutical Sciences, Shandong University of Traditional Chinese Medicine, Jinan, China, [2]Experimental Center, Shandong University of Traditional Chinese Medicine, Jinan, China, [3]Key Laboratory of Traditional Chinese Medicine Classical Theory, Ministry of Education, Shandong University of Traditional Chinese Medicine, Jinan, China, [4]Shandong Provincial Key Laboratory of Traditional Chinese Medicine for Basic Research, Shandong University of Traditional Chinese Medicine, Jinan, China, [5]Innovation Research Institute of Traditional Chinese Medicine, Shandong University of Traditional Chinese Medicine, Jinan, China

Cistanche deserticola Y.C. Ma (*CD*) possesses hepatoprotective activity, while the active ingredients and involved mechanisms have not been fully explored. The objective of this study was to investigate the chemical composition and hepatoprotective mechanisms of *CD*. We primarily used ultra-performance liquid chromatography with quadrupole time-of-flight tandem mass spectrometry (UPLC-Q-TOF-MS/MS) to identify the phenylethanoid glycoside (PhG) components of *CD*. Then, network analysis was used to correlate and predict the pharmacology of the identified active components of PhGs with hepatoprotection. Next, the mechanisms of the core components and targets of action were explored by cellular assays and toll-like receptor 4 (TLR4) target competition assays. Finally, its hepatoprotective effects were further validated in *in vivo* experiments. The results showed that a total of 34 PhGs were identified based on the UPLC-Q-TOF-MS/MS method. Echinacoside (ECH) was identified as the key ingredient, and TLR4 and nuclear factor-kappa B (NF-κB) were speculated as the core targets of the hepatoprotective effect of *CD via* network analysis. The cellular assays confirmed that PhGs had significant anti-inflammatory activity. In addition, the real-time quantitative polymerase chain reaction (RT-qPCR) and Western blot indicated that ECH notably reduced the levels of interleukin 6 (IL-6) and tumor necrosis factor alpha (TNF-α), as well as the mRNA expression of *TLR4*, *TNF-α*, and *IL-6*, and decreased the high expression of the TLR4 protein, which in turn downregulated the myeloid differentiation factor 88 (MyD88), p-P65 and TNF-α proteins in the inflammatory model. The target competition experiments

suggested that ECH and LPS could competitively bind to the TLR4 receptor, thereby reducing the expression of TLR4 downstream proteins. The results of *in vivo* studies showed that ECH significantly ameliorated LPS-induced hepatic inflammatory infiltration and liver tissue damage and reduced serum alanine aminotransferase (ALT) and aspartate aminotransferase (AST) levels in mice. Moreover, ECH remarkably inhibited the release of inflammatory factors such as TNF-α, IL-6, IL-1β, and MCP-1 in the serum of mice, exerting the hepatoprotective effect by the TLR4/NF-κB signaling pathway. More importantly, ECH could act as a potential inhibitor of TLR4 and deserves further in-depth study. Our results could provide a basis for exploring the hepatoprotective properties of *CD*.

KEYWORDS

PhGs, *Cistanche deserticola Y.C. Ma*, UPLC-Q/TOF-MS/MS, network analysis, hepatoprotective effect, TLR4/NF-κB signaling pathway

1 Introduction

The liver, the largest solid organ in the body, is a critical organ performing numerous physiological functions, including detoxification, immune system support, and metabolism and energy regulation (Kubes and Jenne, 2018; Xiao et al., 2019). However, various factors, such as obesity, cholestasis, viral hepatitis, alcohol, drug abuse, and lipopolysaccharide (LPS), can lead to liver diseases such as fatty liver, cirrhosis, hepatocellular carcinoma, and liver failure (Casey, 2016; Albillos et al., 2020; Burra, 2021). As a public health concern, liver disease is a major cause of morbidity and mortality all over the world, affecting millions of people, leading to approximately 2 million deaths every year worldwide. With the increase in liver-related deaths worldwide at present, liver disease led to significant public health problems and a huge medical burden (Hartke et al., 2017; Mundi et al., 2020; Huang et al., 2021; Zheng et al., 2021). The current treatment options for liver disease include lifestyle (dietary and activity) interventions, medical therapies, chemotherapy and targeted therapy agents, and liver transplantation, but overall benefits are modest (Price and Tien, 2017; Chalasani et al., 2018; Chitturi et al., 2018; Sim and Knox, 2018). Both their long-term effect and safety remain unknown, which limits their widespread use. Clearly, there exists an unmet need for innovative drugs. Fortunately, herbal medicine has clear advantages in the prevention and treatment of liver disease, showing good results and few side effects in clinical practice now (Zhang et al., 2018; Xu et al., 2020; Zhang et al., 2020; Xu G. et al., 2021).

CD, a parasitic plant in the mangosteen family, is globally distributed but mainly found in temperate zones. Also, it has been valued since ancient times as the "ginseng of the desert." It was used as a homology of medicine and food and also has been extensively used in the food industry and clinical practice. As the major active components of *CD*, PhGs have been proven to have a wide range of pharmacological effects, such as antioxidant activity, anti-inflammation, anti-apoptosis, and immunological enhancement, and have been frequently prescribed for hepatoprotection (Li et al., 2016; Morikawa et al., 2019; Lei et al., 2020; Jiang et al., 2021). ECH is the major active component of PhGs isolated from *CD* (Liu et al., 2018a). Tao et al. (2021) found that ECH could prevent alcohol-induced liver injury and also had good hepatoprotective effects. Thida et al. (2021) found that ECH could improve the expression of hepatotoxicity by attenuating oxidative stress and inflammatory cytokines. In addition, isoacteoside is also one of the PhGs isolated from *CD* (Li et al., 2008). Isoacteoside's anti-inflammatory effect was found to be dependent on blocking TLR4 dimerization, which activated the MyD88-TAK1–NF-κB/MAPK signaling pathway cascades and the TRIF pathway, according to Gao et al, (2017). However, the mechanism underlying the therapeutic effects of *CD* in hepatoprotection has not been fully elucidated.

Recently, network analysis is widely applied in the study of herb medicine to explore the therapeutic targets and bioactive compounds (Wang et al., 2020a; Yin et al., 2021). As a "drug–target–disease" interaction network, network analysis helps assess the rationality and compatibility through constructing detailed compound–target and target–pathway networks (Guo et al., 2019; Zhang et al., 2019). It is a new research paradigm of drug discovery and has been proven to be effective in screening active components and potential targets in herbal medicine (Wang et al., 2020b; Song et al., 2020; Tian et al., 2020; Zhou et al., 2021; Montano et al., 2022). In addition, network analysis played an important role in screening targets of liver disease. For example, the treatment study of Erchen decoction in nonalcoholic fatty liver disease (NAFLD) has shown that the interactions of active ingredients of Erchen decoction with 77 targets related to NAFLD mainly reduces inflammation's stimulation of the liver through the TLR4 signaling pathway (Liu et al., 2021). Xu et al. (2021b) used the network pharmacological method to analyze the mechanism of schisandrol B in the treatment of CCl4-induced liver injury. Therefore, we applied network analysis to screen new active components for

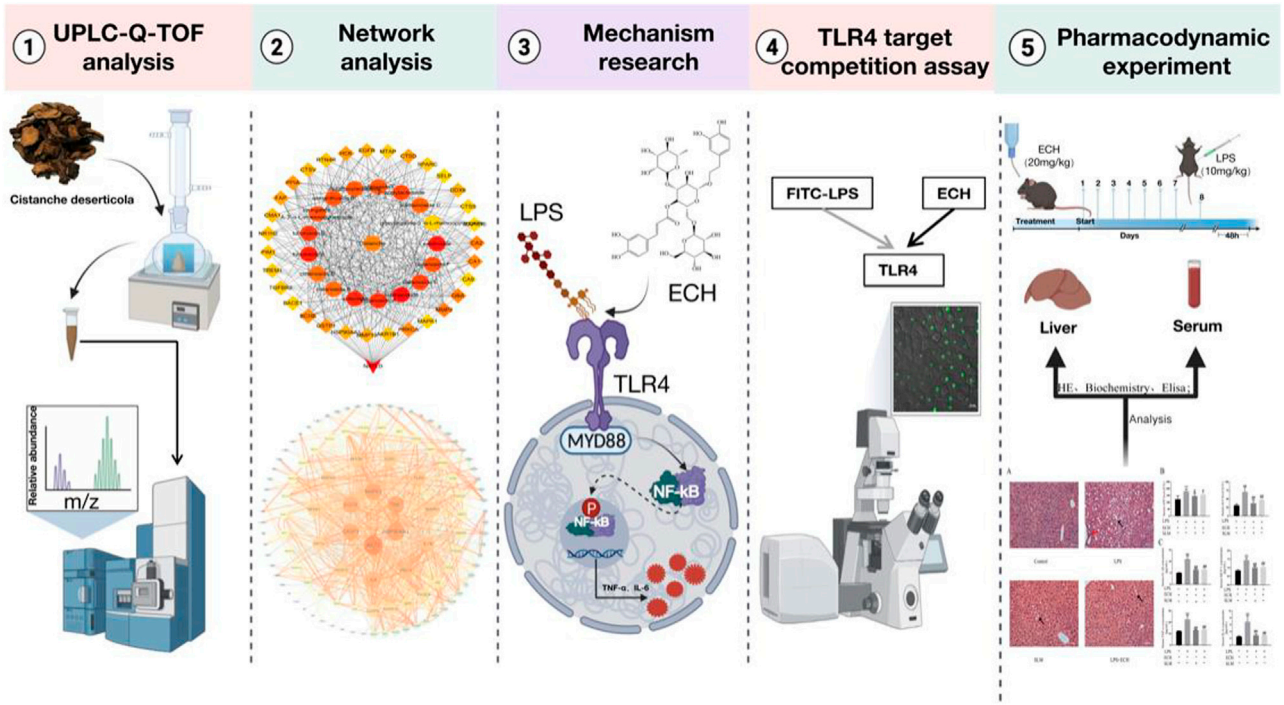

FIGURE 1
Comprehensive strategy diagram.

hepatoprotection from PhGs of *CD* and predicted the potential mechanism of hepatoprotective activity. Finally, studies of the hepatoprotective activity of PhGs were carried out in *in vivo* and *in vitro* experiments.

Using UPLC-Q/TOF-MS/MS technology combined with network analysis, we investigated the main components and potential targets of *CD* on hepatoprotection. The inflammatory model was established by inducing L02 cells with LPS, and the relevant pathways were studied through molecular biology and target competition experiments. Finally, the results from pharmacology were validated *in vivo*. In this study, we investigated the hepatoprotective effect and its potential mechanism of ECH so as to find a novel medicine for hepatoprotection from *CD*. The comprehensive strategy diagram is shown in Figure 1.

2 Materials and methods

2.1 Materials

CD was purchased from Ningxia province and identified by Professor Jun Chen from the Institute of Medicinal Plant Development. The reference standards of echinacoside, 2'-acetylacteoside, tubuloside A, acteoside, salidroside, and isoacteoside were purchased from Chengdu Munster Biotechnology Co., Ltd. (Chengdu, China); osmanthuside B, tubuloside B, cistanoside A, and poliumoside were supplied by Chengdu Keloma Biotechnology Co., Ltd. (Chengdu, China). The purities of all standards were above 98.0% as elucidated, and the details of the reference substances are given in Supplementary Table S1.

Thermo Fisher Scientific in the United States provided HPLC-grade methanol, acetonitrile, and formic acid. Watsons provided distilled water (Watsons Food and Beverage Co., Ltd., Guangzhou, China). The materials obtained are as follows: 1640 medium and fetal bovine serum (FBS) (Gibco, United States); penicillin–streptomycin liquid (Bioharp, Hefei, China); ECH (Chengdu Must Bio-technology Co., Ltd.; Chengdu, China); LPS (Meilunbio, Dalian, China); FITC-LPS (Sigma, United States); CCK-8 Kit and Simply P Total RNA Extraction Kit (Bioss, Beijing, China); MCP-1, IL-1β, IL-6, TNF-α, and NO Elisa Kits (Shanghai Enzyme-linked Biotechnology Co., Ltd., Shanghai, China); ALT and AST reagents (URIT Medical Electronic Co., Ltd., Guilin, China); StarLighter SYBR Green qPCR MIX and StarLighter Script RT all-in-one MIX (Beijing Foreverstar Biotech Co., Ltd., Beijing, China); PMSF, RIPA tissue/cell lysate (Beijing Solarbio Science and Technology Co., Ltd., Beijing, China); SDS-PAGE Sample Loading Buffer and BCA Protein Assay Kit (Beyotime Biotechnology Company,

Beijing, China); PAGE Gel Fast Preparation Kit, Tris-glycine/SDS running buffer, transfer buffer, and TBST (Shanghai Epizyme Biomedical Technology Co., Ltd., Shanghai, China); primary antibody and secondary antibody dilution for Western blot (Absin, Shanghai, China). The detailed information of antibodies is shown in Supplementary Table S2.

2.2 Qualitative analysis of PhGs

2.2.1 Preparation of the sample solution

The medicinal herbs (5 kg) underwent heated circumfluence extraction three times with 10 times the volume of 70% ethanol for 2 h each time, and the filtrates were combined and concentrated under reduced pressure to a thick paste. It was further purified by D101 macroporous resin and eluted sequentially with water and 50% ethanol. The fractions eluted with 50% ethanol were collected, concentrated, and dried under vacuum at 60°C to obtain the total glycoside fraction. The total glycoside (200 mg) was dissolved in 10 ml of 0.1% formic acid. After sonication, the sample solution was centrifuged at 12,000 rpm for 10 min, and the supernatant was subjected to LC–MS analysis.

2.2.2 Preparation of the standard solution

Reference compounds were weighed separately to prepare the standard stock solution (1 mg/ml). An appropriate amount of the standard stock solution was taken and mixed, and then the mixed standard solution was analyzed by LC–MS.

2.2.3 Establishment of the constituents' database

To better identify compounds, a compound database of *CD* and its species was established by searching online databases, including TCMSP (http://lsp.nwu.edu.cn/tcmsp.php), PubMed (http://www.ncbi.nlm.nih.gov/pubmed), CNKI (http://www.cnki.net/), ChemSpider (http://www.chemspider.com/), *m/z* Cloud (https://www.mzcloud.org/), and PubChem (https://pubchem.ncbi.nlm.nih.gov/). Finally, 125 compounds, with their English name, molecular formula, molecular weight, and CAS numbers, were summarized.

2.2.4 UPLC-Q-TOF/MS analysis conditions

The samples were separated on the Waters ACQUITY UPLC BEH C18 column (2.1 mm × 100 mm, 1.7 μm); the mobile phase (A) was acetonitrile, and the mobile phase (B) was water with 0.1% formic acid; the flow rate was 0.3 ml/min, the injection volume was 3 μL, and the column temperature was kept at 30°C. The gradient elution program is shown in Supplementary Table S3.

In the MS analysis, the data were obtained on the Synapt G2 high-definition mass spectrometer (HDMS) system (Waters Corporation, Milford, MA, United States) coupled with Q-TOF. The negative ion mode (NIM) has been used for electron spray ionization (ESI). Parameter settings: capillary voltage was 2.5 kV, ion source temperature was 120°C, the sampling cone was 10 V, the extraction cone was 3 V, desolvation temperature was 450°C, desolvation gas flow was 800 L/h, and cone gas flow was 40 L/h. Inter scan time was 0.02 s, scan time was 0.1 s, and scan range was *m/z* 50–1200; data format is centroid, and dynamic range is extended. 2 ng/L of leucine–enkephalin was used as real-time mass number correction (Lockspray mass: *m/z* 554.2615), and the frequency was 20 s. The MS data were collected and analyzed using MassLynx software v4.1.

2.2.5 Identification strategies of chemical composition

Base peak intensity (BPI) chromatograms of *CD* acquired by UPLC-Q-TOF/MS are shown in Figure 2. First, the accurate mass of precursor ions was obtained by high-resolution mass spectrometry (HRMS). Second, the possible element composition (mass tolerance ≤ ± 5 ppm) of the compounds was speculated through MassLynx software v4.1, after which, referring to the double bond equivalents (DBE) and isotope fit (I-Fit), combined with the plant source, the most likely formula is matched with the established database, and the candidates are obtained according to the matching results.

The primary and multistage EICs were extracted and compared with the reference compounds and the MS^n reported in the literature. Also, peak attribution was determined by comparing the structures of the fragment ions with the candidates. For identification of isomers, this can be determined by comparing their retention times and MS^n with the reference substances.

2.3 Network analysis

2.3.1 Prediction of *CD* candidate targets in NAFLD

To identify the targets, four databases were used to retrieve the chemical ingredients tested by UPLC-Q-TOF/MS: TCMSP (https://old.tcmsp-e.com/tcmsp.php), HERB (http://herb.ac.cn/), TCMIP (http://www.tcmip.cn/TCMIP/index.php/), and TCMID (http://www.megabionet.org/tcmid/). Also, SwissTargetPrediction, SEA, TCMSP, and HERB were used to predict the potential targets, where a probability greater than 0.75 is selected as the condition for predicting targets in the SwissTargetPrediction database. The following databases provided information on fatty liver disease-related targets: OMIM (https://www.omim.org/), TTD (http://db.idrblab.net/ttd/), and GeneCards (https://www.genecards.org/), after which, we screened the same targets of NAFLD and *CD*. Using Cytoscape v3.7.1 software, a "drug–target–disease" network was established.

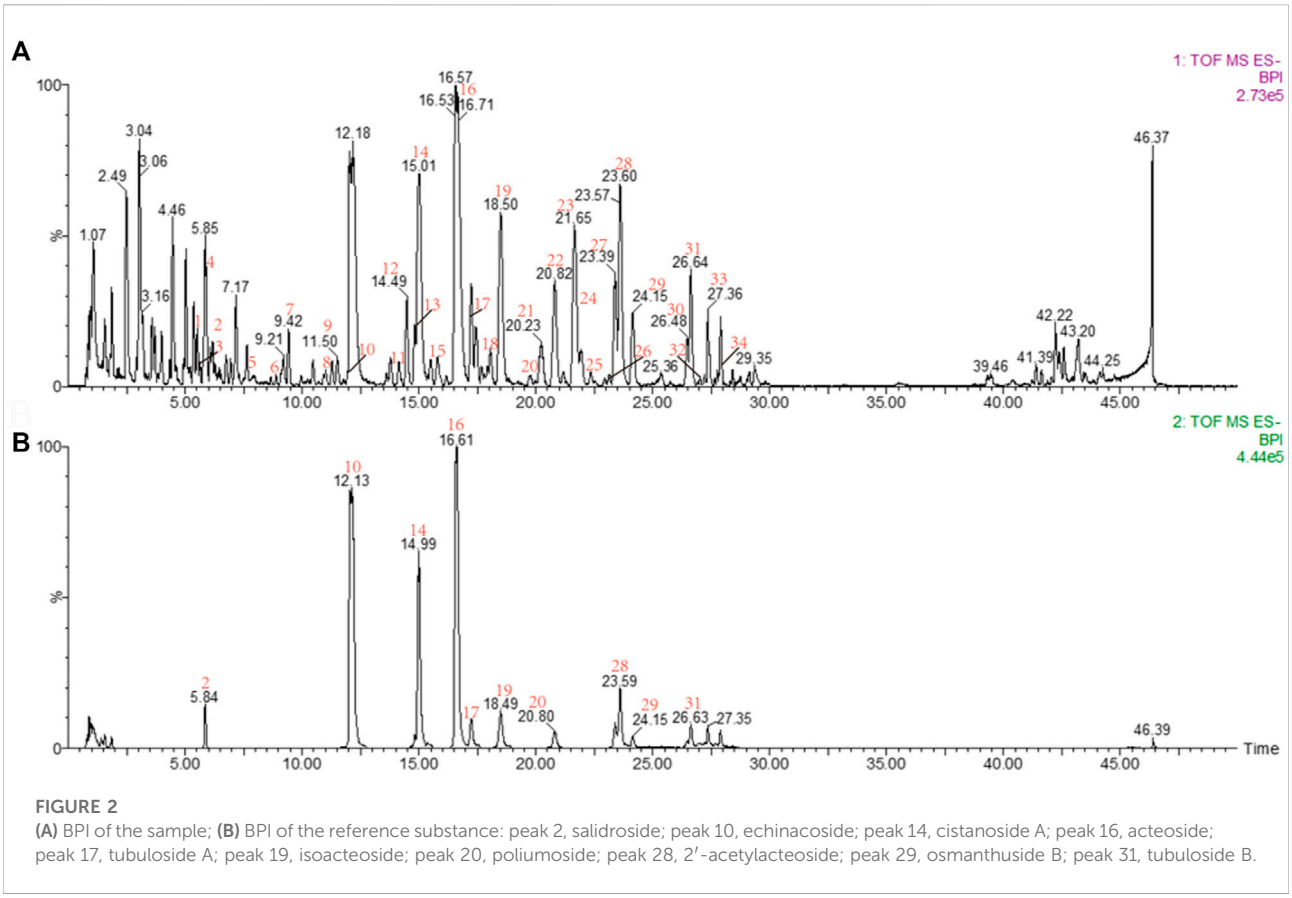

FIGURE 2
(A) BPI of the sample; **(B)** BPI of the reference substance: peak 2, salidroside; peak 10, echinacoside; peak 14, cistanoside A; peak 16, acteoside; peak 17, tubuloside A; peak 19, isoacteoside; peak 20, poliumoside; peak 28, 2′-acetylacteoside; peak 29, osmanthuside B; peak 31, tubuloside B.

2.3.2 Candidate target functional enrichment and protein–protein interaction network analysis

To further understand the molecular activities of prospective targets, functional enrichment analysis was performed using the R package cluster profile. Then, the Kyoto Encyclopedia of Genes and Genomes (KEGG) pathways and Gene Ontology (GO) terms were enriched. In addition, the targets acted upon by the key constituents of *CD* obtained in network analysis were uploaded to the STRING database for protein–protein interaction (PPI) analysis to obtain the PPI network. Using the analysis tools in Cytoscape v3.7.1 software, the color size of the different nodes and the thickness of the lines between the nodes are defined according to the values of their properties.

2.3.3 The molecular docking processing

The protein structures of the core targets were downloaded from the PDB database (http://www.rcsb.org/), separated from the water molecules using PyMOL 2.3.0 software, saved and imported into AutoDock Tools 1.5.6 software for hydrogenation, charge calculation, and atom type settings, and saved in a "pdbqt" format. The 3D structure of the active compound was drawn and energy minimization was performed using ChemOffice 18. 0 software, saved, and imported into AutoDock Tools 1.5.6 in a "mol2" format for hydrogen addition and rotatable bond settings and then saved as a "pdbqt" format file. Molecular docking was performed using AutoDock Vina 1.1.2 software, and the ligand and receptor could bind well at binding energies less than -5 kJ/mol. Finally, the docking results were visualized using PyMOL 2.3.0 software.

2.4 Cell experiment

2.4.1 Cell viability evaluation

The L02 cells were seeded in a 96-well plate overnight at 1×10^4 cells/well and treated with PhGs (200, 100, 50, 25, and 0 μg/ml) and ECH (200, 100, 50, 25, and 0 μM). Following this incubation, the medium was aspirated, and the treated cells were cultivated for 90 min in the 1640 medium containing 10% CCK-8. An automated microplate reader was used to measure the absorbance at 450 nm.

2.4.2 Enzyme-linked immunosorbent assay

The cells treated with drugs were collected, and the cell suspension was diluted with PBS (pH 7.2–7.4) to achieve a cell concentration of about 1 million/mL. Then, ultrasonic crushing was used to destroy cells and release cellular

components, followed by centrifugation at 3000 rpm and 4°C for about 10 min. Also, the supernatant was carefully collected for detection. The content of the inflammatory factors (NO, TNF-α, and IL-6) was detected using ELISA kits in strict accordance with its instructions. First, 50 μL of the standard or sample was added to the appropriate wells, except for the blank well. Then, 100 μl of horseradish peroxidase (HRP) was added to standard wells and sample wells, except for the blank well, covered with an adhesive strip, and incubated for 60 min at 37°C. Next, after washing the microtiter plate five times, substrate A 50 μl and substrate B 50 μl were added to each well, following which, it was gently mixed and incubated for 15 min at 37°C in the dark. Finally, the stop solution was added, and a microplate reader set at a wavelength of 450 nm was used to measure the optical density (*OD*) value of each well in 15 min.

2.4.3 RT-qPCR analysis

The Simply P Total RNA extraction kit was used to extract total RNA from the cells. Reverse transcription was conducted to obtain cDNA. Next, the cDNA was subjected to RT-qPCR instrumentation (Roche LightCycler 480) using amplification reagents. β-ACTB served as an endogenous control. The RT-qPCR primer sequences (Sewell, Wuhan, China) are shown in Supplementary Table S4.

2.4.4 Cell culture and treatment

Beina Bio Co., Ltd (Beijing, China, BNCC35907) provided the L02 normal human liver cell line. L02 cells were cultured in the 1640 complete medium containing 10% FBS and 1% penicillin–streptomycin and maintained in a constant-temperature incubator at 37°C and 5% CO_2. The control group and the LPS group were pretreated with a complete medium, but the ECH group was pretreated with 50 μM ECH. After being incubated for 24 h, both the LPS group and ECH group were cultured for 48 h in a complete medium containing 1 μg/ml LPS.

2.4.5 Western blot

Treated cells were homogenized in RIPA buffer with PMSF and phosphatase inhibitors. The supernatant was obtained by sufficient centrifugation at 4°C (15 min, 14,000 rpm). The protein concentration was quantified with a BCA kit, and protein electrophoresis was performed on a 10% sodium dodecyl sulfate–polyacrylamide gel, following which the protein was transferred to a 0.45-μm PVDF membrane. Subsequently, PVDF membranes were immersed in milk containing 5% skim milk for 2 h at room temperature and incubated with the primary antibody overnight at 4°C. These membranes were washed three times with Tris-buffered saline containing 0.1% Tween 20, and then they were incubated with secondary antibodies for an additional 60 min at room temperature. Relative expression levels of proteins were obtained by delineating the expression levels of specific proteins using a β-actin reference band. Blots were detected using a GE Amersham Imager600 detection device. The experimental data were analyzed using ImageJ 1.8.0 software. Each experiment was repeated three times.

2.4.6 Target competition assay

The cells were cultured in 20-mm confocal dishes and divided into four groups: the control group, the FITC-LPS group, the resatorvid+FITC-LPS group, and the ECH+FITC-LPS group. Only a complete medium was added to the control group. Only a complete medium containing 10 μg/ml of FITC-LPS was added to the FITC-LPS group. The resatorvid+FITC-LPS group was used as the positive control by adding the complete medium containing 150 μM TLR4 inhibitor and 10 μg/ml of FITC-LPS. To the ECH+FITC-LPS group was added the complete medium containing 200 μM of ECH solution and 10 μg/ml of FITC-LPS. After incubating the aforementioned four groups simultaneously for 90 min, the cell cultures were aspirated, discarded, rinsed 3–5 times using PBS, and then the phenol red free medium was added. Each group of experiments was repeated three times. Fluorescence detection was performed using a confocal fluorescence microscope (ZEISS LSM880+Fast Airyscan). The laser pinhole was opened at 100 nm, and the FITC green fluorescence channel was used with an excitation wavelength of 488 nm.

2.5 Animal experiment

2.5.1 Animals and treatment

Male C57BL/6 mice (8-week-old; weight 16–20 g) were obtained from Weitonglihua Laboratory Animal Technology Co., Ltd. (Beijing, China). The animal experiments were carried out under the supervision of the Animal Experiment Center of Shandong University of Traditional Chinese Medicine, and the study protocol was approved by the Laboratory Animal Care and Use Committee of Shandong University of Traditional Chinese Medicine. The mice were housed in an (specified pathogen-free) SPF animal laboratory with standard temperature and humidity and subjected to a 12-h light–dark cycle. All animals had free access to food and water. To compare the efficacy of silymarin (SLM) as a positive drug with that of traditional ECH, all the mice were randomly divided into four groups ($n = 12$): the control group, the LPS group, the SLM+LPS group, and the ECH+LPS group. The LPS group, the SLM+LPS group, and the ECH+LPS group were given LPS at the same frequency at a dose of 10 mg/kg (i.p.), and the control group was given equal amounts of normal saline. To investigate the effect of ECH on LPS-induced liver injury, the mice in SLM and ECH groups were separately treated with SLM (36.4 mg/kg, i. g.) and ECH (20 mg/kg, i. g.) once on a daily basis for 7 days before LPS administration (Jia et al., 2014; Zhang et al., 2021). The control group and the LPS group were only given normal saline. After

TABLE 1 Annotation and analysis of PhGs in *CD*.

No.	RT. (min)	$[M-H]^-$ (*m/z*)	Error (ppm)	Formula	MS/MS fragment ions (*m/z*)	Identification
1	5.52	623.2180	−1.1	$C_{26}H_{39}O_{17}$	461.1651, 315.1106, 179.0349, 135.0449	Unknown
2	5.69	461.1662	0.7	$C_{20}H_{29}O_{12}$	315.1082, 179.0349	Decaffeoylacteoside
3	5.77	299.1133	0.7	$C_{14}H_{19}O_7$	119.0500	Salidroside[a]
4	6.07	487.1456	0.8	$C_{21}H_{27}O_{13}$	179.0353, 161.0244, 135.0453	Cistanoside F
5	7.64	475.1813	−0.6	$C_{21}H_{31}O_{12}$	179.0348, 135.0452	Cistanoside E
6	9.17	503.1761	−0.8	$C_{22}H_{31}O_{13}$	461.1654, 315.1068, 179.0348, 161.0235	Unknown
7	9.42	801.2456	0.4	$C_{35}H_{45}O_{21}$	783.2338, 639.2141, 461.1657, 179.0353,	Cistantubuloside C1/C2
8	11.28	639.1915	−1.6	$C_{29}H_{35}O_{16}$	621.1799, 459.1486, 179.0345, 161.0243	Campneoside II or isomer
9	11.50	639.1929	0.6	$C_{29}H_{35}O_{16}$	621.1825, 459.1520, 179.0349, 161.0246	Campneoside II or isomer
10	12.06	785.2492	−1.5	$C_{35}H_{45}O_{20}$	623.2180, 477.1604, 315.1084, 161.0245	Echinacoside[a]
11	14.14	769.2548	−0.9	$C_{35}H_{45}O_{19}$	607.2213, 461.1665, 179.0350, 161.0244	Cistantubuloside A
12	14.49	769.2541	−1.9	$C_{35}H_{45}O_{19}$	623.2170, 477.1612, 163.0396, 153.0552	Cistantubuloside B1/B2
13	14.82	799.2654	−0.9	$C_{36}H_{47}O_{20}$	785.2506, 623.2183, 461.1643, 193.0504,	Unknown
14	15.01	799.2674	1.6	$C_{36}H_{47}O_{20}$	785.2513, 637.2351, 179.0354, 149.0607	Cistanoside A[a]
15	15.81	755.2387	−1.6	$C_{34}H_{43}O_{19}$	593.2087, 551.1763, 447.1517, 195.0657	Unknown
16	16.58	623.1987	1.8	$C_{29}H_{35}O_{15}$	461.1675, 315.1092, 179.0354, 161.0250	Acteoside[a]
17	17.24	827.2615	0.6	$C_{37}H_{47}O_{21}$	665.2293, 623.2187, 477.1606, 161.0247	Tubuloside A[a]
18	18.06	813.2802	−1.8	$C_{37}H_{49}O_{20}$	799.2632, 637.2350, 193.0506, 175.0397	Cistanoside B
19	18.50	623.1965	−1.8	$C_{29}H_{35}O_{15}$	461.1652, 315.1070, 179.0346, 161.0242	Isoacteoside[a]
20	19.96	769.2549	−0.8	$C_{35}H_{45}O_{19}$	623.1957, 461.1666, 179.0350, 161.0243	Poliumoside[a]
21	20.21	607.2036	1.5	$C_{29}H_{35}O_{14}$	445.1711, 179.0354, 161.0246	Syringalide A-3'-α-L-rhamnopyranoside
22	20.82	607.2015	−2.0	$C_{29}H_{35}O_{14}$	461.1642, 163.0392, 145.0289	Isosyringalide-3'-α-L-rhamnopyranoside or isomer
23	21.65	637.2129	−0.5	$C_{30}H_{37}O_{15}$	623.2010, 475.1826, 329.1222, 161.0244	Cistanoside C
24	21.93	637.2130	−0.3	$C_{30}H_{37}O_{15}$	623.1945, 461.1643, 193.0504, 175.0398	Plantainoside C or isomer
25	22.39	753.2605	−0.1	$C_{35}H_{45}O_{18}$	179.0344, 161.0242, 135.0447	Kankanoside I
26	23.16	607.2015	−2.0	$C_{29}H_{35}O_{14}$	461.1659, 163.0391, 145.0292	Isosyringalide-3'-α-L-rhamnopyranoside or isomer
27	23.39	637.2131	−0.2	$C_{30}H_{38}O_{15}$	623.1999, 461.1659, 193.0508, 175.0391	Plantainoside C or isomer
28	23.60	665.2087	0.8	$C_{31}H_{37}O_{16}$	623.1995, 503.1774, 461.1662, 179.0349	2'-Acetylacteoside[a]
29	24.15	591.2087	1.5	$C_{29}H_{35}O_{13}$	445.1680, 163.0405, 145.0290	Osmanthuside B[a]
30	26.46	651.2292	0.5	$C_{31}H_{39}O_{15}$	475.1805, 193.0660, 175.0399, 149.0602	Cistanoside D
31	26.64	665.2067	−2.3	$C_{31}H_{37}O_{16}$	623.1964, 503.1755, 461.1658, 179.0345	Tubuloside B[a]
32	27.02	649.2117	−2.3	$C_{31}H_{37}O_{15}$	607.2004, 503.1757, 163.0398, 145.0293	Salsaside F
33	27.35	679.2233	−0.7	$C_{32}H_{39}O_{16}$	637.2119, 623.1975, 179.0347, 161.0244	Cistansinenside A or salsaside E
34	27.91	679.2232	−0.9	$C_{32}H_{39}O_{16}$	637.2107, 623.2013, 179.0347, 161.0244	Cistansinenside A or salsaside E

"a" represented the compound confirmed by comparison with the reference standards.

being given LPS 48 h later, the mice were anesthetized and dissected. Blood samples were collected, centrifuged at 3000 rpm for 15 min, and serum was separated for further analysis. Liver tissues were collected and quickly fixed in 4% paraformaldehyde or frozen in liquid nitrogen for further analysis.

2.5.2 Histological evaluation of liver tissues

The liver samples were taken out from 4% paraformaldehyde, embedded in paraffin, and serially sectioned at 4-μm thickness. After routine deparaffinization, they were stained using hematoxylin and eosin (H&E). Histopathological examination was performed under a light microscope.

2.5.3 Determination of biochemical indexes

Serum biochemical indexes, including alanine aminotransferase (ALT) and aspartate aminotransferase (AST), were detected by the automatic biochemical analyzer (URIT-8026; Guangxi, China).

2.5.4 ELISA

The whole blood samples collected in the serum separation tube were placed at 4 °C overnight, centrifuged at 3000 rpm for 20 min, and then the supernatant was diluted twice in PBS for detection. The content of the inflammatory factors (TNF-α, IL-6, IL-1β, and MCP-1) was detected using ELISA kits in strict accordance with its instructions. The procedure is as described in Section 2.4.2.

2.6 Statistical analysis

Data are presented as the mean ± SD. The statistical analysis was carried out using SPSS 19.0 software (SPSS Inc, United States). One-sample t-tests were used to analyze the data after normalizing it to the control. Statistical significance is indicated as $p < 0.05$.

3 Results

3.1 Characterization of the chemical constituents

A total of 34 peaks were identified and determined to be PhGs according to the strategy in "Section 2.2.5" (Supplementary Figure S1). Ten components were validated against their reference compounds, and the chemical structures of the remaining peaks were inferred from the exact mass and MS^n fragment ions. The detailed information on ESI-MS and MS^n is shown in Table 1. The procedures of identification are as follows.

3.1.1 MS cleavage behaviors

In the NIM, the PhGs exhibited similar fragmentation patterns, mainly involving the loss of some characteristic neutral fragments, such as caffeoyl (CA, $C_9H_6O_3$, 162 Da), feruloyl (Fr, $C_{10}H_8O_3$, 174 Da), coumaroyl (Cm, $C_9H_6O_2$, 146 Da), acetyl (Ac, C_2H_2O, 42 Da), glucose (Glu, $C_6H_{10}O_5$, 162 Da), rhamnose (Rha, $C_6H_{10}O_4$, 146 Da), and dehydration (18 Da).

The compositions of PhGs can be quickly identified based on the characteristic fragment ions. In addition to the aforementioned characteristic neutral loss, a series of fragment ions were their moieties (including glycosides and aglycone) in the low *m/z* range. For example, the peak of the fragment ion at *m/z* 179.03 was from caffeoyl, and the peaks of fragment ions at *m/z* 161.02 and *m/z* 135.04 were obtained from the removal of H_2O and CO_2; the peak of the fragment ion from the aglycone (hydroxytyrosol) at *m/z* 153.06 and that at *m/z* 123.04 were generated by the removal of CH_2O.

In this experiment, the fragmentation pathways of reference compounds (Table 1) were analyzed using UPLC-Q-TOF/MS. The characteristic diagnostic ions related to their structures were summarized, and their possible fragmentation pathways were speculated based on the multilevel mass spectra information of the reference substances. The aforementioned results are shown in Supplementary Figure S2.

3.1.2 Identification of PhGs

The relevant literature shows that *CD* contains a large number of PhGs, and the chemical structures of these components are generally glycosides of the phenylethanol group or phenylethanol group with hydroxyl/methoxy substitution attached to β-D-glucopyranose/β-D-glucopyranoside with substituents at the C-2~6 position (Jiang et al., 2009; Han et al., 2012; Holzgrabe and Malet-Martino, 2014). The structural features of PhGs are summarized as follows: the benzene ring is substituted with hydroxyl or methoxy at the C-3 and C-4 positions in the glycosides. Phenylpropenylation often occurs at the C-4 or C-6 position of the medial glucose, and the types of phenylpropenyl groups include caffeoyl, coumaroyl, and feruloyl. Also, the two alkene hydrogens on acryloyl are mostly trans-structures, with occasional acetylation at the C-2 position of the central sugar, and these moieties are linked by ester or glycosidic linkages, which are prone to form the corresponding fragment ions during in-source fragmentation.

In the NIM, both peak 16 and peak 19 (eluted at 16.58 and 18.50 min, respectively) are quasi-molecular ions at *m/z* 623.20 $[M-H]^-$ with a formula of $C_{29}H_{35}O_{15}$, for a pair of isomers, could produce the similar fragment ions *m/z* 461.17, 315.11, 179.03, 161.02, and 135.05 in the MS^2 spectrum. The neutral loss of caffeoyl ($C_9H_6O_3$, -162 Da) forms fragment ions *m/z* 461.17 ($C_{20}H_{29}O_{12}$) by ester bond cleavage, which further loses a neutral molecule of rhamnose ($C_6H_{10}O_4$, -146 Da) and produces the ion *m/z* 315.11 ($C_{14}H_{19}O_8$). In the low range of *m/z*, we found the characteristic fragment ions associated with the caffeoyl structure (*m/z* of 179, 161, and 135) and aglycone structure (*m/z* 153.06 and 123.04). After searching the compound library, acteoside and isoacteoside were matched to them. Peaks 16 and 19 were identified as acteoside and isoacteoside, respectively, by comparing their MS^2 fragmentation pathways and retention times with the reference compounds, and their MS^2 spectrum and fragmentation pathway are shown in Figure 3.

The quasi-molecular ion peaks for both peak 28 and peak 31 (*m/z* 665.21, $C_{31}H_{37}O_{16}$, eluted at 23.60 and 26.64 min, respectively) are at *m/z* 665.21. Compared with peaks 16 and 19, the added mass of 42 Da (C_2H_2O) indicated that peak 28 and peak 31 were both present at the 2-hydroxyl acetylation position of the central sugar (glucose). The neutral loss of the acetyl group (C_2H_2O, -42 Da) in the MS^2 spectrum forms a corresponding fragment ion *m/z* 623.20 ($C_{29}H_{35}O_{15}$). The fragment ion *m/z*

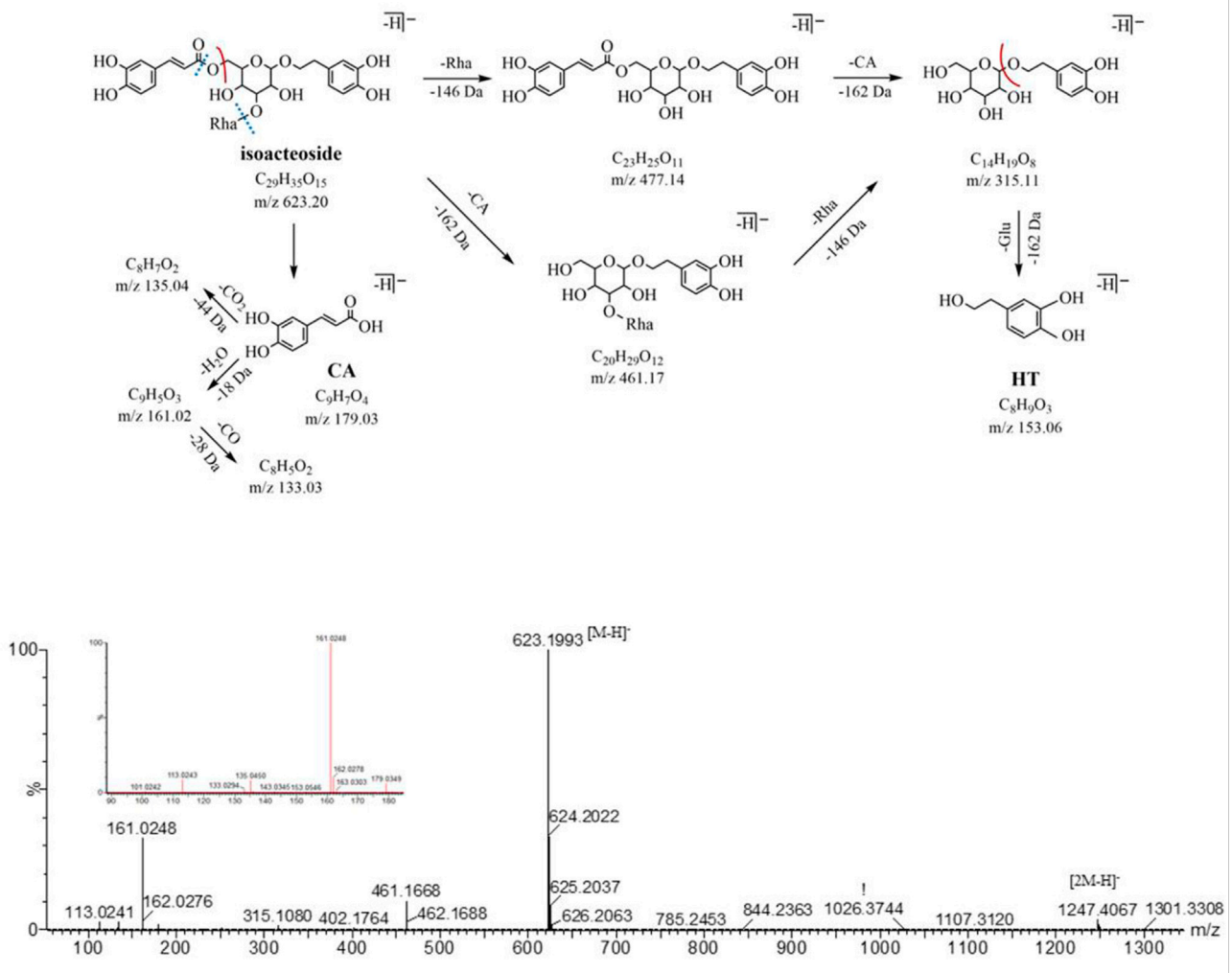

FIGURE 3
MS^2 and the fragmentation pathway of the isoacteoside.

503.18 ($C_{22}H_{31}O_{13}$) attributed to the loss of neutral ($C_9H_6O_3$, -162 Da) and other identical fragment ions *m/z* 461.17 and *m/z* 315.11. The characteristic fragmentation ions *m/z* 179.03, 161.02, and 135.04 related to the caffeoyl structure and the feature fragment ions at *m/z* 153.06 and 123.04 related to the aglycone structure were observed. Peaks 28 and 31 were identified as 2'-acetylacteoside and tubuloside B, respectively, by comparing their MS^2 cleavage behaviors and retention times with those of the reference compounds. The MS^2 profile and fragmentation pathway are shown in Figure 4.

Peak 10 (*m/z* 785.25, $C_{35}H_{45}O_{20}$, 12.06 min) has 162 Da (Glu, $C_6H_{10}O_5$) more than peak 16 and peak 19 (*m/z* 623.20, $C_{29}H_{35}O_{15}$), a glucose glycosyl group, which is presumed to be a triglycoside with another molecule of glucose attached to the central sugar (glucose). The neutral loss of caffeoyl ($C_9H_6O_3$, -162 Da) in the MS^2 spectrum forms fragment ions at *m/z* 623.22 ($C_{26}H_{39}O_{17}$), which further loses the neutral molecules of rhamnose ($C_6H_{10}O_4$, 146 Da) and glucose ($C_6H_{10}O_5$, 162 Da) and yields the corresponding fragment ions *m/z* 477.16 ($C_{20}H_{29}O_{13}$) and *m/z* 461.17 ($C_{20}H_{29}O_{12}$). The characteristic fragmentation ions at *m/z* 179.03, 161.02, and 135.04 related to the caffeoyl structure as well as the feature fragment ions at *m/z* 153.06 and 123.04 related to the aglycone structure were still observed. Peak 10 was identified as ECH by comparing its MS^2 cleavage behavior and retention time with those of the reference compound, and its MS^2 spectrum and cleavage pathway is shown in Figure 5.

Peak 17 (*m/z* 827.26, $C_{37}H_{47}O_{21}$, 17.24 min) has 42 Da (C_2H_2O, an acetyl group) more than peak 10 (*m/z* 785.25, $C_{35}H_{45}O_{20}$), presuming that peak 17 is a triglycoside with hydroxyacetylation at the 2-position of the central sugar (glucose). The neutral loss of caffeoyl ($C_9H_6O_3$, -162 Da) in the MS^2 spectrum forms a fragment ion *m/z* 665.23 ($C_{28}H_{41}O_{18}$), which further loses acetyl (C_2H_2O, -42 Da) and yields the same fragment ions *m/z* 623.22, 477.16, and 461.17 in the peak 10. The characteristic fragment ions *m/z* 179.03, 161.02, and 135.04 related to the caffeoyl structure were observed, as well

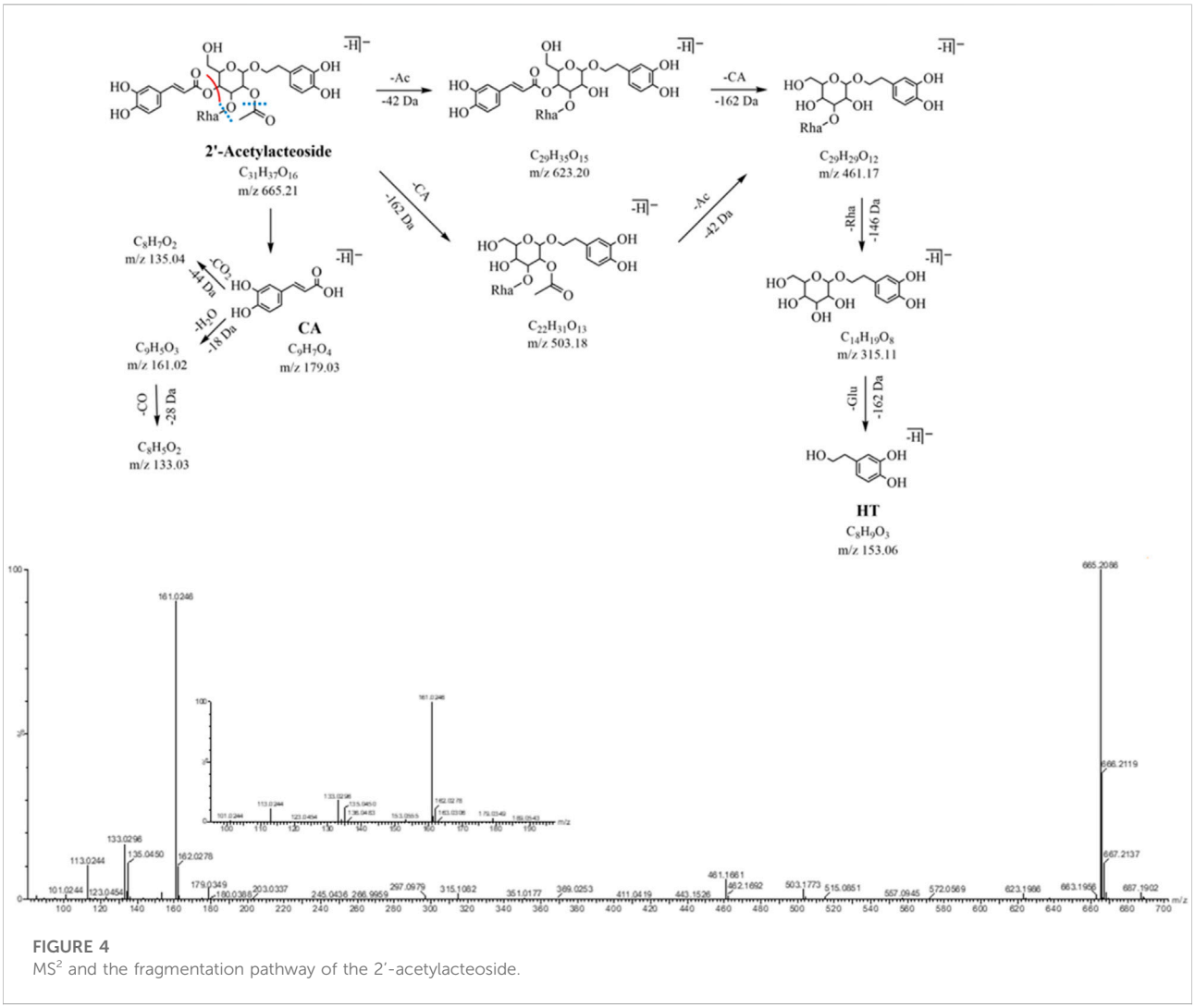

FIGURE 4
MS^2 and the fragmentation pathway of the 2′-acetylacteoside.

as the characteristic fragment ions *m/z* 153.06 and 123.04 related to the aglycone structure. Peak 17 was identified as tubuloside A by comparing their MS^2 cleavage behavior and retention time with those of the reference compounds. The MS^2 spectrum and fragmentation pathway is shown in Figure 6.

The fragmentation patterns of several other typical compounds are described in Supplementary Material S1.

3.2 Results of network analysis

3.2.1 Screening the targets

We further combined the identified 34 compounds with the database of traditional Chinese medicine ingredients to conduct an active compound search and screening to obtain 17 active ingredients. Finally, 189 targets corresponding to these 17 compounds were found in the online database. Also, 1963 NAFLD-related targets were acquired using OMIM, GeneCards, and TTD resources. We screened 135 overlapping targets as prospective targets linked to NAFLD by intersecting the targets of compounds with NAFLD-related targets (Supplementary Figure S3). To illustrate the drug–target–disease network, 135 possible targets and 17 compounds were loaded into Cytoscape 3.7.1 software. In this network, echinacoside, salidroside, and acteoside ranked as the top three compounds, connecting the largest number of targets (Figure 7A). In addition, 15 compounds were bound to the TLR4 target, and the predicted results showed that ECH had the most stable binding effect on the TLR4 protein. The experimental results are shown in Supplementary Table S5.

3.2.2 The PPI network and functional enrichment of candidate targets

We performed PPI network and functional enrichment analyses to reveal interactions between candidate target genes. Also, their associated biological functions and

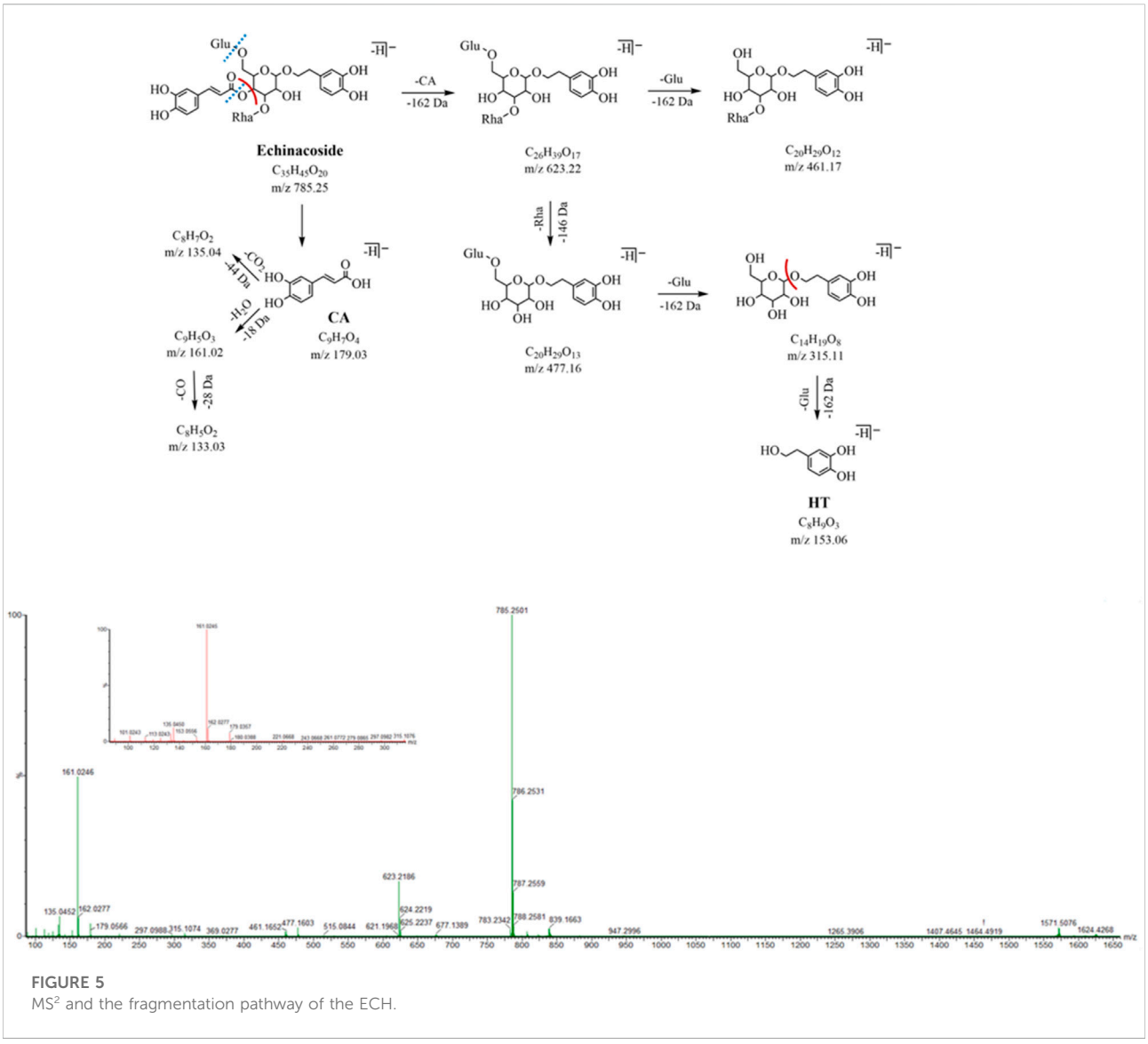

FIGURE 5
MS^2 and the fragmentation pathway of the ECH.

metabolic pathways were investigated. As shown in Figure 7B, the higher the ranking, the larger the circle and the darker the color, indicating higher relevance. AKT1, HSP90AA1, and TNF have been discovered to play key roles in the PPI network. The functions in the KEGG and GO analyses are shown in Figures 8A,B. The results of KEGG pathway enrichment analysis were largely associated with lipid and atherosclerosis, hepatitis B, the AGE-RAGE signaling pathway in diabetic complications, pathways in cancer, Kaposi sarcoma-associated herpesvirus infection, TLR signaling pathway, and so on. The GO biological process was closely related to the response to LPS and so on.

3.3 Results of cell experiments

3.3.1 Optimal intervention condition on L02 cells was determined

To assess the cytotoxicity of PhGs and ECH on L02 cells, CCK-8 assays were performed. The results in Figure 9A indicated that the concentration of PhGs in the range of 25–200 μg/ml and that of ECH in the range of 25–200 μM had no toxic effect on cells. In addition, the effects of LPS on L02 cells are shown in Supplementary Figure S4. In the next step, we treated L02 cells with LPS to establish a cellular inflammation model and performed an RT-qPCR assay. The RT-qPCR assay results showed that with respect to the control group, the mRNA

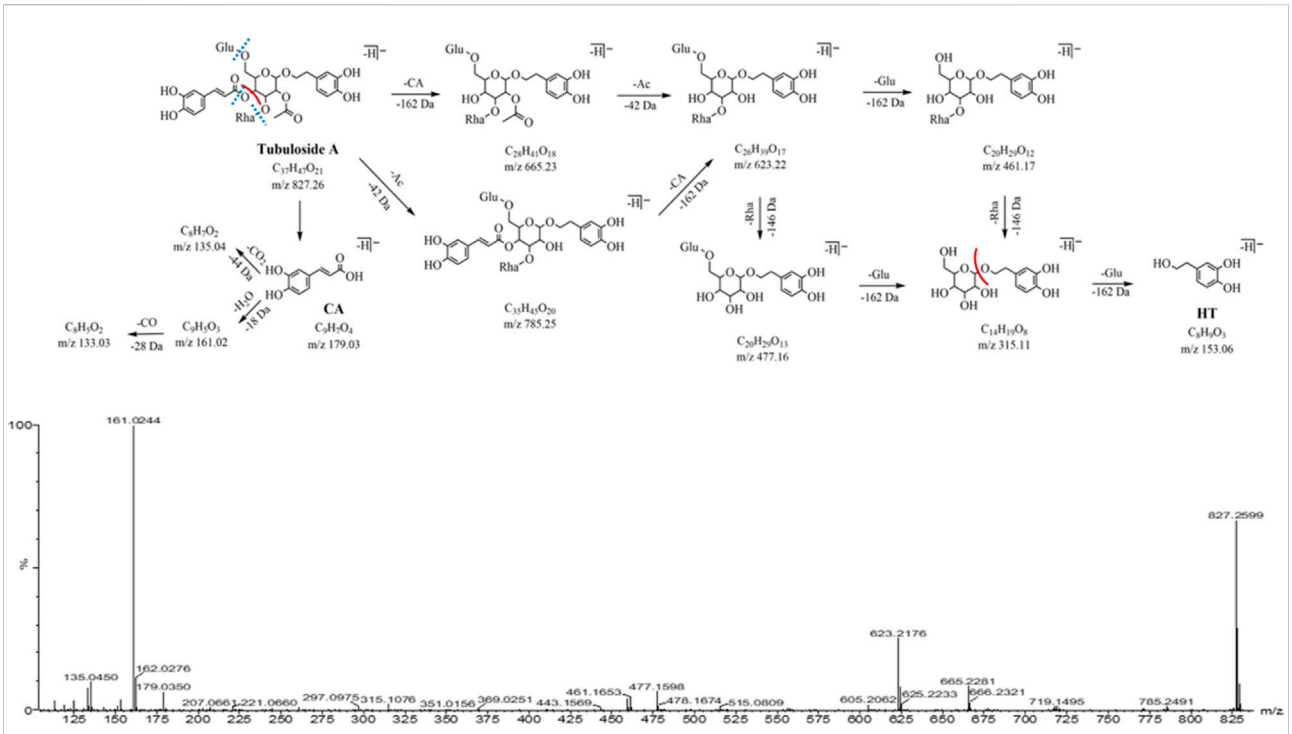

FIGURE 6
MS^2 and the fragmentation pathway of the tubuloside A.

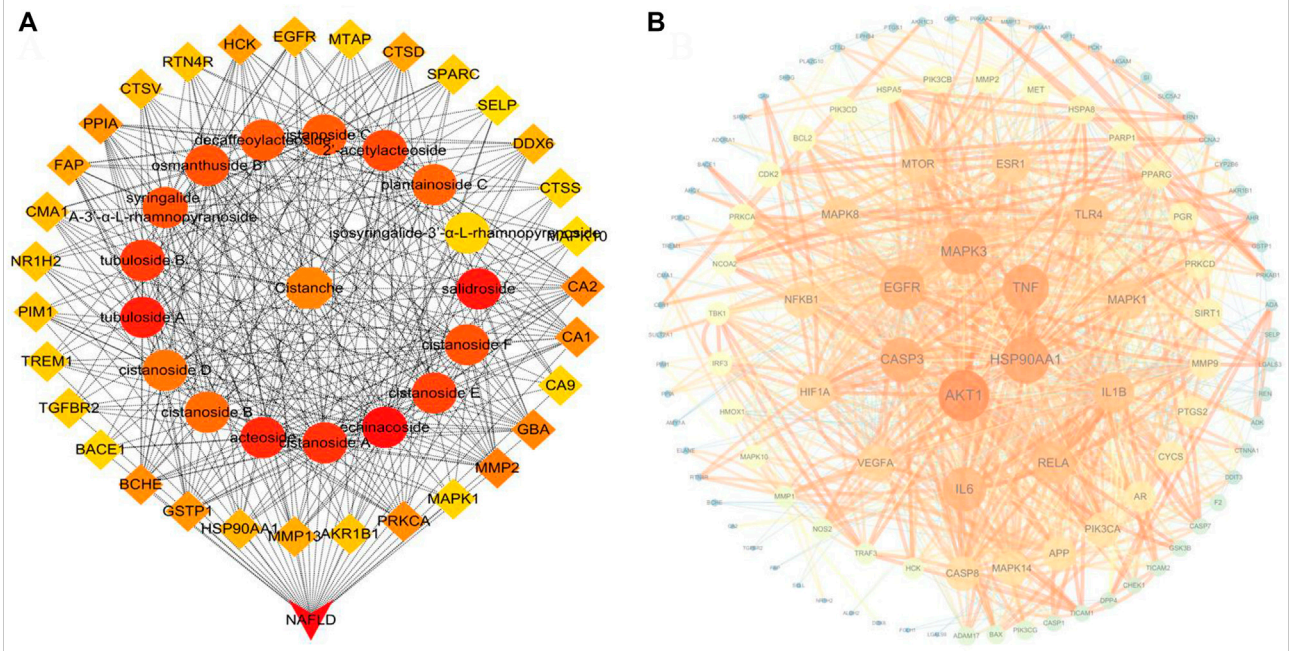

FIGURE 7
(A) Top 50 nodes of the compound–drug–target–disease network; **(B)** PPI network of *CD* candidate targets.

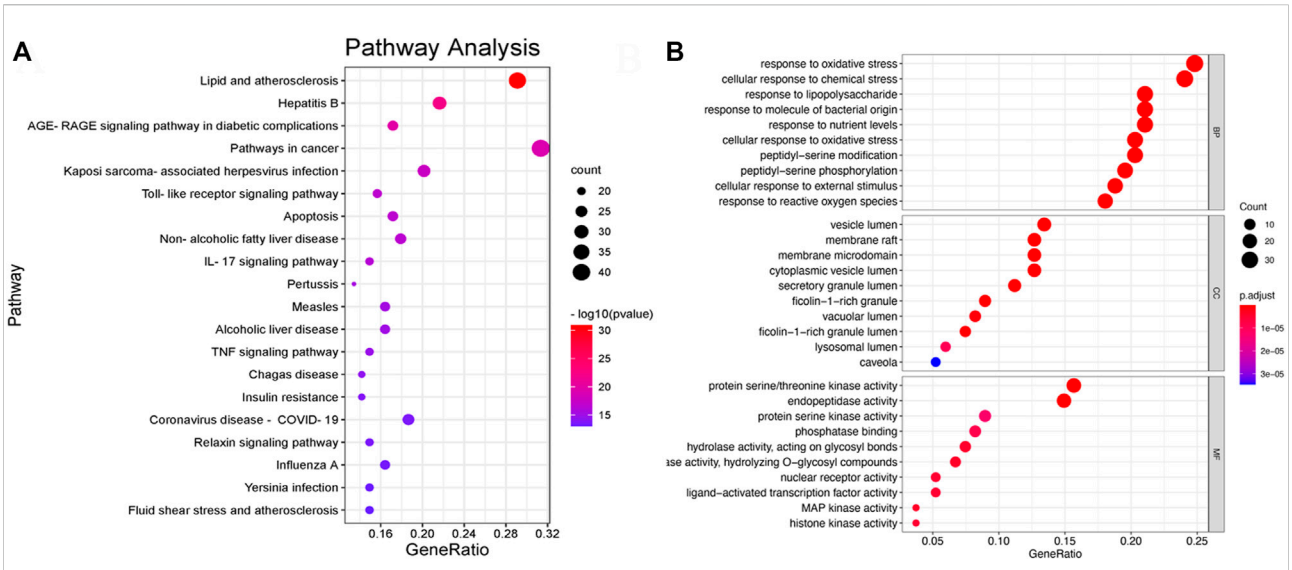

FIGURE 8
(A) Bar plot of KEGG pathway enrichment analysis results, showing the top 20 pathways in the KEGG. **(B)** Bar plot of GO pathway enrichment analysis results, showing the top 10 pathways in the GO.

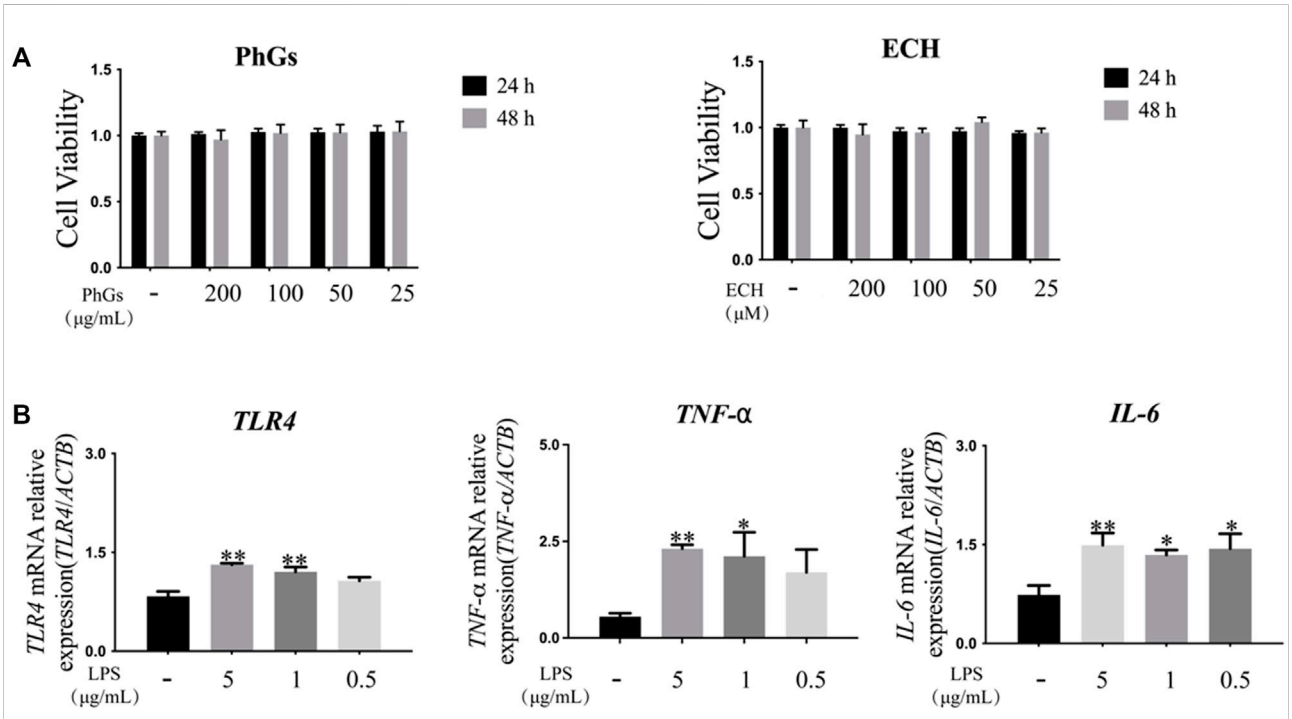

FIGURE 9
Establishment of the inflammation model in L02 cells. **(A)** Cell viability of L02 was affected by different doses and duration of action of PhGs and ECH ($n > 3$). **(B)** Expression of *TLR4*, *IL-6*, and *TNF-α* genes in L02 cells cultured with different concentrations of LPS ($n = 3$). *$p < 0.05$ and **$p < 0.01$ control group compared with the LPS group; all data are presented as mean ± SD.

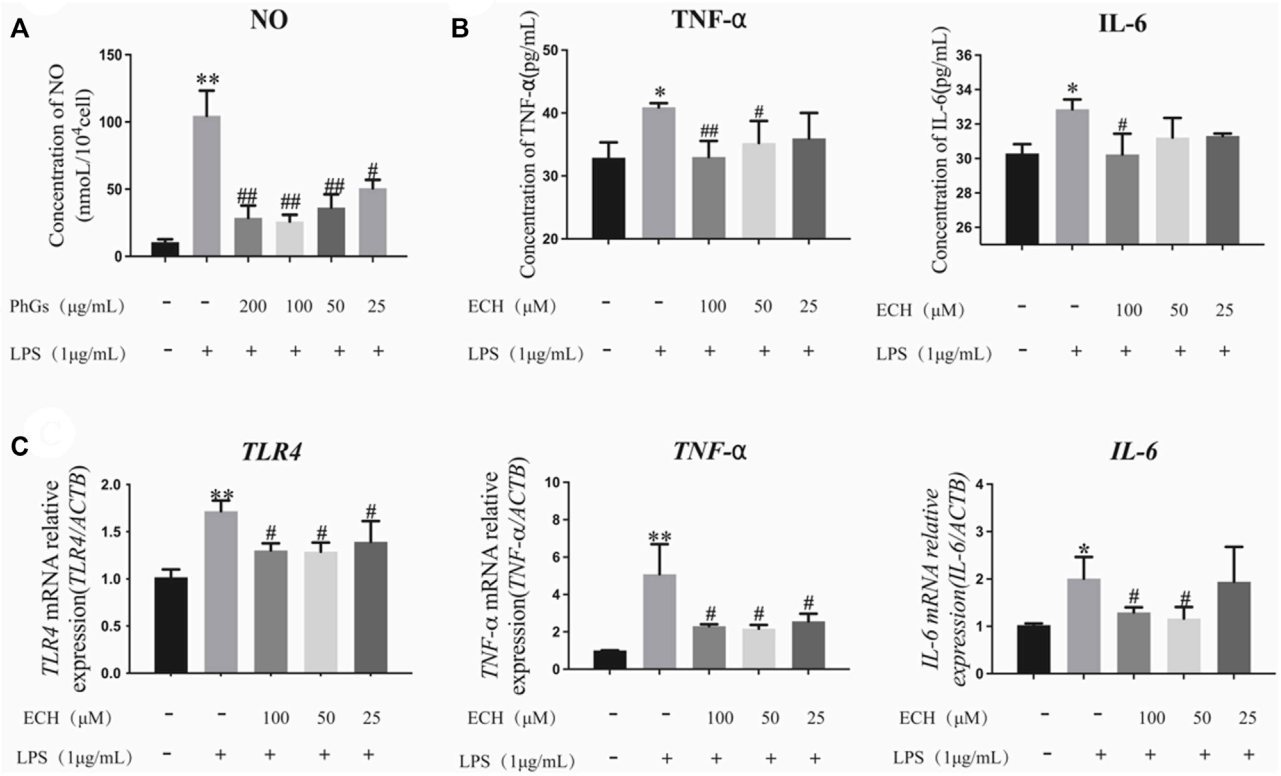

FIGURE 10
Effects of PhGs and ECH on inflammatory factors in L02 cells. **(A)** Expression of NO was analyzed by ELISA. **(B)** IL-6 and TNF-α expression assessed by ELISA. **(C)** Inflammation-related genes *TLR4*, *TNF-α*, and *IL-6* were tested by RT-qPCR; $^{*}p < 0.05$ and $^{**}p < 0.01$ compared with the control group; $^{\#}p < 0.05$ and $^{\#\#}p < 0.01$ compared with the LPS group; all data are presented as mean ± SD ($n = 3$).

expression of *IL-6*, *TLR4*, and *TNF-α* was increased in the LPS group. When choosing an intervention condition, an LPS concentration with the lowest concentration and the best effect should be chosen. Although the lowest concentration was found in the 0.5-μg/ml LPS group, it had an effect only on the mRNA expression of *IL-6* ($p < 0.05$). However, the 1-μg/ml LPS group showed a significant increase in the mRNA expression of *TLR4* ($p < 0.01$), *TNF-α* ($p < 0.05$), and *IL-6* ($p < 0.05$). Therefore, 1 μg/ml (LPS) was chosen for further study (Figure 9B).

3.3.2 PhGs inhibit the production of NO

Echinacoside is the indicative component for the determination of PhGs and is mainly used for liver protection, immune protection, etc. (Pei et al., 2018). Inflammation is closely related to oxidative stress, and with the aim of determining whether PhGs could inhibit LPS-induced inflammation in L02 cells, the level of NO was detected. Our results indicated that PhGs obviously decreased NO levels. 25-μg/mL PhG treatment significantly reduced NO production compared to the LPS group ($p < 0.05$). NO levels were reduced more significantly in the 200, 100, and 50 μg/ml PhG groups ($p < 0.01$, Figure 10A).

3.3.3 ECH inhibits the production of pro-inflammatory cytokines

We measured the secretion of TNF-α and IL-6 using ELISA kits (Figure 10B). ECH administration reduced IL-6 and TNF-α production compared to the LPS group ($p < 0.05$). Among them, 100 μg/ml of ECH administration remarkably decreased the production of IL-6 ($p < 0.05$). TNF-α levels were significantly reduced in the 50-μg/ml ECH administration group ($p < 0.05$), and the 100-μg/ml ECH administration group had a more significant reduction in TNF-α levels ($p < 0.01$).

3.3.4 Effect of ECH on inflammatory gene expression

To determine the expression of inflammation-related genes in L02 cells induced by LPS with different concentrations of ECH, RT-qPCR analyses were performed. As shown in Figure 10C, LPS upregulated the levels of *TLR4*, *TNF-α*, and

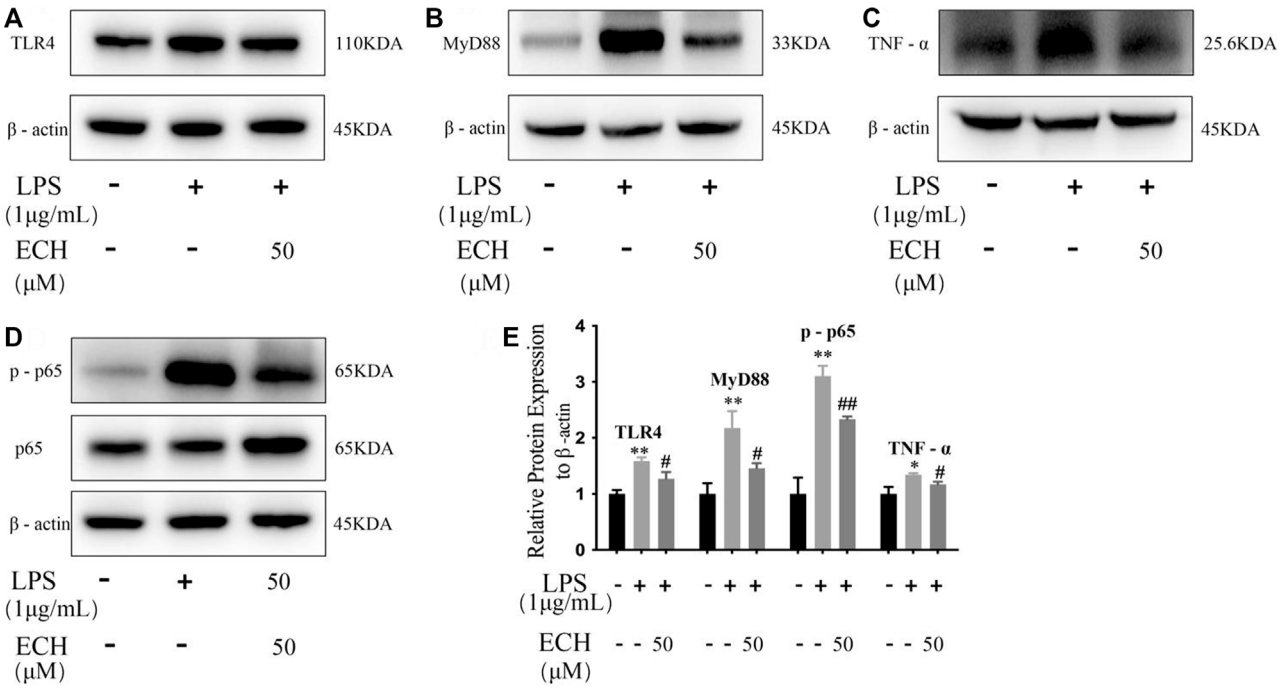

FIGURE 11
Influence of ECH on inflammatory response during the TLR4/NF-κB signaling pathway in L02 cells. **(A)** Protein expressions of TLR4. **(B)** Protein expressions of MyD88. **(C)** Protein expressions of TNF-α. **(D)** Protein expressions of p-P65; **(E)** Protein expression levels of TLR4, MyD88, p-65, and TNF-α the control group compared with the LPS group $^{*}p < 0.05$ and $^{**}p < 0.01$; ECH group compared with the LPS group $^{\#}p < 0.05$ and $^{\#\#}p < 0.01$; all data are presented as mean ± SD ($n = 3$).

IL-6 mRNA in L02 cells ($p < 0.05$), but ECH downregulated these increased mRNA levels. Among them, the high-concentration (100 μg/ml) and medium-concentration (50 μg/ml) administration groups were closer to the control group. These findings suggested that ECH inhibited LPS-induced inflammation in L02 cells.

3.3.5 ECH inhibits the TLR4/NF-κB signaling pathway

To investigate the anti-inflammatory effect of ECH, we detected the expression of TLR4, MyD88, p-P65, and TNF-α to identify whether it regulated inflammation through the TLR4/NF-κB signaling pathway. ECH treatment significantly reduced the TLR4 protein compared to the LPS group ($p < 0.05$). At the same time, ECH also decreased the expression of its downstream proteins MyD88 ($p < 0.05$) and p-P65 ($p < 0.01$). Similarly, ECH decreased TNF-α protein levels in LPS-treated L02 cells ($p < 0.05$). These results indicated that ECH may suppress inflammation by adjusting the TLR4/NF-κB signaling pathway (Figure 11).

3.3.6 ECH competes with FITC-LPS for cellular receptor binding sites

The binding of FITC-LPS to cell membrane surface receptors resulted in enhanced fluorescence at the cell membrane surface, but co-incubation of the compound with FITC-LPS competitively inhibited the binding of FITC-LPS to the membrane surface receptors, resulting in diminished fluorescence intensity (Troelstra et al., 1997; Sauter et al., 2007). As shown in Figure 12, the fluorescence intensity of the FITC-LPS group was the highest after the binding of LPS with fluorescent labeling to cells. When the TLR4 inhibitor was incubated with FITC-LPS, the fluorescence intensity was significantly weaker than that of the FITC-LPS group. When ECH was incubated with FITC-LPS, the fluorescence intensity was close to that of the resatorvid + FITC-LPS group and was significantly weaker than that of the FITC-LPS group, which suggests that ECH could competitively bind to the LPS receptor on the cell membrane surface.

3.4 Animal experiment results

3.4.1 ECH ameliorates LPS-induced liver histopathological damage in mice

To assess the effect of ECH treatment on liver tissue, H&E staining was carried out, which is very straightforward and objective. Compared with the control group, the LPS group developed obvious characteristics of liver injury, abnormal hepatic lobule structure, and infiltration of peripheral

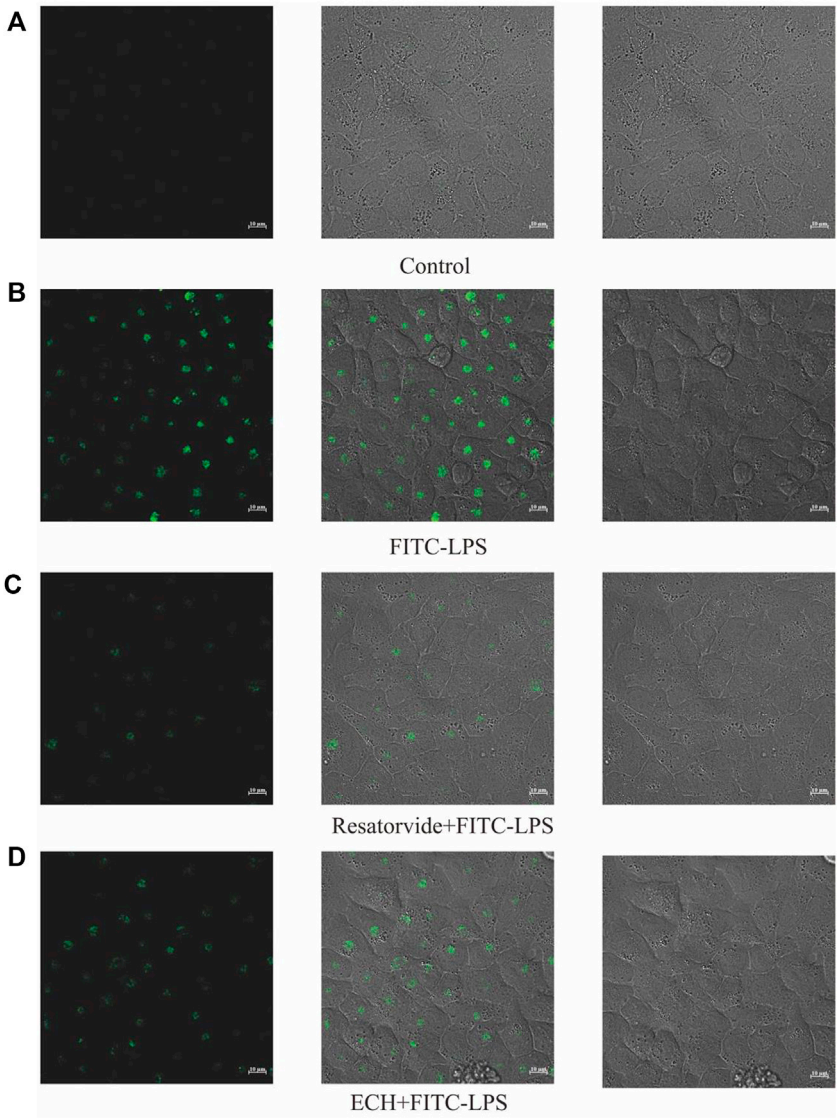

FIGURE 12
Effects of ECH on competitive inhibition of FITC-LPS binding cells. **(A)** Control group; **(B)** FITC-LPS group; **(C)** resatorvide+FITC-LPS group (TLR4 antagonist); **(D)** ECH+FITC-LPS group.

inflammatory. The aforementioned symptoms were effectively relieved after ECH administration (Figure 13A).

3.4.2 ECH significantly decreases the serum ALT and AST levels in mice induced by LPS

According to the changes in the levels of biochemical enzymes in serum, ALT and AST levels in the LPS group were significantly higher than those in the control group ($p < 0.01$), while both enzyme levels in the ECH groups were decreased with a significant statistical difference ($p < 0.01$) (Figure 13B).

3.4.3 ECH decreases secretion of TNF-α, IL-6, IL-1β, and MCP-1 in mice induced by LPS

To assess the effect of ECH pretreatment on the inflammatory response, the serum secretion levels of pro-inflammatory cytokines TNF-α, IL-6, IL-1β, and MCP-1 were detected by ELISA. As shown in Figure 13C, the levels of TNF-α, IL-6, IL-1β, and MCP-1 in serum were significantly upregulated in the LPS group compared with those in the control group ($p < 0.01$), but the ECH group markedly downregulated the secretion of these pro-inflammatory cytokines ($p < 0.01$).

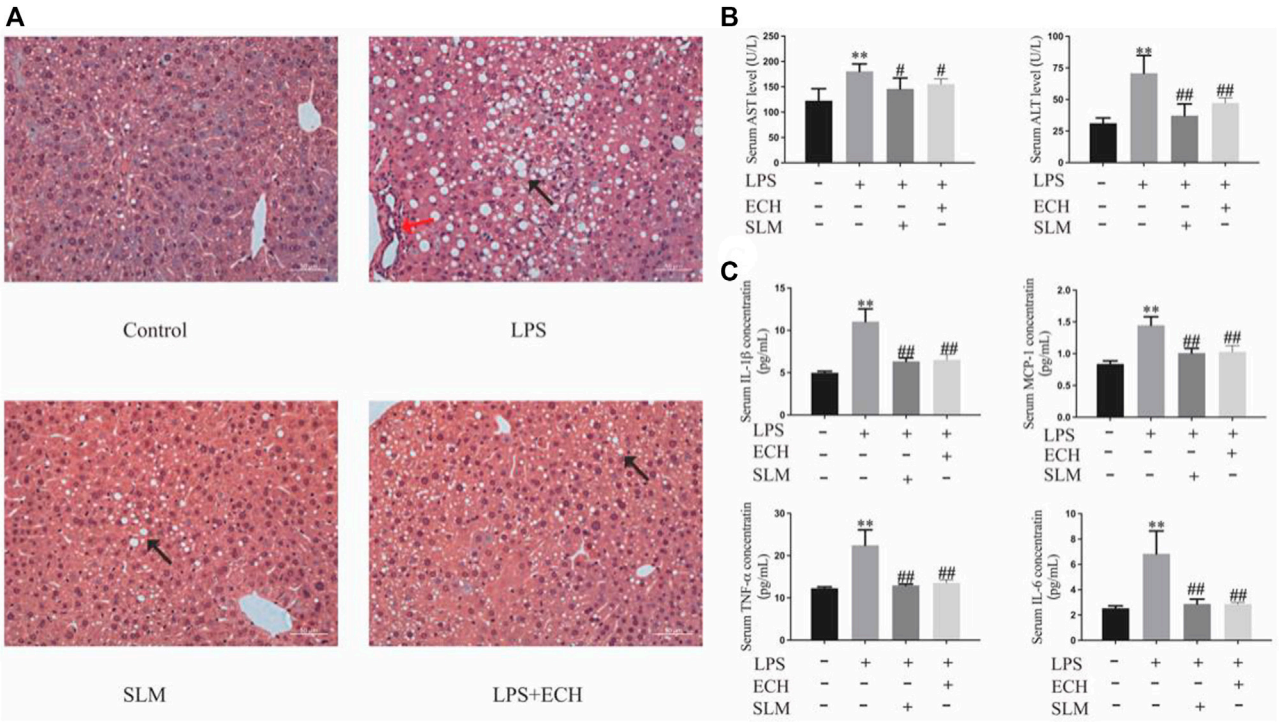

FIGURE 13
Effects of ECH on LPS-induced liver injury. **(A)** H&E staining of liver tissue in each group; **(B)** ALT and AST analysis of the serum; **(C)** serum levels of the inflammatory factors TNF-α, IL-6, IL-1β, and MCP-1. Compared with the control group, $*p < 0.05$ and $**p < 0.01$; in comparison with the LPS group, $^{\#}P < 0.05$ and $\#\#P < 0.01$; all data are presented as mean ± SD (n=4–6/group).

4 Discussion

The inflammatory response is present throughout NAFLD, ranging from nonalcoholic fatty liver to nonalcoholic steatohepatitis (NASH). The inflammatory response has been identified as one of the pathophysiological bases of NAFLD in several studies. Natural products or Chinese herbal medicine are valuable resources for NALFD treatment. Network analysis is an efficient strategy to predict the potential targets of natural products or Chinese herbal medicine (Friedman et al., 2018; Fang et al., 2019; Carpino et al., 2020; Powell et al., 2021). Therefore, the aim of this study was to investigate the hepatoprotective effects of *CD* with network analysis, as well as the *in vitro* and *in vivo* experiments were used to further confirm the results.

First, PhGs have been shown to have good hepatoprotective and immunomodulatory activities (Tian et al., 2021). With the help of the UPLC-Q-TOF/MS/MS technology, we identified the chemical constituents of PhGs in *CD* and further studied their effective components and action mechanism by network analysis. To our knowledge, this is the first report on the integrative strategy of neutral loss and diagnostic ions to identify a total of 34 PhGs from *CD*. Among them, four compounds (compounds 1, 6, 13, and 15) have not been previously reported in *CD*, providing a guide for the identification of other plants of the same genus. Since the PhGs with the same core structure showed the same fragmentation pathway and characteristic fragment ions, we analyzed the fragmentation pathway of typical PhG standards and used the characteristic fragment ions of the standards as diagnostic ions to facilitate the resolution of homologous unknown compounds. Our study not only presented a feasible and generally applicable strategy for the identification of active ingredients in *CD* and other herbal medicines but also laid the foundation for further development and application of PhGs.

Next, we used the 34 components of PhGs identified by UPLC-Q/TOF-MS/MS analysis as candidates for network analysis and a total of 17 active components by database screening for further network analysis. The results of the topological analysis showed that ECH achieved the most targets and that these components were highly correlated with the core targets predicted by NAFLD. Importantly, the levels of nine compounds in the *CD* extract were determined, with ECH having the highest level of 13.45 mg/g. In addition, ECH, as one of the main active components of PhGs, has been well-documented in hepatoprotective studies. For example, Thida et al. (2021). found that ECH attenuated acetaminophen-induced liver injury by reducing oxidative stress and inflammatory cytokines in mice. Li et al. (2014) found that

ECH ameliorated d-galactosamine+LPS-induced acute liver injury in mice by inhibiting apoptosis and inflammation (Pei et al., 2018; Thida et al., 2021). Therefore, we infer that ECH is the most likely chemical component to play a key role in hepatoprotection. PPI network topology analysis revealed the key inflammation-related targets. TNF, IL-6, RELA, IL-1β, and TLR4 are important components in the effect of PhGs on NAFLD. Previous researchers had indicated that inflammatory factors such as IL-6 and TNF-α are associated in the development of NAFLD and critical to reducing the inflammatory response for NAFLD prevention and treatment (Jiang et al., 2016; Hou et al., 2021; Tarantino et al., 2021). Pathway and functional enrichment analyses also suggested that PhGs can exert hepatoprotective effects through modulation of LPS responses and TLR signaling-related pathways. In addition, previous studies had shown that LPS initiated intracellular signaling through binding to cell membrane surface receptors and activated TLR4 to induce downstream inflammatory cytokines (Yuan et al., 2018a; Liu et al., 2018b). Of these, TLR4/NF-κB has been shown to play an important role in liver disease (Henao-Mejia et al., 2012; Miura and Ohnishi, 2014; Carpino et al., 2020; Hu et al., 2020). Therefore, we further used cellular assays to confirm that ECH exerts hepatoprotective effects by inhibiting TLR4/NF-κB activation and attenuating the inflammatory response.

The ELISA, RT-qPCR, and Western blot were used to detect inflammatory factors, and the results showed that both 50 and 100 μM of ECH significantly reduced the expression of TNF-α and IL-6. Tao et al. (2021) found that 25–100 μM of ECH was effective in reducing ethanol-induced lipid accumulation and oxidative damage in HepG2 cells. Ye et al. (2019) found that 20–100 μg/ml of ECH had inhibitory proliferative and pro-apoptotic effects on hepatocellular carcinoma HepG2 cells (Ye et al., 2019; Tao et al., 2021), corresponding to the range of concentrations in this study. Substantial evidence has shown that TLR4 is closely associated with NAFLD (Miura and Ohnishi, 2014; Hu et al., 2020). After RT-qPCR and Western blot analysis, ECH was found to reduce the mRNA and protein level expression of TLR4. The MyD88-dependent TLR4 signaling pathway was activated during NAFLD, leading to rapid activation of NF-κB and the generation of pro-inflammatory mediators such as TNF-α, IL-1β, and IL-6 (Lin et al., 2019; Wang et al., 2020c; Feng et al., 2020; Nishimura et al., 2021; Ye et al., 2021). Reduced levels of TLR4, MyD88, and p-P65 expression were linked to lower levels of pro-inflammatory cytokine production, based on the previous study (Li et al., 2020). In the current study, we observed that a reduction in MyD88, NF-κB, p-P65, and TNF-α expression levels was accompanied by a decrease in inflammatory synthesis after ECH administration treatment. These results suggested that ECH may play a hepatoprotective role by inhibiting the activation of TLR4/NF-κB and alleviating the inflammatory response. These findings demonstrate the protective effect of ECH and its potential to develop hepatoprotective drugs.

ALT and AST are the core biochemical indicators commonly used in the clinical evaluation of liver injury (Yuan et al., 2018b). The serum ALT and AST levels in the mice of the LPS group were significantly higher than those in mice of the control group. ECH significantly reduced the aforementioned biochemical indexes, indicating that LPS successfully established a liver damage model, and ECH has a hepatoprotective effect. H&E pathological sections showed that ECH effectively alleviated liver injury in mice. Pro-inflammatory cytokines are direct indicators reflecting the degree of inflammation (Shah et al., 2018). TNF-α, IL-1β, and IL-6 are typical representatives of multifunctional cytokines, playing an important role in the pathogenesis of acute inflammatory response and liver injury (Liu et al., 2018a). After ECH administration intervention, we found that the secretion of TNF-α, IL-1β, MCP-1, and IL-6 inflammatory factors in the serum of mice was significantly reduced. The *in vivo* experimental index detection showed that ECH could effectively reduce the inflammatory response caused by LPS. However, its specific mechanism has not been elucidated, and we will further study the mechanism of TLR4 and other pathways in the future.

5 Conclusion

A total of 34 PhGs were identified by UPLC-Q/TOF-MS/MS, and we explored the potential hepatoprotective effects of 17 active ingredients by network analysis. Then, the *in vitro* study with the L02 cell model suggested the anti-inflammatory activities and hepatoprotective effects of PhGs. Further *in vitro* experiments found that PhGs had the effect of reducing the NO level, showing a potential anti-inflammatory effect. As the main active component of PhGs, ECH scored highest in network analysis and molecular docking studies. Therefore, we investigated its anti-inflammatory effects through molecular biology experiments. ECH could reduce the expression of inflammatory factors TNF-α and IL-6, as well as decrease LPS-induced *TLR4*, *TNF-α*, and *IL-6* mRNA levels, and inhibit TLR4, MyD88, p-P65, and TNF-α protein expression. These experiments also preliminarily verified that it achieves anti-inflammatory effects through the TLR4/NF-κB signaling pathway. The target competition assay showed that ECH and LPS competitively bound TLR4. Finally, we found that ECH had a hepatoprotective effect on LPS-induced liver injury mice through *in vivo* animal experiments. To sum up, PhGs can be used as anti-inflammatory active components of *CD*, and they play a hepatoprotective role by reducing the inflammatory response. Altogether, the results of this study both explored the anti-inflammatory effect of ECH and provided a novel understanding of the active ingredients and mechanisms of action of herbal medicines. In the long run, it allows the combination of systematic pharmacology with qualitative and quantitative analyses to better grasp the mechanism of herb medicines.

Data availability statement

The datasets presented in this study can be found in online repositories. The names of the repository/repositories and accession number(s) can be found in the article/Supplementary Material.

Ethics statement

The animal study was reviewed and approved by the Experimental Animal Center of Shandong University of Traditional Chinese Medicine.

Author contributions

Conceptualization and methodology, HW and XW; investigation and validation, HW, YYL, and YB; data curation and formal analysis, HW, YYL, YB, and CL; writing—original draft preparation, YW, XL, and KW; writing—review and editing, HW and YYL; supervision, project administration, and funding acquisition, XW and YL.

Funding

This work was supported by the National Natural Science Foundation of China (grant number: 82003917); Natural Science Foundation of Shandong Province (grant number: ZR2020QH323); China Postdoctoral Science Foundation (grant numbers: 2021T140428 and 2020M682228); Shandong Postdoctoral Innovation Project (grant number: 202003028), and Shandong University of Traditional Chinese Medicine undergraduate research training program (grant number: 2021037).

Conflict of interest

The authors declare that the research was conducted in the absence of any commercial or financial relationships that could be construed as a potential conflict of interest.

Publisher's note

All claims expressed in this article are solely those of the authors and do not necessarily represent those of their affiliated organizations, or those of the publisher, the editors, and the reviewers. Any product that may be evaluated in this article, or claim that may be made by its manufacturer, is not guaranteed or endorsed by the publisher.

Supplementary material

The Supplementary Material for this article can be found online at: https://www.frontiersin.org/articles/10.3389/fphar.2022.1018572/full#supplementary-material

References

Albillos, A., de Gottardi, A., and Rescigno, M. (2020). The gut-liver axis in liver disease: Pathophysiological basis for therapy. *J. Hepatol.* 72 (3), 558–577. doi:10.1016/j.jhep.2019.10.003

Burra, P. (2021). Management of complex liver diseases. *Minerva Gastroenterol.* 67 (1), 2–3. doi:10.23736/S2724-5985.20.02803-2

Carpino, G., Del, B. M., Pastori, D., Carnevale, R., Baratta, F., Overi, D., et al. (2020). Increased liver localization of lipopolysaccharides in human and experimental NAFLD. *Hepatology* 72 (2), 470–485. doi:10.1002/hep.31056

Casey, G. (2016). Diseases of the liver. *Nurs. N. Z.* 22 (11), 20–24.

Chalasani, N., Younossi, Z., Lavine, J. E., Charlton, M., Cusi, K., Rinella, M., et al. (2018). The diagnosis and management of nonalcoholic fatty liver disease: Practice guidance from the American Association for the Study of Liver Diseases. *Hepatology* 67 (1), 328–357. doi:10.1002/hep.29367

Chitturi, S., Wong, V. W., Chan, W. K., Wong, G. L., Wong, S. K., Sollano, J., et al. (2018). The asia-pacific working party on non-alcoholic fatty liver disease guidelines 2017-Part 2: Management and special groups. *J. Gastroenterol. Hepatol.* 33 (1), 86–98. doi:10.1111/jgh.13856

Fang, C., Cai, X., Hayashi, S., Hao, S., Sakiyama, H., Wang, X., et al. (2019). Caffeine-stimulated muscle IL-6 mediates alleviation of non-alcoholic fatty liver disease. *Biochim. Biophys. Acta. Mol. Cell Biol. Lipids* 1864 (3), 271–280. doi:10.1016/j.bbalip.2018.12.003

Feng, Z., Pang, L., Chen, S., Pang, X., Huang, Y., Qiao, Q., et al. (2020). Didymin ameliorates dexamethasone-induced non-alcoholic fatty liver disease by inhibiting TLR4/NF-κB and PI3K/Akt pathways in C57BL/6J mice. *Int. Immunopharmacol.* 88, 107003. doi:10.1016/j.intimp.2020.107003

Friedman, S. L., Neuschwander-Tetri, B. A., Rinella, M., and Sanyal, A. J. (2018). Mechanisms of NAFLD development and therapeutic strategies. *Nat. Med.* 24 (7), 908–922. doi:10.1038/s41591-018-0104-9

Gao, H., Cui, Y., Kang, N., Liu, X., Liu, Y., Zou, Y., et al. (2017). Isoacteoside, a dihydroxyphenylethyl glycoside, exhibits anti-inflammatory effects through blocking toll-like receptor 4 dimerization. *Br. J. Pharmacol.* 174 (17), 2880–2896. doi:10.1111/bph.13912

Guo, W., Huang, J., Wang, N., Tan, H. Y., Cheung, F., Chen, F., et al. (2019). Integrating network pharmacology and pharmacological evaluation for deciphering the action mechanism of herbal formula zuojin pill in suppressing hepatocellular carcinoma. *Front. Pharmacol.* 10, 1185. doi:10.3389/fphar.2019.01185

Han, L., Boakye-Yiadom, M., Liu, E., Zhang, Y., Li, W., Song, X., et al. (2012). Structural characterisation and identification of phenylethanoid glycosides from Cistanches deserticola Y.C. Ma by UHPLC/ESI-QTOF-MS/MS. *Phytochem. Anal.* 23 (6), 668–676. doi:10.1002/pca.2371

Hartke, J., Johnson, M., and Ghabril, M. (2017). The diagnosis and treatment of hepatocellular carcinoma. *Semin. Diagn. Pathol.* 34 (2), 153–159. doi:10.1053/j.semdp.2016.12.011

Henao-Mejia, J., Elinav, E., Jin, C., Hao, L., Mehal, W. Z., Strowig, T., et al. (2012). Inflammasome-mediated dysbiosis regulates progression of NAFLD and obesity. *Nature* 482 (7384), 179–185. doi:10.1038/nature10809

Holzgrabe, U., and Malet-Martino, M. (2014). NMR spectroscopy in pharmaceutical and biomedical analysis. *J. Pharm. Biomed. Anal.* 93, 1–2. doi:10.1016/j.jpba.2014.04.007

Hou, X., Yin, S., Ren, R., Liu, S., Yong, L., Liu, Y., et al. (2021). Myeloid-cell-specific IL-6 signaling promotes MicroRNA-223-enriched exosome production to

attenuate NAFLD-associated fibrosis. *Hepatology* 74 (1), 116–132. doi:10.1002/hep.31658

Hu, J., Wang, H., Li, X., Liu, Y., Mi, Y., Kong, H., et al. (2020). Fibrinogen-like protein 2 aggravates nonalcoholic steatohepatitis via interaction with TLR4, eliciting inflammation in macrophages and inducing hepatic lipid metabolism disorder. *Theranostics* 10 (21), 9702–9720. doi:10.7150/thno.44297

Huang, D. Q., El-Serag, H. B., and Loomba, R. (2021). Global epidemiology of NAFLD-related HCC: Trends, predictions, risk factors and prevention. *Nat. Rev. Gastroenterol. Hepatol.* 18 (4), 223–238. doi:10.1038/s41575-020-00381-6

Jia, Y., Guan, Q., Jiang, Y., Salh, B., Guo, Y., Tu, P., et al. (2014). Amelioration of dextran sulphate sodium-induced colitis in mice by echinacoside-enriched extract of Cistanche tubulosa. *Phytother. Res.* 28 (1), 110–119. doi:10.1002/ptr.4967

Jiang, L., Zhou, B., Wang, X., Bi, Y., Guo, W., Wang, J., et al. (2021). The quality monitoring of cistanches herba (Cistanche deserticola ma): A value chain perspective. *Front. Pharmacol.* 12, 782962. doi:10.3389/fphar.2021.782962

Jiang, W., Guo, M. H., and Hai, X. (2016). Hepatoprotective and antioxidant effects of lycopene on non-alcoholic fatty liver disease in rat. *World J. Gastroenterol.* 22 (46), 10180–10188. doi:10.3748/wjg.v22.i46.10180

Jiang, Y., Li, S. P., Wang, Y. T., Chen, X. J., and Tu, P. F. (2009). Differentiation of Herba Cistanches by fingerprint with high-performance liquid chromatography-diode array detection-mass spectrometry. *J. Chromatogr. A* 1216 (11), 2156–2162. doi:10.1016/j.chroma.2008.04.040

Kubes, P., and Jenne, C. (2018). Immune responses in the liver. *Annu. Rev. Immunol.* 36, 247–277. doi:10.1146/annurev-immunol-051116-052415

Lei, H., Wang, X., Zhang, Y., Cheng, T., Mi, R., Xu, X., et al. (2020). Herba Cistanche (rou cong rong): A review of its phytochemistry and pharmacology. *Chem. Pharm. Bull.* 68 (8), 694–712. doi:10.1248/cpb.c20-00057

Li, J., Deng, X., Bai, T., Wang, S., Jiang, Q., and Xu, K. (2020). Resolvin D1 mitigates non-alcoholic steatohepatitis by suppressing the TLR4-MyD88-mediated NF-κB and MAPK pathways and activating the Nrf2 pathway in mice. *Int. Immunopharmacol.* 88, 106961. doi:10.1016/j.intimp.2020.106961

Li, L., Tsao, R., Yang, R., Liu, C., Young, J. C., and Zhu, H. (2008). Isolation and purification of phenylethanoid glycosides from Cistanche deserticola by high-speed counter-current chromatography. *Food Chem.* 108 (2), 702–710. doi:10.1016/j.foodchem.2007.10.082

Li, X., Gou, C., Yang, H., Qiu, J., Gu, T., and Wen, T. (2014). Echinacoside ameliorates D-galactosamine plus lipopolysaccharide-induced acute liver injury in mice via inhibition of apoptosis and inflammation. *Scand. J. Gastroenterol.* 49 (8), 993–1000. doi:10.3109/00365521.2014.913190

Li, Z., Lin, H., Gu, L., Gao, J., and Tzeng, C. M. (2016). Herba Cistanche (rou cong-rong): One of the best pharmaceutical gifts of traditional Chinese medicine. *Front. Pharmacol.* 7, 41. doi:10.3389/fphar.2016.00041

Lin, R., Wu, D., Wu, F. J., Meng, Y., Zhang, J. H., Wang, X. G., et al. (2019). Non-alcoholic fatty liver disease induced by perinatal exposure to bisphenol a is associated with activated mTOR and TLR4/NF-κB signaling pathways in offspring rats. *Front. Endocrinol.* 10, 620. doi:10.3389/fendo.2019.00620

Liu, H., Xu, J., Li, H., Zhang, L., and Xu, P. (2021). Network pharmacology-based investigation to explore the effect and mechanism of Erchen decoction against the nonalcoholic fatty liver disease. *Anat. Rec.* 304 (11), 2605–2619. doi:10.1002/ar.24770

Liu, J., Yang, L., Dong, Y., Zhang, B., and Ma, X. (2018a). Echinacoside, an inestimable natural product in treatment of neurological and other disorders. *Molecules* 23 (5), E1213. doi:10.3390/molecules23051213

Liu, W., Wang, Z., Hou, J. G., Zhou, Y. D., He, Y. F., Jiang, S., et al. (2018b). The liver protection effects of maltol, a flavoring agent, on carbon tetrachloride-induced acute liver injury in mice via inhibiting apoptosis and inflammatory response. *Molecules* 23 (9), E2120. doi:10.3390/molecules23092120

Miura, K., and Ohnishi, H. (2014). Role of gut microbiota and Toll-like receptors in nonalcoholic fatty liver disease. *World J. Gastroenterol.* 20 (23), 7381–7391. doi:10.3748/wjg.v20.i23.7381

Montano, L. M., Sommer, B., Gomez-Verjan, J. C., Morales-Paoli, G. S., Ramirez-Salinas, G. L., Solis-Chagoyan, H., et al. (2022). Theophylline: Old drug in a new light, application in COVID-19 through computational studies. *Int. J. Mol. Sci.* 23 (8), 4167. doi:10.3390/ijms23084167

Morikawa, T., Xie, H., Pan, Y., Ninomiya, K., Yuan, D., Jia, X., et al. (2019). A review of biologically active natural products from a desert plant Cistanche tubulosa. *Chem. Pharm. Bull.* 67 (7), 675–689. doi:10.1248/cpb.c19-00008

Mundi, M. S., Velapati, S., Patel, J., Kellogg, T. A., Abu, D. B., and Hurt, R. T. (2020). Evolution of NAFLD and its management. *Nutr. Clin. Pract.* 35 (1), 72–84. doi:10.1002/ncp.10449

Nishimura, N., Kaji, K., Kitagawa, K., Sawada, Y., Furukawa, M., Ozutsumi, T., et al. (2021). Intestinal permeability is a mechanical rheostat in the pathogenesis of liver cirrhosis. *Int. J. Mol. Sci.* 22 (13), 6921. doi:10.3390/ijms22136921

Pei, W., Guo, R., Zhang, J., and Li, X. (2018). Extraction of phenylethanoid glycosides from Cistanche tubulosa by high-speed shearing homogenization extraction. *J. Aoac Int.* 102, 63–68. doi:10.5740/jaoacint.18-0039

Powell, E. E., Wong, V. W., and Rinella, M. (2021). Non-alcoholic fatty liver disease. *Lancet* 397 (10290), 2212–2224. doi:10.1016/S0140-6736(20)32511-3

Price, J. C., and Tien, P. C. (2017). Editorial: Statins and liver disease: Is it time to recommend statins to prevent liver disease progression? *Am. J. Gastroenterol.* 112 (10), 1506–1507. doi:10.1038/ajg.2017.250

Sauter, K. S., Brcic, M., Franchini, M., and Jungi, T. W. (2007). Stable transduction of bovine TLR4 and bovine MD-2 into LPS-nonresponsive cells and soluble CD14 promote the ability to respond to LPS. *Vet. Immunol. Immunopathol.* 118 (1-2), 92–104. doi:10.1016/j.vetimm.2007.04.017

Shah, K. N., Valand, P., Nauriyal, D. S., and Joshi, C. G. (2018). Immunomodulation of IL-1, IL-6 and IL-8 cytokines by Prosopis juliflora alkaloids during bovine sub-clinical mastitis. *3 Biotech.* 8 (10), 409. doi:10.1007/s13205-018-1438-1

Sim, H. W., and Knox, J. (2018). Hepatocellular carcinoma in the era of immunotherapy. *Curr. Probl. Cancer* 42 (1), 40–48. doi:10.1016/j.currproblcancer.2017.10.007

Song, X., Zhang, Y., Dai, E., Wang, L., and Du, H. (2020). Prediction of triptolide targets in rheumatoid arthritis using network pharmacology and molecular docking. *Int. Immunopharmacol.* 80, 106179. doi:10.1016/j.intimp.2019.106179

Tao, Z., Zhang, L., Wu, T., Fang, X., and Zhao, L. (2021). Echinacoside ameliorates alcohol-induced oxidative stress and hepatic steatosis by affecting SREBP1c/FASN pathway via PPARα. *Food Chem. Toxicol.* 148, 111956. doi:10.1016/j.fct.2020.111956

Tarantino, G., Balsano, C., Santini, S. J., Brienza, G., Clemente, I., Cosimini, B., et al. (2021). It is high time physicians thought of natural products for alleviating NAFLD. Is there sufficient evidence to use them? *Int. J. Mol. Sci.* 22 (24), 13424. doi:10.3390/ijms222413424

Thida, M., Li, B., Zhang, X., Chen, C., and Zhang, X. (2021). Echinacoside alleviates acetaminophen-induced liver injury by attenuating oxidative stress and inflammatory cytokines in mice. *J. Appl. Biomed.* 19 (2), 105–112. doi:10.32725/jab.2021.011

Tian, D., Yang, Y., Yu, M., Han, Z. Z., Wei, M., Zhang, H. W., et al. (2020). Anti-inflammatory chemical constituents of Flos Chrysanthemi Indici determined by UPLC-MS/MS integrated with network pharmacology. *Food Funct.* 11 (7), 6340–6351. doi:10.1039/d0fo01000f

Tian, X. Y., Li, M. X., Lin, T., Qiu, Y., Zhu, Y. T., Li, X. L., et al. (2021). A review on the structure and pharmacological activity of phenylethanoid glycosides. *Eur. J. Med. Chem.* 209, 112563. doi:10.1016/j.ejmech.2020.112563

Troelstra, A., Antal-Szalmas, P., de Graaf-Miltenburg, L. A., Weersink, A. J., Verhoef, J., Van Kessel, K. P., et al. (1997). Saturable CD14-dependent binding of fluorescein-labeled lipopolysaccharide to human monocytes. *Infect. Immun.* 65 (6), 2272–2277. doi:10.1128/iai.65.6.2272-2277.1997

Wang, L., Jia, Z., Wang, B., and Zhang, B. (2020a). Berberine inhibits liver damage in rats with non-alcoholic fatty liver disease by regulating TLR4/MyD88/NF-κB pathway. *Turk. J. Gastroenterol.* 31 (12), 902–909. doi:10.5152/tjg.2020.19568

Wang, L., Li, H., Shen, X., Zeng, J., Yue, L., Lin, J., et al. (2020b). Elucidation of the molecular mechanism of Sanguisorba Officinalis L. against leukopenia based on network pharmacology. *Biomed. Pharmacother.* 132, 110934. doi:10.1016/j.biopha.2020.110934

Wang, Y., Yang, S. H., Zhong, K., Jiang, T., Zhang, M., Kwan, H. Y., et al. (2020c). Network pharmacology-based strategy for the investigation of the anti-obesity effects of an ethanolic extract of zanthoxylum bungeanum maxim. *Front. Pharmacol.* 11, 572387. doi:10.3389/fphar.2020.572387

Xiao, J., Wang, F., Wong, N. K., He, J., Zhang, R., Sun, R., et al. (2019). Global liver disease burdens and research trends: Analysis from a Chinese perspective. *J. Hepatol.* 71 (1), 212–221. doi:10.1016/j.jhep.2019.03.004

Xu, G., Lv, X., Feng, Y., Li, H., Chen, C., Lin, H., et al. (2021a). Study on the effect of active components of Schisandra chinensis on liver injury and its mechanisms in mice based on network pharmacology. *Eur. J. Pharmacol.* 910, 174442. doi:10.1016/j.ejphar.2021.174442

Xu, J., Shen, J., Yuan, R., Jia, B., Zhang, Y., Wang, S., et al. (2021b). Mitochondrial targeting therapeutics: Promising role of natural products in non-alcoholic fatty liver disease. *Front. Pharmacol.* 12, 796207. doi:10.3389/fphar.2021.796207

Xu, Y., Guo, W., Zhang, C., Chen, F., Tan, H. Y., Li, S., et al. (2020). Herbal medicine in the treatment of non-alcoholic fatty liver diseases-efficacy, action

mechanism, and clinical application. *Front. Pharmacol.* 11, 601. doi:10.3389/fphar.2020.00601

Ye, M., Tang, Y., He, J., Yang, Y., Cao, X., Kou, S., et al. (2021). Alleviation of non-alcoholic fatty liver disease by Huazhi Fugan Granules is associated with suppression of TLR4/NF-κB signaling pathway. *Clin. Investig. Arterioscler.* 33 (5), 257–266. doi:10.1016/j.arteri.2020.12.007

Ye, Y., Song, Y., Zhuang, J., Wang, G., Ni, J., and Xia, W. (2019). Anticancer effects of echinacoside in hepatocellular carcinoma mouse model and HepG2 cells. *J. Cell. Physiol.* 234 (2), 1880–1888. doi:10.1002/jcp.27063

Yin, X., Qiu, Y., Li, Z., Guo, L., Wei, H., Liu, B., et al. (2021). Longdan Xiegan Decoction alleviates experimental autoimmune uveitis in rats by inhibiting Notch signaling pathway activation and Th17 cell differentiation. *Biomed. Pharmacother.* 136, 111291. doi:10.1016/j.biopha.2021.111291

Yuan, Q., Zhang, D., Liu, C., Zhang, C., and Yuan, D. (2018a). Chikusetsusaponin V inhibits LPS-activated inflammatory responses via SIRT1/NF-κB signaling pathway in RAW264.7 cells. *Inflammation* 41 (6), 2149–2159. doi:10.1007/s10753-018-0858-8

Yuan, R., Tao, X., Liang, S., Pan, Y., He, L., Sun, J., et al. (2018b). Protective effect of acidic polysaccharide from Schisandra chinensis on acute ethanol-induced liver injury through reducing CYP2E1-dependent oxidative stress. *Biomed. Pharmacother.* 99, 537–542. doi:10.1016/j.biopha.2018.01.079

Zhang, L., Yao, Z., and Ji, G. (2018). Herbal extracts and natural products in alleviating non-alcoholic fatty liver disease via activating autophagy. *Front. Pharmacol.* 9, 1459. doi:10.3389/fphar.2018.01459

Zhang, R., Zhu, X., Bai, H., and Ning, K. (2019). Network pharmacology databases for traditional Chinese medicine: Review and assessment. *Front. Pharmacol.* 10, 123. doi:10.3389/fphar.2019.00123

Zhang, S., Wong, Y. T., Tang, K. Y., Kwan, H. Y., and Su, T. (2020). Chinese medicinal herbs targeting the gut-liver Axis and adipose tissue-liver Axis for non-alcoholic fatty liver disease treatments: The ancient wisdom and modern science. *Front. Endocrinol.* 11, 572729. doi:10.3389/fendo.2020.572729

Zhang, Z. N., Hui, Z., Chen, C., Liang, Y., Tang, L. L., Wang, S. L., et al. (2021). Neuroprotective effects and related mechanisms of echinacoside in MPTP-induced PD mice. *Neuropsychiatr. Dis. Treat.* 17, 1779–1792. doi:10.2147/NDT.S299685

Zheng, S., Yang, Y., Wen, C., Liu, W., Cao, L., Feng, X., et al. (2021). Effects of environmental contaminants in water resources on nonalcoholic fatty liver disease. *Environ. Int.* 154, 106555. doi:10.1016/j.envint.2021.106555

Zhou, W., Lai, X., Wang, X., Yao, X., Wang, W., and Li, S. (2021). Network pharmacology to explore the anti-inflammatory mechanism of Xuebijing in the treatment of sepsis. *Phytomedicine.* 85, 153543. doi:10.1016/j.phymed.2021.153543

frontiers | Frontiers in Pharmacology

TYPE Original Research
PUBLISHED 13 October 2022
DOI 10.3389/fphar.2022.989995

OPEN ACCESS

EDITED BY
Guangyue Su,
Shenyang Pharmaceutical University, China

REVIEWED BY
Daqian Wan,
Tongji Hospital Affiliated to Tongji University, China
Kuo Zhang,
Shenyang Pharmaceutical University, China

*CORRESPONDENCE
Jian Gu,
gujiancd@163.com
Yan Wu,
wuyan1219@yeah.net

SPECIALTY SECTION
This article was submitted to Ethnopharmacology, a section of the journal Frontiers in Pharmacology

RECEIVED 09 July 2022
ACCEPTED 27 September 2022
PUBLISHED 13 October 2022

CITATION
Gong P, Yin K, Luo X, Gu J, Tan R, Wu Y and Li D (2022), Tandem mass tag-based proteomics analysis reveals the multitarget mechanisms of Phyllanthus emblica against liver fibrosis. *Front. Pharmacol.* 13:989995. doi: 10.3389/fphar.2022.989995

Tandem mass tag-based proteomics analysis reveals the multitarget mechanisms of *Phyllanthus emblica* against liver fibrosis

Puyang Gong[1], Kehuan Yin[1], Xiaomin Luo[1], Jian Gu[1]*, Rui Tan[2], Yan Wu[3]* and Dapeng Li[4]

[1]College of Pharmacy, Southwest Minzu University, Chengdu, China, [2]College of Life Science and Engineering, Southwest Jiaotong University, Chengdu, China, [3]College of Pharmacy, Shenzhen Technology University, Shenzhen, China, [4]West China School of Pharmacy, Sichuan University, Chengdu, China

Phyllanthus emblica (PE), a traditional multiethnic herbal medicine, is commonly applied to treat liver diseases. Our previous study demonstrated that aqueous extract of PE (AEPE) could alleviate carbon tetrachloride (CCl_4)-induced liver fibrosis *in vivo*, but the underlying molecular mechanisms are still unclear. The present study was undertaken to clarify the multitarget mechanisms of PE in treating liver fibrosis by proteomics clues. A CCl_4-induced liver fibrosis rat model was established. The anti-liver fibrosis effects of chemical fractions from AEPE were evaluated by serum biochemical indicators and pathological staining. Additionally, tandem mass tag (TMT) -based quantitative proteomics technology was used to detect the hepatic differentially expressed proteins (DEPs). The Kyoto Encyclopedia of Genes and Genomes (KEGG) pathway enrichment, gene ontology (GO) enrichment and protein-protein interaction (PPI) network were used to perform bioinformatics analysis of DEPs. Western blot analysis was used to verify the key potential targets regulated by the effective fraction of AEPE. The low-molecular-weight fraction of AEPE (LWPE) was determined to be the optimal anti-liver fibrosis active fraction, that could significantly improve ALT, AST, HA, Col IV, PCIII, LN, Hyp levels and reduce the pathological fibrotic lesion of liver tissue in model rats. A total of 195 DEPs were screened after LWPE intervention. GO analysis showed that the DEPs were related mostly to extracellular matrix organization, actin binding, and extracellular exosomes. KEGG pathway analysis showed that DEPs are mainly related to ECM-receptor interactions, focal adhesion and PI3K-Akt signaling pathway. Combined with the GO, KEGG

Abbreviations: AEPE, the aqueous extract of PE; ALT, alanine aminotransferase; AST, aspartate aminotransferase; DEPs, differentially expressed proteins; ECM, extracellular matrix; ELISA, enzyme-linked immunosorbent assay; FC, fold change; GO, gene ontology; HA, hyaluronic acid; H&E, hematoxylin and eosin; HWPE, high molecular weight fraction of AEPE; HSC, hepatic stellate cell; Hyp, hydroxyproline; IV-C, collagen IV; KEGG, Kyoto Encyclopedia of Genes and Genomes; LF, liver fibrosis LN, lamininLWPE, low molecular weight fraction of AEPE; PCIII, type III precollagen; PDGF, platelet-derived growth factor; PE, phyllanthus emblica; TGF-β1, transforming growth factor-β1; TMT, tandem mass tag; WB, western blot.

and Western blot results, COL1A2, ITGAV, TLR2, ACE, and PDGFRB may be potential targets for PE treatment of liver fibrosis. In conclusion, LWPE exerts therapeutic effects through multiple pathways and multiple targets regulation in the treatment of liver fibrosis. This study may provide proteomics clues for the continuation of research on liver fibrosis treatment with PE.

KEYWORDS

***Phyllanthus emblica*, liver fibrosis, TMT-based proteomics, multi-target mechanism, differentially expressed proteins**

1 Introduction

Hepatic fibrosis, as a crucial pathological feature, exists in almost all chronic liver diseases triggered by hepatitis virus, alcoholism, cholestasis and lipodystrophy, etc (Shang et al., 2022). Without appropriate therapy, hepatic fibrosis could further deteriorate into cirrhosis, portal hypertension and hepatocellular carcinoma (Anuja et al., 2018). Hepatic fibrosis threatens nearly 2% of the worldwide population and leads to more than one million deaths each year (Qiao et al., 2020). To date, there are still no available drugs approved for the clinical treatment of liver fibrosis (Shi et al., 2020). The development of liver fibrosis comprises mainly inflammation, oxidative stress, hepatic stellate cell (HSC) activation, extracellular matrix (ECM) deposition and formation of fibrillar scar matrix (Qiao et al., 2020). In view of the complicated and dynamic physiopathological mechanism of liver fibrosis, the development of comprehensive medications is urgently needed. Fortunately, traditional Chinese medicine (TCM) has advantages in the treatment of liver fibrosis due to its multiple components and multiple targets (Shan et al., 2019).

Phyllanthus emblica L. (PE), an edible and medicinal dual-purpose plant, belongs to the Euphorbiaceae family which is widely distributed in China, India, Nepal and Malaysia (Muthuraman et al., 2011; Sripanidkulchai and Junlatat, 2014). The fruits of PE first used as a traditional Chinese medicinal material were documented in '*Xin xiu ben cao*' (Newly Revised Materia Medica) in the Tang Dynasty (Huang et al., 2021). PE possesses the traditional efficacies of clearing heat and cooling blood, eliminating food and invigorating the stomach, generating body fluid and relieving cough, and used for treating blood heat, blood stasis and indigestion (Wang et al., 2019). Blood heat and stasis are the main pathogenesis of liver fibrosis according to the theory of TCM (Zhao et al., 2022). Hence, the traditional efficacies of PE are consistent with the basic principle of TCM for the treatment of liver fibrosis. PE was consisted in many herbal medicine compounds for treating the hepatic fibrosis such as *Fuzheng Rougan* formulae (Liu et al., 2014). Furthermore, Tibetans, Uygurs, Mongolians and other ethnic groups in China also use PE to treat blood fever and hepatobiliary diseases (Zhu et al., 2015).

Many modern pharmacological studies have substantiated that PE extract and its active compounds exhibit excellent hepatoprotective effects on various biological models of liver diseases (Yin et al., 2022). Previous studies have shown that PE extract could inhibit the activation of HSC-T6 cells induced by leptin *in vitro* (Lu et al., 2016), and reverse the pathological changes of early liver fibrosis induced by carbon tetrachloride (CCl_4) and thioacetamide *in vivo* (Tasduq et al., 2005; Mir et al., 2007). Our previous study have also demonstrated that the aqueous extract of PE (AEPE) could alleviate CCl_4 induced liver fibrosis through antioxidant and anti-inflammatory effects, inhibiting stellate cell activation and reducing the extracellular matrix (Yin et al., 2021). These evidences suggested that PE may be a potential source of multitarget anti-hepatic fibrosis combination drugs. Importantly, the multitarget mechanism of PE against hepatic fibrosis should be elucidated first.

A great number of protein molecules will be changed in regard to quantity and quality in the development of liver fibrosis (Zardi et al., 2008). Thus, high throughput proteomics combined with bioinformatics for data mining provides a preferable method for large-scale screening and identification of differential proteins for disease, and to predict targets and mechanisms of drugs (Yuan et al., 2020). Tandem mass tag (TMT) - based proteomics is an *in vitro* peptide labelling quantitative technique, that can react with amino labelling, and simultaneously achieve the qualitative and quantitative characterization of multiple sample proteomics through high-precision mass spectrometry analysis. Due to the high repeatability and high sensitivity of the method, it has become one of the most popular proteomic methods for finding biomarkers and screening disease targets (Lan et al., 2021; Yu et al., 2021).

In this study, a rat model of liver fibrosis was established by injection with CCl_4, and the active chemical fraction of AEPE was determined. Further, differentially expressed proteins (DEPs) in liver tissue were analyzed by TMT-based quantitative proteomics. The key targets and underlying mechanisms of regulation by the active fraction of AEPE were explored by bioinformatics analysis. In addition, the key target proteins were verified by Western blotting (Figure 1). The results provide more ideas for the mechanism and targets of PE in the treatment of liver fibrosis.

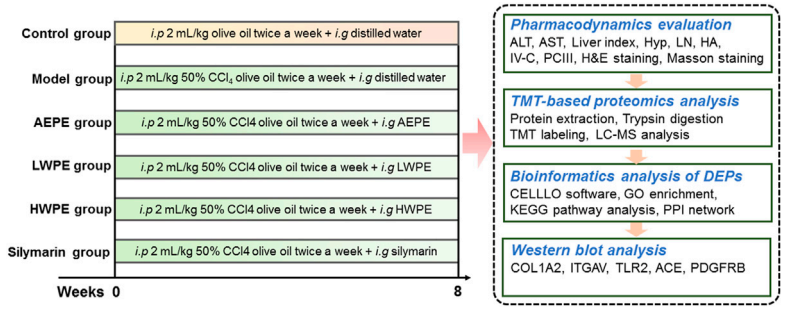

FIGURE 1
Overview of the experimental design of proteomics.

2 Materials and methods

2.1 Chemicals and reagents

Olive oil was obtained from Sigma-Aldrich (St. Louis, MO, United States). CCl_4 was purchased from Shanghai Macklin Biochemical Co., Ltd (Shanghai, China). Silymarin was bought from Madaus (Cologne, Germany). Biochemical assay kits for alanine aminotransferase (ALT), aspartate aminotransferase (AST) and Hydroxyprolin (Hyp) were provided by Institute of Jiancheng Bioengineering (Nanjing, China). Enzyme-linked Immunosorbent Assay (ELISA) and BCA protein quantification kits were obtained by Shanghai Enzyme Link Biotechnology Co., Ltd (Shanghai, China). Rabbit anti-rat polyclonal antibody glyceraldehyde-3-phosphate dehydrogenase (GAPDH), integrin subunit alpha V (ITGAV), platelet derived growth factor receptor beta (PDGFRB), toll-like receptor 2 (TLR2) were purchased from Affinity Biosciences (Changzhou, China). Rabbit anti-rat polyclonal antibody collagen type I alpha 2 chain (COL1A2) and angiotensin I converting enzyme (ACE) were purchased from Beijing Biosynthetic Biotechnology Co., Ltd (Beijing, China) and Wuhan Service biotechnology Co., Ltd (Wuhan, China), respectively. Goat anti-rabbit fluorescently-labeled secondary antibody was purchased from Multi sciences biotechnology Co., Ltd (Shanghai, China).

2.2 Preparation of test drugs

The AEPE and its fractions samples were prepared using the same batch of dried PE fruit (voucher specimens no. 20201212) as in our previous study (Yin et al., 2021; Luo et al., 2022). Briefly, 2000 g of PE was powdered and immersed in distilled water on a rotary shaker for 24 h at a mass ratio of 1:10 at 37°C. Then, the extract was filtered and concentrated to 2000 ml. The 1000 ml extract was precipitated by adding 4 volumes of anhydrous ethanol. The supernatant was concentrated to 1 g (crude drug)/ml to obtain the low-molecular-weight fraction of AEPE (termed LWPE). The resulting precipitate was lyophilized and the high-molecular weight fraction of AEPE (termed HWPE) was obtained. In our previous studies, the main chemical ingredients in AEPE were quantified by high-performance liquid chromatography (HPLC) and the content of crude polysaccharides in HWPE was determined by phenol-sulfuric acid method (Yin et al., 2021; Luo et al., 2022).

2.3 Quantitative analysis of low-molecular-weight fraction of AEPE by high-performance liquid chromatography

The contents of gallic acid and methyl gallate were detected by an Agilent 1260 liquid chromatograph system. The chromatographic separation was performed on a Kromasil 100-5-C_{18} (4.6 × 150mm) column at 37°C.The mobile phase consisted of water containing 0.1% formic acid (solvent A) and acetonitrile (solvent B). The linear gradient elution was as follows: 0–5 min, 3% B; 5–10 min, 3%–4% B; 10–20 min, 4%–12% B; 20–35 min, 12% B; 35–38 min, 12%–18% B; 38–55 min, 18%–40% B. The injection volume was 5 µl. The flow rate was 0.6 ml/min and the wave length was set at 254 nm.

2.4 Animals treatment

Male Wistar rats (180–220 g) were obtained from SPF (Beijing) Biotechnology Co., Ltd (Beijing, China). The animals received food and water allodially and were housed five per cage under well-controlled conditions (12 h light-dark cycle, room temperature 22.0 ± 2°C and room relative humidity 50%–60%) for 1 week for environment adaption. All experimental

procedures were audited and approved by the animal ethics committee of Southwest Minzu University (No. 2021-22).

The rats were randomized into the following six groups (10 rats in each group): the control group, model group, AEPE group, LWPE group, HWPE group and silymarin group. The control group received intraperitoneally injected olive oil at a dose of 2 ml/kg twice each week for eight successive weeks, while the rats in the other groups received 2 ml/kg 50% CCl_4 olive oil. The silymarin group was gavaged daily with 42 mg/kg silymarin aqueous solution. AEPE, LWPE and HWPE aqueous solutions were administered intragastrically to the rats. The dosages of AEPE, LWPE and HWPE were equivalent to their contents in 1.8 g (crude herb)/kg, which was the optimal dose obtained from our previous experiments (Yin et al., 2021). At the end of the 8th week, all rats were anaesthetized with ether, and blood and liver samples were collected for subsequent examination.

2.5 Serum biochemical analyses

The levels of ALT and AST in serum were analyzed by commercially available kits according to the manufacturer's instructions.

2.6 Detection of liver fibrosis biomarkers and hydroxyproline contents

Serum content of HA, LN, IV-C, and PCIII was measured by ELISA. The level of Hyp in each liver tissue was analyzed with the alkaline hydrolysis method by commercial kit.

2.7 Liver histological examination

The liver tissues were fixed with 4% paraformaldehyde, dehydrated, embedded in paraffin, and 4-μm-thick sections were stained with hematoxylin-eosin (H&E) for histopathological evaluation. The severity of fibrosis was evaluated according to the criteria of Liu et al. (2006). Furthermore, Masson staining was applied to observe the changes of collagen deposition in liver tissue.

2.8 Tandem mass tag quantitative proteomics

2.8.1 Protein extraction

Nine liver tissue samples (3 samples per group) collected from the control group, model group, and LWPE group were powdered in liquid nitrogen. The samples were mixed with SDT buffer, then homogenized using an MP homogenizer (24 × 2, 6.0 M/S, 60 s, twice). The homogenate was sonicated by a high-intensity ultrasonic processor and further boiled for 15 min. Next, the samples were centrifuged at 14,000 *g* for 40 min (Wang et al., 2020). The supernatant was collected and filtered with 0.22 μm filters, and the protein concentration of the filtrates was detected by a BCA kit (Zhu et al., 2014).

2.8.2 Trypsin digestion and tandem mass tag labeling

The experimental procedure of this section referred to the literature of Wisniewski et al. (2009). For each sample, 0.2 mg of protein was mixed with 30 μl SDT buffer. Ultrafiltration (Microcon units, 10 kD) was performed to remove the DTT, detergent and other small molecule ingredients using UA buffer (8 M urea, 150 mM Tris-HCl pH 8.0). Then, 100 μL iodoacetamide (100 mM IAA in UA buffer) was added to the sample to intercept reduced cysteine residues, and the sample was incubated in darkness for 0.5 h. The filters were washed three times with 100 μl UA buffer and 100 μl 100 mM TEAB buffer twice. Ultimately, the protein suspensions were digested with 4 μg trypsin in 40 μl TEAB (1:10) buffer at 37°C overnight. According to the calculation of the frequency of tryptophan and tyrosine in vertebrate proteins, the peptide content was estimated by UV spectral density at 280 nm with an extinction coefficient of 1.1 in a 0.1% (g/L) solution. Then, 100 μg of peptide mixture from each sample was labelled according to the instructions of a commercial TMT kit (Thermo Fisher Scientific, United States).

2.8.4 High pH reversed-phase fractionation and LC-MS analysis

TMT-labelled peptides were fractionated into 10 fractions through an incremental acetonitrile step-gradient elution according to the instructions of the Pierce high pH reversed-phase fractionation kit (Thermo scientific, United States). Each fraction was injected for nano liquid chromatography tandem mass spectrometry (LC-MS/MS) analysis performed on an EASY nLC and Q Exactive mass spectrometer (Thermo scientific, United States). Formic acid in 0.1% aqueous solution was used as buffer A, and 0.1% formic acid acetonitrile aqueous solution (84% acetonitrile) was used as buffer B. The samples were separated on a trap column (Thermo, 100 μm × 2 cm) connected to a C_{18} reversed-phase analytical column (Thermo, 75 μm × 10 cm). The flow rate was 300 nl/min. The liquid phase gradient was set as follows: 0–55% buffer B for 80 min, 55–100% buffer B for 5 min, and 100% buffer B for 5 min. On-line mass spectrometry analysis was performed by a Q Exactive mass spectrometer in positive ion mode. The normalized collision energy was 30 eV. The scanning range was 300–1800 m/*z*. The automatic gain control target was set

to 3e6, and the maximum injection time was set to 10 milliseconds. The dynamic exclusion time was 40.0 s.

2.8.6 Database searching

The MASCOT engine version 2.2 embedded into Proteome Discoverer 1.4 software was applied for identification and quantitation analysis of MS raw data of samples. Ensembl_Rattus_29107_20200311. fasta was used as the database. Trypsin was specified as the cleavage enzyme, and the number of missed cleavage sites was 2. The mass error tolerance of the first-level search precursor ion was ±20 ppm; the mass error tolerance of the second-level fragment ion was 0.02 Da. The peptide false discovery rate (FDR) was adjusted to ≤0.01.

2.8.7 Bioinformatics analysis

DEPs were subjected to multiple bioinformatic analyses. Gene Ontology (GO) annotation and Kyoto Encyclopedia of Genes and Genomes (KEGG) pathways enrichment analysis was performed using Database for Annotation, Visualization and Integrated Discovery (DAVID) Bioinformatics Resources (https://david.ncifcrf.gov). The potential protein-protein interactions (PPI) were analyzed *via* the STRING database (https://string-db.org) and CytoScape 3.9.0 software.

2.9 Western blot analysis

Frozen liver tissues were washed 3 times with phosphate buffered saline (PBS), cut into pieces and placed in 10 times the amount of frozen radioimmunoprecipitation assay (RIPA) lysis buffer to prepare tissue homogenates. Then, the protein concentration was determined with a BCA quantification kit. The proteins were separated on sodium dodecyl sulfate-polyacrylamide gel electrophoresis (SDS-PAGE) gel and then transferred to polyvinylidene fluoride membranes. The membrane was blocked with 5% skim milk (prepared with TBST) at room temperature for 60 min and then incubated overnight with rabbit monoclonal antibody (1:1000) at 4°C. After washing 3 times (5 min each time) with TBST, the membranes were incubated with goat antirabbit IgG (1:10000) for 1 h. Finally, enhanced chemiluminescence (ECL) solution was added to adjust the exposure conditions, and images were captured under the chemiluminescence imaging system.

2.10 Statistical analysis

Experimental data are presented as the mean ± standard error of the mean (S.E.M). The multiple comparisons were analyzed by one-way analysis of variance (ANOVA) followed by Dunnett's post-hoc test by GraphPad Prism 9.0 software. A p value <0.05 was the significance threshold.

3 Results

3.1 Phytochemical investigation

The gallic acid and methyl gallate in LWPE were identified and quantified by HPLC, which presenting chromatographic peaks at retention times of 7.207 min for gallic acid and 23.297 min for methyl gallate (Figure 2). Quantifications were carried out by using six-point regression curves of gallic acid (y = 11921 + 828.68, r^2 = 0.9995) and methyl gallate (y = 12752 + 36.651, r^2 = 0.9999). The contents of gallic acid and methyl gallate in LWPE were 14.06 and 3.71 mg/ml, respectively.

3.2 Effects of aqueous extract of PE and its fractions on hepatic lesions in rats administered with carbon tetrachloride

H&E staining and serum biochemical analysis were performed to explore the protective effect of AEPE and its fractions on liver injury induced by CCl_4. As shown in Figure 3A, liver tissues in the control group exhibited natural lobular architecture and cellular structure, and no appreciable pathological changes were observed. In contrast, the model group showed severe hepatocyte swelling and necrosis, lymphocyte infiltration, steatosis and fibrous septum. In the AEPE, LWPE and silymarin groups, the abnormal histological alterations were markedly reduced. Meanwhile, the average severity scores for liver fibrosis in rats treated with AEPE, LWPE and silymarin were significantly lowered compared to CCl_4 controls ($p < 0.05$) (Figure 3B). However, HWPE showed no obvious influences on hepatic histological changes.

Additionally, after treatment with CCl_4, the rat liver was congested and enlarged. As shown in Figure 3C, the increased liver index of the model rat was decreased after AEPE and LWPE treatment ($p < 0.01$). The measurement results of serum biochemical markers are shown in Figure 3D; and Figure 3E. The levels of serum ALT and AST in the model group were significantly higher than the levels of serum ALT and AST in the control group ($p < 0.01$), but decreased following AEPE, LWPE or silymarin treatment ($p < 0.01$). Nevertheless, significant variation of ALT levels was not observed in the HWPE group compared to the model rats.

3.3 Effects of aqueous extract of PE and its fractions on liver fibrosis in rats administered with carbon tetrachloride

Collagen is one of the main components of the ECM, which leads to the development of hepatic fibrosis (Zhang et al., 2020). Hence, collagen deposition in liver tissue was examined by Masson's trichrome staining. As shown in Figure 4A, obvious collagen

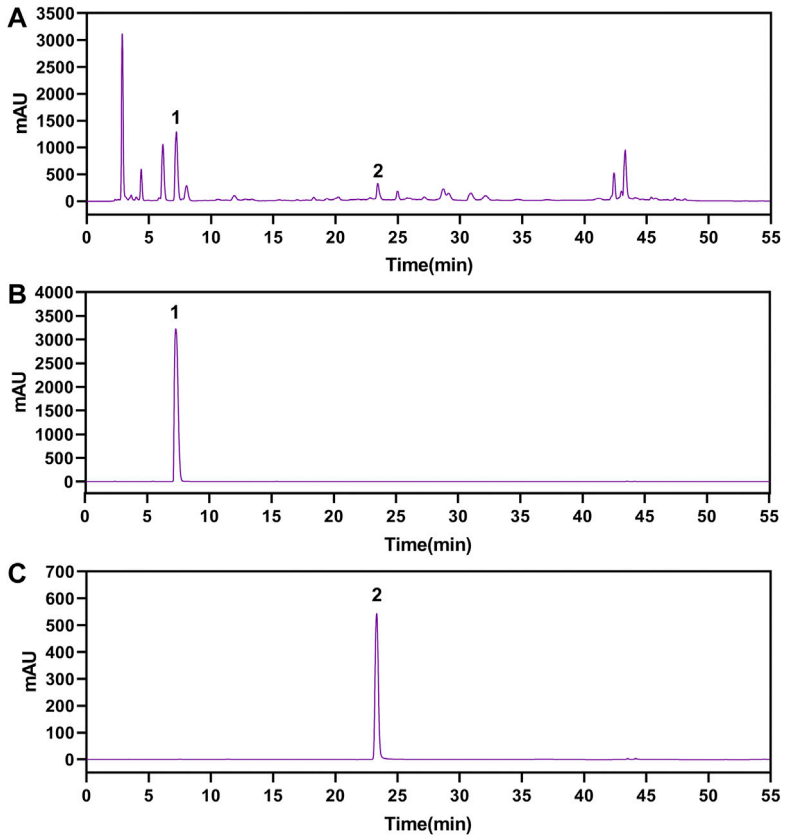

FIGURE 2
The HPLC chromatograms of LWPE **(A)**, gallic acid **(B)** and methyl gallate **(C)**.

accumulation intersected at multiple portal areas in the model group, and pseudo lobule formation was also observed. Collagen deposition was reduced after treatment with AEPE, LWPE or silymarin. The fibrosis area of liver sections in the model group was significantly increased compared to the control group, but decreased in the test drug groups except the HWPE group ($p < 0.01$, Figure 4B). As a unique amino acid in collagen fibers, the Hyp content of liver tissue in the model group was significantly higher than that in the control group, but decreased in the AEPE, LWPE, HWPE and silyamrin groups ($p < 0.05$, Figure 4C).

Meanwhile, the serum biomarkers of fibrogenesis including LN, HA, IV-C, and PCIII were further detected by ELISA, and the results are displayed in Table 1. The levels of these indexes were significantly increased in rat serum after treatment with CCl_4 ($p < 0.01$). Compared with the model group, the levels of LN, NA, PCIII, and IV-C in serum were decreased significantly after treatment with AEPE and LWPE ($p < 0.05$). However, there was no significant difference in the four indicators between the model rat and the HWPE group ($p > 0.05$).

These results indicated that the anti-hepatic fibrosis active ingredients exist mainly in the low molecular weight fraction of the PE water extract, that is, the LWPE fraction. Therefore, the LWPE group was selected for in-depth proteomic analysis to elucidate the multitarget mechanism of PE against hepatic fibrosis.

3.4 Tandem mass tag-based proteomics analysis of liver tissue

A total of 65457 unique peptides and 7550 proteins were detected by TMT quantitative proteomics. Of these proteins, 7525 were quantified (Figure 5A). The relative changes in proteins are visualized in Figures 5B–D. Based on the cutoff value of a 1.2-fold change, in the Model/Control group, 1172 proteins were upregulated and 1310 proteins were downregulated (Supplementary Table S1). In the LWPE/Model group, 281 DEPs (74 upregulated and 207 downregulated) were identified. Importantly, 165 upregulated DEPs in the Model/Control group were downregulated in the LWPE/Model group, and 30 downregulated DEPs in the Model/Control group were upregulated in the LWPE/Model group (Figure 5E). The details of 195 DEPs that were reversely regulated by LWPE treatment are listed in Figure 5F; Supplementary Table S2.

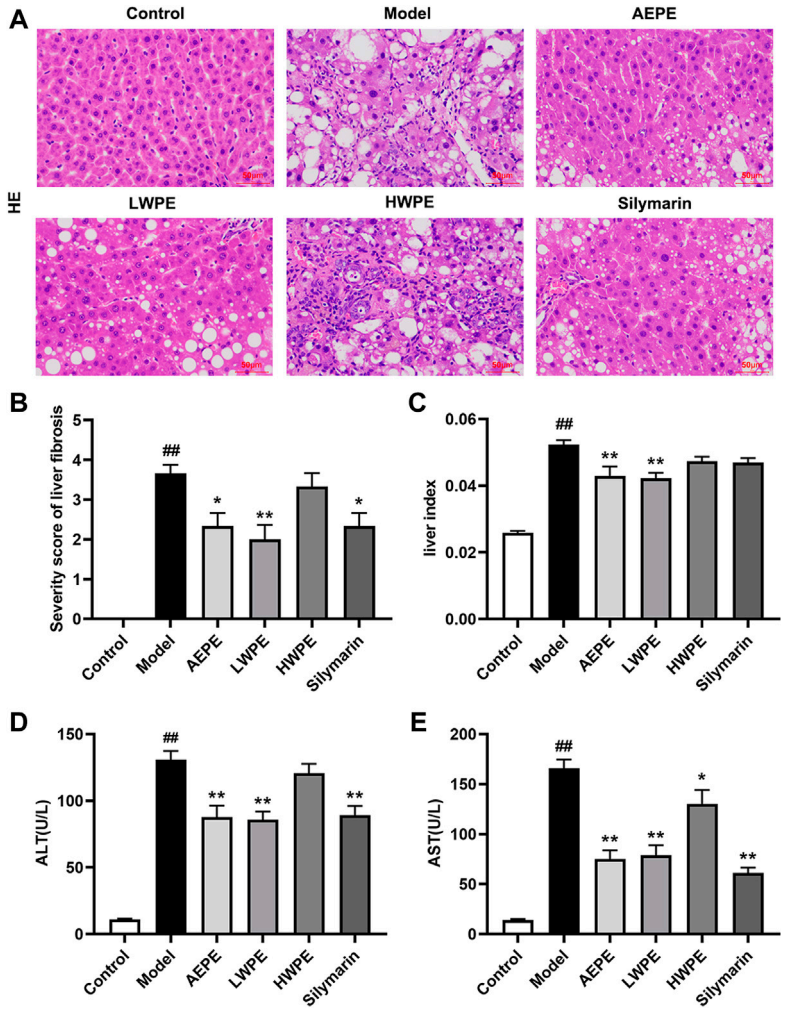

FIGURE 3
Effects of AEPE and its fractions on liver injury in rats administered with CCl_4. **(A)** Representative histopathological sections of liver tissue from each group stained with H&E (magnification, ×200). **(B)** Severity score of hepatic fibrosis in H&E staining. **(C)** The liver-to-body weight ratio of each rat in the groups was calculated. **(D)** ALT levels in serum. **(E)** AST levels in serum. Control, control group. Model, model group. AEPE, aqueous extract of PE group. LWPE, low molecular weight fraction of PE group. HWPE, high molecular weight fraction of PE group. Silymarin, silymarin group. Data are expressed as the mean ± SEM (n = 7–10). ##p < 0.01 vs the control group; *p < 0.05, **p < 0.01 vs the model group.

3.5 Bioinformatics analysis of differentially expressed proteins

3.5.1 Subcellular localization and domain analysis of differentially expressed proteins

The subcellular localization analysis of DEPs is helpful to further comprehend the functions of the proteins in cells. CELLO software was applied to show the number and distribution ratio of DEPs in each subcellular organelle (Figure 6A). The DEPs were located mainly in the nucleus (33.20%), cytoplasmic (28.69%), extracellular (17.62%), and plasma membrane (13.11%). The domain prediction software InterProScan was used to predict the domains of DEPs, and the number of proteins in the domains (top 20) is shown (Figure 6B). The number of DEPs containing the collagen triple helix repeat (20 copies), leucine rich repeat, immunoglobulin I-set domain, leucine rich repeat N-terminal domain and immunoglobulin domain were the largest.

3.5.2 Functional classification of differentially expressed proteins

For a comprehensive understanding of the function, localization and biological pathways of DEPs in living organisms, DEPs were annotated through GO analysis. Set p-value (p) < 0.05, false discovery rate (FDR) < 0.05, and a total of 52 items is obtained, of which 10 are BP, 12 are MF, and

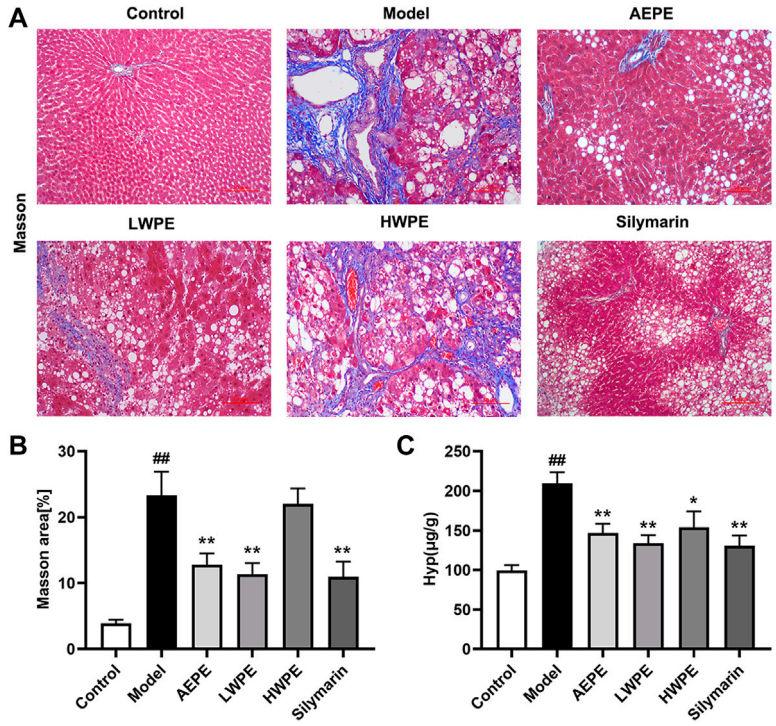

FIGURE 4
Effects of AEPE and its fractions on liver fibrosis in rats administered with CCl_4. **(A)** Representative rat livers stained with Masson (magnification, ×200). **(B)** The positive regions of Masson staining. **(C)** Hyp contents in liver tissues. Data are expressed as the mean ± SEM (n = 7–10). ##p < 0.01 vs the control group; *p < 0.05, **p < 0.01 vs the model group.

TABLE 1 Effects AEPE and its fractions on the serum contents of LN, HA, IV-C and PCIII in CCl_4 induced rat liver fibrosis.

Groups	LN (ng/ml)	HA (ng/ml)	IV-C (ng/ml)	PCIII (ng/ml)
Control	108.85 ± 8.56	88.83 ± 13.35	5.58 ± 0.36	10.41 ± 1.43
Model	142.65 ± 6.83##	120.61 ± 17.79##	7.48 ± 0.91##	14.41 ± 1.64##
AEPE	120.13 ± 8.44**	95.11 ± 13.14**	6.04 ± 1.16*	12.39 ± 1.54*
LWPE	112.90 ± 7.06**	96.42 ± 13.52*	6.01 ± 0.96**	12.47 ± 1.46*
HWPE	138.32 ± 12.18	118.76 ± 10.44	7.30 ± 0.27	14.26 ± 0.96
Silymarin	118.12 ± 11.71**	93.26 ± 16.95**	6.12 ± 1.05*	13.43 ± 1.24

Data were expressed as the mean ± SEM (n = 7–10). ##p < 0.01 vs the control group; *p < 0.05, **p < 0.01 vs the model group.

CC occupies 30, Figure 7A shows an overview of GO analysis, selecting top 10 significantly richer terms in the BP, CC, and MF categories, respectively.

For GO enrichment analysis, the results of BP, MF and the top 20 CC terms with the most significant enrichment are presented in bubble diagrams. In biological processes (Figure 7B), DEPs were primarily involved in extracellular matrix organization and cell adhesion. In molecular function, actin binding, extracellular matrix structural constituent, platelet-derived growth factor binding and protein binding were significantly regulated (Figure 7C). In the cellular component category, the results indicated that DEPs were significantly related to extracellular exosome, extracellular matrix and focal adhesion (Figure 7D).

3.5.3 Kyoto Encyclopedia of Genes and Genomes pathway analysis of differentially expressed proteins

The pathway enrichment of DEPs was analyzed using a KEGG pathway analysis. Fifteen pathways were enriched

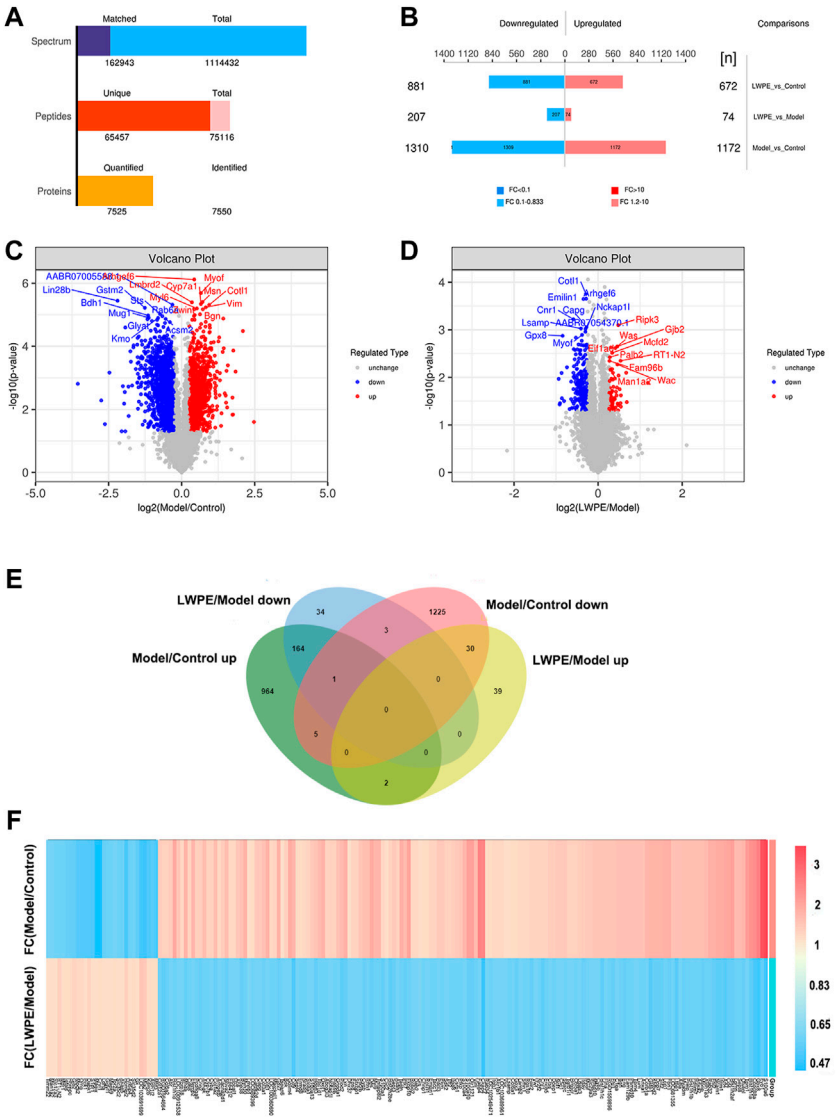

FIGURE 5
Identification of differentially expressed proteins (DEPs) in the livers of control, model and LWPE treated rats. **(A)** Basic statistics of the MS results of the samples. **(B)** The number of DEPs in different comparison groups. **(C** and **D)** Volcano plots of DEPs in different comparison groups. The red dots indicate upregulated proteins and the blue points show downregulated proteins screened based on fold change (FC) > 1.2 or <1/1.2 and a corrected *p*-value of <0.05. **(E)** Venn diagrams showing the distribution of overlapping proteins. **(F)** Hierarchical cluster analysis of 195 DEPs. The color indicates fold changes of proteins, dark blue indicates a decrease, while red indicates an increase.

(p <0.05, Supplementary Table S3). KEGG pathway enrichment bubble chart analyses revealed these DEPs to be enriched in ECM-receptor interaction, focal adhesion and PI3K-Akt signalling pathway (Figure 8A). To further explore the types of pathways enriched, the 15 pathways were classified as shown in Figure 8B, and most of these DEPs were enriched in human disease-related pathways, suggesting that the mechanisms underlying the antifibrotic effects of LWPE are multifunctional and involve multiple pathways.

3.5.4 Protein-protein interaction analysis of differentially expressed proteins

The STRING online database was used to determine the relationship among DEPs to elucidate the molecular mechanism underlying the crosstalk, and the protein interaction parameter score value was "medium confidence >0.4". A total of 172 nodes and 456 edges were interconnected (Figure 8C). The PPI network was further constructed by Cytoscape software to analyze and visualize

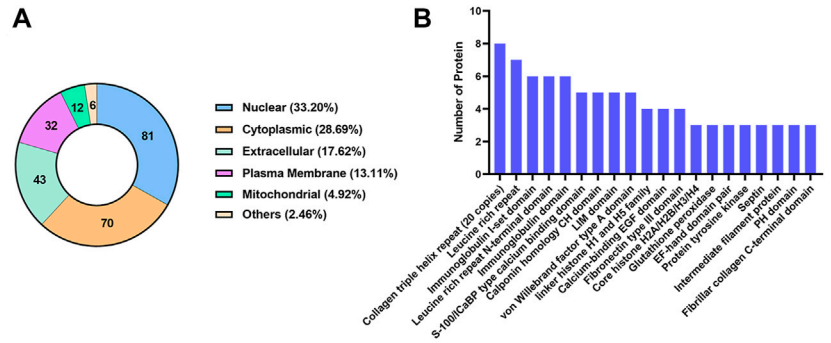

FIGURE 6
Classification of DEPs based on subcellular localization and domain. **(A)** The number and distribution ratio of DEPs in each subcellular organelle. **(B)** The number of proteins in the domains (top 20).

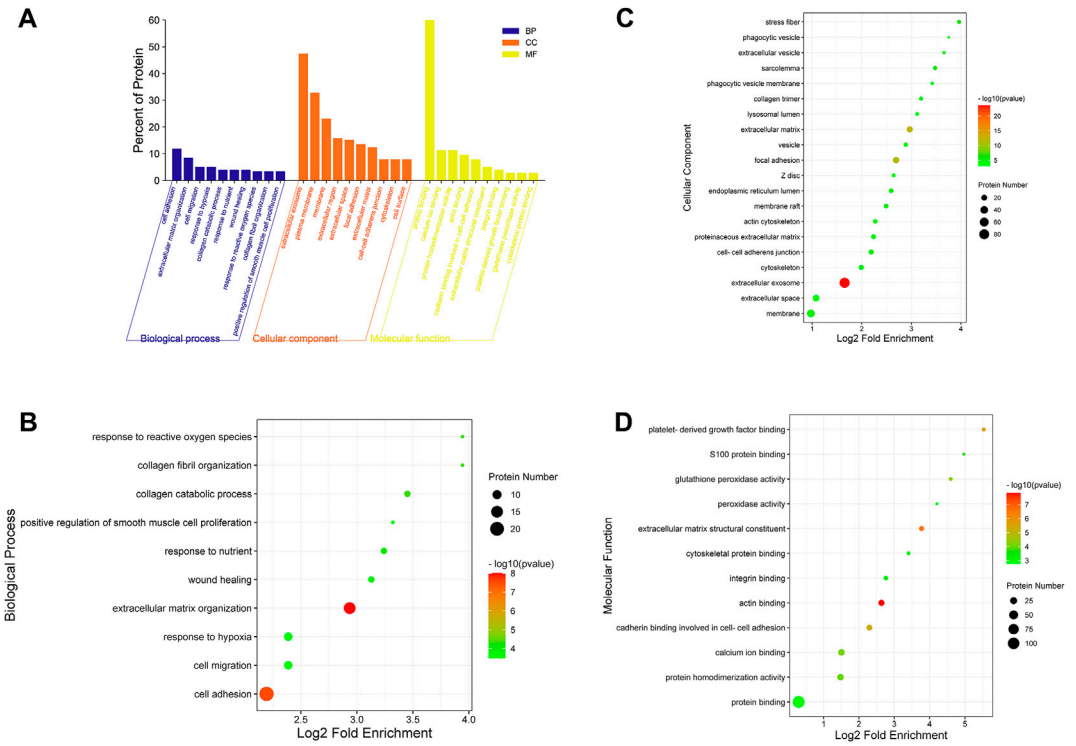

FIGURE 7
GO annotation classification analysis in biological process (BP), cellular component (CC) and molecular function (MF). **(A)** The top 10 significantly richer terms in the BP, CC, and MF categories. **(B)** Enrichment bubble plots of DEPs in BP. **(C)** Enrichment bubble plots of DEPs in the top 20 CC. **(D)** Enrichment bubble plots of DEPs in MF. $p < 0.05$, FDR<0.05.

the importance of target proteins, and the results revealed that ITGB1, COL1A2, ITGAV, TLR2, ACE, and PDGFRB occupy the center of the PPI network and act as hubs for interaction with other differentially expressed proteins (Figure 8D).

3.6 Western blot analysis

The protein expression levels of COL1A2, ITGAV, TLR2, ACE, and PDGFRB in liver tissue were measured by Western blot to further verify the results of quantitative proteomics analysis.

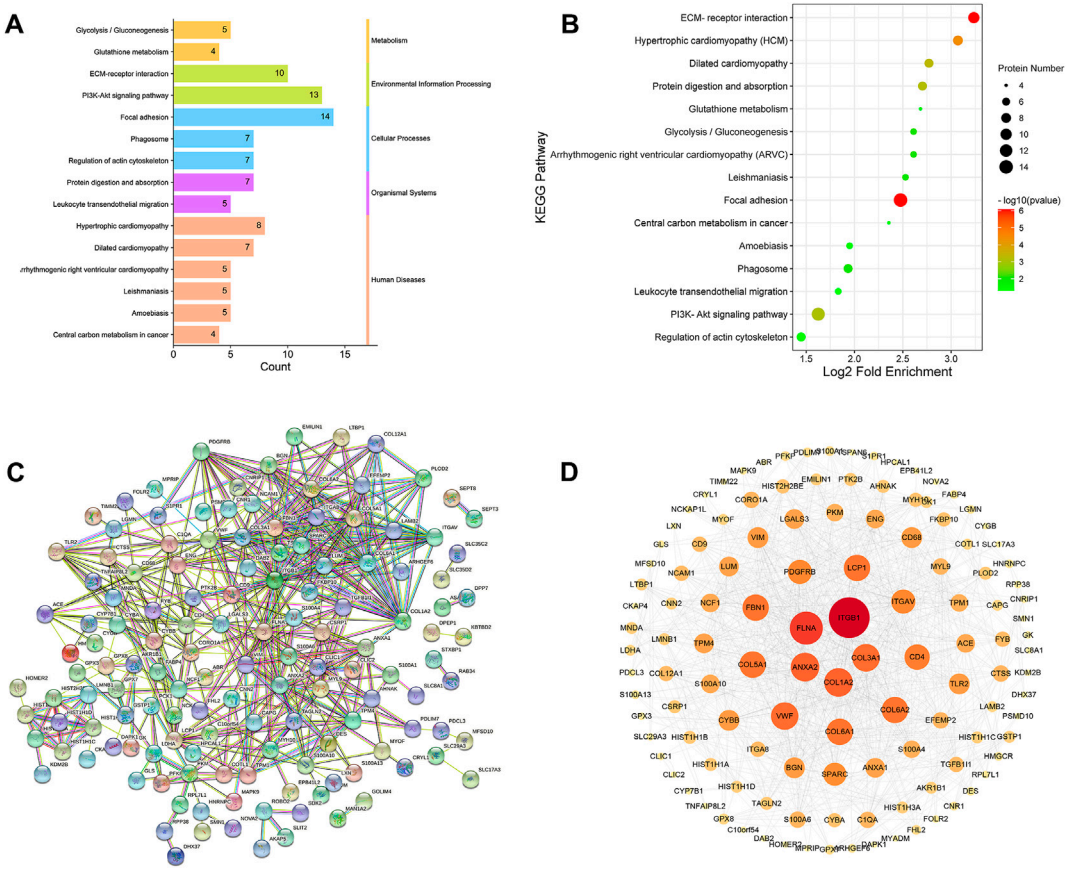

FIGURE 8
Kyoto Encyclopedia of Genes and Genomes (KEGG) pathway analysis and protein-protein interaction (PPI) network analysis of DEPs. **(A)** Classification of KEGG pathways. **(B)** Enrichment bubble plots of DEPs in the KEGG pathway, $p<0.05$. **(C)** PPI analysis among the DEPs of STRING database, medium confidence>0.4. **(D)** Cytoscape analysis of DEPs.

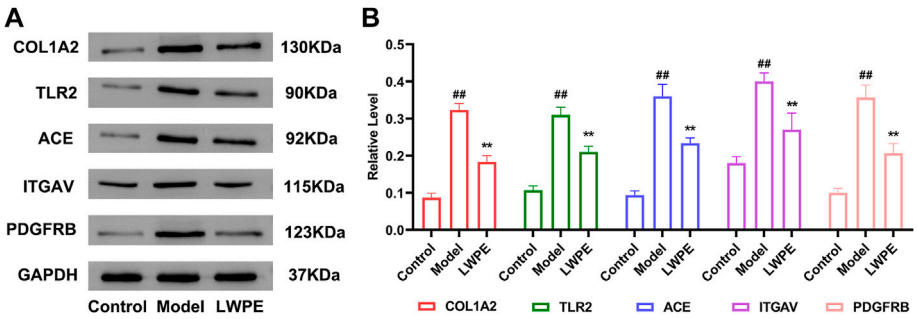

FIGURE 9
Western blot analysis of the key proteins. **(A)** The protein expression levels of GAPDH, COL1A2, ITGAV, TLR2, ACE and PDGFRB; **(B)** The relative levels of the proteins, in the model group vs the LWPE group. Data are expressed as the mean ± SEM ($n = 3$). ##$p < 0.01$ vs the control group; *$p < 0.05$, **$p < 0.01$ vs the model group.

As shown in Figure 9, the expression levels of COL1A2, ITGAV, TLR2, ACE, and PDGFRB in the model group were all significantly increased compared with those in the control group ($p < 0.01$). LWPE treatment significantly downregulated the levels of these proteins compared with those in the model group ($p < 0.01$). The results are consistent with the protein profiles in TMT-based proteomic analysis.

4 Discussion

In the present study, the anti-hepatic fibrosis efficacies of AEPE and its fractions were evaluated using a rat model induced by CCl_4. LWPE contained mainly secondary metabolites proven to be the optimal effective chemical fraction of AEPE by comprehensive serum biochemical analysis and histopathological examination. Our previous work demonstrated that LWPE contains a variety of phenolic acids and flavonoids, such as gallic acid, corilagin, ellagic acid, etc (Yin et al., 2021). These monomeric components have been reported to exert inhibitory effects on liver fibrosis by interfering with different molecular signalling pathways (Yin et al., 2022). Hence, LWPE possesses the characteristics of multicomponent and multitarget integrated therapy for liver fibrosis, which makes it difficult to elucidate the effective mechanism of LWPE.

Currently, high-throughput proteomic technology has been broadly applied to search for biomarkers and drug targets of liver diseases (Cowan et al., 2010), providing an appropriate technical tool for identifying the multitarget mechanism of LWPE on hepatic fibrosis. We identified 195 DEPs regulated by LWPE in liver tissue using TMT-based quantitative proteomics. Through GO enrichment analysis, the DEPs were highly related to ECM organization, ECM structural constituents and extracellular exosomes. During the formation of liver fibrosis, HSC are activated under the stimulation of various biological factors and then transformed into myofibroblasts, leading to excessive ECM deposition, which is a common pathological feature of liver fibrosis (Sun et al., 2018; Zhang et al., 2020). The ECM is composed of a heterogeneous mixture of glycoproteins and proteoglycans (PGs), including LN, fibronectin, collagen, HA and heparan sulfate PGs (Jonathan P. Myers et al., 2011). In our experimental pharmacodynamic results, the contents of HA, LN, IV-C, PCIII, and Hyp in the LWPE group were significantly decreased compared with those in the model group. Therefore, LWPE may alleviate CCl_4-induced liver fibrosis by reducing ECM synthesis and accumulation.

KEGG pathway enrichment showed that DEPs are related to ECM-receptor interaction, focal adhesion and the PI3K-Akt signalling pathway. Interestingly, the ECM-receptor interaction and PI3K-Akt signalling pathways are involved in the focal adhesion (Chen et al., 2017). Studies have proven that focal adhesion plays an important role in HSC activation, and the disintegration of focal adhesions in activated HSCs may contribute to reversing liver fibrosis (Kumar et al., 2014). Besides, ECM is mainly distributed and aggregates on the cell surface and intercellular substances (Yumeng and Shenghua, 2017), and cell adhesion to ECM is mediated by ECM receptors namely integrins, discoidin domains and syndecans (Khurana et al., 2021). Integrins activate focal adhesion kinase (FAK) and Src-family kinases, and subsequently stimulate downstream signalling cascades such as the PI3K/Akt signalling pathway (Mitra et al., 2005). The expression of ECM in various cell types can be induced by activating the PI3K/Akt pathway (Sun et al., 2016). Inhibition of PI3K signalling in HSCs restrained collagen synthesis and ECM deposition, and decreased the expression of profibrogenic factors (Tu et al., 2016). Studies have shown that PE extract can inhibit Akt overactivity, thereby inhibiting the dysregulation of PI3K/Akt (Kunchana et al., 2021). We speculate that LWPE can alleviate liver fibrosis by regulating multiple pathways, including ECM-receptor interaction, focal adhesion and the PI3K-Akt signalling pathway.

In addition, according to the PPI network analysis, COL1A2, ITGAV, TLR2, ACE, and PDGFRB located in the center of the network and presented in multiple enriched signalling pathways. Therefore, these representative proteins were selected for further molecular biotechnology verification, and the results proved that LWPE can decrease the abovementioned proteins expression caused by CCl_4.

Collagen is the most abundant ECM protein when fibrosis occurs, accounting for approximately 50% of the dry liver weight in cirrhosis (Kunchana et al., 2021). Among the 28 known types of collagen, at least 11 are expressed in liver tissue (Kunchana et al., 2021). In this study, quantitative protein analysis showed that various collagen proteins (including Col5a1, Col3a1, Col1a2, Col6a1, and Col6a2) in the liver tissue of model rats were decreased after treatment with LWPE. To date, there are no recognized most important proteins of the ECM specifically addressed in fibrosis, type I and III collagens are the most abundant collagens, followed by type IV, V, and VI collagens (Karsdal et al., 2015). Among these collagens, the type I collagen subunit molecule is a fibril-forming heterotrimeric protein consisting of two α1 chains and one α2 chain, which fold into a highly ordered and steady triple-helix (Blackstock et al., 2014). Col1a1 is a valid target for the treatment of liver fibrosis by inhibiting the synthesis of type I collagen, which has been proven in many studies (Calvente et al., 2015; Tao et al., 2018). To the best of our knowledge, the role of Col1a2 in liver fibrosis is still poorly understood. We validated that LWPE could reduce the expression of

Col1a2 by Western blotting, suggesting that Col1a2 may be a potential effective target for the treatment of liver fibrosis.

Toll-like receptors (TLRs), a class of pattern recognition receptors, play a specific role in the regulation of the inflammatory response and liver fibrosis (Raby et al., 2017; Gan et al., 2018). TLR2 is one of the most common TLRs and is widely expressed on parenchymal and nonparenchymal liver cells mediating liver disease pathogenesis, including alcoholic liver disease and the nonalcoholic steatohepatitis (Getachew et al., 2021). TLR2 signalling pathways induce translocation of NF-κB into the nucleus and eventually modulate transcription of genes, as well as the production of inflammatory cytokines, considered to be the major hepatotoxic mediators that participate in the pathological process of liver fibrosis (Simeonova et al., 2001; Yang et al., 2020; Getachew et al., 2021). Knockout of TLR2 has been reported to be able to relieve CCl_4-induced hepatic fibrosis in mice by downregulating the expression of profibrotic and proinflammatory genes (Ji et al., 2014). Previous studies have shown that various extracts and ingredients of PE possess anti-inflammatory properties (Li et al., 2020); hence, we speculated that TLR2 may be the key target that mediates the anti-inflammatory effects of LWPE in treating liver fibrosis. Moreover, the effects of LWPE on the TLR2/NF-κB signalling pathway in hepatic fibrosis rats also deserve further verification.

Inhibiting the activation and proliferation of HSCs in damaged livers has been widely recognized as a suitable treatment strategy for hepatic fibrosis (Yang et al., 2020). PDGF, which is the most potent mitogen for activated HSCs, binds to PDGF α and *ß* receptors and activates the downstream ERK/MAPK and Akt/PKB signalling pathways, leading to stimulation of HSCs proliferation (Borkham-Kamphorst and Weiskichen, 2016). However, only PDGF *ß* receptor (PDGFBR) is specifically overexpressed on activated HSCs (Chen et al., 2020). Reducing PDGFBR expression by siRNA effectively reduced the activation and proliferation of HSCs *in vitro* and suppressed liver fibrosis in an animal model (Chen et al., 2008). ITGAV, namely αV integrins, are heterodimeric cell-surface proteins, that play a central role in the progression of liver fibrosis as they activate latent TGF-β which is a known profibrogenic cytokine (Rahman et al., 2022). Experimental evidence demonstrates that depletion of the ITGAV subunit in HSCs protects mice from liver fibrosis induced by CCl_4 (Henderson et al., 2013). ACE is a key proteolytic enzyme of the renin-angiotensin system (RAS), converting the decapeptide angiotensin I (Ang I) into the active octapeptide angiotensin II (Ang II) (Henderson et al., 2013). Ang II could induce contraction and proliferation of HSCs through the Ang II type 1 (AT1) receptor and motivate the activation and differentiation of quiescent HSCs into myofibroblasts (Saber et al., 2018). Several studies applied the method of ACE inhibition and showed that reducing Ang II formation could significantly ameliorate bile duct ligation or CCl_4 induced liver fibrosis in rats (Simeonova et al., 2001). Therefore, we speculated that LWPE likely inhibited HSCs *via* interfering the expression of PDGFBR, ITGAV and ACE according to the results of proteomic analysis and Western blotting assays.

Taken together, these key DEPs are closely associated with the pathophysiology of hepatic fibrosis involving ECM sedimentation, inflammation, activation and proliferation of HSCs, which suggests that LWPE regulates liver fibrosis through multiple targets and multiple pathways. Additionally, many previous *in vivo* toxicity evaluation studies reported that PE extracts have no obvious toxic effects though hematological and histopathological examination, behavioral observation and biochemical marker analysis (Saini et al., 2022). Hence, PE is expected to be a potential source for the development of anti-liver fibrosis multitarget drugs that are safe and have no side effects.

5 Conclusion

In this study, we determined that LWPE is the main effective fraction of AEPE against liver fibrosis, and proteomics and bioinformatics analysis showed that LWPE can regulate multiple targets including COL1A2, ITGAV, TLR2, ACE, and PDGFRB, etc., ECM-receptor interaction, focal adhesion and the PI3K-Akt signalling pathway and other pathways to exert antifibrosis effects.

Data availability statement

The datasets presented in this study can be found in online repositories. The names of the repository/repositories and accession number(s) can be found in the article/Supplementary Material.

Ethics statement

The animal study was reviewed and approved by animal ethics committee of Southwest Minzu University.

Author contributions

PG, JG, and YW conceived the study and designed the experiments. KY and XL performed the experiments. KY, PG, and YW analyzed the data, prepared the figures, and wrote the manuscript. DL and RT guided the experiment. All authors have read and agreed to the final version of the manuscript.

Funding

This study was supported by grants from the National Natural Science Foundation of China (No. 82004069), the Natural Science Foundation of Sichuan Province (No. 2022NSFSC1524) and the Fundamental Research Funds for the Central Universities of Southwest Minzu University (No. 2021121).

Conflict of interest

The authors declare that the research was conducted in the absence of any commercial or financial relationships that could be construed as a potential conflict of interest.

Publisher's note

All claims expressed in this article are solely those of the authors and do not necessarily represent those of their affiliated organizations, or those of the publisher, the editors and the reviewers. Any product that may be evaluated in this article, or claim that may be made by its manufacturer, is not guaranteed or endorsed by the publisher.

Supplementary material

The Supplementary Material for this article can be found online at: https://www.frontiersin.org/articles/10.3389/fphar.2022.989995/full#supplementary-material

References

Anuja, G. I., Shine, V. J., Latha, P. G., and Suja, S. R. (2018). Protective effect of ethyl acetate fraction of Drynaria quercifolia against CCl4 induced rat liver fibrosis via Nrf2/ARE and NFκB signalling pathway. *J. Ethnopharmacol.* 216, 79–88. doi:10.1016/j.jep.2017.11.015

Blackstock, C. D., Higashi, Y., Sukhanov, S., Shai, S. Y., Stefanovic, B., Tabony, A. M., et al. (2014). Insulin-like growth factor-1 increases synthesis of collagen type I via induction of the mRNA-binding protein LARP6 expression and binding to the 5′ stem-loop of COL1a1 and COL1a2 mRNA. *J. Biol. Chem.* 289, 7264–7274. doi:10.1074/jbc.M113.518951

Borkham-Kamphorst, E., and Weiskirchen, R. (2016). The PDGF system and its antagonists in liver fibrosis. *Cytokine Growth Factor Rev.* 28, 53–61. doi:10.1016/j.cytogfr.2015.10.002

Calvente, C. J., Sehgal, A., Popov, Y., Kim, Y. O., Zevallos, V., Sahin, U., et al. (2015). Specific hepatic delivery of procollagen α1(I) siRNA in lipid-like nanoparticles resolves liver fibrosis. *Hepatology* 62, 1285–1297. doi:10.1002/hep.27936.Specific

Chen, C., Li, X., and Wang, L. (2020). Thymosinβ4 alleviates cholestatic liver fibrosis in mice through downregulating PDGF/PDGFR and TGFβ/Smad pathways. *Dig. Liver Dis.* 52, 324–330. doi:10.1016/j.dld.2019.08.014

Chen, S. W., Zhang, X. R., Wang, C. Z., Chen, W. Z., Xie, W. F., and Chen, Y. X. (2008). RNA interference targeting the platelet-derived growth factor receptor β subunit ameliorates experimental hepatic fibrosis in rats. *Liver Int.* 28, 1446–1457. doi:10.1111/j.1478-3231.2008.01759.x

Chen, W., Zhao, W., Yang, A., Xu, A., Wang, H., Cong, M., et al. (2017). Integrated analysis of microRNA and gene expression profiles reveals a functional regulatory module associated with liver fibrosis. *Gene* 636, 87–95. doi:10.1016/j.gene.2017.09.027

Cowan, M. L., Rahman, T. M., and Krishna, S. (2010). Proteomic approaches in the search for biomarkers of liver fibrosis. *Trends Mol. Med.* 16, 171–183. doi:10.1016/j.molmed.2010.01.006

Gan, F., Liu, Q., Liu, Y., Huang, D., Pan, C., Song, S., et al. (2018). Lycium barbarum polysaccharides improve CCl4-induced liver fibrosis, inflammatory response and TLRs/NF-kB signaling pathway expression in wistar rats. *Life Sci.* 192, 205–212. doi:10.1016/j.lfs.2017.11.047

Getachew, A., Hussain, M., Huang, X., and Li, Y. (2021). Toll-like receptor 2 signaling in liver pathophysiology. *Life Sci.* 284, 119941. doi:10.1016/j.lfs.2021.119941

Henderson, N., Arnold, T., Katamura, Y., Giacomini, M., Rodriguez, J., McCarty, J., et al. (2013). OC-002 Selective alpha V integrin deletion identifies a core, targetable molecular pathway that regulates fibrosis across solid organs. *Gut* 62, A1.2–A1. doi:10.1136/gutjnl-2013-304907.002

Huang, H., Chen, J., Zhang, D., Li, M., Xian, Q., Fan, S., et al. (2021). Research progress of phyllanthi fructus and prediction of its Q-markers. *China J. Chin. Mat. Medica* 46, 5533–5544. doi:10.19540/j.cnki.cjcmm.20210810.201

Ji, L., Xue, R., Tang, W., Wu, W., Hu, T., Liu, X., et al. (2014). Toll like receptor 2 knock-out attenuates carbon tetrachloride (CCl 4)-induced liver fibrosis by downregulating MAPK and NF-κB signaling pathways. *FEBS Lett.* 588, 2095–2100. doi:10.1016/j.febslet.2014.04.042

Karsdal, M. A., Manon-Jensen, T., Genovese, F., Kristensen, J. H., Nielsen, M. J., Sand, J. M. B., et al. (2015). Novel insights into the function and dynamics of extracellular matrix in liver fibrosis. *Am. J. Physiol. Gastrointest. Liver Physiol.* 308, G807–G830. doi:10.1152/ajpgi.00447.2014

Khurana, A., Sayed, N., Allawadhi, P., and Weiskirchen, R. (2021). It's all about the spaces between cells: Role of extracellular matrix in liver fibrosis. *Ann. Transl. Med.* 9, 728. doi:10.21037/atm-20-2948

Kumar, P., Smith, T., Rahman, K., Mells, J. E., Thorn, N. E., Saxena, N. K., et al. (2014). Adiponectin modulates focal adhesion disassembly in activated hepatic stellate cells: Implication for reversing hepatic fibrosis. *FASEB J.* 28, 5172–5183. doi:10.1096/fj.14-253229

Kunchana, K., Jarisarapurin, W., Chularojmontri, L., and Wattanapitayakul, S. K. (2021). Potential use of amla (Phyllanthus emblica l.) fruit extract to protect skin keratinocytes from inflammation and apoptosis after uvb irradiation. *Antioxidants* 10, 703. doi:10.3390/antiox10050703

Lan, Y., Zeng, X., Xiao, J., Hu, L., Tan, L., Liang, M., et al. (2021). New advances in quantitative proteomics research and current applications in asthma. *Expert Rev. Proteomics* 18, 1045–1057. doi:10.1080/14789450.2021.2017777

Li, W., Zhang, X., Chen, R., Li, Y., Miao, J., Liu, G., et al. (2020). HPLC fingerprint analysis of Phyllanthus emblica ethanol extract and their antioxidant and anti-inflammatory properties. *J. Ethnopharmacol.* 254, 112740. doi:10.1016/j.jep.2020.112740

Liu, J., Wang, L., and Wang, M. (2014). 30 cases of liver fibrosis in chronic Hepatitis B treated with fuzheng rougan formulae. *Tradit. Chin. Med. Res.* 27, 19–21. doi:10.3969/j.issn.1001-6910.2014.06.09

Liu, J. Y., Chen, C. C., Wang, W. H., Hsu, J. D., Yang, M. Y., and Wang, C. J. (2006). The protective effects of Hibiscus sabdariffa extract on CCl 4-induced liver fibrosis in rats. *Food Chem. Toxicol.* 44, 336–343. doi:10.1016/j.fct.2005.08.003

Lu, C. C., Yang, S. H., Hsia, S. M., Wu, C. H., and Yen, G. C. (2016). Inhibitory effects of Phyllanthus emblica L. on hepatic steatosis and liver fibrosis *in vitro*. *J. Funct. Foods* 20, 20–30. doi:10.1016/j.jff.2015.10.012

Luo, X., Zhang, B., Pan, Y., Gu, J., Tan, R., and Gong, P. (2022). Phyllanthus emblica aqueous extract retards hepatic steatosis and fi brosis in NAFLD mice in association with the reshaping of intestinal microecology. *Front. Pharmacol.* 13, 893561. doi:10.3389/fphar.2022.893561

Mir, A. I., Kumar, B., Tasduq, S. A., Gupta, D. K., Bhardwaj, S., and Johri, R. K. (2007). Reversal of hepatotoxin-induced pre-fibrogenic events by Emblica officinalis - a histological study. *Indian J. Exp. Biol.* 45, 626–629.

Mitra, S. K., Hanson, D. A., and Schlaepfer, D. D. (2005). Focal adhesion kinase: In command and control of cell motility. *Nat. Rev. Mol. Cell Biol.* 6, 56–68. doi:10.1038/nrm1549

Muthuraman, A., Sood, S., and Singla, S. K. (2011). The antiinflammatory potential of phenolic compounds from Emblica officinalis L. in rat. *Inflammopharmacology* 19, 327–334. doi:10.1007/s10787-010-0041-9

Myers, Jonathan P., Santiago-Medina, M., and Gomez, T. M. (2011). Regulation of axonal outgrowth and pathfinding by integrin-ECM interactions. *Dev. Neurobiol.* 71, 901–923. doi:10.1002/dneu.20931

Qiao, M., Yang, J., Zhu, Y., Zhao, Y., and Hu, J. (2020). Transcriptomics and proteomics analysis of system-level mechanisms in the liver of apigenin-treated fibrotic rats. *Life Sci.* 248, 117475. doi:10.1016/j.lfs.2020.117475

Raby, A. C., Colmont, C. S., Kift-Morgan, A., Köhl, J., Eberl, M., Fraser, D., et al. (2017). Toll-like receptors 2 and 4 are potential therapeutic targets in peritoneal dialysis-associated fibrosis. *J. Am. Soc. Nephrol.* 28, 461–478. doi:10.1681/ASN.2015080923

Rahman, S. R., Roper, J. A., Grove, J. I., Aithal, G. P., Pun, K. T., and Bennett, A. J. (2022). Integrins as a drug target in liver fibrosis. *Liver Int.* 42, 507–521. –15. doi:10.1111/liv.15157

Saber, S., Mahmoud, Amr A. A., Helal, N. S., El-ahwany, E., and Abdelghany, R. H. (2018). Renin-angiotensin system inhibition ameliorates CCl4-induced liver fibrosis in mice through the inactivation of nuclear transcription factor kappa-B. *Can. J. Physiol. Pharmacol.* 96, 569–576. doi:10.1139/cjpp-2017-0728

Saini, R., Sharma, N., Oladeji, O. S., Sourirajan, A., Dev, K., Zengin, G., et al. (2022). Traditional uses, bioactive composition, pharmacology, and toxicology of Phyllanthus emblica fruits: A comprehensive review. *J. Ethnopharmacol.* 282, 114570. doi:10.1016/j.jep.2021.114570

Shan, L., Liu, Z., Ci, L., Shuai, C., Lv, X., and Li, J. (2019). Research progress on the anti-hepatic fibrosis action and mechanism of natural products. *Int. Immunopharmacol.* 75, 105765. doi:10.1016/j.intimp.2019.105765

Shang, X., Yuan, H., Dai, L., Liu, Y., He, J., Chen, H., et al. (2022). Anti-liver fibrosis activity and the potential mode of action of ruangan granules: Integrated network pharmacology and metabolomics. *Front. Pharmacol.* 12, 754807. doi:10.3389/fphar.2021.754807

Shi, M. J., Yan, X. L., Dong, B. S., Yang, W. N., Su, S. B., and Zhang, H. (2020). A network pharmacology approach to investigating the mechanism of Tanshinone IIA for the treatment of liver fibrosis. *J. Ethnopharmacol.* 253, 112689. doi:10.1016/j.jep.2020.112689

Simeonova, P. P., Gallucci, R. M., Hulderman, T., Wilson, R., Kommineni, C., Rao, M., et al. (2001). The role of tumor necrosis factor-α in liver toxicity, inflammation, and fibrosis induced by carbon tetrachloride. *Toxicol. Appl. Pharmacol.* 177, 112–120. doi:10.1006/taap.2001.9304

Sripanidkulchai, B., and Junlatat, J. (2014). Bioactivities of alcohol based extracts of Phyllanthus emblica branches: Antioxidation, antimelanogenesis and anti-inflammation. *J. Nat. Med.* 68, 615–622. doi:10.1007/s11418-014-0824-1

Sun, J., Wu, Y., Long, C., He, P., Gu, J., Yang, L., et al. (2018). Anthocyanins isolated from blueberry ameliorates CCl4 induced liver fibrosis by modulation of oxidative stress, inflammation and stellate cell activation in mice. *Food Chem. Toxicol.* 120, 491–499. doi:10.1016/j.fct.2018.07.048

Sun, L., Dong, Y., Zhao, J., Yin, Y., and Zheng, Y. (2016). The CLC-2 chloride channel modulates ECM synthesis, differentiation, and migration of human conjunctival fibroblasts via the PI3K/Akt signaling pathway. *Int. J. Mol. Sci.* 17, E910. doi:10.3390/ijms17060910

Tao, R., Fan, X. X., Yu, H. J., Ai, G., Zhang, H. Y., Kong, H. Y., et al. (2018). MicroRNA-29b-3p prevents Schistosoma japonicum-induced liver fibrosis by targeting COL1A1 and COL3A1. *J. Cell Biochem.* 119, 3199–3209. doi:10.1002/jcb.26475

Tasduq, S. A., Mondhe, D. M., Gupta, D. K., Baleshwar, M., and Johri, R. K. (2005). Reversal of fibrogenic events in liver by Emblica officinalis (fruit), an Indian natural drug. *Biol. Pharm. Bull.* 28, 1304–1306. doi:10.1248/bpb.28.1304

Tu, W., Ye, J., and Wang, Z. J. (2016). Embryonic liver fordin is involved in glucose glycolysis of hepatic stellate cell by regulating PI3K/Akt signaling. *World J. Gastroenterol.* 22, 8519–8527. doi:10.3748/wjg.v22.i38.8519

Wang, B., Lu, S., Zhang, C., Zhu, L., Li, Y., Bai, M., et al. (2020). Quantitative proteomic analysis of the liver reveals antidepressant potential protein targets of Sinisan in a mouse CUMS model of depression. *Biomed. Pharmacother.* 130, 110565. doi:10.1016/j.biopha.2020.110565

Wang, S. H., Cheng, J. T., Guo, C., Cui, W. J., Shi, J., and Liu, A. (2019). Chemical constituents of Phyllanthus emblica and its anti-inflammation activities. *Chin. Tradit. Herb. Drugs* 50, 4873–4878. doi:10.7501/j.issn.0253-2670.2019.20.005

Wiśniewski, J. R., Zougman, A., Nagaraj, N., and Mann, M. (2009). Universal sample preparation method for proteome analysis. *Nat. Methods* 6, 359–362. doi:10.1038/nmeth.1322

Yang, J., Gao, J., Yu, W., Hao, R., Fan, J., and Wei, J. (2020). The effects and mechanism of Aronia melanocarpa Elliot anthocyanins on hepatic fibrosis. *J. Funct. Foods* 68, 103897–103898. doi:10.1016/j.jff.2020.103897

Yin, K. H., Luo, X. M., Ding, Y., Que, H. Y., Tan, R., Li, D. P., et al. (2022). Research progress on hepatoprotective effect and mechanism of Phyllanthus emblica and its active components. *Chin. Tradit. Herb. Drugs* 53, 295–307. doi:10.7501/j.issn.0253-2670.2022.01.034

Yin, K., Li, X., Luo, X., Sha, Y., Gong, P., Gu, J., et al. (2021). Hepatoprotective effect and potential mechanism of aqueous extract from Phyllanthus emblica on carbon-tetrachloride-induced liver fibrosis in rats. *Evid. Based. Complement. Altern. Med.* 2021, 5345821. doi:10.1155/2021/5345821

Yu, D., Wang, Z., Cupp-Sutton, K. A., Guo, Y., Kou, Q., Smith, K., et al. (2021). Quantitative top-down proteomics in complex samples using protein-level tandem mass tag labeling. *J. Am. Soc. Mass Spectrom.* 32, 1336–1344. doi:10.1021/jasms.0c00464

Yuan, Z. H., Yu, X., Duan, Y. D., Liu, P., Jiang, Y. Y., Zhang, W., et al. (2020). Method and application of proteomics in study of targets of traditional Chinese medicines. *Zhongguo Zhongyao Zazhi* 45, 1034–1038. doi:10.19540/j.cnki.cjcmm.20191206.201,

Yumeng, Q., and Shenghua, C. (2017). Influence of extracellular matrix on hepatic stellate cells during liver fibrosis process. *J. Pract. Hepatol.* 20, 381–384. doi:10.3969/j.issn.1672

Zardi, E. M., Dobrina, A., Ambrosino, G., Margiotta, D., Polistina, F., and Afeltra, A. (2008). New therapeutic approaches to liver fibrosis: A practicable route?. *Curr. Med. Chem.* 15 (16), 1628–1644. doi:10.2174/092986708784911560

Zhang, B., Lai, L., Tan, Y., Liang, Q., Bai, F., Mai, W., et al. (2020). Hepatoprotective effect of total flavonoids of Mallotus apelta (Lour.) Muell.Arg. leaf against carbon tetrachloride-induced liver fibrosis in rats via modulation of TGF-β1/Smad and NF-κB signaling pathways. *J. Ethnopharmacol.* 254, 112714. doi:10.1016/j.jep.2020.112714

Zhao, Q., Bai, J., Chen, Y., Liu, X., Zhao, S., Ling, G., et al. (2022). An optimized herbal combination for the treatment of liver fibrosis: Hub genes, bioactive ingredients, and molecular mechanisms. *J. Ethnopharmacol.* 297, 115567. doi:10.1016/j.jep.2022.115567

Zhu, Y., Xu, H., Chen, H., Xie, J., Shi, M., Shen, B., et al. (2014). Proteomic analysis of solid pseudopapillary tumor of the pancreas reveals dysfunction of the endoplasmic reticulum protein processing pathway. *Mol. Cell. Proteomics* 13, 2593–2603. doi:10.1074/mcp.M114.038786

Zhu, Z., bao, Z., Huang, J., and Tang, D. (2015). Comparison of similarities and differences in the clinical application of Phyllanthus emblica in traditional Chinese pharmacy and ethnopharmacology. *Chin. J. Ethn. Med.* 21, 40–42. doi:10.16041/j.cnki.cn15-1175.2015.04.031

frontiers | Frontiers in Pharmacology

TYPE Review
PUBLISHED 17 October 2022
DOI 10.3389/fphar.2022.1030173

OPEN ACCESS

EDITED BY
Guangyue Su,
Shenyang Pharmaceutical University, China

REVIEWED BY
Sherin Zakaria,
Kafrelsheikh University, Egypt
Hartmut Jaeschke,
University of Kansas Medical Center Research Institute, United States

*CORRESPONDENCE
Jianjun Liu,
Jianjun_liu2020@163.com
Xiongwen Lv,
xiongwen_lv2019@163.com

SPECIALTY SECTION
This article was submitted to Ethnopharmacology, a section of the journal Frontiers in Pharmacology

RECEIVED 28 August 2022
ACCEPTED 05 October 2022
PUBLISHED 17 October 2022

CITATION
Shan L, Wang F, Zhai D, Meng X, Liu J and Lv X (2022), Caffeine in liver diseases: Pharmacology and toxicology. *Front. Pharmacol.* 13:1030173. doi: 10.3389/fphar.2022.1030173

Caffeine in liver diseases: Pharmacology and toxicology

Liang Shan[1,2,3,4], Fengling Wang[1], Dandan Zhai[1], Xiangyun Meng[1], Jianjun Liu[1]* and Xiongwen Lv[2,3,4]*

[1]Department of Pharmacy, The Second People's Hospital of Hefei, Hefei Hospital Affiliated to Anhui Medical University, Hefei, Anhui, China, [2]Anhui Province Key Laboratory of Major Autoimmune Diseases, Anhui Medical University, Hefei, Anhui, China, [3]Inflammation and Immune Mediated Diseases Laboratory of Anhui Province, Hefei, Anhui, China, [4]The Key Laboratory of Major Autoimmune Diseases, Hefei, Anhui, China

We have previously shown that adenosine A1AR antagonists, adenosine A2aAR antagonists, and caffeine have significant inhibitory effects on the activation and proliferation of hepatic stellate cells in alcoholic liver fibrosis. Many recent studies have found that moderate coffee consumption is beneficial for various liver diseases. The main active ingredient of coffee is caffeine, which is a natural non-selective adenosine receptor antagonist. Moreover, numerous preclinical epidemiological studies and clinical trials have examined the association between frequent coffee consumption and the risk of developing different liver diseases. In this review, we summarize and analyze the prophylactic and therapeutic effects of caffeine on various liver diseases, with an emphasis on cellular assays, animal experiments, and clinical trials. To review the prevention and treatment effects of caffeine on different liver diseases, we searched all literature before 19 July 2022, using "caffeine" and "liver disease" as keywords from the PubMed and ScienceDirect databases. We found that moderate coffee consumption has beneficial effects on various liver diseases, possibly by inhibiting adenosine binding to its receptors. Caffeine is a potential drug for the prevention and treatment of various liver diseases.

KEYWORDS

caffeine, liver diseases, pharmacology, toxicology, adenosine, adenosine receptor

1 Introduction

Caffeine, one of the most widely consumed pharmacologically active ingredients in the world, is the main component of coffee and tea (Rawat et al., 2018; Alehaideb et al., 2021). One gram of Nescafe contains approximately 35 mg of caffeine, while 1 g of tea contains approximately 20–35 mg of caffeine. Most western countries, such as the United States, Britain, and France, have a greater tendency to drink coffee, while most eastern countries, such as China, India, and Japan, tend to favor tea (Alshabi et al., 2021). Scientists have paid increased attention to the relationship between caffeine and health because it is closely related to people's daily lives (Leung et al., 2011). Traditionally, caffeine has been described as a potential drug of abuse, and it is widely stated that consuming too many caffeinated drinks is unhealthy (Barcelos et al., 2014). However, in recent years, an increasing number of interesting and

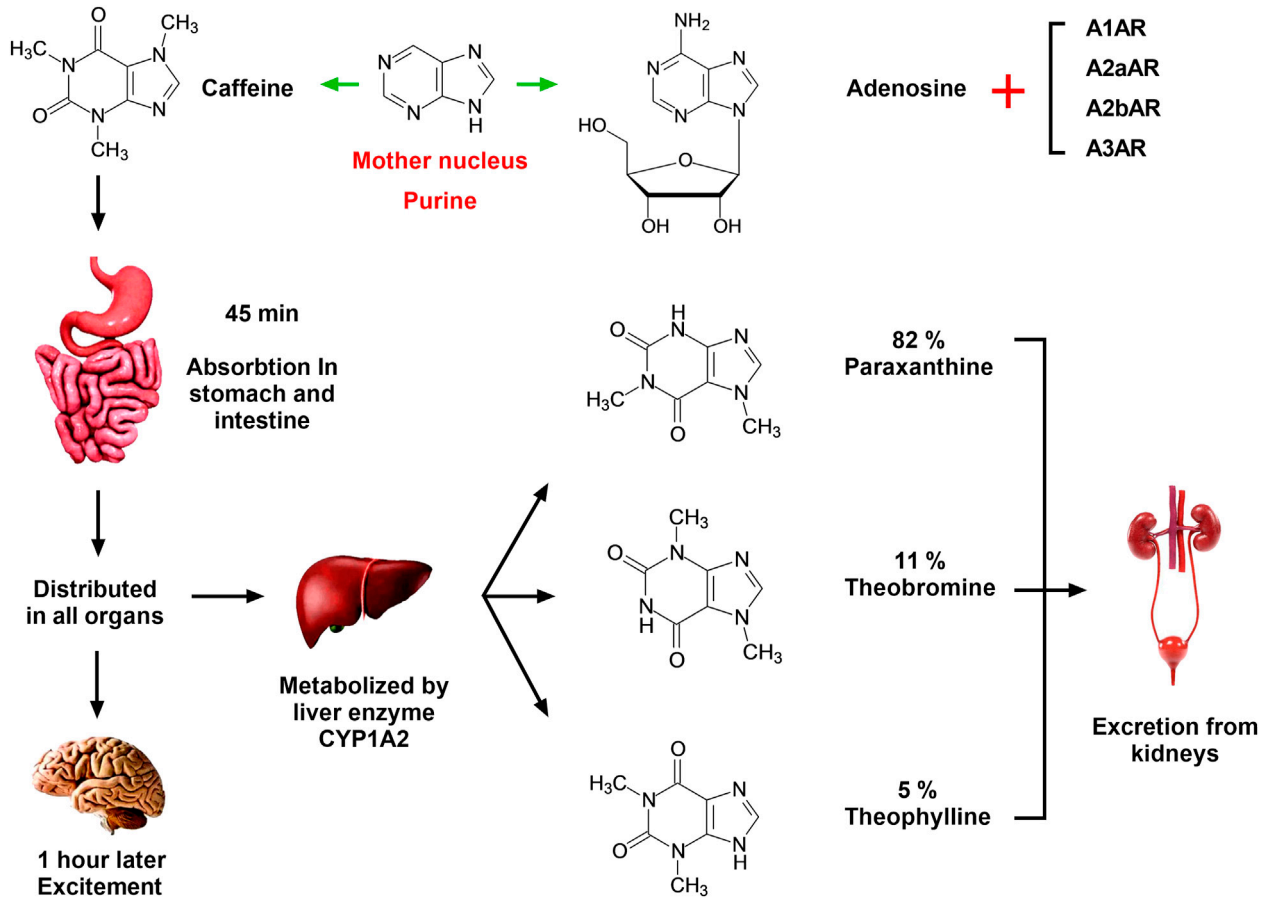

FIGURE 1
Absorption, distribution, metabolism, and excretion of caffeine in the human body. Caffeine has a similar chemical structure to adenosine, and the mother nucleus of both is purine. Therefore, caffeine is a natural non-selective antagonist of adenosine, which can competitively inhibit the binding of adenosine and ARs *in vivo* and play different physiological functions. Caffeine is completely absorbed by the stomach and small intestine within 45 min of oral administration, following which it is distributed in all organs of the body and enters the central nervous system through the blood within 1 h. In the central nervous system, caffeine can combine with ARs and cause central nervous system excitement. Caffeine is catalyzed by CYP1A2 in the liver to produce three primary metabolites: parxanthine (82%), theobromine (11%), and theophylline (5%). The conversion process is a first-order chemical kinetic reaction, and these compounds are further metabolized and eventually excreted in the urine.

controversial studies have stated that drinking caffeine can reduce the risk of various liver diseases, especially in alcoholics. Further research suggests that drinking more than two cups of coffee or tea per day significantly reduces the risk of chronic liver diseases in people at high risk of alcoholism, overweight, and diabetes (Higdon and Frei, 2006; Duseja, 2012).

The chemical structure of caffeine contains a purine ring, which chemically resembles adenosine and is a natural non-selective receptor antagonist of adenosine (Figure 1) (Eltzschig et al., 2012). Previous studies by our research team have shown that caffeine has a certain preventive effect on alcoholic liver fibrosis in rats, in which the cAMP-PKA-CREB signaling pathway is thought to play a role (Wang et al., 2015; Yang et al., 2015). We have previously used acetaldehyde to stimulate Hepatic Stellate cell-T6 (HSC-T6) cells in rats to establish an *in vitro* model of alcoholic liver fibrosis, and the results implicated the cAMP/PKA/SRC/ERK1/2/P38 MAPK signaling pathway as playing a key role, confirming the involvement of the adenosine signaling pathway in alcoholic liver fibrosis (Wang et al., 2014; Wang et al., 2015; Yang et al., 2015).

Recently, there are increasing reports that regular oral coffee is associated with reduced risk of various liver diseases (Saab et al., 2014). Therefore, to update the data in this field, we developed a research synthesis that includes the pathophysiological mechanisms, results of experimental and clinical studies, mechanisms of drug resistance and ways to overcome them, adverse effects of caffeine, recent patents in this field, and future developments. We conducted a small review of articles published before 19 July 2022 in PubMed and Web of Science, which were searched using the keywords “caffeine” and

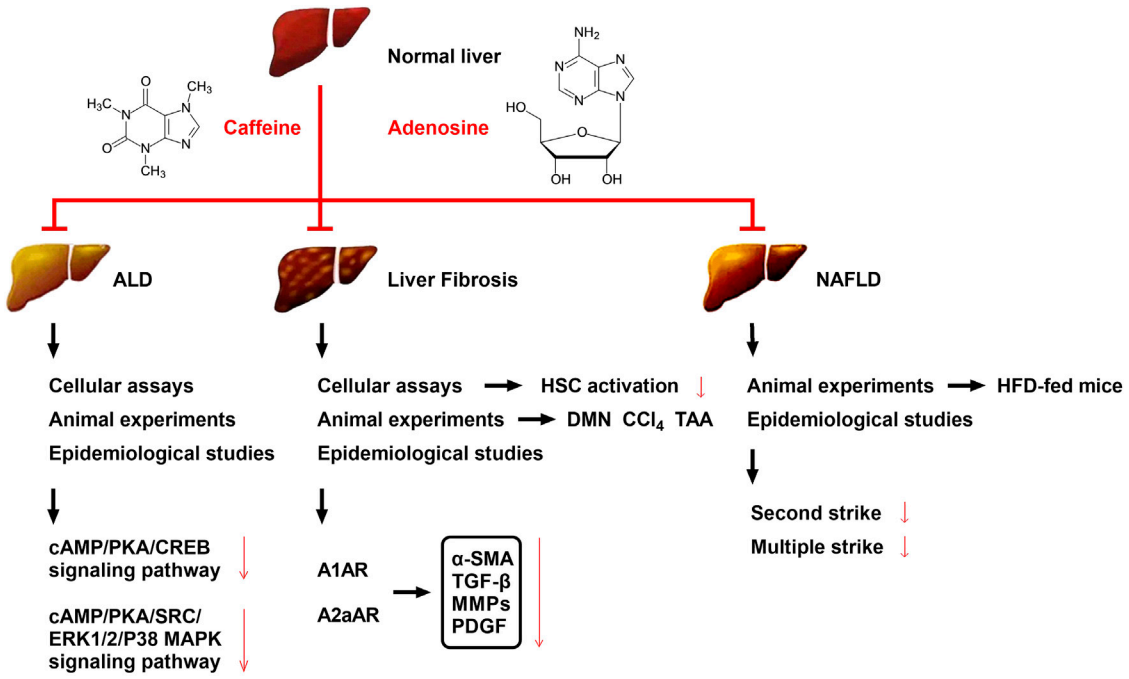

FIGURE 2
Effects and possible mechanisms of caffeine on reducing ALD, liver fibrosis, and NAFLD. The mechanism by which caffeine attenuates ALD may be related to its inhibition of the cAMP/PKA/CREB and cAMP/PKA/SRC/ERK1/2/P38 MAPK signaling pathways. The mechanism by which caffeine attenuates liver fibrosis may be related to its competitive inhibition of adenosine and AR binding (mainly A1AR, A2aAR, and A2bAR) in HSCs, which serves to reduce the levels of the extracellular fibrotic cytokines α-SMA, TGF-β, MMPs, and PDGF. Caffeine has been shown to reduce chemical toxicant-induced liver fibrosis in three animal models of liver fibrosis (DMN, CCl_4, and TAA), and its effect on liver fibrosis has been further confirmed by multiple clinical trials. Caffeine attenuates HFD-induced NAFLD in mice, which has also been confirmed in several clinical trials; its mechanism may be related to the reduction of liver damage caused by the second strike and/or multiple strike.

"liver disease." As a result, we found caffeine to be a potential drug for preventing and treating various liver diseases.

2 Adenosine signaling in the liver

Caffeine is structurally similar to adenosine and is a non-selective adenosine receptor (AR) inhibitor that competently inhibits adenosine both *in vitro* and *in vivo* (van Dam et al., 2020). The release of adenosine triphosphate (ATP) from various cells in the liver (hepatocytes, Kupfer cells, and HSCs) increases when stimulated by various factors, including alcohol, acetaldehyde, chemical toxins, and radiation (Eltzschig et al., 2012; van Dam et al., 2020). When ATP is released extracellularly from stressed or damaged cells, it is rapidly hydrolyzed to adenosine monophosphate (AMP) and phosphoric acid by CD39/ENTPD1 expressed on the cell surface, releasing energy simultaneously, before being further hydrolyzed to adenosine by Ecto-5′-nucleotidase (NT5E, CD73). Adenosine binds to ARs to exert various physiological effects, while adenosine deaminase (ADA) plays a negative regulatory role, which hydrolyzes and inactivates adenosine. ARs have four subtypes, namely, A1AR, A2aAR, A2bAR, and A3AR, which are widely distributed in the body and play different physiological roles after binding with adenosine. Thus, the cascade of extracellular enzyme CD39-CD73-ADA co-regulates and stabilizes the adenosine level (Eltzschig et al., 2012; van Dam et al., 2020). We have previously shown that adenosine A1AR and A2AR of HSCs promote the activation and proliferation of HSCs after activation under the action of acetaldehyde; however, A1AR and A2AR have opposite regulatory effects on the cAMP-PKA-CREB signaling pathway. Additionally, adenosine A1AR antagonists, adenosine A2AR antagonists, and caffeine have significant inhibitory effects on the activation and proliferation of HSCs in alcoholic liver fibrosis (Wang et al., 2015; Yang et al., 2015). An overview of the relationship between the adenosine signaling pathway and various liver diseases is shown in Figures 2, 3.

2.1 Caffeine in alcoholic liver disease

Alcoholic liver disease (ALD) occurs as a result of the interaction of many factors, including oxidative stress, intestinal endotoxin, inflammatory mediators, and nutritional

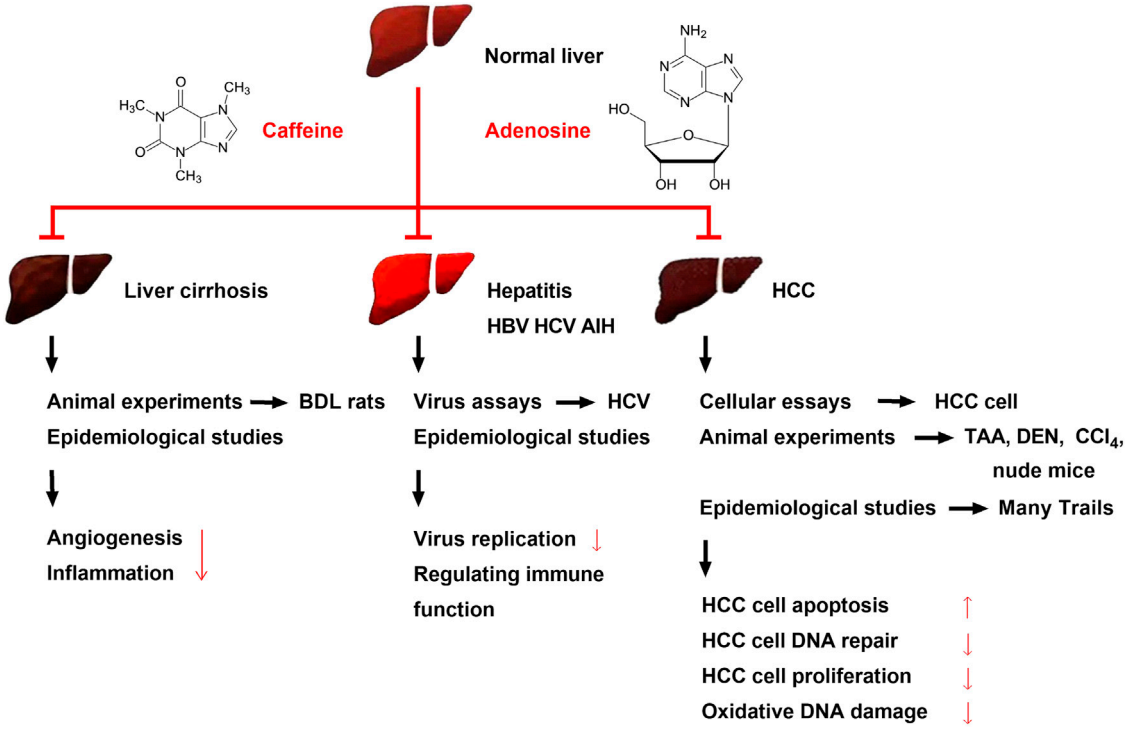

FIGURE 3
Effects of caffeine on alleviating liver cirrhosis, different types of hepatitis, and HCC and its possible mechanisms. Caffeine attenuates BDL-induced liver cirrhosis in rats. Several clinical trials have shown the same result, and the mechanism may be related to the ability of caffeine to inhibit inflammation and angiogenesis. Viral assays have found that caffeine can inhibit HBV and HCV, while clinical trials have found that caffeine can alleviate hepatitis B, C, and AIH; its mechanism may be related to the inhibition of hepatitis virus replication and regulation of immune function. Recent preclinical studies and multiple clinical trials have found that caffeine attenuates HCC. Caffeine inhibits the proliferation of various HCC cells and attenuates chemical toxicant (TAA, DEN, and CCl_4)-induced HCC and xenograft HCC in nude mice. Large clinical trials initiated in several countries have found that the risk of HCC is reduced in people with an oral coffee consumption habit; this may be due to the ability of caffeine to inhibit HCC cell proliferation and oxidative DNA damage and reduce HCC cell DNA repair.

imbalance, which are directly or indirectly induced by the metabolism of ethanol and its derivatives (Li et al., 2021). Additionally, acetaldehyde, a metabolite of ethanol, has strong immunogenicity with the acetaldehyde adduct formed by various proteins, which can stimulate the body to produce antibodies and cause immune damage, leading to damage of important proteins, including protease and DNA (Li et al., 2021). Epidemiological studies have shown that coffee consumption can slow the development of chronic liver disease, including alcoholic cirrhosis (van Dam et al., 2020). Wang et al. established an alcoholic liver fibrosis rat model by intragastric administration of ethanol, followed by treatment with varying concentrations of caffeine (5, 10, and 20 mg/kg/day). The results showed that after 8–12 weeks of treatment, the levels of serum alanine aminotransferase (ALT), aspartate transaminase (AST), hyaluronic acid (HA), laminin (LN), N-terminal peptide of type III procollagen (PIIINP), and type IV collagen in the high-dose group were significantly reduced. Additionally, in an *in vitro* culture model of primary rat HSCs induced by acetaldehyde, it was confirmed that caffeine inhibits acetaldehyde-induced activation and proliferation of HSCs through the A2AR-mediated cAMP/PKA/CREB signaling pathway (Eltzschig et al., 2012; Wang et al., 2015). In conclusion, previous studies, both *in vivo* and *in vitro*, all support the conclusion that caffeine alleviates ALD (Figure 2).

2.2 Caffeine in liver fibrosis

Liver fibrosis is a pathophysiological process that refers to the abnormal proliferation of connective tissues in the liver induced by various pathogenic factors, including viral hepatitis, alcohol, fatty liver, and autoimmune diseases (Arauz et al., 2014; Ebadi et al., 2021). However, any liver injury also involves a process of liver fibrosis during repair and healing (Eraky et al., 2018; Romualdo et al., 2020). The beneficial effects of caffeine and coffee extracts on liver fibrosis have been demonstrated in several standard rodent models of experimental liver fibrosis induced by dimethylnitrosamine (DMN), carbon tetrachloride (CCl_4),

and thioacetamide (TAA), and protective effects of filtered coffee were found in most of the published studies (Furtado et al., 2012; Arauz et al., 2014; Eraky et al., 2018). Recently, researchers have found that caffeine can prevent CCl_4-induced hepatic damage in mice through its antioxidant capacities (Pan et al., 2018). In contrast, one study showed that the intake of unfiltered Turkish coffee not only had no protective effect on CCl_4-induced liver fibrosis but also significantly increased AST/ALT levels, thereby exacerbating CCl_4-induced hepatotoxicity (Dranoff, 2018). As a caveat, given that the underlying mechanisms responsible for these differences have not been studied, more accurate animal studies are needed to confirm them.

Persistent inflammatory factors stimulate HSCs in the liver to secrete fibrotic factors that increase extracellular matrix (ECM) formation and ultimately lead to liver fibrosis (Eraky et al., 2018). In three rat models of CCl_4, DMN, and TAA-induced hepatic fibrosis, coffee and caffeine intake reduced transforming growth factor-β (TGF-β) levels and thus inhibited HSC activation and proliferation (Arauz et al., 2014). During the progress of hepatic fibrosis, HSCs differentiated into myofibroblasts and promoted ECM secretion, a process commonly referred to as HSC activation. Caffeine intake can reduce the total content of hepatic collagen in rodent models of hepatic fibrosis. Activated HSCs also secrete matrix metalloproteinases (MMPs), whose activity is important in maintaining a balance between tissue repair and scar formation in hepatic fibrosis. Caffeine can significantly reduce the total MMP secretion in the liver. Besides, the expression of α-smooth muscle actin (α-SMA) is often a marker of HSC activation in hepatic fibrosis. Caffeine can decrease α-SMA expression in the whole liver, which may indicate decreased HSC activation and slow disease progression. In summary, *in vivo* studies have shown that the anti-fibrosis properties of caffeine converge with a reduction in HSC activation and proliferation (Amer et al., 2017).

HSCs are deemed the main effector cells in liver fibrosis (Eraky et al., 2018). Interestingly, human HSCs express all four ARs (A1AR, A2aAR, A2bAR, and A3AR), while mouse HSCs express all receptors, except A3AR. A2aAR, which regulates the function of HSCs, has been most widely studied (Yang et al., 2015). Indeed, following activation by extracellular adenosine, A2aAR on HSCs significantly upregulates collagen and TGF-β secretion, decreases MMP expression, and prevents the chemotaxis of HSCs to platelet-derived growth factor (PDGF). Additionally, liver inflammation activates HSCs, and the effect of PGE2 on HSC activation is changed from facilitatory to inhibitory when combined with caffeine, suggesting that caffeine effectively suppresses liver fibrosis during inflammation (Yamaguchi et al., 2021). These results suggest that the inhibition of the prefibrotic adenosine signal in HSCs is the mechanism underlying the anti-liver fibrosis effects of caffeine. The main possible mechanisms of the anti-liver fibrosis effects of caffeine are shown in Figure 2.

2.3 Caffeine in non-alcoholic fatty liver disease

Non-alcoholic fatty liver disease (NAFLD) refers to a clinicopathological syndrome characterized by hepatic steatosis, which is caused by other than alcohol and other unclear liver damage factors. The disease spectrum of NAFLD includes non-alcoholic fatty liver, also known as simple fatty liver, non-alcoholic fatty hepatitis, fatty liver fibrosis, cirrhosis, and hepatocellular carcinoma (HCC) (Fang et al., 2019; Mansour et al., 2021). CYP1A2 is an important enzyme in the liver, which catalyzes caffeine to form paraxanthine (82%), theobromine (11%), and theophylline (5%) (Perera et al., 2013; Garduno and Wu, 2021). Apparent caffeine clearance is considered a gold standard measurement of CYP1A2 activity. Previous studies have found that decreased CYP1A2 activity is associated with NAFLD progression, although more research is needed (Perera et al., 2013; Garduno and Wu, 2021). A study in 2019 showed that the prevalence rate of NAFLD in China was approximately 29.2%, with an increase of 14% in the past decade. However, the specific pathogenesis of NAFLD remains to be explored. The doctrine of the "multiple strike" theory, based on the "second strike" theory, is currently widely accepted, and includes lipotoxicity, mitochondrial dysfunction, endoplasmic reticulum stress, adipose tissue dysfunction, inflammatory cytokines, and enteric endotoxin multiple strike factors. Despite advances in research, there remain limited effective therapeutic drugs for NAFLD in clinical practice; thus, it is crucial to fully determine the pathogenesis of NAFLD to establish effective therapeutic targets (Sewter et al., 2021).

Many preclinical studies have shown that caffeine intake alleviates NAFLD and can even prevent NAFLD in high-fat-diet (HFD)-fed mice (Fang et al., 2019; Velázquez et al., 2020). Other studies have shown that Pu-erh tea extract (PTE) protected HFD-fed mice from developing NAFLD, whereas decaffeinated PTE showed no such anti-NAFLD effects (Helal et al., 2018; Fang et al., 2019). Additionally, further studies found that caffeine-stimulated muscle IL-6 mediates the alleviation of NAFLD. Researchers have found that consuming caffeine at a concentration of 0.5 mg/ml in drinking water for 16 weeks has a strong protective effect on HFD-induced NAFLD without affecting HFD-induced oxidative stress. The same method was used to feed IL-6 knockout and wild-type mice, with comparable levels of hepatic steatosis in HFD-fed IL-$6^{-/-}$ and HFD-fed WT mice. The results showed that caffeine consistently protected against HFD-induced NAFLD in the wild-type mice, while the protective effects were abrogated in IL-$6^{-/-}$ mice. Moreover, caffeine-induced STAT3 phosphorylation in the liver was

inhibited in HFD-fed IL-6$^{-/-}$ mice, and caffeine treatment reduced the ALT and AST levels in the HFD-fed control mice but not in the IL-6$^{-/-}$ mice after 12 weeks. These results suggest that IL-6 is necessary for the protective effect of caffeine on NAFLD in mice (Fang et al., 2019).

Caffeine has shown inhibitory effects in most of the preclinical studies on the effects of caffeine on NAFLD/non-alcoholic steatohepatitis (NASH) (Dungubat et al., 2020; Velázquez et al., 2020). New studies have confirmed that 75 mg/kg caffeine per day, which is equivalent to 6 mg/kg per day in humans, could significantly improve liver lipid deposition, glucose metabolism, inflammation, and fibrosis in a mouse model of NASH induced by a high-trans fatty acid/high-carbohydrate diet, with the mechanism thought to be related to the improvement of abnormal gene expression in NASH by caffeine (Konstantinou et al., 2014). However, numerous studies have shown conflicting results on the effects of caffeine on humans and animals. Dungubat et al. used C57BL/6J mice fed a choline-deficient, L-amino acid-defined, high-fat diet (CDAHFD) as an animal model of NASH. Seven-week-old male C57BL/6J received 0.05% (w/w) caffeine and CDAHFD supplemented with 0.1% (w/w) caffeine and chlorogenic acid (CGA) for 7 weeks, and the results showed that caffeine and CGA significantly worsened the markers of liver cell injury, inflammation, and/or steatosis in NASH lesions in mice (Dungubat et al., 2020). Differences in experimental conditions may account for the conflicting results of studies on the effects of caffeine and CGA on NAFLD/NASH. Moreover, in humans, Birerdinc et al. (2012) reported a protective effect of caffeine on patients with NAFLD, but Shen et al. (2016) reported that total caffeine intake was not associated with the prevalence of hepatic fibrosis in NAFLD. Therefore, the use of caffeine in the prevention and treatment of NAFLD still needs further research.

However, another researcher investigated the effects of caffeine and green coffee extract (GCE) on hepatic lipids in lean female rats with steatosis (Velázquez et al., 2020). Female SD rats were fed a standard diet or a cocoa butter-based HFD plus 10% liquid fructose for 3 months, which induced hepatic steatosis without obesity, inflammation, endoplasmic reticulum stress, or hepatic insulin resistance. In the third month, the HFD was supplemented with caffeine (5 mg/kg/day) or GCE. However, the experimental results indicated that neither caffeine nor GCE alleviated hepatic steatosis, but the GCE-treated rats showed lower hepatic triglyceride levels compared with the caffeine group. The experimental results show that a low dose of caffeine did not reduce hepatic steatosis in lean female rats, but the same dose provided as a GCE reduced liver triglyceride levels. Thus, a moderate dose of caffeine, equivalent to 1 cup of coffee a day in humans, did not alleviate liver lipid deposition in a model of diet-induced hepatic steatosis without obesity and inflammation. Differences in experimental conditions may account for the conflicting results of studies on the effects of caffeine on NAFLD/NASH. Various NAFLD/NASH animal models have been used in various studies, mainly including nutritional models, such as high fat, high cholesterol, and high fructose diet, and genetic models such as KK-AY mice (Figure 2) (Birerdinc et al., 2012; Velázquez et al., 2020). Additionally, various caffeine administration methods are used in experimental studies, including *via* drinking water, diet, and gavage, and the doses vary across studies. Therefore, various factors lead to contradictory experimental results across different experiments.

2.4 Caffeine in cirrhosis

Cirrhosis is a common clinical chronic progressive liver disease, which is caused by one or more etiologies of chronic or repeated action of diffuse liver damage. The histopathology of cirrhosis shows extensive necrosis of hepatocytes, nodular regeneration of residual hepatocytes, connective tissue hyperplasia, and fibrous septum formation, resulting in the destruction of the liver lobule structure and formation of pseudolobules (Feld et al., 2015). The liver gradually becomes deformed and hardened before ultimately developing into cirrhosis. Earlier studies have found that caffeine clearance in cirrhosis can be used to measure liver metabolic capacity (Lewis and Rector, 1992; Tangkijvanich et al., 1999). For example, the 13C-caffeine breath test is a non-invasive, quantitative test of liver function, which can reliably differentiate patients with decompensated cirrhosis from non-cirrhotic patients with chronic liver diseases (Xin et al., 2021). Additionally, previous studies have assessed the effect of caffeinated beverage consumption on the risk of symptomatic liver cirrhosis (Corrao et al., 2001). The results demonstrated a significant reduction in the risk of liver cirrhosis with increased coffee intake. The liver cirrhosis odds ratios (ORs) decreased from 1.0 (reference category: lifetime abstainers from coffee) to 0.47 (95% confidence interval: 0.20, 1.10), 0.23 (0.10, 0.53), 0.21 (0.06, 0.74), and 0.16 (0.05, 0.50) in individuals who drank 1, 2, 3, and ≥4 cups of coffee, respectively. Caffeine (250 mg) is also commonly administered orally to investigate the effect of cirrhosis on the disposition of the liver and the elimination of drugs from it (Desmond et al., 1980). These findings suggest that coffee, but not other caffeinated beverages, inhibits the onset of alcoholic and nonalcoholic liver cirrhosis (Corrao et al., 2001).

The anti-inflammatory effect of caffeine varies with the treatment protocols and doses (Feld et al., 2015; de Alcântara Almeida et al., 2021). Bile duct ligation (BDL) in rats is a common animal model of liver cirrhosis, and previous studies have demonstrated that BDL rats have significantly higher

portal pressure, elevated total bilirubin (TB), AST, and ALT compared to sham-operated rats, indicating the typical presentation of liver cirrhosis (Chang et al., 2019). Researchers have found that treatment with high doses of caffeine (50 mg/kg/day) for 2 weeks eased liver fibrosis, alleviated intrahepatic angiogenesis, and reduced portal pressure in rats with BDL-induced cirrhosis without adversely affecting systemic hemodynamics, supporting the benefit of using caffeine treatment in patients with cirrhosis (Chang et al., 2019). The underlying mechanisms might be related to inhibiting angiogenesis and inflammation. However, the plasma levels of ALT, AST, and TB were not influenced by 50 mg/kg/day dose of caffeine treatment in common BDL rats; therefore, the specific mechanisms require further study. It has been reported that 250 mg of caffeine administered orally can prolong the elimination half-life by approximately 1 h in patients with cirrhosis compared to healthy controls, but the result did not reach statistical significance (Desmond et al., 1980). Therefore, the adverse effects of prolonged plasma clearance should be considered prior to long-term oral administration of coffee in patients with cirrhosis (Lewis and Rector, 1992).

In the early stage of liver cirrhosis, there are no obvious symptoms due to the strong liver compensatory function, while in the later stage, liver function damage and portal hypertension are the main manifestations, and multiple systems are involved. In the late stage, complications, such as upper gastrointestinal bleeding, hepatic encephalopathy, secondary infection, hypersplenism, ascites, and cancer are common (Hsu et al., 2015). Oral caffeine at 50 mg/kg/day alleviates hemodynamic derangements and portal hypertension in cirrhotic rats induced by BDL compared to vehicle (sham rats). Additionally, 28 days after administration, caffeine increased systemic vascular resistance and reduced superior mesenteric artery flow, mesenteric vascular density, portosystemic shunting, intrahepatic angiogenesis, and fibrosis, without affecting liver and renal biochemistry (Hsu et al., 2015). Further research found that the selective adenosine A1 agonist N6-cyclopentyladenosine (CPA) (1 mg/kg/day, i.p.) or A2A agonist GCS21680 (0.5 mg/kg/day, i.p.) could reverse these treatment effects. Researchers then used oral gavage administration of TAA (200 mg/kg, thrice-weekly for 8 weeks)-induced cirrhotic rats, and the results demonstrated that caffeine downregulated endothelial NO synthase, vascular endothelial growth factor (VEGF), phospho-VEGFR2, and phospho-Akt mesenteric protein expression compared to vehicle (distilled water). Further *in vivo* studies have also found that caffeine inhibited the activation of hepatic stellate and sinusoidal endothelial cells, which was reversed by CPA (1 mg/kg/day, i.p.) and GCS21680 (0.5 mg/kg/day, i.p.) (Figure 3) (Hsu et al., 2015). However, caffeine did not modify the vascular response to vasoconstrictors in splanchnic, hepatic, and collateral vascular beds in this study, although the specific reasons for this remain to be determined (Hsu et al., 2015).

2.5 Caffeine in (autoimmune) hepatitis

Hepatitis is a general term for liver inflammation, which usually refers to liver cells destroyed by various pathogenic factors, such as viruses, bacteria, parasites, chemicals, poisons, drugs, alcohol, and autoimmune factors. The function of the liver is damaged, causing a series of uncomfortable symptoms and abnormal liver function indicators (Jaruvongvanich et al., 2017; Wijarnpreecha et al., 2017). A case control study, which employed 234 hepatitis B virus (HBV) chronic carriers (109 cases and 125 controls) investigated whether moderate coffee consumption reduces the risk of HCC in hepatitis B chronic carriers. The results indicated that coffee consumption significantly reduced the risk of HCC by almost half [OR: 0.54, 95% confidence interval (CI): 0.30–0.97] in HBV chronic carriers, with the risk to moderate drinkers reduced by almost 60% (OR: 0.41, 95% CI: 0.19–0.89) compared to those with no coffee-drinking habit (Leung et al., 2011). Caffeine inhibits hepatitis C virus (HCV) replication *in vitro* and has been shown to dose-dependently inhibit HCV replication at non-cytotoxic concentrations, with an IC50 value of 0.7263 mM after 48 h of incubation. These results implicate caffeine as a novel agent for anti-HCV therapies due to its efficient inhibition of HCV replication at non-toxic concentrations (Batista et al., 2015). Additionally, previous studies have demonstrated that caffeine intake is significantly associated with decreased odds of advanced hepatic fibrosis in patients with chronic hepatitis C. Future prospective studies should focus on assessing the optimal dose and preparation of caffeinated beverages for the prevention of hepatitis (Jaruvongvanich et al., 2017; Wijarnpreecha et al., 2017).

Autoimmune hepatitis (AIH) is one of the three major autoimmune liver diseases, in addition to biliary cirrhosis and primary sclerosing cholangitis. AIH is a chronic inflammation of the liver of unknown etiology and presents with hyperimmunoglobulinemia and/or circulating autoantibodies (Lammert et al., 2022). The basic pathology of AIH is detrital necrosis in the perilobular area of the liver, which may also be accompanied by bridging necrosis with marked infiltration of lymphocytes and monocytes. AIH is more common in females, with a male to female ratio of approximately 1:4. AIH can occur at any age and is often accompanied by extrahepatic autoimmune disease, which can be effectively treated with immunosuppressive therapy (Lammert et al., 2022). A recent study found that patients with AIH reported lower lifetime coffee consumption. Researchers investigated the lifetime coffee consumption of 358 patients with AIH (cases) and 564 volunteers (controls), as well as its associations with age, sex, education, smoking status,

BMI, and daily activity. The results showed that 24.6% of patients with AIH never drank coffee compared to 15.7% of controls ($p < 0.001$). Additionally, only 65.6% were current drinkers compared to 77% of controls ($p < 0.001$). Besides, patients with AIH consumed fewer lifetime cups of coffee per month (45 vs. 47 for controls, $p < 0.001$) and spent a lower percentage of their lives drinking coffee (62.5% vs. 69.1% for controls, $p < 0.001$). Furthermore, the relationship between coffee consumption and the risk of AIH development was dose-dependent (Figure 3). However, the major limitations of this study include the memory bias of the patients with AIH and the low population of patients. Future studies should consider the association between coffee intake and outcomes related to non-transplanted AIH livers (Lammert et al., 2022).

2.6 Caffeine in HCC

HCC is a primary liver cancer with a high mortality rate and represents the most common malignancy worldwide, especially in Asia, Africa, and southern Europe (Johnson et al., 2011; Kawano et al., 2012). Viral hepatitis (hepatitis B or C), cirrhosis, diabetes mellitus, and chronic alcoholism are the most common causes of HCC (Johnson et al., 2022; Salem et al., 2022). Tumor size and stage are the two key factors affecting the treatment and prognosis of HCC, and the prognosis of advanced HCC is poor. Primary HCC is rare in the United States, with most cases being metastatic HCC (Higdon and Frei, 2006; Kennedy et al., 2017). Sorafenib was approved by the FDA in 2007 for treating unresectable HCC, while in 2017, regorafenib and nivolumab were approved for HCC. Lenvatinib was approved in 2018 for patients with unresectable HCC. All four of these drugs have drug resistance and toxicity, and their therapeutic effects remain incompletely satisfactory. According to recent reports, 60% of the anticancer medications in current use have been obtained from natural sources (Rawat et al., 2018). Dietary phytochemical caffeine has been found to be useful for treating HCC and other diseases (Fujimaki et al., 2012; Estari et al., 2021). As early as 1989, studies reported on the use of caffeine-potentiated chemotherapy (Kawano et al., 2012). Recent cellular assays, animal experiments, and clinical trials have shown that caffeine has a protective effect on the liver and reduces the risk of HCC. Caffeine may be developed as a drug to prevent and treat HCC in the future (Figure 3) (Okano et al., 2011; Wang et al., 2019).

2.6.1 Cellular assays

Previous studies have found that caffeine inhibits DNA repair and can increase the antitumor effect of cisplatin (Chae et al., 2012; Kawano et al., 2012). Researchers have demonstrated that caffeine (0.5 mM) increased the antitumor effect of cisplatin (0.4, 0.6, 1.2, 0.9 μg/ml) on the proliferation of various HCC cells (Li-7, HLF, HuH-7, HepG2). However, caffeine treatment alone did not increase cell apoptosis in the four HCC cell lines (Chae et al., 2012; Kawano et al., 2012). Currently, the idea that caffeine reduces the risk of HCC is controversial (Wang et al., 2011). Caffeine is a well-known radiosensitizer, which eliminates radiation-induced G2 block and promotes cancer cell apoptosis. Caffeine can increase the radiosensitivity of McA-RH7777 rat hepatocellular cancer cells but had no effect on BRL3A rat normal liver cells and irradiated normal liver tissues *in vivo*. However, caffeine has been shown to enhance the radiosensitivity of ortho topically transplanted human HCC in a nude mouse model, suggesting that it may be effective intreating liver cancer, although the dosage and method require further study (Wang et al., 2011). Chae et al. demonstrated that paclitaxel combined with caffeine is effective in the reversal of paclitaxel resistance through the inhibition of the DNA damage checkpoint *in vitro* (Chae et al., 2012). The results of these cell assays support the use of caffeine as an adjunctive therapy for HCC (Wang et al., 2011; Chae et al., 2012). Another cellular assay found that the non-selective AR antagonist caffeine and its analog CGS 15943 inhibited human HCC cell growth and the proliferation of four HCC cell lines (HLF and SK-Hep-1 cell lines, HepG2 and PLC-PRF-5 cells) by targeting the phosphoinositide 3-kinase/Akt pathway; however, CGS 15943 only slightly induced apoptosis in these cell lines, suggesting that caffeine has a chemopreventive effect against HCC (Edling et al., 2014). Moreover, an *in vitro* study showed that a low concentration of caffeine inhibits the progression of HCC *via* the Akt signaling pathway (Dong et al., 2015), while another study showed that caffeine inhibited the proliferation of liver cancer cells and activated the MEK/ERK/EGFR signaling pathway (Okano et al., 2008).

2.6.2 Animal experiments

Currently, three chemical toxins, namely CCl_4, TAA, and DEN, are commonly used to induce HCC in rodents, while there are more than 1,000 chemical compounds in coffee (Bravi et al., 2013; Rawat et al., 2018; Zhang et al., 2021). The anticancer effect of coffee may be the result of the combined action of several chemical components such as caffeine, trigonelline (TRI), and CGA (Kennedy et al., 2017; Romualdo et al., 2020). Indeed, researchers have demonstrated that a combination of CAF+TRI+CGA (50, 25, and 25 mg/kg) administered intragastrically for 10 weeks reduced the incidence, number, and proliferation (Ki-67) of hepatocellular preneoplastic foci while enhancing apoptosis (cleaved caspase-3) in the adjacent parenchyma in HCC rats induced by DEN/CCl_4 (Romualdo et al., 2020). The mechanism by which the three component combination attenuates fibrosis-associated hepatocarcinogenesis may be related to reduced DNA expression. Different types of coffee may produce different results. It has also been shown that intake of conventional coffee, decaffeinated coffee, and 0.1% caffeine for 8 weeks significantly reduced serum ALT ($p <$

0.001), oxidized glutathione ($p < 0.05$), fibrosis/inflammation scores ($p < 0.001$), collagen volume fraction ($p < 0.01$), and TGF-β1 protein expression ($p \leq 0.001$) in the livers from TAA (200 mg/kg b.w., i.p.)-treated Wistar rats (Amer et al., 2017).

2.6.3 Clinical trials

Many epidemiological surveys and clinical studies have found that moderate coffee consumption reduces the risk of HCC, with similar results found in the North American population, the European population, the Japanese population, the Singaporean population, and the Hong Kong population (Bamia et al., 2015; Petrick et al., 2015; Di Maso et al., 2021). However, no such study has been conducted in the Chinese mainland population, which may be related to the fact that the Chinese population is not used to drinking coffee but prefers drinking tea (Johnson et al., 2011; Di Maso et al., 2021). From 1993 to 1998, the Singapore Chinese Health Study enrolled a prospective cohort of 63,257 middle-aged and older Chinese men and women with a relatively high-risk for HCC. The researchers found that 362 of the cohort had developed HCC by the end of 31 December 2006 and that individuals who consumed ≥3 cups of coffee per day experienced a statistically significant reduction in the risk of HCC [44%; hazard ratio (HR): 0.56, 95% CI: 0.31–1.00; $p = 0.049$] after adjustment for potential confounders and tea consumption compared to non-drinkers of coffee (Johnson et al., 2011). A recently published systematic review and dose-response meta-analysis enrolled 2,272,642 participants and 2,905 cases to explore the effects of coffee, including caffeinated and decaffeinated coffee, on the risk of HCC and found that an extra two cups of coffee per day was associated with a 35% reduction in the risk of HCC [relative risk (RR): 0.65, 95% CI: 0.59–0.72], while an extra two cups of caffeinated and decaffeinated coffee (2 and 3 cohort studies, respectively) was associated with reductions of 27% (RR: 0.73, 95% CI: 0.63–0.85) and 14% (RR: 0.86, 95% CI: 0.74–1.00) in the risk of HCC, respectively (Kennedy et al., 2017). The researchers believe that the mechanism of action of caffeine against HCC might be related to the inhibition of HCC cell proliferation and the alleviation of oxidative DNA damage, although opposing results have also been published (Kennedy et al., 2017). Indeed, another *in vitro* study found that caffeine alone at tested concentrations was not cytotoxic and did not induce DNA damage in HepG2 cells (Leão et al., 2021). Coffee consumption may have a protective effect on chronic liver disease, which needs to be confirmed in larger populations (Johnson et al., 2011). A Hong Kong, China, case-control study enrolled 234 chronic carriers of hepatitis B (109 vs. 125 controls) and found that moderate coffee consumption was associated with a reduced risk of HCC in chronic carriers of hepatitis B; however, the study was limited by a small sample size (Leung et al., 2011). Recent studies have demonstrated that the methylxanthine derivative caffeine upregulated peroxisome proliferator-activated receptor gamma (PPARγ) expression in hepatocytes of Caucasian patients with ongoing hepatic fibrogenesis and Chinese patients with fully developed HCC, suggesting that the effects of caffeine vary among ethnic groups; thus, further studies are necessary to fully understand the underlying mechanisms (Gressner et al., 2009).

The number of large clinical trials linking coffee consumption to a reduced risk of chronic liver disease has increased recently (Kennedy et al., 2017). A study published in 2015 recruited a total of 1,212,893 subjects [HCC, $n = 860$; intrahepatic cholangiocarcinoma (ICC), $n = 260$] and found that higher coffee consumption (>3 cups/day) was associated with lower risk of HCC compared to non-drinkers (HR: 0.73, 95% CI: 0.53–0.99; $p < 0.0001$). Additionally, coffee with or without caffeine and sex may have influenced the results, but there was no relationship between coffee consumption and ICC. Moreover, the large clinical trials did not consider ethnic differences in people from different regions and how the coffee was prepared (Petrick et al., 2015). Another multi-center, prospective cohort study identified 201 HCC cases among 486,799 men/women, after a median follow-up of 11 years and calculated the adjusted HR for HCC incidence in relation to quintiles/categories of coffee/tea intakes. The results showed that the coffee consumers in the highest quintile compared to the lowest quintile had a 72% reduced risk of HCC (HR: 0.28; 95% CI: 0.16–0.50, P-trend<0.001) (Bamia et al., 2015). Mechanistic studies could clarify whether these significant associations can be attributed to caffeine or other components in these drinks (Bamia et al., 2015). Two reviews published in 2021 analyzed and summarized the Caffeinated Coffee Consumption and Health Outcomes in the US Population and found that caffeinated coffee consumption decreased the incidence/mortality of cardiovascular disease, as well as the incidence of type 2 diabetes and HCC, with a recommended dose of 3–4 cups per day (120 ml/cup) (Di Maso et al., 2021; Kolb et al., 2021). Interestingly, coffee consumption has also been shown to reduce HCC recurrence after orthotopic liver transplantation, in that those with postoperative coffee intake ≥3 cups/day had a longer overall survival than those who consumed less or no coffee. An *in vitro* study showed that the antagonist activity of caffeine has adenosine A2AR-mediated growth-promoting effects on HCC cells associated with the MAPK and NF-kappa B pathways (Wiltberger et al., 2019). The specific mechanism by which coffee consumption reduces the risk of HCC still needs further study. In conclusion, recent cellular assays, animal experiments, and epidemiological studies have found that oral coffee consumption reduces the risk of HCC.

2.7 Toxicity or adverse effects of caffeine

Maternal caffeine intake during pregnancy is associated with an increased risk of childhood obesity. Studies in adults suggest

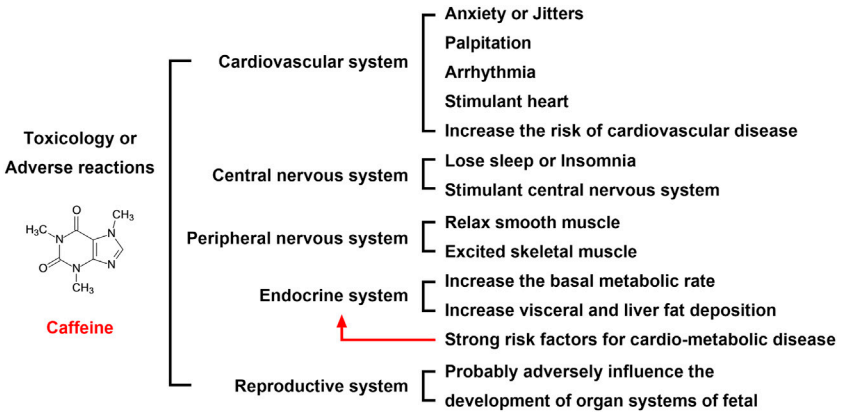

FIGURE 4
Toxicology or adverse reactions of caffeine. The adverse reactions of caffeine on the cardiovascular, nervous, and reproductive systems are serious. Although most of the adverse reactions disappear after discontinuing oral administration, the impact on the fetus is more serious, which requires expecting mothers to be vigilant. Therefore, an oral dose of coffee is not recommended for women who are trying to become pregnant or who are pregnant.

that caffeine intake also directly affects the visceral and liver fat deposition, which are strong risk factors for cardio-metabolic disease (Voerman et al., 2020) (Figure 4). A recent population-based prospective cohort study recruited 4,770 pregnant women, and of the 4,770 women included, 2,780 (58.3%), 1,583 (33.2%), 329 (6.9%), and 78 (1.6%) consumed <2 units, 2–3.9 units, 4–5.9 units, and ≥6 units of caffeine per day, respectively, during pregnancy. The results showed that high maternal caffeine intake during pregnancy was associated with higher childhood general body fat mass, abdominal fat mass, and liver fat fraction at the age of 10 years, while differential fat accumulation in these depots may increase susceptibility to cardio-metabolic disease in later life (Voerman et al., 2020). However, the mechanisms underlying these findings are poorly understood.

According to the World Health Organization (WHO), epidemiological evidence indicates that in pregnant women, a caffeine intake of 300 mg/day (5 mg/kg × day) is associated with an increased risk of intrauterine growth retardation (IUGR) (He et al., 2019). Previous studies have demonstrated that prenatal caffeine exposure (PCE) induces IUGR and high susceptibility to NAFLD in offspring rats, with the underlying mechanisms considered to be associated with fetal overexposure to maternal glucocorticoids (He et al., 2019). Further research found that PCE structurally and functionally inhibited the fetal liver and induced catch-up growth after birth in rat offspring with IUGR, and the mechanisms underlying these phenomena were associated with the inhibition of GR/C/EBPα/IGF1R signaling by intrauterine maternal glucocorticoid overexposure. The effects of caffeine exposure during pregnancy on the increased risk of liver disease in offspring remain controversial and require further study. Another study showed that PCE increased the serum total cholesterol levels in adult offspring rats *via* impacting histone acetylation and cholesterol synthesis-related gene expression *via* regulation of the A2AR/cAMP/PKA pathway and SIRT1 expression at the cellular level (Hu et al., 2019). Therefore, oral caffeine (including caffeinated, decaffeinated, or a combination of both) consumption at any dose is not recommended for women who are trying to become pregnant or who are already pregnant. Interestingly, maternal caffeine intake, but not paternal caffeine intake, has been found to be associated with childhood obesity (Voerman et al., 2020).

3 Discussion

The present study examined the beneficial use of caffeine in different liver diseases and its toxity. The pharmacokinetics of caffeine in human body and possible adverse effects of coffee/caffeine consumption have been investigated in great details. This systematic review of studies on the effects of coffee on ALD, viral (autoimmune) hepatitis, NAFLD, cirrhosis and HCC was performed to examine the association of coffee consumption with various chronic liver diseases. Many questions however remain unanswered before we conclude that coffee can take care of our livers. Amount of coffee, and type of coffee no doubt would be important but equally important might be the race of the population being studied for the beneficial effects of coffee. Additional animal and cell culture studies have also further elucidated the biochemical basis by which coffee may inhibit adenosine and AR binding in patients with various liver diseases, and the mechanism involves multiple signaling pathways. Besides, at present, the experimental results on the effects of coffee exposure during pregnancy on the fetus are still

controversial and need further study. There is still a long way to go before all the above problems can be solved.

Numerous preclinical studies and epidemiological investigations have found that oral caffeine has preventive and therapeutic effects on various liver diseases. However, the current research on caffeine dosage remains controversial. In humans with a moderate to high caffeine intake, daily doses are approximately 10–20 mg/kg. It is estimated that an adult human (mean weight, 70 kg) with moderate coffee intake consumes approximately 400 mg of caffeine per day, which is equivalent to 6 mg/kg per day or three cups of coffee. The average green tea drinker could be defined as a 60 kg man who consumes 10 g of green tea in four cups every day. In the future, caffeine may be developed as a drug to prevent and treat liver diseases. Future research should focus on identifying the explicit dose and mechanisms.

Author contributions

Writing the manuscript: LS, FW, and DZ; developing the idea for the article and critically revising it: XM and JL; supervision: XL. All authors have read and approved the final version of the manuscript.

Funding

This study was supported by the National Natural Science Foundation of China (Grant No. 82003849), the National Natural Science Foundation of China (Grant No. 81970518), and the Special Doctoral Fund of Hefei Hospital Affiliated to Anhui Medical University (The 2nd People's Hospital of Hefei) (Grant No. 2020BSZX04).

Acknowledgments

We thank LetPub (www.letpub.com) for its linguistic assistance during the preparation of this manuscript.

Conflict of interest

The authors declare that the research was conducted in the absence of any commercial or financial relationships that could be construed as a potential conflict of interest.

Publisher's note

All claims expressed in this article are solely those of the authors and do not necessarily represent those of their affiliated organizations, or those of the publisher, the editors and the reviewers. Any product that may be evaluated in this article, or claim that may be made by its manufacturer, is not guaranteed or endorsed by the publisher.

References

Alehaideb, Z., Sheriffdeen, M., and Law, F. (2021). Inhibition of caffeine metabolism by apiaceous and rutaceae families of plant products in humans: *In vivo* and *in vitro* studies. *Front. Pharmacol.* 12, 641090. doi:10.3389/fphar.2021.641090

Alshabi, A. M., Alkahtani, S. A., Shaikh, I. A., and Habeeb, M. S. (2021). Caffeine modulates pharmacokinetic and pharmacodynamic profiles of pioglitazone in diabetic rats: Impact on therapeutics. *Saudi Med. J.* 42 (2), 151–160. doi:10.15537/smj.2021.2.25695

Amer, M. G., Mazen, N. F., and Mohamed, A. M. (2017). Caffeine intake decreases oxidative stress and inflammatory biomarkers in experimental liver diseases induced by thioacetamide: Biochemical and histological study. *Int. J. Immunopathol. Pharmacol.* 30 (1), 13–24. doi:10.1177/0394632017694898

Arauz, J., Zarco, N., Segovia, J., Shibayama, M., Tsutsumi, V., and Muriel, P. (2014). Caffeine prevents experimental liver fibrosis by blocking the expression of TGF-β. *Eur. J. Gastroenterol. Hepatol.* 26 (2), 164–173. doi:10.1097/MEG.0b013e3283644e26

Bamia, C., Lagiou, P., Jenab, M., Trichopoulou, A., Fedirko, V., Aleksandrova, K., et al. (2015). Coffee, tea and decaffeinated coffee in relation to hepatocellular carcinoma in a European population: Multicentre, prospective cohort study. *Int. J. Cancer* 136 (8), 1899–1908. doi:10.1002/ijc.29214

Barcelos, R. P., Souza, M. A., Amaral, G. P., Stefanello, S. T., Bresciani, G., Fighera, M. R., et al. (2014). Caffeine supplementation modulates oxidative stress markers in the liver of trained rats. *Life Sci.* 96 (1-2), 40–45. doi:10.1016/j.lfs.2013.12.002

Batista, M. N., Carneiro, B. M., Braga, A. C., and Rahal, P. (2015). Caffeine inhibits hepatitis C virus replication *in vitro*. *Arch. Virol.* 160 (2), 399–407. doi:10.1007/s00705-014-2302-1

Birerdinc, A., Stepanova, M., Pawloski, L., and Younossi, Z. M. (2012). Caffeine is protective in patients with non-alcoholic fatty liver disease. *Aliment. Pharmacol. Ther.* 35 (1), 76–82. doi:10.1111/j.1365-2036.2011.04916.x

Bravi, F., Bosetti, C., Tavani, A., Gallus, S., and La Vecchia, C. (2013). Coffee reduces risk for hepatocellular carcinoma: An updated meta-analysis. *Clin. Gastroenterol. Hepatol.* 11 (11), 1413–1421. doi:10.1016/j.cgh.2013.04.039

Chae, S., Kim, Y. B., Lee, J. S., and Cho, H. (2012). Resistance to paclitaxel in hepatoma cells is related to static JNK activation and prohibition into entry of mitosis. *Am. J. Physiol. Gastrointest. Liver Physiol.* 302 (9), G1016–G1024. doi:10.1152/ajpgi.00449.2011

Chang, C. C., Chuang, C. L., Tsai, M. H., Hsin, I. F., Hsu, S. J., Huang, H. C., et al. (2019). Effects of caffeine treatment on hepatopulmonary syndrome in biliary cirrhotic rats. *Int. J. Mol. Sci.* 20 (7), 1566. doi:10.3390/ijms20071566

Corrao, G., Zambon, A., Bagnardi, V., D'Amicis, A., Klatsky, A., and D'Amicis, A.Collaborative SIDECIR Group (2001). Coffee, caffeine, and the risk of liver cirrhosis. *Ann. Epidemiol.* 11 (7), 458–465. doi:10.1016/s1047-2797(01)00223-x

de Alcântara Almeida, I., Mancebo Dorvigny, B., Souza Tavares, L., Nunes Santana, L., and Vitor Lima-Filho, J. (2021). Anti-inflammatory activity of caffeine (1, 3, 7-trimethylxanthine) after experimental challenge with virulent Listeria monocytogenes in Swiss mice. *Int. Immunopharmacol.* 100, 108090. doi:10.1016/j.intimp.2021.108090

Desmond, P. V., Patwardhan, R. V., Johnson, R. F., and Schenker, S. (1980). Impaired elimination of caffeine in cirrhosis. *Dig. Dis. Sci.* 25 (3), 193–197. doi:10.1007/BF01308138

Di Maso, M., Boffetta, P., Negri, E., La Vecchia, C., and Bravi, F. (2021). Caffeinated coffee consumption and health outcomes in the US population: A dose-response meta-analysis and estimation of disease cases and deaths avoided. *Adv. Nutr.* 12 (4), 1160–1176. doi:10.1093/advances/nmaa177

Dong, S., Kong, J., Kong, J., Shen, Q., Kong, F., Sun, W., et al. (2015). Low concentration of caffeine inhibits the progression of the hepatocellular carcinoma via Akt signaling pathway. *Anticancer. Agents Med. Chem.* 15 (4), 484–492. doi:10.2174/1871520615666150209110832

Dranoff, J. A. (2018). Coffee consumption and prevention of cirrhosis: In support of the caffeine hypothesis. *Gene Expr.* 18 (1), 1–3. doi:10.3727/105221617X15046391179559

Dungubat, E., Watabe, S., Togashi-Kumagai, A., Watanabe, M., Kobayashi, Y., Harada, N., et al. (2020). Effects of caffeine and chlorogenic acid on nonalcoholic steatohepatitis in mice induced by choline-deficient, L-amino acid-defined, high-fat diet. *Nutrients* 12 (12), 3886. doi:10.3390/nu12123886

Duseja, A. K. (2012). Coffee and liver - long way to go. *J. Clin. Exp. Hepatol.* 2 (3), 291–294. doi:10.1016/j.jceh.2012.07.006

Ebadi, M., Ip, S., Bhanji, R. A., and Montano-Loza, A. J. (2021). Effect of coffee consumption on non-alcoholic fatty liver disease incidence, prevalence and risk of significant liver fibrosis: Systematic review with meta-analysis of observational studies. *Nutrients* 13 (9), 3042. doi:10.3390/nu13093042

Edling, C. E., Selvaggi, F., Ghonaim, R., Maffucci, T., and Falasca, M. (2014). Caffeine and the analog CGS 15943 inhibit cancer cell growth by targeting the phosphoinositide 3-kinase/Akt pathway. *Cancer Biol. Ther.* 15 (5), 524–532. doi:10.4161/cbt.28018

Eltzschig, H. K., Sitkovsky, M. V., and Robson, S. C. (2012). Purinergic signaling during inflammation. *N. Engl. J. Med.* 367 (24), 2322–2333. doi:10.1056/NEJMra1205750

Eraky, S. M., El-Mesery, M., El-Karef, A., Eissa, L. A., and El-Gayar, A. M. (2018). Silymarin and caffeine combination ameliorates experimentally-induced hepatic fibrosis through down-regulation of LPAR1 expression. *Biomed. Pharmacother.* 101, 49–57. doi:10.1016/j.biopha.2018.02.064

Estari, R. K., Dong, J., Chan, W. K., Park, M. S., and Zhou, Z. (2021). Time effect of rutaecarpine on caffeine pharmacokinetics in rats. *Biochem. Biophys. Rep.* 28, 101121. doi:10.1016/j.bbrep.2021.101121

Fang, C., Cai, X., Hayashi, S., Hao, S., Sakiyama, H., Wang, X., et al. (2019). Caffeine-stimulated muscle IL-6 mediates alleviation of non-alcoholic fatty liver disease. *Biochim. Biophys. Acta. Mol. Cell Biol. Lipids* 1864 (3), 271–280. doi:10.1016/j.bbalip.2018.12.003

Feld, J. J., Lavoie, É. G., Fausther, M., and Dranoff, J. A. (2015). I drink for my liver, doc: Emerging evidence that coffee prevents cirrhosis. *F1000Res.* 4, 95. doi:10.12688/f1000research.6368.2

Fujimaki, S., Matsuda, Y., Wakai, T., Sanpei, A., Kubota, M., Takamura, M., et al. (2012). Blockade of ataxia telangiectasia mutated sensitizes hepatoma cell lines to sorafenib by interfering with Akt signaling. *Cancer Lett.* 319 (1), 98–108. doi:10.1016/j.canlet.2011.12.043

Furtado, K. S., Prado, M. G., Aguiar E Silva, M. A., Dias, M. C., Rivelli, D. P., Rodrigues, M. A., et al. (2012). Coffee and caffeine protect against liver injury induced by thioacetamide in male Wistar rats. *Basic Clin. Pharmacol. Toxicol.* 111 (5), 339–347. doi:10.1111/j.1742-7843.2012.00903.x

Garduno, A., and Wu, T. (2021). Tobacco smoke and CYP1A2 activity in a US population with normal liver enzyme levels. *Int. J. Environ. Res. Public Health* 18 (5), 2225. doi:10.3390/ijerph18052225

Gressner, O. A., Gao, C., Rehbein, K., Lahme, B., Siluschek, M., Berg, T., et al. (2009). Elevated concentrations of 15-deoxy-Delta12, 14-prostaglandin J2 in chronic liver disease propose therapeutic trials with peroxisome proliferator activated receptor gamma-inducing drugs. *Liver Int.* 29 (5), 730–735. doi:10.1111/j.1478-3231.2008.01895.x

He, B., Wen, Y., Hu, S., Wang, G., Hu, W., Magdalou, J., et al. (2019). Prenatal caffeine exposure induces liver developmental dysfunction in offspring rats. *J. Endocrinol.* 242 (3), 211–226. doi:10.1530/JOE-19-0066

Helal, M. G., Ayoub, S. E., Elkashefand, W. F., and Ibrahim, T. M. (2018). Caffeine affects HFD-induced hepatic steatosis by multifactorial intervention. *Hum. Exp. Toxicol.* 37 (9), 983–990. doi:10.1177/0960327117747026

Higdon, J. V., and Frei, B. (2006). Coffee and health: A review of recent human research. *Crit. Rev. Food Sci. Nutr.* 46 (2), 101–123. doi:10.1080/10408390500400009

Hsu, S. J., Lee, F. Y., Wang, S. S., Hsin, I. F., Lin, T. Y., Huang, H. C., et al. (2015). Caffeine ameliorates hemodynamic derangements and portosystemic collaterals in cirrhotic rats. *Hepatology* 61 (5), 1672–1684. doi:10.1002/hep.27679

Hu, S., Liu, K., Luo, H., Xu, D., Chen, L., Zhang, L., et al. (2019). Caffeine programs hepatic SIRT1-related cholesterol synthesis and hypercholesterolemia via A2AR/cAMP/PKA pathway in adult male offspring rats. *Toxicology* 418, 11–21. doi:10.1016/j.tox.2019.02.015

Jaruvongvanich, V., Sanguankeo, A., Klomjit, N., and Upala, S. (2017). Effects of caffeine consumption in patients with chronic hepatitis C: A systematic review and meta-analysis. *Clin. Res. Hepatol. Gastroenterol.* 41 (1), 46–55. doi:10.1016/j.clinre.2016.05.012

Johnson, P., Zhou, Q., Dao, D. Y., and Lo, Y. (2022). Circulating biomarkers in the diagnosis and management of hepatocellular carcinoma. *Nat. Rev. Gastroenterol. Hepatol.* 19, 670–681. doi:10.1038/s41575-022-00620-y

Johnson, S., Koh, W. P., Wang, R., Govindarajan, S., Yu, M. C., and Yuan, J. M. (2011). Coffee consumption and reduced risk of hepatocellular carcinoma: Findings from the Singapore Chinese health study. *Cancer Causes Control* 22 (3), 503–510. doi:10.1007/s10552-010-9725-0

Kawano, Y., Nagata, M., Kohno, T., Ichimiya, A., Iwakiri, T., Okumura, M., et al. (2012). Caffeine increases the antitumor effect of Cisplatin in human hepatocellular carcinoma cells. *Biol. Pharm. Bull.* 35 (3), 400–407. doi:10.1248/bpb.35.400

Kennedy, O. J., Roderick, P., Buchanan, R., Fallowfield, J. A., Hayes, P. C., and Parkes, J. (2017). Coffee, including caffeinated and decaffeinated coffee, and the risk of hepatocellular carcinoma: A systematic review and dose-response meta-analysis. *BMJ open* 7 (5), e013739. doi:10.1136/bmjopen-2016-013739

Kolb, H., Martin, S., and Kempf, K. (2021). Coffee and lower risk of type 2 diabetes: Arguments for a causal relationship. *Nutrients* 13 (4), E1842. doi:10.3390/nu12061842

Konstantinou, D., Margariti, E., Hadziyannis, E., Pectasides, D., and Papatheodoridis, G. V. (2014). Significance of the 13C-caffeine breath test for patients with cirrhosis. *Ann. Gastroenterol.* 27 (1), 53–59.

Lammert, C., Chalasani, S. N., Green, K., Atkinson, E., McCauley, B., and Lazaridis, K. N. (2022). Patients with autoimmune hepatitis report lower lifetime coffee consumption. *Dig. Dis. Sci.* 67 (6), 2594–2599. doi:10.1007/s10620-021-06989-1

Leão, T. K., Ribeiro, D. L., Machado, A., Costa, T. R., Sampaio, S. V., and Antunes, L. (2021). Synephrine and caffeine combination promotes cytotoxicity, DNA damage and transcriptional modulation of apoptosis-related genes in human HepG2 cells. *Mutat. Res. Genet. Toxicol. Environ. Mutagen.* 868, 503375. doi:10.1016/j.mrgentox.2021.503375

Leung, W. W., Ho, S. C., Chan, H. L., Wong, V., Yeo, W., and Mok, T. S. (2011). Moderate coffee consumption reduces the risk of hepatocellular carcinoma in Hepatitis B chronic carriers: A case-control study. *J. Epidemiol. Community Health* 65 (6), 556–558. doi:10.1136/jech.2009.104125

Lewis, F. W., and Rector, W. G., Jr. (1992). Caffeine clearance in cirrhosis. The value of simplified determinations of liver metabolic capacity. *J. Hepatol.* 14 (2-3), 157–162. doi:10.1016/0168-8278(92)90152-f

Li, B. Y., Mao, Q. Q., Gan, R. Y., Cao, S. Y., Xu, X. Y., Luo, M., et al. (2021). Protective effects of tea extracts against alcoholic fatty liver disease in mice via modulating cytochrome P450 2E1 expression and ameliorating oxidative damage. *Food Sci. Nutr.* 9 (10), 5626–5640. doi:10.1002/fsn3.2526

Mansour, A., Mohajeri-Tehrani, M. R., Samadi, M., Qorbani, M., Merat, S., Adibi, H., et al. (2021). Effects of supplementation with main coffee components including caffeine and/or chlorogenic acid on hepatic, metabolic, and inflammatory indices in patients with non-alcoholic fatty liver disease and type 2 diabetes: A randomized, double-blind, placebo-controlled, clinical trial. *Nutr. J.* 20 (1), 35. doi:10.1186/s12937-021-00694-5

Okano, J. I., Fujise, Y., Abe, R., Imamoto, R., and Murawaki, Y. (2011). Chemoprevention against hepatocellular carcinoma. *Clin. J. Gastroenterol.* 4 (4), 185–197. doi:10.1007/s12328-011-0227-8

Okano, J., Nagahara, T., Matsumoto, K., and Murawaki, Y. (2008). Caffeine inhibits the proliferation of liver cancer cells and activates the MEK/ERK/EGFR signalling pathway. *Basic Clin. Pharmacol. Toxicol.* 102 (6), 543–551. doi:10.1111/j.1742-7843.2008.00231.x

Pan, Y., Long, X., Yi, R., and Zhao, X. (2018). Polyphenols in liubao tea can prevent CCl_4-Induced hepatic damage in mice through its antioxidant capacities. *Nutrients* 10 (9), 1280. doi:10.3390/nu10091280

Perera, V., Gross, A. S., Forrest, A., Landersdorfer, C. B., Xu, H., Ait-Oudhia, S., et al. (2013). A pharmacometric approach to investigate the impact of methylxanthine abstinence and caffeine consumption on CYP1A2 activity. *Drug Metab. Dispos.* 41 (11), 1957–1966. doi:10.1124/dmd.113.053074

Petrick, J. L., Freedman, N. D., Graubard, B. I., Sahasrabuddhe, V. V., Lai, G. Y., Alavanja, M. C., et al. (2015). Coffee consumption and risk of hepatocellular carcinoma and intrahepatic cholangiocarcinoma by sex: The liver cancer pooling project. *Cancer Epidemiol. Biomarkers Prev.* 24 (9), 1398–1406. doi:10.1158/1055-9965.EPI-15-0137

Rawat, D., Shrivastava, S., Naik, R. A., Chhonker, S. K., Mehrotra, A., and Koiri, R. K. (2018). An overview of natural plant products in the treatment of hepatocellular carcinoma. *Anticancer. Agents Med. Chem.* 18 (13), 1838–1859. doi:10.2174/1871520618666180604085612

Romualdo, G. R., Prata, G. B., da Silva, T. C., Evangelista, A. F., Reis, R. M., Vinken, M., et al. (2020). The combination of coffee compounds attenuates early fibrosis-associated hepatocarcinogenesis in mice: Involvement of miRNA profile modulation. *J. Nutr. Biochem.* 85, 108479. doi:10.1016/j.jnutbio.2020.108479

Saab, S., Mallam, D., Cox, G. A., and Tong, M. J. (2014). Impact of coffee on liver diseases: A systematic review. *Liver Int.* 34 (4), 495–504. doi:10.1111/liv.12304

Salem, R., Tselikas, L., and De Baere, T. (2022). Interventional treatment of hepatocellular carcinoma. *J. Hepatol.* S0168 (22), 1205–1206. Advance online publication. doi:10.1016/j.jhep.2022.03.037

Sewter, R., Heaney, S., and Patterson, A. (2021). Coffee consumption and the progression of NAFLD: A systematic review. *Nutrients* 13 (7), 2381. doi:10.3390/nu13072381

Shen, H., Rodriguez, A. C., Shiani, A., Lipka, S., Shahzad, G., Kumar, A., et al. (2016). Association between caffeine consumption and nonalcoholic fatty liver disease: A systemic review and meta-analysis. *Ther. Adv. Gastroenterol.* 9 (1), 113–120. doi:10.1177/1756283X15593700

Tangkijvanich, P., Wittayalertpanya, S., Kusonsolboon, T., Thong-Ngam, D., and Mahachai, V. (1999). Caffeine clearance study in hepatocellular carcinoma. *J. Med. Assoc. Thai* 82 (3), 297–303.

van Dam, R. M., Hu, F. B., and Willett, W. C. (2020). Coffee, caffeine, and health. *N. Engl. J. Med.* 383 (4), 369–378. doi:10.1056/NEJMra1816604

Velázquez, A. M., Roglans, N., Bentanachs, R., Gené, M., Sala-Vila, A., Lázaro, I., et al. (2020). Effects of a low dose of caffeine alone or as part of a green coffee extract, in a rat dietary model of lean non-alcoholic fatty liver disease without inflammation. *Nutrients* 12 (11), 3240. doi:10.3390/nu12113240

Voerman, E., Jaddoe, V. W., Hulst, M. E., Oei, E. H., and Gaillard, R. (2020). Associations of maternal caffeine intake during pregnancy with abdominal and liver fat deposition in childhood. *Pediatr. Obes.* 15 (5), e12607. doi:10.1111/ijpo.12607

Wang, H., Guan, W., Yang, W., Wang, Q., Zhao, H., Yang, F., et al. (2014). Caffeine inhibits the activation of hepatic stellate cells induced by acetaldehyde via adenosine A2A receptor mediated by the cAMP/PKA/SRC/ERK1/2/P38 MAPK signal pathway. *PloS one* 9 (3), e92482. doi:10.1371/journal.pone.0092482

Wang, Q., Dai, X., Yang, W., Wang, H., Zhao, H., Yang, F., et al. (2015). Caffeine protects against alcohol-induced liver fibrosis by dampening the cAMP/PKA/CREB pathway in rat hepatic stellate cells. *Int. Immunopharmacol.* 25 (2), 340–352. doi:10.1016/j.intimp.2015.02.012

Wang, T. J., Liu, Z. S., Zeng, Z. C., Du, S. S., Qiang, M., Jiang, W., et al. (2011). Caffeine does not enhance radiosensitivity of normal liver tissue *in vivo*. *Mol. Biol. Rep.* 38 (7), 4359–4367. doi:10.1007/s11033-010-0563-7

Wang, Z., Gu, C., Wang, X., Lang, Y., Wu, Y., Wu, X., et al. (2019). Caffeine enhances the anti-tumor effect of 5-fluorouracil via increasing the production of reactive oxygen species in hepatocellular carcinoma. *Med. Oncol.* 36 (12), 97. doi:10.1007/s12032-019-1323-8

Wijarnpreecha, K., Thongprayoon, C., and Ungprasert, P. (2017). Impact of caffeine in hepatitis C virus infection: A systematic review and meta-analysis. *Eur. J. Gastroenterol. Hepatol.* 29 (1), 17–22. doi:10.1097/MEG.0000000000000757

Wiltberger, G., Wu, Y., Lange, U., Hau, H. M., Tapper, E., Krenzien, F., et al. (2019). Protective effects of coffee consumption following liver transplantation for hepatocellular carcinoma in cirrhosis. *Aliment. Pharmacol. Ther.* 49 (6), 779–788. doi:10.1111/apt.15089

Xin, X., Cheng, C., Bei-Yu, C., Hong-Shan, L., Hua-Jie, T., Xin, W., et al. (2021). Caffeine and EGCG alleviate high-trans fatty acid and high-carbohydrate diet-induced NASH in mice: Commonality and specificity. *Front. Nutr.* 8, 784354. doi:10.3389/fnut.2021.784354

Yamaguchi, M., Dohi, N., Ooka, A., Saito, S. Y., and Ishikawa, T. (2021). Caffeine-induced inversion of prostaglandin E2 effects on hepatic stellate cell activation. *Biomed. Pharmacother.* 142, 111989. doi:10.1016/j.biopha.2021.111989

Yang, Y., Wang, H., Lv, X., Wang, Q., Zhao, H., Yang, F., et al. (2015). Involvement of cAMP-PKA pathway in adenosine A1 and A2A receptor-mediated regulation of acetaldehyde-induced activation of HSCs. *Biochimie* 115, 59–70. doi:10.1016/j.biochi.2015.04.019

Zhang, Y., Liu, Z., Choudhury, T., Cornelis, M. C., and Liu, W. (2021). Habitual coffee intake and risk for nonalcoholic fatty liver disease: A two-sample mendelian randomization study. *Eur. J. Nutr.* 60 (4), 1761–1767. doi:10.1007/s00394-020-02369-z

frontiers | Frontiers in Pharmacology

TYPE Original Research
PUBLISHED 20 October 2022
DOI 10.3389/fphar.2022.965914

OPEN ACCESS

EDITED BY
Yuzhi Zhou,
Shanxi University, China

REVIEWED BY
You Yun,
Institute of Chinese Materia Medica, China Academy of Chinese Medical Sciences, China
Qicai Xiao,
Sun Yat-sen University, China

*CORRESPONDENCE
Ping Liu,
liuliver@vip.sina.com
Jiamei Chen,
cjm0102@126.com
Wei Liu,
lwhzayl@163.com

†These authors have contributed equally to this work and share first authorship

SPECIALTY SECTION
This article was submitted to Ethnopharmacology, a section of the journal Frontiers in Pharmacology

RECEIVED 10 June 2022
ACCEPTED 11 October 2022
PUBLISHED 20 October 2022

CITATION
Zhang L, Hu Y, Qi S, Zhang C, Zhou Q, Zhang D, Mu Y, Zhang H, Chen G, Liu P, Chen J and Liu W (2022), Astragalus saponins and its main constituents ameliorate ductular reaction and liver fibrosis in a mouse model of DDC-induced cholestatic liver disease. *Front. Pharmacol.* 13:965914. doi: 10.3389/fphar.2022.965914

Astragalus saponins and its main constituents ameliorate ductular reaction and liver fibrosis in a mouse model of DDC-induced cholestatic liver disease

Linzhang Zhang[1†], Yonghong Hu[1†], Shenglan Qi[2], Congcong Zhang[2], Qun Zhou[1], Dingqi Zhang[1], Yongping Mu[1], Hua Zhang[1], Gaofeng Chen[1], Ping Liu[1*], Jiamei Chen[1*] and Wei Liu[1,2*]

[1]Key Laboratory of Liver and Kidney Diseases (Ministry of Education), Shanghai Key Laboratory of Traditional Chinese Clinical Medicine, Institute of Liver Diseases, Shuguang Hospital Affiliated to Shanghai University of Traditional Chinese Medicine, Shanghai, China, [2]The MOE Key Laboratory for Standardization of Chinese Medicines and the SATCM Key Laboratory for New Resources and Quality Evaluation of Chinese Medicines, Institute of Chinese Materia Medica, Shanghai University of Traditional Chinese Medicine, Shanghai, China

Cholestatic liver disease (CLD) is a chronic liver disease characterized by ductular reaction, inflammation and fibrosis. As there are no effective chemical or biological drugs now, majority of CLD patients eventually require liver transplantation. Astragali radix (AR) is commonly used in the clinical treatment of cholestatic liver disease and its related liver fibrosis in traditional Chinese medicine, however its specific active constituents are not clear. Total astragalus saponins (ASTs) were considered to be the main active components of AR. The aim of this study is to investigate the improvement effects of the total astragalus saponins (ASTs) and its main constituents in cholestatic liver disease. The ASTs from AR was prepared by macroporous resin, the content of saponins was measured at 60.19 ± 1.68%. The ameliorative effects of ASTs (14, 28, 56 mg/kg) were evaluated by 3, 5-Diethoxycarbonyl-1, 4-dihydrocollidine (DDC)-induced CLD mouse model. The contents of hydroxyproline (Hyp), the mRNA and protein expression of cytokeratin 19 (CK19) and α-smooth muscle actin (α-SMA) in liver tissue were dose-dependently improved after treatment for ASTs. 45 astragalus saponins were identified in ASTs by UHPLC-Q-Exactive Orbitrap HRMS, including astragaloside I, astragaloside II, astragaloside III, astragaloside IV, isoastragaloside I, isoastragaloside II, cycloastragenol, etc. And, it was found that ductular reaction in sodium butyrate-induced WB-F344 cell model were obviously inhibited by these main constituents. Finally, the improvement effects of astragaloside I, astragaloside II, astragaloside IV and cycloastragenol (50 mg/kg) were evaluated in DDC-induced CLD mice model. The results showed that astragaloside I and cycloastragenol significantly improved mRNA and protein expression of CK19 and α-SMA in liver tissue. It suggested that astragaloside I and cycloastragenol could alleviate ductular reaction and liver fibrosis. In summary, this study revealed that ASTs could

significantly inhibit ductular reaction and liver fibrosis, and astragaloside I and cycloastragenol were the key substances of ASTs for treating cholestatic liver disease.

KEYWORDS

astragalus saponins, DDC, cholestatic liver disease, astragaloside I, cycloastragenol

Introduction

Cholestasis is a pathological condition in which bile formation, secretion and excretion are impaired inside and outside the liver due to various reasons, and bile flow cannot flow properly into the duodenum and enters the bloodstream (Hasegawa et al., 2021). Hepatobiliary diseases in which cholestasis is the main manifestation of liver lesions for various reasons are named cholestatic liver disease, which itself can further aggravate liver damage (Brevini et al., 2020; Stättermayer et al., 2020). Ductular reaction and liver fibrosis are typical pathological manifestations of cholestatic liver disease (Kummen et al., 2021). There are no definitive data on the incidence of cholestatic liver disease. A study about patients with initially diagnosed chronic liver disease showed that cholestasis occurred in 882 of 2,520 patients (35%) with chronic liver disease and was more likely to be seen in PBC and PSC (Wagner and Fickert, 2020). UDCA is the common clinical drug for PBC, but there is still a significant unmet need for treatment of patients with poor response, and there are no chemical or biological drugs for PSC, liver transplantation is currently the only effective treatment (Weismüller et al., 2017), it is an urgent need for developing new drugs.

Astragali radix (AR) has been used commonly in traditional Chinese medicine for more than 2000 years (Yu et al., 2018). It is the dried root of *Astragalus membranaceus* (Fisch.) Bge. var. mongholicus (Bge.) Hsiao. or *Astragalus membranaceus* (Fisch.) Bge. Pharmacological studies and clinical practices indicate that AR had various medicinal effects including anti-inflammatory, anti-cancer, hepatoprotective, cardioprotective, neurological, and antiviral. It is widely used for the treatment of anemia, liver fibrosis and cirrhosis, allergy, chronic fatigue, loss of appetite, uterine prolapse and other diseases (Fu et al., 2014; Zhang L. et al., 2017). *Astragalus* saponins (ASTs) are considered to be the main active components of AR, more than 200 AR compounds have been independently reported (Guo et al., 2019). Studies have shown that AR and its components had good protective effects against various liver disease models induced by carbon tetrachloride (CCl_4), dimethylnitrosamine (DMN), and α-naphthyl isothiocyanate (ANIT) (Vitcheva et al., 2013; Zhou et al., 2016; Qiu et al., 2021). And ASTs are effective in improving cardiovascular diseases, diabetes, neurological degeneration, and other diseases (Xia et al., 2020; Meng et al., 2021; Su et al., 2021). However, few results have reported the effects of ASTs on cholestatic liver disease. Therefore, we investigate the effects and active constituents of ASTs in cholestatic liver disease.

In this study, ASTs are assessed *in vivo* by 3,5-diethoxycarbonyl-1,4-dihydrocollidine (DDC)-induced CLD mouse model, which is a classical animal model of cholestatic liver disease induced by toxicant (Fickert et al., 2007). Meanwhile, the chemical profiling of ASTs and absorbed chemical constituents are analysed by ultra-high-performance liquid chromatography-Q exactive hybrid quadrupole orbitrap high-resolution accurate mass spectrometriy (UHPLC-Q-Exactive Orbitrap HRMS) after oral aderministration of ASTs. Further, the effect of inhibiting ductular reaction of main constituents is evaluated by sodium butyrate (SB)-induced WB-F344 cell model *in vitro*. Finally, the improvement effects of main absorbed chemical constituents (astragaloside I, astragaloside II, astragaloside IV and cycloastragenol) are evaluated by DDC-induced CLD mice model. The results clarify the major active constituents of ASTs for the treatment of cholestatic liver disease, and with a view to provide references for clinical application and further research of AR.

Materials and methods

Materials and reagents

DDC and SB are purchased from Sigma-Aldrich (STBK3562, B5887, St. Louis, MO, United States). The DDC diet ingredients were normal chow (which contains 203.5 g/kg crude protein, 43.1 g/kg crude fat, 48.9 g/kg crude fiber, 91.8 g/kg moisture, 59.3 g/kg ash, 14.8 g/kg calcium, 9.1 g/kg phosphorus. Energy was about 3,600 kcal/kg) and 0.1% DDC. The DDC diet was prepared by Fanbo biotechnology Co. (M2011, Jiangsu, China). Astragaloside I, astragaloside II, astragaloside III, astragaloside IV, isoastragaloside I, isoastragaloside II and cycloastragenol are purchased from Chengdu Biopurify. Co. Obeticholic acid and D101 macroporous resin are purchased from Dalian Melan Co. DMEM and FBS are purchased from Gibco Life Technology (Gibco Invitgen Corporation, Barcelona, Spain). Alanine aminotransferase (ALT), aspertate aminotransferase (AST), total bilirubin (TBiL), direct bilirubin (DBiL), indirect bilirubin (IBiL) kits, hematoxylin eosin (H&E) staining kits and hydroxyproline (Hyp) kits are purchased from Nanjing Jiancheng Institute of Biological Engineering. The reverse transcriptase assay kit, Trizol reagent, and SYBR Green Realtime PCR MASTER Mix are purchased from Takara Biotech Co. RIPA lysis buffer and BCA protein concentration assay kits are purchased from Beyotime BioLtd. The antibodies cytokeratin 19 (#10712-1-

TABLE 1 qRT-PCR primer sequences.

Species	Gene	Forward primer (5′–3′)	Reverse primer (5′–3′)
Mouse	CK19	GGAAGGTGATATTGTGTTCGCC	CTATGGTCTCCTCTGTAGAAGGC
Mouse	CK7	AGGAACAGAAGTCAGCCAAGAG	GCAACACAAACTCATTCTCAGC
Mouse	α-SMA	CACTGTAACTGGGGGCAACT	CACTTCTTGTCAGCGTCGAA
Mouse	Col1A1	GATTCCCTGGACCTAAAGGTGC	AGCCTCTCCATCTTTGCCAGCA
Mouse	GAPDH	AGCCAGAGCTGTGCAGATGA	GCAGGCTGGCATTTGTGGTT
Rat	CK19	CCCCAAAGGGATGAGAAGTT	CACTTGGTGGTTTGCTACGA
Rat	GAPDH	CCATCAACGACCCCTTCATT	GACCAGCTTCCCATTCTCAG

AP), α-smooth muscle actin (#ab124964) and GAPDH (#60004-1-Ig) are purchased from Proteintech (Wuhan, China). Astragali radix (AR) (No. 220120) was purchased from Shanghai Hongqiao Traditional Chinese Medicine Decoction Piecess Co., Ltd. (Shanghai, China), and the herb was authenticated as *Astragalus membranaceus* (Fisch.) Bge. var. mongholicus (Bge.) Hsiao. by associate professor LIU Wei, from the Institute of Liver Diseases, Shuguang Hospital Affiliated to Shanghai University of Traditional Chinese Medicine.

Animals

Three batches of male C57/BL6J mice, 48, 6, and 56 mice, with a body mass of 20 ± 2 g, are purchased from Beijing Vital River Laboratory Animal Co. The animals are housed in the Experimental Animal Center of Shanghai University of Traditional Chinese Medicine. The experiments are approved by the Experimental Animal Ethics Committee of Shanghai University of Traditional Chinese Medicine with the following ethics number: PZSHUTCM201016007. The ambient temperature is 22 ± 2°C, and the duration of daylight and darkness are 12 h each, with free access to water and food.

Preparation of astragalus saponins

The preparation procedures of ASTs from AR by macroporous resin column chromatography are described in previous report (Chu et al., 2022). Dried AR (2 kg) is sheared into segments and extracted with 20 L of 70% ethanol (*v*/*v*) thrice in reflux, each for 2 h. Extracts are combined, filtered, and concentrated under reduced pressure at 45°C to afford 4 L concentrated extract of AR. The concentrated extract is separated and prepared ASTs by macroporous resin column chromatography (4 kg, column volume is about 3 L), being eluted with a gradient system of water - ethanol (100:0, 70:30, 10:90), 20 L per elution segment. Finally, the 90% ethanol fraction (mainly contains saponins) is collected, and evaporated under reduced pressure with the rotary evaporator at 45°C and the concentrate freeze-dried to yield solid material (10.23 g, extract yield is 0.51% from AR). The average content of total saponins in the preparation ASTs is determined as 60.19 ± 1.68% using the method reported in the literature (Kong et al., 2010). Identification and characterization of chemical constituents from ASTs is using UHPLC-Q-Exactive Orbitrap HRMS (Supplementary Table S1).

Intervention effects of ASTs on 0.1% DDC-induced mouse model

Forty-eight mice are randomly divided into normal control group (n = 8) and model group (n = 40). The normal control group is fed normal chow, the model group is fed chow containing 0.1% DDC. After 4 weeks of feeding, the 40 model mice are further randomly divided into five groups of eight mice each: CLD model group, 14 mg/kg ASTs group, 28 mg/kg ASTs group, 56 mg/kg ASTs group (the dose is used human equivalent dose [65 kg, 15, 30, 60 g recipe per day]), and 10 mg/kg obeticholic acid group (positive control). The normal and model groups are gavaged 0.4% CMC-Na solution from week five to week eight once a day, and the treatment groups are given the corresponding drug by gavage once a day. At the end of week 8, the mice are executed, blood and liver specimens are collected for further experiments.

Characterization of the absorbed chemical constituents in mice serum and liver after oral administration of ASTs

After 7 days of acclimatization, six male mice are randomly divided into two groups (3 mice for each group). ASTs group is oral administered 56 mg/kg ASTs solution; control group is oral administered 0.4% CMC-Na solution. All animals are fasted overnight before the experiment and have free access to water. One hour after once oral administration of ASTs, all mice are anesthetized. Blood samples are collected from the abdominal aorta, and liver tissues are quickly removed. Serum samples are obtained by centrifuged at 8,000 × g for 10 min at 4°C. All

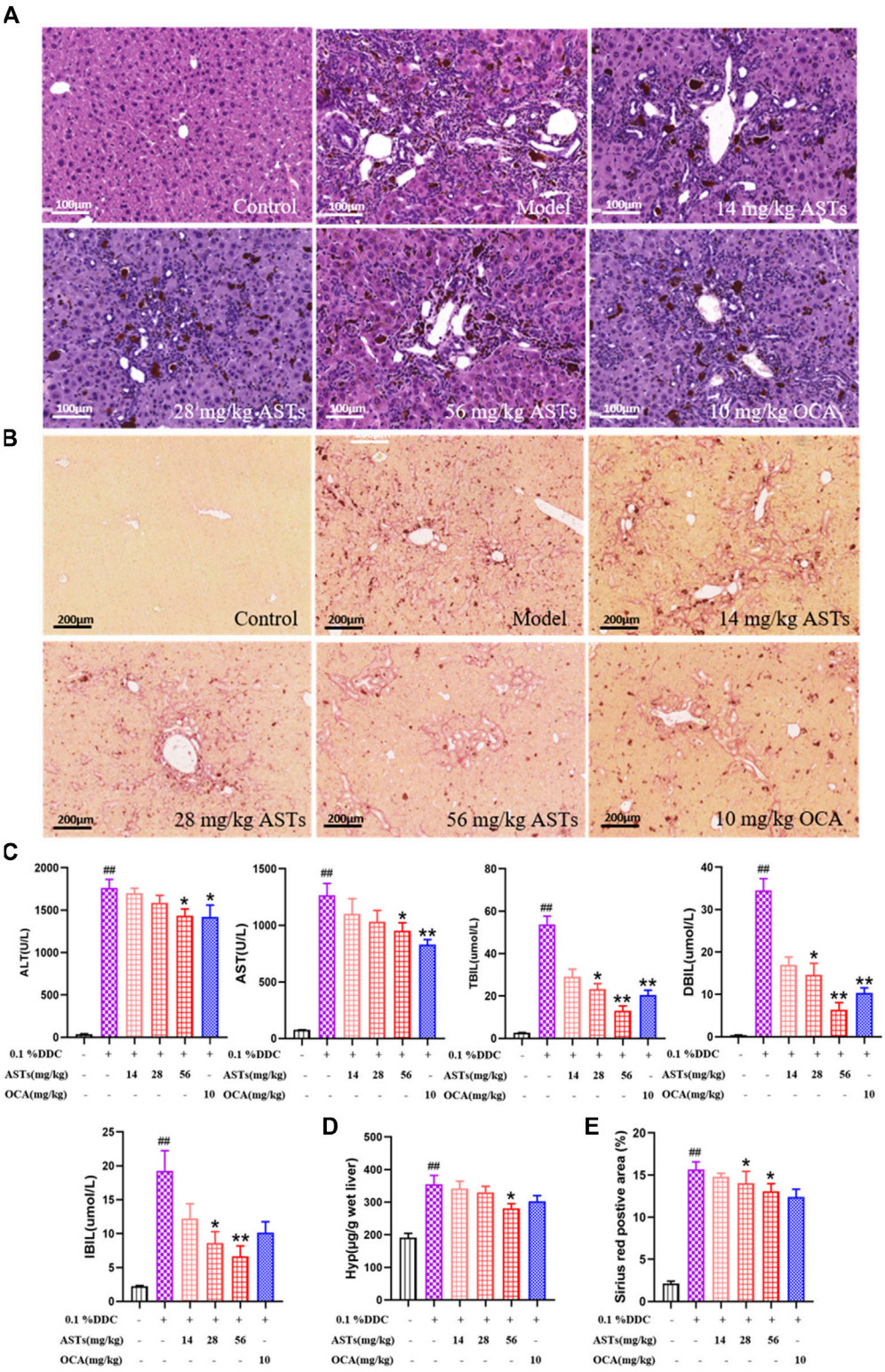

FIGURE 1
Effects of ASTs on serum biochemistry and collagen deposition in 0.1% DDC-induced CLD mice. **(A,B)** Representative images of H&E staining (×20x) (scale bar 100 μm), sirius red staining (×10x) (scale bar 200 μm) are performed to observe the histopathological characteristics of liver tissues after the treatment of ASTs and OCA. **(C)** Measurement of serum ALT, AST, TBiL, DBiL and IBiL levels in mice are deceted. **(D)** Hyp levels in liver tissues are determined, **(E)** Area (%) of positive sirius red is assessed by quantitative imaging of sirius red staining. $^{\#\#}p < 0.01$ vs. the normal group. $^{**}p < 0.01$ and $^{*}p < 0.05$ vs. 0.1% DDC group. Values were expressed as mean ± SD.

10.3389/fphar.2022.965914

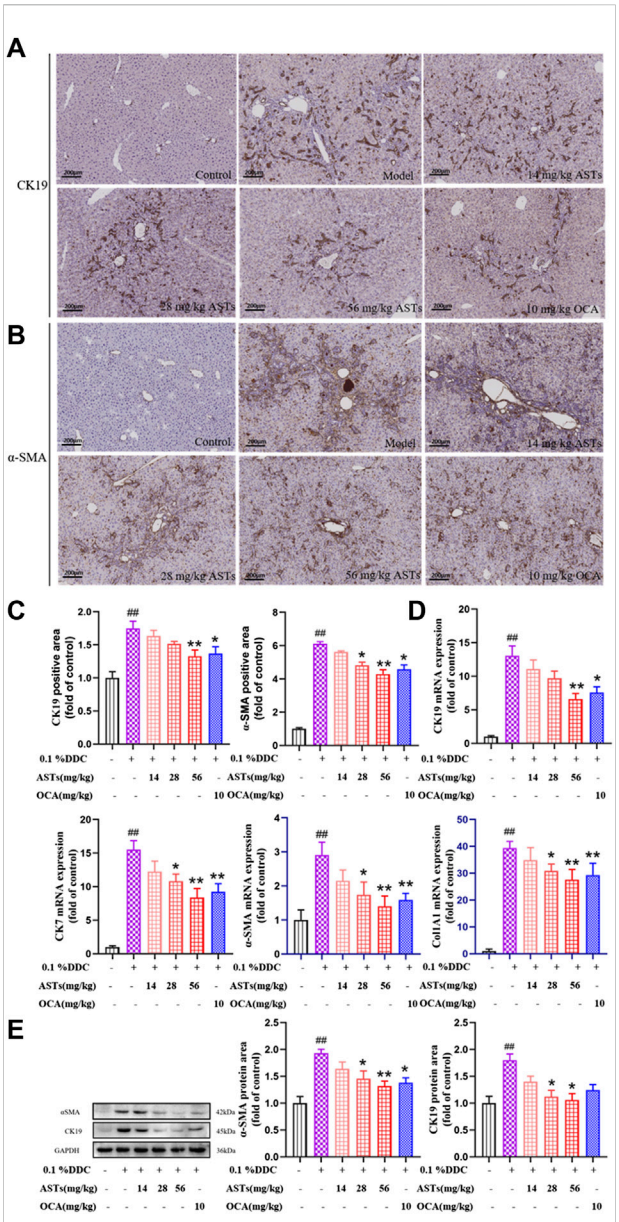

FIGURE 2
Effects of ASTs on the expressions of CK19, CK7, α-SMA, Col1A1 in 0.1% DDC-induced CLD mice. **(A,B)** Immunohistochemical method is used to detect the effects of ASTs and OCA on hepatic α-SMA and CK19 expressions in the liver (×10x) (scale bar 200 μm). **(C)** α-SMA and CK19 positive areas are assessed by immunohistochemical quantification. **(D)** Effects of ASTs on the gene expressions of CK19, CK7, α-SMA and Col1A1 are evaluated by qRT-PCR, and normalized against GAPDH level. **(E)** Protein expressions of α-SMA and CK19 in liver are assessed by western blot and normalized to GAPDH protein. $^{\#\#}p <$ 0.01 vs. the normal group. $^{**}p < 0.01$ and $^{*}p < 0.05$ vs. 0.1% DDC group. Values were expressed as mean ± SD.

samples are stored at −80°C until analysis. The serum samples (200 μL) are added five times methanol (1 ml), vortexed and then, centrifuged at 12,000 × g for 10 min. The supernatant (960 μL) is dried with nitrogen gas. The residue is redissolved in 80 μL 10% methanol, vortexed and then, centrifuged at 12,000 × g for 10 min, and the supernatant is used in the UHPLC-Q-Exactive Orbitrap HRMS analysis. The 100 mg liver tissue is homogenized in 1 ml methanol on ice, the homogenate of them is centrifuged at 4°C at 12,000 × g for 10 min, The supernatant (800 μL) is dried with nitrogen gas. The residue is redissolved in 80 μL 10% methanol, vortexed and then, centrifuged at 12,000 × g for 10 min, and the supernatant is used in the UHPLC-Q-Exactive Orbitrap HRMS analysis.

The inhibitory effects of the main chemical constituents of ASTs on ductular reaction in sodium butyrate-induced WB-F344 cell model

The cell viability assay of main chemical constituents of ASTs is evaluated by CCK-8. WB-F344 cells are plated at 5×10^3 cells/well in 96-well plates and cultured in culture medium containing 10% FBS. After 24 h, the cells are incubated with ASTs and its seven components at different concentrations (ASTs at concentrations of 10, 20, 40, 60, 80 and 100 μg/ml. Astragaloside I, astragaloside II, astragaloside III, astragaloside IV, isoastragaloside I, isoastragaloside II and cycloastragenol at concentrations of 6.25, 12.5, 25, 50 and 100 μM, respectively for 24 h). Subsequently, all wells are added into CCK-8 solution. After 1 h incubation, the absorbance is read at 450 nm, and the cell viability is calculated.

The effect of main constituents of ASTs is evaluated in sodium butyrate-induced WB-F344 cell model. WB-F344 cells are inoculated in 6-well plates with 3×10^4 cells and cultured in DMEM medium containing 10% FBS. The cells are divided into DMSO control group, SB (3.75 μM) group, SB + astragaloside I (10 μM) group, SB + astragaloside II (10 μM) group, SB + astragaloside III (10 μM) group, SB + astragaloside IV (10 μM) group, SB + isoastragaloside I (10 μM) group, SB + isoastragaloside II (10 μM) group, SB + cycloastragenol (10 μM) group and SB + ASTs (10 μg/ml) group. Drug-containing medium and fresh medium are replaced after 2 days. All cells are maintained for 4 days and collected for mRNA analysis by qRT-PCR.

Intervention effects of astragaloside I, astragaloside II, astragaloside IV, cyclogalactol on 0.1 %DDC-induced CLD mouse model

Fifty-six mice are randomly divided into normal control group (n = 8) and CLD model group (n = 48). The normal control group is fed normal chow, the model group is fed chow containing 0.1% DDC. After 4 weeks of feeding, the

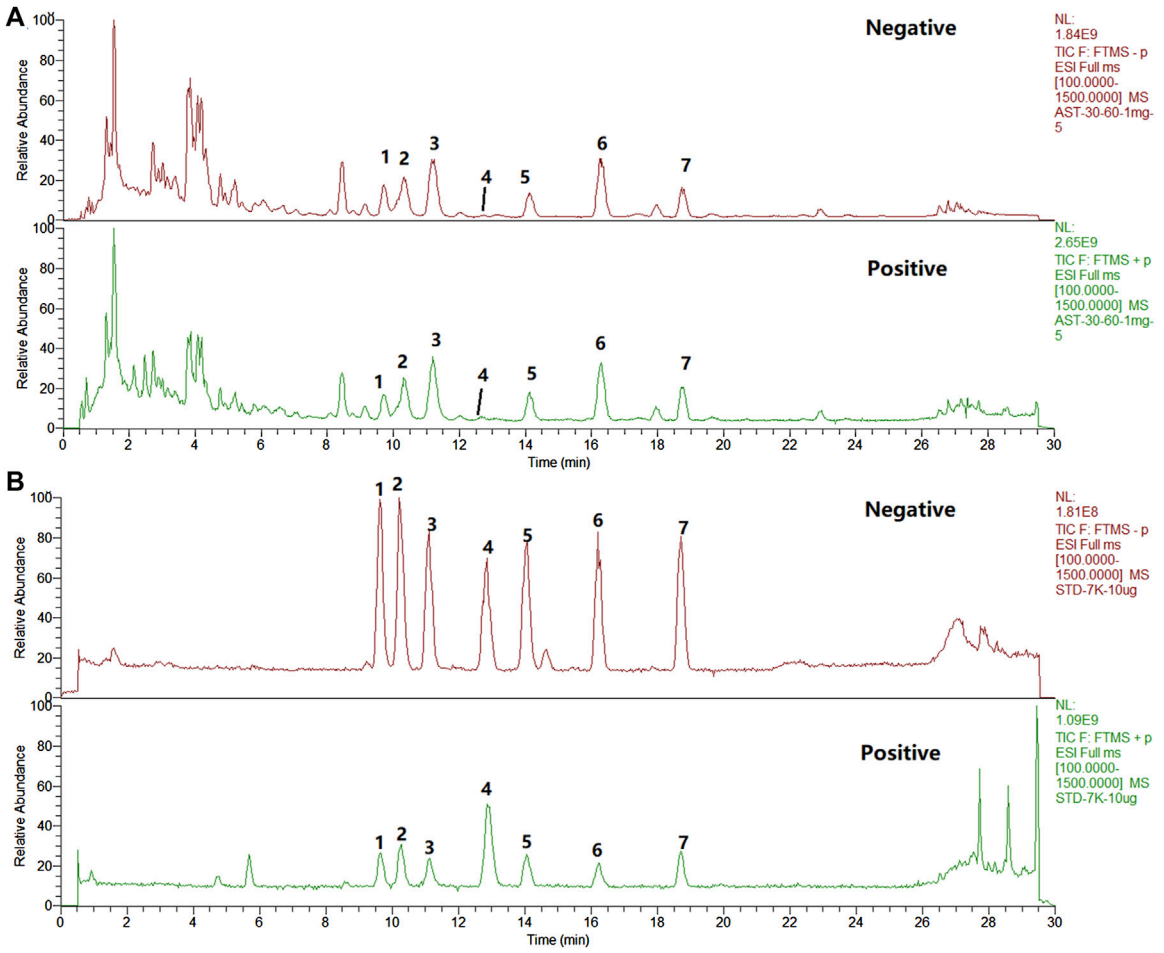

FIGURE 3
The total ion chromatograms (TICs) of the extract of ASTs and seven reference substances by UHPLC-Q-Exactive Orbitrap HRMS. **(A)**, ASTs solution; **(B)**, standard solution; 1, astragaloside III; 2, astragaloside IV; 3, astragaloside II; 4, cycloastragenol; 5, isoastragaloside II; 6, astragaloside I; 7, isoastragaloside I.

48 model mice are further randomly divided into six groups of eight mice each: CLD model group, 50 mg/kg astragaloside I group, 50 mg/kg astragaloside II group, 50 mg/kg astragaloside IV group, 50 mg/kg cycloastragenol group, and 56 mg/kg ASTs group. From week five to week 8, normal group and model group are given 0.4% CMC-Na solution by gavage once a day, and drug groups are given the corresponding drug by gavage once a day. The mice are executed at the end of week 8, blood and liver specimens are collected for subsequent experiments.

Serum biochemistry and pathology analysis

Serum samples are thawed at 4°C one night in advance and placed in the autoanalyzer according to the labeling order, followed by adding the corresponding assay reagents to the assay vials to detect serum ALT, AST, TBiL, DBiL and IBiL levels. Liver tissues are fixed in neutral formalin, embedded in paraffin, sectioned, stained with H&E and Sirius Red. They are processed for quantitative analysis of the positive area of SR staining by using Image Analysis.

Hepatic hydroxyproline content assays

The liver tissue (50.0 mg) is weighed into a 1.5 ml centrifuge tube. Each sample is added to 1 ml of hydrolysate, then incubated in a water bath at 95°C for 10 min. After cooling to room temperature, the pH is adjusted to 6.0–6.8. The supernatant (4 ml) is added to 30 mg of activated carbon and centrifuged. Then each tube is added to agents I, II and III respectively. 200 μL of the mixture is used to determine the OD value at 550 nm, and the hyp content of each sample is calculated.

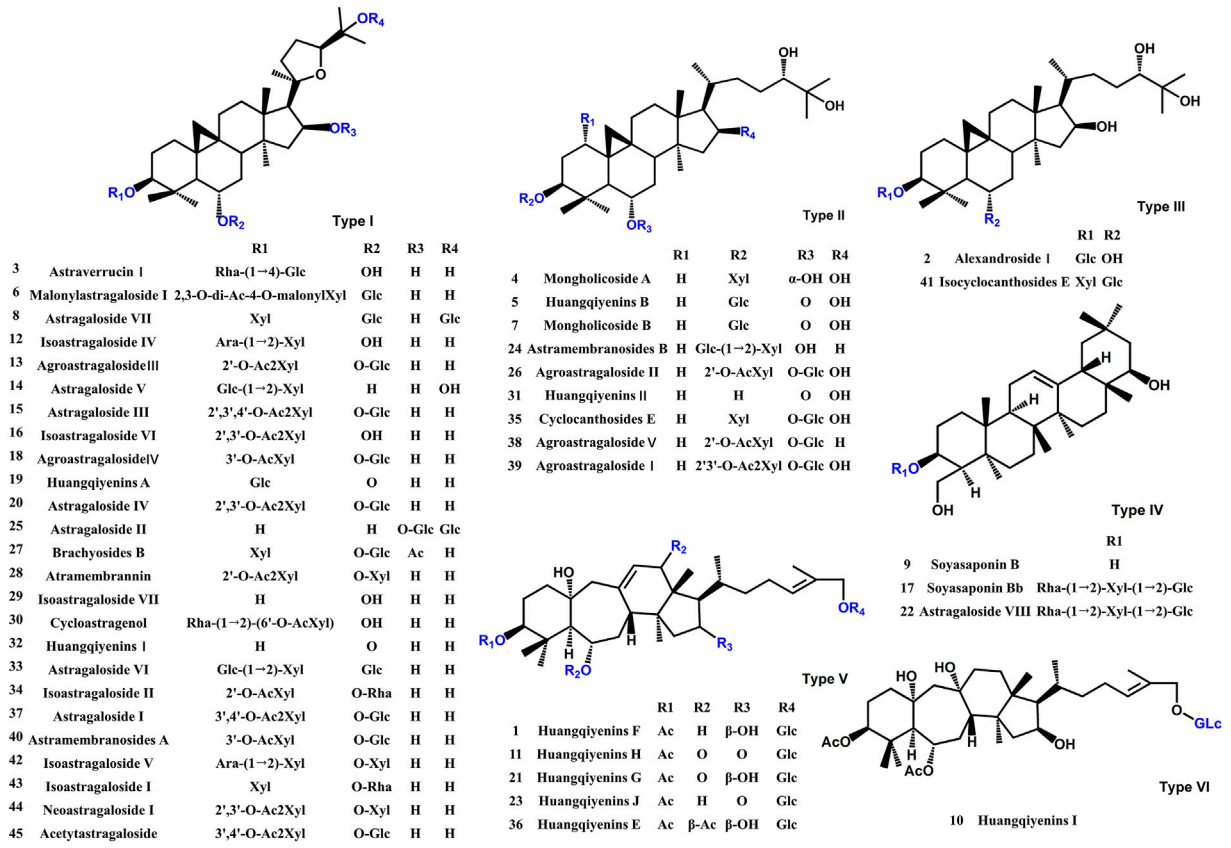

		R1	R2	R3	R4
3	Astraverrucin I	Rha-(1→4)-Glc	OH	H	H
6	Malonylastragaloside I	2,3-O-di-Ac-4-O-malonylXyl	Glc	H	H
8	Astragaloside VII	Xyl	Glc	H	Glc
12	Isoastragaloside IV	Ara-(1→2)-Xyl	OH	H	H
13	AgroastragalosideIII	2'-O-Ac2Xyl	O-Glc	H	H
14	Astragaloside V	Glc-(1→2)-Xyl	H	H	OH
15	Astragaloside III	2',3',4'-O-Ac2Xyl	O-Glc	H	H
16	Isoastragaloside VI	2',3'-O-Ac2Xyl	OH	H	H
18	AgroastragalosidelV	3'-O-AcXyl	O-Glc	H	H
19	Huangqiyenins A	Glc	O	H	H
20	Astragaloside IV	2',3'-O-Ac2Xyl	O-Glc	H	H
25	Astragaloside II	H	H	O-Glc	Glc
27	Brachyosides B	Xyl	O-Glc	Ac	H
28	Atramembrannin	2'-O-Ac2Xyl	O-Xyl	H	H
29	Isoastragaloside VII	H	OH	H	H
30	Cycloastragenol	Rha-(1→2)-(6'-O-AcXyl)	OH	H	H
32	Huangqiyenins I	H	O	H	H
33	Astragaloside VI	Glc-(1→2)-Xyl	Glc	H	H
34	Isoastragaloside II	2'-O-AcXyl	O-Rha	H	H
37	Astragaloside I	3',4'-O-Ac2Xyl	O-Glc	H	H
40	Astramembranosides A	3'-O-AcXyl	O-Glc	H	H
42	Isoastragaloside V	Ara-(1→2)-Xyl	O-Xyl	H	H
43	Isoastragaloside I	Xyl	O-Rha	H	H
44	Neoastragaloside I	2',3'-O-Ac2Xyl	O-Xyl	H	H
45	Acetytastragaloside	3',4'-O-Ac2Xyl	O-Glc	H	H

		R1	R2	R3	R4
4	Mongholicoside A	H	Xyl	α-OH	OH
5	Huangqiyenins B	H	Glc	O	OH
7	Mongholicoside B	H	Glc	O	OH
24	Astramembranosides B	H	Glc-(1→2)-Xyl	OH	H
26	Agroastragaloside II	H	2'-O-AcXyl	O-Glc	OH
31	Huangqiyenins II	H	H	O	OH
35	Cyclocanthosides E	H	Xyl	O-Glc	OH
38	Agroastragaloside V	H	2'-O-AcXyl	O-Glc	H
39	Agroastragaloside I	H	2'3'-O-Ac2Xyl	O-Glc	OH

		R1	R2
2	Alexandroside I	Glc	OH
41	Isocyclocanthosides E	Xyl	Glc

		R1
9	Soyasaponin B	H
17	Soyasaponin Bb	Rha-(1→2)-Xyl-(1→2)-Glc
22	Astragaloside VIII	Rha-(1→2)-Xyl-(1→2)-Glc

		R1	R2	R3	R4
1	Huangqiyenins F	Ac	H	β-OH	Glc
11	Huangqiyenins H	Ac	O	O	Glc
21	Huangqiyenins G	Ac	O	β-OH	Glc
23	Huangqiyenins J	Ac	H	O	Glc
36	Huangqiyenins E	Ac	β-Ac	β-OH	Glc

10 Huangqiyenins I

FIGURE 4
The chemical structures of identified *Astragalus* saponins.

Immunohistochemistry assays

Paraffin tissue sections are dewaxed, dehydrated and antigen repair is performed with 4% citrate buffer. Sections are incubated with 3% H_2O_2 for 20 min and 10% goat serum for 30 min. Anti-CK19 (1:500) and anti-α-SMA (1:1,000) are incubated at 4°C overnight. Sections are incubated with HRP-labeled secondary antibody in the next day. The tissue sections are stained by 3, 3-diaminobenzidine (DAB) and H&E staining. The positive area of tissue staining is quantified using Image Analysis.

Quantitative real-time PCR analysis

Mouse liver tissue and WB-F344 cells are lysed with Trizol reagent. Then chloroform, isopropanol, 75% ethanol and anhydrous ethanol are added respectively. Finally DEPC water is added. The NanoVue concentration detector is applied to detect the RNA concentration. Total RNA is reverse transcribed using reverse transcription kit to obtain cDNA. 384-well PCR plates are spiked, and the corresponding indexes are detected by Real-time PCR method. The expression of each mRNA is calculated by $2^{-\Delta\Delta}$Ct method. The amount of mRNA is normalized using GAPDH as an internal standard. qRT-PCR primer sequences are shown in Table 1.

Western blot analysis

The liver tissue (40.0–60.0 mg) is weighed and added to 1 ml of protein lysate. The lysed tissues are centrifuged at 12,000 rpm for 30 min, and the protein concentration is measured by BCA protein assay kit. Equal amounts of protein samples are separated by SDS-PAGE and transferred to polyvinylidene fluoride (PVDF) membranes. The membranes are blocked for 1 h at room temperature in Western blocking solution. The primary antibody is incubated at 4°C overnight and the secondary antibody is incubated at room temperature for 1 h in the following day. The primary antibody dilutions are incubated with anti-CK19 (1:1,000), anti-α-SMA (1:1,000), GAPDH (1:

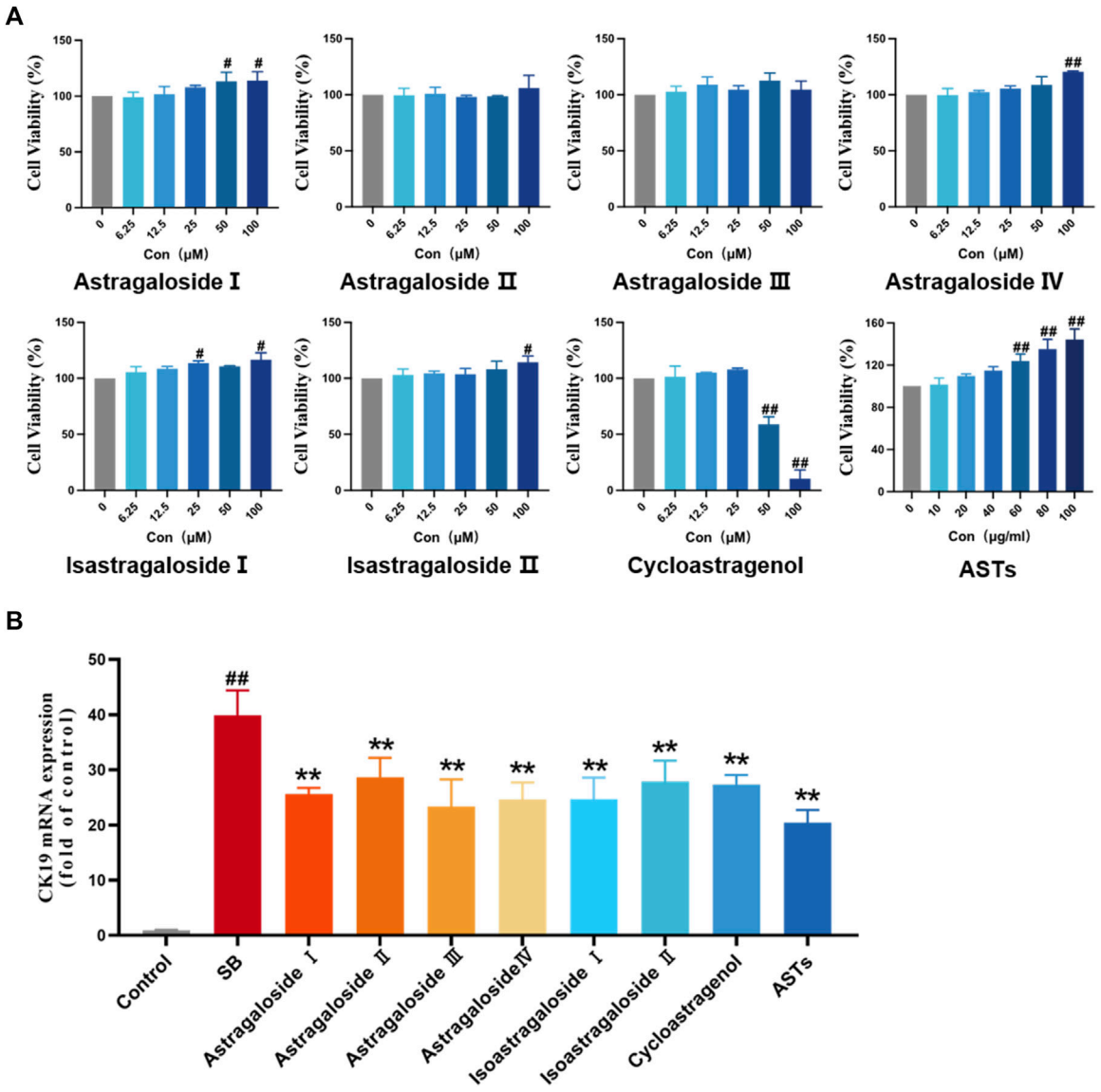

FIGURE 5
Effects of ASTs and main components in SB-induced WB-F344 cell model. **(A)** Cell viability is determined by CCK8 assay. **(B)** Expression of CK19 is determined by qRT-PCR. $^{\#\#}p < 0.01$ and $^{\#}p < 0.05$ vs. the control group. $^{**}p < 0.01$ vs. SB model group. Values were expressed as mean ± SD.

5,000) and secondary antibody (1:1,000). The target bands are scanned and compared with GAPDH bands for statistical analysis.

Statistical analysis

SPSS 23.0 software is used to statistically analyze the data. The data is expressed as mean ± standard deviation (SD), and $p < 0.05$ is considered statistically significant. One-way ANOVA analysis is used for the comparative analysis of multiple groups, and Student's t-test is used for the statistical comparison between two groups.

Results

ASTs improves serum biochemistry and collagen deposition in DDC-induced CLD mice

Normal morphology and regular arrangement of hepatocytes in the normal group are shown in H&E staining (Figure 1A). Compared with the normal group, porphyrin deposition, cell necrosis and inflammatory cell infiltration are increased in the model group, and the number of hyperplastic bile ducts is

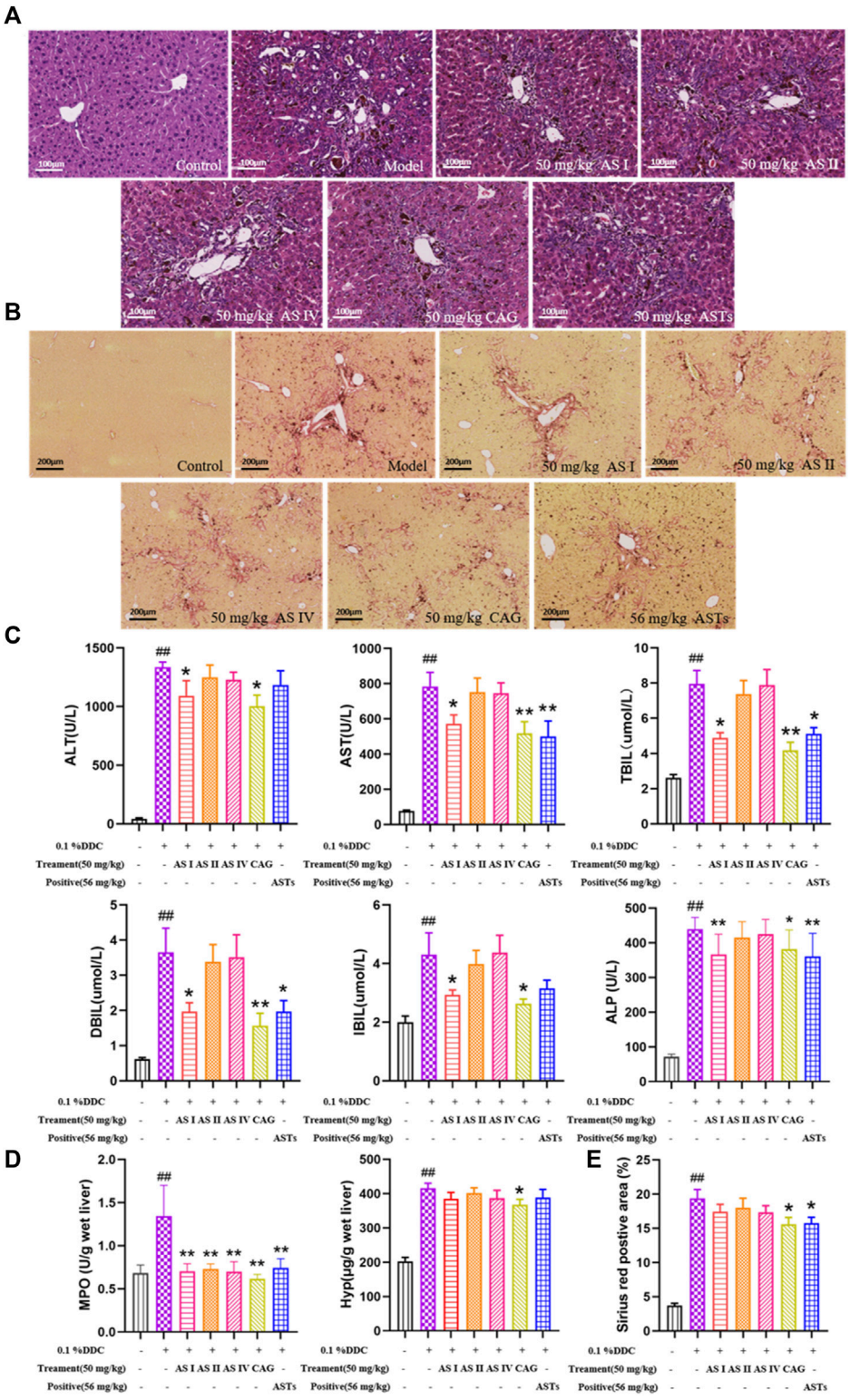

FIGURE 6
Effects of astragaloside I, astragaloside II, astragaloside IV and cyclogalactol on liver injury and collagen deposition of 0.1% DDC-induced mice. **(A,B)** Representative images of H&E staining of liver tissue (×20x) (scale bar 100 μm), sirius red staining (×10x) (scale bar 200 μm) are performed to observe the histopathological characteristics of liver tissues. **(C)** Measurement of serum ALT, AST, TBiL, DBiL, IBiL and ALP levels are deceted in mice. **(D)** MPO and Hyp content in liver tissues are determinated. **(E)** Area (%) of positive collagen is assessed by quantitative imaging of sirius red staining. $^{\#\#}p < 0.01$ vs. the normal group. $^{**}p < 0.01$ and $^{*}p < 0.05$ vs. 0.1% DDC group. Values were expressed as mean ± SD.

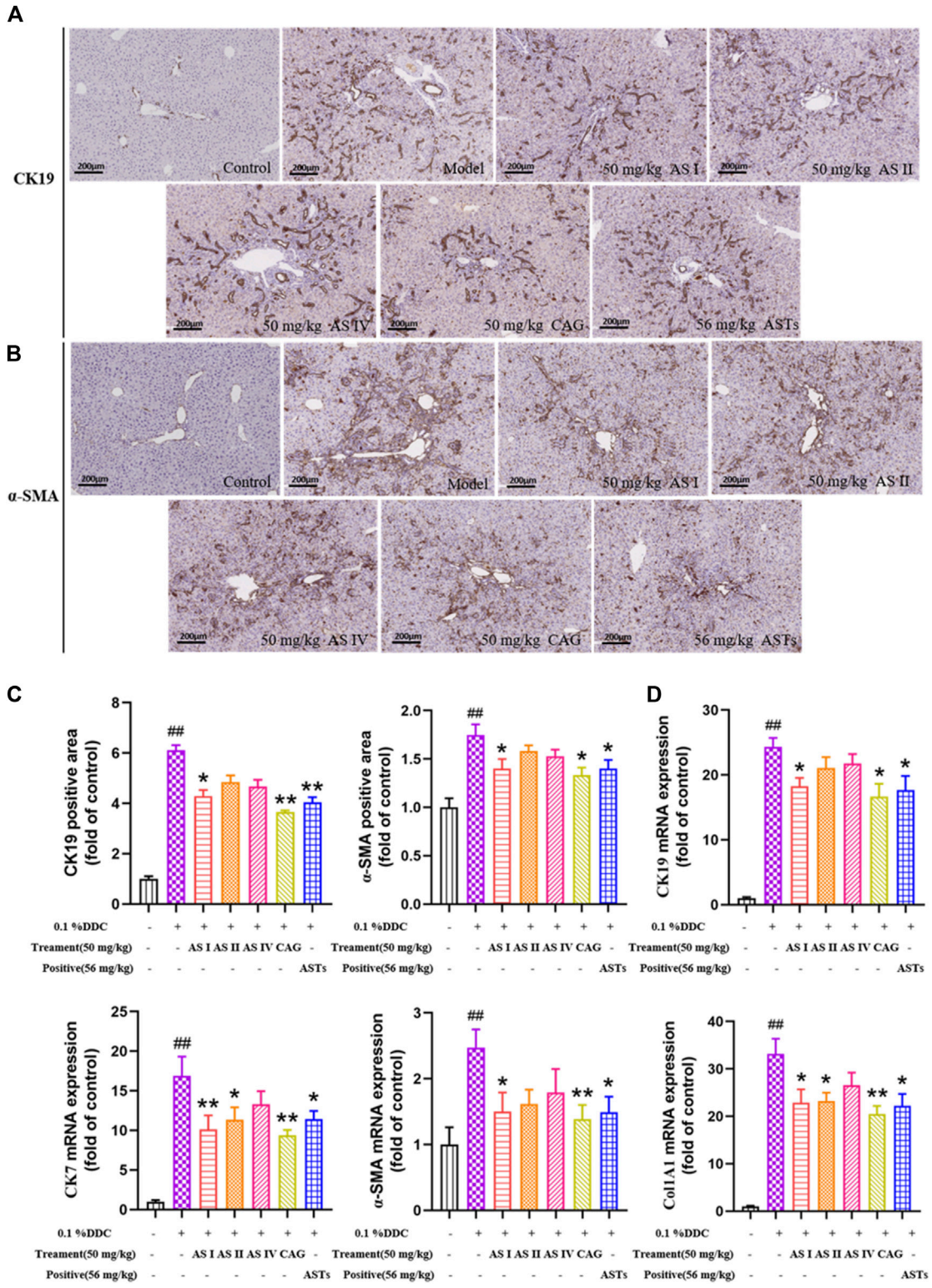

FIGURE 7
Effects of astragaloside I, astragaloside II, astragaloside IV and cyclogalactol on the expressions of CK19, CK7, α-SMA and Col1A1 in 0.1% DDC-induced CLD mice. **(A,B)** Immunohistochemical method is used to detect the effects of different astragalus saponins on hepatic α-SMA and CK19 protein expressions (×10x) (scale bar 200 μm). **(C)** Morphometric quantification of the α-SMA and CK19-positive area (%). **(D)** Effects of different astragalus saponins on the gene expressions of CK19, CK7, α-SMA and Col1A1 are evaluated by qRT-PCR, and normalized to GAPDH gene. $^{\#\#}p < 0.01$ vs. the normal group. $^{**}p < 0.01$ and $^{*}p < 0.05$ vs. 0.1% DDC group. Values were expressed as mean ± SD.

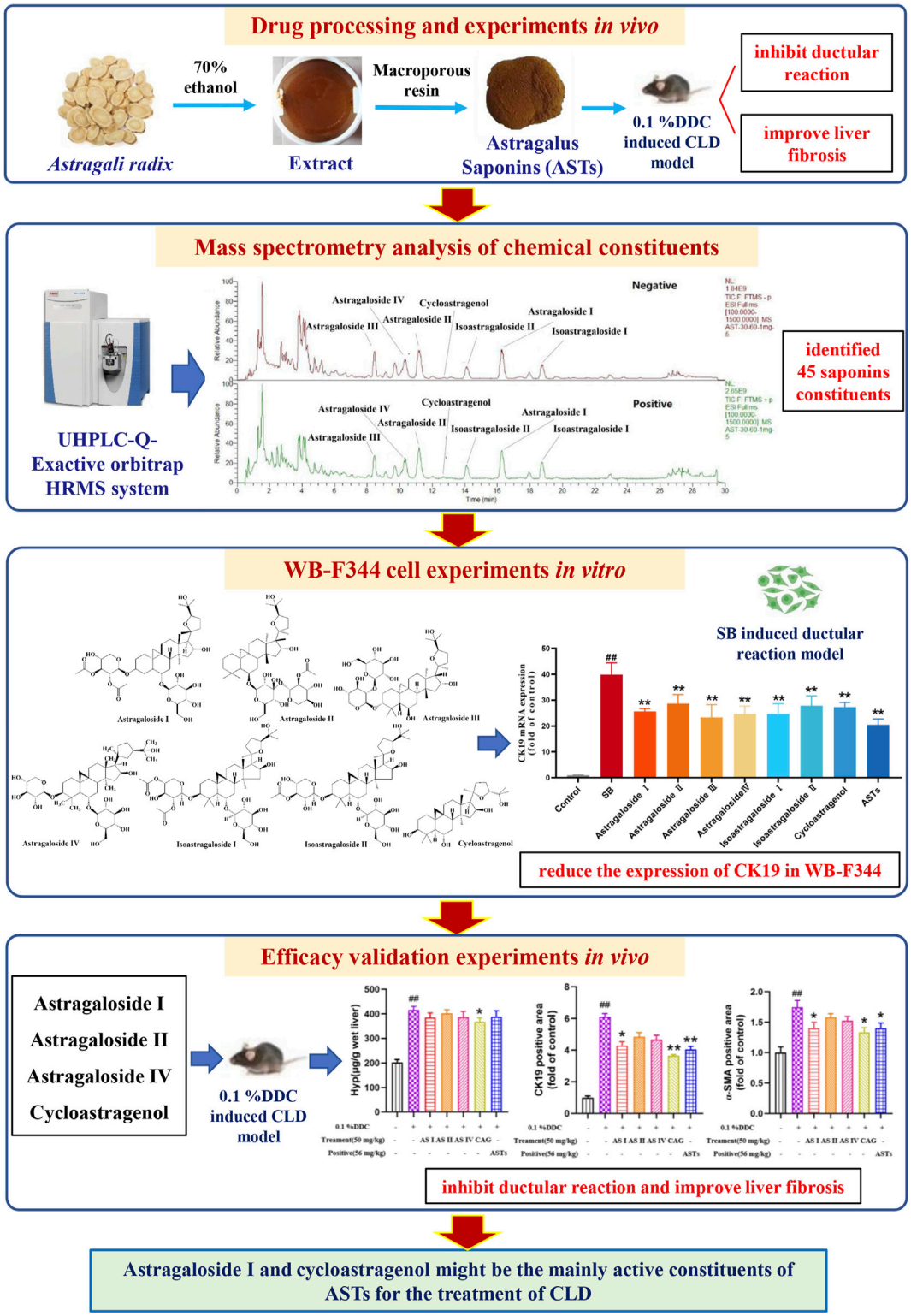

FIGURE 8
Scheme of the study. The main experiments in sequence include drug processing and *in vivo* experiments, mass spectrometry analysis of chemical constituents, *in vitro* WB-F344 cell experiments, and *in vivo* efficacy validation experiments.

increased. Compared with the model group, the ductular reaction and inflammation are reduced to different degrees in ASTs-treated groups. In addition, sirius red staining shows that (Figure 1B), collagen deposition is rarely seen in the normal group, and compared with the normal group, a large number of collagen are deposited around the hyperplastic bile ducts in the model group, while collagen deposition is alleviated in ASTs-treated groups.

Serum ALT, AST, TBiL, DBiL and IBiL levels are significantly increased in the model group ($p < 0.01$) than these in the normol group, the elevation of each index is remarkablely reduced after ASTs and obeticholic acid treatment ($p < 0.01$ or $p < 0.05$) (Figure 1C). In addition, liver Hyp content and Sirius red positive area are significantly reduced after ASTs treatment ($p < 0.05$). However, there is no significant difference between the obeticholic acid group and the model group (Figures 1D,E).

ASTs regulates the expressions of CK19, CK7, α-SMA, COL1A1 in DDC-induced CLD mice

Hepatic α-SMA and CK19 are abundantly expressed in the liver of the model group by immunohistochemical staining (Figures 2A,B). Compared with the normal group, the positive areas of α-SMA and CK19 are significantly higher in the model group ($p < 0.01$), and significantly attenuated in the ASTs-treated and obeticholic acid-treated groups ($p < 0.01$ or $p < 0.05$) (Figure 2C).

The mRNA expressions of CK19, CK7, α-SMA and Col1A1 are significantly increased in the model group ($p < 0.01$) (Figure 2D), while the expressions of CK19, CK7, α-SMA and Col1A1 are significantly reduced in the ASTs-treated group ($p < 0.01$ or $p < 0.05$). Likewise, the protein expressions of CK19 and α-SMA are consistent with the qRT-PCR results (Figure 2E).

Identification of the chemical constituents in ASTs and the absorbed chemical constituents in mice serum and liver after oral administration of ASTs

A comprehensive analysis of the components in ASTs is performed by UHPLC-Q-Exactive Orbitrap HRMS under the above optimal conditions. The total ion chromatograms (TICs) of the ASTs and seven astragalus saponins standards in positive and negative ion mode are shown in Figure 3A. The calculated errors of the protonated molecular weights of all identified compounds are within 10 ppm. 45 kinds of astragalus saponins are identified or tentatively determined from the ASTs after careful comparison with the retention times and MS/MS profiles of standards, references and chemistry books. Detailed information on the identified chemical components in the ASTs, including retention times, precise molecular weights, MS/MS fragment ions and peak areas of each component are listed in Supplementary Table S1. And specific structures of identified 45 astragalus saponins are shown in Figure 4. The TICs of seven astragalus saponins reference standards in positive and negative ion mode are shown in Figure 3B, and the contents of astragaloside III, astragaloside IV, astragaloside II, cycloastragenol, isoastragaloside II, astragaloside I, and isoastragaloside I are 23.81 mg/g, 25.98 mg/g, 66.17 mg/g, 0.42 mg/g, 27.19 mg/g, 79.46 mg/g and 34.29 mg/g in the ASTs, respectively. The serum and liver samples collected from ASTs-treated mice at 1 h are collected for LC-MS analysis to detect the absorbed prototypes as more as possible. With the help of the key information of the constituents (as listed in Supplementary Table S1) and the identification of the chemical constituents in ASTs, astragaloside IV, astragaloside II, cycloastragenol, and astragaloside I are obviously detected in serum or liver after oral administration 56 mg/kg ASTs. Other saponins constituents are not detected in serum or liver, it may be related with the relatively low contents of them in ASTs.

Effects of main chemical constituents of ASTs on SB-induced WB-F344 cell model

On the basis of effects of ASTs *in vivo* and the chemical analysis results of UHPLC-Q-Exactive Orbitrap HRMS, the effects of main seven chemical constituents of AST on SB-induced WB-F344 cell are evaluated. First, the cell viability is evaluated by CCK8 assay. Compared with the control group, cell viability is not significantly inhibited within 12.5 μM of these compound, but is obviously inhibited by isoastragaloside I treatment with 25 μM, astragaloside I and cycloastragenol treatment with 50 μM ($p < 0.01$ or $p < 0.05$) (Figure 5A). Consistent with the *in vivo* experiments, the expression of CK19 is evaluated *in vitro*. The elevated mRNA expression of CK19 in SB-induced WB-F344 cell is significantly decreased in these compounds (10 μM) and ASTs groups (10 μg/ml) ($p < 0.01$) (Figure 5B).

Astragaloside I and cycloastragenol improve serum biochemistry and collagen deposition in DDC-induced CLD mice

Normal morphology of hepatocytes without degeneration and necrosis are showed in the normal group by H&E staining (Figure 6A). Compared with the normal group, the ductular reaction phenomenons are increased in the model group, including bile duct dilatation, increase in the number of hyperplastic bile ducts, structural disorder, massive inflammatory cell infiltration, and focal necrosis of hepatocytes. The above phenomenons in four saponins and ASTs groups are improved in different degrees. Sirius red staining (Figure 6B) showed that a large amount of collagen fibers are deposited around the

hyperplastic bile ducts. The collagen deposition is reduced in each treatment group, and the best improvement effect is observed in the astragaloside I, cycloastragenol and ASTs groups.

Serum ALT, AST, TBiL, DBiL, IBiL and ALP levels are significantly elevated in the CLD model mice compared with the normal mice ($p < 0.01$), and the elevation of each index is significantly reduced in the astragaloside I, cycloastragenol and ASTs group ($p < 0.01$ or $p < 0.05$) (Figure 6C). Liver MPO, liver Hyp content and sirius red positive area are significantly elevated in the model group ($p < 0.01$), and significantly alleviated in the cycloastragenol and ASTs group ($p < 0.05$) (Figures 6D,E).

Astragaloside I and cycloastragenol supppressed the expressions of CK19, CK7, α-SMA, COL1A1, IL-1β, and IL-6 in DDC-induced CLD mice

As shown in immunohistochemical staining (Figures 7A,B, Supplementary Figures S2 A,B), little or no α-SMA, CK19, IL-1β and IL-6 are expressed in the normal group, while a large amount of α-SMA, CK19, IL-1β and IL-6 are expressed in the model group. The positive areas of α-SMA, CK19, IL-1β and IL-6 are significantly increased in the model group ($p < 0.01$), and significantly attenuated in the astragaloside I, cycloastragenol and ASTs groups ($p < 0.01$ or $p < 0.05$, Figure 7C, Supplementary Figures S2 C,D).

qRT-PCR results show that the mRNA expressions of CK19, CK7, α-SMA and Col1A1 are significantly reduced in the astragaloside I, cycloastragenol and ASTs groups compared with the model group. And the mRNA expressions of CK7 and Col1A1 are also significantly reduced in the astragaloside II group ($p < 0.01$ or $p < 0.05$) (Figure 7D).

Discussion

Cholestatic liver disease is a chronic liver disease that causes liver damage and fibrosis owing to bile stasis. (Karlsen et al., 2014). Ductular reaction and liver fibrosis are typical pathological manifestations of cholestatic liver disease (Fricker and Lichtenstein, 2019). Ursodeoxycholic acid (UDCA) is currently the first-line clinical drug of choice, but fails to improve disease progression at a later stage (Lindor et al., 2009). Clinical study has found that the combination of fibrates and UDCA improved serum biochemistry indices in CLD patients who responded poorly to UDCA, but had little or no effect on inhibition of disease progression (Lemoinne et al., 2018). Since no single drug or treatment has been proven to prolong transplant-free survival in CLD patients, finding a new drug has clinical values.

Recent studies have found Huangqi decoction (the main ingredient is AR) could alleviate chronic cholestatic liver injury in DDC-induced mice by improving intestinal microbiota dysbiosis and inhibiting bile acid-stimulated inflammation (Li et al., 2019; Zou et al., 2021). And Huangqi decoction also can reduce bile duct hyperplasia, and relieve liver fibrosis in bile duct ligation (BDL) rats. The mechanism may be related to regulate Numb expression and inhibit Notch signaling pathway (Zhang X. et al., 2017; Xu et al., 2020). But these studies mainly focus on the effective mechanism, without identifying the active pharmaceutical constituents of AR. In this study, ductular reaction and liver fibrosis are able to dose-dependently improved in DDC-induced CLD mice after ASTs treatment. Cholestatic liver injury is often accompanied by significant bile duct hyperplasia in the protal area (Tacke and Zimmermann, 2014). Bile duct hyperplasia is a compensatory response of the liver in response to impaired bile acid circulation. CK19 and CK7 are specific biomarkers of biliary epithelial cells (Mishra et al., 2009). And during the pathogenesis of liver fibrosis, activated hepatic stellate cells and fibroblasts express α-SMA, synthesize collagen and produce extracellular matrix (Parola and Pinzani, 2019; Zahedifard et al., 2020). The expressions of CK19 and α-SMA in liver tissues of CLD mice are significantly decreased after continuous oral administration of ASTs for 4 weeks. These results suggest that ASTs has a significant improvement effect on CLD mice.

UHPLC-Q-Orbitrap Exactive HRMS system is now widely used for the identification and quantitative analysis of components in TCM or compound prescriptions (Liu et al., 2021; Zhang C. et al., 2022). In this study, 45 kinds of astragalus saponins are identified in ASTs by UHPLC-Q-Orbitrap Exactive HRMS technology, seven kinds of astragalus saponins are identified by standards, including astragaloside I, astragaloside II, astragaloside III, astragaloside IV, isoastragaloside I, isoastragaloside II and cycloastragenol. And astragaloside I, astragaloside II, astragaloside IV and cycloastragenol are found in mice serum or liver tissues after oral administration of ASTs. Next, the transdifferentiation of WB-F344 cell model induced by SB is to evaluate the effects of ASTs and main components (Wang et al., 2010). qRT-PCR results revealed that the expression of CK19 in SB-induced WB-F344 cell is significantly decreased in these seven saponins constituents treatment groups. Astragaloside I can be sequentially converted to astragaloside II, astragaloside IV and cycloastragenol in rats after oral administration of AR (Li et al., 2017). Consistent with this, a little astragaloside I is found in the serum and liver tissues in our experiments, it has probably converted to other saponins *in vivo*. Combining the results of the absorbed chemical analysis *in vivo* and the activity screening *in vitro* experiments, astragaloside I, astragaloside II, astragaloside IV and cycloastragenol are finally selected, and the improvement effects of them are evaluated on cholestatic liver disease mouse model.

It is found that astragaloside IV is able to inhibit liver inflammation *via* mitogen-activated protein kinase (MAPK)/ nuclear factor kappa-B (NF-κB) signaling pathway, which in turn reduce lipid levels, hepatic steatosis in hyperlipidemic mice (Zhang Y. et al., 2022). Astragaloside IV significantly reduces body weight, white fat and liver/body weight ratio in senescent mice by targeting mitochondrial activity, and promotes fatty acid in white adipose

tissue mobilization in aging mice (Luo et al., 2021). Cycloastragenol activates Farnesoid X receptor (FXR) to reduce hepatic lipid accumulation, blood glucose, serum triacylglycerol levels and bile acids in high-fat diet mice. And cycloastragenol also attenuates hepatic steatosis in mice with methionine choline-deficient diet-induced nonalcoholic steatohepatitis (Gu et al., 2017). However, there are few studies related to astragaloside I and astragaloside II in liver diseases, especially cholestatic liver disease. Our experimental results show that Hyp content, abnormalities of serum biochemistry and the hepatic expressions of CK19 and α-SMA in CLD mice are significantly alleviated in cycloastragenol and astragaloside I treatment groups. It is reported that AR could regulate arachidonic acid metabolism and ether lipid metabolism by modulating the expressions of cytochrome P450 1A2 (CYP1A2), phosphate Cytidylyltransferase 1A (PCYT1A) and cytochrome P450 Family one Subfamily B Member 1 (CYP1B1) through network pharmacology techniques, to effectively ameliorate liver fibrosis (Wang et al., 2019). And network pharmacology study also found that astragalus flavonoids exerted anti-fibrosis effects by inhibiting IκB kinase β (IKKβ)/NF-κB pathway (An et al., 2020). However, these network pharmacology studies have not explored in-depth to find out the active constituents, and further validation experiments were lacking. In this study, we innovatively use UHPLC-Q-Orbitrap Exactive HRMS technology, combined with *in vivo* and *in vitro* experiments to find out the active constituents of ASTs exerting the therapeutic effects in cholestatic liver disease (Figure 8). And this strategy is promising for further investigation of other TCM herbs and formulaes.

However, the relationship between different effective constituents of ASTs and the protective mechanism against cholestatic liver disease should be further studied. In additional, the second *in vivo* experiment is not able to set up multiple doses of drug concentrations, which is also a shortcoming of the present study.

Conclusion

In this study, ASTs are found to have significant therapeutic effects on cholestatic liver disease, which are the main active site of AR against CLD, astragaloside I and cycloastragenol significantly inhibit the progression of cholestatic liver disease, which may the most important active constituents of ASTs for CLD. These findings not only provide a scientific basis for clarifying the active constituents of ASTs in the treatment of CLD, but also suggest novel promising therapeutic drugs for CLD.

Data availability statement

The original contributions presented in the study are included in the article/Supplementary Materials, further inquiries can be directed to the corresponding authors.

Ethics statement

The animal study was reviewed and approved by Animal Experimentation of Shanghai University of Traditional Chinese Medicine.

Author contributions

LZ, PL, JC, and WL participated in research design. LZ, YH, SQ, CZ, QZ, and DZ conducted experiments. YM, HZ, and GC performed data analysis. LZ, YH, PL, JC, and WL edited and writed of the manuscript, designed and drawed of tables and figures. All authors agree to be accountable for all aspects of work ensuring integrity and accuracy.

Funding

This work was supported by the National Natural Science Foundation of China (No. 81973613, and No. 82130120), Shanghai Science and Technology Committee Rising-Star Program (19QA1408900), “Chen Guang” project supported by Shanghai Municipal Education Commission and Shanghai Education Development Foundation (No. 20CG50), Young Elite Scientists Sponsorship Program by CAST (No. 2020QNRC001), China Postdoctoral Science Foundation (2021M702218), Shanghai Post-doctoral Excellence Program (2020372).

Conflict of interest

The authors declare that the research was conducted in the absence of any commercial or financial relationships that could be construed as a potential conflict of interest.

Publisher’s note

Supplementary material

The Supplementary Material for this article can be found online at: https://www.frontiersin.org/articles/10.3389/fphar.2022.965914/full#supplementary-material

References

An, L., Lin, Y., Li, L., Kong, M., Lou, Y., Wu, J., et al. (2020). Integrating network pharmacology and experimental validation to investigate the effects and mechanism of *Astragalus* flavonoids against hepatic fibrosis. *Front. Pharmacol.* 11, 618262–262. doi:10.3389/fphar.2020.618262

Brevini, T., Tysoe, O. C., and Sampaziotis, F. (2020). Tissue engineering of the biliary tract and modelling of cholestatic disorders. *J. Hepatol.* 73 (4), 918–932. doi:10.1016/j.jhep.2020.05.049

Chu, J., Abulimiti, A., Wong, B., Zhao, G., Xiong, S., Zhao, M., et al. (2022). Sigesbeckia orientalis L. Derived active fraction ameliorates perioperative neurocognitive disorders through alleviating hippocampal neuroinflammation. *Front. Pharmacol.* 13, 846631–631. doi:10.3389/fphar.2022.846631

Fickert, P., Stöger, U., Fuchsbichler, A., Moustafa, T., Marschall, H., Weiglein, A., et al. (2007). A new xenobiotic-induced mouse model of sclerosing cholangitis and biliary fibrosis. *Am. J. Pathol.* 171 (2), 525–536. doi:10.2353/ajpath.2007.061133

Fricker, Z., and Lichtenstein, D. (2019). Primary sclerosing cholangitis: A concise review of diagnosis and management. *Dig. Dis. Sci.* 64 (3), 632–642. doi:10.1007/s10620-019-05484-y

Fu, J., Wang, Z., Huang, L., Zheng, S., Wang, D., Chen, S., et al. (2014). Review of the botanical characteristics, phytochemistry, and pharmacology of Astragalus membranaceus (Huangqi). *Phytother. Res.* 28 (9), 1275–1283. doi:10.1002/ptr.5188

Gu, M., Zhang, S., Zhao, Y., Huang, J., Wang, Y., Li, Y., et al. (2017). Cycloastragenol improves hepatic steatosis by activating farnesoid X receptor signalling. *Pharmacol. Res.* 121, 22–32. doi:10.1016/j.phrs.2017.04.021

Guo, Z., Lou, Y., Kong, M., Luo, Q., Liu, Z., and Wu, J. (2019). A systematic review of phytochemistry, pharmacology and pharmacokinetics on astragali radix: Implications for astragali radix as a personalized medicine. *Int. J. Mol. Sci.* 20 (6), E1463. doi:10.3390/ijms20061463

Hasegawa, S., Yoneda, M., Kurita, Y., Nogami, A., Honda, Y., Hosono, K., et al. (2021). Cholestatic liver disease: Current treatment strategies and new therapeutic agents. *Drugs* 81 (10), 1181–1192. doi:10.1007/s40265-021-01545-7

Karlsen, T., Vesterhus, M., and Boberg, K. (2014). Review article: Controversies in the management of primary biliary cirrhosis and primary sclerosing cholangitis. *Aliment Pharmacol Ther.* 39 (3), 282–301. doi:10.1111/apt.12581

Kong, Y., Yan, M., Liu, W., Chen, C., Zhao, B., Zu, Y., et al. (2010). Preparative enrichment and separation of astragalosides from Radix Astragali extracts using macroporous resins. *J. Sep. Sci.* 33 (15), 2278–2286. doi:10.1002/jssc.201000083

Kummen, M., Thingholm, L., Rühlemann, M., Holm, K., Hansen, S., Moitinho-Silva, L., et al. (2021). Altered gut microbial metabolism of essential nutrients in primary sclerosing cholangitis. *Gastroenterology* 160 (5), 1784–1798.e0. doi:10.1053/j.gastro.2020.12.058

Lemoinne, S., Pares, A., Reig, A., Ben Belkacem, K., Kemgang Fankem, A. D., Gaouar, F., et al. (2018). Primary sclerosing cholangitis response to the combination of fibrates with ursodeoxycholic acid: French-Spanish experience. *Clin. Res. Hepatol. Gastroenterol.* 42 (6), 521–528. doi:10.1016/j.clinre.2018.06.009

Li, H. F., Xu, F., Yang, P., Liu, G. X., Shang, M. Y., Wang, X., et al. (2017). Systematic screening and characterization of prototype constituents and metabolites of total astragalosides using HPLC-ESI-IT-TOF-MSn after oral administration to rats. *J. Pharm. Biomed. Anal.* 142, 102–112. doi:10.1016/j.jpba.2017.05.009

Li, W. K., Wang, G. F., Wang, T. M., Li, Y. Y., Li, Y. F., Lu, X. Y., et al. (2019). Protective effect of herbal medicine Huangqi decoction against chronic cholestatic liver injury by inhibiting bile acid-stimulated inflammation in DDC-induced mice. *Phytomedicine* 62, 152948–948. doi:10.1016/j.phymed.2019.152948

Lindor, K. D., Kowdley, K. V., Luketic, V. A. C., Harrison, M. E., McCashland, T., Befeler, A. S., et al. (2009). High-dose ursodeoxycholic acid for the treatment of primary sclerosing cholangitis. *Hepatology* 50 (3), 808–814. doi:10.1002/hep.23082

Liu, W., Huang, J., Zhang, F., Zhang, C. C., Li, R. S., Wang, Y. L., et al. (2021). Comprehensive profiling and characterization of the absorbed components and metabolites in mice serum and tissues following oral administration of Qing-Fei-Pai-Du decoction by UHPLC-Q-Exactive-Orbitrap HRMS. *Chin. J. Nat. Med.* 19 (4), 305–320. doi:10.1016/S1875-5364(21)60031-6

Luo, Z., Wang, Y., Xue, M., Xia, F., Zhu, L., Li, Y., et al. (2021). Astragaloside IV ameliorates fat metabolism in the liver of ageing mice through targeting mitochondrial activity. *J. Cell. Mol. Med.* 25 (18), 8863–8876. doi:10.1111/jcmm.16847

Meng, P., Yang, R., Jiang, F., Guo, J., Lu, X., Yang, T., et al. (2021). Molecular mechanism of astragaloside IV in improving endothelial dysfunction of cardiovascular diseases mediated by oxidative stress. *Oxid. Med. Cell. Longev.* 2021, 1481236. doi:10.1155/2021/1481236

Mishra, L., Banker, T., Murray, J., Byers, S., Thenappan, A., He, A., et al. (2009). Liver stem cells and hepatocellular carcinoma. *Hepatology* 49 (1), 318–329. doi:10.1002/hep.22704

Parola, M., and Pinzani, M. (2019). Liver fibrosis: Pathophysiology, pathogenetic targets and clinical issues. *Mol. Asp. Med.* 65, 37–55. doi:10.1016/j.mam.2018.09.002

Qiu, J., Yan, J., Liu, W., Liu, X., Lin, J., Du, Z., et al. (2021). Metabolomics analysis delineates the therapeutic effects of Huangqi decoction and astragalosides on α-naphthylisothiocyanate (ANIT) -induced cholestasis in rats. *J. Ethnopharmacol.* 268, 113658–658. doi:10.1016/j.jep.2020.113658

Stättermayer, A. F., Halilbasic, E., Wrba, F., Ferenci, P., and Trauner, M. (2020). Variants in ABCB4 (MDR3) across the spectrum of cholestatic liver diseases in adults. *J. Hepatol.* 73 (3), 651–663. doi:10.1016/j.jhep.2020.04.036

Su, J., Gao, C., Xie, L., Fan, Y., Shen, Y., Huang, Q., et al. (2021). Astragaloside II ameliorated podocyte injury and mitochondrial dysfunction in streptozotocin-induced diabetic rats. *Front. Pharmacol.* 12, 638422–422. doi:10.3389/fphar.2021.638422

Tacke, F., and Zimmermann, H. (2014). Macrophage heterogeneity in liver injury and fibrosis. *J. Hepatol.* 60 (5), 1090–1096. doi:10.1016/j.jhep.2013.12.025

Vitcheva, V., Simeonova, R., Krasteva, I., Nikolov, S., and Mitcheva, M. (2013). Protective effects of a purified saponin mixture from Astragalus corniculatus Bieb., *in vivo* hepatotoxicity models. *Phytother. Res.* 27 (5), 731–736. doi:10.1002/ptr.4785

Wagner, M., and Fickert, P. (2020). Drug therapies for chronic cholestatic liver diseases. *Annu. Rev. Pharmacol. Toxicol.* 60 (5), 503–527. doi:10.1146/annurev-pharmtox-010818-021059

Wang, D., Li, R., Wei, S., Gao, S., Xu, Z., Liu, H., et al. (2019). Metabolomics combined with network pharmacology exploration reveals the modulatory properties of Astragali Radix extract in the treatment of liver fibrosis. *Chin. Med.* 14, 30. doi:10.1186/s13020-019-0251-z

Wang, P., Cong, M., Liu, T., Yang, A., Cong, R., Wu, P., et al. (2010). Primary isolated hepatic oval cells maintain progenitor cell phenotypes after two-year prolonged cultivation. *J. Hepatol.* 53 (5), 863–871. doi:10.1016/j.jhep.2010.05.014

Weismüller, T., Trivedi, P., Bergquist, A., Imam, M., Lenzen, H., Ponsioen, C., et al. (2017). Patient Age, sex, and inflammatory bowel disease phenotype Associate with course of primary sclerosing cholangitis. *Gastroenterology* 152 (8), 1975–1984. doi:10.1053/j.gastro.2017.02.038

Xia, M., Xie, X., Ding, J., Du, R., and Hu, G. (2020). Astragaloside IV inhibits astrocyte senescence: Implication in Parkinson's disease. *J. Neuroinflammation* 17 (1), 105. doi:10.1186/s12974-020-01791-8

Xu, W., Xu, Y. N., Zhang, X., Xu, Y., Jian, X., Chen, J. M., et al. (2020). Hepatic stem cell Numb gene is a potential target of Huang Qi Decoction against cholestatic liver fibrosis. *Sci. Rep.* 10 (1), 17486. doi:10.1038/s41598-020-74324-1

Yu, J., Ji, H., and Liu, A. (2018). Alcohol-soluble polysaccharide from Astragalus membranaceus: Preparation, characteristics and antitumor activity. *Int. J. Biol. Macromol.* 118, 2057–2064. doi:10.1016/j.ijbiomac.2018.07.073

Zahedifard, F., Lee, H., No, J., Salimi, M., Seyed, N., Asoodeh, A., et al. (2020). Comparative study of different forms of Jellein antimicrobial peptide on Leishmania parasite. *Exp. Parasitol.* 209, 107823–823. doi:10.1016/j.exppara.2019.107823

Zhang, C., Zhang, D., Wang, Y., Zhang, L., Qi, S., Fang, Q., et al. (2022). Pharmacokinetics and anti-liver fibrosis characteristics of amygdalin: Key role of the deglycosylated metabolite prunasin. *Phytomedicine.* 99, 154018–018. doi:10.1016/j.phymed.2022.154018

Zhang, L., Gong, A., Riaz, K., Deng, J., Ho, C., Lin, H., et al. (2017). A novel combination of four flavonoids derived from Astragali Radix relieves the symptoms of cyclophosphamide-induced anemic rats. *FEBS open bio* 7 (3), 318–323. doi:10.1002/2211-5463.12146

Zhang, X., Xu, Y., Chen, J. M., Liu, C., Du, G.-L., Zhang, H., et al. (2017). Huang qi decoction prevents BDL-induced liver fibrosis through inhibition of Notch signaling activation. *Am. J. Chin. Med.* 45 (1), 85–104. doi:10.1142/S0192415X17500070

Zhang, Y., Du, M., Wang, J., and Liu, P. (2022). Astragaloside IV relieves atherosclerosis and hepatic steatosis *via* MAPK/NF-κB signaling pathway in LDLR$^{-/-}$ mice. *Front. Pharmacol.* 13, 828161–161. doi:10.3389/fphar.2022.828161

Zhou, Y., Tong, X., Ren, S., Wang, X., Chen, J., Mu, Y., et al. (2016). Synergistic anti-liver fibrosis actions of total astragalus saponins and glycyrrhizic acid via TGF-β1/Smads signaling pathway modulation. *J. Ethnopharmacol.* 190, 83–90. doi:10.1016/j.jep.2016.06.011

Zou, J., Li, W., Wang, G., Fang, S., Cai, J., Wang, T., et al. (2021). Hepatoprotective effects of Huangqi decoction (Astragali Radix and Glycyrrhizae Radix et Rhizoma) on cholestatic liver injury in mice: Involvement of alleviating intestinal microbiota dysbiosis. *J. Ethnopharmacol.* 267, 113544–544. doi:10.1016/j.jep.2020.113544

frontiers | Frontiers in Pharmacology

TYPE Original Research
PUBLISHED 09 November 2022
DOI 10.3389/fphar.2022.1058480

OPEN ACCESS

EDITED BY
Yi Wu,
Nanjing Agricultural University, China

REVIEWED BY
Liwei Guo,
Yangtze University, China
Cui Liu,
South China Agricultural University, China
Yanyu Huang,
University of California, Davis, United States
Adelijiang Wusiman,
Xinjiang Agricultural University, China

*CORRESPONDENCE
Xuemei Tian,
txm@qau.edu.cn
Ranran Hou,
rrhou@qau.edu.cn

SPECIALTY SECTION
This article was submitted to Ethnopharmacology, a section of the journal Frontiers in Pharmacology

RECEIVED 30 September 2022
ACCEPTED 26 October 2022
PUBLISHED 09 November 2022

CITATION
Gao F, Liu H, Han H, Wang X, Qu L, Liu C, Tian X and Hou R (2022), Ameliorative effect of Berberidis radix polysaccharide selenium nanoparticles against carbon tetrachloride induced oxidative stress and inflammation.
Front. Pharmacol. 13:1058480.
doi: 10.3389/fphar.2022.1058480

Ameliorative effect of *Berberidis radix* polysaccharide selenium nanoparticles against carbon tetrachloride induced oxidative stress and inflammation

Fei Gao[1,2], Huimin Liu[2,3], Hao Han[2,3], Xin Wang[3], Lihua Qu[1,2], Congmin Liu[1,2], Xuemei Tian[4]* and Ranran Hou[1,2]*

[1]College of Chemistry and Pharmaceutical Sciences, Qingdao Agricultural University, Qingdao, China, [2]Agricultural Bio-Pharmaceutical Laboratory, Qingdao Agricultural University, Qingdao, China, [3]College of Veterinary Medicine, Qingdao Agricultural University, Qingdao, China, [4]Shandong Provincial Key Laboratory of Applied Mycology, Qingdao Agricultural University, Qingdao, China

Berberidis radix polysaccharide (BRP) extracted as capping agents was applied to prepare BRP-selenium nanoparticles (BRP-SeNPs) in the redox reaction system of sodium selenite and ascorbic acid. The stability and characterization of BRP-SeNPs were investigated by physical analysis method. The results revealed that BRP were tightly wrapped on the surface of SeNPs by forming C-O···Se bonds or hydrogen bonding interaction (O-H···Se). BRP-SeNPs presented irregular, fragmented and smooth surface morphology and polycrystalline nanoring structure, and its particle size was 89.4 nm in the optimal preparation condition. The pharmacologic functions of BRP-SeNPs were explored *in vitro* and *in vivo*. The results showed that BRP-SeNPs could heighten the cell viabilities and the enzyme activity of GSH-Px and decrease the content of MDA on H_2O_2-induced AML-12 cells injury model. *In vivo* tests, the results displayed that BRP-SeNPs could increase the body weight of mice, promote the enzyme activity like SOD and GSH-Px, decrease the liver organ index and the hepatic function index such as ALT, AST, CYP2E1, reduce the content of MDA, and relieve the proinflammation factors of NO, IL-1β and TNF-α in CCl_4-induced mice injury model. Liver tissue histopathological studies corroborated the improvement of BRP-SeNPs on liver of CCl_4-induced mice. The results of Western blot showed that BRP-SeNPs could attenuate oxidant

Abbreviations: BRP, *Berberidis radix* polysaccharide; BRP-SeNPs, BRP-selenium nanoparticles; GSH-Px, Glutathione peroxidase; MDA, Malondialdehyde; ALT, Alanine aminotransferase; AST, Aspartate aminotransferase; CYP, Cytochrome P450; TLR4, Toll-like receptor 4; p-JNK, Phosphorylation-Jun kinase; p-ERK, Phosphorylation-extracellular regulated protein kinases; p-p38, Phosphorylation-p38; p-ASK1, Phosphorylation-Apoptosis signal-regulating kinase 1; Keap1, Kelch-like ECH-associated protein 1; Nrf2, Nuclear factor erythroid 2-related factor 2; p-MKK4, Phosphorylation-mitogen activated protein kinase 4; ARE, Antioxidant response element; PMSF, Phenylmethylsulfonyl fluoride; SDS-PAGE, Sodium dodecyl sulfate polyacrylamide gel electrophoresis; PVDF, Polyvinylidene fluoride; TBST, Tris Buffered Saline Tween; ROS, Reactive oxygen species; DLS, Dynamic light scattering; FT-IR, Fourier transform infrared spectroscopy; UV-Vis, Ultraviolet-visible spectroscopy; XPS, X-ray photoelectron spectrometer; SEM, Scanning electron microscope; STEM, Scanning transmission electron microscopy; HAADF, High-angle annular dark field; TEM, Transmission electron microscopy; EDX, Energy Dispersive X-Ray Spectroscopy.

stress by the Nrf2/Keap1/MKP1/JNK pathways, and downregulate the proinflammatory factors by TLR4/MAPK pathway. These findings suggested that BRP-SeNPs possess the hepatoprotection and have the potential to be a green liver-protecting and auxiliary liver inflammation drugs.

KEYWORDS

Berberidis radix polysaccharide, selenium nanoparticles, oxidative stress, hepatoprotection, anti-inflammation

1 Introduction

Liver, the major metabolic and excretory organ in mammals, plays an important role in maintaining homeostasis (Li et al., 2015). Lots of factors such as drugs, viruses, environmental toxicants, alcohol, or metabolic diseases could lead to liver injury (Kanhar and Sahoo, 2019). Carbon tetrachloride (CCl_4), a representative hepatotoxin, is commonly served as inducement of liver injury model which is used to evaluate the therapeutic potential of drug for liver injury (Song et al., 2021). Numerous studies have shown that the hepatotoxicity of CCl_4 is the result of oxidative stress and meanwhile it can lead to hepatitis (Che et al., 2019). In liver tissue, CCl_4 can be catalyzed by cytochrome P450 to form CCl_3, $OOCCl_3$ and reactive oxygen species (ROS) (Liu et al., 2018a). The long-term accumulation of ROS in the body can also lead to various serious chronic liver diseases (Xu et al., 2017). Subsequently, inflammatory cells in liver tissue would be activated by a large number of free radicals, causing liver cell damage and inflammatory response (Faure-Dupuy et al., 2019; Wang W. et al., 2019). At present, the drugs used to treat the liver impairment diseases usually have many side effects and limited curative effect (Wang et al., 2021). It is urgent to find new products to prevent chemical-induced liver oxidative stress damage and relieve liver inflammation.

Selenium is an indispensable micronutrient in living organisms and plays an important role in the prevention of cancer (Sun et al., 2016), diabetes (Liu et al., 2018b), and immune modulation capabilities (Bagheri-Josheghani and Bakhshi, 2022). At same time, selenium is involved in the antioxidant defense systems of the liver and plays an important role in protecting against oxidative stress. Many studies demonstrated that Se supplementation can increase the level of enzymes such as GPx, prevent the accumulation of free radical species, and reduce the cellular damage (Qin et al., 2015). However, the narrow margin between the effective and toxic doses limited the application of this substance. It has been reported that orange-red and zero-valence selenium nanoparticles (SeNPs) have better bioavailability and chemical stability, and are less toxic than other forms of inorganic selenium (Wadhwani et al., 2016). Nevertheless, poor water solubility and the ability to easily transform into a grey analogue, that is, thermodynamically stable but biologically inert, makes Se^0 difficult to be used in food and medicine fields. Therefore, a kind of material as stabilizer or capping agent is needed for nano-selenium composites. Polysaccharides are rich in hydrophilic groups (such as hydroxyl groups) and can be used as stabilizers to synthesize selenium nanoparticles and improve their stability. Meanwhile, polysaccharides have received extensive attention due to their diverse biological activities and low side-effects (Cheng et al., 2018). Therefore, polysaccharide was selected to synthesize nano-selenium complex, hoping to exert better biological activity and synergistic effect (Huang S. et al., 2020).

Berberidis radix, a commonly used Chinese herbal medicine, is the root or stem bark the Berberidaceae, including *Berberis soulieana* Schneid., *Berberis wilsonae* Hemsl., and *Berberis poiretii* Schneid. Or *Berberis vernae* Schneid. And others in the same genus. In traditional Chinese medicine, it is defined bitter in taste and attributive to liver, stomach, and large intestine. It has the function of clearing away heat and draining dampness, and dissipating blood stasis. It is mainly used to treat dysentery, jaundice, pharyngalgia, conjunctival congestion and traumatic injury. *Berberidis radix* polysaccharide (BRP) as the main functional component of *Berberidis radix* may have the similar effect and abundant branch structure and hydroxyl groups, which can be used as stabilizers for the preparation of SeNPs.

In this experiment, we obtained a new polysaccharide from *Berberidis radix*, greenly synthesized and characterizes BRP-SeNPs, and then test the antioxidant activities and anti-inflammation activities *in vitro* and *in vivo*. Therefore, this study aimed to explore whether the *Berberidis radix* polysaccharide-selenium nanoparticles (BRP-SeNPs) have the effect of relieving liver injury and anti-inflammatory activities and its action mechanism, and finally provide a theoretical basis for the research and development of new green liver-protecting and anti-inflammatory drugs.

2 Materials and methods

2.1 Materials and chemicals

The herbal of *Berberidis radix* was the product from Tibet (China). Sodium selenite (Na_2SeO_3), ascorbic acid, hydrogen peroxide (H_2O_2) and carbon tetrachloride (CCl_4) were obtained from Aladdin Industrial Corporation (Shanghai, China). DMEM, FBS, PBS, and Trypsin were purchased from Beyotime Biotechnology Co., Ltd. (Shanghai, China). The

ELISA assay kits of AST, ALT, SOD, GSH-Px, MDA, CYP2E1, NO, TNF-α and IL-1β were purchased from Jiangsu Meimian Industrial Co., Ltd. (Yancheng, China). Antibodies of mouse TLR4, p-JNK, p-ERK, p-p38, p-ASK, p-MKK4, Keap1, Nrf2 were purchased from Cell Signaling Technology (Beverly, MA, United States). Antibodies of mouse β-actin and secondary antibody (HRP labeled goat anti-mouse IgG antibody) were purchased from Zhongshan Golden Bridge Biotechnology Co., Ltd. (Beijing, China). In addition, all other chemicals and solvents were analytical grade chemicals and sourced from Sinopharm Chemical Reagent Co., Ltd. (Shanghai, China).

2.2 Preparation and characterization of BRP and BRP-SeNPs

2.2.1 Preparation of BRP

50 g *Berberidis radix* power was immersed in 100 ml of 95% petroleum ether solution and refluxed at 60°C for 3 h. The filtered and dried residue was extracted three times with distilled water (1:30 g/ml) at 100°C for 2 h and the filtrates were combined. After that, the filtrate was further condensed to 200 ml with a rotary evaporator at 55°C and then added to four times volume of ethyl alcohol. After standing for 12 h at 4°C, polysaccharides of *Berberidis radix* was precipitated and deproteinated with Sevag reagent ($V_{N\text{-butyl alcohol}}$:$V_{Trichloromethane}$ = 1:4). The resulting solution was freeze-dried to obtain the *Berberidis radix* polysaccharide (BRP).

2.2.2 Preparation of BRP-SeNPs

According to the previous reports, the BRP-SeNPs were prepared (Zeng et al., 2019). Briefly, 10 mM sodium selenite was added to prepared BRP (2.0 mg/ml) solution and stirred at 25°C for 30 min. Then, 4 times of fresh ascorbic acid (40 mM) was slowly added in and magnetically stirred for 12 h. The resulting product was dialyzed (MWCO: 8000–14000 Da) with distilled water for 72 h and finally lyophilized to obtain BRP-SeNPs.

2.2.3 Characterization of BRP-SeNPs

The color change of the prepared BRP-SeNPs was recorded by a digital camera (Exterior, EOS 1500D, Canon, Japan). Measurement of mean diameter (particle size), dispersibility index (PDI) and Zeta potential of nanoparticles was used dynamic light scattering (DLS, ZS90, Malvern, United Kingdom). The Fourier transform infrared spectroscopy was obtained by FT-IR spectrometer (FI-IR, NicoletiS10, Thermo Fisher, United States). The UV-Vis spectra were scanned from 200 to 800 nm using UV-Vis spectrophotometer (UV, V-3900, HITACHI, Japan). The XPS spectra of BRP and BRP-SeNPs were analyzed by X-ray electron spectrometer (XPS, AXIS SUPRA+, Shimadzu, Japan). The morphology of BRP and BRP-SeNPs was observed by scanning electron microscopy (SEM, Quanta60, FEI, United States) and transmission electron microscopy (TEM, Talos F200S, FEI, United States). The composition of the samples was analyzed using STEM-HAADF detector and EDX equipped with a transmission electron microscope (HRTEM, Talos F200S, FEI, United States).

2.3 Antioxidant activity of BRP-SeNPs *in vitro*

2.3.1 Cell culture

The normal mouse hepatocytes AML-12 cell line (CRL-2254) used herein was purchased from the ATCC. The cells were cultured in DMEM/F12 containing 10% FBS, 100 μg/ml streptomycin and 100 U/mL penicillin in cell incubator (5% CO_2, 37°C). 100 μL of AML-12 cell suspension (2×10^5 cells/mL) was inoculated in a 96-well plate for 12 h.

2.3.2 Establishment of cells injury model induced by H_2O_2

AML-12 cells were treated with different concentrations of H_2O_2 (0, 25, 50, 100, 150, 200, 250 μM) for 4 h to induce oxidative injure. After that, 10 μL of CCK-8 was added to each well, and the cells were continued to incubate for 2 h at 37°C. The absorbance value of each well was determined at 450 nm by microplate reader (OD, MD/Spectra Max M2e, Molecular Devices, United States).

2.3.3 Cytotoxicity and protective assays of BRP-SeNPs

AML-12 cells were treated with different concentrations of BRP-SeNPs (0, 50, 100, 200, 300, 400, 500 μg/ml) for 24 h. The cytotoxicity was detected by CCK-8 assays.

In the protection assay, AML-12 cells were cultured with different concentrations of BRP-SeNPs (100, 200, 400 μg/ml) for 24 h and then treated with 100 μM H_2O_2 for 4 h. The protective function of BRP-SeNPs was determined by CCK-8 assays.

2.3.4 Changes of intracellular GSH-Px and MDA content

According to the previous procedure, AML-12 cells were cultured in 6-well plates, and then treated with or without BRP-SeNPs and H_2O_2. The cells were collected and lysed, and centrifuged to obtain the supernatant. The enzyme activity of GSH-Px and content of MDA was determined according to the manufacturer's instructions.

2.4 Animal treatment and dosage regimen

SPF Kunming mice (female, 20 ± 2 g) were purchased from Jinan Pengyue Laboratory Animal Breeding Co., Ltd. (Shandong,

China). Animals were reared under the conditions of standard 12-h light, ambient temperature of 25 ± 2°C, and relative humidity of 60 ± 5%. After 3 days of acclimatization, all animals were used for experiments. All experimental protocols strictly followed the Qingdao Agricultural University guidelines for the care and use of laboratory animals.

25 mice were randomly divided into 5 groups (n = 5). Blank control group (BC), model group (MG), positive control group (PC), high dose groups (H) and low dose groups (L). The mice in the H, L groups were intragastric administration with BRP-SeNPs (200, 50 mg/kgbw) and PC group with Silymarin (200 mg/kgbw) for 21 days. The mice in the BC and MG groups were given the same volume of distilled water at the same time. All mice, except BC group, were intraperitoneally injected with 0.2% CCl_4 ($V_{Carbon\ tetrachloride}/V_{Olive\ oil}$) at a dose of 0.1 ml/10 gbw after the last intragastric administration, and the BC group mice were intraperitoneally injected with the same volume of olive oil. After a 12 h fast, all mice were sacrificed under anesthesia. Blood samples were collected from the orbits, and serum was harvested by centrifugation (3000 rpm, 10 min, 4°C). The liver was washed with 0.9% normal saline and used for biochemical index determination, histopathology analysis and Western blot analysis.

2.5 Biochemical index determination

Biochemical analysis of serum was performed, and serum ALT and AST were detected according to the manufacturer's instructions.

The liver samples with saline solution were homogenized at a ratio of 1:9 (g/ml). The supernatant was obtained by centrifugation at 8000 rpm for 10 min. Liver oxidation index was determined using SOD, GSH-Px, MDA and CYP2E1 Elisa kits, and inflammation index was tested using NO, TNF-α, IL-1β Elisa kits. All Elisa assays were performed according to the kit's instructions.

2.6 Histopathology analysis

A part of fresh liver was cut and fixed in 4% paraformaldehyde solution and stored for 48 h. After dehydration and transparency, the tissues were embedded in wax block, cut into 5 μm slices and stained with H&E assay.

2.7 Western blot analysis

Liver sample was added into 1 mM PMSF (Phenylmethylsulfonyl fluoride) (10 mg: 100 uL). The tissue homogenate was centrifugated (12,000 g, 4°C) for 5 min to obtained the supernatant. The concentration of protein in the supernatant was detected by BCA kit, and then denaturized with the Western-IP loading buffer at 100°C for 5 min to finally get protein sample.

Denatured proteins were separated on 10% sodium lauryl sulfate-polyacrylamide gel electrophoresis (SDS-PAGE) and moved to the membranes of polyvinylidene fluoride (PVDF) (Millipore, United States). After that, the PVDF was blocked with 5% BSA-TBST (Tris Buffered Saline Tween) solution (v/v) for 1 h and then incubated with the corresponding antibodies at 4°C overnight. The membranes were washed with TBST. After washing with TBST, the membranes were incubated with an HRP-IgG antibody at room temperature for 4 h. Then, the membranes were washed three times with TBST. Finally, images were got using a chemiluminescence imaging system and analyzed by ImageJ software.

2.8 Statistical analysis

All data were repeated three times and data analysis was performed using SPSS 23.0 analysis software. Data were expressed as Mean ± SD, analyzed by one-way analysis of variance (ANOVA) and Duncan's multiple range test.

3 Results and discussion

3.1 Preparation of BRP-SeNPs

As shown in Figure 1A, Na_2SeO_3 was added to the BRP solution and mixed well. The reduction reaction of the precursor SeO_3^{2-} to selenium (Se) atoms was triggered when ascorbic acid was added, resulting in the formation of SeNPs stabilized by BRP macromolecules. The synthesis process of BRP-SeNPs could be clearly detected by monitoring the dark red color-light yellow or reddish brown. When the polysaccharide concentration was 0 mg/ml to 1.0 mg/ml, the solution was dark red and turbid, and a lot of precipitates were formed. However, when the polysaccharide concentration reached 2.0 mg/ml, the clear and bright orange-red solution was obtained. And then as the polysaccharide concentration increased, the color of the solution gradually brightly deepened.

3.2 Stability of BRP-SeNPs

The stability and the size of BRP-SeNPs are always important to affect their biological activity. Therefore, BRP-SeNPs need to be experimentally determined to screen the optimal synthesis conditions. As shown in Figure 1B, the concentration of BRP affected the particle size, PDI and Zeta potential of BRP-SeNPs. When the BRP concentration was 2.0 mg/ml, the particle size (89.4 nm) and PDI (0.24) of synthesized BRP-SeNPs were

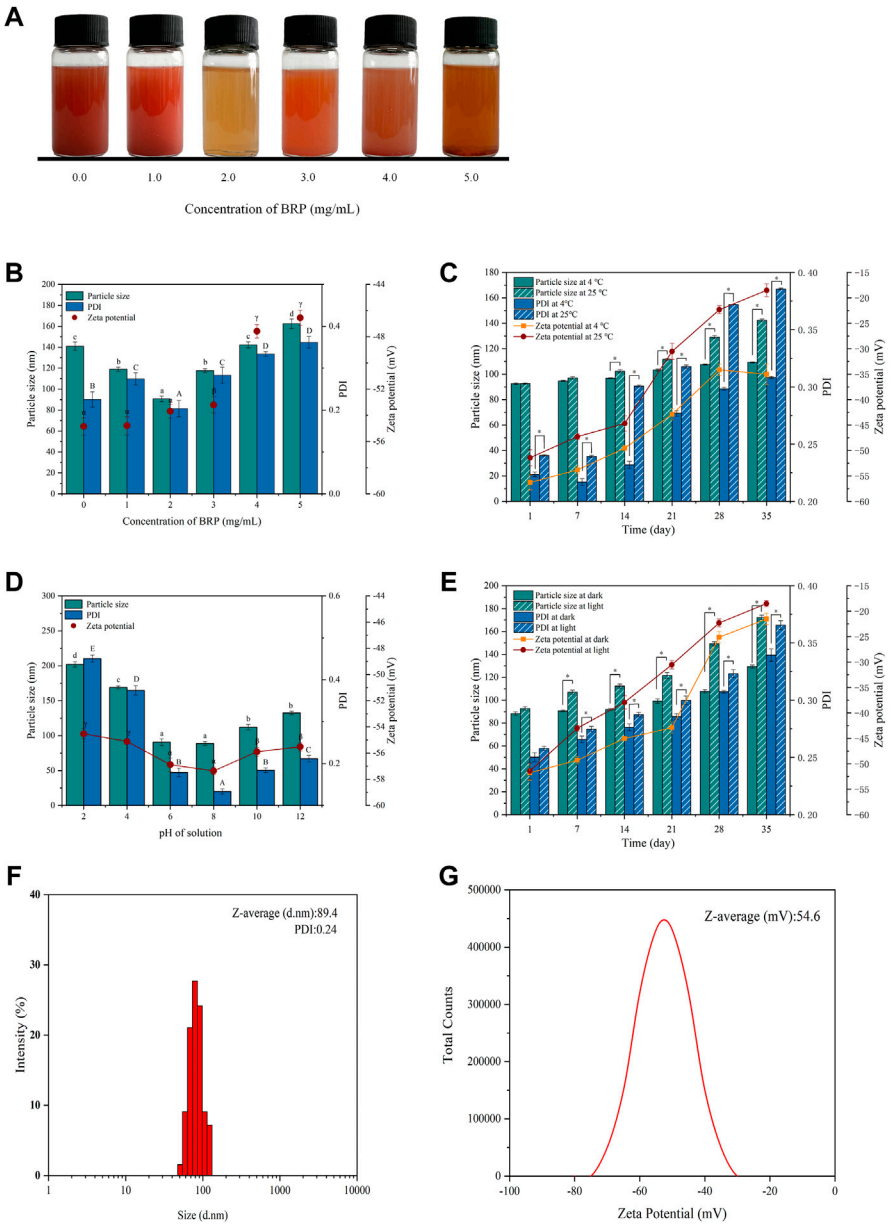

FIGURE 1
(A) Selenium nanoparticles synthesized with different concentrations BRP. **(B)** The influence of BRP concentration on the particle size, PDI and zeta potential of SeNPs. The influence of **(C)** temperature, **(D)** pH and **(E)** light conditions on the stability of SeNPs during 35 days of storage. **(F)** The particle size, PDI and **(G)** Zeta potential of BRP-SeNPs. The different letters indicate significant differences ($p < 0.05$). Comparisons between experimental groups were conducted by using one-way ANOVA, $^*p < 0.05$.

significant smaller than other groups. The results demonstrated that BRP-SeNPs had comparatively centralized distribution of the particles diameter when BRP used at 2.0 mg/ml. Comparing to the concentration of BRP in 4.0–5.0 mg/ml, the zeta potential of BRP-SeNPs prepared with BRP in 0–3.0 mg/ml were significant higher. The results meant that BRP-SeNPs possessed high Zeta potential had low aggregation and high stability. However, some studies reported that with the increasing of concentration of polysaccharide, the particle size of synthetic polysaccharide-SeNPs would get smaller (Chen et al., 2022). We speculated that the strong molecular interaction between polysaccharides was likely to lead to the weakened binding ability of BRP to SeNPs in our research. The results in Figure 1B demonstrated that the particle size and stability of SeNPs can be successfully regulated by adjusting the concentration of BRP. On this basis, the storage time was

extended to 35 days to study the potential effects of temperature, pH, and light on the stability of BRP-SeNPs.

As shown in Figure 1C, when the solution was stored at 25°C, the particle size of BRP-SeNPs increased significantly from 92.6 to 138.4 nm in 35 days, while there was only varied 16.5 nm (92.6–109.1 nm) at 4°C during the same time. The changes of PDI and Zeta potential of BRP-SeNPs were dramatically increased after 14 days whether it was stored at 4°C or 25°C. Comparing with the BRP-SeNPs stored at 25°C, the PDI and Zeta potential of BRP-SeNPs stored at 4°C were significant lower. Those results indicated that the BRP-SeNPs stored at 25°C had poor stability. The reason may be that the surface charge of spherical SeNPs is weakened by the high temperature, which reduces the stability and makes the SeNPs nanoparticles turbid and unstable (Song et al., 2020).

As shown in Figure 1D, pH also had a significant effect on particle size and PDI. It was found that the particle size of BRP-SeNPs increased significantly and was unstable under acidic conditions. The reason might be that BRP is protonated under strongly acidic conditions, which weakens the electrostatic interaction between BRP and SeNPs, resulting in the aggregation of SeNPs. In contrast, under weakly alkaline conditions, the particles of the BRP-SeNPs solution have less aggregation and better stability.

In addition, as shown in Figure 1E, the effects of light conditions (500 ± 40 Lx) on the physicochemical stability of BRP-SeNPs were also determined. The results of particle size and PDI slightly increased when the storage time was extended to 35 days under dark conditions. In contrast, under illumination, the particle size of BRP-SeNPs significantly increased. This phenomenon may be due to the photosensitivity of the O-H which likely conjugated to the SeNPs, thereby affecting the stability of the solution (Gao et al., 2020). In order to obtain BRP-SeNPs with smaller size and better stability, the optimal synthesis and storage conditions were as follows. The reaction system contained 10 mM, 2.0 mg/ml BRP, and 40 mM ascorbic acid. The solution system could store in 4°C without light. Under these conditions, the particle size of BRP-SeNPs was 89.4 nm, the PDI was 0.24, and the Zeta potential was −54.6 mV, as shown in Figures 1F,G.

3.3 Characterization of BRP-SeNPs

The BRP-SeNPs were further characterized by FT-IR spectroscopy. As shown in Figure 2A, the peak of BRP at 3380 cm^{-1} represented the stretching vibration of the hydroxy group, which slightly shifted to 3402 cm^{-1} in the IR spectrum of BRP-SeNPs (Wang L. et al., 2019). The sharp band at 2940 and 2340 cm^{-1} were the C-H stretching vibration in methylene group and carbon dioxide peak in the testing environment (Shi et al., 2021). The absorption band at 1650 cm^{-1} could be assigned to the absorption of water, and the absorption peaks at 1400 cm^{-1} represented the bending vibration of -OH (Zhang et al., 2021). Meanwhile, the peak of BRP at 1035 cm^{-1} was caused by the stretching vibration of C-O-C and C-O-H, which slightly shifted to 1081 cm^{-1} in the IR spectrum of BRP-SeNPs (Xiao et al., 2017). Moreover, the characteristic band of BRP-SeNPs at 3402 cm^{-1} was relatively lower than that of BRP (3380 cm^{-1}), with an obvious blue shift (Liu et al., 2012), indicating that the hydroxyl groups of BRP were bound by hydrogen bonding (O-H···Se) between the surface atoms of SeNPs (Zhang et al., 2015). In addition, the absorption band of C-O-H of BRP-SeNP appeared at higher wavelength at 1081 cm^{-1} (Liu et al., 2012) compared with the BRP, indicating that some hydroxy groups of BRP were conjugated with SeNPs to disrupt hydrogen bond in native BRP and formed new C-O···Se bonds (Liu et al., 2017; Hui et al., 2019). FT-IR spectroscopy showed the interaction mechanism between BRP and SeNPs. As shown in Figure 2B, UV-Vis absorption spectrum of BRP and BRP-SeNPs was detected in the range of 200–800 nm. The UV-Vis spectrum of BRP did not exhibit obvious absorption peaks between 200 and 400 nm, and thus illustrated its contained minimal proteins and nucleic acids. However, the UV-Vis spectrum result of BRP-SeNPs showed an obvious absorption peak near 270 nm and that explained the formation of SeNPs and the interaction between BRP and SeNPs which had been werified in previous results (Zhai et al., 2017).

In order to explain the interaction mechanism between BRP and SeNPs, XPS was used to further explore. As shown in Figure 2C, there was a typical Se 3 days peak in the full spectrum of BRP-SeNPs compared with BRP, indicating that the selenium was successfully introduced into BRP-SeNPs. In addition, according to the NIST X-ray photoelectron spectroscopy database (standard reference database 20, version 4.1) and the high-resolution of Se 3 days spectrum of BRP-SeNPs, two dominant peaks at 56.1 eV (Se $3d_{3/2}$) and 55.6 eV (Se $3d_{5/2}$) were observed in Figure 2D, indicating the selenium in the BRP-SeNPs was zero valence selenium (Se^0) (Gao et al., 2020). Besides, the Se 3 days spectrum of BRP-SeNPs had no electron binding energy peak at 59.1 eV, indicating that all Se^{4+} were reduced to Se^0 in this reaction system (Jiang et al., 2022).

As shown in Figures 2E,F, the O1s spectra of BRP and BRP-SeNPs displayed that the binding energy was increased from 532.7 to 532.3 eV in BRP to 534.3 and 533.9 eV in BRP-SeNP, which might be attributed to the strong interactions and the formation of C–O···Se bonds between SeNPs and BRP (Ren et al., 2021). The results mentioned-above indicated that the strong interaction between BRP and SeNPs during the formation of BRP-SeNPs reduced the electron density around the O atom, which in turn weakened the shielding effect on the inner electrons, making the O atom's binding energy increase and the formation of C-O···Se bonds (Cai et al., 2018). This result of the formation of C-O···Se bonds in BRP-SeNPs was consistent with that showed in FT-IR analysis. Combined with all results, the formation mechanism of BRP-SeNPs was showed in

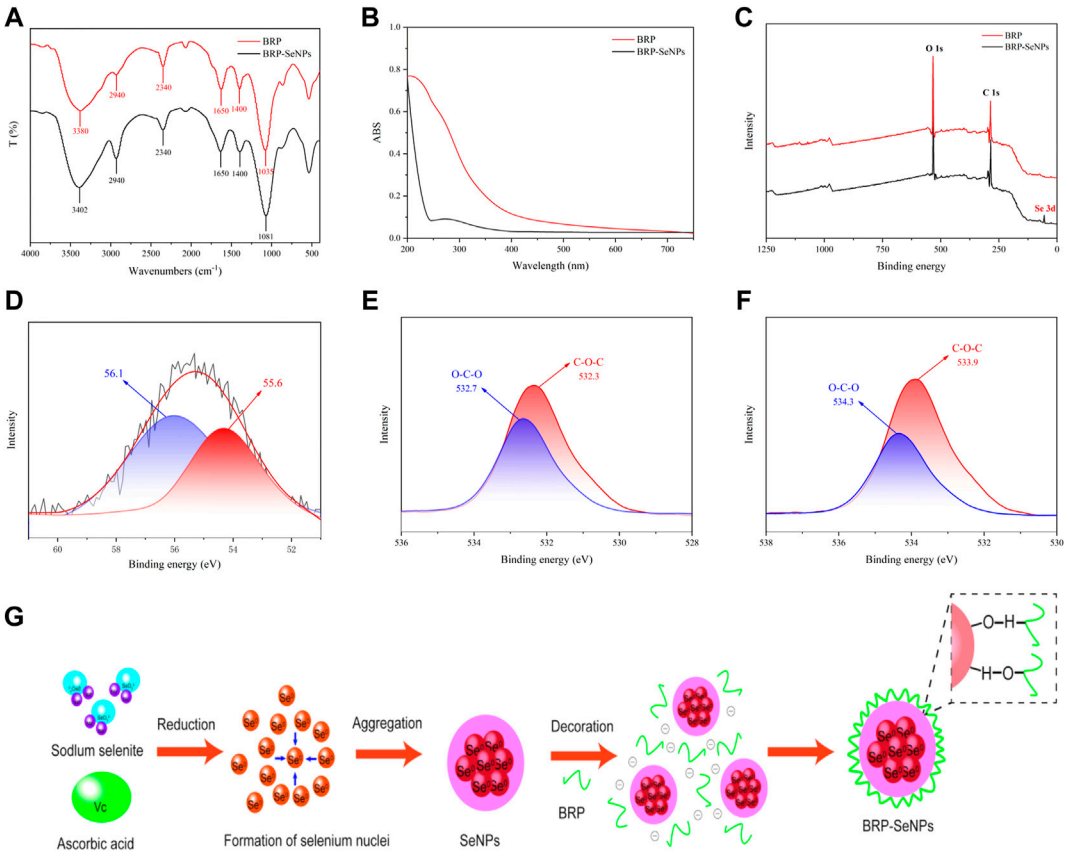

FIGURE 2
Characterization of BRP-SeNPs. **(A)** FT-IR spectrum. **(B)** UV-vis absorption spectrum. **(C)** XPS spectrum of BRP and BRP-SeNPs. **(D)** High-resolution Se 3 days spectrum of BRP-SeNPs. O1s spectrum of **(E)** BRP and **(F)** BRP-SeNPs. **(G)** Schematic diagrams of formation mechanism of BRP-SeNP.

Figure 2G. In the reaction system, free Se^{4+} (SeO_3^{2-}) was firstly reduced to form Se^0 by ascorbic acid, then the original Se core was subsequently generated and amount of Se^0 finally aggregated into SeNPs. Next, BRP wrapped on the surface of SeNPs through the formation of C-O···Se bonds or the strong interaction by the hydroxyl group between BRP and SeNPs to produce BRP-SeNPs.

The surface morphology and elemental composition of BRP-SeNPs were analyzed by SEM and EDX techniques. As shown in Figures 3A–F, BRP presented areatus, foveolate and rough surface morphology. However, BRP-SeNPs revealed irregular, fragmented and smooth surface morphology. Then we determined the three elements of C, O, and Se in BRP and BRP-SeNPs. The results showed that C and O in BRP were 42.74% and 57.26%, and C, O, and Se in BRP-SeNPs were 32.66%, 48.05% and 19.29%, respectively. After that, a small amount of BRP-SeNPs solution was placed on a copper grid and dried, and then observed by transmission electron microscopy (Zhang et al., 2014). As shown in Figure 3G, the BRP-SeNPs presented well-dispersed spherical particles with a diameter of about 60 nm. Interestingly, the size of particle measured by DLS was bigger than that by TEM, which is due to that DLS measured the size of the polysaccharide-conjugated selenium nanoparticles while TEM only observed SeNPs without polysaccharides visualization which supports the preceding research result (Bai et al., 2020). Under the observation of HRTEM, as shown in Figures 3H,I, there were a lot of crystal structures on the spherical surface of BRP-SeNPs. After selected area electron diffraction (SAED) analysis, as shown in Figures 3J,K, bright light bands could be clearly seen, which appeared as circular aperture, indicating that the BRP-SeNPs possessed polycrystalline nanoring structures.

3.4 Antioxidant activities of BRP-SeNPs *in vitro*

3.4.1 Effects of H_2O_2 and BRP-SeNPs on the viability of AML-12 cells

The effect of BRP-SeNPs on the viability of AML-12 cells was detected by CCK-8 method. As shown in Figure 4A, when

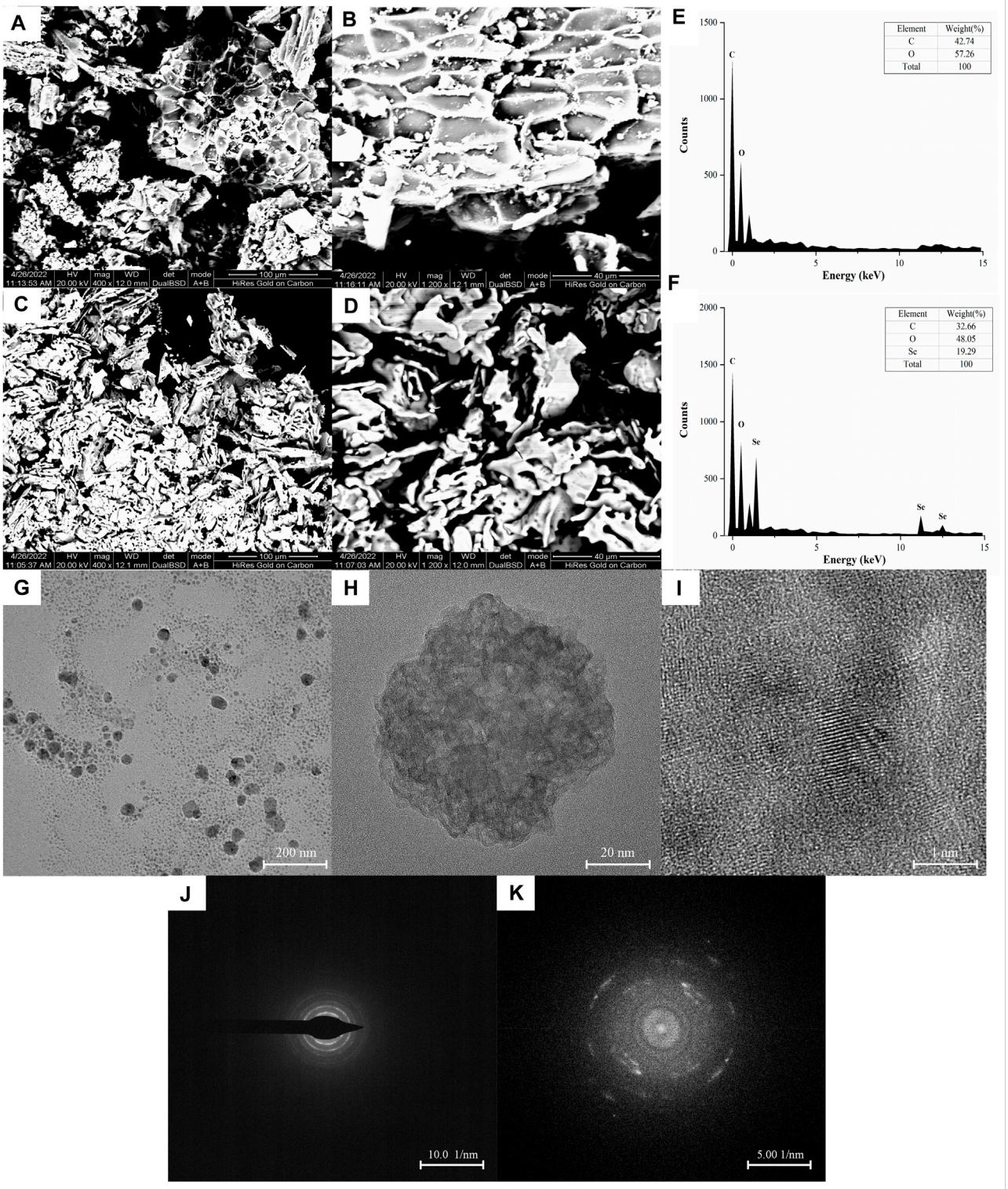

FIGURE 3
SEM images of **(A,B)** BRP and **(C,D)** BRP-SeNPs, A and C under ×400 magnification, B and D under 1200 × magnification. The distribution of C, O, and Se in **(E)** BRP and **(F)** BRP-SeNP by EDX analysis. Representative **(G)** TEM and **(H,I)** HRTEM images of BRP-SeNPs and its corresponding **(J,K)** SAED pattern.

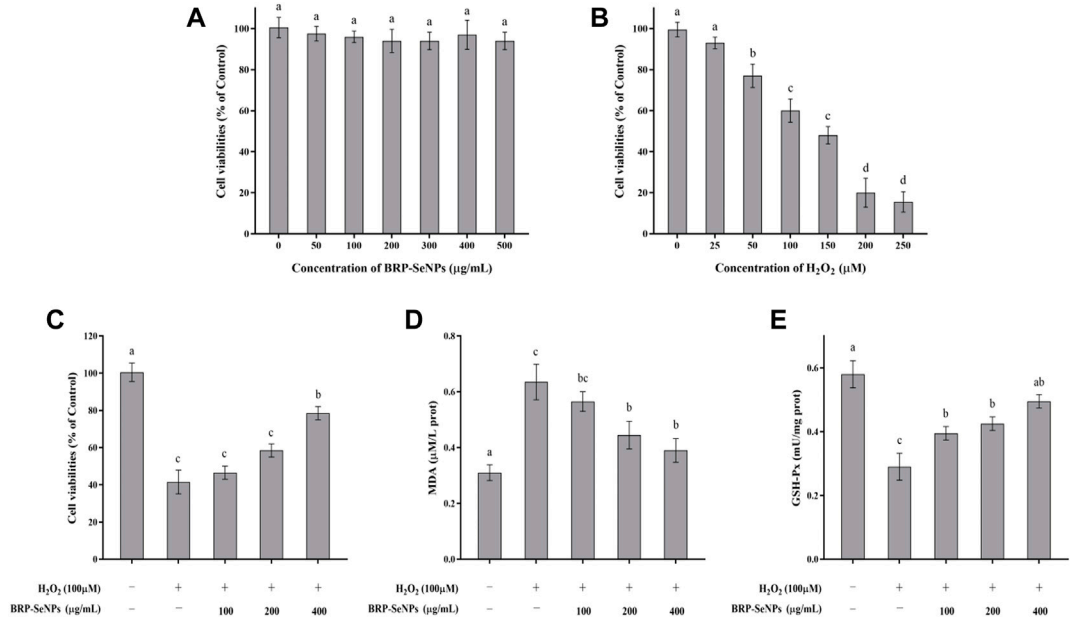

FIGURE 4
(A) Evaluation of toxicity of BRP-SeNPs on AML-12 cells. **(B)** Test of H_2O_2 concentration on AML-12 cells. **(C)** Protective effect of BRP-SeNPs on the H_2O_2-induced AML-12 cells model. **(D)** Effect of BRP-SeNPs on the level of MDA on H_2O_2-induced AML-12 cells model. **(E)** Effect on the activity of GSH-Px on H_2O_2-induced AML-12 cells model. The different letters indicate significant differences ($p < 0.05$).

AML-12 cells were stimulated with different concentrations of BRP-SeNPs, the cell viabilities of BRP-SeNPs groups had no significant difference compared with the BC group. It indicated that BRP-SeNPs had no toxic effect on AML-12 cells in the concentration range of 0–500 μg/ml. Therefore, BRP-SeNPs at concentrations of 100, 200, and 400 μg/ml were used in subsequent experiments. After that, AML-12 cells were stimulated with 0–250 μM H_2O_2 for 4 h, as shown in Figure 4B, the cell viability decreased as with the increase of H_2O_2 concentration. When the H_2O_2 concentration was 25 μM, there was no significant difference on cell viability. When the H_2O_2 concentration reached 100 μM, the cell viability was 60.30 ± 2.39% of BC group, and the cell was in a reversible state. Therefore, we selected 100 μM of H_2O_2 to stimulate AML-12 cells for 4 h as cellular oxidative injury model.

3.4.2 Effects of BRP-SeNPs on H_2O_2-induced oxidative injury model

AML-12 cells were pretreated with BRP-SeNPs at 0, 100, 200, 400 μg/ml for 24 h, and then stimulated with H_2O_2 for 4 h. As shown in Figure 4C, after treatment with 100, 200, and 400 μg/ml of BRP-SeNPs, the cell viability was significantly higher than that in the MG group in a dose-dependent manner. This indicated that BRP-SeNPs could alleviate the decrease in cell viability induced by H_2O_2.

The effect of BRP-SeNPs on MDA production was shown in Figure 4D. Compared with the BC group, the MDA content of the cells stimulated by H_2O_2 was significantly increased. However, BRP-SeNPs pretreatment significantly decreased the MDA content of H_2O_2-induced AML-12 cells. The results showed that BRP-SeNPs could markedly reduce intracellular MDA production.

The changes of intracellular GSH-Px activity during H_2O_2-induced cell injury were shown in Figure 4E. GSH-Px is an antioxidant enzyme that catalyzes the decomposition of hydrogen peroxide. Compared with the BC group, the GSH-Px activity of H_2O_2-induced AML-12 cells was significantly decreased, however, BRP-SeNPs restored the GSH-Px activity and even showed no significant difference at 400 μg/ml compared with BC group. This suggested that BRP-SeNPs may recover AML-12 cells by protecting against H_2O_2-induced reduction in antioxidant enzyme activity.

3.5 Effect of BRP-SeNPs on body weight and relative organ index *in vivo*

Animal experiment process in mice as shown in Figure 5A. The effect of BRP-SeNPs on the body weight of mice was shown in Figure 5B. During the first 3 weeks, the average body weight of each group in the natural growth state gradually increased. Compared with the BC group, the MG, PC, and BRP-SeNPs groups had no significant effect on the body weight of the mice. After the injection with CCl_4 and fasting treatment, the body

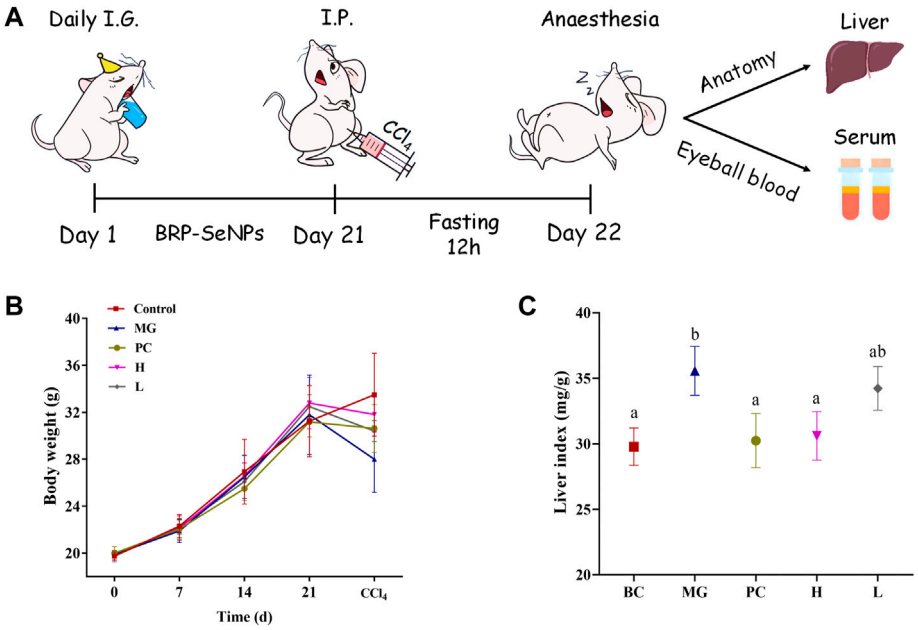

FIGURE 5
(A) Animal experiment process in mice. **(B)** Effect of BRP-SeNPs on body weight of mice. **(C)** Effect of BRP-SeNPs on organ index in CCl_4-induced mice. The different letters indicate significant differences ($p < 0.05$).

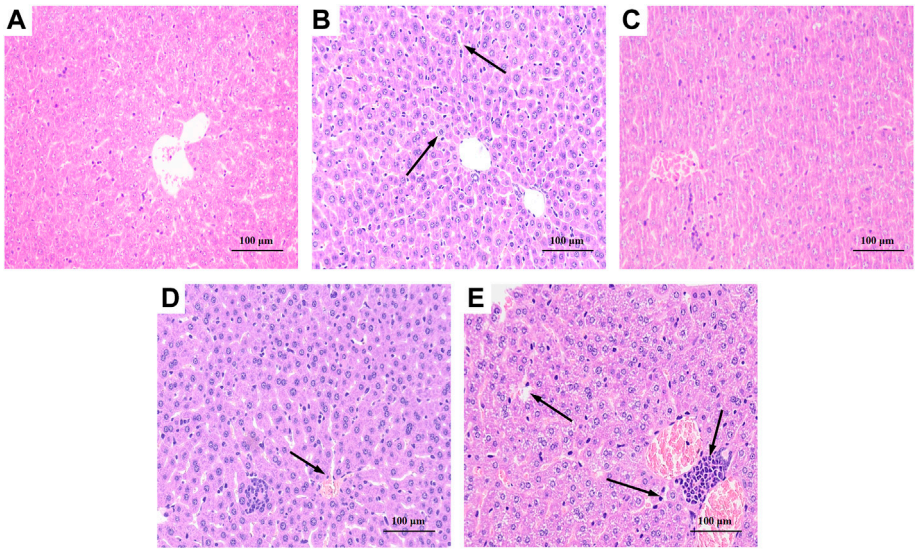

FIGURE 6
Effect of BRP-SeNPs on liver histopathological changes in CCl_4-induced mice (×200 Magnification). **(A)** BC, **(B)** MG, **(C)** PC, **(D)** H, and **(E)** L group. Areas of severe histopathological changes were marked by black arrows.

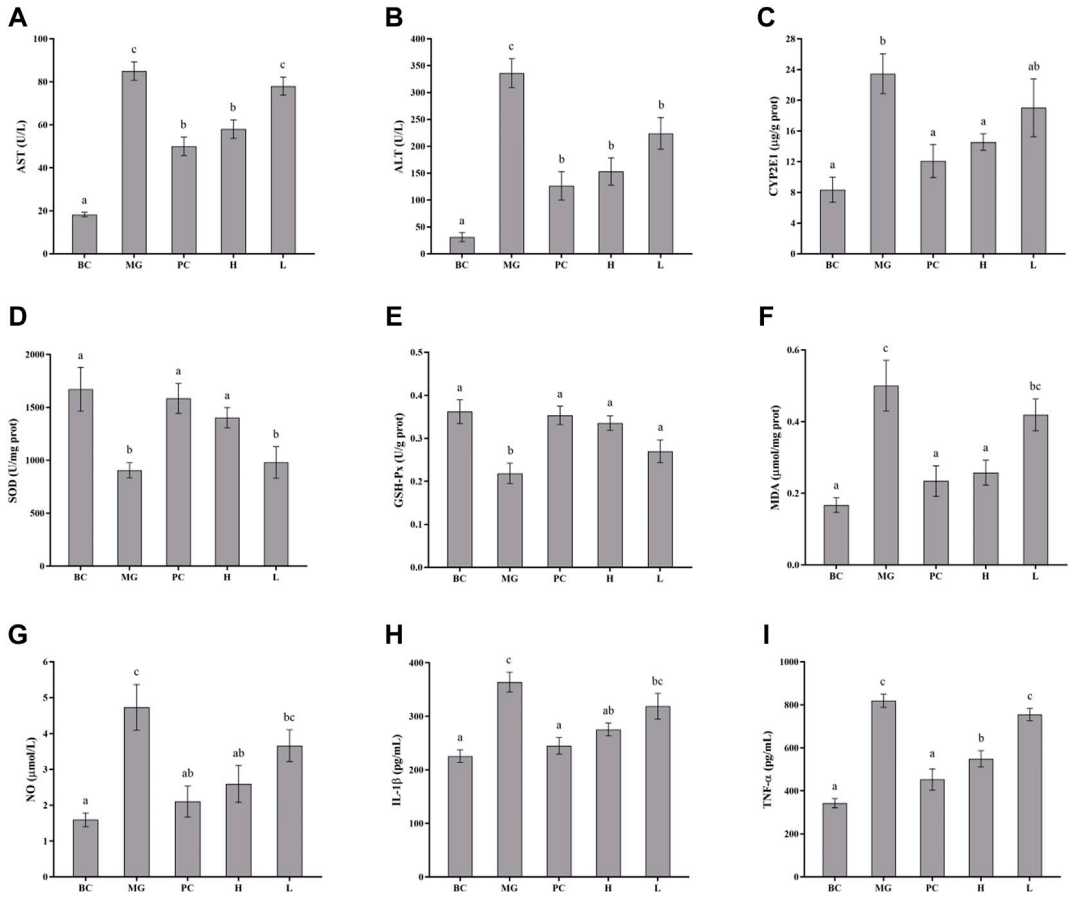

FIGURE 7
Effect of BRP-SeNPs on the contents of **(A)** AST, and **(B)** ALT in serum of mice induced by CCl_4. **(C)** Represents the content of CYP2E1 in the liver. **(D–I)** Effect of BRP-SeNPs on indicators of liver oxidative stress and inflammatory mediators induced by CCl_4. **(D–F)** Represent the content of SOD, GSH-Px and MDA, and **(G–I)** represent the content of NO, IL-1β and TNF-α in the liver, respectively. The different letters indicate significant differences ($p < 0.05$).

weight of mouse was obviously decreased. The weight loss rate of H group and L group was lower than that of MG group. It revealed that the mice pretreated with BRP-SeNPs possessed stronger protective functions against CCl_4-induce damage. The liver index of the MG group was significantly higher than that of the BC group (Figure 5C), indicating that CCl_4 could cause changes in the liver, loss its function and even clog in the organ. The liver indexes of mice treated with BRP-SeNPs were lower than that of MG group, and H group was significantly lower than that of MG group. The results suggested that BRP-SeNPs may promote the function of liver and gain the weight body to protect against injury induced by CCl_4.

3.6 Liver histopathological

As shown in Figure 6A, the liver tissue of the BC group was observed after staining, and the hepatocytes were arranged regularly and the morphology was normal. The liver tissue of the MG group, as shown in Figure 6B, exhibited hepatocyte degeneration, blurred cell boundaries, inflammatory cell infiltration, plasma vacuolization, hepatocyte necrosis, and all that indicated that intraperitoneal injection of CCl_4 would cause severe damage to the liver of mice. Figure 6C showed that the liver of PC basically returned to a normal state except for loose arrangement. As shown in Figures 6D,E, BRP-SeNPs pretreatment could significantly resist the invasion and damage of the liver by CCl_4-induced histopathological changes, especially for the high-dose group.

3.7 Biochemical assays detected in blood serum

The effects of BRP-SeNPs on serum marker levels in mice were demonstrated in Figures 7A,B. The levels of serum ALT and

AST in the MG group were significantly higher than that in the BC group. After the mice treated with different concentrations of BRP-SeNPs for 21 days and induced by CCl_4, the serum AST and ALT levels were decreased to a certain extent. Concretely speaking, the serum AST levels of H groups was significantly lower than MG and the serum ALT levels of L and H groups were significantly reduced compared with MG. The serum parameters indicated that BRP-SeNPs could improve the function and activity of hepatocyte stimulated by exogenous injury-inducing factor to suppress the release of ALT and AST.

3.8 CYP2E1 changes in liver

CYP2E1 is a major drug metabolizing enzyme, and its overexpression in the liver can lead to oxidative stress (Song et al., 2011). As shown in Figure 7C, the CYP2E1 enzyme content in the MG group was significantly higher than BC group ($p < 0.05$), and it confirmed that CCl_4 caused significant increase in the expression of CYP2E1 enzyme in the liver of mice. Silymarin could restore CYP2E1 levels in the mice induced by CCl_4. BRP-SeNPs could significantly reduce the rise of CYP2E1 expression induced by CCl_4 ($p < 0.05$). When the mice were given BRP-SeNPs of 200 mg/kgbw, the CYP2E1 level in liver of the mice induced by CCl_4 was similar as PC group. This indicated that BRP-SeNPs could enhance the function of liver and restrain the expression of hepatic CYP2E1 to relieve oxidative stress.

3.9 Biochemical assays detected in liver

Oxidative damage caused by reactive oxygen species (ROS) is an important part of CCl_4-induced liver damage. When ROS rise in the body, excess free radicals could lead to lipid peroxidation reaction that damages cell membranes and organic damage. At the same time, ROS also reduced the activity of antioxidant enzymes *in vivo*, resulting in a further increase in oxidative damage. When the liver is damaged by external factors, it will cause a series of stress responses. Thus, we determined the antioxidant enzyme activity such as SOD and GSH-Px, and the content of MDA. Besides, in order to investigate whether BRP-SeNPs have therapeutic effect on the inflammation caused by CCl_4-induced liver injury, detection kits were also used to test the relative pro-inflammatory cytokines (NO, IL-1β, TNF-α) in the liver.

3.9.1 Effects on SOD and GSH-Px activity and MDA levels in liver

SOD and GSH-Px are antioxidant enzymes that could reduce the oxidation caused by ROS, and play an important role in maintaining ROS balance in the body. As shown in Figures 7D–E, CCl_4 decreased the SOD and GSH-Px activities in MG compared with the BC group, indicating that CCl_4 may cause damage to the hepatocyte and further inhibit the express of the two antioxidant enzymes. While the mice administrated with BRP-SeNPs could significantly recover the activities of SOD and GSH-Px in a concentration-dependent manner. This indicated that BRP-SeNPs could strengthen the liver function and the expression of antioxidant enzyme to attenuate the injury induced by CCl_4.

Hyperoxidation of lipids is a hallmark of oxidative stress. As shown in Figure 7F, compared with the MG group, the content of MDA in H and PC group was significantly decreased and had no significant difference with BC. This indicated that BRP-SeNPs could effectively alleviate CCl_4-induced lipid peroxidation. So far, we could speculate from the results mentioned above that BRP-SeNPs could improve the liver function, heighten the hepatocellular activity and activate the antioxidant system to relieve the liver injury evoked by exogenous pathogenic factors such as CCl_4.

3.9.2 Effects on NO, IL-1β and TNF-α levels in liver

As shown in Figure 7G, CCl_4 could significantly increase the NO production compared with normal mice. However, BRP-SeNPs displayed good inhibitory effect on the NO concentration in a dose-dependent manner. As shown in Figures 7H,I, the levels of IL-1β and TNF-α in BC, PC and H group were significantly lower than that in the MG. All the results of proinflammatory cytokines showed that BRP-SeNPs possessed the anti-inflammatory activity by inhibiting the production of NO, L-1β and TNF-α in CCl_4-induced liver injury model.

3.10 Cell signaling pathway

Activated Nrf2 transferred into nucleus, interacts with ARE, and induces the expression of downstream targets to regulate oxidative stress (Ning et al., 2018). In general, the liver is a metabolically active organ possessing a wide range of antioxidant systems, and correspondingly, it is likely that oxidative stress plays a key role in promoting the development of acute liver injury. In this experiment, in order to elucidate the molecular mechanism of the protective effect of BRP-SeNPs on the liver and the inhibitory effect on inflammation, we analyzed the expression of Nrf2, Keap1, MKP1, p-JNK, p-ASK1, p-MKK4, TLR4, p-38, p-ERK. Inactive state Nrf2 interacts with actin-binding protein Keap1 in the cytoplasm and is rapidly degraded by the ubiquitin-proteasome pathway. However, when Nrf2 is exposed to oxidative or electrophilic stress, the phosphorylation of Nrf2 leads to the dissociation of the Nrf2-Keap1 complex, and then, stable Nrf2 translocates to the nucleus. In the nucleus, Nrf2 binds to the ARE sequence and promotes the expression of many antioxidant proteins and phase II detoxifying enzymes including GSH-Px and SOD, which are closely related to

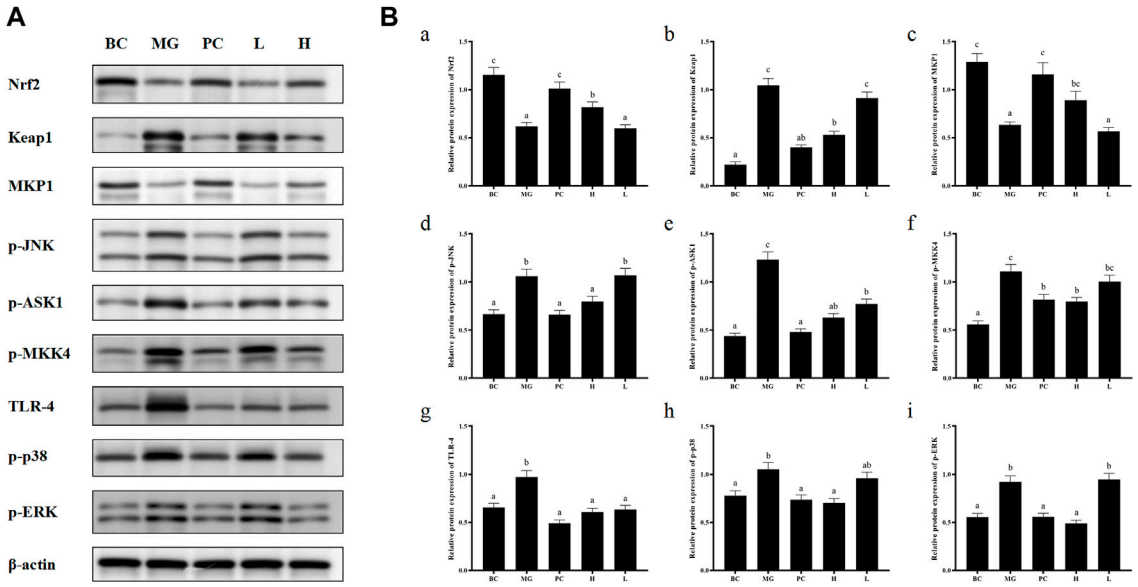

FIGURE 8
(A) BRP-SeNPs protected mice from CCl_4-induced liver injury *via* Nrf2/Keap1/MKP1/JNK and TLR4/MAPK signaling pathways. **(B)** Quantification of **(A)** Nrf2, **(B)**Keap1, **(C)**MKP1, **(D)** p-JNK, **(E)** p-ASK1, **(F)** p-MKK4, **(G)** TLR4, **(H)** p-p38, **(I)** p-ERK expression in cytoplasm. The different letters indicate significant differences ($p < 0.05$).

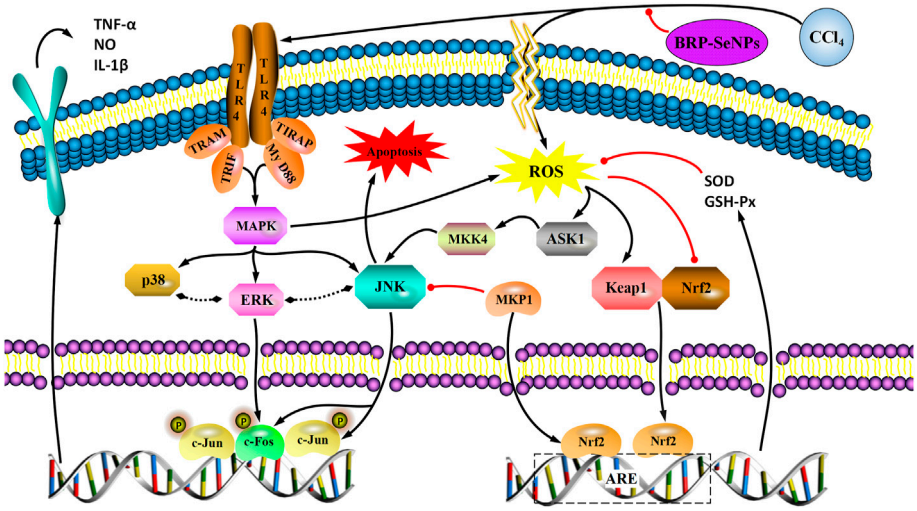

FIGURE 9
A proposed mechanism for the hepatoprotective effect of BRP-SeNPs on CCl_4-induced liver injury *in vivo*. Black arrow represents the activation and red line the inhibition.

eliminating excessive free radicals and protecting against oxidative stress. The results showed that BRP-SeNPs attenuated liver injury by upregulating Nrf2 and downregulating Keap1 in the Nrf2/ARE signaling pathway in Figure 8. It was in keeping with the activity changes of SOD and GSH-Px tested in our research and the report (Meng et al., 2021). It was in keeping with the activity changes of SOD and GSH-Px tested in our research. It indicated that BRP-SeNPs could regulate and control Nrf2/ARE pathway, and finally showed hepatoprotective effect on CCl_4-induced liver injury.

In the anti-inflammatory mechanism, we explored the TLR4/MAPK pathway. CCl_4 significantly increased the expression of TLR4 protein in mouse liver, and BRP-SeNPs could inhibit CCl_4-induced up-regulation of TLR4 protein expression in mouse liver. Stimulated TLR4 can activate the MAPK signaling pathway and accordingly lead to the expression of p-p38, p-ERK, and p-JNK protein. Further, they promote the synthesis and release of inflammatory factors. However, it can be seen that BRP-SeNPs can reduce the release of NO, IL-1β and TNF-α by down-regulating the expression of TLR4/MAPK pathway in the liver of mice induced by CCl_4 in Figure 8.

In the anti-apoptosis mechanism, we determined the ASK1/MKK4/JNK pathway. BRP-SeNPs could inhibit the expression of p-ASK1 and p-MKK4 in the CCl_4-induced damage. As we all know, JNK plays an important role in the ROS-induced apoptosis, including mitochondrial apoptotic pathway in the cytoplasmic and transcription factor pathway in the nuclear. However, BRP-SeNPs suppressed the expression of p-JNK by ASK1/MKK4 pathway and finally maintained the activity and function of hepatocyte and liver. It was consistent to histopathological changes in our study.

In addition, MKP1 is another important protein in protecting liver injury. It upregulates the expression of Nrf2, interacts directly with Nrf2 and promotes the Nrf2/ARE pathway during hepatoprotection (Wang M. et al., 2019). Meanwhile, MKP1 is an endogenous key hepatoprotective factor, which can upregulate antioxidant pathways and inhibit the activation of JNK during liver injury (Li et al., 2017). High-dose BRP-SeNPs could significantly reduce CCl_4-induced hepatic JNK-activating protein expression and reverse it to normal levels achieving therapeutic effect. After detecting the expression of MKP1 protein, the results showed that CCl_4 significantly inhibited the expression of MKP1 in mice liver, and high-dose BRP-SeNPs could increase the expression of MKP1 protein in turn.

Taken all the results of mechanism, we found that BRP-SeNPs possessed hepatoprotection by the Nrf2/Keap1/MKP1/JNK pathways, and anti-inflammatory by TLR4/MAPK pathway in Figures 8, 9.

4 Conclusion

In summary, *Berberidis radix* polysaccharide (BRP) as a stabilizer obtained from *Berberidis radix* was used to prepare the BRP-selenium nanoparticles (BRP-SeNPs) in the redox reaction system of sodium selenite and ascorbic acid. The stability and characterization of BRP-SeNPs were investigated by DLS, FT-IR, UV-Vis, XPS, SEM, TEM, STEM-HAADF, EDX. The optimal preparation condition was established and the BRP-SeNPs were successfully synthesized. Then, *in vitro* tests, BRP-SeNPs had protective effects on H_2O_2-induced AML-12 cells injury model. Subsequently, the preventive effect of BRP-SeNPs on in CCl_4-induced mice liver injury was explored. BRP-SeNPs could increase the body weight of mice, the activity of SOD and GSH-Px in liver, and meanwhile decrease the liver organ index, ALT and AST in serum, CYP2E1, the content of MDA and the level of NO, IL-1β, and TNF-α in the liver of CCl_4-induced damage. The histomorphology of liver was restored under the stimulating of BRP-SeNPs. Finally, the hepatoprotective mechanism against CCl_4-induced liver injury was elucidated. The results indicated that BRP-SeNPs could attenuate oxidant stress by the Nrf2/Keap1/MKP1/JNK pathways, and downregulate the proinflammatory factors by TLR4/MAPK pathway. Hence, BRP-SeNPs possess the hepatoprotection and have the potential to be a green liver-protecting and auxiliary liver inflammation drugs.

Data availability statement

The original contributions presented in the study are included in the article/Supplementary Material, further inquiries can be directed to the corresponding authors.

Ethics statement

The animal study was reviewed and approved by Experimental Animal Ethical Committee of Qingdao Agricultural University.

Author contributions

FG completed the animal experiment, biochemical indexes, pathological results, western blotting, ELISA kits, designed diagrams, created the manuscript. HL and HH participated in the animal experiment and western blotting, ELISA kits. LQ and CL helped design the experiment and provided supervision. XW reviewed the manuscript. XT helped design the experiment, provided supervision and reviewed the manuscript. RH conceived the experimental design, reviewed the manuscript and acquired funding.

Funding

This work was supported by the Key R and D Program of Shandong Province (Major Scientific and Technological Innovation Project) (2021CXGC011305), Natural Science Foundation of Shandong Province of China (ZR2020QC198), Qingdao Agricultural University Doctoral Start-Up Fund (6631121044, 6631118020), National Natural Science Foundation of China (82003941, 31802229), Special Foundation for Taishan Scholar of Shandong Province.

Conflict of interest

The authors declare that the research was conducted in the absence of any commercial or financial relationships that could be construed as a potential conflict of interest.

Publisher's note

All claims expressed in this article are solely those of the authors and do not necessarily represent those of their affiliated organizations, or those of the publisher, the editors and the reviewers. Any product that may be evaluated in this article, or claim that may be made by its manufacturer, is not guaranteed or endorsed by the publisher.

Supplementary material

The Supplementary Material for this article can be found online at: https://www.frontiersin.org/articles/10.3389/fphar.2022.1058480/full#supplementary-material

References

Bagheri-Josheghani, S., and Bakhshi, B. (2022). Formulation of selenium nanoparticles encapsulated by alginate-chitosan for controlled delivery of Vibrio cholerae LPS: a novel delivery system candidate for nanovaccine. *Int. J. Biol. Macromol.* 208, 494–508. doi:10.1016/j.ijbiomac.2022.03.087

Bai, K., Hong, B., He, J., and Huang, W. (2020). Antioxidant capacity and hepatoprotective role of chitosan-stabilized Selenium nanoparticles in concanavalin a-induced liver injury in mice. *Nutrients* 12, E857. doi:10.3390/nu12030857

Cai, W., Hu, T., Bakry, A. M., Zheng, Z., Xiao, Y., and Huang, Q. (2018). Effect of ultrasound on size, morphology, stability and antioxidant activity of selenium nanoparticles dispersed by a hyperbranched polysaccharide from Lignosus rhinocerotis. *Ultrason. Sonochem.* 42, 823–831. doi:10.1016/j.ultsonch.2017.12.022

Che, J., Yang, S., Qiao, Z., Li, H., Sun, J., Zhuang, W., et al. (2019). Schisandra chinensis acidic polysaccharide partialy reverses acetaminophen-induced liver injury in mice. *J. Pharmacol. Sci.* 140, 248–254. doi:10.1016/j.jphs.2019.07.008

Chen, G., Yang, F., Fan, S., Jin, H., Liao, K., Li, X., et al. (2022). Immunomodulatory roles of selenium nanoparticles: Novel arts for potential immunotherapy strategy development. *Front. Immunol.* 13, 956181. doi:10.3389/fimmu.2022.956181

Cheng, L., Wang, Y., He, X., and Wei, X. (2018). Preparation, structural characterization and bioactivities of Se-containing polysaccharide: A review. *Int. J. Biol. Macromol.* 120, 82–92. doi:10.1016/j.ijbiomac.2018.07.106

Faure-Dupuy, S., Delphin, M., Aillot, L., Dimier, L., Lebossé, F., Fresquet, J., et al. (2019). Hepatitis B virus-induced modulation of liver macrophage function promotes hepatocyte infection. *J. Hepatol.* 71, 1086–1098. doi:10.1016/j.jhep.2019.06.032

Gao, X., Li, X., Mu, J., Ho, C. T., Su, J., Zhang, Y., et al. (2020). Preparation, physicochemical characterization, and anti-proliferation of selenium nanoparticles stabilized by Polyporus umbellatus polysaccharide. *Int. J. Biol. Macromol.* 152, 605–615. doi:10.1016/j.ijbiomac.2020.02.199

Huang, S., Yang, W., and Huang, G. (2020). Preparation and activities of selenium polysaccharide from plant such as Grifola frondosa. *Carbohydr. Polym.* 242, 116409. doi:10.1016/j.carbpol.2020.116409

Hui, H., Li, X., Jin, H., Yang, X., Xin, A., Zhao, R., et al. (2019). Structural characterization, antioxidant and antibacterial activities of two heteropolysaccharides purified from the bulbs of Lilium davidii var. unicolor Cotton. *Int. J. Biol. Macromol.* 133, 306–315. doi:10.1016/j.ijbiomac.2019.04.082

Jiang, H., Wang, R., Zhou, F., Wu, Y., Li, S., Huo, G., et al. (2022). Preparation, physicochemical characterization, and cytotoxicity of selenium nanoparticles stabilized by Oudemansiella raphanipies polysaccharide. *Int. J. Biol. Macromol.* 211, 35–46. doi:10.1016/j.ijbiomac.2022.05.011

Kanhar, S., and Sahoo, A. K. (2019). Ameliorative effect of Homalium zeylanicum against carbon tetrachloride-induced oxidative stress and liver injury in rats. *Biomed. Pharmacother.* 111, 305–314. doi:10.1016/j.biopha.2018.12.045

Li, S., Tan, H. Y., Wang, N., Zhang, Z. J., Lao, L., Wong, C. W., et al. (2015). The role of oxidative stress and antioxidants in liver diseases. *Int. J. Mol. Sci.* 16, 26087–26124. doi:10.3390/ijms161125942

Li, Y., Tang, R., Leung, P. S. C., Gershwin, M. E., and Ma, X. (2017). Bile acids and intestinal microbiota in autoimmune cholestatic liver diseases. *Autoimmun. Rev.* 16, 885–896. doi:10.1016/j.autrev.2017.07.002

Liu, W., Li, X., Wong, Y. S., Zheng, W., Zhang, Y., Cao, W., et al. (2012). Selenium nanoparticles as a carrier of 5-fluorouracil to achieve anticancer synergism. *ACS Nano* 6, 6578–6591. doi:10.1021/nn202452c

Liu, F., Zhu, Z. Y., Sun, X., Gao, H., and Zhang, Y. M. (2017). The preparation of three selenium-containing Cordyceps militaris polysaccharides: Characterization and anti-tumor activities. *Int. J. Biol. Macromol.* 99, 196–204. doi:10.1016/j.ijbiomac.2017.02.064

Liu, Y., Wen, P. H., Zhang, X. X., Dai, Y., and He, Q. (2018a). Breviscapine ameliorates CCl_4-induced liver injury in mice through inhibiting inflammatory apoptotic response and ROS generation. *Int. J. Mol. Med.* 42, 755–768. doi:10.3892/ijmm.2018.3651

Liu, Y., Zeng, S., Liu, Y., Wu, W., Shen, Y., Zhang, L., et al. (2018b). Synthesis and antidiabetic activity of selenium nanoparticles in the presence of polysaccharides from Catathelasma ventricosum. *Int. J. Biol. Macromol.* 114, 632–639. doi:10.1016/j.ijbiomac.2018.03.161

Meng, M., Zhang, R., Han, R., Kong, Y., Wang, R., and Hou, L. (2021). The polysaccharides from the Grifola frondosa fruiting body prevent lipopolysaccharide/D-galactosamine-induced acute liver injury via the miR-122-Nrf2/ARE pathways. *Food Funct.* 12, 1973–1982. doi:10.1039/d0fo03327h

Ning, C., Gao, X., Wang, C., Huo, X., Liu, Z., Sun, H., et al. (2018). Hepatoprotective effect of ginsenoside Rg1 from Panax ginseng on carbon tetrachloride-induced acute liver injury by activating Nrf2 signaling pathway in mice. *Environ. Toxicol.* 33, 1050–1060. doi:10.1002/tox.22616

Qin, S., Huang, B., Ma, J., Wang, X., Zhang, J., Li, L., et al. (2015). Effects of selenium-chitosan on blood selenium concentration, antioxidation status, and cellular and humoral immunity in mice. *Biol. Trace Elem. Res.* 165, 145–152. doi:10.1007/s12011-015-0243-5

Ren, L., Wu, Z., Ma, Y., Jian, W., Xiong, H., and Zhou, L. (2021). Preparation and growth-promoting effect of selenium nanoparticles capped by polysaccharide-protein complexes on tilapia. *J. Sci. Food Agric.* 101, 476–485. doi:10.1002/jsfa.10656

Shi, X. D., Tian, Y. Q., Wu, J. L., and Wang, S. Y. (2021). Synthesis, characterization, and biological activity of selenium nanoparticles conjugated with polysaccharides. *Crit. Rev. Food Sci. Nutr.* 61, 2225–2236. doi:10.1080/10408398.2020.1774497

Song, B. J., Abdelmegeed, M. A., Yoo, S. H., Kim, B. J., Jo, S. A., Jo, I., et al. (2011). Post-translational modifications of mitochondrial aldehyde dehydrogenase and biomedical implications. *J. Proteomics* 74, 2691–2702. doi:10.1016/j.jprot.2011.05.013

Song, X., Chen, Y., Sun, H., Liu, X., and Leng, X. (2020). Physicochemical and functional properties of chitosan-stabilized selenium nanoparticles under different processing treatments. *Food Chem.* 331, 127378. doi:10.1016/j.foodchem.2020.127378

Song, X., Cui, W., Gao, Z., Zhang, J., and Jia, L. (2021). Structural characterization and amelioration of sulfated polysaccharides from Ganoderma applanatum residue against CCl(4)-induced hepatotoxicity. *Int. Immunopharmacol.* 96, 107554. doi:10.1016/j.intimp.2021.107554

Sun, Q., Dong, M., Wang, Z., Wang, C., Sheng, D., Li, Z., et al. (2016). Selenium-enriched polysaccharides from Pyracantha fortuneana (Se-PFPs) inhibit the growth and invasive potential of ovarian cancer cells through inhibiting β-catenin signaling. *Oncotarget* 7, 28369–28383. doi:10.18632/oncotarget.8619

Wadhwani, S. A., Shedbalkar, U. U., Singh, R., and Chopade, B. A. (2016). Biogenic selenium nanoparticles: current status and future prospects. *Appl. Microbiol. Biotechnol.* 100, 2555–2566. doi:10.1007/s00253-016-7300-7

Wang, L., Li, C., Huang, Q., and Fu, X. (2019a). Biofunctionalization of selenium nanoparticles with a polysaccharide from Rosa roxburghii fruit and their protective effect against H(2)O(2)-induced apoptosis in INS-1 cells. *Food Funct.* 10, 539–553. doi:10.1039/c8fo01958d

Wang, M., Niu, J., Ou, L., Deng, B., Wang, Y., and Li, S. (2019b). Zerumbone protects against carbon tetrachloride (CCl(4))-induced acute liver injury in mice via inhibiting oxidative stress and the inflammatory response: involving the TLR4/NF-κB/COX-2 pathway. *Molecules* 24, E1964. doi:10.3390/molecules24101964

Wang, W., Jiang, L., Ren, Y., Shen, M., and Xie, J. (2019c). Characterizations and hepatoprotective effect of polysaccharides from Mesona blumes against tetrachloride-induced acute liver injury in mice. *Int. J. Biol. Macromol.* 124, 788–795. doi:10.1016/j.ijbiomac.2018.11.260

Wang, N., Wu, Y., Jia, G., Wang, C., Xiao, D., Goff, H. D., et al. (2021). Structural characterization and immunomodulatory activity of mycelium polysaccharide from liquid fermentation of Monascus purpureus (Hong Qu). *Carbohydr. Polym.* 262, 117945. doi:10.1016/j.carbpol.2021.117945

Xiao, Y., Huang, Q., Zheng, Z., Guan, H., and Liu, S. (2017). Construction of a Cordyceps sinensis exopolysaccharide-conjugated selenium nanoparticles and enhancement of their antioxidant activities. *Int. J. Biol. Macromol.* 99, 483–491. doi:10.1016/j.ijbiomac.2017.03.016

Xu, G., Han, X., Yuan, G., An, L., and Du, P. (2017). Screening for the protective effect target of deproteinized extract of calf blood and its mechanisms in mice with CCl4-induced acute liver injury. *PLoS One* 12, e0180899. doi:10.1371/journal.pone.0180899

Zeng, D., Zhao, J., Luk, K. H., Cheung, S. T., Wong, K. H., and Chen, T. (2019). Potentiation of *in vivo* anticancer efficacy of selenium nanoparticles by mushroom polysaccharides surface decoration. *J. Agric. Food Chem.* 67, 2865–2876. doi:10.1021/acs.jafc.9b00193

Zhai, X., Zhang, C., Zhao, G., Stoll, S., Ren, F., and Leng, X. (2017). Antioxidant capacities of the selenium nanoparticles stabilized by chitosan. *J. Nanobiotechnology* 15, 4. doi:10.1186/s12951-016-0243-4

Zhang, C., Pan, D., Luo, K., She, W., Guo, C., Yang, Y., et al. (2014). Peptide dendrimer-Doxorubicin conjugate-based nanoparticles as an enzyme-responsive drug delivery system for cancer therapy. *Adv. Healthc. Mater.* 3, 1299–1308. doi:10.1002/adhm.201300601

Zhang, C., Zhai, X., Zhao, G., Ren, F., and Leng, X. (2015). Synthesis, characterization, and controlled release of selenium nanoparticles stabilized by chitosan of different molecular weights. *Carbohydr. Polym.* 134, 158–166. doi:10.1016/j.carbpol.2015.07.065

Zhang, S., Song, Z., Shi, L., Zhou, L., Zhang, J., Cui, J., et al. (2021). A dandelion polysaccharide and its selenium nanoparticles: Structure features and evaluation of anti-tumor activity in zebrafish models. *Carbohydr. Polym.* 270, 118365. doi:10.1016/j.carbpol.2021.118365

frontiers | Frontiers in Pharmacology

TYPE Original Research
PUBLISHED 24 November 2022
DOI 10.3389/fphar.2022.1026912

OPEN ACCESS

EDITED BY
Guangyue Su,
Shenyang Pharmaceutical University, China

REVIEWED BY
Ziyi Song,
Guangxi University, China
Xiao Ma,
Chengdu University of Traditional Chinese Medicine, China

*CORRESPONDENCE
Chia-Jung Lee,
cjlee@tmu.edu.tw

SPECIALTY SECTION
This article was submitted to Ethnopharmacology, a section of the journal Frontiers in Pharmacology

RECEIVED 24 August 2022
ACCEPTED 31 October 2022
PUBLISHED 24 November 2022

CITATION
Ning D-S, Chen Y-J, Lin C-J, Wang C-C, Zhao H-W, Wang K-T, Lee M-C, Tayo LL, Chiu W-C, Yeh C-L and Lee C-J (2022), Hepatoprotective effect of botanical drug formula on high-fat diet-induced non-alcoholic fatty liver disease by inhibiting lipogenesis and promoting anti-oxidation. *Front. Pharmacol.* 13:1026912. doi: 10.3389/fphar.2022.1026912

Hepatoprotective effect of botanical drug formula on high-fat diet-induced non-alcoholic fatty liver disease by inhibiting lipogenesis and promoting anti-oxidation

De-Shan Ning[1], Yu-Ju Chen[2], Chien-Ju Lin[3], Ching-Chiung Wang[2,4,5,6], Hong-Wei Zhao[1], Kun-Teng Wang[7], Ming-Chung Lee[7], Lemmuel L. Tayo[8], Wan-Chun Chiu[9,10], Chiu-Li Yeh[9] and Chia-Jung Lee[2,4,6]*

[1]Infinitus (China) Company Ltd., Guangzhou, China, [2]Ph.D. Program in Clinical Drug Development of Herbal Medicine, Taipei Medical University, Taipei, Taiwan, [3]School of Pharmacy, College of Pharmacy, Kaohsiung Medical University, Kaohsiung, Taiwan, [4]Graduate Institute of Pharmacognosy, Taipei Medical University, Taipei, Taiwan, [5]School of Pharmacy, Taipei Medical University, Taipei, Taiwan, [6]Traditional Herbal Medicine Research Center, Taipei Medical University Hospital, Taipei, Taiwan, [7]Herbiotek Co., Ltd., New Taipei City, Taiwan, [8]School of Chemical, Biological Materials Science and Engineering, Mapúa University, Manila, Philippines, [9]School of Nutrition and Health Sciences, College of Nutrition, Taipei Medical University, Taipei, Taiwan, [10]Department of Nutrition, Wan Fang Hospital, Taipei Medical University, Taipei, Taiwan

With the prevalence of obesity and other components of metabolic syndrome, Non-alcoholic fatty liver disease (NAFLD) has become increasingly common. In recent years, much attention has been paid to various plant sources, hoping to find a treatment for NAFLD in plants. The Livsooth authentic herbal formula (LAH, 樂悠本草), a botanical drug formula combined with Puerariae lobatae radix, Lonicerae japonicae flos, Hoveniae semen, and Siraitiae fructus. This study used a network pharmacology approach to predict the potential mechanisms of LAH against NAFLD. Gene Ontology (GO) and KEGG pathway enrichment analyses have identified potential biochemical and signaling pathways. Subsequently, the potential mechanism of action of LAH on NAFLD predicted by network pharmacology analysis was validated in a high-fat diet (HFD)-induced NAFLD model in C57BL/6 mice. Our results demonstrated that LAH ameliorated hepatocyte steatosis in liver tissue by activating the AMPK pathway and decreasing serum triglycerides, low-density lipoprotein, glucose, and cholesterol. Besides, LAH increased the hepatic antioxidant enzymes

Abbreviations: ALT, Alanine aminotransferase; CAT, Catalase; CHOL, Cholesterol; DMEM, Dulbecco's Modified Eagle Medium; FBS, Fetal bovine serum; FFAs, Free fatty acids; GLU, Glucose; GO, Gene Ontology; GPx, Glutathione peroxidase; GR, Glutathione reductase; GSH, Glutathione; HFD, High-fat diet; HPLC, High-performance liquid chromatography; KEGG, Kyoto Encyclopedia of Genes and Genomes; LAH, Livsooth authentic herbal formula; NAFLD, Non-alcoholic fatty liver disease; NASH, Non-alcoholic steatohepatitis; ND, Chow diet; OA, Oleic acid; PBS, Phosphate-buffered saline; PVDF, Polyvinylidene difluoride; ROS, Reactive oxygen species; SOD, Superoxide dismutase; TCM, Traditional Chinese medicine.

activities, suggested that LAH improved oxidative stress markers in HFD induced NAFLD mice. *In vitro* experiments confirmed that the active component of LAH, puerarin, regulates lipid accumulation through the AMPK pathway. In conclusion, our study shows that network pharmacology predictions are consistent with experimental validation. LAH can be a candidate supplement for the prevention of NAFLD.

KEYWORDS

non-alcoholic fatty liver disease (NAFLD), network pharmacology, herb-based supplements, puerarin, AMPK pathway, anti-oxidation

Introduction

Two In the past few decades, liver disease has become one of the leading causes of death worldwide. By 2010, it was estimated that approximately 4% of deaths worldwide were due to liver diseases, such as liver cancer and cirrhosis. Non-alcoholic fatty liver disease (NAFLD) is the main cause of cirrhosis, including a variety of pathological liver diseases, which are characterized by hyperlipidemia, inflammation, and fibrosis (steatohepatitis and steatosis, respectively). With the prevalence of obesity and other components of metabolic syndrome, NAFLD has become increasingly common (Byass, 2014; Brunt et al., 2015; Rinella, 2015). The steps of developing NAFLD includes liver triglyceride (TG) accumulation to develop into non-alcoholic steatohepatitis (NASH) followed by oxidative stress, autophagy, and inflammation, causing further damage. Overweight or obese individuals are prone to insulin resistance which can negate insulin signaling, increase lipolysis of adipose tissue in excess free fatty acids (FFAs) and induction fatty tissue inflammation (Eigentler et al., 2020; Stefan, 2020). Along with the hepatic lipid accumulation, the high levels of FFA, cholesterol, and lipid metabolites present in the liver induce lipotoxicity. Furthermore, free fatty acids increase the risk of oxidative stress and produce reactive oxygen species (ROS). Thus, research on ways to improve the clinical outcome of fatty liver disease is critical. Livsooth authentic herbal formula (LAH, 樂悠本草) consists of four botanical drugs, *Pueraria montana* var. *lobata* (Willd.) Maesen and S.M.Almeida ex Sanjappa & Predeep [Leguminosae; Puerariae lobatae radix], *Lonicera japonica* Thunb. [Caprifoliaceae; Lonicerae japonicae flos], *Hovenia dulcis* Thunb. [Rhamnaceae; Hoveniae semen] and *Siraitia grosvenorii* (Swingle) C.Jeffrey ex A.M.Lu & Zhi Y.Zhang [Cucurbitaceae; Siraitiae fructus]. Puerariae lobatae radix is a very useful Traditional Chinese medicine (TCM) for relieving head and neck pain, reducing fever, clearing measles, promoting body fluid, and relieving diarrhea (Ehrman et al., 2007; Zhao et al., 2016). Modern pharmacological investigations have shown that this botanical cocktail has extensive biological activities such as hepatoprotective (Zhou et al., 2018; Sun et al., 2019), antioxidant (Jiang et al., 2005), anti-inflammatory (Jin et al., 2012) and anti-cancer (Ahn et al., 2019). Lonicerae japonicae flos is well-known as clearing heat and detoxifying. Many studies have described the anti-inflammatory (Yang et al., 2019a; Yang et al., 2021) and antiviral activities (Zhou et al., 2017) of honeysuckle. It inhibits oxidative damage to hepatocytes by increasing the activity of antioxidant enzymes which scavenge reactive oxygen species and other free radicals (Gao et al., 2018). Hoveniae semen has been used in the treatment of ethanol-induced liver disease for centuries. Hoveniae semen could modulate abnormalities of the gut-liver axis and inhibits TLR4-associated inflammatory mediator activation to exert its hepatoprotective properties (Cho et al., 2016; Jeong et al., 2019; Qiu et al., 2019). Siraitiae fructus is a medicinal and edible plant with various health-promoting properties. It serves as a promising antiglycative agent against diabetic complications by inhibiting protein glycation and glycoxidation (Chen et al., 2011; Liu et al., 2018). These four botanical drugs have been reported to have protective effects on the liver, suggesting a potential therapeutic effect on NAFLD. However, no scientific experiments and clinical trials have been conducted to verify its effectiveness or to explore its potential mechanism against NAFLD.

In recent years, much attention has been paid to various plant sources, hoping to find a treatment for NAFLD in plants. TCM has been used in China and other countries for thousands of years. A specific and basic feature of TCM is the use of formulas containing several botanical drugs to ameliorate the abnormal symptoms associated with a particular disease (Guo et al., 2017). A wide variety of botanical remedies have traditionally been used to treat NAFLD and metabolic syndromes. Having multiple biological targets and multiple therapeutic mechanisms are characteristic features of TCM formula, and these substances may provide potential therapeutic effects on the multifactorial NAFLD (Xu et al., 2020; Fan et al., 2021). Network pharmacology is a new approach to predict or reveal complex mechanisms of TCM formula, which updates the research model from the current "one target, one drug" model to a new "network-target, multiple-component" model (Zhang et al., 2019). By providing a detailed composite target and target pathway network, it is helpful to evaluate the integrity, systemic and interaction of TCM. Therefore, the application of network pharmacology to TCM compounds can be used to explain the mechanism of action of TCM, discover medicinal active ingredients, and provide new ideas for the development and research of new drugs.

In this study, we used a network pharmacology approach to predict potential pathways of LAH to NAFLD. In addition, a

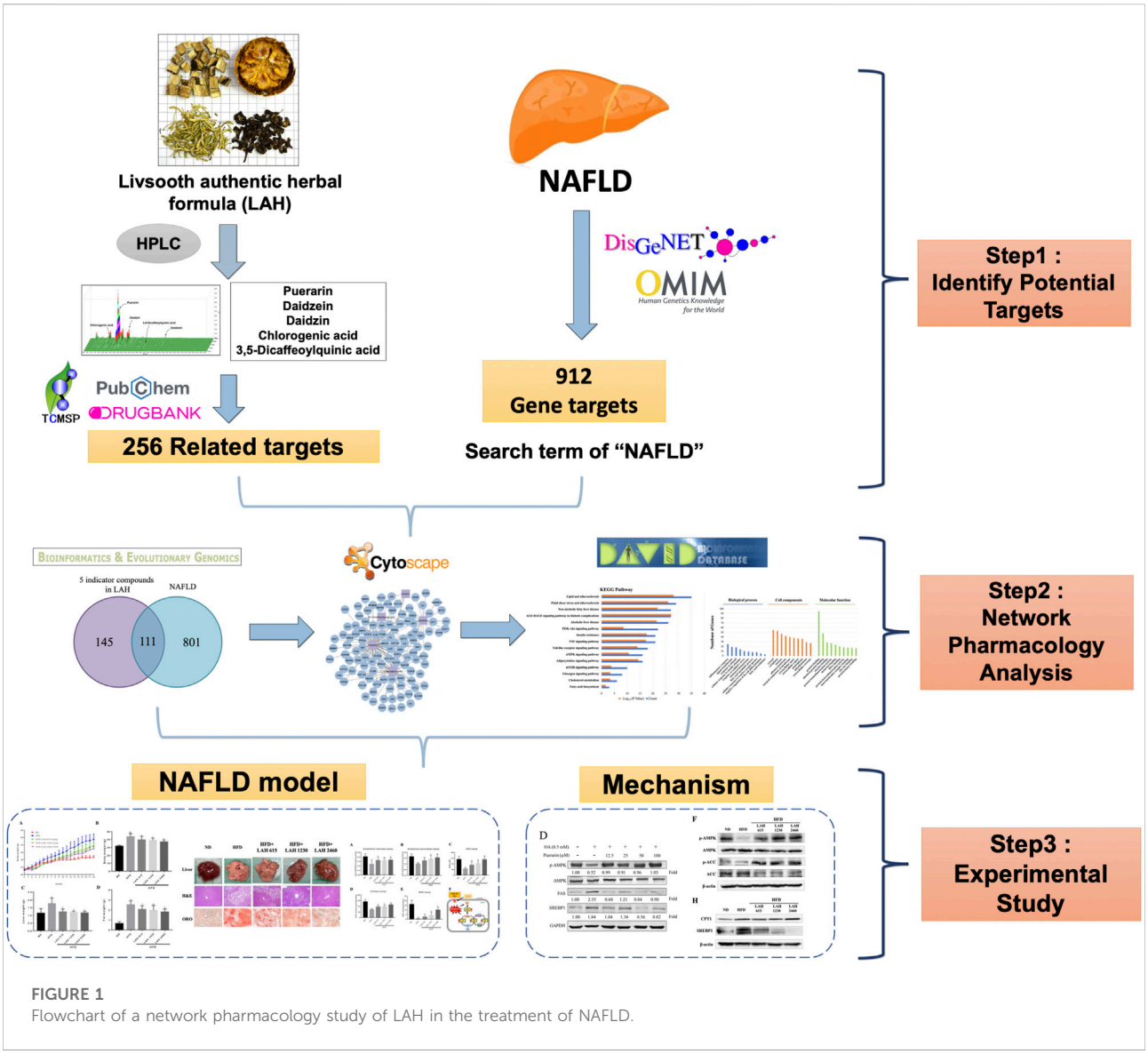

FIGURE 1
Flowchart of a network pharmacology study of LAH in the treatment of NAFLD.

mouse model of NAFLD was established by feeding a high-fat diet (HFD) and used to verify whether the effect and mechanism of LAH on NAFLD *in vivo* was as predicted by the network pharmacology approach. The detailed research flowchart is shown in Figure 1.

Materials and methods

Preparation of Livsooth authentic herbal mix

The Livsooth authentic herbal formula (LAH) prescription from Infinitus Pharmaceutical combines *Pueraria montana* var. *lobata* (Willd.) Maesen and S.M.Almeida ex Sanjappa & Predeep [Leguminosae; Puerariae lobatae radix], *Lonicera japonica* Thunb. [Caprifoliaceae; Lonicerae japonicae flos], *Hovenia dulcis* Thunb. [Rhamnaceae; Hoveniae semen] and *Siraitia grosvenorii* (Swingle) C.Jeffrey ex A.M.Lu & Zhi Y.Zhang [Cucurbitaceae; Siraitiae fructus]. The medicinal materials were authenticated by a non-profit organization, the Brion Research Institute of Taiwan. Voucher specimens (No. PR-20180001 for Puerariae lobatae radix, No. LJF-20180001 for Lonicerae japonicae flos, No. HS-20180001 for Hoveniae semen and No. SF-20180001 for Siraitiae fructus) was deposited at the College of Pharmacy, Taipei Medical University. Botanical drugs of LAH (Puerariae lobatae radix: Lonicerae japonicae flos: Hoveniae semen: Siraitiae fructus = 48: 26: 8: 1) were extracted with 10-fold boiling water for 2 h, twice. Combined extraction solution was removed excess water to the

solid content about 60% by vacuum concentration. The LAH granules were obtained by 80°C dry granulation. The above extraction procedure was under Good Manufacturing Practice (GMP) in China.

High-performance liquid chromatography sample preparation

For high-performance liquid chromatography (HPLC) analysis, a 0.5 g sample was extracted using 20 ml of 70% methanol through ultrasonic oscillation at 25°C for 20 min. The sample was then filtered through a 0.45 μm syringe filter.

High-performance liquid chromatography analysis of marker substances in LAH

The Waters HPLC system (Milford, Massachusetts, United States) was comprised of Waters 600 pump system, Waters 2996 Photodiode array detector, Waters 717 plus Autosampler, and Sugai U-620 Column oven (Wakayama City, Japan). Cosmosil 5C18-MS-II reversed phase column (5 μm, 4.6 × 250 mm, Nacalai tesque, Japan) equipped with Lichrospher RP-18 end-capped guard column (5 μm, 4.0 × 10 mm, Merck, Germany) was used as the stationary phase. The gradient elution was composed of eluents A, B, and C (A: H_2O/KH_2PO_4/10% H_3PO_4 = 1000 ml/2.72 g/1 ml; B: Acetonitrile; C: H_2O) according to the following profile: 0–30 min, 90%–75% A and 10%–25% B; 30–40 min, 75%–65% A and 25%–35% B; 40–55 min, 65%–0% A, 35%–75% B and 0%–25% C; 55–60 min, 75%–10% B and 25%–90% C; 60–65 min, 0%–90% A, 10% B and 90%–0% C. The gradient elution was used for 3D fingerprint analysis and quantification of puerarin (250 nm), daidzin (250 nm), daidzein (250 nm), chlorogenic acid (320 nm) and 3,5-dicaffeoylquinic acid (325 nm). The flow rate was 1 ml/min, and the column temperature was maintained at 35°C.

Predicting the mechanism of action of the five major components of LAH in non-alcoholic fatty liver disease based on network pharmacology

This study recruited compound names which were used as keywords in TCMSP (http://tcmspw.com/tcmsp.php), DrugBank (https://go.drugbank.com/) and PubChem (https://pubchem.ncbi.nlm.nih). gov/) database search components for gene targets, standardized using UniProt KB database while deleting duplicates to obtain 256 potential targets. A list of NAFLD-related targets was collected from the OMIM (https://omim.org/) (Amberger et al., 2014; Zhang et al., 2020) and DisGeNET (https://www.disgenet.org/) (Piñero et al., 2016) repositories using the search term "non-alcoholic fatty liver disease" or "NAFLD" or "fatty liver, nonalcoholic" or "liver, nonalcoholic fatty" or "livers, nonalcoholic fatty" or "nonalcoholic fatty liver" or "nonalcoholic steatohepatitis" or "steatohepatitis, nonalcoholic," delete duplicates to obtain 912 gene targets. To understand the mechanism of LAH in NAFLD, network analysis was performed. Component-Target network was established and visualized by Cytoscape 3.9.1 software. For predicting the mechanism of action of LAH in NAFLD, putative targets were loaded into DAVID (https://david.ncifcrf.gov/) for enrichment analyses in KEGG (Kyoto Encyclopedia of Genes and Genomes) pathways and the GO (Gene Ontology) enrichments. Adjusted p-value ≤ 0.05 and count ≥2 was chosen in functional annotation clustering.

Animals and experimental protocol

Five-week-old male C57BL/6 mice were procured from the National Laboratory Animal Center in Taiwan and kept on a 12-h light/12-h dark cycle at 21 ± 2°C with food and water ad libitum. C57BL/6 mice were randomized into a ND group: fed with chow diet (ND) and oral administration ddH_2O, a high-fat diet group (HFD) fed a commercial diet containing 60% fat and oral administration ddH_2O (High-fat diet (No. 58Y1) was purchased from TestDiet, Inc.), and three LAH groups: fed with a high-fat diet and oral administration of LAH at doses of 615 mg/kg, 1230 mg/kg, and 2460 mg/kg; each group n = 10. All experiments were carried out for 18 weeks, and body weight and obesity-related biomarkers were periodically recorded. At the end of the experiment, the mice were euthanized with CO_2 after fasting for 12 h, and then blood and tissue samples were collected. The animal use protocol was reviewed and approved by the Institutional Animal Care and Use Committee or Panel (IACUC/IACUP), Taipei Medical University (IACUC Approval no. LAC-2019-0070). All methods involved in the animal experiments were performed in accordance with the relevant guidelines and regulations.

Histological and oil red O analysis

Liver tissue was fixed in 4% formaldehyde and embedded in paraffin. All tissues were sliced into 10-μm sections and stained with hematoxylin and eosin (H&E). OCT-embedded frozen liver sections were stained with Oil Red O. Briefly, liver sections were fixed with 4% formaldehyde at room temperature for 15 min. After fixation, the cells were washed three times with phosphate-buffered saline (PBS) and stained with 0.6% (w/v) Oil Red O solution for 15 min at room temperature. The sections were quickly washed with 60% isopropanol one time, washed three times with PBS, and photographed using a Nikon microscope.

Serum biochemical analysis

Blood was obtained from the heart after the end of the 18-weeks, centrifuged blood samples at 13,000 rpm for 10 min to separate the serum. Serum levels of glucose (GLU), triglyceride (TRIG), total cholesterol (CHOL), alanine aminotransferase (ALT), aspartate aminotransferase (AST), and albumin (ALB) were analyzed using VetTest 8008 (IDEXX Lab Inc., Westbrook, ME, United States) according to the manufacturer's protocol.

Western blot assay

Tissues and cells were lysed in ice-cold RIPA buffer, and protein quantification was performed using the Bradford assay (Bio-Rad Laboratories, Hercules, CA, United States). Lysates were electrophoresed on 8%–10% SDS-PAGE gels and transferred to an immunoblot polyvinylidene difluoride (PVDF) membrane using a semi-dry transfer system (Bio-Rad, Hercules, CA, United States). The PVDF membranes were blocked with 5% BSA at room temperature for 1 h and incubated at 4°C overnight with the following primary antibodies. These membranes were several washed with TBST buffer, secondary antibodies and chemiluminescent detection reagents were applied sequentially. Primary specific antibodies included β-actin (Santa Cruz Biotechnology, CA, United States), CPT1, SREBP1, phospho-AMPK, AMPK, and phospho-ACC (Cell Signaling Technology, Danvers, MA, United States). Western blots were quantified by ImageJ.

Assay for oxidative stress-related parameters in liver

Liver tissue homogenates were prepared by high-speed stirring of liver tissue in ice-cold buffer (0.25 M sucrose, 1 mM EDTA, 10 mM Tris-HCl), then centrifuged for 10 min (4500 × g, 4°C), and the liver cytoplasm separated and stored at −80°C for further analysis. Superoxide dismutase (SOD, Rondox SD125, Antrim, United Kingdom), glutathione reductase (GR, Randox GR 2368, Goldberg, DM), glutathione peroxidase (GPx, Randox RS 504, Paglia), glutathione (GSH, Catalog No.703002), catalase (CAT, Cayman No.707002), LDL and HDL (Randox CH201, Antrim, United Kingdom), and triglyceride (TRIG, TR213, Antrim, United Kingdom) levels in the liver homogenates were determined using biochemical kits.

Cell culture and fatty liver cells treatment

The HepG2 hepatocyte cell line was purchased from the Bioresource Collection and Research Center (BCRC, Taiwan) and cultured at 37°C in a 5% CO_2 atmosphere in DMEM medium supplemented with 1% penicillin/streptomycin, 1% l-glutamine and 10% fetal bovine serum (FBS). HepG2 cells were incubated with 0.5 mM oleic acid (St. Louis, MO, United States) and co-treated with LAH (12.5–400 μg/ml) to stimulate lipid accumulation for 24 h then evaluate the mechanism of lipid metabolism.

Cell viability assay

HepG2 cells were incubated with various concentrations of LAH for 24 h to determine cell viability using MTT solution (Sigma). Next, the culture plates were treated with DMSO to evaluate cell viability. Absorbance was then measured at 600 nm using an ELISA plate reader (BioTek, Winooski, VT, United States).

Oil red O staining

HepG2 cells were seeded and grown in 48-well plates and co-treated with 0.5 mM oleic acid and LAH (12.5–400 μg/ml) for 24 h. Cells were washed three times with PBS and fixed with 4% formaldehyde at room temperature for 1 h. After fixation, cells were stained with Oil Red O solution for 1 h and washed with 60% isopropanol to detect oil droplets. For quantitative analysis of cellular lipids, Oil Red O was eluted with 100% isopropanol and quantified spectrophotometrically at 520 nm using an ELISA plate reader (BioTek, Winooski, VT, United States).

Statistical analysis

All data are presented as mean ± SD. The difference between multiple groups was analyzed using one-way analysis of variance (ANOVA) followed by Tukey's multiple comparison test. A p value <0.05 was considered statistically significant. All statistical analyses were using GraphPad Prism Software version 7.0 (GraphPad Software Inc., San Diego, CA, United States).

Results

Analysis of the main components of LAH using high-performance liquid chromatography

The contents of the components in LAH were analyzed using the HPLC method. The HPLC chromate-graphic profile indicated that LAH contained chlorogenic acid, puerarin, daidzin, daidzein and 3,5-dicaffeoylquinic acid. The contents of the investigated analytes were as follows: chlorogenic acid for 3.87 mg/g, puerarin for 57.33 mg/g, daidzin for 14.82 mg/g, 3,5-

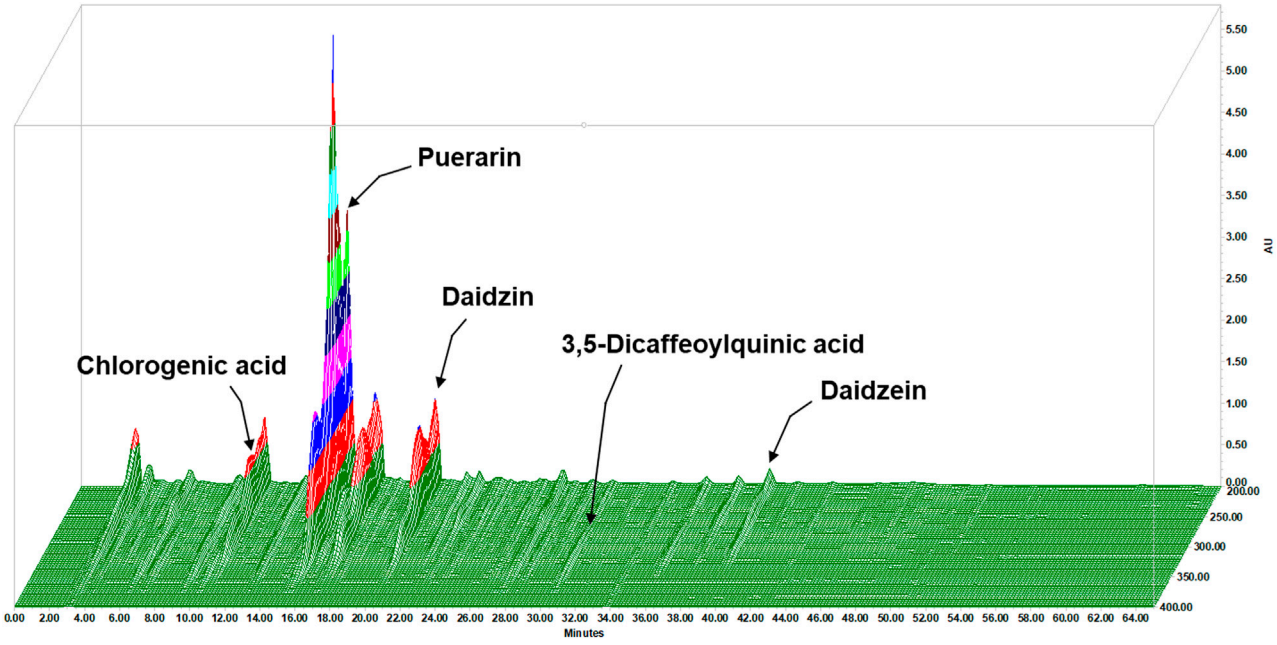

FIGURE 2
3D fingerprint analysis of the LAH by using high-performance liquid chromatography (HPLC).

dicaffeoylquinic acid for 0.46 mg/g and daidzein for 1.70 mg/g in LAH, as well as the peaks of retention times were at 11.36, 15.40, 20.31, 30.22, and 39.32 min, respectively (Figure 2).

Network pharmacology analysis of LAH treating non-alcoholic fatty liver disease

According to HPLC analysis, chlorogenic acid, puerarin, daidzin, 3,5-dicaffeoylquinic acid and daidzein are the major components in LAH. To further study the mechanism of action of LAH against NAFLD, it is crucial to understand the target genes of these 5 components. Network pharmacology provides an effective tool for the study of TCM pharmacology. A total of 256 potential targets were retrieved from the TCMSP, DrugBank and PubChem databases of LAH. Further, a total of 912 gene targets associated with NAFLD were retrieved from OMIM and DisGeNET databases. Using Venn diagram to analyze the gene targets of LAH and the gene targets related to NAFLD in the database, it was found that 111 targets overlapped, which were considered as potential targets of LAH against NAFLD (Figure 3A). To predict the underlying mechanism of LAH to NAFLD, these targets were constructed using Cytoscape to plot a Component-Target network (Figure 3B). To identify biological signatures of LAH-related targets of NAFLD, KEGG pathway and GO enrichment analysis was performed on the involved targets. The significantly enriched KEGG pathways of 111 putative targets contained lipid and atherosclerosis, non-alcoholic fatty liver disease, AMPK signaling pathway, PI3K-Akt signaling pathway, adipocytokine signaling pathway, etc, demonstrate the effect of LAH against NAFLD was closely related to lipogenesis and promoting anti-oxidation effect (Figure 3C). In terms of GO enrichment analysis, it was also shown that LAH may exert its ameliorating effect on NAFLD by regulating fatty acid metabolism and response to oxidative stress *via* protein binding, the identical protein binding and enzyme binding (Figure 3D).

LAH reduces lipid accumulation in HepG2 cells

We used the MTT assay to determine the cytotoxicity of LAH in HepG2 cells to investigate whether LAH regulates lipid metabolism in hepatocytes *in vitro*. There was no cell cytotoxicity in the range of 0–400 μg/ml (Figure 4A). To investigate the effect of LAH on hepatic lipid accumulation, cellular lipid deposits were induced by oleic acid (OA) in HepG2 cells. Oil red O staining confirmed that 0.5 mM OA increase lipid droplets accumulation in HepG2 cells, compared with the Blank group. LAH alleviated intracellular lipid droplets in a dose-dependent compared to OA induced HepG2 cells (Figures 4B,C).

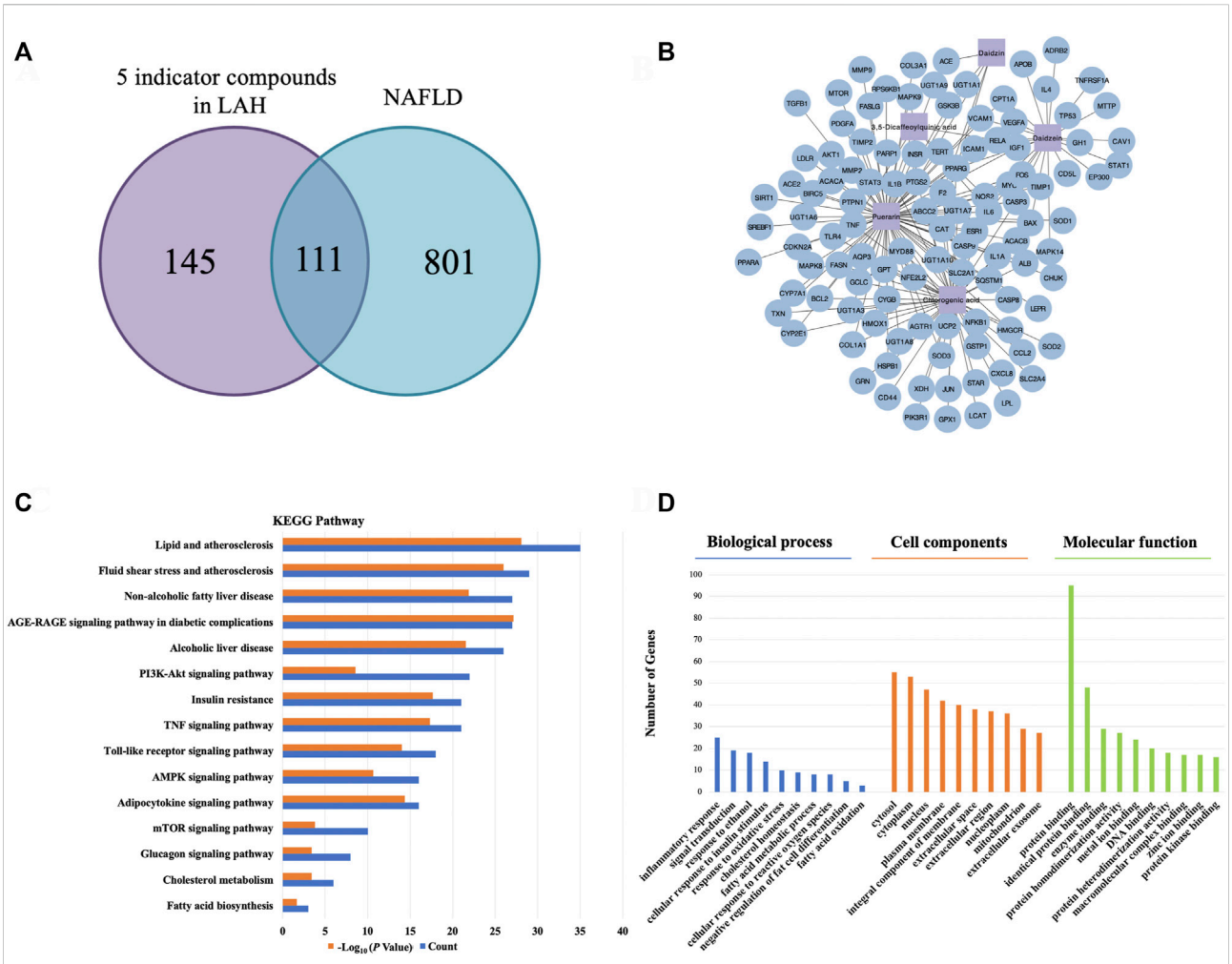

FIGURE 3
Network pharmacology analysis for LAH on NAFLD. **(A)** Venn diagrams of potential genes in LAH and NAFLD. **(B)** LAH Component-Target network. The purple square represents the 5 major components, and the blue circle represent the target genes. **(C)** The KEGG pathway enrichment analyses of 111 target proteins. **(D)** The GO enrichment analyses of 111 target proteins.

Effect of puerarin on lipogenesis-related proteins in the HepG2 cells

To prove puerarin is the major active component of LAH, we investigate its capability in regulating lipid accumulation, expression of lipogenesis-related proteins, phospho-AMPK, SREBP1, and FAS via western blot analyses. OA downregulated the protein expression levels of phospho-AMPK. The puerarin cotreatment was a significant increase phospho-AMPK protein level in HepG2 cells. The FAS, and SREBP1 protein expressions were found inhibited by puerarin, compared with OA group. (Figure 4D). Therefore, these results indicate that puerarin reduces lipid accumulation in OA-treated HepG2 cells by regulating AMPK/SREBP1 and lipogenesis synthesis pathway. It is suggested that puerarin can be used as an active indicator component of LAH.

Effect of LAH on body weight, fat weight, liver weight and hepatic histological changes in high-fat diet fed mice

Before administration of LAH and HFD, the body weight values were not different between the groups. After feeding with a high-fat diet, the body weight of the HFD group was significantly higher than that of the ND group. In LAH-treated groups were significantly decrease the body weight compared with the HFD group (Figures 5A,B). The weight of the liver and fat presented the same result. Liver weight in all LAH groups were significantly lower than the HFD group and close to the ND group. Fat weights were significantly lower in all LAH groups than in the HFD group (Figures 5C,D). In addition, to determine the histological effects of LAH on hepatic steatosis, liver histological slices used H&E staining to detect lipid accumulation and hepatocyte damage. Significant histological

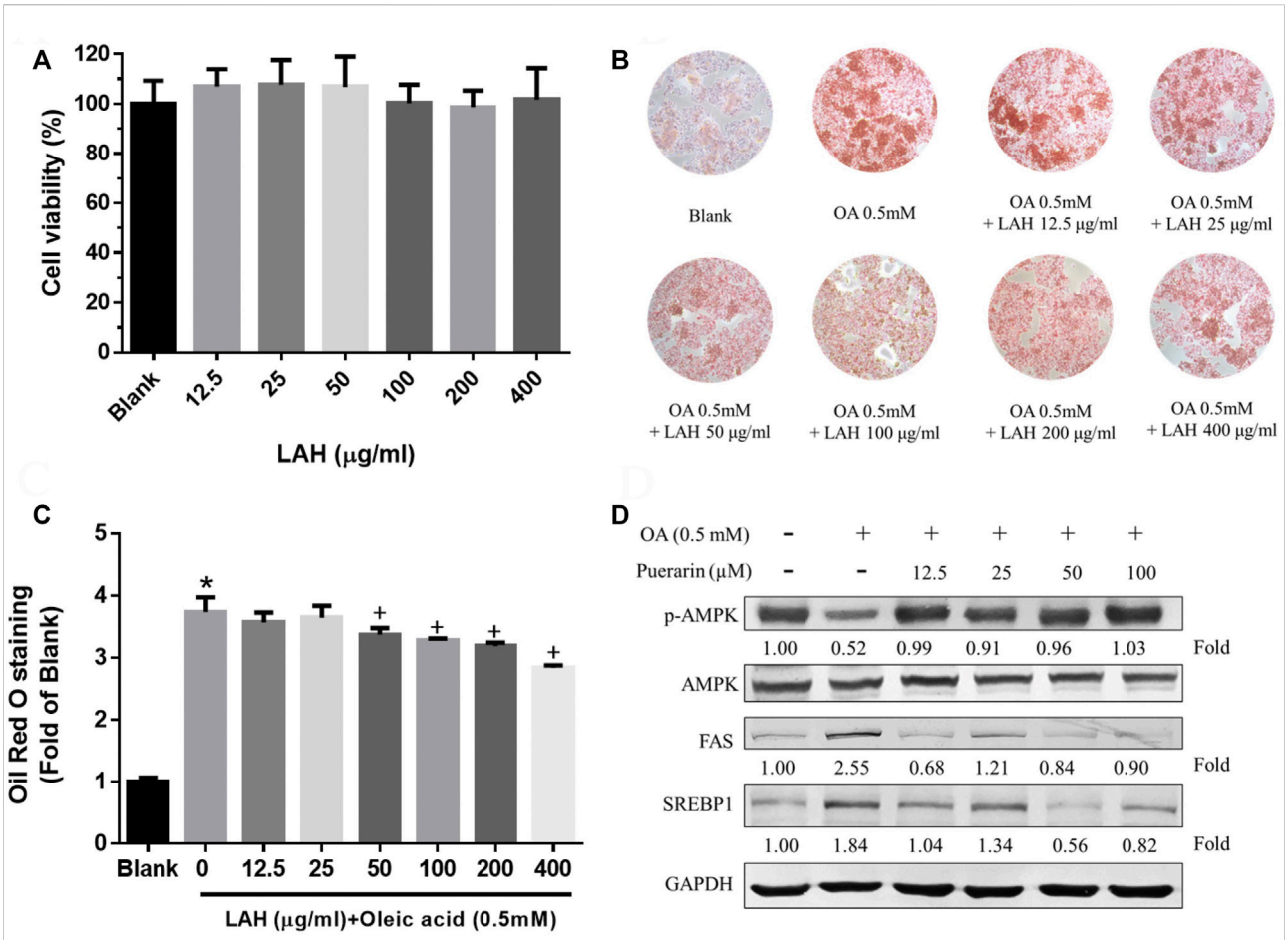

FIGURE 4
LAH and puerarin regulate OA-induced lipogenesis in HepG2 cells. **(A)** Cell viability of HepG2 cell treated with LAH, determined over 24 h using an MTT assay. **(B)** Cells were plated into 24well plate and treated with different doses of LAH in the presence of OA (0.5 mM) for 24 h. ORO staining of HepG2 cells after treatment with OA and LAH. **(C)** Quantitative lipid accumulation of Oil Red O contents at 520 nm. **(D)** Phosphorylated AMPK, AMPK, FA, and SREBP1 protein levels by western blot analysis. Protein expression was normalized to GAPDH. Values are expressed as mean ± SD (n = 3/group). *$p < 0.05$ compared with Blank group. + $p < 0.05$ compared with OA group.

abnormalities, including fat deposition in hepatocytes and inflammatory cell infiltration, were observed in the HFD group liver tissue, as compared with the ND group. However, these changes in pathology were alleviated in LAH-treated (615 mg/kg, 1230 mg/kg, or 2460 mg/kg) groups. Furthermore, Oil Red O staining observed that the lipid deposition in hepatocytes of the HFD group was significantly increased compared to the ND group; the deposition of lipid droplets in the hepatocytes of the LAH group was significantly decreased (Figure 5E).

Effects of LAH on the biochemical parameters

The levels of blood glucose, CHOL, TC, ALT, and AST in HFD group were higher than those in ND group. This means that HFD-induced mice develop hyperglycemia, dyslipidemia, and liver damage. The results showed that LAH treatment (615 mg/kg, 1230 mg/kg, or 2460 mg/kg) significantly reduced HFD-induced increases of blood glucose, CHOL, TC, ALT, and AST levels in a dose-dependent manner. These results suggest that LAH may prevent HFD-induced hyperglycemia, dyslipidemia, and liver damage (Figures 6A–E).

Effects of LAH on the hepatic lipid accumulation

We next investigated the effect of LAH on hepatic lipid accumulation. Mice fed the HFD showed markedly increased LDL and HDL levels in the liver compared to the ND mice. The mice administered with LAH (615 mg/kg, 1230 mg/kg, or

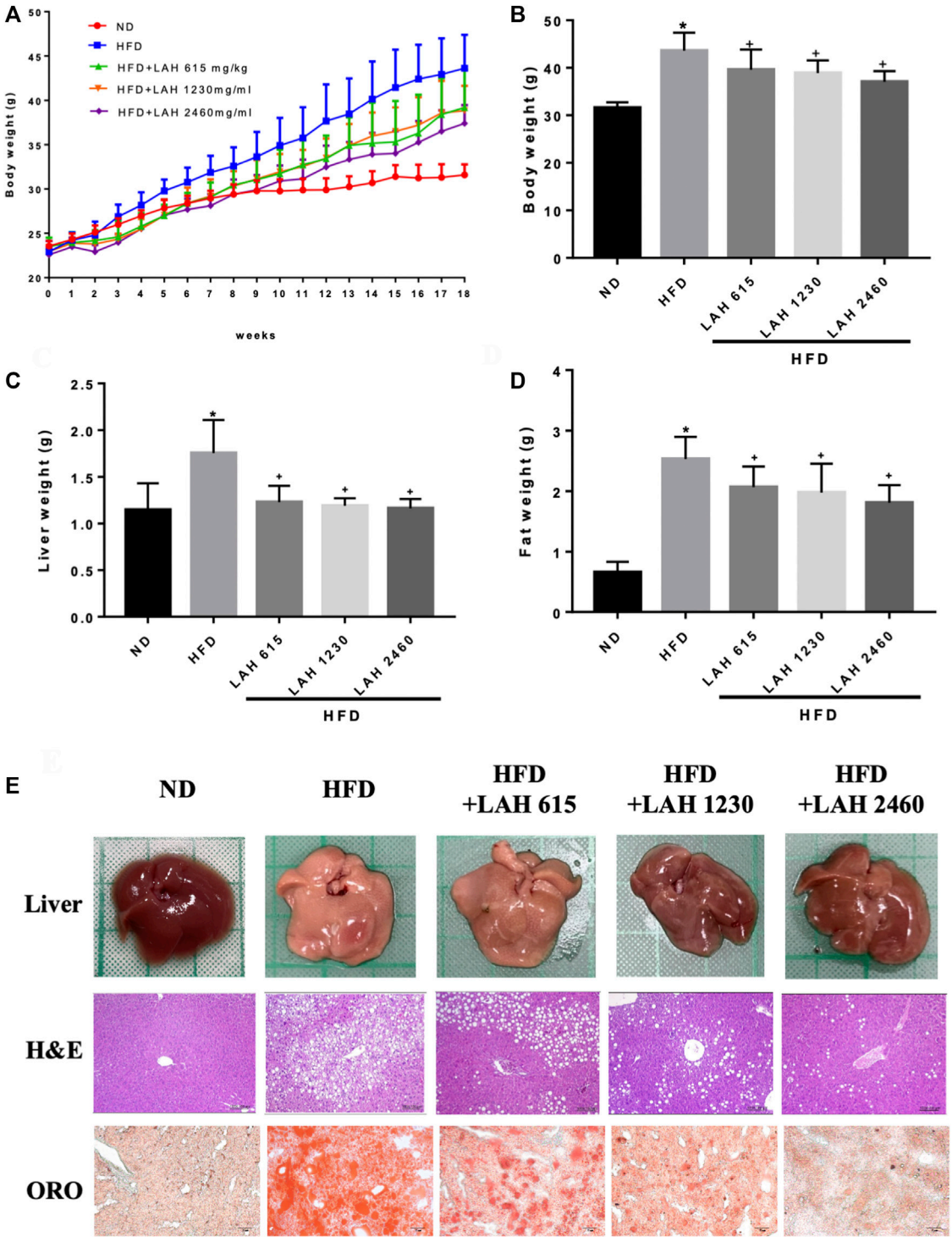

FIGURE 5
LAH ameliorated hepatic steatosis in HFD-induced mice. **(A)** Changes in body weight of mice fed either chow diet (ND), high-fat diet (HFD), or HFD containing 615 mg/kg, 1230 mg/kg, or 2460 mg/kg LAH extract for 18 weeks, **(B)** final body weight, **(C)** final liver and **(D)** inguinal adipose tissue weights, **(E)** Morphological photographs of livers. Histological analysis of liver sections stained with hematoxylin-eosin (H&E) staining and oil red O (100 × magnification). Values are expressed as mean ± SD (n = 10/group). *$p < 0.05$ compared with ND group. + $p < 0.05$ compared with HFD group.

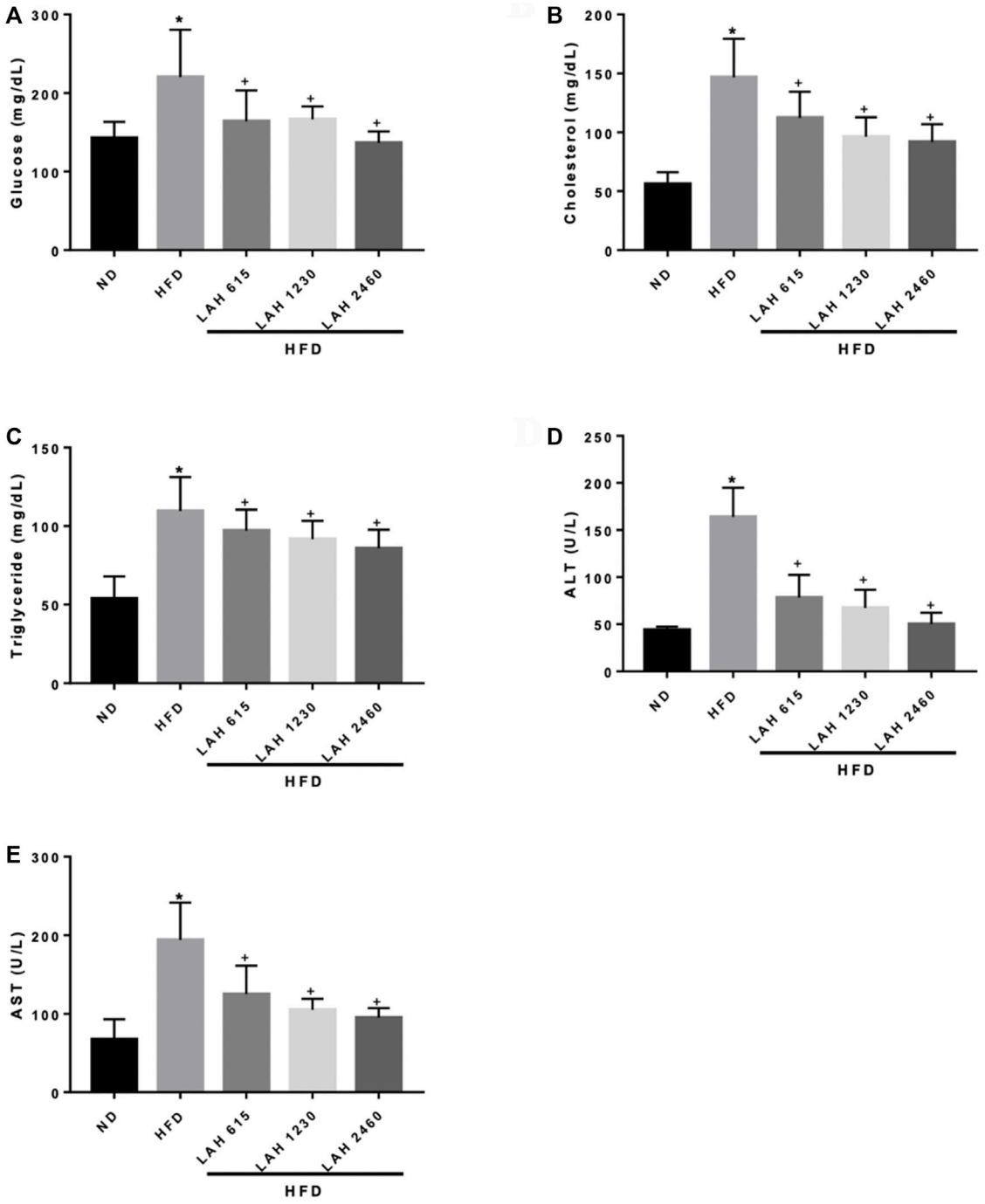

FIGURE 6
Serum biochemical analysis after 18 weeks of supplementation with LAH. Biochemical analysis of serum samples. Levels of **(A)** Fasting blood glucose, **(B)** CHOL, **(C)** TG, **(D)** ALT, and **(E)** AST were measured in the serum of mice in different experimental groups. Values are expressed as mean ± SD (n = 10/group). *$p < 0.05$ compared with ND group. + $p < 0.05$, compared with HFD group.

2460 mg/kg) had significantly decreased LDL and HDL levels in the liver compared to the HFD mice (Figures 7A,B). In addition, the LDL-to-HDL ratio of HFD-fed mice was significantly higher than that of ND mice, and this ratio was markedly reduced by LAH treatment (Figure 7C). The levels of hepatic TC and TG in the HFD mice were significantly higher than those in the ND mice. In comparison to the HFD mice, hepatic TC and TG levels in the LAH mice were lower (Figures 7D,E).

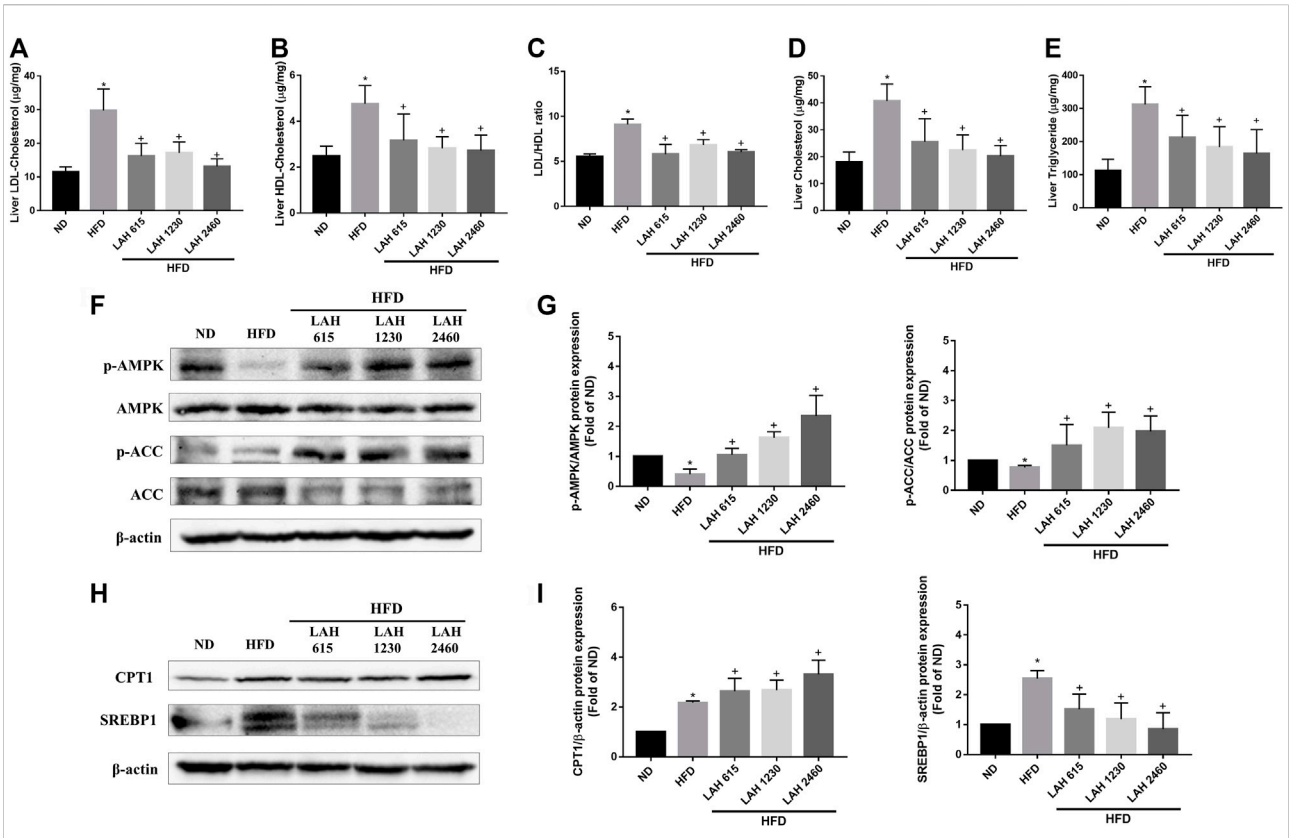

FIGURE 7
LAH treatment ameliorates HFD-induced hepatic lipids accumulation via AMPK-SREBP1 pathway. Liver content of **(A)** LDL, **(B)** HDL, **(C)** LDL/HDL ratio, **(D)** CHOL, and **(E)** TG in the ND, HFD, or HFD containing 615 mg/kg, 1230 mg/kg, and 2460 mg/kg LAH extract groups are shown (***n*** = 10 per group). **(F)** Phosphorylated AMPK, AMPK, Phosphorylated ACC, ACC protein levels by western blot analysis. **(G)** Phospho-AMPK and phospho-ACC protein expression was normalized to total AMPK and ACC, respectively. **(H)** CPT1, and SREBP-1 protein levels by western blot analysis. **(I)** CPT1 and SREBP1 protein expression was normalized to β-actin. Values are expressed as mean ± SD (n = 3/group). *$p < 0.05$, compared with ND group. + $p < 0.05$ compared with HFD group.

To investigate the molecular mechanisms, we evaluated protein expression during hepatic lipogenesis by Western blotting. LAH supplemented group caused increases in fatty acid oxidation-related protein expression as well as phospho-AMPK, phospho-ACC and CPT1 levels, compared to the HFD group (Figures 7F–I). Furthermore, SREBP1 protein levels increased significantly in the HFD group compared with the ND group. LAH treatment downregulated the SREBP1 protein expression compared with HFD group (Figures 7H,I). These results indicate that LAH can protect against lipid accumulation in the liver and enhance fatty acid oxidation by regulating AMPK-SREBP1 pathway.

Anti-oxidative effects of LAH on liver tissue

Excessive accumulation of fatty acids will increase the production of ROS. To understand the anti-oxidative effect of LAH on HFD-induced mouse liver tissues, we evaluated glutathione reductase (GR), glutathione peroxidase (GPx), GSH, CAT, and SOD (Figures 8A–E) levels. The activity of these enzymes was significantly reduced by the HFD. However, LAH treatment (615 mg/kg, 1230 mg/kg, or 2460 mg/kg) upregulates these enzymes activity which is like the ND group. The results suggest that LAH attenuates HFD-induced oxidative stress in hepatocytes by increasing the potential of antioxidant enzymes. (Figure 8F).

Discussion

The essence of Chinese medicine lies in the use of formulas containing several botanical drugs to achieve better effects and improve abnormal symptoms associated with a specific disease. Previous studies have shown that TCM formulas have a protective effect against NAFLD (Yang et al., 2019b; Li et al., 2020). Puerariae lobatae radix, Lonicerae japonicae

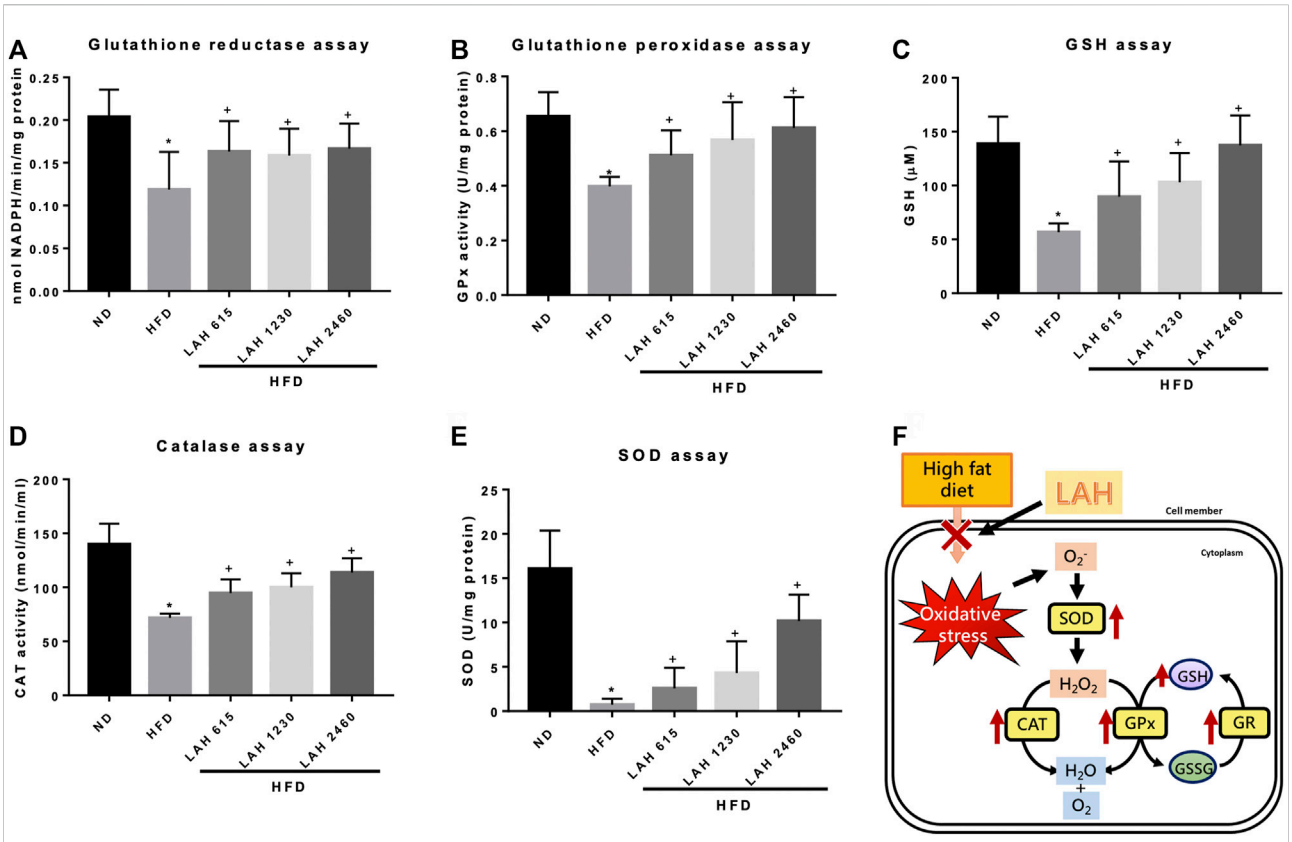

FIGURE 8
LAH attenuates hepatic oxidative stress and enhances antioxidant enzyme activity in HFD-mice. Levels of **(A)** Glutathione reductase (GR), **(B)** Glutathione peroxidase (GPx), **(C)** GSH, **(D)** CAT, and **(E)** SOD in liver tissue. **(F)** A schematic illustration of the antioxidant effect of LAH. Values are expressed as mean ± SD (n = 10/group). *$p < 0.05$ compared with ND group. + $p < 0.05$ compared with HFD group.

flos, Hoveniae semen, and Siraitiae fructus have been used to treat metabolic diseases. Recent research suggests that Puerariae lobatae radix improves glucose and lipid metabolism and exerts protective effects against hepatic steatosis in high-fat diet-fed rodent models (Zhang et al., 2018a), while Lonicerae japonicae flos extracts lower the triglyceride levels in serum and liver tissues of an animal model of hyperlipidemia (Li et al., 2015), and Hoveniae semen exhibited protective properties against ALD by reducing oxidative stress and preventing lipid dysmetabolism *in vivo* (Meng et al., 2020). Siraitiae fructus has been hypothesized to protect against NAFLD development by inhibiting fat droplet formation in the liver (Zhang et al., 2018b). Based on previous clinical experiences and animal experiments, we combined the four botanical drugs to form LAH for the first time and used network pharmacology to predict the mechanism of action of LAH, providing a new direction for the mechanism study of TCM formulas.

HPLC analysis revealed that chlorogenic acid, puerarin, daidzin, 3,5-dicaffeoylquinic acid and daidzein are the major components in LAH. In our network pharmacology approach, we focus on the potential targets of these five components for NAFLD. The results of KEGG and GO enrichment analysis showed that the pathways were mainly enriched in cancer, oxidative stress, non-alcoholic fatty liver disease, AMPK signaling pathway and other signal pathways, which indicated that LAH may regulated fatty liver *via* AMPK signaling pathway. Puerarin, which was the most abundant component of LAH. Puerarin has more target proteins in the interaction network, it may be the key component of LAH that plays the role of hepatoprotective. Previous studies have reported that puerarin increased serum insulin and decreased fasting serum glucose levels in ob/ob mice and STZ-induced diabetic rats, which are related to the activation of AMPK and PI3K/Akt pathways (Zhou et al., 2014). Furthermore, puerarin has a protective effect on alcohol-induced liver injury which may be related to the inhibition of oxidative stress (Zhou et al., 2014). Many studies have shown that puerarin has a variety of biological activities, but there are few studies focusing on the pharmacological action of puerarin and the underlying mechanisms and its antioxidant effect in NAFLD. To

investigate the underlying mechanism, we performed OA-induced hepatic steatosis in HepG2 cells as an *in vitro* model of NAFLD. The results showed that puerarin treatment significantly decreased OA-induced HepG2 cells lipid droplets accumulation. In addition, puerarin increased the protein expression of phosphorylated AMPK and decreased SREBP1 and FAS protein expression in OA-induced HepG2 cells. As reported, AMPK phosphorylation can regulate lipid and carbohydrate metabolism in liver cells, which blocks SREBP1 expression to reduce fatty acid synthesis (Zhang et al., 2017). The protective effect of LAH is likely attributed to its regulatory role in the AMPK-SREBP1 signaling pathway.

We investigated the mechanism involved in the hepatoprotective effects of LAH in HFD-induced mice. The characteristics of NAFLD induced by HFD are the presence of higher concentrations of blood sugar, cholesterol, and TG in the blood circulation, as well as higher concentrations of liver damage markers, such as AST, ALT and LDH. (Eisinger et al., 2014). AST and ALT are important indices related to liver function, and the abnormally increased serum levels of AST and ALT imply the occurrence of hepatotoxicity and liver injury, which are closely associated with hyperlipidemia and hepatic steatosis (Sachdev et al., 2006). LAH administration lowered HFD-induced high serum levels of AST and ALT, indicating that LAH could protect mice against HFD-induced liver damage. Accumulated evidence has demonstrated that LAH improves hyperglycemia and dyslipidemia in HFD-induced mice, as indicated by lower circulating concentrations of cholesterol, glucose, and TG. It also decreased both liver and adipose tissue weight, decreased lipid accumulation in the liver, and ameliorated NAFLD in HFD-induced obese mice. Hepatic steatosis is defined by the excessive accumulation of triglycerides, causing more than 5% of hepatocytes containing visible lipid droplets in either a micro- or macrovesicular pattern (Ress and Kaser, 2016). LAH was able to reduce lipid accumulation and fat vacuoles as visualized using H&E staining and Oil Red O staining of liver histological slices. This effect can be attributed to a reduction in triglyceride levels in the blood and liver tissues.

SREBP1 is the most important transcription factor regulating *de novo* lipogenesis in the liver, and it specifically regulates the expression of many key enzymes in the fatty acid biosynthesis pathway (Wang et al., 2017). AMPK suppresses various anabolic pathways, stimulates catabolic pathways, it is considered to be the main therapeutic target for the treatment of non-alcoholic fatty liver (Kim et al., 2016). In addition, AMPK also the upstream kinase of SREBP1 in the liver. Therefore, activation of AMPK leads to the suppression of SREBP1 and reduces hepatocyte adipogenesis (Juszczak et al., 2020). *In vivo* studies confirmed that LAH increased AMPK phosphorylation, ACC phosphorylation and inhibited SREBP1 expression compared to the HFD group. In addition, we found that LAH improves CPT1 expression. CPT-1 is responsible for the transport of activated fatty acids into the mitochondria for β-oxidation (Qu et al., 2016). We found that LAH improved NAFLD in HFD-induced mice by enhancing AMPK expression to suppress SREBP1 activity and increasing β-oxidation for lipolysis. As predicted by network pharmacology approach, LAH may exert therapeutic effects on NAFLD by regulating the AMPK signaling pathway and decrease fatty acid synthesis.

HFD induces excessive accumulation of TC, cholesterol, free fatty acids, and lipids, leading to the production of reactive oxygen species (ROS) in the liver and accelerating oxidative stress (Tan and Norhaizan, 2019). Oxidative stress plays a vital role in the pathogenesis of NAFLD from steatosis to NASH, fibrosis, and cirrhosis and therefore, enhancing the cellular antioxidant system may have beneficial effects on NAFLD. AMPK activity is implicated in cellular redox homeostasis and plays a critical role in maintaining cell integrity by the inhibition of ROS and promote defense against oxidative stress (Hinchy et al., 2018). Our data indicated that LAH could increase AMPK phosphorylation in HFD mice. In order to explore the antioxidant effect of LAH, we measured the activity of antioxidant enzymes. Glutathione (GSH), one of the most abundant low molecular weight non-protein thiols, modulates physiological levels of ROS and is involved in the cell's oxidative stress response. Glutathione reductase (GR) is responsible for maintaining the supply of reduced glutathione, and glutathione peroxidase (GPX) catalyzes the detoxification of H_2O_2 and lipid peroxides by reduced glutathione (Panday et al., 2020). Therefore, the activity of these antioxidants can be used as indicators of antioxidant activity (Perlemuter et al., 2005). In this study, the antioxidant enzyme activity of liver tissue in the HFD group was significantly reduced compared with that in the ND group, suggesting that NAFLD increased oxidative stress and decreased antioxidant capacity. However, LAH administration enhanced antioxidant capacity by increasing GR, GPX, and GSH activities. In addition, SOD and catalase levels were increased by LAH administration. Through these results, we confirmed the inhibitory effect of LAH on fatty liver by improving the antioxidant effect of the liver. In our future study, the research direction will explore the antioxidant mechanism of LAH.

In conclusion, this study demonstrates that supplementation with LAH efficiently inhibits fatty liver development and hepatotoxicity in HFD-induced NAFLD and prevents abnormal lipid accumulation by regulating AMPK/ACC activation, increasing β-oxidation, and downregulating FAS and SREBP1. Moreover, LAH also showed antioxidant activities and improves hyperglycemia and dyslipidaemia in NAFLD mice. This experimental evidence indicates that LAH has a potential protective effect in the prevention and improvement of NAFLD.

Data availability statement

The original contributions presented in the study are included in the article/Supplementary Material, further inquiries can be directed to the corresponding author.

Ethics statement

The animal study was reviewed and approved by Institutional Animal Care and Use Committee or Panel (IACUC/IACUP), Taipei Medical University (IACUC Approval no. LAC-2019-0070).

Author contributions

D-SN, Y-JC, and C-JL designed experiments, analyzed data and wrote the manuscript. H-WZ, K-TW, and M-CL designed the research. C-CW, W-CC, C-LY, and C-JL contributed the experimental design and discussion. L-LT revised the final manuscript as submmited. Y-JC was responsible for animal care. All authors have read and agreed to the published version of manuscript.

Funding

This work was supported by grants from Infinitus (China) Company Ltd. and Herbiotek Co., Ltd. (Project code: A-109-003).

Acknowledgments

We thank all the participants and the coordination staff in the study gratefully.

Conflict of interest

Authors D-SN and H-WZ were employed by Infinitus (China) Company Ltd.; Authors K-TW, M-CL were employed by Herbiotek Co., Ltd.

The remaining authors declare that the research was conducted in the absence of any commercial or financial relationships that could be construed as a potential conflict of interest.

Publisher's note

All claims expressed in this article are solely those of the authors and do not necessarily represent those of their affiliated organizations, or those of the publisher, the editors and the reviewers. Any product that may be evaluated in this article, or claim that may be made by its manufacturer, is not guaranteed or endorsed by the publisher.

Supplementary material

The Supplementary Material for this article can be found online at: https://www.frontiersin.org/articles/10.3389/fphar.2022.1026912/full#supplementary-material.

References

Ahn, S. Y., Jo, M. S., Lee, D., Baek, S. E., Baek, J., Yu, J. S., et al. (2019). Dual effects of isoflavonoids from Pueraria lobata roots on estrogenic activity and anti-proliferation of MCF-7 human breast carcinoma cells. *Bioorg. Chem.* 83, 135–144. doi:10.1016/j.bioorg.2018.10.017

Amberger, J. S., Bocchini, C. A., Schiettecatte, F., Scott, A. F., and Hamosh, A. (2014). OMIM.org: Online Mendelian Inheritance in Man (OMIM®), an online catalog of human genes and genetic disorders. *Nucleic Acids Res.* 43 (D1), D789–D798. doi:10.1093/nar/gku1205

Brunt, E. M., Wong, V. W., Nobili, V., Day, C. P., Sookoian, S., Maher, J. J., et al. (2015). Nonalcoholic fatty liver disease. *Nat. Rev. Dis. Prim.* 1, 15080. doi:10.1038/nrdp.2015.80

Byass, P. (2014). The global burden of liver disease: A challenge for methods and for public health. *BMC Med.* 12, 159. doi:10.1186/s12916-014-0159-5

Chen, X. B., Zhuang, J. J., Liu, J. H., Lei, M., Ma, L., Chen, J., et al. (2011). Potential AMPK activators of cucurbitane triterpenoids from Siraitia grosvenorii Swingle. *Bioorg. Med. Chem.* 19 (19), 5776–5781. doi:10.1016/j.bmc.2011.08.030

Cho, I., Kim, J., Jung, J., Sung, S., Kim, J., Lee, N., et al. (2016). Hepatoprotective effects of hoveniae semen cum fructus extracts in ethanol intoxicated mice. *J. Exerc. Nutr. Biochem.* 20 (1), 49–64. doi:10.20463/jenb.2016.03.20.1.4

Ehrman, T. M., Barlow, D. J., and Hylands, P. J. (2007). Phytochemical informatics of traditional Chinese medicine and therapeutic relevance. *J. Chem. Inf. Model.* 47 (6), 2316–2334. doi:10.1021/ci700155t

Eigentler, T., Lomberg, D., Machann, J., and Stefan, N. (2020). Lipodystrophic nonalcoholic fatty liver disease induced by immune checkpoint blockade. *Ann. Intern. Med.* 172 (12), 836–837. doi:10.7326/L19-0635

Eisinger, K., Liebisch, G., Schmitz, G., Aslanidis, C., Krautbauer, S., and Buechler, C. (2014). Lipidomic analysis of serum from high fat diet induced obese mice. *Int. J. Mol. Sci.* 15 (2), 2991–3002. doi:10.3390/ijms15022991

Fan, Q., Xu, F., Liang, B., and Zou, X. (2021). The anti-obesity effect of traditional Chinese medicine on lipid metabolism. *Front. Pharmacol.* 12, 696603. doi:10.3389/fphar.2021.696603

Gao, Y., Tang, H., Xiong, L., Zou, L., Dai, W., Liu, H., et al. (2018). Protective effects of aqueous extracts of flos lonicerae japonicae against hydroquinone-induced toxicity in hepatic L02 cells. *Oxid. Med. Cell. Longev.* 2018, 4528581. doi:10.1155/2018/4528581

Guo, Y., Li, J. X., Mao, T. Y., Zhao, W. H., Liu, L. J., and Wang, Y. L. (2017). Targeting Sirt1 in a rat model of high-fat diet-induced non-alcoholic fatty liver disease: Comparison of Gegen Qinlian decoction and resveratrol. *Exp. Ther. Med.* 14 (5), 4279–4287. doi:10.3892/etm.2017.5076

Hinchy, E. C., Gruszczyk, A. V., Willows, R., Navaratnam, N., Hall, A. R., Bates, G., et al. (2018). Mitochondria-derived ROS activate AMP-activated protein kinase (AMPK) indirectly. *J. Biol. Chem.* 293 (44), 17208–17217. doi:10.1074/jbc.RA118.002579

Jeong, Y. H., Oh, Y. C., Cho, W. K., Yim, N. H., and Ma, J. Y. (2019). Hoveniae semen seu fructus ethanol extract exhibits anti-inflammatory activity via MAPK, AP-1, and STAT signaling pathways in LPS-stimulated RAW 264.7 and mouse

peritoneal macrophages. *Mediat. Inflamm.* 2019, 9184769. doi:10.1155/2019/9184769

Jiang, R. W., Lau, K. M., Lam, H. M., Yam, W. S., Leung, L. K., Choi, K. L., et al. (2005). A comparative study on aqueous root extracts of Pueraria thomsonii and Pueraria lobata by antioxidant assay and HPLC fingerprint analysis. *J. Ethnopharmacol.* 96 (1-2), 133–138. doi:10.1016/j.jep.2004.08.029

Jin, S. E., Son, Y. K., Min, B. S., Jung, H. A., and Choi, J. S. (2012). Anti-inflammatory and antioxidant activities of constituents isolated from Pueraria lobata roots. *Arch. Pharm. Res.* 35 (5), 823–837. doi:10.1007/s12272-012-0508-x

Juszczak, F., Caron, N., Mathew, A. V., and Decleves, A. E. (2020). Critical role for AMPK in metabolic disease-induced chronic kidney disease. *Int. J. Mol. Sci.* 21 (21), E7994. doi:10.3390/ijms21217994

Kim, J., Yang, G., Kim, Y., Kim, J., and Ha, J. (2016). AMPK activators: Mechanisms of action and physiological activities. *Exp. Mol. Med.* 48, e224. doi:10.1038/emm.2016.16

Li, S., Xu, Y., Guo, W., Chen, F., Zhang, C., Tan, H. Y., et al. (2020). The impacts of herbal medicines and natural products on regulating the hepatic lipid metabolism. *Front. Pharmacol.* 11, 351. doi:10.3389/fphar.2020.00351

Li, Y., Cai, W., Weng, X., Li, Q., Wang, Y., Chen, Y., et al. (2015). Lonicerae japonicae flos and lonicerae flos: A systematic pharmacology review. *Evidence-based complementary Altern. Med.*, 2015., 905063. doi:10.1155/2015/905063

Liu, H., Wang, C., Qi, X., Zou, J., and Sun, Z. (2018). Antiglycation and antioxidant activities of mogroside extract from Siraitia grosvenorii (Swingle) fruits. *J. Food Sci. Technol.* 55 (5), 1880–1888. doi:10.1007/s13197-018-3105-2

Meng, X., Tang, G. Y., Zhao, C. N., Liu, Q., Xu, X. Y., and Cao, S. Y. (2020). Hepatoprotective effects of Hovenia dulcis seeds against alcoholic liver injury and related mechanisms investigated via network pharmacology. *World J. Gastroenterol.* 26 (24), 3432–3446. doi:10.3748/wjg.v26.i24.3432

Panday, S., Talreja, R., and Kavdia, M. (2020). The role of glutathione and glutathione peroxidase in regulating cellular level of reactive oxygen and nitrogen species. *Microvasc. Res.* 131, 104010. doi:10.1016/j.mvr.2020.104010

Perlemuter, G., Davit-Spraul, A., Cosson, C., Conti, M., Bigorgne, A., Paradis, V., et al. (2005). Increase in liver antioxidant enzyme activities in non-alcoholic fatty liver disease. *Liver Int.* 25 (5), 946–953. doi:10.1111/j.1478-3231.2005.01126.x

Piñero, J., À, Bravo, Queralt-Rosinach, N., Gutiérrez-Sacristán, A., Deu-Pons, J., Centeno, E., et al. (2016). DisGeNET: A comprehensive platform integrating information on human disease-associated genes and variants. *Nucleic Acids Res.* 45 (D1), D833–D839. doi:10.1093/nar/gkw943

Qiu, P., Dong, Y., Zhu, T., Luo, Y. Y., Kang, X. J., Pang, M. X., et al. (2019). Semen hoveniae extract ameliorates alcohol-induced chronic liver damage in rats via modulation of the abnormalities of gut-liver axis. *Phytomedicine* 52, 40–50. doi:10.1016/j.phymed.2018.09.209

Qu, Q., Zeng, F., Liu, X., Wang, Q. J., and Deng, F. (2016). Fatty acid oxidation and carnitine palmitoyltransferase I: Emerging therapeutic targets in cancer. *Cell Death Dis.* 7 (5), e2226–e. doi:10.1038/cddis.2016.132

Ress, C., and Kaser, S. (2016). Mechanisms of intrahepatic triglyceride accumulation. *World J. Gastroenterol.* 22 (4), 1664–1673. doi:10.3748/wjg.v22.i4.1664

Rinella, M. E. (2015). Nonalcoholic fatty liver disease: A systematic review. *JAMA* 313 (22), 2263–2273. doi:10.1001/jama.2015.5370

Sachdev, M. S., Riely, C. A., and Madan, A. K. (2006). Nonalcoholic fatty liver disease of obesity. *Obes. Surg.* 16 (11), 1412–1419. doi:10.1381/096089206778870012

Stefan, N. (2020). Causes, consequences, and treatment of metabolically unhealthy fat distribution. *Lancet. Diabetes Endocrinol.* 8 (7), 616–627. doi:10.1016/S2213-8587(20)30110-8

Sun, Y., Zhang, H., Cheng, M., Cao, S., Qiao, M., Zhang, B., et al. (2019). New hepatoprotective isoflavone glucosides from Pueraria lobata (Willd.) Ohwi. *Nat. Prod. Res.* 33 (24), 3485–3492. doi:10.1080/14786419.2018.1484461

Tan, B. L., and Norhaizan, M. E. (2019). Effect of high-fat diets on oxidative stress, cellular inflammatory response and cognitive function. *Nutrients* 11 (11), E2579. doi:10.3390/nu11112579

Wang, L-F., Wang, X-N., Huang, C-C., Hu, L., Xiao, Y-F., Guan, X-H., et al. (2017). Inhibition of NAMPT aggravates high fat diet-induced hepatic steatosis in mice through regulating Sirt1/AMPKα/SREBP1 signaling pathway. *Lipids Health Dis.* 16 (1), 82. doi:10.1186/s12944-017-0464-z

Xu, Y., Guo, W., Zhang, C., Chen, F., Tan, H. Y., Li, S., et al. (2020). Herbal medicine in the treatment of non-alcoholic fatty liver diseases-efficacy, action mechanism, and clinical application. *Front. Pharmacol.* 11, 601. doi:10.3389/fphar.2020.00601

Yang, J. M., Sun, Y., Wang, M., Zhang, X. L., Zhang, S. J., Gao, Y. S., et al. (2019). Regulatory effect of a Chinese herbal medicine formula on non-alcoholic fatty liver disease. *World J. Gastroenterol.* 25 (34), 5105–5119. doi:10.3748/wjg.v25.i34.5105

Yang, R., Fang, L., Li, J., and Zhang, Y. Q. (2021). A new anti-inflammatory lignan from Lonicerae Japonicae flos. *Nat. Prod. Res.* 35 (4), 587–592. doi:10.1080/14786419.2019.1587430

Yang, R., Fang, L., Li, J., Zhao, Z., Zhang, H., and Zhang, Y. (2019). Separation of five iridoid glycosides from lonicerae japonicae flos using high-speed counter-current chromatography and their anti-inflammatory and antibacterial activities. *Molecules* 24 (1), E197. doi:10.3390/molecules24010197

Zhang, M., Yuan, Y., Zhou, W., Qin, Y., Xu, K., Men, J., et al. (2020). Network pharmacology analysis of Chaihu Lizhong Tang treating non-alcoholic fatty liver disease. *Comput. Biol. Chem.* 86, 107248. doi:10.1016/j.compbiolchem.2020.107248

Zhang, R., Zhu, X., Bai, H., and Ning, K. (2019). Network pharmacology databases for traditional Chinese medicine: Review and assessment. *Front. Pharmacol.* 10, 123. doi:10.3389/fphar.2019.00123

Zhang, S., Wang, J., Zhao, H., and Luo, Y. (2018). Effects of three flavonoids from an ancient traditional Chinese medicine Radix puerariae on geriatric diseases. *Brain Circ.* 4 (4), 174–184. doi:10.4103/bc.bc_13_18

Zhang, X., Song, Y., Ding, Y., Wang, W., Liao, L., Zhong, J., et al. (2018). Effects of mogrosides on high-fat-diet-induced obesity and nonalcoholic fatty liver disease in mice. *Molecules* 23 (8), E1894. doi:10.3390/molecules23081894

Zhang, Y., Meng, T., Zuo, L., Bei, Y., Zhang, Q., Su, Z., et al. (2017). Xyloketal B attenuates fatty acid-induced lipid accumulation via the SREBP-1c pathway in NAFLD models. *Mar. Drugs* 15 (6), E163. doi:10.3390/md15060163

Zhao, L., Wang, Y., Liu, J., Wang, K., Guo, X., Ji, B., et al. (2016). Protective effects of genistein and puerarin against chronic alcohol-induced liver injury in mice via antioxidant, anti-inflammatory, and anti-apoptotic mechanisms. *J. Agric. Food Chem.* 64 (38), 7291–7297. doi:10.1021/acs.jafc.6b02907

Zhou, B. G., Zhao, H. M., Lu, X. Y., Zhou, W., Liu, F. C., Liu, X. K., et al. (2018). Effect of puerarin regulated mTOR signaling pathway in experimental liver injury. *Front. Pharmacol.* 9, 1165. doi:10.3389/fphar.2018.01165

Zhou, W., Yin, A., Shan, J., Wang, S., Cai, B., and Di, L. (2017). Study on the rationality for antiviral activity of flos lonicerae japonicae-fructus forsythiae herb chito-oligosaccharide via integral pharmacokinetics. *Molecules* 22 (4), E654. doi:10.3390/molecules22040654

Zhou, Y. X., Zhang, H., and Peng, C. (2014). Puerarin: A review of pharmacological effects. *Phytother. Res.* 28 (7), 961–975. doi:10.1002/ptr.5083

frontiers | Frontiers in Pharmacology

TYPE Original Research
PUBLISHED 28 November 2022
DOI 10.3389/fphar.2022.1084435

OPEN ACCESS

EDITED BY
Yi Wu,
Nanjing Agricultural University, China

REVIEWED BY
Weijie Lv,
South China Agricultural University, China
Xinghua Zhao,
Agricultural University of Hebei, China
Jian Li,
Fujian Agriculture and Forestry University, China

*CORRESPONDENCE
Xiaowen Jiang,
jiangxianwen@neau.edu.cn
Wenhui Yu,
yuwenhui@neau.edu.cn

†These authors share first authorship

SPECIALTY SECTION
This article was submitted to Ethnopharmacology, a section of the journal Frontiers in Pharmacology

RECEIVED 30 October 2022
ACCEPTED 15 November 2022
PUBLISHED 28 November 2022

CITATION
Liang M, Huo M, Guo Y, Zhang Y, Xiao X, Xv J, Fang L, Li T, Wang H, Dong S, Jiang X and Yu W (2022), Aqueous extract of Artemisia capillaris improves non-alcoholic fatty liver and obesity in mice induced by high-fat diet. *Front. Pharmacol.* 13:1084435. doi: 10.3389/fphar.2022.1084435

Aqueous extract of Artemisia capillaris improves non-alcoholic fatty liver and obesity in mice induced by high-fat diet

Meng Liang[1†], Mohan Huo[2], Yi Guo[1], Yuyi Zhang[1], Xiao Xiao[1], Jianwen Xv[1], Lixue Fang[1], Tianqi Li[1], Huan Wang[1], Siyu Dong[1], Xiaowen Jiang[1*] and Wenhui Yu[1,3,4*]

[1]Department of Veterinary Medicine, Northeast Agricultural University, Harbin, China, [2]Department of Life Sciences, Northeast Agricultural University, Harbin, China, [3]Institute of Chinese Veterinary Medicine, Northeast Agricultural University, Harbin, China, [4]Heilongjiang Provincial Key Laboratory for Prevention and Control of Common Animal Diseases, Northeast Agricultural University, Harbin, China

Non-alcoholic fatty liver disease (NAFLD) is one of the most common chronic liver diseases and is a nutritional metabolic disease. *Artemisia capillaris* (AC) is the above-ground dried part of *Artemisia capillaris Thunb.* or *Artemisia scoparia Waldst. et Kit.*, a natural medicinal plant with pharmacological effects of heat-clearing and biliary-promoting. In order to evaluate the therapeutic effect of Artemisia capillaris on NAFLD and obesity, experiments were conducted using aqueous extracts of Artemisia capillaris (WAC) to intervene in NAFLD models *in vivo* and *in vitro*. *In vivo* experiments were performed using HFD-fed (high fat diet) C57BL/6 mice to induce NAFLD model, and *in vitro* experiments were performed using oleic acid to induce HepG2 cells to construct NAFLD cell model. H.E. staining and oil red O staining of liver tissue were used to observe hepatocytes. Blood biochemistry analyzer was used to detect serum lipid levels in mice. The drug targets and mechanism of action of AC to improve NAFLD were investigated by western blotting, qRT-PCR and immunofluorescence. The results showed that C57BL/6 mice fed HFD continuously for 16 weeks met the criteria for NAFLD in terms of lipid index and hepatocyte fat accumulation. WAC was able to reverse the elevation of serum lipid levels induced by high-fat diet in mice. WAC promoted the phosphorylation levels of PI3K/AKT and AMPK in liver and HepG2 cells of NAFLD mice, inhibited SREBP-1c expression, reduced TG and lipogenesis, and decreased lipid accumulation. In summary, WAC extract activates PI3K/AKT pathway, reduces SREBP-1c protein expression by promoting AMPK phosphorylation, and decreases fatty acid synthesis and TG content in hepatocytes. AC can be used as a potential health herb to improve NAFLD and obesity.

KEYWORDS

aqueous extracts of Artemisia capillaris, NAFLD, lipid metabolism, PI3K/AKT, AMPK, SREBP-1c

1 Introduction

Non-alcoholic fatty liver disease (NAFLD) is a clinicopathologic syndrome of hepatic steatosis. It is characterized by excessive accumulation of lipids, mainly triglycerides (TG), in hepatocytes. However, NAFLD does not include a history of excessive alcohol consumption and definite liver damage factors (Cohen et al., 2011; Chalasani et al., 2018). NAFLD is a chronic nutritional metabolic disease that can develop into hepatitis, cirrhosis, and even liver cancer (Diehl and Day, 2017; Huang et al., 2021; Ratziu et al., 2022). Studies have shown that the incidence of NAFLD has shown a high development worldwide (Lonardo et al., 2016). It is closely associated with other metabolic diseases such as obesity, type 2 diabetes, dyslipidemia and hypertension, so NAFLD has become a global health problem of concern (Chalasani et al., 2018). Currently, clinical treatment is mostly carried out with lipid-lowering drugs, antioxidants and insulin sensitizers, but long-term use of these drugs produces toxic side effects. Natural medicines as alternative therapies have their unique advantages in the treatment of NAFLD, and there are some herbal medicines that have potential applications in the treatment of NAFLD.

The occurrence of NAFLD is closely related to insulin resistance (IR). When IR occurs in the body, in order to meet the body's energy supply needs, fat becomes the main mode of energy supply. After the increased breakdown of peripheral adipose tissue in the body, the uptake of free fatty acids by hepatocytes increases and they are deposited in the form of TG in the cells, and eventually NAFLD occurs. The phosphatidylinositol-3-kinase (PI3K) signaling pathway (PI3K/AKT) is the classical hepatic insulin signaling pathway (Fukuda et al., 2016). Activation of the PI3K/AKT transduction pathway improves IR and alleviates NAFLD. AMP-activated protein kinase (AMPK) is an important factor in the development of NAFLD and regulation of hepatic lipid metabolism. Activation of AMPK has an important regulatory role on lipid metabolism (Kamikubo et al., 2016; Garcia et al., 2019). Activated AMPK promotes lipid catabolism and ATP production, reduces mitochondrial ATP consumption to maintain the steady state of cellular energy, and regulates the activity of lipid metabolism-related enzymes to regulate fatty acid synthesis and oxidation in the liver (Hardie, 2015; Garcia and Shaw, 2017). AMPK inhibits sterol-regulatory element binding proteins-1c (SREBP-1c) activity, inhibits lipid synthesis, and reduces lipid deposition in the liver (Day et al., 2017). SREBP is an endoplasmic reticulum (ER) membrane-bound transcription factor that activates genes encoding fatty acid synthesis and regulating cholesterol (Horton et al., 2002). SREBP-1c, one of the isoforms of the SREBP family, is a key transcription factor with the function of enhancing the expression of genes related to hepatic adipogenesis (Irimia et al., 2017). It is mainly distributed in the liver and adipose tissue. Overexpression of SREBP-1c will cause lipid metabolism disorders. Activation of AMPK can downregulate SREBP-1c expression, control fatty acid oxidation (Samovski et al., 2015). TG and TC production in the liver, reduce lipid accumulation in hepatocytes, improve lipid metabolism disorders in the liver, and alleviate NAFLD (Tang et al., 2016).

Artemisia capillaris (AC) is a dried above-ground part of Artemisia capillaris Thunb. or Artemisia scoparia Waldst. et Kit. which is commonly used in traditional medicine for the treatment of clearing heat and gallbladder. It mainly contains coumarins, flavonoids, organic acids, volatile oils, terpenoids and other chemical components (Yuan et al., 2017). Recent studies have found that, in addition to its pharmacological effects such as choleretic and hepatoprotective, AC also has a variety of pharmacological activities such as antipyretic, anti-inflammatory, analgesic, and regulating lipid metabolism (Hsueh et al., 2021)。 Organic acids such as chlorogenic acid and caffeic acid contained in AC exhibited potential anti-obesity effects in mice induced by high-fat diet (HFD) (Cho et al., 2010). In addition, Ethanol extract of Artemisia scoparia (Galluzzi et al., 2018) has a modulating effect on lipid metabolism. The addition of SCO to HFD significantly reduced the levels of circulating glycerol and free fatty acids, and *in vitro* experiments revealed that SCO attenuated the lipolytic effect in TNF-α-induced cultured adipocytes (Boudreau et al., 2018).

In the present study, we evaluated the effects of WAC on a high-fat diet-induced mouse model of NAFLD and an oleic acid-induced HepG2 cell model. Then we explored the mechanisms by which WAC improves lipid accumulation *in vivo* and *in vitro*.

2 Materials and methods

2.1 Preparation of WAC

The air-dried AC used in this study, produced in Gansu Province, China, was purchased from Harbin Songshantang Pharmaceutical Company, China. AC was identified by a professor from the Institute of Chinese Veterinary Medicine, Northeastern Agricultural University. Weigh 100 g of dried AC, add 800 ml of distilled water, soak for 30 min at room temperature, decoct for 1 h, and collect the decoction solution. Then, 600 ml of distilled water was added and the decoction was decocted again for 1 h. The decoction was collected. The decoction solution collected twice was mixed, and the decoction solution was filtered, centrifuged to remove insoluble substances, and lyophilized at -50°C for 48 h to a powdered solid (Huang et al., 2022). The average yield of AC was 15.6% (W/W). The lyophilized product was stored at -20°C. For cellular experiments, WAC was dissolved in DMEM and filtered (0.22 μm).

2.2 Identification of WAC active ingredients by LC-MS

WAC (100 mg) were individually grounded with liquid nitrogen and the homogenate was resuspended with prechilled 80% methanol by well vortex. The samples were incubated on ice for 5 min and then were centrifuged at 15,000 g, 4°C for 20 min. Some of supernatant was diluted to final concentration containing 53% methanol by LC-MS grade water. The samples were subsequently transferred to a fresh Eppendorf tube and then were centrifuged at 15000 g, 4°C for 20 min (Want et al., 2013). Finally, the supernatant was injected into the LC-MS/MS system analysis LC-MS/MS analyses were performed using an ExionLCTM AD system (SCIEX) coupled with a QTRAP® 6,500 + mass spectrometer (SCIEX). Samples were injected onto a Xselect HSS T3 (2.1 × 150 mm, 2.5 μm) using a 20-min linear gradient at a flow rate of 0.4 ml/min for the positive/negative polarity mode. The eluents were eluent A (0.1% Formic acid-water) and eluent B (0.1%Formic acid-acetonitrile) (Luo et al., 2015). The solvent gradient was set as follows: 2% B, 2 min; 2–100% B, 15.0 min; 100% B, 17.0 min; 100–2% B, 17.1 min;2% B, 20 min. QTRAP® 6,500 + mass spectrometer was operated in positive polarity mode with Curtain Gas of 35 psi, Collision Gas of Medium, Ion Spray Voltage of 5500V, Temperature of 550°C, Ion Source Gas of 1:60, Ion Source Gas of 2:60. QTRAP® 6,500 + mass spectrometer was operated in negative polarity mode with Curtain Gas of 35 psi, Collision Gas of Medium, Ion Spray Voltage of -4500V, Temperature of 550°C, Ion Source Gas of 1:60, Ion Source Gas of 2:60.

2.3 Experimental grouping and sample collection

Five-week-old male C57BL/6 mice were purchased from Changsheng Biotechnology (Changsheng, Liaoning, China). Animal experimental design strictly followed the guidelines of the International Association for the Evaluation and Accreditation of Laboratory Animal Care and was licensed by the Research Animal Protection Committee of Northeast Agricultural University. Mice were housed at 25 ± 1°C and in humidity-controlled chambers with natural light and dark cycles. After a 1-week adaptation period, mice were randomly divided into two groups: normal diet (ND) group (n = 6); and high-fat diet (HFD) group (n = 12). The nutritional analysis values and energy supply ratios of the high-fat diet are shown in Tables 1, 2, respectively. Mice in the high-fat diet group at week 16 formed a model of NAFLD (Li et al., 2022). Twelve mice in the high-fat diet group were randomly divided into two groups: the NAFLD model group (n = 6), and the NAFLD + WAC group (HFD + WAC, 50 mg/kg/d, WAC gavage twice a week, n = 6). WAC gavage lasted for 6 weeks. The experimental period was 22 weeks. The doses administered in this experiment were selected based on the experiments of Choi (Choi et al., 2013). All mice were fed and watered *ad libitum*, and body weight and food intake were recorded weekly. At the end of the animal experimental period, all mice were fasted and watered *ad libitum* for 12 h. Then, blood was collected from the eyes after anesthesia with ether, and serum was obtained by centrifugation at 3,000 rpm for 5 min at 4°C. Livers were immediately excised, collected and stored at -80°C for analysis, or stored in 4% paraformaldehyde for histological studies.

TABLE 1 Nutritional analysis values.

Feed components	Ratio (%)
Crude protein	19.2
Crude fat	14.4
Crude fiber	3.8
Crude ash content	4.0
Water content	9.2
Calcium	0.82
Total phosphorus	0.69

TABLE 2 Energy supply ratio.

Energy value	Ratio (%)
Protein	20.8
Fat	34.9
Carbaohydrate	44.3

2.4 Detection of major lipid indicators and glucose in blood and liver tissues

Serum TC, TG, Glucose, HDL and LDL levels were measured by a fully automated biochemical analyzer, and liver TC and TG levels were measured by a commercially available kit (Jiancheng, Nanjing, China). The liver tissue samples were accurately weighed, mechanically homogenized under ice and water bath conditions, centrifuged at 2,500 rpm for 10 min, and the supernatant was extracted and used to assay TG and TC levels.

2.5 Histological tests for liver pathology

Immediately after execution of the mice, liver tissue was fixed in 4% paraformaldehyde, paraffin-embedded, and sections were stained for H&E. The tissues were sectioned using a fcryostat and stained for Oil Red O. Light was observed using an optical microscope (Nikon, Tokyo, Japan).

TABLE 3 mRNA primer sequences.

Name	Forward 5–3'	Reverse 5–3'
FASN	TAAAGCATGACCTCGTGATGAA	GAAGTTCAGTGAGGCGTAGTAG
ACC	GGCCAGTGCTATGCTGAGAT	AGGGTCAAGTGCTGCTCCA
SREBP-1c	GCTACCGGTCTTCTATCAATGA	CGCAAGACAGCAGATTTATTCA
SCD-1	AACATTCAATCCCGGGAGAATA	GAAACTTTCTTCCGGTCGTAAG

2.6 Western blot analysis

Total protein samples were prepared using RIPA lysis buffer containing protease inhibitors and phosphatase inhibitors and quantified by the BCA protein assay kit. Equal amounts of proteins were separated by sodium dodecyl sulfate-polyacrylamide gel electrophoresis (SDS-PAGE). The molecular weight region of the target protein indicated by the pre-stained Marker was cut off and transferred to PVDF membrane or NC membrane, and the skimmed milk powder was closed at room temperature for 2 hours, and the primary antibody was added at the end of closure and incubated in the refrigerator at 4°C overnight. The primary antibodies are shown in Table 4. Then incubation with secondary antibody IgG (1:10,000) and preparation of ECL luminescent solution (meilunbio, Dalian, China) was performed for strip exposure. The strips were exposed using a 5,200 Tanon imaging system (Tanon science and technology, Shanghai, China). The developed protein bands were further quantified by ImageJ software and then compared with the grayscale values of the internal reference gene β-tubulin to calculate the relative expression levels of the target proteins measured in each of the above experimental groups.

2.7 HepG2 cell culture and drug treatment

HepG2 cells were provided by Dr. Zhang, College of Food, Northeastern Agricultural University. HepG2 cells were cultured in DMEM medium supplemented with 10% fetal bovine serum and 1% penicillin/streptomycin at 37°C and 5% CO_2 atmosphere. In the experiments, cells were starved in DMEM without FBS for 12 h. Subsequently, cells were cultured with DMEM containing FBS (negative control), OA-BSA complex (0.5 mM) (Xie et al., 2016) alone for 24 h to develop steatosis, and OA (0.5 mM) and WAC (1.5 mg/ml) were co-treated for 24 h. Next, cells were collected for subsequent experimental analysis. OA-BSA complexes were prepared by first dissolving OA in NaOH at 75°C by saponification and then adding the saponified OA to the medium containing 5% BSA and heating at 55°C until the solution became clear and transparent, resulting in a final concentration of 0.5 mM OA-BSA complexes.

2.8 HepG2 cell viability assay

Cell viability was assessed by cck-8 assay. HepG2 cells were inoculated at a density of 5 × 104 per well in 96-well plates with 100 μL of medium per well. Six replicate wells were set up and HepG2 cells were pre-cultured in an incubator at 37°C for 24 h. Then OA was co-treated with WAC (0.5 mg/ml, 1 mg/ml, 1.5 mg/ml, 2 mg/ml, 2.5 mg/ml, 3 mg/ml) for 24 h. 10 μL of cck-8 working solution was added to each well, protected from light, and incubated for 0.5 h in an incubator at 37°C. The absorbance at 450 nm was measured by an enzyme marker, and the cell survival rate (%) was calculated relative to the control group.

2.9 HepG2 cell lipid droplet observation

Oil Red O staining was used to assess the level of intracellular lipid droplets. The cells were washed 3 times with PBS, fixed with 4% paraformaldehyde for 10 min, and washed 3 times with PBS. The appropriate amount of staining washing solution was added to cover cells for 20 s and then aspirated and stained with modified Oil Red O staining solution for 20 min, and then the modified Oil Red O staining solution was removed with staining washing solution and washed with PBS. Finally, stained HepG2 cells were observed with an E100 light microscope (Nikon, Tokyo, Japan). For BODIPY staining, HepG2 cells were first inoculated in 24-well plates and treated with OA and WAC when the density reached 60%–70% for 24 h. Cells were fixed with 4% paraformaldehyde PBS for 1 h at room temperature, then washed 3 times with PBS for 5 min each, stained with 4 μM BODIPY493/503 at 37°C for 30 min, washed with PBS for 3 times, re-stained with DAPI for 5 min, and washed with PBS for 3 times. After blocking with PBS, the cell plates were placed on an inverted fluorescence microscope and the fluorescence signal was acquired and quantified using Image-Pro Plus software (version 3.0, Media Cybernetics, Bethesda, MD, United States) and the same parameters.

TABLE 4 Antibodies and reagents.

Antibodies and Reagents	Producer
Rabbit anti-PI3K(A11402, 1:500)	Abclonal, Wuhan, China
Rabbit anti-p-PI3K(A4992, 1:500)	Abclonal, Wuhan, China
Rabbit anti-AKT(A18120, 1:500)	Abclonal, Wuhan, China
Rabbit anti-p-AKT(AP1068, 1:500)	Abclonal, Wuhan, China
Rabbit anti-AMPK(WL02254, 1:1000)	Wanleibio, Shenyang, China
Rabbit anti-p-AMPK(WL05103, 1:1000)	Wanleibio, Shenyang, China
Rabbit anti-SREBP-1c(WL02093, 1:1000)	Biodragon, Suzhou, China
Rabbit anti-SCD1(A15606, 1:1000)	Abclonal, Wuhan, China
Rabbit anti-FAS(WL03376, 1:1000)	Wanleibio, Shenyang, China
Rabbit anti-DGAT2(A13891, 1:1000)	Abclonal, Wuhan, China
Rabbit anti-β-tubulin(AC008, 1:10000)	Abclonal, Wuhan, China
Rabbit anti-SREBP-1c(A15586, 1:200)	Abclonal, Wuhan, China
Goat Anti-rabbit IgG/FITC antibody(bs-0295G-FITC)	Bioss, Beijing, China
BODIPY 493/503	yuanye, Shanghai, China
DAPI staining solution(BL105A)	Biosharp, Hefei, China
Fatostatin (125B11)	MCE, Shanghai, China
BioRT Master HiSensi cDNA First Strand Synthesis kit	Boster, USA
BioEasy Master Mix (SYBR Green)(BSB25L1B)	Boster, USA
High glucose DMEM(cat.no.SH30022.01)	HyClone, Shanghai, China
Fetal Bovine Serum(WHRTNA101-1)	Wohong, Shijiazhuang, China
Penicillin-Streptomycin mixture	Solarbio, Beijing, China
Oleic acid	yuanye, Shanghai, China
High fat diet and normal diet	Xiaoshuyoutai, Beijing, China

2.10 Detection of TC and TG content in HepG2 cells

Commercially available kits (Nanjing Jiancheng Bioengineering Co., Ltd. Nanjing, China) were used to determine intracellular TC and TG levels and to assess the extent of lipid accumulation. TG and TC levels were measured according to the manufacturer's instructions, and protein concentrations were determined by the Enhanced BCA Protein Assay Kit. Then, lipid levels/protein concentrations were calculated.

2.11 Immunofluorescence assay

HepG2 cells were plated in 24-well plates and treated with OA and WAC when the density reached 60%–70% for 24 h. Cells were fixed with 4% paraformaldehyde, washed, permeabilized, and closed. Cells were incubated with SREBP-1c (1:200) primary antibody overnight at 4°C in the refrigerator. Secondary antibody goat anti-rabbit IgG HampL/HRP (1:200) was added to the cells for 1 h. The nuclei were stained with DAPI (BL105A, Biosharp, Hefei, China) for 5 min. After blocking with PBS, the cell plates were placed on an inverted fluorescence microscope and the fluorescence signal was acquired and quantified using Image-Pro Plus software (version 3.0, Media Cybernetics, Bethesda, MD, United States) and the same parameters.

2.12 qRT-PCR analysis

0.1 g of liver tissue was weighed, total RNA was extracted and RNA concentration was detected according to the kit. RNA was reverse transcribed into cDNA using the kit, primers were synthesized by Sangon Biotech (Sangon Biotech Co., Ltd. Shanghai, China), primer design is shown in Table 3 qRT-PCR was performed using SYBR Green in a Light Cycler@480 System (Roche, Switzerland). reaction conditions were: pre-denaturation at 95°C for 10 min; denaturation at 95°C for 15 s, denaturation at 60°C for 1 min, 40 cycles; and finally melting reaction. The mRNA expression level was quantified using β-actin as the control. The calculation method used was $2^{-\Delta\Delta Ct}$ method.

2.13 Statistical analysis of data

Data were expressed as mean ± standard deviation, and statistical analysis was performed using SPSS software 22.0. Statistical differences in quantitative data between groups and

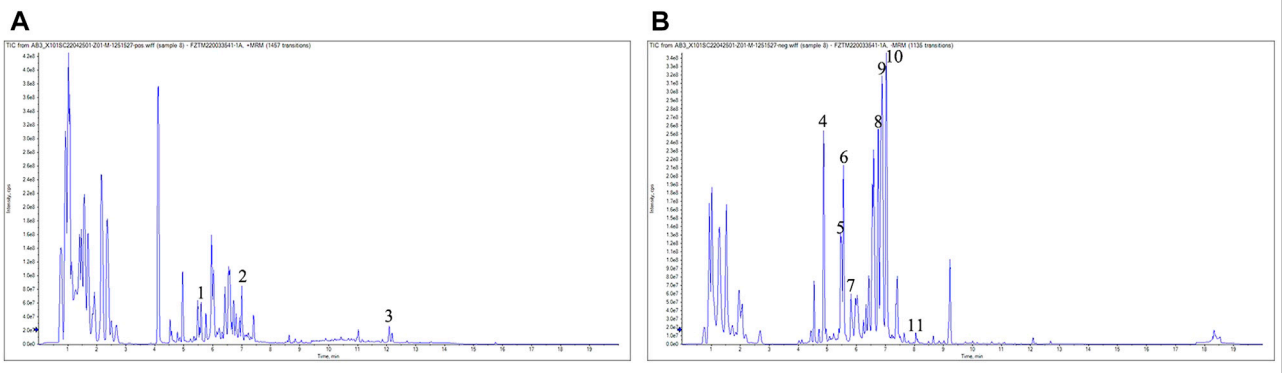

FIGURE 1
LC-MS analysis. **(A)** positive mode **(B)** negative mode. 1) 1-Caffeoylquinic acid (rt = 5.46 min), 2) Isoferulic Acid (rt = 7.008 min),3) Costunolide (rt = 12.083 min), 4) Neochlorogenic acid (rt = 4.879 min), 5) Chlorogenic Acid (rt = 5.37 min), 6) 3-O-Feruloylquinic acid (rt = 5.55 min), 7) Caffeic acid (rt = 5.801 min), 8) Isochlorogenic acid B (rt = 6.768 min), 9) 1,5-Dicaffeoylquinic acid (rt = 7.676 min), 10) Isochlorogenic acid C (rt = 7.053 min), 11) Scoparone (rt = 7.935 min).

significance of nonparametric comparisons between groups were analyzed using one-way ANOVA and Tukey's test. Plots were performed using Origin 2019. $p < 0.05$ was considered statistically significant.

3 Results

3.1 LC-MS analysis of WAC

As shown in Figure 1A,B, 11 compounds were characterized by LC/MS, including 1) 1-Caffeoylquinic acid (rt = 5.46 min), 2) Isoferulic Acid (rt = 7.008 min), 3) Costunolide (rt = 12.083 min), 4) Neochlorogenic acid (rt = 4.879 min), 5) Chlorogenic Acid (rt = 5.37 min), 6) 3-O-Feruloylquinic acid (rt = 5.55 min), 7) Caffeic acid (rt = 5.801 min), 8) Isochlorogenic acid B (rt = 6.768 min), 9) 1,5-Dicaffeoylquinic acid (rt = 7.676 min), 10) Isochlorogenic acid C (rt = 7.053 min), and 11) Scoparone (rt = 7.935 min). The WAC extract samples used in this study contained the active ingredients described in previous reports (Dai et al., 2021; Hsueh et al., 2021).

3.2 WAC alleviates high fat diet-induced obesity and hepatic steatosis in non-alcoholic fatty liver disease mice

To determine the effect of WAC on NAFLD *in vivo*, a mouse model of NAFLD was constructed by feeding mice with HFD for 16 weeks, and WAC was given by gavage at 50 mg/kg/d for the next 6 weeks (Figure 2A). In terms of histopathology, WAC treatment significantly improved fat accumulation in the liver of HFD-fed mice (Figures 2B,I). Mice fed with HFD showed higher weight gain. weight gain was reduced after WAC treatment (Figures 2C–E). The liver index, inguinal adiposity index and epididymal adiposity index were significantly increased in HFD-fed mice, and the above indices were significantly reduced after 6 weeks of WAC treatment. HFD enhanced the adiposity index and WAC treatment reduced the adiposity index, suggesting that the weight loss was associated with a reduction in the amount of adiposity (Figures 2F–H). These results suggest that WAC treatment alleviates obesity and hepatic steatosis in HFD-induced NAFLD mice.

3.3 WAC ameliorates lipid metabolism disorders in high fat diet-induced non-alcoholic fatty liver disease mice

Excessive accumulation of hepatic lipids is due to a dysregulation of lipid metabolic homeostasis, which ultimately leads to hepatic steatosis. Mice fed HFD exhibited significantly higher serum TG and TC levels compared to mice in the ND group, and WAC treatment restored serum triglyceride and cholesterol levels to normal levels (Figures 3A,B). Elevated serum glucose in mice fed HFD was also reversed by WAC, restoring normal levels (Figure 3C), suggesting that WAC may regulate glucose metabolism in mice. Compared with mice in the ND group, serum levels of HDL were reduced and LDL levels were increased in mice fed HFD, and both reduced HDL levels and increased LDL levels were reversed after 6 weeks of WAC treatment (Figures 3D,E). In addition, the liver of HFD-induced NAFLD mice exhibited elevated TG and TC levels, which were significantly reduced after WAC treatment (Figures 3F,G). These results suggest that WAC treatment ameliorates metabolic disorders in HFD-induced NAFLD mice.

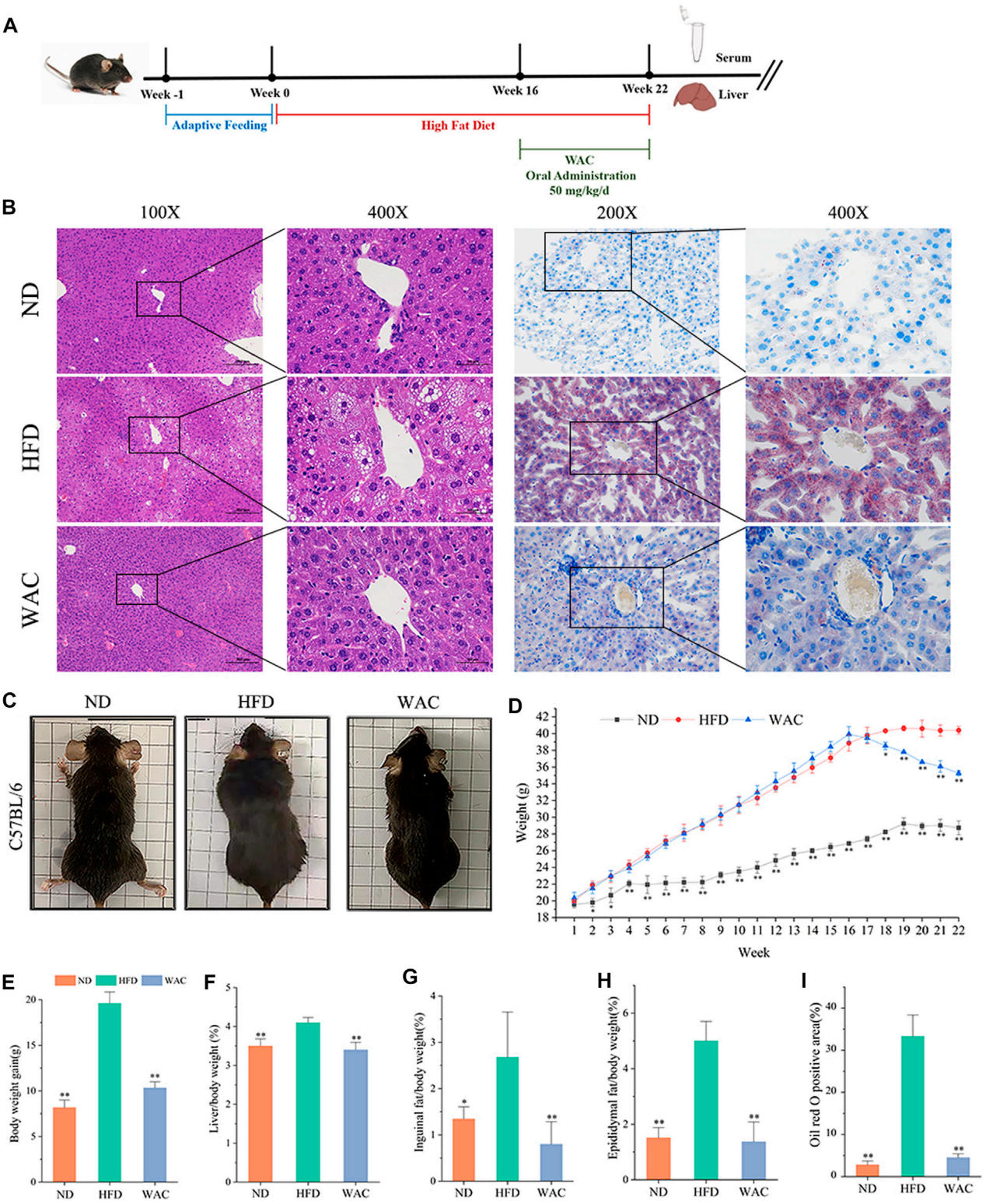

FIGURE 2
Effect of WAC on obesity and hepatic steatosis in HFD-induced NAFLD mice. **(A)** Animal experimentation process. **(B)** Pictures of liver morphology, HE staining and oil red O staining of liver sections after 6 weeks of WAC gavage. **(C)** Body condition of mice in each group after 6 weeks of WAC gavage. **(D)** Body weight changes in mice over 22 weeks. **(E)** Body weight gain in mice over 22 weeks. **(F)** Mouse liver index. **(G)** Index of inguinal adipose tissue in mice. **(H)** Adipose tissue index of mouse epididymis. **(I)** The positive areas of oil-red O staining were analyzed using ImageJ. Compared with HFD, * indicates $p < 0.05$ and ** indicates $p < 0.01$.

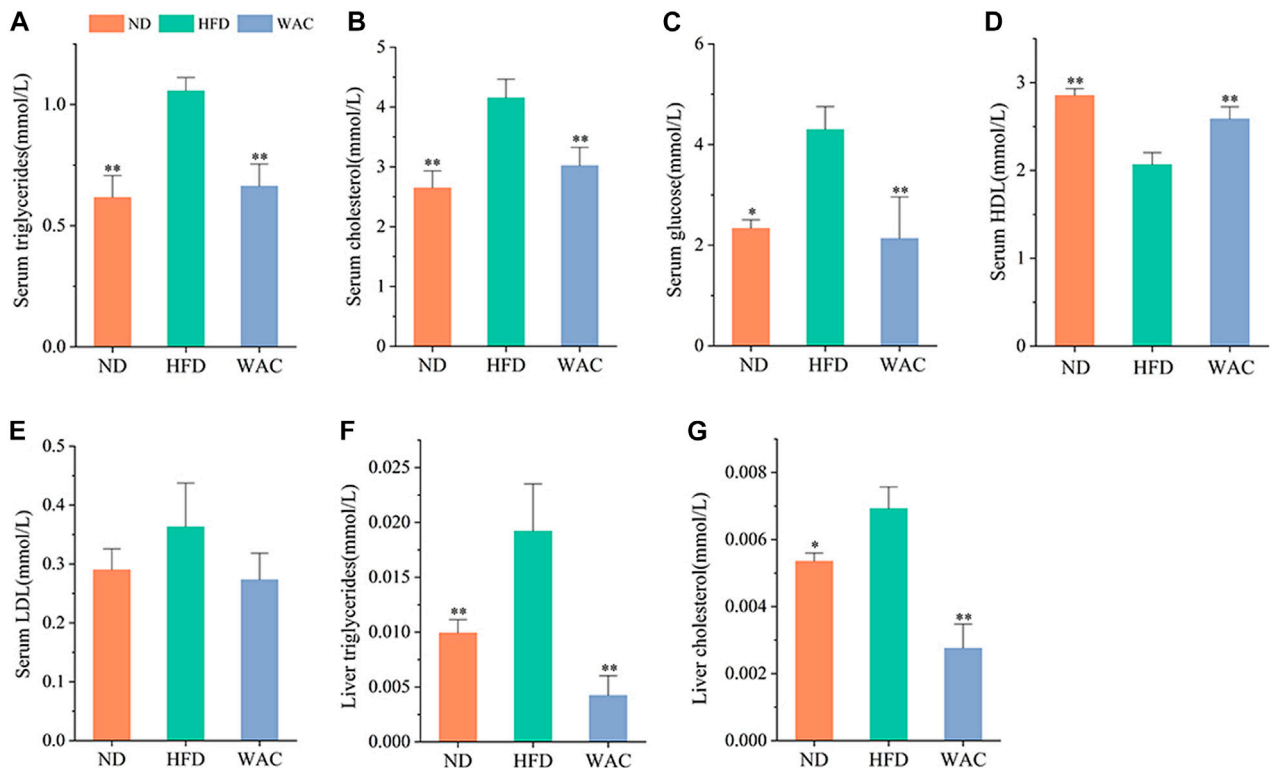

FIGURE 3
Effect of WAC on metabolic disorders in HFD-induced NAFLD mice. **(A)** Serum triglyceride levels. **(B)** Serum cholesterol levels. **(C)** Serum glucose levels. **(D)** Serum HDL levels. **(E)** Serum LDL levels. **(F)** Liver triglyceride levels in mice. **(G)** Liver cholesterol levels in mice. Compared with HFD, * indicates $p < 0.05$ and ** indicates $p < 0.01$.

3.4 WAC ameliorates OA-induced lipid accumulation in HepG2 cells

The cytotoxic effect of WAC was determined by cck-8, and 1.5 mg/ml was selected as the WAC concentration for the following *in vitro* experiments (Figure 4B). *In vitro*, lipid accumulation in HepG2 cells was induced with 0.5 mM OA. The effect of WAC on lipid accumulation in HepG2 cells was assayed by co-treatment of HepG2 cells with WAC and OA (Figure 4A). Compared with the NC group, the TG content of HepG2 cells in the OA group was significantly higher, whereas the TG content was significantly lower after treatment of HepG2 cells with WAC (Figure 4C). In contrast to the *in vivo* results, the OA-induced TC of HepG2 cells did not change, nor did WAC treatment cause changes in the TC of HepG2 cells (Figure 4D). The results of cytosolic oil red O staining showed a significant increase in lipid droplets in HepG2 cells in the OA group compared to the NC group. There was a decrease in lipid droplets in HepG2 cells in the WAC group compared to the OA group (Figure 4E). After HepG2 cells were incubated with OA for 24 h, lipid accumulation was detected by staining with BODIPY493/503 (a specific lipophilic probe), which showed that OA significantly promoted lipid accumulation in HepG2 cells, and the green fluorescence intensity of HepG2 cells in the WAC group was diminished (Figure 4F). These results suggest that *in vitro*, WAC ameliorates OA-induced lipid accumulation in HepG2 cells.

3.5 WAC activates PI3K/AKT and AMPK *in vivo*

Total PI3K and AKT and their phosphorylation levels, AMPK and its phosphorylation levels were detected *in vivo* by western blotting. Mice in the HFD group had elevated PI3K and AKT protein levels, decreased phosphorylated PI3K and AKT protein levels, decreased p-PI3K/PI3K and p-AKT/AKT levels, and significantly increased AMPK and p-AMPK protein levels in the liver. Mice in the WAC group had decreased PI3K and AKT protein levels, increased phosphorylated PI3K and AKT protein levels, increased p-PI3K/PI3K and p-AKT/AKT levels, and increased p-AMPK/AMPK (Figures 5A,B). Liver SREBP-1c protein

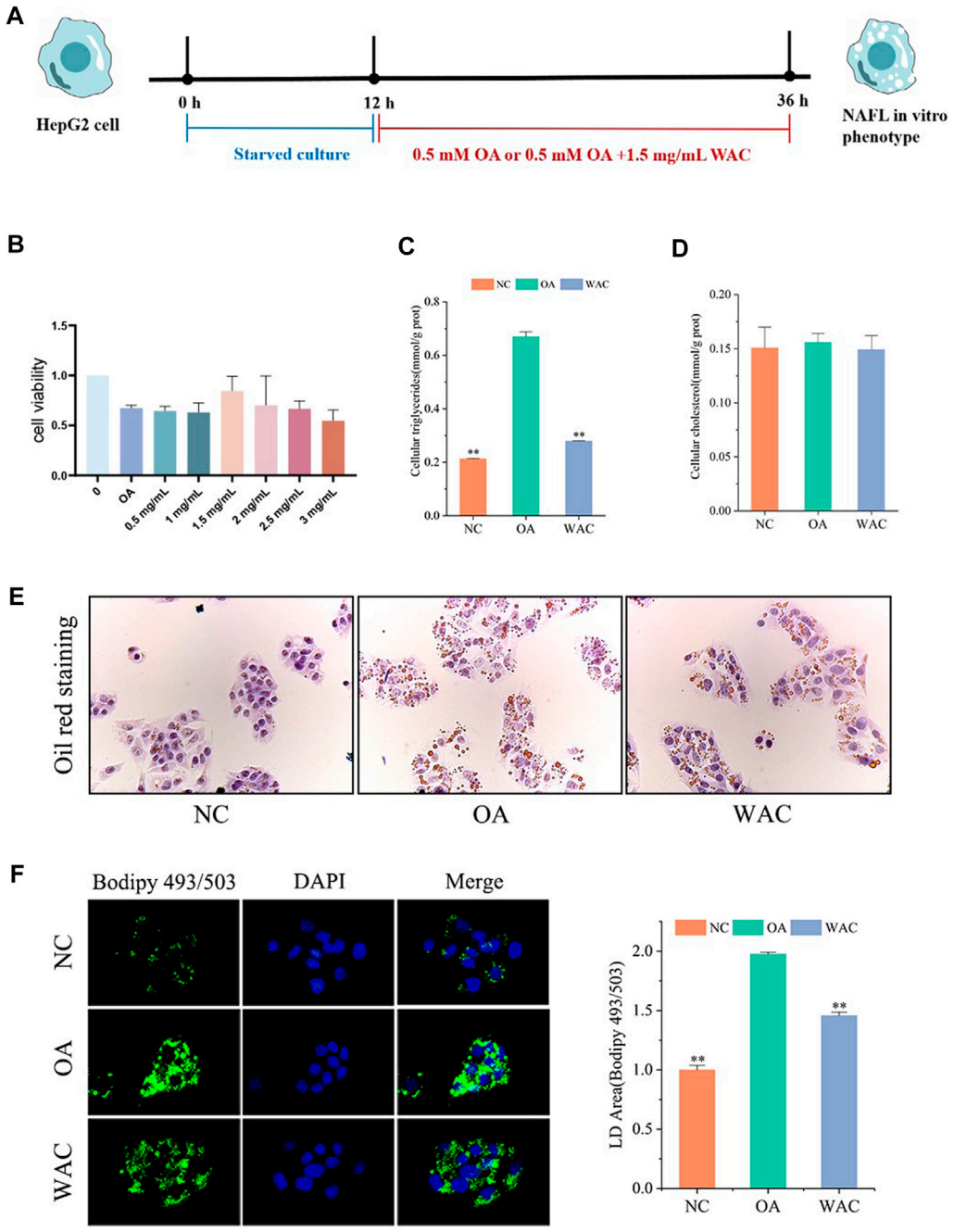

FIGURE 4
Effect of WAC on lipid accumulation in OA-induced HepG2 cells. **(A)** Cellular experimental procedures. **(B)** Cell viability. **(C,D)** Triglyceride and cholesterol levels in HepG2 cells. **(E)** Graph of oil red O staining results. **(F)** Graph of BODIPY staining results. Compared with OA, * indicates $p < 0.05$ and ** indicates $p < 0.01$.

levels were significantly elevated in mice in the HFD group, and WAC treatment significantly decreased the elevated SREBP-1c protein levels (Figures 5C,D). The qRT-PCR results showed that WAC decreased the expression of the lipid synthesis genes *FASN*, *ACC*, *SREBP-1c* and *SCD-1* caused by the high-fat diet (Figure 5E). These results suggest that WAC activates PI3K/AKT and AMPK and decreases SREBP-1c expression.

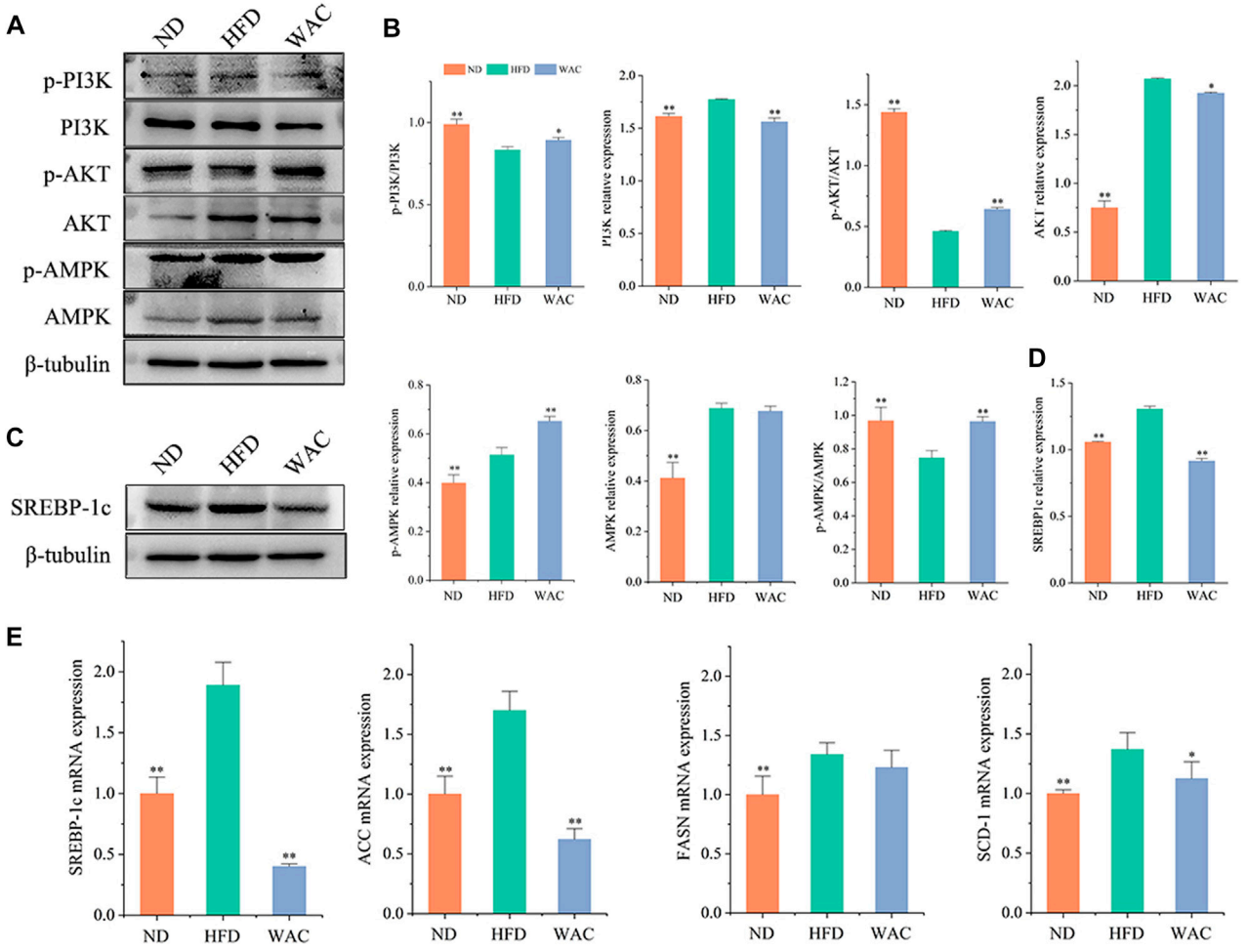

FIGURE 5
Effect of WAC on PI3K, AKT, AMPK phosphorylation and SREBP-1c protein expression in HFD-induced NAFLD mice. **(A,B)** Phosphorylation and total protein levels of PI3K, AKT, and AMPK in mouse liver. **(C,D)** Protein levels of SREBP-1c in mouse liver. **(E)** The mRNA levels of mouse liver FASN, ACC, SREBP-1c and SCD-1. Compared with HFD, * indicates $p < 0.05$ and ** indicates $p < 0.01$.

3.6 WAC activates PI3K/AKT and AMPK *in vitro*

In vitro, total PI3K and AKT and their phosphorylation levels, AMPK and p-AMPK protein levels were measured by protein blotting, and the trends were the same as *in vivo*. The phosphorylated PI3K and AKT protein levels were decreased, p-PI3K/PI3K levels were decreased, AMPK protein levels were significantly increased and p-AMPK protein levels were decreased in HepG2 cells of OA group. After WAC treatment of HepG2 cells, the above results were reversed (Figures 6A–D). As with the results of *in vivo* experiments, SREBP-1c protein levels were significantly elevated in HepG2 cells in the OA group compared with the NC group, and WAC treatment reversed the elevated SREBP-1 protein levels (Figures 6C,D). Immunofluorescence staining of OA and WAC-treated cells using SREBP-1c antibody showed that WAC significantly reduced SREBP-1c expression in HepG2 cells (Figure 6E). WAC decreased OA-induced mRNA expression of the elevated expression of the lipid synthesis genes *FASN*, *ACC*, *SREBP-1c* and *SCD-1* (Figure 6F).

3.7 WAC reduces lipogenesis in HepG2 cells

We further verified whether SREBP-1c acts as a target of WAC to reduce lipid synthesis. We treated HepG2 cells with the SREBP-1c inhibitor Fatostatin (FATO) *in vitro* and performed subsequent experiments (Figure 7A). After WAC treatment of HepG2 cells, TG was significantly reduced, but

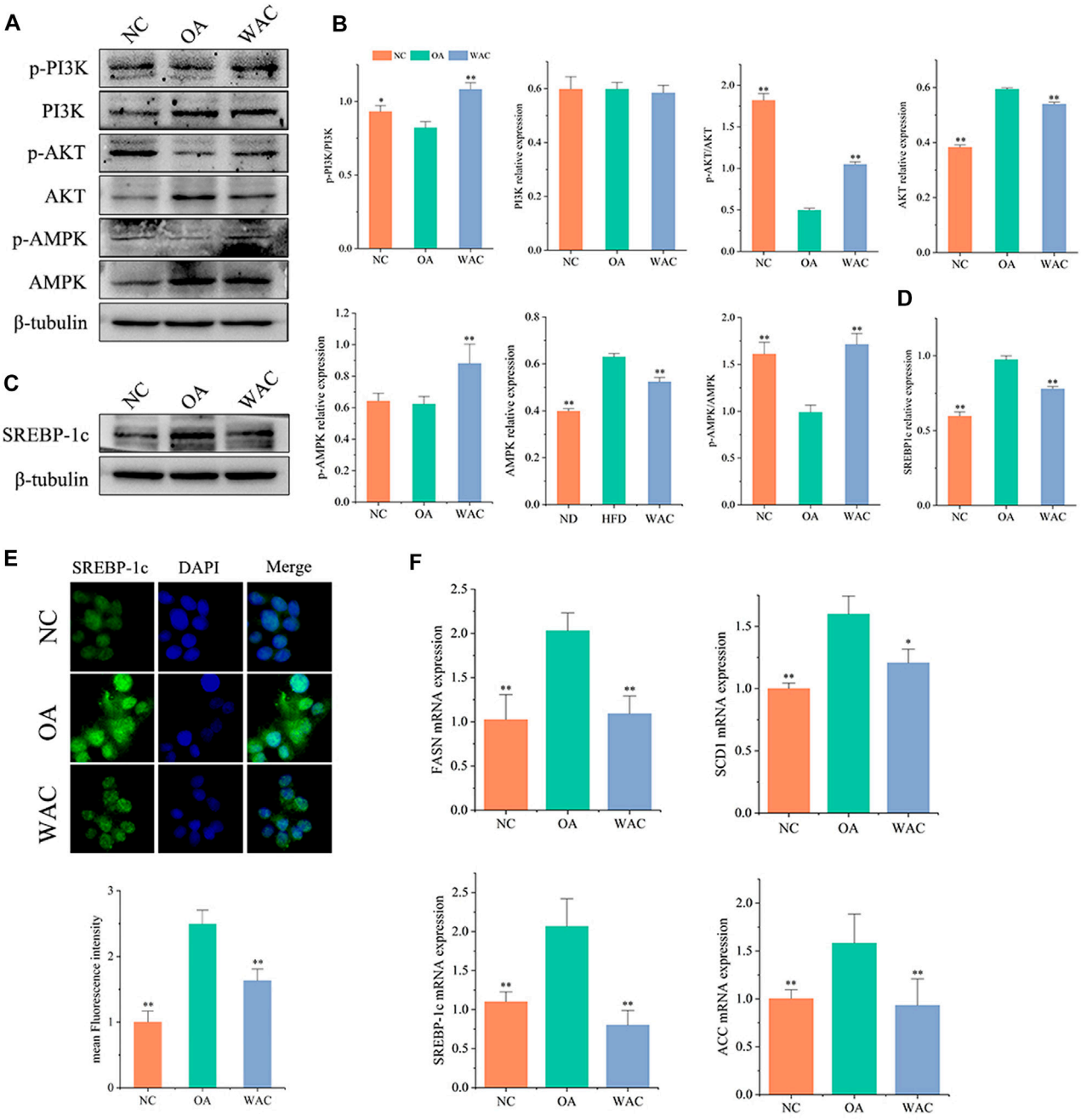

FIGURE 6
Effect of WAC on OA-induced PI3K, AKT, AMPK phosphorylation and SREBP-1c protein expression in HepG2 cells. **(A,B)** Phosphorylation of PI3K, AKT, AMPK and total protein levels in HepG2 cells. **(C,D)** Protein levels of SREBP-1c in HepG2 cells. **(E)** Graph of SREBP-1c immunofluorescence results. **(F)** mRNA levels of FASN, ACC, SREBP-1c and SCD-1 in HepG2 cells. Compared with OA, * indicates $p < 0.05$ and ** indicates $p < 0.01$.

TC remained unchanged significantly (Figures 7B,C). Oil red staining and BODIPY493/503 staining also demonstrated that WAC reduced the number of lipid droplets and lipid accumulation (Figures 7D,E). The expression of adipogenesis-related proteins SCD1, FAS and DGAT2 was also examined, and WAC reduced the protein

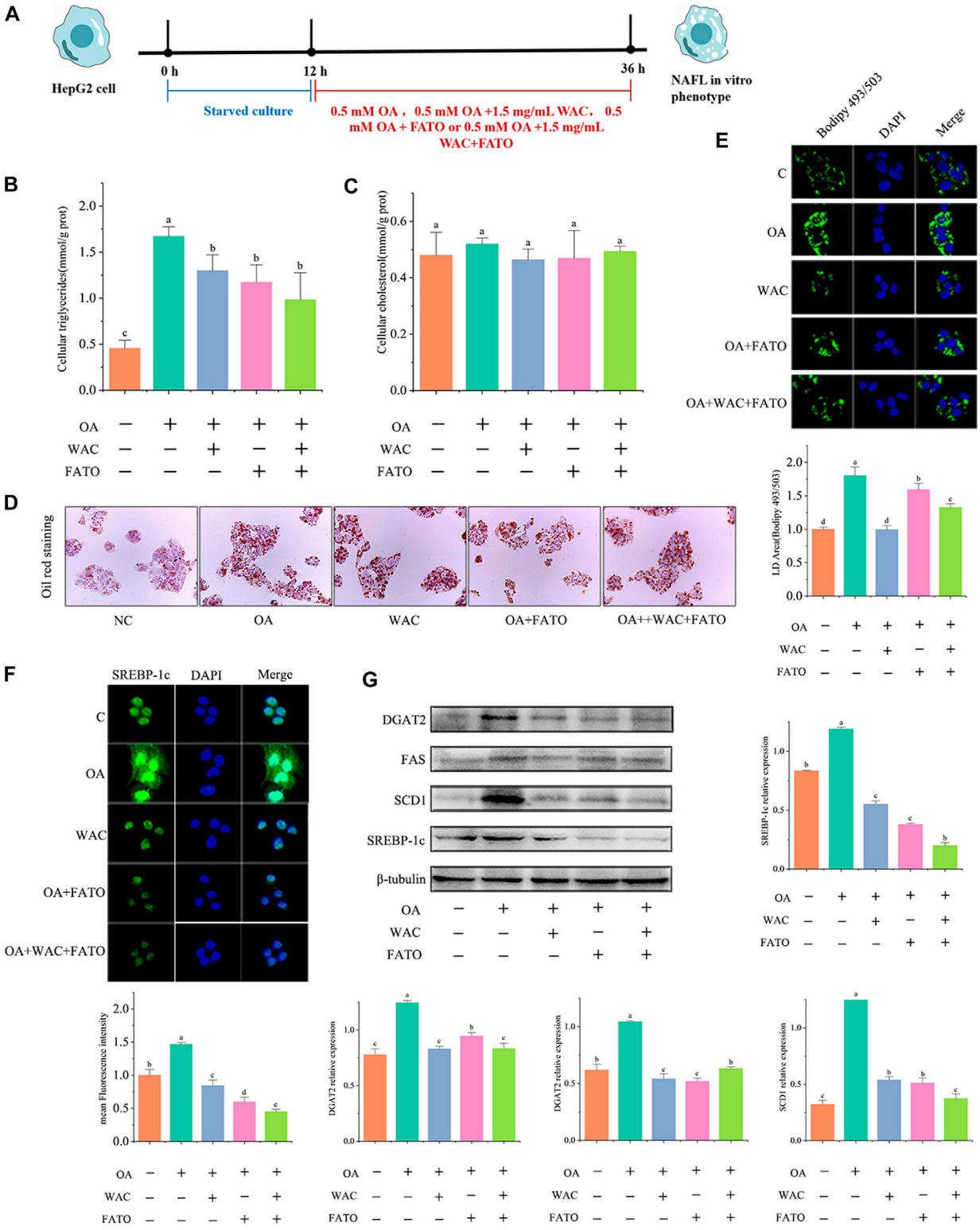

FIGURE 7
Effect of WAC on SREBP-1c in HepG2 cells. **(A)** Experimental procedure of cells after the addition of FATO. **(B,C)** Triglyceride and cholesterol levels in HepG2 cells. **(D)** Graph of oil red O staining results. **(E)** Graph of BODIPY staining results. **(F)** Graph of SREBP-1c immunofluorescence results. **(G)** SREBP-1c, SCD1, FAS, DGAT2 protein levels in HepG2 cells. Different letters represent significant differences.

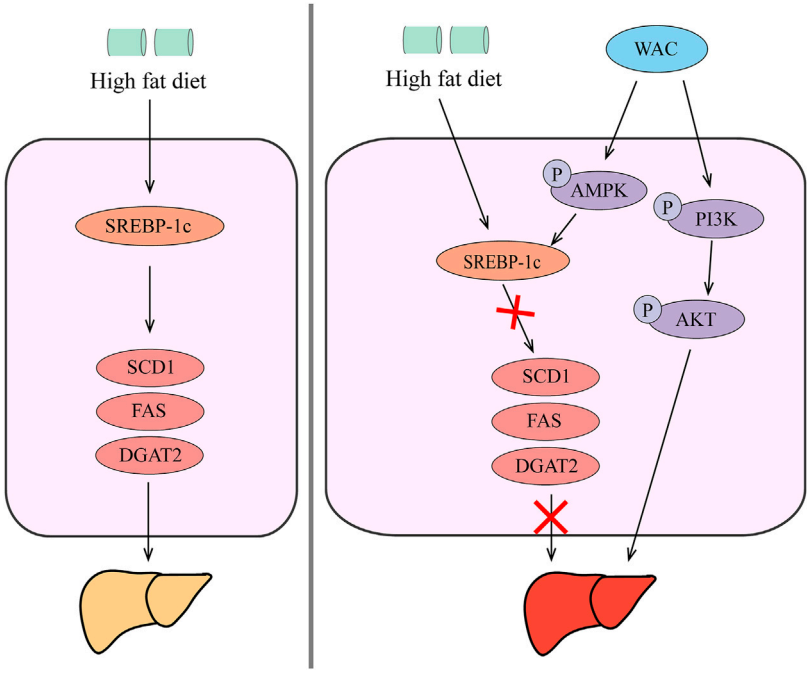

FIGURE 8
Schematic diagram of the mechanism by which WAC improves NAFLD. WAC activates PI3K/AKT pathway, activates AMPK to promote SREBP-1c expression, thereby reducing hepatic TG synthesis and lipid synthesis.

expression levels of SCD1, FAS and DGAT2 compared with the model group (Figure 7G). With the SREBP-1c inhibitor FATO, the trend of action was the same as that of WAC. The above results suggest that WAC reduces lipogenesis in HepG2 cells and is able to regulate the SREBP-1c pathway.

4 Discussion

HFD-fed C57BL/6 mice for 16 weeks were successfully constructed as a model of NAFLD. WAC intervention reversed the abnormal levels of TG, TC, GLU, HDL, LDL in serum and TG and TC in liver of mice induced by high-fat diet, and the results of liver pathology tests indicated that WAC reduced the number of hepatic lipid droplets. The results of *in vitro* experiments were also similar, indicating that WAC has the effect of promoting lipid metabolism and reducing the accumulation of lipids in the liver. By using LC/MS technology, Zhao et al. detected nine Nine chlorogenic acid analogues of AC, including chlorogenic acid, cryptochlorogenic acid, neochlorogenic acid, 3,5-dicaffeoylquinic acid, 4,5-dicaffeoylquinic acid, 3,4-dicaffeoylquinic acid, chlorogenic acid methyl ester, cryptochlorogenic acid methyl ester, neochlorogenic acid methyl ester (Zhao et al., 2014). The active components of WAC were identified by LC-MS. Recent studies have found that chlorogenic acid (CGA) inhibits adipocyte differentiation and triglyceride (TG) accumulation (Liu et al., 2021), and caffeic acid (CA) reduces gene expression related to fatty acid synthesis and improves hepatic steatosis (Kim et al., 2018), therefore, we hypothesize that the active substances of WAC that promote lipid metabolism are chlorogenic acid analogues.

PI3K/AKT signaling pathway plays an important role in the development of NAFLD (Huang et al., 2018; Santoleri and Titchenell, 2019). Insulin is recruited through insulin receptor substrate (IRS) and activates PI3K. Activated PI3K signals to its downstream target kinase AKT (Osorio-Fuentealba and Klip, 2015), which inhibits GSK3. GSK3 promotes the degradation of mature SREBP-1c (Cross et al., 1995), which mediates lipid metabolism (Lagathu et al., 2006). SREBP-1c is a major regulator of fatty acid synthesis in the liver (Osborne and Espenshade, 2022). It can control the amount of TG *in vivo* by regulating acetyl coenzyme A carboxylase 1 (ACC1), fatty acid synthase (FASN), stearoyl coenzyme A desaturase (SCD-1) and other enzymes or proteins related to fatty acid synthesis (Wang et al., 2015). In mouse liver and *in vitro* cultured HepG2 cells, we observed that HFD and OA impaired PI3K/AKT signaling pathway and up-regulated SREBP-1c protein expression, whereas WAC increased PI3K/AKT phosphorylation and decreased SREBP-1c expression. WAC decreased TG content and reduced lipid deposition in liver and HepG2 cells. Although there are no reports of WAC affecting

NAFLD through the PI3K/AKT signaling pathway, it has been shown that chlorogenic acid prevents HFD-induced hepatic steatosis and may achieve this effect by modulating intestinal flora and increasing GLP-1 secretion (Jiang et al., 2022).

AMPK is a member of the serine/threonine kinase family and has the role of SREBP-1c, a factor that regulates energy homeostasis (Desjardins and Steinberg, 2018). In recent years, the AMPK signaling pathway has been shown to be associated with the alleviation of metabolic disorders in many studies on the treatment of NAFLD. Activation of AMPK signaling pathway is a common feature of NAFLD treatment (Chen et al., 2019; Zhou et al., 2021; Chen et al., 2022; Kim et al., 2022; Liao et al., 2022; Zhang and Feng, 2022). Activated AMPK signaling pathway in the liver reduces NAFLD mainly by reducing lipid production in the liver and regulating fatty acid oxidation in the liver (Day et al., 2017; von Loeffelholz et al., 2021). AMPK is an upstream kinase of SREBP-1c (Zhao et al., 2022). It can inhibit the expression of genes related to lipid synthesis such as SREBP-1c (Kim et al., 2020), and reduce hepatic TG synthesis. In this experiments, p-AMPK/AMPK and SREBP-1c protein expression were detected by western blotting. The results showed that WAC reversed the trend of decreased p-AMPK/AMPK protein expression and increased SREBP-1c expression in HFD mouse hepatocytes and OA-induced HepG2 cells. This indicated that the AMPK/SREBP-1c pathway was activated by WAC. The mRNA expression of the lipid synthesis genes FASN, ACC, SREBP-1c and SCD-1 was also observed by qRT-PCR. This showed that WAC significantly reduced the expression of the above lipid synthesis genes. In summary, WAC reduces TG synthesis in liver and HepG2 cells by activating PI3K/AKT pathway and AMPK to decrease SREBP-1c expression and alleviate hepatic steatosis.

SCD1, FAS and DGAT2 are all downstream factors of SREBP-1c. FAS and SCD1 are known to be involved in the *ab initio* synthesis, esterification and desaturation of fatty acids. DGAT2 catalyzes the final step of TG production and accelerates hepatic lipid synthesis (Liu et al., 2012; Shimano and Sato, 2017). We found that AMPK could regulate the expression of SREBP-1c. To verify whether SREBP-1c is the target of WAC action, we further inhibited SREBP-1c with inhibitors *in vitro* and found that the results after inhibition were consistent with the trend of WAC action results. The expression of SCD1, FAS, and DGAT2 were all inhibited after inhibition of SREBP-1c. The above results indicate that SREBP-1c is the pathway of WAC action, and WAC can regulate the SREBP-1c pathway and reduce lipogenesis in HepG2 cells.

Our experiments showed that WAC can activate PI3K/AKT pathway and AMPK and thus reduce hepatic TG synthesis, but there are some limitations. In this experiment, we did not investigate the specific relationship between PI3K/AKT pathway and AMPK each with SREBP-1c expression by further experiments. This is the focus of our follow-up study.

In summary, our *in vivo* and *in vitro* studies showed that WAC activates PI3K/AKT pathway, activates AMPK to promote SREBP-1c expression, thereby reducing hepatic TG synthesis and lipid synthesis (Figure 8). Therefore, AC could be used as a potential health herb for improving NAFLD and obesity.

Data availability statement

The raw data supporting the conclusions of this article will be made available by the authors, without undue reservation.

Ethics statement

All experiments were conducted in accordance with the NEAU animal use and ethics policy. All animal experiments were approved by the Northeastern Agricultural University Experimental Animal Welfare and Ethics Committee (NEAUEC-20210219).

Author contributions

ML: Conceptualization; Data curation and analysis; Writing. MH: Validation; Data analysis. YG: Validation. YZ: Data curation. XX: Data curation. JX: Data curation. LF: Data curation. HW: Data curation. XJ: Review. WY: Review and editing.

Conflict of interest

The authors declare that the research was conducted in the absence of any commercial or financial relationships that could be construed as a potential conflict of interest.

Publisher's note

All claims expressed in this article are solely those of the authors and do not necessarily represent those of their affiliated organizations, or those of the publisher, the editors and the reviewers. Any product that may be evaluated in this article, or claim that may be made by its manufacturer, is not guaranteed or endorsed by the publisher.

Supplementary material

The Supplementary Material for this article can be found online at: https://www.frontiersin.org/articles/10.3389/fphar.2022.1084435/full#supplementary-material

References

Boudreau, A., Richard, A. J., Burrell, J. A., King, W. T., Dunn, R., Schwarz, J. M., et al. (2018). An ethanolic extract of Artemisia scoparia inhibits lipolysis *in vivo* and has antilipolytic effects on murine adipocytes *in vitro*. *Am. J. Physiol. Endocrinol. Metab.* 315 (5), E1053–e1061. doi:10.1152/ajpendo.00177.2018

Chalasani, N., Younossi, Z., Lavine, J. E., Charlton, M., Cusi, K., Rinella, M., et al. (2018). The diagnosis and management of nonalcoholic fatty liver disease: Practice guidance from the American Association for the Study of Liver Diseases. *Hepatology* 67 (1), 328–357. doi:10.1002/hep.29367

Chen, K., Chen, X., Xue, H., Zhang, P., Fang, W., Chen, X., et al. (2019). Coenzyme Q10 attenuates high-fat diet-induced non-alcoholic fatty liver disease through activation of the AMPK pathway. *Food Funct.* 10 (2), 814–823. doi:10.1039/c8fo01236a

Chen, H., Nie, T., Zhang, P., Ma, J., and Shan, A. (2022). Hesperidin attenuates hepatic lipid accumulation in mice fed high-fat diet and oleic acid induced HepG2 via AMPK activation. *Life Sci.* 296, 120428. doi:10.1016/j.lfs.2022.120428

Cho, A. S., Jeon, S. M., Kim, M. J., Yeo, J., Seo, K. I., Choi, M. S., et al. (2010). Chlorogenic acid exhibits anti-obesity property and improves lipid metabolism in high-fat diet-induced-obese mice. *Food Chem. Toxicol.* 48 (3), 937–943. doi:10.1016/j.fct.2010.01.003

Choi, M. K., Han, J. M., Kim, H. G., Lee, J. S., Lee, J. S., Wang, J. H., et al. (2013). Aqueous extract of Artemisia capillaris exerts hepatoprotective action in alcohol-pyrazole-fed rat model. *J. Ethnopharmacol.* 147 (3), 662–670. doi:10.1016/j.jep.2013.03.065

Cohen, J. C., Horton, J. D., and Hobbs, H. H. (2011). Human fatty liver disease: old questions and new insights. *Science* 332 (6037), 1519–1523. doi:10.1126/science.1204265

Cross, D. A., Alessi, D. R., Cohen, P., Andjelkovich, M., and Hemmings, B. A. (1995). Inhibition of glycogen synthase kinase-3 by insulin mediated by protein kinase B. *Nature* 378 (6559), 785–789. doi:10.1038/378785a0

Dai, Y., Dou, Z., Zhou, R., Luo, L., Bian, L., Chen, Y., et al. (2021). Quality evaluation of Artemisia capillaris Thunb. Based on qualitative analysis of the HPLC fingerprint and UFLC-Q-TOF-MS/MS combined with quantitative analysis of multicomponents. *J. Anal. Methods Chem.* 2021, 5546446. doi:10.1155/2021/5546446

Day, E. A., Ford, R. J., and Steinberg, G. R. (2017). AMPK as a therapeutic target for treating metabolic diseases. *Trends Endocrinol. Metab.* 28 (8), 545–560. doi:10.1016/j.tem.2017.05.004

Desjardins, E. M., and Steinberg, G. R. (2018). Emerging role of AMPK in Brown and beige adipose tissue (BAT): Implications for obesity, insulin resistance, and type 2 diabetes. *Curr. Diab. Rep.* 18 (10), 80. doi:10.1007/s11892-018-1049-6

Diehl, A. M., and Day, C. (2017). Cause, pathogenesis, and treatment of nonalcoholic steatohepatitis. *N. Engl. J. Med.* 377 (21), 2063–2072. doi:10.1056/NEJMra1503519

Fukuda, T., Hamaguchi, M., Kojima, T., Mitsuhashi, K., Hashimoto, Y., Ohbora, A., et al. (2016). Transient remission of nonalcoholic fatty liver disease decreases the risk of incident type 2 diabetes mellitus in Japanese men. *Eur. J. Gastroenterol. Hepatol.* 28 (12), 1443–1449. doi:10.1097/meg.0000000000000736

Galluzzi, L., Vitale, I., Aaronson, S. A., Abrams, J. M., Adam, D., Agostinis, P., et al. (2018). Molecular mechanisms of cell death: Recommendations of the nomenclature committee on cell death 2018. *Cell Death Differ.* 25 (3), 486–541. doi:10.1038/s41418-017-0012-4

Garcia, D., and Shaw, R. J. (2017). AMPK: Mechanisms of cellular energy sensing and restoration of metabolic balance. *Mol. Cell* 66 (6), 789–800. doi:10.1016/j.molcel.2017.05.032

Garcia, D., Hellberg, K., Chaix, A., Wallace, M., Herzig, S., Badur, M. G., et al. (2019). Genetic liver-specific AMPK activation protects against diet-induced obesity and NAFLD. *Cell Rep.* 26 (1), 192–208. doi:10.1016/j.celrep.2018.12.036

Hardie, D. G. (2015). AMPK: Positive and negative regulation, and its role in whole-body energy homeostasis. *Curr. Opin. Cell Biol.* 33, 1–7. doi:10.1016/j.ceb.2014.09.004

Horton, J. D., Goldstein, J. L., and Brown, M. S. (2002). SREBPs: activators of the complete program of cholesterol and fatty acid synthesis in the liver. *J. Clin. Invest.* 109 (9), 1125–1131. doi:10.1172/jci15593

Hsueh, T. P., Lin, W. L., Dalley, J. W., and Tsai, T. H. (2021). The pharmacological effects and pharmacokinetics of active compounds of Artemisia capillaris. *Biomedicines* 9 (10), 1412. doi:10.3390/biomedicines9101412

Huang, X., Liu, G., Guo, J., and Su, Z. (2018). The PI3K/AKT pathway in obesity and type 2 diabetes. *Int. J. Biol. Sci.* 14 (11), 1483–1496. doi:10.7150/ijbs.27173

Huang, D. Q., El-Serag, H. B., and Loomba, R. (2021). Global epidemiology of NAFLD-related HCC: trends, predictions, risk factors and prevention. *Nat. Rev. Gastroenterol. Hepatol.* 18 (4), 223–238. doi:10.1038/s41575-020-00381-6

Huang, G., Zhu, Y., Yong, C., Tian, F., Liu, L., Wu, Q., et al. (2022). Artemisia capillaris Thunb. water extract attenuates adriamycin-induced renal injury by regulating apoptosis through the ROS/MAPK axis. *J. Food Biochem.* 46 (2), e14065. doi:10.1111/jfbc.14065

Irimia, J. M., Meyer, C. M., Segvich, D. M., Surendran, S., DePaoli-Roach, A. A., Morral, N., et al. (2017). Lack of liver glycogen causes hepatic insulin resistance and steatosis in mice. *J. Biol. Chem.* 292 (25), 10455–10464. doi:10.1074/jbc.M117.786525

Jiang, H., Mao, T., Liu, Y., Tan, X., Sun, Z., Cheng, Y., et al. (2022). Protective effects and mechanisms of yinchen linggui zhugan decoction in HFD-induced nonalcoholic fatty liver disease rats based on network Pharmacology and experimental verification. *Front. Pharmacol.* 13, 908128. doi:10.3389/fphar.2022.908128

Kamikubo, R., Kai, K., Tsuji-Naito, K., and Akagawa, M. (2016). β-Caryophyllene attenuates palmitate-induced lipid accumulation through AMPK signaling by activating CB2 receptor in human HepG2 hepatocytes. *Mol. Nutr. Food Res.* 60 (10), 2228–2242. doi:10.1002/mnfr.201600197

Kim, H. M., Kim, Y., Lee, E. S., Huh, J. H., and Chung, C. H. (2018). Caffeic acid ameliorates hepatic steatosis and reduces ER stress in high fat diet-induced obese mice by regulating autophagy. *Nutrition* 55-56, 63–70. doi:10.1016/j.nut.2018.03.010

Kim, M. H., Seong, J. B., Huh, J. W., Bae, Y. C., Lee, H. S., and Lee, D. S. (2020). Peroxiredoxin 5 ameliorates obesity-induced non-alcoholic fatty liver disease through the regulation of oxidative stress and AMP-activated protein kinase signaling. *Redox Biol.* 28, 101315. doi:10.1016/j.redox.2019.101315

Kim, E., Jang, E., and Lee, J. H. (2022). Potential roles and key mechanisms of hawthorn extract against various liver diseases. *Nutrients* 14 (4), 867. doi:10.3390/nu14040867

Lagathu, C., Yvan-Charvet, L., Bastard, J. P., Maachi, M., Quignard-Boulangé, A., Capeau, J., et al. (2006). Long-term treatment with interleukin-1beta induces insulin resistance in murine and human adipocytes. *Diabetologia* 49 (9), 2162–2173. doi:10.1007/s00125-006-0335-z

Li, X., Yao, Y., Wang, Y., Hua, L., Wu, M., Chen, F., et al. (2022). Effect of hesperidin supplementation on liver metabolomics and gut microbiota in a high-fat diet-induced NAFLD mice model. *J. Agric. Food Chem.* 70 (36), 11224–11235. doi:10.1021/acs.jafc.2c02334

Liao, M., Sun, C., Li, R., Li, W., Ge, Z., Adu-Frimpong, M., et al. (2022). Amelioration action of gastrodigenin rhamno-pyranoside from Moringa seeds on non-alcoholic fatty liver disease. *Food Chem.* 379, 132087. doi:10.1016/j.foodchem.2022.132087

Liu, Q., Siloto, R. M., Lehner, R., Stone, S. J., and Weselake, R. J. (2012). Acyl-CoA: diacylglycerol acyltransferase: molecular biology, biochemistry and biotechnology. *Prog. Lipid Res.* 51 (4), 350–377. doi:10.1016/j.plipres.2012.06.001

Liu, M., Qin, J., Cong, J., and Yang, Y. (2021). Chlorogenic acids inhibit adipogenesis: Implications of wnt/β-catenin signaling pathway. *Int. J. Endocrinol.* 2021, 2215274. doi:10.1155/2021/2215274

Lonardo, A., Byrne, C. D., Caldwell, S. H., Cortez-Pinto, H., and Targher, G. (2016). Global epidemiology of nonalcoholic fatty liver disease: Meta-analytic assessment of prevalence, incidence, and outcomes. *Hepatology* 64 (4), 1388–1389. doi:10.1002/hep.28584

Luo, P., Dai, W., Yin, P., Zeng, Z., Kong, H., Zhou, L., et al. (2015). Multiple reaction monitoring-ion pair finder: a systematic approach to transform nontargeted mode to pseudotargeted mode for metabolomics study based on liquid chromatography-mass spectrometry. *Anal. Chem.* 87 (10), 5050–5055. doi:10.1021/acs.analchem.5b00615

Osborne, T. F., and Espenshade, P. J. (2022). Lipid balance must be just right to prevent development of severe liver damage. *J. Clin. Invest.* 132 (11), e160326. doi:10.1172/jci160326

Osorio-Fuentealba, C., and Klip, A. (2015). Dissecting signalling by individual Akt/PKB isoforms, three steps at once. *Biochem. J.* 470 (2), e13–e16. doi:10.1042/bj20150750

Ratziu, V., Francque, S., and Sanyal, A. (2022). Breakthroughs in therapies for NASH and remaining challenges. *J. Hepatol.* 76 (6), 1263–1278. doi:10.1016/j.jhep.2022.04.002

Samovski, D., Sun, J., Pietka, T., Gross, R. W., Eckel, R. H., Su, X., et al. (2015). Regulation of AMPK activation by CD36 links fatty acid uptake to β-oxidation. *Diabetes* 64 (2), 353–359. doi:10.2337/db14-0582

Santoleri, D., and Titchenell, P. M. (2019). Resolving the paradox of hepatic insulin resistance. *Cell. Mol. Gastroenterol. Hepatol.* 7 (2), 447–456. doi:10.1016/j.jcmgh.2018.10.016

Shimano, H., and Sato, R. (2017). SREBP-Regulated lipid metabolism: convergent physiology - divergent pathophysiology. *Nat. Rev. Endocrinol.* 13 (12), 710–730. doi:10.1038/nrendo.2017.91

Tang, H., Yu, R., Liu, S., Huwatibieke, B., Li, Z., and Zhang, W. (2016). Irisin inhibits hepatic cholesterol synthesis via AMPK-SREBP2 signaling. *EBioMedicine* 6, 139–148. doi:10.1016/j.ebiom.2016.02.041

von Loeffelholz, C., Coldewey, S. M., and Birkenfeld, A. L. (2021). A narrative review on the role of AMPK on de novo lipogenesis in non-alcoholic fatty liver disease: Evidence from human studies. *Cells* 10 (7), 1822. doi:10.3390/cells10071822

Wang, Y., Viscarra, J., Kim, S. J., and Sul, H. S. (2015). Transcriptional regulation of hepatic lipogenesis. *Nat. Rev. Mol. Cell Biol.* 16 (11), 678–689. doi:10.1038/nrm4074

Want, E. J., Masson, P., Michopoulos, F., Wilson, I. D., Theodoridis, G., Plumb, R. S., et al. (2013). Global metabolic profiling of animal and human tissues via UPLC-MS. *Nat. Protoc.* 8 (1), 17–32. doi:10.1038/nprot.2012.135

Xie, C., Chen, Z., Zhang, C., Xu, X., Jin, J., Zhan, W., et al. (2016). Dihydromyricetin ameliorates oleic acid-induced lipid accumulation in L02 and HepG2 cells by inhibiting lipogenesis and oxidative stress. *Life Sci.* 157, 131–139. doi:10.1016/j.lfs.2016.06.001

Yuan, H. J., Li, W., Jin, J. M., Chen, J. J., Jiang, J., Wang, H., et al. (2017). Research progress on chemical constituents, pharmacological mechanism and clinical application of Guizhi decoction. *Zhongguo Zhong Yao Za Zhi* 42 (23), 4556–4564. doi:10.19540/j.cnki.cjcmm.20170928.010

Zhang, J., and Feng, Q. (2022). Pharmacological effects and molecular protective mechanisms of Astragalus polysaccharides on nonalcoholic fatty liver disease. *Front. Pharmacol.* 13, 854674. doi:10.3389/fphar.2022.854674

Zhao, Y., Geng, C. A., Ma, Y. B., Huang, X. Y., Chen, H., Cao, T. W., et al. (2014). UFLC/MS-IT-TOF guided isolation of anti-HBV active chlorogenic acid analogues from Artemisia capillaris as a traditional Chinese herb for the treatment of hepatitis. *J. Ethnopharmacol.* 156, 147–154. doi:10.1016/j.jep.2014.08.043

Zhao, X., Xue, X., Wang, C., Wang, J., Peng, C., and Li, Y. (2022). Emerging roles of sirtuins in alleviating alcoholic liver disease: A comprehensive review. *Int. Immunopharmacol.* 108, 108712. doi:10.1016/j.intimp.2022.108712

Zhou, F., Ding, M., Gu, Y., Fan, G., Liu, C., Li, Y., et al. (2021). Aurantio-obtusin attenuates non-alcoholic fatty liver disease through AMPK-mediated autophagy and fatty acid oxidation pathways. *Front. Pharmacol.* 12, 826628. doi:10.3389/fphar.2021.826628

frontiers | Frontiers in Pharmacology

TYPE Review
PUBLISHED 09 January 2023
DOI 10.3389/fphar.2022.1094405

OPEN ACCESS

EDITED BY
Guangyue Su,
Shenyang Pharmaceutical University, China

REVIEWED BY
Xu-Dong Zhou,
Hunan University of Chinese Medicine, China
Jianhua Xu,
Fujian Medical University, China

*CORRESPONDENCE
Jianyou Shi,
shijianyoude@126.com
Lan Bai,
blci@163.com

†These authors have contributed equally to this work

SPECIALTY SECTION
This article was submitted to Ethnopharmacology, a section of the journal Frontiers in Pharmacology

RECEIVED 10 November 2022
ACCEPTED 23 December 2022
PUBLISHED 09 January 2023

CITATION
Peng H, Zhong L, Cheng L, Chen L, Tong R, Shi J and Bai L (2023), *Ganoderma lucidum*: Current advancements of characteristic components and experimental progress in anti-liver fibrosis. *Front. Pharmacol.* 13:1094405. doi: 10.3389/fphar.2022.1094405

Ganoderma lucidum: Current advancements of characteristic components and experimental progress in anti-liver fibrosis

Haoyuan Peng[1†], Lei Zhong[2†], Lin Cheng[3†], Lu Chen[2], Rongsheng Tong[2,1], Jianyou Shi[2,1]* and Lan Bai[2,1]*

[1]The State Key Laboratory of Southwestern Chinese Medicine Resources, Department of Pharmacy, Chengdu University of Traditional Chinese Medicine, Chengdu, China, [2]Department of Pharmacy, Personalized Drug Therapy Key Laboratory of Sichuan Province, Sichuan Provincial People's Hospital, School of Medicine, University of Electronic Science and Technology of China, Chengdu, China, [3]College of Medicine, Southwest Jiaotong University, Chengdu, Sichuan, China

Ganoderma lucidum (G. lucidum, Lingzhi) is a well-known herbal medicine with a variety of pharmacological effects. Studies have found that *G. lucidum* has pharmacological effects such as antioxidant, antitumor, anti-aging, anti-liver fibrosis, and immunomodulation. The main active components of *G. lucidum* include triterpenoids, polysaccharides, sterols, peptides and other bioactive components. Among them, the triterpenoids and polysaccharide components of *G. lucidum* have a wide range of anti-liver fibrotic effects. Currently, there have been more reviews and studies on the antioxidant, antitumor, and anti-aging properties of *G. lucidum*. Based on the current trend of increasing number of liver fibrosis patients in the world, we summarized the role of *G.lucidum* extract in anti-liver fibrosis and the effect of *G. lucidum* extract on liver fibrosis induced by different pathogenesis, which were discussed and analyzed. Research and development ideas and references are provided for the subsequent application of *G. lucidum* extracts in anti-liver fibrosis treatment.

KEYWORDS

***Ganoderma lucidum*, liver fibrosis, triterpenes, polysaccharide, chromatography, pharmacology**

1 Introduction

Ganoderma lucidum is the dried fruiting entity of *G. lucidum (Leyss. ex Fr.) Karst.* or *Ganoderma purpurea* Zhao, Xu et Zhang, a fungus of the family Polyporaceae, which are one of the most well-known kinds of therapeutic fungi in China and a very representative large species of Chinese herbal medicine (Wang et al., 2017). *G. lucidum* has been utilized for over 2,000 years in China and has been recorded in Shennong Ben Cao Jing (Eastern Han Dynasty), Baopu Zi—Immortal Medicine (Eastern Jin Dynasty), Compendium of Materia Medica (Ming Dynasty), the Pharmacopoeia of the People's Republic of China (2000 edition), etc., (Luo et al., 2021) in various ancient books and modern standards. With both medicinal and edible properties, *G. lucidum* has been considered to have broad development prospects. In 2020, the State Administration for Market Regulation (China) included healthy food products such as *G. lucidum* in the raw material catalog (Luo et al., 2021), indicating that *G. lucidum* occupies an important position in the health food market in China. Meanwhile, *G. lucidum* has been added to the US Pharmacopoeia and the European Pharmacopoeia, indicating that *G. lucidum* is also widely used internationally. The bioactive substances of *G. lucidum*

TABLE 1 The main anti-fibrosis ingredients of *Ganoderma lucidum*.

Number	Category	Compound name	Ganoderma species	References
1	Triterpenes	Ganoderic acid A	*G. lucidum*	El-Mekkawy et al. (1998)
2	Triterpenes	Ganoderic acid B	*G. lucidum*	Kubota et al. (1982)
3	Triterpenes	Ganoderic acid C	*G. lucidum*	Seo et al. (2009)
4	Triterpenes	Ganoderic acid D	*G. lucidum*	Qiao et al. (2007)
5	Triterpenes	Ganoderic acid F	*G. lucidum*	Yang et al. (2012)
6	Triterpenes	Ganoderic acid G	*G. lucidum*	Kikuchi et al. (1985)
7	Triterpenes	Ganoderic acid H	*G. lucidum*	Yang et al. (2012)
8	Triterpenes	Ganoderic acid DM	*G. lucidum*	Adams et al. (2010)
9	Triterpenes	Ganoderic acid X	*G. lucidum*	Li et al. (2009)
10	Triterpenes	Lucidone A	*G. amboinense*	Gan et al. (1998)
11	Triterpenes	Lucidone B	*G. lucidum*	Nishitoba et al. (1985)
12	Triterpenes	Lucidone C	*G. lucidum*	Nishitoba et al. (1986)
13	Triterpenes	Lucidone D2	*G. lucidum*	Nishitoba et al. (1986)
14	Triterpenes	Ganoderal A	*G. lucidum*	Niedermeyer et al. (2005)
15	Triterpenes	Ganoderal B	*G. lucidum*	Nishitoba et al. (1988)
16	Triterpenes	Ganoderma lactone A	Ganoderma sp	Lakornwong et al. (2014)
17	Triterpeness	Ganoderma lactone D	Ganoderma sp	Lakornwong et al. (2014)
18	Triterpenes	Ganoderma lactone F	Ganoderma sp	Lakornwong et al. (2014)
19	Triterpenes	Ganoderma lactone G	Ganoderma sp	Lakornwong et al. (2014)
20	Triterpene	12-Hydroxy G-A C2	*G. lucidum*	Yang et al. (2007)
21	Triterpene	20-Hydroxy L-A A	*G. lucidum*	Ma et al. (2002)
22	Triterpene	20-Hydroxy L-A D2	*G. lucidum*	Akihisa et al. (2005)
23	Triterpene	20-Hydroxy L-A E2	*G. lucidum*	Akihisa et al. (2005)
24	Triterpene	20-Hydroxy L-A F	*G. lucidum*	Akihisa et al. (2005)
25	Triterpene	20-Hydroxy L-A N	*G. lucidum*	Akihisa et al. (2005)

include polysaccharides, triterpenes, sterols, peptides, and so on. The pharmacological effects of *G. lucidum* include antioxidant (Ferreira et al., 2009), antitumor/anticancer (Moradali et al., 2007), antimicrobial (Barros et al., 2007), immunomodulatory (Borchers et al., 2004), anti-inflammatory (Moro et al., 2012), antiatherogenic (Mori et al., 2008), and hypoglycemic effects (Hu et al., 2006). In recent years, a growing number of research have discovered that Ganoderma has multiple hepatoprotective benefits on different liver injuries, including alcoholic liver disease, viral hepatitis, autoimmune hepatitis, non-alcoholic fatty liver disease (NAFLD), hepatitis B, inflammation, fibrosis, and cholestatic liver diseases (Aydın and Akçalı, 2018).

The number of people with liver fibrosis is currently on the rise worldwide, and there is an urgent need to develop preventive and therapeutic measures against liver fibrosis. Therefore, in this paper, we searched databases such as PubMed and Web of Science for keywords such as *G. lucidum*, liver fibrosis, *G. lucidum* polysaccharides, and *G. lucidum* triterpenes for the discussion. Firstly, we summarized the reported anti-fibrotic components of *G. lucidum*. Secondly, we outlined the anti-fibrotic effects of *G. lucidum* extracts according to different pathogenic models and influencing factors of liver fibrosis. Finally, the discussions of existing studies showed the possible research directions that were proposed to provide research ideas and references for further development of the application of *G. lucidum* in anti-liver fibrotic diseases.

2 The main anti-fibrosis ingredients of *G. lucidum*

Fibrosis of the liver is a reversible liver disease. Modern research has found that *G. lucidum* encompasses *G. lucidum* polysaccharides, triterpenes, and other bioactive components, which have apparent anti-liver fibrosis pharmacological effects (Zhan et al., 2015; Xu et al., 2016). We summarized the specific components of *G. lucidum* anti-liver fibrosis reported in the

10.3389/fphar.2022.1094405

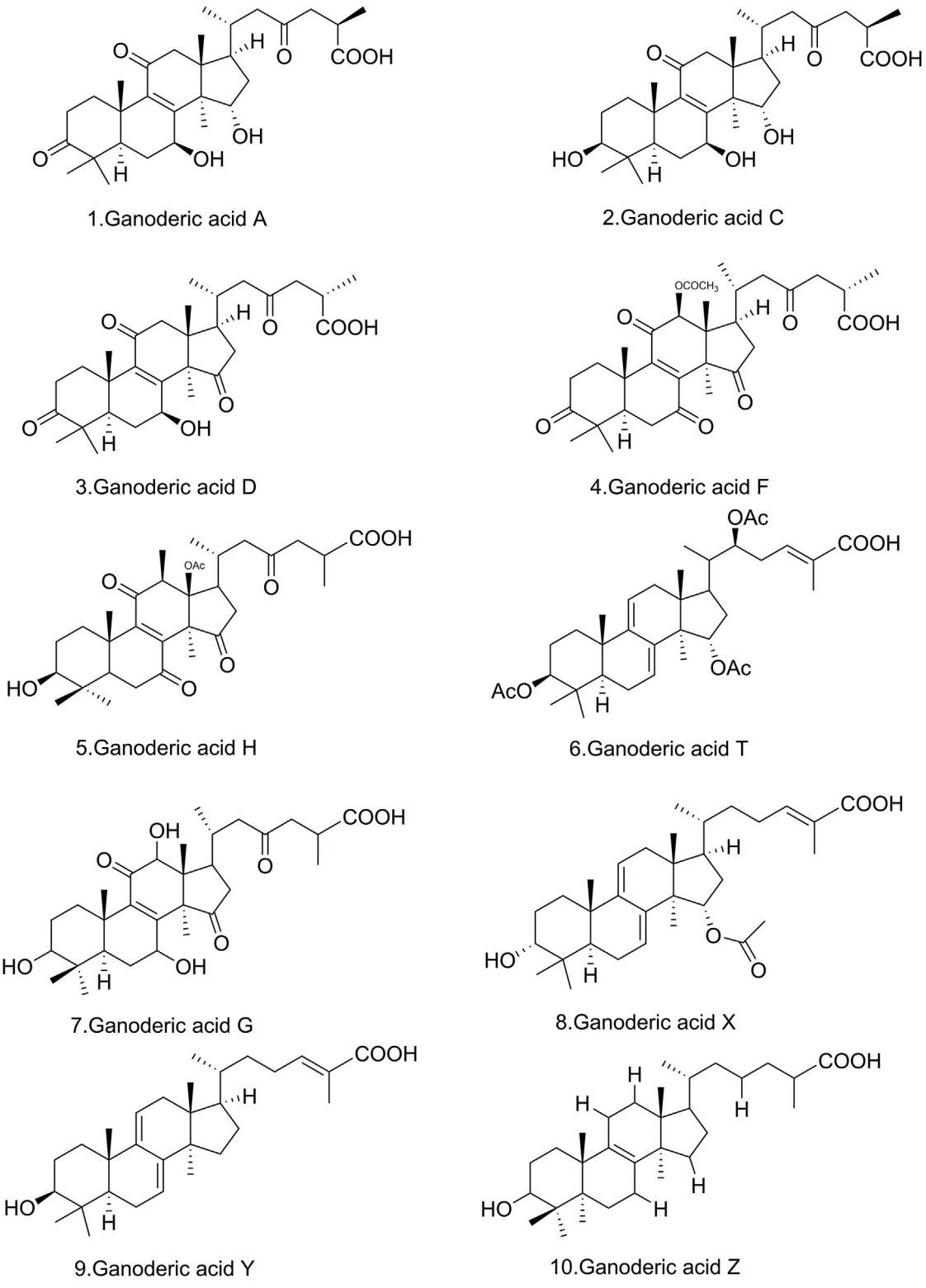

FIGURE 1
Chemical structure of the main active components of Ganoderma triterpenes.

literature so far, almost all of them are triterpenoids, and extracts of *G. lucidum* polysaccharides have also been reported to have anti-liver fibrosis effects, but the isolation of monomer components remains to be studied (Table 1).

G. lucidum triterpenes were found to have significant inhibitory proliferative effects on platelet-derived growth factor (PDGF)-BB-stimulated HSC-T6 (rat HSC) cell lines. 25 μg/mL *G. lucidum* triterpenes inhibited HSC-T6 cell proliferation and triggered

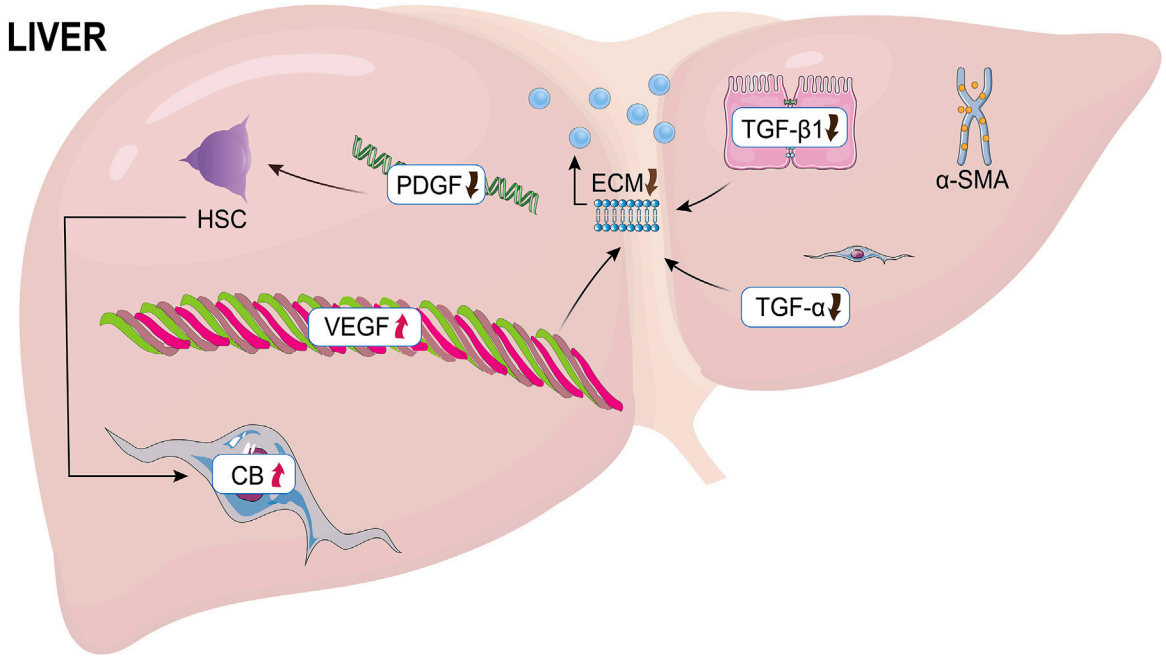

FIGURE 2
The causes of liver fibrosis. HSC, hepatic stellate cells; PDGF, Platelet-derived growth factor; ECM, extracellular matrix; VEGF, vascular endothelial growth factor; CB, cannabinoid.

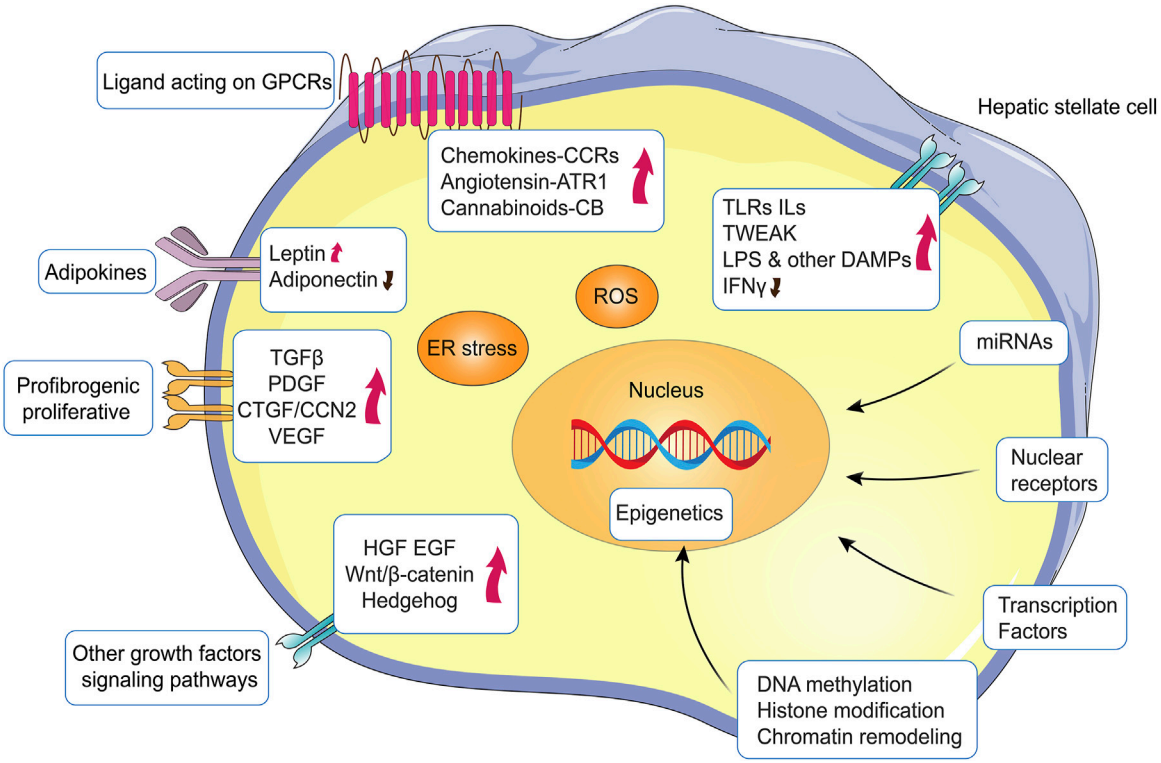

FIGURE 3
Major signaling pathways, molecules and mechanisms regulating HSC activation. HSC activation is regulated by a multitude of pathways and signaling molecules or events that can either sustain or inhibit HSC activation and subsequent proliferative and/or profibrogenic responses.

TABLE 2 Anti-hepatic fibrosis model of *G. lucidum* and the factors affecting it.

Pretreatment and liver fibrosis inducer	Influence parameter
D-Galactosamine	AST, ALT, SOD
Ethanol	MDA
CCl_4	GOT, GPT
High-fat food	TG, LDL
Formaldehyde	ALP, AST, ALT

AST, aspartate aminotransferase; ALT, alanine aminotransferase; SOD, superoxide dismutase; MDA, malondialdehyde; GPT, pyruvate aminotransferase; GOT, glutamate oxaloacetate transaminase; TG, triglycerides; LDL, low-density lipoprotein; ALP, alkaline phosphatase.

apoptosis. Meanwhile, the phosphorylation of cell cycle proteins D1, D2, and PDGFβR was inhibited, while the phosphorylation of *ß* was enhanced. Thus, the expression of α-SMA was inhibited. *G. lucidum* triterpene extract may inhibit the multiplication of PDGFβR-activated hepatic stellate cells by preventing the phosphorylation of platelet-derived growth factor, thus showing its effect against liver fibrosis (Wang et al., 2009; Qiu et al., 2019). *G. lucidum* triterpenes exerts anti-fibrotic effects on liver fibrosis through several mechanisms. They inhibited HSC proliferation and upregulated collagenase expression, thus inhibiting collagen deposition; *G. lucidum* was anti-oxidant activity, on the other hand, is crucial to its hepatoprotective impact (Qiu et al., 2019). These two methods combined successfully to slow the development of liver fibrosis (Wang et al., 2009; Qiu et al., 2019).

Several highly oxidized and pharmacologically active triterpenoids can be extracted from *G. lucidum* at present. *G. lucidum* acids were the primary source of pharmacological activity of *G. lucidum*; on the contrary, their triterpenoids containing carboxyl groups were generally called *G. lucidum* acids, which are highly oxidized derivatives of lanolin (Satria et al., 2019). These substances have complicated structures, high molecular weights, and high lipophilicity (Lin et al., 2003). Their main chemical structures are shown in Figure 1. The triterpenoids found naturally in Ganoderma originated from the intermediate wool sterol backbone. The cyclization of squalene-2,3-epoxide gives protosterol, a carbon-cationic intermediate that undergoes a further skeleton rearrangement, produces a tetracyclic wool sterol ($C_{30}H_{54}$) skeleton. Tetracyclic wool sterols play the role of intermediate molecules in the biosynthesis of various wool sterane triterpenes. The triterpenoids were uncommon secondary metabolites in the genus Ganoderma and were the products of side-chain degradation of wool sterane-type triterpenoids. The common triterpenoids in the genus Ganoderma have a carbon skeleton of 24 or 27 carbon atoms (Koo et al., 2021). The activity relationship analysis of triterpenoids isolated from *G. lucidum* revealed that the type of side chain, the C-3 carbonyl group, the number of double bonds, and the number of hydroxyl groups have a crucial impact in cytotoxicity (Wu et al., 2013).

Ganoderic acid's action may be mostly attributable to the hydroxylation of its fuzzy sterane triterpene structure. As illustrated in Figure 1, Ganoderic acid A (GA-A) is hydroxylated at positions 7 and 15, while Ganoderic acid H (GA-H) is hydroxylated at C-3, and inactive Ganoderic acid F (GAF) is not hydroxylated. Other triterpenes have hydroxyl or acetoxy groups at positions 3, 7, and 15, including Ganoderic acid C1 (GA-C1), Ganoderic acid C2 (GA-C2), and Ganoderic acid C3 (GA-C3) (GA-C2) (Siwulski et al., 2015), Ganoderic acid D (GA-D), Ganoderic acid T (GA-T) (Tang et al., 2006), Ganoderic acid X (GA-X), Ganoderic acid Y (GA-Y) (Hajjaj et al., 2005), Ganoderol A (Liu et al., 2006), Ganoderol B (Hajjaj et al., 2005), Ganoderol B (Liu et al., 2006), and Ganoderol glycol (Liu et al., 2006), were also shown to be inhibitors (Jiang et al., 2008). The structure and anti-liver fibrosis effect of *G. lucidum* triterpene extracts after isolation is also an urgent need for development and research nowadays.

3 Pathology, signal pathways and experimental models of hepatic fibrosis

Hepatic fibrosis formation demands the stimulation and proliferation of hepatic stellate cells (HSCs), as well as the accumulation of extracellular matrix (ECM), and simultaneous creation of α-smooth muscle actin (α-SMA) and type I collagen. PDGF-BB homodimers are strong ligands for PDGF receptors (PDGFRs), hence boosting the expansion of HSC. Inhibiting the activation and proliferation of activated HSCs, as well as inducing their death, are considered therapeutic methods for the prevention and therapy of liver fibrosis (Wang et al., 2009). Moreover, fibrogenesis is triggered by the activation and proliferation of myofibroblasts, which are the main supply of ECM in wounded livers (Bataller and Brenner, 2005; Kisseleva and Brenner, 2008). In fibrotic livers, activated hepatic stellate cells (aHSCs) were the main source of myoblasts, although they are one of their precursors. Endogenous portal fibroblasts, fibroblasts, bone marrow-originating cells, and myofibroblasts produced from hepatic parenchymal cells go through the epithelial-mesenchymal transition (EMT) and produce a large number of myofibroblasts in fibrotic livers. According to the cause of liver fibrosis, several types of cells trigger myofibroblasts (Iwaisako et al., 2014). In the resting state, hematopoietic stem cells, called resting hematopoietic stem cells, are responsible for storing vitamin A in the liver. Hematopoietic stem cells are activated by inflammatory mediators due to liver injury, which in turn differentiate into myofibroblasts (Zhang et al., 2016). Thus, tissue remodeling in the liver is begun by ECM proteins and matrix metalloproteinases (MMPs) released by hematopoietic stem cells (Puche et al., 2013; Li et al., 2015). HSC proliferation is also boosted by growth factors like TGF-α and epidermal growth factor (Meyer et al., 1990). A healthy liver includes collagen IV and collagen VI in the Disse area. During fibrosis, however, they are exchanged for collagens I and II and fibronectin (Brown et al., 2006). TGF-β1 is normally dormant, but upon excitation, it triggers a signaling pathway including Smad proteins that results in the creation of collagen. In addition, TGF-β1 promotes the transformation of dormant hematopoietic stem cells into ECM-secreting myofibroblasts (Breitkopf et al., 2006). Also, the initiation of hepatic angiogenesis is recognition of the vascular endothelial growth factor receptor (VEGF). Overall, these expansion factors induce ECM remodeling, leading to collagen synthesis (Schuppan et al., 2001). In liver fibrosis, neurochemical and neurotrophic substances also have an influence on HSCs. The neuroendocrine system is upregulated by liver damage, and stimulated HSCs begin to display receptors that govern cannabinoid (CB) signaling (Figure 2) (Mukhopadhyay et al., 2010).

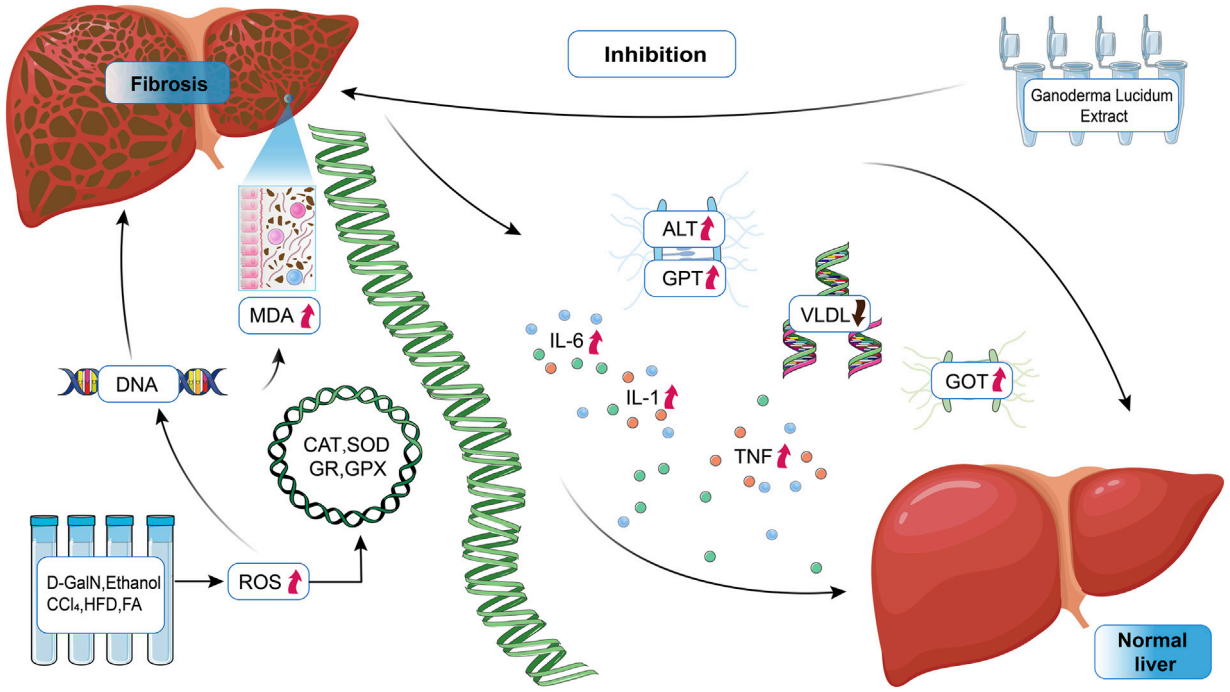

FIGURE 4
Mechanism of action of *Ganoderma lucidum* in the treatment of liver fibrosis. ALT, alanine aminotransferase; MDA, malondialdehyde; GPT, pyruvate aminotransferase; GOT, glutamate oxaloacetate transaminase; ROS, reactive oxygen species; CAT, catalase; GR, glutathione reductase; GPX, glutathione peroxidase; VLDL, very-low-density lipoprotein.

HSC activation may also be dependent on contact with altered ECM (shifting from basal-like to fibrillary ECM) *via* integrin-mediated signals (Henderson et al., 2013), to promote HSC activation *via* peptide mediators (PDGF, FGF, HGF, VEGF) that stay trapped in the altered ECM (Lee et al., 2015). By interacting with their cognate receptor(s), multiple peptide growth factors can affect and sustain one or more of the phenotypic responses of activated HSC (Figure 3) (Parola and Pinzani, 2019). A typical example is the signaling pathways elicited by TGβ1 or PDGF, growth factors that act on myofibroblasts but are also released by these cells. Similar considerations can be made for other ligand-receptor-induced signaling pathways, such as those involving HGF, EGF/EGFR, VEGF/VEGFR, Wnt/β-catenin, Hedgehog, endotelins, cannabinoids, adipokines, retinoid and vitamin D receptors, integrins, and TLRs (Higashi et al., 2017). As a pertinent example, connective tissue growth factor (CTGF) is believed to be crucial in mediating TGFβ1 pro-fibrogenic effects (Jun and Lau, 2011) and experimental targeting of CTGF can impact HSC activation and suppress experimental fibrosis (Hao et al., 2014). Another example is the use of losartan, an inhibitor of the angiotensin II receptor ATR1, which is strongly expressed by activated HSC, with angiotensin II boosting proliferation, migration, contractility, and TGFβ1 and collagen I production in these cells (Moreno and Bataller, 2008). Losartan has been shown in animal studies (Moreno et al., 2010) and maybe in hepatitis C virus (HCV) patients (Salama et al., 2016) to prevent fibrosis *via* modulating non-phagocytic NADPH-oxidase and profibrogenic genes (Colmenero et al., 2009).

HSC express a number of nuclear transcription factor receptors, including PPAR-γ and PPAR-δ, farnesoid X receptor (FXR), liver X receptor (LXR), vitamin D receptor (VDR), nuclear receptor subfamily 4 group A member 1 (NR4A1), and nuclear receptor subfamily 1 group D member 1 (REV-ERB) (Tsuchida and Friedman, 2017). These nuclear receptors, which control energy fluxes and metabolic pathways, are dysregulated in chronic liver diseases (CLD), especially in progressive NAFLD (Wang et al., 2015), and have been shown to limit HSC activation and fibrosis development.

G. lucidum anti-fibrotic activity could also result from the enhancement of collagenase (CLG), as therapy with *G. lucidum* extracts (GLE) decreased the gene expression of collagen (α1)(I), smooth muscle α-actin, metalloproteinase tissue inhibitor, and metalloproteinase-13 in liver fibrosis-induced rats (Wu et al., 2010). Consequently, decreasing hepatic hydroxyproline (HYP) concentration and enhancing liver histology, GLE restored thioacetamide (TAA)-induced reduction in collagenase activity and enhanced collagen clearance (Wu et al., 2010; Qiu et al., 2019). Several substances are known to produce liver fibrosis and are therefore frequently employed to develop animal models for the research of this specific kind of lesions. For most cases, intraperitoneal administration of these substances causes liver fibrosis within a comparatively brief time frame (Smith, 2013). When taken orally or by inhalation, the development of fibrosis is restricted and delayed. Popular as a result of their great repeatability, convenience of use, and accurate portrayal of the pathways participating in human liver fibrosis, these chemically-based animal models are widely utilized (Crespo Yanguas et al.,

TABLE 3 Effect of *G. lucidum* extracts (GL) on lipid peroxidation in mouse (untreated with ethanol) liver homogenates.

Groups	MDA (nmole/mg protein)	Inhibition rate (%)
Saline	0.162 ± 0.006	—
GL (10 mg/kg)	0.129 ± 0.02	20.37
GL (25 mg/kg)	0.125 ± 0.0005*	22.84
GL (50 mg/kg)	0.121 ± 0.008*	25.31

Data source: (Shieh et al., 2001) Each number indicates mean ± S.E., (n = 10). *p < .001, notably distinct from the standard control group. *p < .05, notably distinct from the standard control group. Analysis of variance with Dunnett's test. p-values below .05 were considered significant.

TABLE 4 Inhibitory effect of *G. lucidum* extracts (GL) on ethanol-induced lipid peroxidation in mouse liver homogenates.

Groups	MDA (nmole/mg protein)	Inhibition rate (%)
Saline	0.046 ± 0.01	—
95% Ethanol (0.1 mL)	0.095 ± 0.01*	—
95% Ethanol (0.1 mL)+GL (10 mg/kg)	0.058 ± 0.03	38.9
95% Ethanol (0.1 mL)+GL (25 mg/kg)	0.048 ± 0.02	49.5
95% Ethanol(0.1 mL)+GL(50 mg/kg)	0.045 ± 0.01*	52.6

Data source: (Shieh et al., 2001) Each number indicates mean ± S.E., (n = 10). *p < .05, notably distinct from the standard control group. *p < .05, notably distinct from the ethanol group. Analysis of variance with Dunnett's test. p-values below .05 were considered significant.

TABLE 5 Hepatoprotective effect of raw herbal extracts on CCl_4-induced increase in GOT GPT levels.

Groups	Dose (mg/kg)	GOT	GPT	Protection (%)	LDH
Normal	—	120.83 ± 4.02	44.18 ± 2.45	—	—
CCl_4	—	263.58 ± 8.11*	84.93 ± 2.29*	—	552.83 ± 57.58
GL	10	253.05 ± 16.26	77.07 ± 8.47	7.38	484.67 ± 70.13
	30	198.13 ± 19.32	64.37 ± 5.32	45.85	464.33 ± 22.40
	100	169.52 ± 14.82	52.68 ± 6.20	65.89	310.17 ± 100.41

Data source: (Lin et al., 1995) Significantly apart from the norm. *p < .001, Student's t-test. Notably distinct from the CCl_4-control group; % of protection: p = (C - 120.83) - (T - 120.83)/(C - 120.83); C, the GOT value of CCl_4-controlled group; T, the GOT value of the drug-treated group.

2016). Therefore, we summarized the model of liver fibrosis caused by d-galactosamine, ethanol, CCl_4, high-fat food, and formaldehyde and the factors influencing the anti-liver fibrosis experiment with *G. lucidum* (Table 2).

G. lucidum extracts could significantly increase the activity of certain enzymes or decrease specific indicators. We summarized the mechanisms that usually cause liver fibrosis, as shown in Figure 4, as well as the therapeutic effects of Ganoderma on them for the review summary and to provide ideas for subsequent studies.

4 Protective effect of *G. lucidum* on different liver fibrosis models in experiments

There are many causative factors of liver fibrosis, and the changes in the levels of the influencing factors in different liver fibrosis model experiments demonstrate the good anti-fibrotic effect of *G. lucidum*.

4.1 Protective effect of *G. lucidum* on D-galactosamine-induced hepatic fibrosis

The effect of total triterpenes extracted from *G. lucidum* on a model of experimental liver fibrosis induced by D-galactosamine (D-GalN) was extensively studied in mice (Shieh et al., 2001; Shi et al., 2008). *G. lucidum* triterpene extract (80 mg/kg) strongly prevented the elevation of blood alanine aminotransferase (ALT) and the hepatic models' triglyceride levels, with outcomes comparable to malic acid, a reference material known for its protective benefits (Ala-Kokko et al., 1987). Oxidative stress was primarily caused by the manufacturing of reactive oxygen species (ROS), which was an imbalance between free radical exposure and antioxidant defenses. ROS also play an important role in cell proliferation and signaling (Zhu et al., 2020). Free radicals damage hepatocytes by directly damaged key biomolecules, included DNA, lipids, and proteins (Alía et al., 2003). *G. lucidum* triterpene extract also prevented the decline in superoxide dismutase (SOD) activity and glutathione (GSH)

TABLE 6 ***G. lucidum*** **(GL) attenuates perirenal fat accumulation in the liver weight of mice fed a high-fat diet (HFD).**

Groups	Liver weight (g)	Perirenal fat weight (g)
ND	1.25	0.62
ND + GL	1.05	0.59
HFD	1.92	1.66
HFD + GL	1.41	1.17

Data source: (Jung et al., 2018) Five times per week, GL (50 mg/kg) or a placebo was orally delivered to mice fed a normal diet (ND) or an HFD. Dietary consumption was assessed every 10 days for 16 weeks. After 16 weeks of GL, therapy, the mice were slaughtered and their tissues were weighed (n = 8–9 per group). The data is the mean.

TABLE 7 ***G. lucidum*** **(GL) reduces fasting glucose levels, glucose tolerance, and insulin tolerance in HFD-fed mice.**

Groups	Fasting blood glucose (mg/dl)	Glucose tolerance (mg/dL)	Insulin tolerance (mg/dL)
ND	90	122	166
ND + GL	98	116	169
HFD	168	218	247
HFD + GL	118	171	168

Data source: (Jung et al., 2018) In HFD-fed, animals, GL, decreased fasting blood glucose, glucose tolerance, and insulin tolerance. Oral administration of GL (50 mg/kg) or vehicle five times per week to mice fed a normal diet (ND) or a high-fat diet (HFD). Once every 2 weeks, the mice were fasted for 16 h to assess their blood glucose levels. At 14 weeks of GL, therapy, mice (n = 8–9) were fasted for 16 h to conduct the GTT, and ITT (n = 8–9 for each group). Statistics are the mean.

content and inhibited the increase in malondialdehyde (MDA) content in mice with D-galactosamine-induced liver fibrosis. It likewise improved histopathological changes.

D-GalN-induced liver fibrosis was characterized by a large rise in serum marker enzyme (AST, ALT) activity, liver MDA levels, and a significant decline in liver SOD and GSH activity (Shi et al., 2008). Pretreatment of mice with *G. lucidum* total triterpene extracted kept these parameters at their normal values. Histopathological examination of liver sections complemented these biochemical findings. From the biological parameters and the histopathological examination of the liver, it was inferred that the optimal hepatoprotective effect of *G. lucidum* total triterpene extracted was noticed following therapy at a dose of 180 mg/kg (Shi et al., 2008; Soares et al., 2013). The results might indicate that the triterpenoids isolated from *G. lucidum* had powerful defensive effects against D-galactosamine-induced liver fibrosis. *G. lucidum* triterpene extract's hepatoprotective effect might be related to the activity of enzymes that neutralize free radicals, thus improving anti-oxidant capacity (Kim et al., 1999).

4.2 Protective effect of *G. lucidum* on alcoholic-induced hepatic fibrosis

Liver fibrosis caused by alcohol consumption is among the major risk factors for developing of many liver disorders. Alcohol misuse causes 10%–35% of alcoholic hepatitis and around 10% of cirrhosis (Stickel et al., 2017). *G. lucidum* had certain anti-oxidant effects on ethanolic liver fibrosis. It was postulated that among the primary causes of ethanol-induced liver fibrosis is free radical-induced lipid peroxidation, which is mostly caused by chronic alcohol consumption (Bautista and Spitzer, 1999; Meagher et al., 1999).

ICR mice were used to research the preventive effect of *G. lucidum* against ethanol-induced liver fibrosis and its mode of action (Shieh et al., 2001). It has been disclosed that ethanol increases lipid peroxidation in the liver (Kera et al., 1985). It was also shown that *G. lucidum* prevented ethanol-induced lipid peroxidation by 95% in a dose-dependent way. *G. lucidum* inhibited lipid peroxidation and dramatically reduced MDA production in the liver homogenates of control mice (untreated with ethanol), as shown in Table 3. These findings disclosed that *G. lucidum* was protective effect against ethanol-induced liver fibrosis was at least partially attributable to a reduction in MDA production. Their findings suggested that free radical generation might contribute to etiology of ethanol-induced liver damage and liver fibrosis. These effects may be attributable to its capacity to reduce membrane lipid peroxidation and free radical production or to scavenge free radicals (Table 4) (Bautista and Spitzer, 1999; Shieh et al., 2001).

4.3 Protective effect of *G. lucidum* on CCl_4-induced hepatic fibrosis

In the liver, cytochrome P450-dependent oxidases activate CCl_4 to produce CCl_3 radicals, which bind to cytosolic lipids and proteins under the influence of oxygen and trigger lipid peroxidation *via* hydrogen extraction (Kadiiska et al., 2000; Lim et al., 2000). These factors lead to alterations in the structure of the endoplasmic reticulum and other membranes, and loss of metabolic enzyme activity, which impairs liver function (Soares et al., 2013). And regards the activity of reducing elevated glutamate pyruvate aminotransferase (GPT) levels, *G. lucidum* treatment showed therapeutic activity, as shown in Table 5, where a single injection

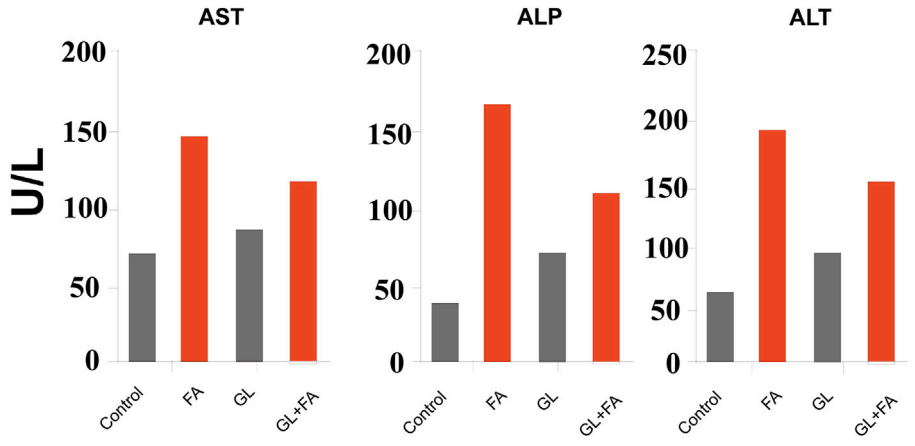

FIGURE 5
Data source: (Oluwafemi Adetuyi et al., 2020) formaldehyde and GL's effect on hepatic enzyme markers. The data are displayed as the mean (n = 7). AST, aspartate aminotransferase; ALP, alkaline phosphatase; ALT, alanine aminotransferase.

TABLE 8 Effects of *G. lucidum* and formaldehyde on the mean body weight and relative organ weight of rats.

Groups	Average body weight (g)	Relative organ weight (g)
Control	42.35 ± 4.52	7.32 ± 0.47
FA	18.75 ± 5.45	4.76 ± 0.78
GL	36.74 ± 6.32	8.76 ± 0.95
GL + FA	25.45 ± 6.32	6.75 ± 0.52

Data source: (Oluwafemi Adetuyi et al., 2020) Significantly different from control.

of CCl_4 induced a significant increase in serum glutamate oxaloacetate transaminase (GOT) and GPT levels 72 h after intoxication against the control group (Lin et al., 1995). Lactate dehydrogenase (LDH) values were statistically significantly lower in the drug-treated group than in the CCl_4-treated control rats, except in rats treated with *G. lucidum* (10 mg/kg). The results also indicated that Ganoderma showed potent hepatoprotective effects by observing a reduction in serum LDH levels (Lin et al., 1995). The targeted conjugates can protect mice, according to a preliminary biological review from acute liver fibrosis generated by carbon tetrachloride (Jin et al., 2014). The histological changes observed in the drug treatment group were smaller than those noticed inside the group. Administration of *G. lucidum* in an attempt to lessen the hepatotoxic effects of CCl_4 was shown to be effective in reducing CCl_4-induced liver fibrosis. In the LDH assay, rats administered *G. lucidum* (10, 30, and 100 mg/kg) showed better activity (Recknagel et al., 1974; Lin et al., 1995). The effect of *G. lucidum* extracts on GOT and serum lactate dehydrogenase showned that CCl_4 combined with *G. lucidum* extracts significantly decreased liver damage in rats (Lin et al., 1995).

GLE therapy significantly alleviated CCl_4-induced living fibrosis, accompanied by increases in plasma transaminases, hepatic malondialdehyde and hydroxyproline (HP) levels, and decreases in plasma albumin A/G ratio and hepatoproteins (Lin and Lin, 2006). Additionally, GLE therapy lowered TGF-β1 expression and changed MAT1A and MAT2 expression. *G. lucidum* fermentation filtrate (FGL) was found to have the same pharmacological activity against CCl_4-induced liver fibrosis (Kwon and Kim, 2011).

4.4 Protective effect of *G. lucidum* on non-alcoholic obesity-induced hepatic fibrosis

Non-alcoholic fatty liver disease (NAFLD) can result in severe fibrosis of the liver. Early detection and early treatment of NAFLD can significantly enhance therapy success rates (Zhou et al., 2021). Mice-fed high-fat food (HFD) showed signs of non-alcoholic steatosis, as evidenced by increased liver-to-body weight ratio, hepatic fat, and serum ALT levels. However, GL treatment was successful in ameliorating these abnormalities. An aqueous extract of GL effectively reduced obesity *via* modulation of the intestinal microbiota in rodents (Chang et al., 2015), as shown in Table 6. Other studies have reported that GL substrate extracts could effectively treat obesity by altering the expression of metabolic enzymes (Thyagarajan-Sahu et al., 2011).

In the liver, insulin resistance is associated with the amount of subcutaneous abdominal fat (Abate et al., 1995). Increased levels of cellular fatty acid derivatives stimulate stress kinases, resulting in the phosphorylation of insulin receptor substrate (IRS) proteins with serine (Capeau, 2008). A clinical investigation demonstrated that insulin resistance and hepatic steatosis are closely linked. Reduced glucose tolerance is indicative of insulin resistance and inappropriate glucose handling (Shulman et al., 1990). Glucose transporter protein 4 (GLUT4) plays a crucial part in glucose transport in muscle and adipose tissue (Zhao and Keating, 2007). Glucose translocation by GLUT4 is an insulin-dependent mechanism and a rate-limiting step in glucose consumption. According to the literature research in Table 7,

after 6 weeks, GL therapy lowered fasting glucose levels and enhanced glucose and insulin sensitivity in HFD-fed rats. In addition, GL increased adipocyte GLUT4 protein levels. These findings imply that GL's anti-adipogenic action may mitigate hyperglycemia (Jung et al., 2018).

Cholesterol and triglycerides accumulate in liver cells, causing their deposition in the liver cells. They were generally considered the culprits of fatty liver (Zhai et al., 2008). Thus, in the context of steatosis, an excessive buildup of triglycerides (TG) inside the hepatocytes was released as very-low-density lipoprotein (VLDL), an essential precursor of LDL that possessed atherogenic features (Venkatesan et al., 1993; Jung et al., 2018). It was widely assumed that excessive liver production of VLDL contributed to numerous hyperlipidemic conditions in humans, such as familial combination hyperlipidemia and diabetes (Venkatesan et al., 1993). Total blood cholesterol (TC) and LDL levels were decreased in HFD-fed mice by GL. Consequently, the data revealed that GL may enhance the serum lipid profile and prevent the evolution of non-alcoholic steatosis. In conclusion, GL regulated energy metabolic processes and fat accumulation in the liver and adipocytes directly. It enhanced insulin sensitivity and metabolic problems in a diet-induced obese animal model. GL was a viable eligible for prevention or treatment metabolic disorders including NAFLD.

4.5 Protective effect of *G. lucidum* on formaldehyde-induced hepatic fibrosis

G. lucidum extract exerts a preventive and therapeutic effect in experiments on liver fibrosis caused by formaldehyde (FA) exposure (Oluwafemi Adetuyi et al., 2020). By evaluating alanine aminotransferase (ALT), aspartate aminotransferase (AST), and alkaline phosphatase (ALP), the hepatoprotective efficacy of *G. lucidum* against FA-induced liver fibrosis was determined. ALT was an essential liver fibrosis enzyme responsible for catalyzing the transamination process. This increase in the number of enzymes will aggravate liver fibrosis (Kodavanti et al., 1989). AST and ALP were indicators of liver fibrosis; they were cytosolic and mitochondrial enzymes whose levels were frequently raised in the presence of persistent disease and necrosis resulting from lack of hepatocyte integrity. Such enzymes facilitated the exchange of α-amino acids from alanine and aspartate to the α-keto group of ketoglutarate, leading to the formation of pyruvate and oxaloacetate, respectively (Schiff et al., 2007). The FA group had considerably higher levels of these enzymes in contrast to the control group. Moreover, treatment with 100 mg/kg of *G. lucidum* considerably decreased the increased levels in Figure 5, demonstrating that *G. lucidum* protects rats from FA-induced liver fibrosis, as shown in Table 8. Ganoderma administration significantly reduced the elevated liver function enzymes (Lakshmi et al., 2006).

TNF, IL-1β, and IL-6 have a significant impact on the etiology of liver fibrosis. TNF is largely a set of pro-inflammatory cytokines recognized to play an essential part in inducing liver fibrosis, and there is evidence that oxidative stress and endotoxins may work together to promote TNF production (Feagins et al., 2008). Interleukins 1β and 6 are potential indicators of hepatotoxicity, either acute or chronic. The liver secreted pro-inflammatory cytokines TNF, IL-1β, and IL-6 into the bloodstream during hepatotoxic fibrosis. Consequently, biological therapies that block these cytokines demonstrated considerable therapeutic potential. When FA was delivered to rats, the levels of these cytokines were dramatically increased in the liver. A substantial decrease in cytokine levels was confirmed in the group administered 100 mg/kg of *G.lucidum*. These findings provide more evidence of the hepatoprotective action of *G. lucidum*. *G. lucidum* was able to counteract this impact, since the FA-treated rats exhibited extensive periportal cell infiltration and significant congestion (Batiha et al., 2020a; Oluwafemi Adetuyi et al., 2020).

This study showed that exposure to FA resulted in a significant decrease in anti-oxidant markers (Batiha et al., 2020b) and hepatic transaminases, triglycerides, and inflammatory markers increased. *G. lucidum* was ability to restore anti-oxidant, lipid, and anti-inflammatory status conferred a protective impact (El-Rahman et al., 2020).

5 Conclusion and perspective

G. lucidum has reached more than two thousand years of medicinal use in China and is also a traditional and valuable herb commonly used in our folklore, playing an important role in maintaining human health. The effective hepatoprotective activity of the natural active ingredients isolated from Ganoderma may represent an exciting advance in the search for effective hepatoprotective agents, particularly given the urgent need for the development of novel and innovative drugs as well as additional research, including clinical trials, to identify these natural compounds as good alternatives to conventional drugs. Therefore, most current studies on *G. lucidum* against liver fibrosis were conducted with the crude extract of *G. lucidum*. In the subsequent development, the components of *G. lucidum* can be purified and separated, and in the case of promising components, such as *G. lucidum* triterpenes can be finely separated. 1) The active components should be identified, and then performed cytotoxicity experiments. Subsequently, *in vitro* and *in vivo* experiments should be conducted to clarify the mechanism of action and the conformational relationships of its compounds. 2) We can optimize the scaffolds or moieties of natural drugs through synthetic reconstitution to stabilize or enhance their pharmacodynamic activities. 3) In the subsequent development of Ganoderma drugs, we can achieve the optimal therapeutic effect of the Chinese herbal formulas by using different ratios of ingredients based on the clear mechanism of the anti-liver fibrosis action of Ganoderma.

For example, the pharmacological effects of Ganoderma triterpenes are mainly focused on single components such as ganoderic acid A, ganoderic acid D, ganoderol F, or semi-purified components of the extract to analyze the pharmacological activities, followed by the ratio of various components in the triterpenes, i.e., the ratio of ganoderic acid to ganoderol, whether the two components have synergistic pharmacological effects, or the pharmacological effects of the ratio with traditional drug combinations are often neglected, i.e., at what ratio the anti-liver fibrosis activity is the strongest, which is not only in the development and utilization of single components of *G. lucidum*.

Therefore, these studies provide valuable insights and a certain working basis in the research of new drugs for *G. lucidum* against liver fibrosis. With the rising trend in the number of patients with liver fibrosis worldwide, there is a large market for effective drugs to treat

liver disease. As a medicinal food source, *G. lucidum* is a drug with potential to be developed as an anti-liver fibrosis agent. The role of *G. lucidum* in maintaining liver function will be better applied and will receive more attention and application in the field of healthcare and pharmaceutical research, believing that it will make an important contribution to the human health industry.

Author contributions

HP, LZ, and LIC contributed to the conception of this review and preparation of the manuscript, tables, and figures; LUC and RT revised tables, figures and reviewed manuscript; JS and LB contributed to the conception, supervision, and revision of the manuscript. All authors have approved the final article and are included in the disclosure.

Funding

This work is funded by the National Natural Science Foundation of China (No. 82073311); Natural Science Foundation of Sichuan Province (No.2022JDTD0025); The Open Research Fund of State Key Laboratory of Southwestern Chinese Medicine Resources (SKLTCM2022019, ZYXK2011011 and the study of vacuum freeze-drying technology of chuanxiong based on intelligent control algorithm neural network model).

Conflict of interest

The authors declare that the research was conducted in the absence of any commercial or financial relationships that could be construed as a potential conflict of interest.

Publisher's note

All claims expressed in this article are solely those of the authors and do not necessarily represent those of their affiliated organizations, or those of the publisher, the editors and the reviewers. Any product that may be evaluated in this article, or claim that may be made by its manufacturer, is not guaranteed or endorsed by the publisher.

References

Abate, N., Garg, A., Peshock, R. M., Stray-Gundersen, J., and Grundy, S. M. (1995). Relationships of generalized and regional adiposity to insulin sensitivity in men. *J. Clin. Invest.* 96 (1), 88–98. doi:10.1172/jci118083

Adams, M., Christen, M., Plitzko, I., Zimmermann, S., Brun, R., Kaiser, M., et al. (2010). Antiplasmodial lanostanes from the Ganoderma lucidum mushroom. *J. Nat. Prod.* 73 (5), 897–900. doi:10.1021/np100031c

Akihisa, T., Tagata, M., Ukiya, M., Tokuda, H., Suzuki, T., and Kimura, Y. (2005). Oxygenated lanostane-type triterpenoids from the fungus Ganoderma l ucidum. *J. Nat. Prod.* 68 (4), 559–563. doi:10.1021/np040230h

Ala-Kokko, L., Stenbäck, F., and Ryhänen, L. (1987). Preventive effect of malotilate on carbon tetrachloride-induced liver damage and collagen accumulation in the rat. *Biochem. J.* 246 (2), 503–509. doi:10.1042/bj2460503

Alía, M., Horcajo, C., Bravo, L., and Goya, L. (2003). Effect of grape antioxidant dietary fiber on the total antioxidant capacity and the activity of liver antioxidant enzymes in rats. *Nutr. Res.* 23 (9), 1251–1267. doi:10.1016/s0271-5317(03)00131-3

Aydın, M. M., and Akçalı, K. C. (2018). Liver fibrosis. *Turkish J. Gastroenterology* 29 (1), 14–21. doi:10.5152/tjg.2018.17330

Barros, L., Baptista, P., Estevinho, L. M., and Ferreira, I. C. (2007). Effect of fruiting body maturity stage on chemical composition and antimicrobial activity of Lactarius sp. mushrooms. *J. Agric. Food Chem.* 55 (21), 8766–8771. doi:10.1021/jf071435+

Bataller, R., and Brenner, D. A. (2005). Liver fibrosis. *J. Clin. investigation* 115 (2), 209–218. doi:10.1172/JCI24282

Batiha, G. E.-S., Beshbishy, A. M., El-Mleeh, A., Abdel-Daim, M. M., and Devkota, H. P. (2020a). Traditional uses, bioactive chemical constituents, and pharmacological and toxicological activities of Glycyrrhiza glabra L.(Fabaceae). *Biomolecules* 10 (3), 352. doi:10.3390/biom10030352

Batiha, G. E.-S., Magdy Beshbishy, A., Wasef, L., Elewa, Y. H., El-Hack, A., Mohamed, E., et al. (2020b). Uncaria tomentosa (willd. Ex schult.) dc. A review on chemical constituents and biological activities. *Appl. Sci.* 10 (8), 2668. doi:10.3390/app10082668

Bautista, A. P., and Spitzer, J. J. (1999). Role of Kupffer cells in the ethanol-induced oxidative stress in the liver. *Front. Biosci.* 4, D589–D595. doi:10.2741/bautista

Borchers, A. T., Keen, C. L., and Gershwin, M. E. (2004). Mushrooms, tumors, and immunity: An update. *Exp. Biol. Med.* 229 (5), 393–406. doi:10.1177/153537020422900507

Breitkopf, K., Godoy, P., Ciuclan, L., Singer, M., and Dooley, S. (2006). TGF-beta/Smad signaling in the injured liver. *Z. für Gastroenterol.* 44 (01), 57–66. doi:10.1055/s-2005-858989

Brown, B., Lindberg, K., Reing, J., Stolz, D. B., and Badylak, S. F. (2006). The basement membrane component of biologic scaffolds derived from extracellular matrix. *Tissue Eng.* 12 (3), 519–526. doi:10.1089/ten.2006.12.519

Capeau, J. (2008). Insulin resistance and steatosis in humans. *Diabetes & metabolism* 34 (6), 649–657. doi:10.1016/S1262-3636(08)74600-7

Chang, C.-J., Lin, C.-S., Lu, C.-C., Martel, J., Ko, Y.-F., Ojcius, D. M., et al. (2015). Ganoderma lucidum reduces obesity in mice by modulating the composition of the gut microbiota. *Nat. Commun.* 6 (1), 7489–7519. doi:10.1038/ncomms8489

Colmenero, J., Bataller, R., Sancho-Bru, P., Domínguez, M., Moreno, M., Forns, X., et al. (2009). Effects of losartan on hepatic expression of nonphagocytic NADPH oxidase and fibrogenic genes in patients with chronic hepatitis C. *Am. J. Physiology-Gastrointestinal Liver Physiology* 297 (4), G726–G734. doi:10.1152/ajpgi.00162.2009

Crespo Yanguas, S., Cogliati, B., Willebrords, J., Maes, M., Colle, I., Van den Bossche, B., et al. (2016). Experimental models of liver fibrosis. *Archives Toxicol.* 90 (5), 1025–1048. doi:10.1007/s00204-015-1543-4

El-Mekkawy, S., Meselhy, M. R., Nakamura, N., Tezuka, Y., Hattori, M., Kakiuchi, N., et al. (1998). Anti-HIV-1 and anti-HIV-1-protease substances from Ganoderma lucidum. *Phytochemistry* 49 (6), 1651–1657. doi:10.1016/s0031-9422(98)00254-4

El-Rahman, A., Ghada, I., Behairy, A., Elseddawy, N. M., Batiha, G. E.-S., Hozzein, W. N., et al. (2020). Saussurea lappa ethanolic extract attenuates triamcinolone acetonide-induced pulmonary and splenic tissue damage in rats via modulation of oxidative stress, inflammation, and apoptosis. *Antioxidants* 9 (5), 396. doi:10.3390/antiox9050396

Feagins, A., Opriessnig, T., Guenette, D., Halbur, P., and Meng, X. (2008). Inactivation of infectious hepatitis E virus present in commercial pig livers sold in local grocery stores in the United States. *Int. J. food Microbiol.* 123 (1-2), 32–37. doi:10.1016/j.ijfoodmicro.2007.11.068

Ferreira, I. C., Barros, L., and Abreu, R. (2009). Antioxidants in wild mushrooms. *Curr. Med. Chem.* 16 (12), 1543–1560. doi:10.2174/092986709787909587

Gan, K.-H., Kuo, S.-H., and Lin, C.-N. (1998). Steroidal constituents of Ganoderma a pplanatum and Ganoderma n eo-japonicum. *J. Nat. Prod.* 61 (11), 1421–1422. doi:10.1021/np980184j

Hajjaj, H., Macé, C., Roberts, M., Niederberger, P., and Fay, L. B. (2005). Effect of 26-oxygenosterols from Ganoderma lucidum and their activity as cholesterol synthesis inhibitors. *Appl. Environ. Microbiol.* 71 (7), 3653–3658. doi:10.1128/AEM.71.7.3653-3658.2005

Hao, C., Xie, Y., Peng, M., Ma, L., Zhou, Y., Zhang, Y., et al. (2014). Inhibition of connective tissue growth factor suppresses hepatic stellate cell activation *in vitro* and prevents liver fibrosis *in vivo*. *Clin. Exp. Med.* 14 (2), 141–150. doi:10.1007/s10238-013-0229-6

Henderson, N. C., Arnold, T. D., Katamura, Y., Giacomini, M. M., Rodriguez, J. D., McCarty, J. H., et al. (2013). Targeting of αv integrin identifies a core molecular pathway that regulates fibrosis in several organs. *Nat. Med.* 19 (12), 1617–1624. doi:10.1038/nm.3282

Higashi, T., Friedman, S. L., and Hoshida, Y. (2017). Hepatic stellate cells as key target in liver fibrosis. *Adv. drug Deliv. Rev.* 121, 27–42. doi:10.1016/j.addr.2017.05.007

Hu, S.-H., Wang, J.-C., Lien, J.-L., Liaw, E.-T., and Lee, M.-Y. (2006). Antihyperglycemic effect of polysaccharide from fermented broth of Pleurotus citrinopileatus. *Appl. Microbiol. Biotechnol.* 70 (1), 107–113. doi:10.1007/s00253-005-0043-5

Iwaisako, K., Jiang, C., Zhang, M., Cong, M., Moore-Morris, T. J., Park, T. J., et al. (2014). Origin of myofibroblasts in the fibrotic liver in mice. *Proc. Natl. Acad. Sci.* 111 (32), E3297–E3305. doi:10.1073/pnas.1400062111

Jiang, J., Grieb, B., Thyagarajan, A., and Sliva, D. (2008). Ganoderic acids suppress growth and invasive behavior of breast cancer cells by modulating AP-1 and NF-kappaB signaling. *Int. J. Mol. Med.* 21 (5), 577–584. doi:10.3892/ijmm.21.5.577

Jin, X.-Y., Fan, S.-Y., Li, H.-W., Shi, W.-G., Chen, W., Wang, H.-F., et al. (2014). Novel liver-specific nitric oxide (NO) releasing drugs with bile acid as both NO carrier and targeting ligand. *Chin. Chem. Lett.* 25 (5), 787–790. doi:10.1016/j.cclet.2014.04.001

Jun, J.-I., and Lau, L. F. (2011). Taking aim at the extracellular matrix: CCN proteins as emerging therapeutic targets. *Nat. Rev. Drug Discov.* 10 (12), 945–963. doi:10.1038/nrd3599

Jung, S., Son, H., Hwang, C. E., Cho, K. M., Park, S. W., and Kim, H. J. (2018). Ganoderma lucidum ameliorates non-alcoholic steatosis by upregulating energy metabolizing enzymes in the liver. *J. Clin. Med.* 7 (6), 152. doi:10.3390/jcm7060152

Kadiiska, M. B., Gladen, B. C., Baird, D. D., Dikalova, A. E., Sohal, R. S., Hatch, G. E., et al. (2000). Biomarkers of oxidative stress study: Are plasma antioxidants markers of CCl4 poisoning? *Free Radic. Biol. Med.* 28 (6), 838–845. doi:10.1016/s0891-5849(00)00198-2

Kera, Y., Komura, S., Ohbora, Y., Kiriyama, T., and Inoue, K. (1985). Ethanol induced changes in lipid peroxidation and nonprotein sulfhydryl content. Different sensitivities in rat liver and kidney. *Res. Commun. Chem. pathology Pharmacol.* 47 (2), 203–209.

Kikuchi, T., Matsuda, S., Murai, Y., and Ogita, Z. (1985). Ganoderic acid G and I and ganolucidic acid A and B, new triterpenoids from Ganoderma lucidum. *Chem. Pharm. Bull.* 33 (6), 2628–2631. doi:10.1248/cpb.33.2628

Kim, D.-H., Shim, S.-B., Kim, N.-J., and Jang, I.-S. (1999). Beta-glucuronidase-inhibitory activity and hepatoprotective effect of Ganoderma lucidum. *Biol. Pharm. Bull.* 22 (2), 162–164. doi:10.1248/bpb.22.162

Kisseleva, T., and Brenner, D. A. (2008). Mechanisms of fibrogenesis. *Exp. Biol. Med.* 233 (2), 109–122. doi:10.3181/0707-MR-190

Kodavanti, P. R. S., Joshi, U. M., Young, R. A., Meydrech, E. F., and Mehendale, H. M. (1989). Protection of hepatotoxic and lethal effects of CCl4 by partial hepatectomy. *Toxicol. Pathol.* 17 (3), 494–505. doi:10.1177/019262338901700304

Koo, M. H., Chae, H.-J., Lee, J. H., Suh, S.-S., and Youn, U. J. (2021). Antiinflammatory lanostane triterpenoids from Ganoderma lucidum. *Nat. Prod. Res.* 35 (22), 4295–4302. doi:10.1080/14786419.2019.1705815

Kubota, T., Asaka, Y., Miura, I., and Mori, H. (1982). Structures of ganoderic acid A and B, two new lanostane type bitter triterpenes from Ganoderma lucidum (FR.) KARST. *Helvetica Chim. Acta* 65 (2), 611–619. doi:10.1002/hlca.19820650221

Kwon, S.-C., and Kim, Y.-B. (2011). Antifibrotic activity a fermentation filtrate of Ganoderma lucidum. *Laboratory animal Res.* 27 (4), 369–371. doi:10.5625/lar.2011.27.4.369

Lakornwong, W., Kanokmedhakul, K., Kanokmedhakul, S., Kongsaeree, P., Prabpai, S., Sibounnavong, P., et al. (2014). Triterpene lactones from cultures of Ganoderma sp. KM01. *J. Nat. Prod.* 77 (7), 1545–1553. doi:10.1021/np400846k

Lakshmi, B., Ajith, T., Jose, N., and Janardhanan, K. (2006). Antimutagenic activity of methanolic extract of Ganoderma lucidum and its effect on hepatic damage caused by benzo [a] pyrene. *J. Ethnopharmacol.* 107 (2), 297–303. doi:10.1016/j.jep.2006.03.027

Lee, Y. A., Wallace, M. C., and Friedman, S. L. (2015). Pathobiology of liver fibrosis: A translational success story. *Gut* 64 (5), 830–841. doi:10.1136/gutjnl-2014-306842

Li, D., He, L., Guo, H., Chen, H., and Shan, H. (2015). Targeting activated hepatic stellate cells (aHSCs) for liver fibrosis imaging. *EJNMMI Res.* 5 (1), 71–10. doi:10.1186/s13550-015-0151-x

Li, Y. Y., Mi, Z. Y., Tang, Y., Wang, G., Li, D. S., and Tang, Y. J. (2009). Lanostanoids isolated from Ganoderma lucidum mycelium cultured by submerged fermentation. *Helvetica Chim. Acta* 92 (8), 1586–1593. doi:10.1002/hlca.200900028

Lim, H.-K., Kim, H.-S., Choi, H.-S., Oh, S., Jang, C.-G., Choi, J., et al. (2000). Effects of acetylbergenin against D-galactosamine-induced hepatotoxicity in rats. *Pharmacol. Res.* 42 (5), 471–474. doi:10.1006/phrs.2000.0730

Lin, J.-M., Lin, C.-C., Chen, M.-F., Ujiie, T., and Takada, A. (1995). Radical scavenger and antihepatotoxic activity of Ganoderma formosanum, Ganoderma lucidum and Ganoderma neo-japonicum. *J. Ethnopharmacol.* 47 (1), 33–41. doi:10.1016/0378-8741(95)01251-8

Lin, M., Feng, W., and Ruoyun, C. (2003). Analysis of triterpene constituents from Ganoderma lucidum. *Yao xue xue bao= Acta Pharm. Sin.* 38 (1), 50–52.

Lin, W.-C., and Lin, W.-L. (2006). Ameliorative effect of Ganoderma lucidum on carbon tetrachloride-induced liver fibrosis in rats. *World J. Gastroenterology WJG* 12 (2), 265–270. doi:10.3748/wjg.v12.i2.265

Liu, J., Kurashiki, K., Shimizu, K., and Kondo, R. (2006). 5alpha-reductase inhibitory effect of triterpenoids isolated from Ganoderma lucidum. *Biol. Pharm. Bull.* 29 (2), 392–395. doi:10.1248/bpb.29.392

Luo, Y., Lin, C., Xue-lian, Z., Jin, L., Fei, W., and Xiaobo, S. (2021). Advances in the pharmacological activity of triterpenoid components of Ganoderma lucidum. *Chin. Pharmacol. Bull.* 37 (09), 1185–1188.

Ma, J., Ye, Q., Hua, Y., Zhang, D., Cooper, R., Chang, M. N., et al. (2002). New lanostanoids from the mushroom Ganoderma l ucidum. *J. Nat. Prod.* 65 (1), 72–75. doi:10.1021/np010385e

Meagher, E. A., Barry, O. P., Burke, A., Lucey, M. R., Lawson, J. A., Rokach, J., et al. (1999). Alcohol-induced generation of lipid peroxidation products in humans. *J. Clin. investigation* 104 (6), 805–813. doi:10.1172/JCI5584

Meyer, D. H., Bachem, M. G., and Gressner, A. M. (1990). Modulation of hepatic lipocyte proteoglycan synthesis and proliferation by Kupffer cell-derived transforming growth factors type beta 1 and type alpha. *Biochem. biophysical Res. Commun.* 171 (3), 1122–1129. doi:10.1016/0006-291x(90)90801-s

Moradali, M.-F., Mostafavi, H., Ghods, S., and Hedjaroude, G.-A. (2007). Immunomodulating and anticancer agents in the realm of macromycetes fungi (macrofungi). *Int. Immunopharmacol.* 7 (6), 701–724. doi:10.1016/j.intimp.2007.01.008

Moreno, M., and Bataller, R. (2008). Cytokines and renin-angiotensin system signaling in hepatic fibrosis. *Clin. liver Dis.* 12 (4), 825–852. doi:10.1016/j.cld.2008.07.013

Moreno, M., Gonzalo, T., Kok, R. J., Sancho-Bru, P., Van Beuge, M., Swart, J., et al. (2010). Reduction of advanced liver fibrosis by short-term targeted delivery of an angiotensin receptor blocker to hepatic stellate cells in rats. *Hepatology* 51 (3), 942–952. doi:10.1002/hep.23419

Mori, K., Kobayashi, C., Tomita, T., Inatomi, S., and Ikeda, M. (2008). Antiatherosclerotic effect of the edible mushrooms Pleurotus eryngii (Eringi), Grifola frondosa (Maitake), and Hypsizygus marmoreus (Bunashimeji) in apolipoprotein E–deficient mice. *Nutr. Res.* 28 (5), 335–342. doi:10.1016/j.nutres.2008.03.010

Moro, C., Palacios, I., Lozano, M., D'Arrigo, M., Guillamón, E., Villares, A., et al. (2012). Anti-inflammatory activity of methanolic extracts from edible mushrooms in LPS activated RAW 264.7 macrophages. *Food Chem.* 130 (2), 350–355. doi:10.1016/j.foodchem.2011.07.049

Mukhopadhyay, B., Liu, J., Osei-Hyiaman, D., Godlewski, G., Mukhopadhyay, P., Wang, L., et al. (2010). Transcriptional regulation of cannabinoid receptor-1 expression in the liver by retinoic acid acting via retinoic acid receptor-γ. *J. Biol. Chem.* 285 (25), 19002–19011. doi:10.1074/jbc.m109.068460

Niedermeyer, T. H., Lindequist, U., Mentel, R., Gördes, D., Schmidt, E., Thurow, K., et al. (2005). Antiviral Terpenoid constituents of Ganoderma p feifferi. *J. Nat. Prod.* 68 (12), 1728–1731. doi:10.1021/np0501886

Nishitoba, T., Oda, K., Sato, H., and Sakamura, S. (1988). Novel triterpenoids from the fungus Ganoderma lucidum. *Agric. Biol. Chem.* 52 (2), 367–372. doi:10.1080/00021369.1988.10868655

Nishitoba, T., Sato, H., and Sakamura, S. (1986). New terpenoids, ganolucidic acid D, ganoderic acid L, lucidone C and lucidenic acid G, from the fungus Ganoderma lucidum. *Agric. Biol. Chem.* 50 (3), 809–811. doi:10.1271/bbb1961.50.809

Nishitoba, T., Sato, S., and Sakamura, S. (1985). New terpenoids from Ganoderma lucidum and their bitterness. *Agric. Biol. Chem.* 49 (5), 1547–1549. doi:10.1080/00021369.1985.10866944

Oluwafemi Adetuyi, B., Olamide Okeowo, T., Adefunke Adetuyi, O., Abraham Adebisi, O., Ogunlana, O. O., Janet Oretade, O., et al. (2020). Ganoderma lucidum from red mushroom attenuates formaldehyde-induced liver damage in experimental male rat model. *Biology* 9 (10), 313. doi:10.3390/biology9100313

Parola, M., and Pinzani, M. (2019). Liver fibrosis: Pathophysiology, pathogenetic targets and clinical issues. *Mol. aspects Med.* 65, 37–55. doi:10.1016/j.mam.2018.09.002

Puche, J. E., Saiman, Y., and Friedman, S. L. (2013). Hepatic stellate cells and liver fibrosis. *Compr. Physiol.* 3 (4), 1473–1492. doi:10.1002/cphy.c120035

Qiao, Y., Zhang, X.-m., and Qiu, M.-h. (2007). Two novel lanostane triterpenoids from Ganoderma sinense. *Molecules* 12 (8), 2038–2046. doi:10.3390/12082038

Qiu, Z., Zhong, D., and Yang, B. (2019). Preventive and therapeutic effect of Ganoderma (lingzhi) on liver injury. *Ganoderma Health* 1182, 217–242. doi:10.1007/978-981-32-9421-9_9

Recknagel, R., Glende, E., Ugazio, G., Koch, R., and Srinivasan, S. (1974). New data in support of lipoperoxidation theory for carbon-tetrachloride liver-injury. *Israel J. Med. Sci.* 10 (4), 301–311.

Salama, Z. A., Sadek, A., Abdelhady, A. M., Darweesh, S. K., Morsy, S. A., and Esmat, G. (2016). Losartan may inhibit the progression of liver fibrosis in chronic HCV patients. *Hepatobiliary Surg. Nutr.* 5 (3), 249–255. doi:10.21037/hbsn.2016.02.06

Satria, D., Amen, Y., Niwa, Y., Ashour, A., Allam, A. E., and Shimizu, K. (2019). Lucidumol D, a new lanostane-type triterpene from fruiting bodies of Reishi (Ganoderma lingzhi). *Nat. Prod. Res.* 33 (2), 189–195. doi:10.1080/14786419.2018.1440229

Schiff, N. D., Giacino, J. T., Kalmar, K., Victor, J., Baker, K., Gerber, M., et al. (2007). Behavioural improvements with thalamic stimulation after severe traumatic brain injury. *Nature* 448 (7153), 600–603. doi:10.1038/nature06041

Schuppan, D., Ruehl, M., Somasundaram, R., and Hahn, E. G. (2001). Matrix as a modulator of hepatic fibrogenesis. *Seminars liver Dis.* 21, 351–372. doi:10.1055/s-2001-17556()

Seo, H. W., Hung, T. M., Na, M., Jung, H. J., Kim, J. C., Choi, J. S., et al. (2009). Steroids and triterpenes from the fruit bodies of Ganoderma lucidum and their anti-complement activity. *Archives Pharmacal Res.* 32 (11), 1573–1579. doi:10.1007/s12272-009-2109-x

Shi, Y., Sun, J., He, H., Guo, H., and Zhang, S. (2008). Hepatoprotective effects of Ganoderma lucidum peptides against D-galactosamine-induced liver injury in mice. *J. Ethnopharmacol.* 117 (3), 415–419. doi:10.1016/j.jep.2008.02.023

Shieh, Y.-H., Liu, C.-F., Huang, Y.-K., Yang, J.-Y., Wu, I.-L., Lin, C.-H., et al. (2001). Evaluation of the hepatic and renal-protective effects of Ganoderma lucidum in mice. *Am. J. Chin. Med.* 29, 501–507. doi:10.1142/S0192415X01000526

Shulman, G. I., Rothman, D. L., Jue, T., Stein, P., DeFronzo, R. A., and Shulman, R. G. (1990). Quantitation of muscle glycogen synthesis in normal subjects and subjects with non-insulin-dependent diabetes by 13C nuclear magnetic resonance spectroscopy. *N. Engl. J. Med.* 322 (4), 223–228. doi:10.1056/nejm199001253220403

Siwulski, M., Sobieralski, K., Golak-Siwulska, I., Sokol, S., and Sekara, A. (2015). Ganoderma lucidum (curt. Fr.) karst.-health-promoting properties. A review. *Herba Pol.* 61 (3), 105–118. doi:10.1515/hepo-2015-0026

Smith, G. P. (2013). "Animal models for the study of human disease: Chapter 19," in *Animal models of fibrosis in human disease* (Netherland: Elsevier).

Soares, A. A., de Sá-Nakanishi, A. B., Bracht, A., da Costa, S. M. G., Koehnlein, E. A., de Souza, C. G. M., et al. (2013). Hepatoprotective effects of mushrooms. *Molecules* 18 (7), 7609–7630. doi:10.3390/molecules18077609

Stickel, F., Moreno, C., Hampe, J., and Morgan, M. Y. (2017). The genetics of alcohol dependence and alcohol-related liver disease. *J. hepatology* 66 (1), 195–211. doi:10.1016/j.jhep.2016.08.011

Tang, W., Liu, J.-W., Zhao, W.-M., Wei, D.-Z., and Zhong, J.-J. (2006). Ganoderic acid T from Ganoderma lucidum mycelia induces mitochondria mediated apoptosis in lung cancer cells. *Life Sci.* 80 (3), 205–211. doi:10.1016/j.lfs.2006.09.001

Thyagarajan-Sahu, A., Lane, B., and Sliva, D. (2011). ReishiMax, mushroom based dietary supplement, inhibits adipocyte differentiation, stimulates glucose uptake and activates AMPK. *BMC Complementary Altern. Med.* 11 (1), 74–14. doi:10.1186/1472-6882-11-74

Tsuchida, T., and Friedman, S. L. (2017). Mechanisms of hepatic stellate cell activation. *Nat. Rev. Gastroenterology hepatology* 14 (7), 397–411. doi:10.1038/nrgastro.2017.38

Venkatesan, S., Cullen, P., Pacy, P., Halliday, D., and Scott, J. (1993). Stable isotopes show a direct relation between VLDL apoB overproduction and serum triglyceride levels and indicate a metabolically and biochemically coherent basis for familial combined hyperlipidemia. *Arterioscler. Thromb.* 13 (7), 1110–1118. doi:10.1161/01.atv.13.7.1110

Wang, G. J., Huang, Y. J., Chen, D. H., and Lin, Y. L. (2009). Ganoderma lucidum extract attenuates the proliferation of hepatic stellate cells by blocking the PDGF receptor. *Phytotherapy Res. Int. J. Devoted Pharmacol. Toxicol. Eval. Nat. Prod. Deriv.* 23 (6), 833–839. doi:10.1002/ptr.2687

Wang, J., Cao, B., Zhao, H., and Feng, J. (2017). Emerging roles of Ganoderma lucidum in anti-aging. *Aging Dis.* 8 (6), 691–707. doi:10.14336/AD.2017.0410

Wang, Y., Viscarra, J., Kim, S.-J., and Sul, H. S. (2015). Transcriptional regulation of hepatic lipogenesis. *Nat. Rev. Mol. Cell Biol.* 16 (11), 678–689. doi:10.1038/nrm4074

Wu, G.-S., Guo, J.-J., Bao, J.-L., Li, X.-W., Chen, X.-P., Lu, J.-J., et al. (2013). Anti-cancer properties of triterpenoids isolated from Ganoderma lucidum–a review. *Expert Opin. investigational drugs* 22 (8), 981–992. doi:10.1517/13543784.2013.805202

Wu, Y. W., Fang, H. L., and Lin, W. C. (2010). Post-treatment of Ganoderma lucidum reduced liver fibrosis induced by thioacetamide in mice. *Phytotherapy Res. Int. J. Devoted Pharmacol. Toxicol. Eval. Nat. Prod. Deriv.* 24 (4), 494–499. doi:10.1002/ptr.2949

Xu, F., Zhou, D., Meng, X., Wang, X., Liu, C., Huang, C., et al. (2016). Smad2 increases the apoptosis of activated human hepatic stellate cells induced by TRAIL. *Int. Immunopharmacol.* 32, 76–86. doi:10.1016/j.intimp.2016.01.013

Yang, M., Wang, X., Guan, S., Xia, J., Sun, J., Guo, H., et al. (2007). Analysis of triterpenoids in Ganoderma lucidum using liquid chromatography coupled with electrospray ionization mass spectrometry. *J. Am. Soc. Mass Spectrom.* 18 (5), 927–939. doi:10.1016/j.jasms.2007.01.012

Yang, S.-X., Yu, Z.-C., Lu, Q.-Q., Shi, W.-Q., Laatsch, H., and Gao, J.-M. (2012). Toxic lanostane triterpenes from the basidiomycete Ganoderma amboinense. *Phytochem. Lett.* 5 (3), 576–580. doi:10.1016/j.phytol.2012.05.017

Zhai, C. X., Gu, H. N., Tian, J., and Zhou, Q. Z. (2008). Deaggregation of long chain alkyl β-naphthoic acid ester with β-CD and α-CD: A mimic way to remove excessive fat from fatty liver. *Chin. Chem. Lett.* 19 (6), 720–724. doi:10.1016/j.cclet.2008.04.018

Zhan, L., Huang, C., Meng, X.-M., Song, Y., Wu, X. Q., Yang, Y., et al. (2015). Hypoxia-inducible factor-1alpha in hepatic fibrosis: A promising therapeutic target. *Biochimie* 108, 1–7. doi:10.1016/j.biochi.2014.10.013

Zhang, C.-Y., Yuan, W.-G., He, P., Lei, J.-H., and Wang, C.-X. (2016). Liver fibrosis and hepatic stellate cells: Etiology, pathological hallmarks and therapeutic targets. *World J. gastroenterology* 22 (48), 10512–10522. doi:10.3748/wjg.v22.i48.10512

Zhao, F.-Q., and Keating, A. F. (2007). Functional properties and genomics of glucose transporters. *Curr. genomics* 8 (2), 113–128. doi:10.2174/138920207780368187

Zhou, Y., Liu, Z., Qiao, G., Tang, B., and Li, P. (2021). Visualization of endoplasmic reticulum viscosity in the liver of mice with nonalcoholic fatty liver disease by a near-infrared fluorescence probe. *Chin. Chem. Lett.* 32 (11), 3641–3645. doi:10.1016/j.cclet.2021.04.035

Zhu, P., Qian, J., Xu, Z., Meng, C., Liu, J., Shan, W., et al. (2020). Piperlonguminine and piperine analogues as TrxR inhibitors that promote ROS and autophagy and regulate p38 and Akt/mTOR signaling. *J. Nat. Prod.* 83 (10), 3041–3049. doi:10.1021/acs.jnatprod.0c00599

frontiers | Frontiers in Pharmacology

TYPE Original Research
PUBLISHED 08 February 2023
DOI 10.3389/fphar.2023.1093934

OPEN ACCESS

EDITED BY
Guangyue Su,
Shenyang Pharmaceutical University, China

REVIEWED BY
Lu Yifei,
Shanghai University of Traditional Chinese Medicine, China
Ming-Hua Zheng,
First Affiliated Hospital of Wenzhou Medical University, China

*CORRESPONDENCE
Shuo Zhang,
zhangshuotcm@126.com
Zhiyun Chen,
zhiyunchen63@163.com

†These authors share first authorship

SPECIALTY SECTION
This article was submitted to Ethnopharmacology, a section of the journal Frontiers in Pharmacology

RECEIVED 09 November 2022
ACCEPTED 20 January 2023
PUBLISHED 08 February 2023

CITATION
Yan J, Nie Y, Chen Z, Yao J, Zhang S and Chen Z (2023), The IDI1/SREBP2 axis drives intrahepatic cholestasis and is a treatment target of San-Huang-Cai-Zhu formula identified by sequencing and experiments. *Front. Pharmacol.* 14:1093934. doi: 10.3389/fphar.2023.1093934

The IDI1/SREBP2 axis drives intrahepatic cholestasis and is a treatment target of San-Huang-Cai-Zhu formula identified by sequencing and experiments

Junbin Yan[1,2†], Yunmeng Nie[3†], Zheng Chen[1,4†], Jiaming Yao[5], Shuo Zhang[2*] and Zhiyun Chen[1,4*]

[1]The First Affiliated Hospital of Zhejiang Chinese Medical University, Zhejiang Provincial Hospital of Chinese Medicine, Hangzhou, China, [2]The Second Affiliated Hospital of Zhejiang Chinese Medical University, The Xin Hua Hospital of Zhejiang Province, Hangzhou, China, [3]School of Basic Medical Sciences, Zhejiang Chinese Medical University, Hangzhou, China, [4]Key Laboratory of Integrative Chinese and Western Medicine for the Diagnosis and Treatment of Circulatory Diseases of Zhejiang Province, Hangzhou, China, [5]Hangzhou Hospital of Traditional Chinese Medicine, Hangzhou, China

San-Huang-Chai-Zhu formula (SHCZF), originates from Da-Huang-Xiao-Shi decoction (DHXSD) for the treatment of jaundice as recorded in the Chinese traditional Chinese medicine book *Jin Gui Yao Lue*. In the clinic, SHCZF has been used to treat cholestasis-related liver disease by improving intrahepatic cholestasis, but the treatment mechanism has not been elucidated. In this study, 24 Sprague-Dawley (SD) rats were randomly assigned to the normal, acute intrahepatic cholestasis (AIC), SHCZF, and ursodeoxycholic acid (UDCA) groups. In addition, 36 SD rats were divided into dynamic groups, namely, normal 24 h, AIC 24 h, normal 48 h, AIC 48 h, normal 72 h, and AIC 72 h groups. Alpha-naphthylisothiocyanate (ANIT) was used to induce an AIC rat model. Serum biochemical indices and hepatic pathology were detected. Part of the hepatic tissues was used for sequencing, and others were used for subsequent experiments. Sequencing data combined with bioinformatics analysis were used to screen target genes and identify the mechanisms of SHCZF in treating AIC rats. Quantitative real-time PCR (qRT-PCR) and Western blotting (WB) were used to detect the RNA/Protein expression levels of screened genes. Rats in the dynamic group were used to determine the sequence of cholestasis and liver injury. High-performance liquid chromatography (HPLC) was used to determine the representative bioingredients of SHCZF. Sequencing and bioinformatics analysis suggested that IDI1 and SREBP2 are hub target genes of

Abbreviations: AIC, Acute intrahepatic cholestasis; ANTI, Alpha-naphthylisothiocyanate; AAAALAC, Association for Assessment and Accreditation of Laboratory Animal Care; CLD, Cholestatic liver diseases; DHXSD, Da-Huang-Xiao-Shi decoction; DEGs, differential expressed genes; GGT, Gamma-glutamyl transaminase; HPLC, High-performance liquid chromatography; IACUC, Institutional Animal Care and Use Committee; ICP, Intrahepatic cholestasis of pregnancy; IHC, Intrahepatic Cholestasis; IDI1, Isopentenyl-Diphosphate Delta Isomerase 1; IL-1β, Interleukin 1 Beta; LCA, Lithocholic acid; LCN2, Lipocalin 2; LDLr, Low-Density Lipoprotein Receptor; PLS-DA, Partial least squares discrimination analysis; PFIC, Progressive familial intrahepatic cholestasis; qRT-PCR, Quantitative real-time PCR; SD, Sprague-Dawley; SHCZF, San-Huang-Cai-Zhu formula; SREBP2, Sterol Regulatory Element-Binding Protein 2; TCM, Traditional Chinese medicine; TI, Therapeutic index; TNF-α, Tumor Necrosis Factor Alpha; UDCA, Ursodeoxycholic Acid; HPLC-MS/MS, High-Performance Liquid Chromatography with Tandem Mass Spectrometry; WB, Western blotting.

SHCZF to ameliorate ANTI-induced intrahepatic cholestasis in rats. The treatment mechanism is associated with the regulation of lipoprotein receptor (LDLr) to reduce cholesterol intake and 3-Hydroxy-3-Methylglutaryl-CoA reductase (HMGCR), and 3-Hydroxy-3-Methylglutaryl-CoA synthase 1 (HMGCS1) to decrease cholesterol synthesis. Animal experiments showed that SHCZF significantly reduced the expression levels of the above genes and proinflammatory cytokine lipocalin 2 (LCN2), inflammatory cytokines interleukin 1 beta (IL-1β) and tumor necrosis factor alpha (TNF-α), thereby improving intrahepatic cholestasis and inflammation and liver injury.

KEYWORDS

intrahepatic cholestasis, traditional Chinese medicine, San-Huang-Chai-Zhu formula, cholesterol metabolism, IDI1, SREBP2

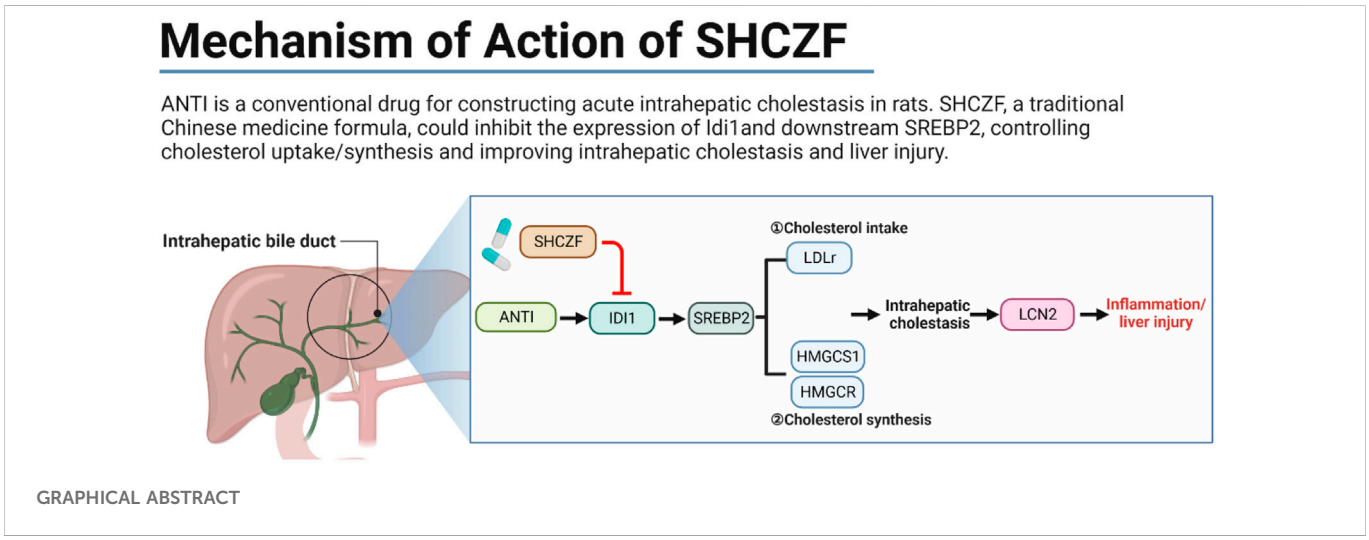

GRAPHICAL ABSTRACT

Highlights

- Elevated expression of IDI1, and SREBP2 will cause intrahepatic cholestasis in rats.
- Excessive intrahepatic cholestasis may activate the expression of the pro-inflammatory gene LCN2, causing hepatic inflammation and injury.
- The effect of San-Huang-Cai-Zhu formula (SHCZF) in improving intrahepatic cholestasis is similar to that of Ursodeoxycholic Acid (UDCA). The effect of SHCZF in improving liver injury is better than UDCA.
- The regulatory pathways of SHCZF include IDI1/SREBP2 and its downstream LDLr (reduces free cholesterol uptake) and HMGCR/HMGCS1 (reduces cholesterol synthesis in the liver).

1 Introduction

Intrahepatic cholestasis (IHC) is a pathological process caused by hepatic-disordered bile synthesis/absorption (Meier-Abt, 1990). Clinically, the prevalence of IHC is high. 35% of patients diagnosed with chronic liver disease have concurrent IHC (Bortolini et al., 1992). Patients with cholestatic liver diseases (CLDs), intrahepatic cholestasis of pregnancy (ICP), neonatal cholestasis, or progressive familial intrahepatic cholestasis (PFIC) have a high probability of IHC (Balistreri, 1985; Gossard and Talwalkar, 2014; Williamson and Geenes, 2014; Hassan and Hertel, 2022). In addition, the diagnosis of cholestasis is difficult. In the early stages, patients with IHC present normal or slightly elevated serum alkaline phosphatase (ALP) and gamma-glutamyl transaminase (GGT). A series of clinical manifestations, such as jaundice, will only gradually emerge in the progressive stage (Kuntz and Kuntz, 2008). Prolonged IHC will induce further fibrosis and cirrhosis in CLD patients, eventually causing liver failure (Guo et al., 2020; Ginès et al., 2021).

Because IHC is classified as jaundice in Chinese medicine, Da-Huang-Xiao-Shi decoction (DHXSD), the traditional formula for jaundice treatment, which originated from Jin Gui Yao Lue, is usually used to treat IHC in clinics (He et al., 1990; Chen et al., 2018). DHXSD is composed of *Mirabilitum* (Mang xiao), *Phellodendron chinense Schneid.* (Huang bai), *Rheum officinale Baill.* (Da Huang) and *Gardenia jasminoides Ellis.* (Zhi Zi). Studies have shown that DHXSD effectively improves cholestasis in mice and rats (Zhu and Feng, 2019; Xue et al., 2021). We removed *Mirabilitum* (Mang xiao) in the clinical application instead of adding *Atractylodes macrocephala Koidz.* (Bai Zhu) and *Bupleurum chinensis DC.* (Chai Hu), which dredge the liver and strengthen the spleen. Thus, San-Huang-Chai-Zhu formula (SHCZF), originating from DHXSD, was formed.

We have confirmed that SHCZF can ameliorate IHC in rats by regulating the expression of CYP4A1, HACL1, and F11R (Yao et al., 2021) and dose-dependently improve IHC-induced liver injury by inhibiting SIRT1/PGC-1α and mitochondrial oxidative stress (Liu et al., 2022b). Through network pharmacology and molecular docking, we also identified possible bioactive components in SHCZF, such as chrysin and rhodopsin, that can target AKT1 and TP53 for the treatment of AIC in rats (Liu et al., 2022a). To provide more convincing data supporting the clinical promotion of SHCZF, we screened and validated the mechanisms of SHCZF in treating AIC from a more comprehensive perspective through sequencing and bioinformatics analysis.

2 Materials and animals

2.1 Preparation of SHCZF

SHCZF is composed of five traditional Chinese herbs: *Rheum officinale Baill.* (Da Huang), *Phellodendron chinense Schneid.* (Huang Bai), *Gardenia jasminoides Ellis.* (Zhi Zi), *Bupleurum chinensis DC.* (Chai Hu), and *Atractylodes macrocephala Koidz.* (Bai Zhu) with the ratio of 4:4:3:3:4. SHCZF was prepared by the pharmaceutical center of The First Affiliated Hospital of Zhejiang Chinese Medical University. The traditional decoction method (three-decoction) was used to extract as many bioactive ingredients from herbs as possible (Wang and Liu, 1997; Lin et al., 2011). The process is as follows: 1) add ten times the volume of water to the herbs, steep for 30 min, boil and decoct for 1.5 h; 2) add eight times the volume of water to the dregs, boil and decoct for 1 h; 3) add six times the volume of water to the dregs, boil and decoct for 0.5 h. The liquids obtained from the three decoctions were combined and concentrated into SHCZF extract (2 g·ml^{-1}).

2.2 Bioactive ingredients analysis of SHCZF

High-Performance Liquid Chromatography with Tandem Mass Spectrometry (HPLC-MS/MS), used to analyze the bioactive ingredients of SHCZF, was performed by Qingdao Sci-tech Innovation Quality Testing Co., Ltd. liquid Chromatograph Mass Spectrometer.

100 mg SHCZF extract was diluted in 1 mL 70% methanol. The automatic grinder was used for crushing the above samples, followed by low-temperature sonication (40 KHZ) for 10 min. The mixture was centrifuged for 10 min (4°C, 12,000 rmp) to acquire the supernatant. Agilent Zorbax Eclipse C18 column (1.8 μm, 2.1 × 100 mm, USA) was used for chromatographic separation. The mobile phase consisted of A (0.1% formic acid aqueous solution) and B (pure acetonitrile). The column temperature was 30°C. The injection volume was 2 μL. The liquid chromatography (LC) mobile phase conditions are shown in Table 1.

Mass spectrometry (MS) monitoring was operated in positive and negative ion modes. The conditions of the different modes can be found in our previous studies (Hong et al., 2020). Refer to Thermo mzCloud and Thermo mzValut databases for identifying SHCZF bioactive ingredients.

TABLE 1 Liquid chromatography mobile phase conditions.

Time (min)	Flow rate (μL/min)	Gradient	B (%)	A (%)
0–2	300	/	5	95
2–6	300	Linear gradient	30	70
6–7	300	/	30	70
7–12	300	Linear gradient	78	22
12–14	300	/	78	22
14–17	300	Linear gradient	95	5
17–20	300	/	95	5
20–21	300	Linear gradient	5	95
21–25	300	/	5	95

2.3 Reagents of experiments

The reagents used in the experiments are as follows. Hepatic cholesterol test kit (E1015) was purchased from APPLYGEN. Protein Extraction Kit (KGP2100), 2xSDS-PAGE protein loading buffer (KGP1012) were purchased from KeyGEN Biotech. Bicinchoninic acid (BCA) protein assay kit (A20312), Goat Anti-Mouse IgG (H + L) HRP conjugated (GAM007) and Goat Anti-Rabbit IgG (H + L) HRP conjugated (GAR007) were purchased from MULTI SCIENCES. TGX Stain-Free™ FastCast ™ Acrylamide kit 7.5% (#1610181), TGX Stain-Free™ FastCast ™ Acrylamide kit 12% (#1610185), and Trans-Blot Turbo 5x Transfer Buffer (#10026938) were purchased from BIO-RAD. Polyvinylidene difluoride (PVDF) membranes (IPVH00010) were purchased fromMillipore. Anti-GAPDH monoclonal antibody (YM3029), IDI1 rabbit Pab (YT7476), SREBP2 Polyclonal antibody (YN0037), and LCN2 rabbit pAb (YT7924) were purchased from Immunoway. Tissue RNA purification kit plus (RN002plus) was purchased from ES Science. PrimeScript™ RT reagent Kit with gDNA Eraser (RR047A) and TB Green® Premix Ex Taq™ II (RR820A) were purchased from Takara.

2.4 Establishment of animal model

A total of 60 male Sprague-Dawley (SD) rats (SPF grade, 8 weeks, 140 ± 10 g) were provided by Shanghai SIPPR-Bk Laboratory Animal Co., Ltd. (SCXK (Hu) 2013-0016). All rats were housed in an environment with a temperature of 22°C ± 2°C and humidity of 60 ± 5%. After 1 week of acclimatizing feeding, rats were randomly divided into disease (n = 24) and dynamic groups (n = 36). After receiving the appropriate interventions rats were intraperitoneally injected with 50 mg·kg^{-1} pentobarbital sodium and then sacrificed (Figure 1). Hepatic tissues and serum were collected for subsequent analysis. All animal research was conducted following Association for Assessment and Accreditation of Laboratory Animal Care (AAAALAC) and Institutional Animal Care and Use Committee (IACUC) guidelines and approved by the Animal Experimentation Ethics Committee of Zhejiang Chinese medical university (ZSLL-2015-195). The modeling conditions used in this study were long-used by the research group with literature support (Chisholm and

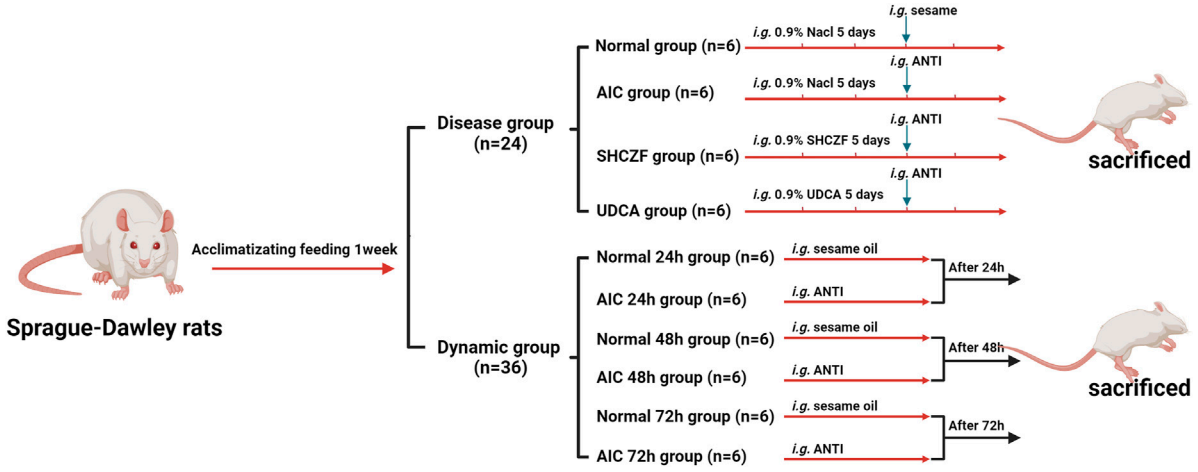

FIGURE 1
The flow of animal grouping and modeling.

Dolphin, 1996; Yao et al., 2021), resulting in low mortality (0%) and a high success rate of modeling (100%).

2.4.1 Disease model and drugs intervention

The rats in the disease group were randomly divided into the normal, AIC, SHCZF, and UDCA groups (6 rats in each group). Rats in AIC groups were given 4% alpha-naphthylisothiocyanate (ANIT) (J&K Scientific, Lot: 249447) 100 mg·kg^{-1} (the dosage of ANTI referred to the literature and our previous studies) (Chisholm and Dolphin, 1996; Yao et al., 2021). Rats in the SHCZF and UDCA groups were gavaged 20 g·kg^{-1} of SHCZF or 90 mg·kg^{-1} of UDCA, respectively. The doses of the above therapeutic drugs are obtained by equivalence conversion concerning the optimal clinical using amounts.

2.4.2 Dynamic model

The rats in the dynamic group were divided into normal 24 h, AIC 24 h, normal 48 h, AIC 48 h, normal 72 h, and AIC 72 h groups (6 rats in each group). Rats were respectively executed after injecting ANTI (100 mg·kg^{-1}) 24 h, 48 h, and 72 h.

3 Sequencing and bioinformatics analysis

Further, we used hepatic tissues for sequencing to determine the treating mechanism and target genes of SHCZF. Based on whole-genome sequencing and bioinformatics analysis, we combined the existing literature to screen the potential mechanism and target genes of SHCZF in treating AIC rats.

3.1 Sequencing

Sequencing was performed by Shanghai Yuanzi Biotechnology Co., Ltd., of China. The analysis process was as follows: total hepatic RNA was extracted with TRIzol reagent (Invitrogen, USA). Total RNA was analyzed for purity and concentration using an Agilent 2100 Bioanalyzer and RNA 6000 Nano LabChip Kit (Agilent, USA). Quality RNA was amplified to construct libraries, which were subsequently sequenced by Illumina high-throughput sequencing analysis.

3.2 Bioinformatics analysis

3.2.1 Screening of target genes

The genes with zero expression were deleted, while log2 (exp+1) transformation was performed. Boxplot, partial least squares discrimination analysis (PLS-DA), and dendrogram (R package ropls and ggplot2 were selected (Thévenot et al., 2015)) were used to determine whether the genes' expression data needed to be normalized and whether there was an expression convergence between groups and differences outside the groups.

Rats were screened for differential expressed genes (DEGs) before and after modeling (Normal vs. AIC) and treatment (AIC vs. SHCZF), respectively, using the ebayes analysis of the R package limma (Ritchie et al., 2015). |logFC|>1.5, p-value < 0.05 were used as the screening condition. Genes with opposite expression changes in Normal vs. AIC and AIC vs. SHCZF were intersected to screen for genes whose expression significantly changed in the progression of Normal to AIC and improved after SHCZF intervention. These intersected genes were considered target genes of SHCZF to improve AIC. The expression changes of the above genes in different groups of rats were further analyzed.

3.2.2 Screening of treatment mechanisms

The genes with expression changes before and after modeling (Normal vs. AIC) and treatment (AIC vs. SHCZF) (|logFC|>0, p-value < 0.05) were analyzed by Gene Set Enrichment Analysis (GSEA). C2 gene sets of the MSigDB database (*https://www.gsea-msigdb.org/gsea/msigdb/human/collections.jsp#C2*) were used as background data sets to infer which genes and pathways are most closely related to the disease and SHCZF intervention. Gene sets in the collection are curated from various sources, including online pathway databases and literature. The top three pathways with the lowest p-value will be further analyzed.

4 Experimental validation

4.1 Biochemical indices

After the rats were anesthetized, blood was taken from abdominal veins. Centrifugation was used to separate serum. ALT, AST, ALP, TPA, and TBIL levels were detected with an automatic biochemical analyzer. ALT and AST were used to reflect the degree of hepatic injury in rats. ALP, TPA, and TBIL values were used to reflect the intrahepatic cholestasis in rats.

4.2 Liver histopathological analysis

4.2.1 Hematoxylin and eosin (HE) staining

Rat hepatic tissues were fixed with 10% formaldehyde for 48 h and dehydrated with alcohol. Then, hepatic tissues were embedded in paraffin and cut into sections with a thickness of 4 μM (Leica, Germany). After dewaxing and rehydration, the sections were stained with hematoxylin for 5 min and eosin for 2 min. Finally, the sections were observed under an optical microscope (Olympus, Japan).

4.2.2 Immunohistochemistry to detect CK19

Paraffin-embedded sections of rat liver tissue were first dewaxed and hydrated. Then, antigen repair and blocking were performed. The sections were incubated separately with primary antibody (overnight at 4°C) and secondary antibody (1 h at room temperature). DAB was used as a staining agent. Hematoxylin was used for restaining. At last, the staining of sections was observed under an optical microscope (Olympus, Japan).

4.3 Hepatic cholesterol content analysis

Before lysis, PBS was used to wash hepatic tissues twice to remove residual blood. Adding 10 μL lysate per 1 mg of tissue. The supernatant was heated at 70°C for 10 min, and then centrifuged at room temperature of 2,000 g for 5 min. The supernatant was used for TC detection. The BCA method was used to determine the protein concentration in the above tissues. The ratio of cholesterol and protein concentrations was seen as the cholesterol content in rat liver tissue.

4.4 Western blot analysis

A total protein extraction kit was used to extract proteins from hepatic tissues. Protein concentrations were determined using the BCA method and uniformly diluted to 8 ng/μL. SDS loading buffer (×2) was used to configure the protein for electrophoresis. The loading protein (40 ng) was added to SDS-PAGE gels (7.5% or 12.5%). Electrophoresis was performed for 50 min at a consistent voltage (180 V). Then, the proteins were transferred to PVDF membranes using a semi-dry transfer machine (Bio-Rad, USA). PVDF membranes were incubated with the corresponding primary antibodies overnight (4°C). Primary antibodies were used at the described concentrations: LCN2 (1:800), SREBP2 (1:1000), IDI1 (1:1500), and GAPDH (1:3000). The next day, the PVDF membranes were incubated with secondary antibody (1:5000) for 1 h at room temperature. An Odyssey Infrared Imaging System was used to analyze images and corresponding gray values. Subsequently, Spearman correlation analysis was used to confirm correlations between the relative protein expression of IDI1, SREBP2 and AIC related biochemical indicators (ALP, AST, ALT) to further judge the relationship between IDI1/SREBP2 axis and AIC.

4.5 Quantitative real-time (qRT) PCR

The RNA extraction kit was used to extract RNA from hepatic tissues. RNA concentrations were determined by Micro-Volume Measurement Platforms (BioDrop, USA) and uniformly diluted to 125 ng/μL. Completing DNA removal and RNA reverse transcription, respectively, with the RNA reverse transcription kit. The reverse transcription conditions is 37°C for 15 min and 85°C for 5 s. Next, amplification was performed. The amplification system includes 2 μL cDNA, 5 μL 2 × TB green, 0.4 μL forward primer (10 μm), 0.4 μL reverse primer (10 μm), and 2.2 μL ddH_2O. The amplification condition is 95°C for 3 min, 40 cycles of 95°C for 12 s, and 62°C for 40 s. Each sample has three multiple holes. Its mean value was used for analysis. Livak ($2^{-\Delta\Delta CT}$) method was used to calculate RNA relative expression (Livak and Schmittgen, 2001). Primer sequences were designed and synthesized by Sangon Biotech (Shanghai) Co., Ltd. (Table 2).

4.6 Statistical analysis

Data were analyzed in IBM SPSS Statistics 25. Data were expressed as mean ± SD. One-way analysis of variance (ANOVA) was used to

TABLE 2 Sequencing information of hub genes.

Gene	Gene id	Primers (5′→3′)
IDI1	89784	F: GCT GCC GAG GTT GAA GTA C
		R: GCT GGC ATT GAT TTC AGG CAT TGT G
SREBP2	300095	F: AGC AAC AAC AGC AGT GGC AGA G
		R: GGT GGA TGA GGG AGA GAA GGT AGA C
LDLr	300438	F: CTT GTC CAT CTT CCT CCC CAT TGC
		R: ATC TCG TCC TCC GTG GTC TTC TG
HMGCR	25675	F: GAC CAA CCT TCT ACC TCA GCA AGC
		R: GGA CAA CTC ACC AGC CAT CAC AG
HMGCS1	29637	F: CGG TTC CCT TGC TTC TGT TCT GG
		R: CCT GGT GTG GCA TCT TGT GTG AC
LCN2	170496	F: AGC GAA TGC GGT CCA GAA AGA AAG
		R: CGA GGA TGG AAG TGA CGT TGT AGC
IL-1β	24494	F: CCC TGA ACT CAA CTG TGA AAT AGC A
		R: CCC AAG TCA AGG GCT TGG AA
TNF-α	24835	F: ATA CAC TGG CCC GAG GCA AC
		R: CCA CAT CTC GGA TCA TGC TTT C
Actin	81822	F:TGT TGC CCT AGA CTT CGA GCA
		R: CCA TAC CCA GGA AGG AAG GCT

determine if there was a difference in results. A post-ANOVA Tukey (HSD) multiple mean comparison test was used to assess the specificity of the differences. p-value < 0.05 suggest the difference is significant.

5 Results

5.1 Results of HPLC-MS/MS

In the negative and positive modes, 240 and 207 bioactive substances in SHCZF were identified, respectively. Among them, geniposide and 3-(3-Nitrophenyl)-2′-acrylonaphthone were the most concentrated bioactive ingredients obtained in negative and positive ion modes (Figure 2). The relative concentration of geniposide was as high as 7114.3 μg/g, while that of 3-(3-Nitrophenyl)-2′-acrylonaphthone was 3460.4 μg/g. Geniposide, the bioactive ingredient of *Gardenia jasminoides Ellis.* (Zhi Zi), showed the highest concentration in SHCZF, which suggests that gardenia or Zhi Zi may be the critical component in SHCZF to develop its efficacy.

In addition, we further summarized the active ingredients with the highest concentration (top 10) in positive and negative ion modes. Table 3 shows that in addition to geniposide, the concentrations of rheic acid (1271.2 μg/g), the primary bioactive ingredient of *Rheum officinale Baill* (Da Huang) was equally high. The above results suggest that SHCZF may acquire tits he unique advantages in treating diseases through multiple targets and mechanisms because of the simultaneous cross-action of multiple herbs.

5.2 Results of bioinformatics analysis

Standardization analysis aims to remove biases in sequencing data caused by technology and their possible impact on subsequent analysis. Figure 3A suggests that the sequencing data used for analysis have been normalized. Figures 3B, C indicate that the expression levels in the normal, AIC, and SHCZF rats has a distribution difference, suggesting that the intervention of ANTI and SHCZF significantly affects the gene expression of rats.

The results of DEGs screening showed that, 241 genes were upregulated, and 211 genes were downregulated in AIC rats

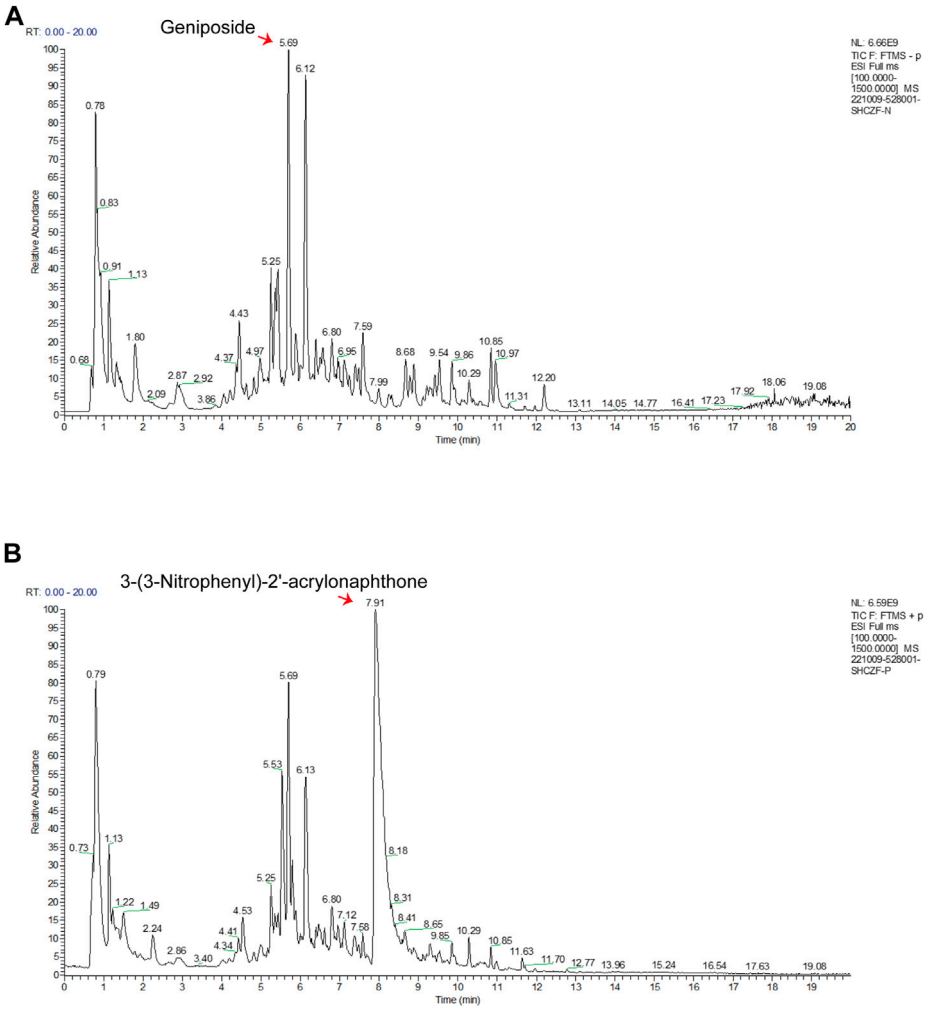

FIGURE 2
The results of HPLC-MS/MS. **(A)** Total ion current (TIC) chromatograms in negative mode, **(B)** TIC chromatograms in positive mode.

TABLE 3 Top 10 bioactive ingredients with the highest relative concentrations in SHCZF.

Bioacitve ingredient	Molecular	Class	Concentration (μg/g)
Geniposide	$C_{17}H_{24}O_{10}$	Prenol lipids	7114.3
(3R,5R)-1,3,5-Trihydroxy-4-{[(2E)-3-(4-hydroxy-3-methoxyphenyl)-2-propenoyl]oxy} cyclohexanecarboxylic acid	$C_{17}H_{20}O_9$	Organooxygen compounds	5782.4
3-(3-Nitrophenyl)-2′-acrylonaphthone	$C_{19}H_{13}NO_3$	Linear 1,3-diarylpropanoids	3460.4
Gallic acid	$C_7H_6O_5$	Benzene and substituted derivatives	2924.1
Methyl chlorogenate	$C_{17}H_{20}O_9$	Organooxygen compounds	2510.9
Catechin	$C_{15}H_{14}O_6$	Flavonoids	1887.4
N-[4-(Acetylsulfamoyl)phenyl]-2-phenyl-2-(phenylsulfanyl)acetamide	$C_{22}H_{20}N_2O_4S_2$	Benzene and substituted derivatives	1672.7
6-O-[(2E)-3-Phenyl-2-propenoyl]-1-O-(3,4,5-trihydroxybenzoyl)-β-D-glucopyranose	$C_{22}H_{22}O_{11}$	Tannins	1437.5
Rheic acid	$C_{15}H_8O_6$	Anthracenes	1271.2
Sinapoylglucose	$C_{17}H_{22}O_{10}$	Cinnamic acids and derivatives	1136.3

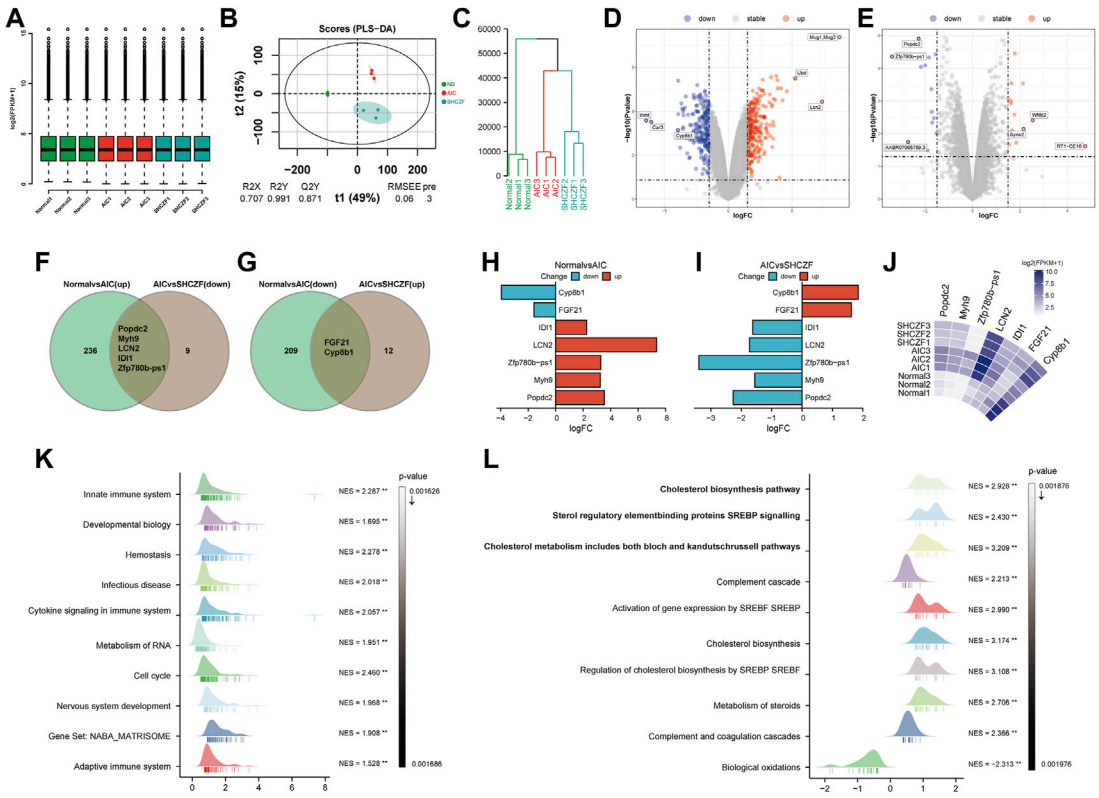

FIGURE 3
The results of bioinformatics analysis. **(A)** Boxplot, **(B)** PLS-DA plot, **(C)** Dendrogram, **(D,E)** Volcano plots, **(F,G)** Veen plots, **(H–J)** Crucial gene expression analysis plots, **(K,L)** GSEA analysis results.

compared with normal rats. Mug1, LCN2, Ubd/Inmt, Car3, and Cyp8b1 were the top 3 genes with the most significant up/downregulation of expression (Figure 3D). Compared with AIC rats, SHCZF intervention resulted in upregulation of 14 genes and downregulation of 14 genes. RT1-CE16, syne2, Wfdc2, Zfp780b-ps1, AABR07065789.3, and Popdc2 were the top 3 genes with the most significant up/downregulation of expression, respectively (Figure 3E). A total of 7 genes were screened from the above genes by taking

intersections, including Popdc2, Myh9, Zfp780b-ps1, LCN2, IDI1, FGF21, and Cyp8b1 (Figures 3F, G). The expression levels of Popdc2, Myh9, Zfp780b-ps1, Lcn2, and Idi1 were increased in the ANTI-induced AIC rats (Normal vs. AIC) and decreased after SHCZF treatment (AIC vs. SHCZF). The expression of FGF21 and Cyp8b1 was downregulated after ANTI stimulation (Normal vs. AIC) and upregulated after SHCZF treatment (Figures 3H–J). Based on the expression changes of the above genes in the normal, AIC, and SHCZF rats (elevated or decreased in the disease model and reversed after SHCZF treatment), we speculated that the above genes might be AIC-related disease genes and therapeutic target genes of SHCZF.

GSEA results suggested that the mechanism of ANTI-induced AIC in rats may be immune-related (Figure 3K). The process of cholestasis induced by toxic ANTI in rats is an invasion of a foreign substance, which will activate the immune system of rats. SHCZF treats the AIC of rats by improving the metabolism of sterols, especially cholesterol (Figure 3L). GSEA enrichment results (AIC vs. SHCZF) showed that IIDI1, Sqle, Hmgcs1, Cyp51, Fdps, and Fdft1 simultaneously exist in the top 3 significant pathways (p-value minimum), suggesting that these genes may be the core genes in SHCZF-related cholesterol regulatory pathways (Table 4).

Among the above genes, only IDI1 is a target gene of both ANTI, SHCZF and the core gene in cholesterol metabolism-related pathways. The change in the expression of IDI1 may be the key to SHCZF treating AIC rats and may be related to cholesterol metabolism.

5.3 Formulation of a hypothesis

IHC is a pathophysiological process caused by bile secretion and excretion disorders, characterized by excessive accumulation of bile components such as cholesterol and bilirubin in intrahepatic bile ducts, causing damage to the liver.

IDI1 is an essential metabolic gene related to cholesterol synthesis and transport (Yang et al., 2022). IDI1 can regulate cholesterol synthesis and transport through SREBP2 (Tremblay et al., 2011; Zhang et al., 2012; Zhang et al., 2018). The upregulation of LDLr caused by SREBP2 activation promotes the uptake of free cholesterol, which is an essential reason for cholesterol accumulation (Van Rooyen et al., 2011). SREBP2 can also directly regulate the rate of cholesterol synthesis by regulating the expression of the rate-limiting enzymes HMGCR (Poornima et al., 2022) and HMGCS1 (Vock et al., 2008; Madison, 2016). Excessive accumulation of cholesterol in the liver will stimulate the expression of LCN2, causing inflammation and subsequent hepatic damage (Ye et al., 2016; Currò et al., 2020).

Therefore, we propose the following hypothesis based on bioinformatics and literature analysis results. SHCZF reduces LDL-c uptake by regulating IDI1/SREBP2/LDLR pathway. SHCZF can also lower cholesterol synthesis in the liver by regulating IDI1/SREBP2/HMGCR (HMGCS1) pathway (Figure 4).

5.4 Results of experiments

5.4.1 SHCZF protects rats from ANTI-induced AIC

Figures 5A–C showe that the cholestasis-related indicators ALP, TBA, and TBIL were significantly higher in the serum of AIC rats than in the serum of normal rats ($p < 0.05$). After SHCZF and UDCA administration, the concentration of these indicators in the serum of rats was reduced. Intrahepatic cholesterol levels were significantly higher in AIC rats than that in normal rats ($p < 0.05$) and decreased after UDCA and SHCZF treatment ($p < 0.05$). SHCZF restored hepatic cholesterol to levels similar to those in normal rats, while UDCA restored cholesterol to levels below those in normal rats (Figure 5D). The common pathological manifestations of IHC include cholestasis starting from hepatocytes in the third region of the hepatic lobules, manifesting as feathery degeneration of hepatocytes with dilated bile ducts (Nakanuma et al., 2012). Cytokeratin 19 (CK19) is a bile duct type cytokeratin. Immunohistochemistry of CK19 can effectively reflect bile duct dilatation in the liver. Figure 5E shows increased bile duct dilatation in AIC rats compared to normal rats and significant improvement after SHCZF and UDCA treatment.

The above results suggest that both SHFZF and UDCA can improve hepatic cholestasis in rats. The efficacy of UDCA is better than that of SHCZF.

5.4.2 SHCZF protects rats from hepatic injury

Figures 6A, B show that the hepatic injury-related indicators ALT and AST were significantly upregulated in AIC rats compared with normal rats ($p < 0.05$). After the administration of SHCZF and UDCA, ALT and AST were significantly reduced ($p < 0.05$). Figure 6C shows that AIC rats had significant inflammatory cell infiltration in the portal area, while SHCZF and UDCA effectively improved inflammation in the rat liver.

The above results suggest that both SHFZF and UDCA can improve hepatic inflammation and injury in rats. The efficacy of SHCZF is better than that of UDCA.

5.4.3 Cholestasis precedes hepatic injury

When the liver is damaged, the transaminase in liver cells will be released into the blood, causing an increase in serum ALT and AST levels (Pol et al., 1991; Prati et al., 2002). The production of ALP can be induced when bile is not efficiently excreted and the internal pressure of bile capillaries is increased. Subsequently, bile acid dissolves ALP from the lipid membrane, increasing serum ALP levels (Siddique and Kowdley, 2012). Therefore, serum ALT and

TABLE 4 GSEA crucial pathways information Table (AIC vs. SHCZF).

ID	p-value	Core genes
Cholesterol biosynthesis pathway	0.001876	IID1, Sqle, Hmgcs1, Cyp51, Fdps, Fdft1, Msmo1, Mvd, Sc5d, Mvk, Pmvk
Sterol regulatory element binding proteins SREBP signaling	0.001883	IDI1, Sqle, Hmgcs1, Cyp51, Fdps, Fdft1, Insig1, Mvd, Fasn
Cholesterol metabolism includes both bloch and kandutschrussell pathways	0.001894	IDI1, Sqle, Hmgcs1, Cyp51, Fdps, Fdft1, Hsd17b7, Msmo1, Mvd, Ebp, Sc5d, Dhcr24, Fasn, Mvk, Pmvk

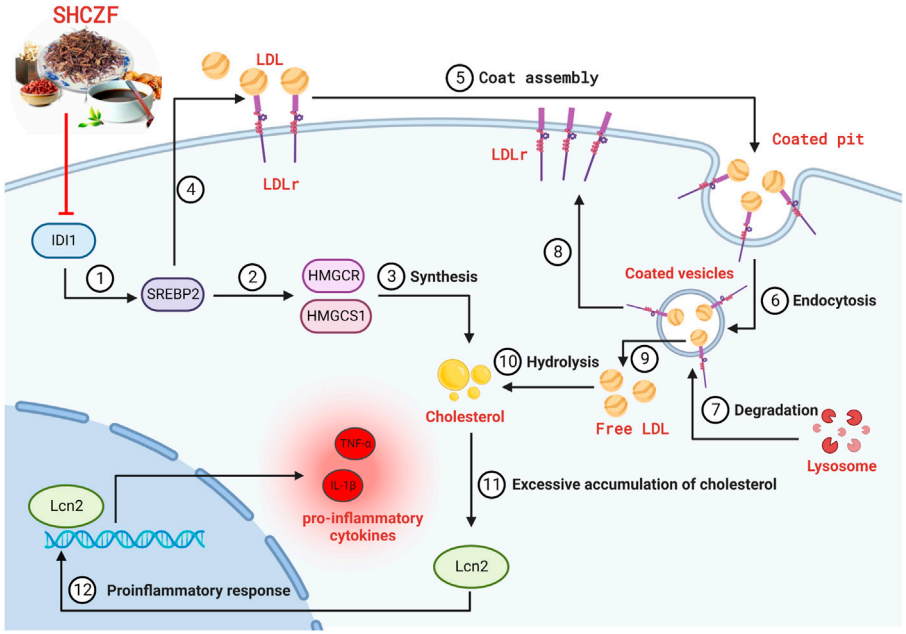

FIGURE 4
The hypothesis of SHCZF in treating AIC rats. ②, ③The mechanism of cholesterol synthesis, ④–⑨The mechanism of cholesterol uptake: Endocytosis mediated by the LDLr on the cell surface can absorb cholesterol-rich LDL from the blood, called the LDLr pathway. LDLr can combine with free LDL in plasma to form an LDL-LDLr complex, which appears in the coated pit, and forms coated vesicles to enter the cell. The outer skin of coated vesicles is then depolymerized, causing the separation of LDL and LDLr. LDLr returns to the cellular membrane for the next cycle, while LDL is degraded by lysosomes and hydrolyzed into free cholesterol.

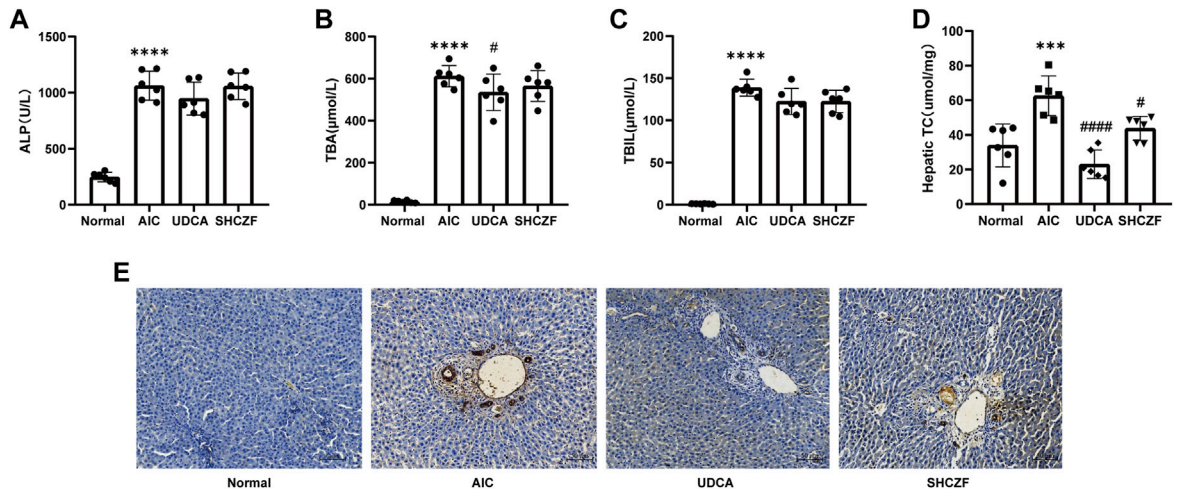

FIGURE 5
The results of cholestasis levels in rats. **(A)** ALP level, **(B)** TBA level, **(C)** TBIL level, **(D)** Hepatic cholesterol content level, **(E)** CK19 immunohistochemistry (400x).

AST levels always reflect the degree of hepatic injury, while ALP demonstrates the level of cholestasis.

To clarify the sequence of cholestasis and hepatic injury, we constructed 24, 48, 72 h AIC rat models and corresponding normal controls. Then, we detected the dynamic changes in ALT, AST, and ALP in rat serum. The results showed that compared with normal rats, the level of serum ALP in AIC rats increased significantly at 24 h (Figure 7A). In comparison, ALT and AST levels increased dramatically after 24 h, reaching the peak at 48 h (Figures 7B, C). The ALP level was significantly higher in AIC rats than that in normal rats at 24 h, while ALT and AST did not increase considerably, suggesting that cholestasis may precede hepatic injury in rats.

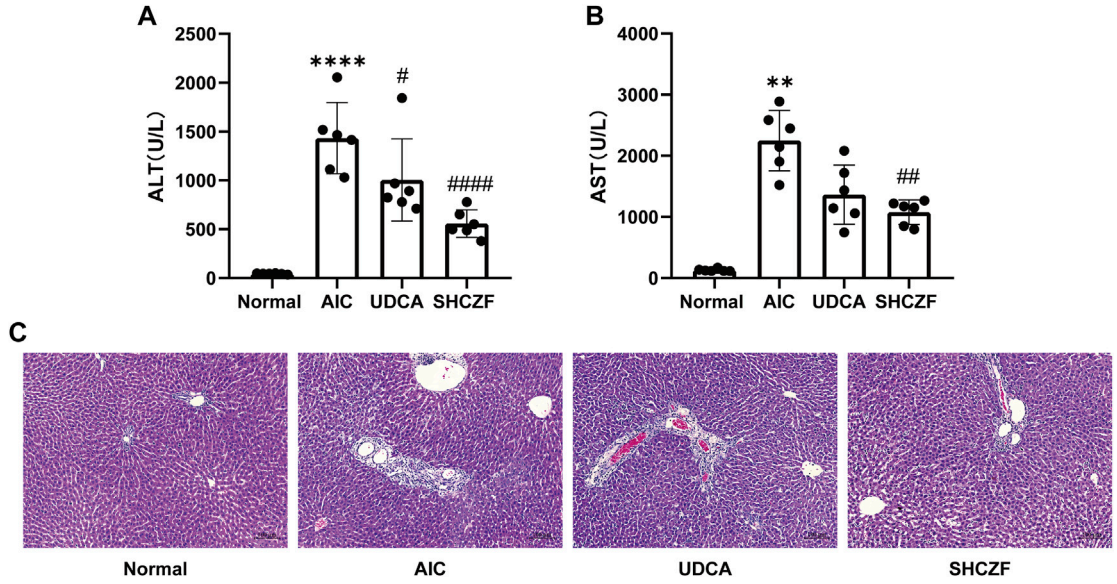

FIGURE 6
The results of hepatic injury in rats. **(A)** ALT level, **(B)** AST level, **(C)** HE staining (200x).

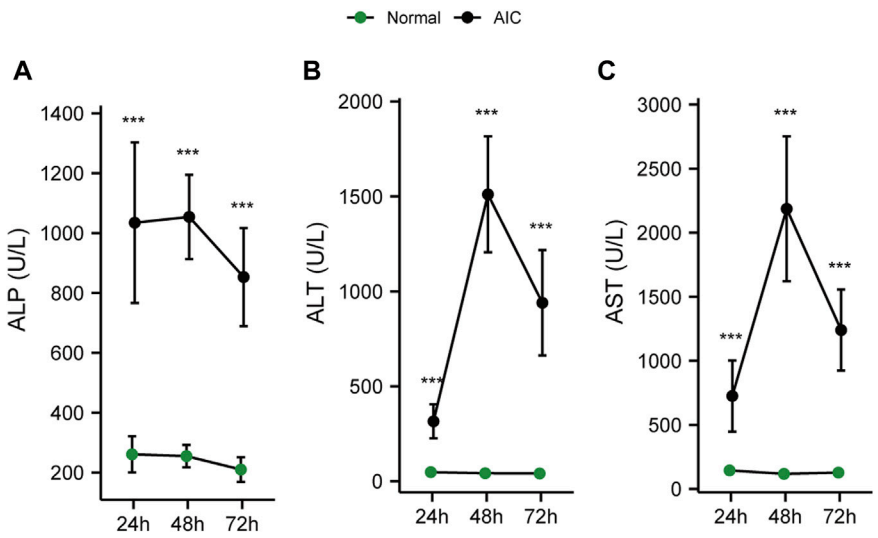

FIGURE 7
Dynamic chart of serum cholesterol and hepatic injury-related indicators in rats. **(A)** ALP dynamic change, **(B)** ALT dynamic change, **(C)** AST dynamic change.

5.4.4 SHCZF inhibits IDI1/SREBP2/LDLr and IDI1/SREBP2/HMGCR/HMGCS1

IDI1 and SREBP2 are the crucial target genes of SHCZF for the treatment of cholestasis, as clarified by bioinformatics and literature analysis. Downstream LDLr (cholesterol uptake) and HMGCR/HMGCS1 (cholesterol synthesis) are controlled by SREBP2 for the critical genes for regulating cholesterol metabolism (Haskins et al., 2015; Che et al., 2020; Lebeau et al., 2022).

The correlation coefficient (R) > 0 indicates a positive correlation between the two variables; Conversely, it is a negative correlation. The absolute value of correlation coefficient reflects the degree of correlation: 0–0.3 represents weak or uncorrelated; 0.3–0.5 represents weak correlation; 0.5–0.8 represents moderate correlation; 0.8–1 stands for strong correlation. The results of correlation analysis indicated that the expression of IDI1 and SREBP2 were at least weakly correlated with ALP, AST, and ALT levels (Figures 8A–C).

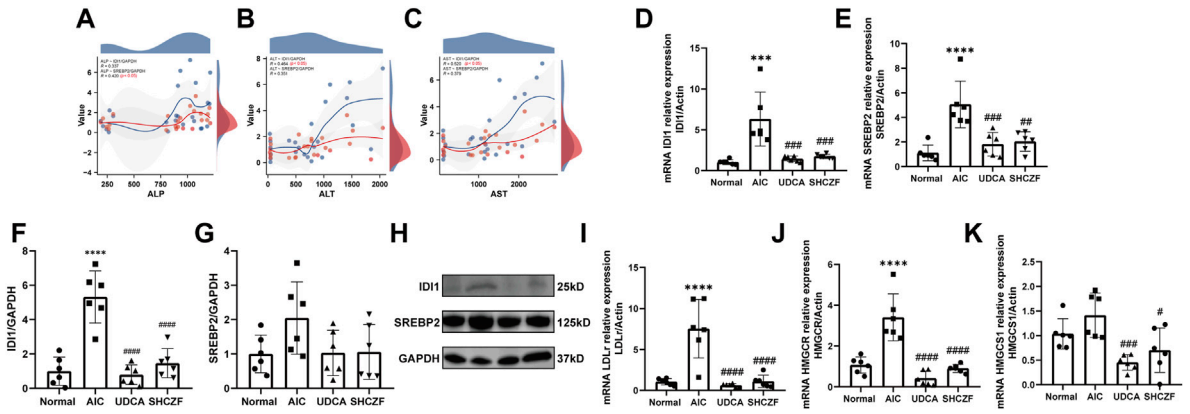

FIGURE 8
Expression of SHCZF target genes and cholesterol metabolism-related genes. **(A)** Correlation between IDI1, SREBP2, and ALP, **(B)** Correlation between IDI1, SREBP2, and ALT, **(C)** Correlation between IDI1, SREBP2, and AST, **(D)** mRNA expression of IDI1, **(E)** mRNA expression of SREBP2, **(F)** protein expression of IDI1, **(G)** protein expression of SREBP2, **(H)** WB bands of IDI1, SREBP2, and GAPDH, **(I)** mRNA expression of LDLr, **(J)** mRNA expression of HMGCR, **(K)** mRNA expression of HMGCS1.

Figures 8D–H show that both the mRNA and protein expression of IDI1 and SREBP2 were increased after ANTI induction ($p < 0.05$), while intervention with SHCZF and UDCA significantly decreased their expression ($p < 0.05$). The expression of LDLr, HMGCR, and HMGCS1 was substantially higher in the liver tissues of AIC rats compared with normal rats ($p < 0.05$), while SHCZF and UDCA treatment significantly reduced the expression of these genes ($p < 0.05$) (Figures 8I–K). The expression change in the IDI1/SREBP2 pathway and downstream cholesterol uptake and synthesis-related hub genes met expectations. In addition, the efficacy of SHCZF in improving cholesterol metabolism was similar to that of UDCA.

5.4.5 SHCZF reduces the release of inflammatory cytokines

Excessive accumulation of cholesterol activates the expression of LCN2. LCN2 substantially activates proinflammatory cytokines (TNF-α and IL-1β), causing hepatic inflammation (Weerachayaphorn et al., 2014; Ye et al., 2016).

Both the mRNA and protein expression levels of LCN2 increased after ANTI induction ($p < 0.05$), whereas intervention with SHCZF and UDCA decreased LCN2 expression ($p < 0.05$) (Figures 9A–C). Figures 9D, E shows that TNF-α and IL-1β were upregulated in AIC rats compared with normal rats ($p < 0.05$). SHCZF and UDCA treatment significantly reduced the expression levels of these proinflammatory cytokines ($p < 0.05$). The expression changes of LCN2 and downstream proinflammatory cytokines meets expectations. In addition, the efficacy of SHCZF in improving inflammation was better than that of UDCA.

6 Discussion

IHC is gaining increasing attention due to its high morbidity and severe outcome. However, until now, the drugs available for treating IHC have been quite limited. UDCA is one of the few prescription drugs approved by the U.S. Food and Drug Administration (FDA) for clinical use in treating IHC (Beuers et al., 1998). However, the therapeutic index (TI) of UDCA is narrow. Inappropriate therapeutic doses may cause "unintended" adverse reactions, such as hepatitis, ascites, severe diarrhea, and immunosuppression, etc. (Chapman, 2010; Sinakos et al., 2010). *In vivo*, UDCA can even transform into toxic lithocholic acid (LCA), which may induce death from liver failure in patients with impaired sulfation (one of the major conjugation pathways in the body with an essential role in human metabolism (Alnouti, 2009;

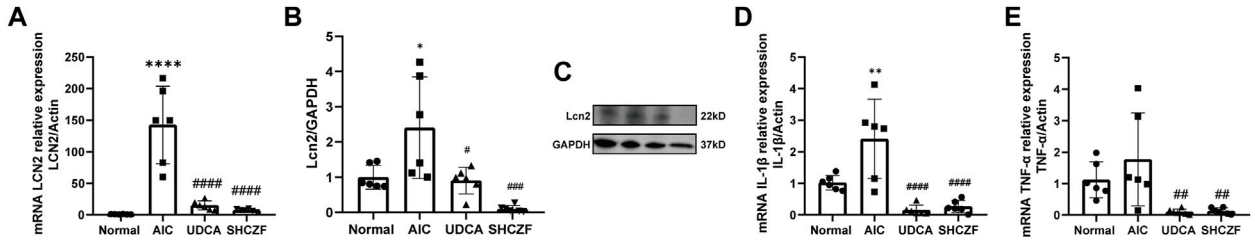

FIGURE 9
Expression of LCN2 and pro-inflammatory cytokines. **(A)** mRNA expression of LCN2, **(B)** protein expression of LCN2, **(C)** WB bands of Lcn2 and GAPDH, **(D)** mRNA expression of TNF-α, **(E)** mRNA expression of IL-1β.

Kotb, 2012). Finding reliable drugs for the treatment of cholestasis is critical.

In China, traditional Chinese medicine has been used to treat diseases for thousands of years and shows great value for rediscovery. Among the medicines, SHZCF, originating from *Jin Gui Yao Lue*, is a traditional Chinese formula used for treating cholestasis in the clinic. In a previous study, we have clarified the mechanism by which SHCZF improves cholestasis through mitochondrial oxidative stress (Liu et al., 2022b). We also screened essential bioactive ingredients and possible target genes of SHCZF through network pharmacology (Liu et al., 2022a). However, no study has directly confirmed the effect of SHCZF on cholesterol metabolism-related pathways. In addition, the relationship between cholestasis and liver inflammation and the improvement effect of SHCZF is also unclear.

In this study, through transcriptome sequencing data and bioinformatics analysis, we preliminarily determined that IDI1/SREBP2, a cholesterol metabolism pathway, may be the therapeutic target of SHCZF. The results of CK19 immunohistochemistry, TC, and evaluation of cholestasis-related indicators showed that the intervention of SHCZF and UDCA effectively improved the bile duct dilatation and cholestasis in the rat liver. The effect of UDCA on improving cholesterol was significantly higher than that of SHCZF, which could reduce cholesterol to a level lower than that of normal rats. However, a moderate amount of cholesterol is beneficial. Studies have found that cholesterol can induce oxidative stress, mitochondrial damage, and the death of hepatic stellate cells to reduce the degree of fibrosis (Rauchbach et al., 2022). Moderate cholesterol can also activate Nrf-2 and HIF-1α and promote hepatocyte proliferation and liver regeneration, improving hepatic fibrosis (Kaminsky-Kolesnikov et al., 2020). SHCZF, which restored the cholesterol level in the liver of rats to approximately that in normal rats, may be more suitable for the treatment of cholestasis. The dynamic rat model confirmed that continuous cholestasis further led to hepatic inflammation and subsequent damage, reflecting the importance of timely treatment of cholestasis. Assessment of hepatic injury indicators (transaminase) and pro-inflammatory cytokines showed that both SHCZF and UDCA improved hepatic inflammation and injury, but the improvement effect of SHCZF was better. Based on the analysis of the experimental results, we confirmed that SHCZF can indeed improve cholestasis and subsequent hepatic inflammation and injury by regulating IDI1/SREBP2 pathway. Simultaneously, through the comparison of curative effects, we believe that SHCZF may be more effective than the positive drug UDCA. However, the above analysis results only come from rat experiments, lacking the support of clinical research. As a complex drug composed of various traditional Chinese herbs, SHCZF quality control is also an unavoidable problem.

7 Conclusion

In this study, we confirmed the efficacy of SHCZF improving ANTI-induced AIC in rats: 1) Cholesterol sludge and inflammatory infiltration in the rat liver were alleviated; 2) IDI1/SREBP2 expression was reduced, and cholesterol uptake (LDLr), synthesis (HMGCR/HMGCS1)-related gene expression was inhibited; 3) Excessive accumulation of cholesterol in the liver may further induce the expression of LCN2, causing hepatic inflammation and injury; 4) The expression of LCN2 was significantly reduced, and the levels of proinflammatory cytokines TNF-α and IL-1β were suppressed.

Data availability statement

The datasets presented in this study can be found in online repositories. The names of the repository/repositories and accession number(s) can be found below: NCBI BioProject https://www.ncbi.nlm.nih.gov/bioproject/, PRJNA906447.

Ethics statement

The animal study was reviewed and approved by The Animal Experimentation Ethics Committee of Zhejiang Chinese medical university (ZSLL-2015-195).

Author contributions

JY: Investigation, Software, Validation, Writing—original draft. ZC: Investigation, Visualization. YN: Investigation, Software. JMY: Visualization. SZ: Conceptualization, Methodology. ZYC: Conceptualization, Methodology.

Funding

This work was supported by the Zhejiang Science and Technology Program of Traditional Chinese Medicine (2023ZR016).

Conflict of interest

The authors declare that the research was conducted in the absence of any commercial or financial relationships that could be construed as a potential conflict of interest.

Publisher's note

Supplementary material

The Supplementary Material for this article can be found online at: https://www.frontiersin.org/articles/10.3389/fphar.2023.1093934/full#supplementary-material

SUPPLEMENTARY TABLE 1
UHPLC-MSMS results.

SUPPLEMENTARY TABLE 2
WB original data.

SUPPLEMENTARY TABLE 3
GSEA results (AIC vs SHCZF).

SUPPLEMENTARY TABLE 4
Biochemical index of disease model.

SUPPLEMENTARY TABLE 5
Biochemical index of dynamic model.

SUPPLEMENTARY TABLE 6
GSEA results (ND vs AIC).

SUPPLEMENTARY TABLE 7
PCR original data.

SUPPLEMENTARY TABLE 8
RNA control.

SUPPLEMENTARY TABLE 9
TC original data.

SUPPLEMENTARY TABLE 10
WB original bands.

References

Alnouti, Y. (2009). Bile acid sulfation: A pathway of bile acid elimination and detoxification. *Toxicol. Sci.* 108 (2), 225–246. doi:10.1093/toxsci/kfn268

Balistreri, W. F. (1985). Neonatal cholestasis. *J. Pediatr.* 106 (2), 171–184. doi:10.1016/s0022-3476(85)80282-1

Beuers, U., Boyer, J. L., and Paumgartner, G. (1998). Ursodeoxycholic acid in cholestasis: Potential mechanisms of action and therapeutic applications. *Hepatology* 28 (6), 1449–1453. doi:10.1002/hep.510280601

Bortolini, M., Almasio, P., Bray, G., Budillon, G., Coltorti, M., Frezza, M., et al. (1992). Multicentre survey of the prevalence of intrahepatic cholestasis in 2520 consecutive patients with newly diagnosed chronic liver disease. *Drug Investig.* 4 (4), 83–89. doi:10.1007/BF03258368

Chapman, R. W. (2010). Primary sclerosing cholangitis: What is the role of ursodeoxycholic acid in therapy for PSC? *Nat. Rev. Gastroenterol. Hepatol.* 7 (2), 74–75. doi:10.1038/nrgastro.2009.235

Che, L., Chi, W., Qiao, Y., Zhang, J., Song, X., Liu, Y., et al. (2020). Cholesterol biosynthesis supports the growth of hepatocarcinoma lesions depleted of fatty acid synthase in mice and humans. *Gut* 69 (1), 177–186. doi:10.1136/gutjnl-2018-317581

Chen, J. L., Yang, X., Zhang, Q., Sun, L., Liu, Y., Zhu, B. B., et al. (2018). Effect of ursodeoxycholic acid with traditional Chinese medicine on biochemical response in patients with primary biliary cholangitis: A real-world cohort study. *Zhonghua Gan Zang Bing Za Zhi* 26 (12), 909–915. doi:10.3760/cma.j.issn.1007-3418.2018.12.007

Chisholm, J. W., and Dolphin, P. J. (1996). Abnormal lipoproteins in the ANIT-treated rat: A transient and reversible animal model of intrahepatic cholestasis. *J. Lipid Res.* 37 (5), 1086–1098. doi:10.1016/s0022-2275(20)42018-8

Currò, D., Vergani, E., Bruno, C., Comi, S., D'abate, C., and Mancini, A. (2020). Plasmatic lipocalin-2 levels in chronic low-grade inflammation syndromes: Comparison between metabolic syndrome, total and partial adult growth hormone deficiency. *Biofactors* 46 (4), 629–636. doi:10.1002/biof.1628

Ginès, P., Krag, A., Abraldes, J. G., Solà, E., Fabrellas, N., and Kamath, P. S. (2021). Liver cirrhosis. *Lancet* 398 (10308), 1359–1376. doi:10.1016/S0140-6736(21)01374-X

Gossard, A. A., and Talwalkar, J. A. (2014). Cholestatic liver disease. *Med. Clin. North Am.* 98 (1), 73–85. doi:10.1016/j.mcna.2013.09.002

Guo, H., Liao, M., Jin, J., Zeng, J., Li, S., Schroeder, D. R., et al. (2020). How intrahepatic cholestasis affects liver stiffness in patients with chronic Hepatitis B: A study of 1197 patients with liver biopsy. *Eur. Radiol.* 30 (2), 1096–1104. doi:10.1007/s00330-019-06451-x

Haskins, J. W., Zhang, S., Means, R. E., Kelleher, J. K., Cline, G. W., Canfrán-Duque, A., et al. (2015). Neuregulin-activated ERBB4 induces the SREBP-2 cholesterol biosynthetic pathway and increases low-density lipoprotein uptake. *Sci. Signal* 8 (401), ra111. doi:10.1126/scisignal.aac5124

Hassan, S., and Hertel, P. (2022). Overview of progressive familial intrahepatic cholestasis. *Clin. Liver Dis.* 26 (3), 371–390. doi:10.1016/j.cld.2022.03.003

He, J., Wang, C., and Xu, J. (1990). Relation of changes in plasma cAMP, cGMP and the clinical conditions, pathology and the type of traditional Chinese medicine in 50 cases of chronic severe icteric hepatitis (in Chinese). *Zhong Xi Yi Jie He Za Zhi* 10 (2), 7567–7577.

Hong, W., Li, S., Cai, Y., Zhang, T., Yang, Q., He, B., et al. (2020). The target MicroRNAs and potential underlying mechanisms of yiqi-bushen-tiaozhi recipe against-non-alcoholic steatohepatitis. *Front. Pharmacol.* 11, 529553. doi:10.3389/fphar.2020.529553

Kaminsky-Kolesnikov, Y., Rauchbach, E., Abu-Halaka, D., Hahn, M., García-Ruiz, C., Fernandez-Checa, J. C., et al. (2020). Cholesterol induces nrf-2- and HIF-1α-Dependent hepatocyte proliferation and liver regeneration to ameliorate bile acid toxicity in mouse models of NASH and fibrosis. *Oxid. Med. Cell Longev.* 2020, 5393761. doi:10.1155/2020/5393761

Kotb, M. A. (2012). Molecular mechanisms of ursodeoxycholic acid toxicity & side effects: Ursodeoxycholic acid freezes regeneration & induces hibernation mode. *Int. J. Mol. Sci.* 13 (7), 8882–8914. doi:10.3390/ijms13078882

Kuntz, M., and Kuntz, H. D. J. S. B. H. (2008). *Hepatology textbook and atlas*.

Lebeau, P. F., Byun, J. H., Platko, K., Saliba, P., Sguazzin, M., Macdonald, M. E., et al. (2022). Caffeine blocks SREBP2-induced hepatic PCSK9 expression to enhance LDLR-mediated cholesterol clearance. *Nat. Commun.* 13 (1), 770. doi:10.1038/s41467-022-28240-9

Lin, Y., Zhou, L., and Wu, S. (2011). Reflections on the research of reforming the dosage form of traditional Chinese medicine soup (in Chines). *Chin. J. Exp. Traditional Med. Formulae* 17 (5), 3.

Liu, B., Zhang, J., Shao, L., and Yao, J. (2022a). Network pharmacology analysis and molecular docking to unveil the potential mechanisms of San-Huang-Chai-Zhu formula treating cholestasis. *PLoS One* 17 (2), e0264398. doi:10.1371/journal.pone.0264398

Liu, B., Zhang, J., Shao, L., and Yao, J. (2022b). San-huang-chai-zhu formula ameliorates liver injury in intrahepatic cholestasis through suppressing SIRT1/PGC-1α-regulated mitochondrial oxidative stress. *Evid. Based Complement. Altern. Med.* 2022, 7832540. doi:10.1155/2022/7832540

Livak, K. J., and Schmittgen, T. D. (2001). Analysis of relative gene expression data using real-time quantitative PCR and the 2(-Delta Delta C(T)) Method. *Methods* 25 (4), 402–408. doi:10.1006/meth.2001.1262

Madison, B. B. (2016). Srebp2: A master regulator of sterol and fatty acid synthesis. *J. Lipid Res.* 57 (3), 333–335. doi:10.1194/jlr.C066712

Meier-Abt, P. J. (1990). Cellular mechanisms of intrahepatic cholestasis. *Drugs* 40 (3), 84–97. doi:10.2165/00003495-199000403-00009

Nakanuma, Y., Zen, Y., and Portmann, B. C. J. M. P. O. T. L. (2012). Diseases of the bile ducts - MacSween's pathology of the liver. *Sixth Ed.* 20 (2), 491–562.

Pol, S., Nalpas, B., Vassault, A., Bousquet-Lemercier, B., Franco, D., Lacour, B., et al. (1991). Hepatic activity and mRNA expression of aspartate aminotransferase isoenzymes in alcoholic and nonalcoholic liver disease. *Hepatology* 14 (4), 620–625. doi:10.1016/0270-9139(91)90048-z

Poornima, M. S., Sindhu, G., Billu, A., Sruthi, C. R., Nisha, P., Gogoi, P., et al. (2022). Pretreatment of hydroethanolic extract of Dillenia indica L. attenuates oleic acid induced NAFLD in HepG2 cells via modulating SIRT-1/p-LKB-1/AMPK, HMGCR & PPAR-α signaling pathways. *J. Ethnopharmacol.* 292, 115237. doi:10.1016/j.jep.2022.115237

Prati, D., Taioli, E., Zanella, A., Della Torre, E., Butelli, S., Del Vecchio, E., et al. (2002). Updated definitions of healthy ranges for serum alanine aminotransferase levels. *Ann. Intern Med.* 137 (1), 1–10. doi:10.7326/0003-4819-137-1-200207020-00006

Rauchbach, E., Zeigerman, H., Abu-Halaka, D., and Tirosh, O. (2022). Cholesterol induces oxidative stress, mitochondrial damage and death in hepatic stellate cells to mitigate liver fibrosis in mice model of NASH. *Antioxidants (Basel)* 11 (3), 536. doi:10.3390/antiox11030536

Ritchie, M. E., Phipson, B., Wu, D., Hu, Y., Law, C. W., Shi, W., et al. (2015). Limma powers differential expression analyses for RNA-sequencing and microarray studies. *Nucleic Acids Res.* 43 (7), e47. doi:10.1093/nar/gkv007

Siddique, A., and Kowdley, K. V. (2012). Approach to a patient with elevated serum alkaline phosphatase. *Clin. Liver Dis.* 16 (2), 199–229. doi:10.1016/j.cld.2012.03.012

Sinakos, E., Marschall, H. U., Kowdley, K. V., Befeler, A., Keach, J., and Lindor, K. (2010). Bile acid changes after high-dose ursodeoxycholic acid treatment in primary sclerosing cholangitis: Relation to disease progression. *Hepatology* 52 (1), 197–203. doi:10.1002/hep.23631

Thévenot, E. A., Roux, A., Xu, Y., Ezan, E., and Junot, C. (2015). Analysis of the human adult urinary metabolome variations with age, body Mass index, and gender by implementing a comprehensive workflow for univariate and OPLS statistical analyses. *J. Proteome Res.* 14 (8), 3322–3335. doi:10.1021/acs.jproteome.5b00354

Tremblay, A. J., Lamarche, B., Lemelin, V., Hoos, L., Benjannet, S., Seidah, N. G., et al. (2011). Atorvastatin increases intestinal expression of NPC1L1 in hyperlipidemic men. *J. Lipid Res.* 52 (3), 558–565. doi:10.1194/jlr.M011080

Van Rooyen, D. M., Larter, C. Z., Haigh, W. G., Yeh, M. M., Ioannou, G., Kuver, R., et al. (2011). Hepatic free cholesterol accumulates in obese, diabetic mice and causes nonalcoholic steatohepatitis. *Gastroenterology* 141 (4), 1393e1391–14031395. doi:10.1053/j.gastro.2011.06.040

Vock, C., Döring, F., and Nitz, I. (2008). Transcriptional regulation of HMG-CoA synthase and HMG-CoA reductase genes by human ACBP. *Cell Physiol. Biochem.* 22 (5-6), 515–524. doi:10.1159/000185525

Wang, L., and Liu, B. (1997). Experimental investigation on the relationship between the amount of herbal decoction, water addition, fire, decoction time and decoction volume (in Chinese)CNKI:SUN:ZGYA. *China Pharm.* 8 (2), 2.

Weerachayaphorn, J., Luo, Y., Mennone, A., Soroka, C. J., Harry, K., and Boyer, J. L. (2014). Deleterious effect of oltipraz on extrahepatic cholestasis in bile duct-ligated mice. *J. Hepatol.* 60 (1), 160–166. doi:10.1016/j.jhep.2013.08.015

Williamson, C., and Geenes, V. (2014). Intrahepatic cholestasis of pregnancy. *Obstet. Gynecol.* 124 (1), 120–133. doi:10.1097/aog.0000000000000346

Xue, H., Fang, S., Zheng, M., Wu, J., Li, H., Zhang, M., et al. (2021). Da-Huang-Xiao-Shi decoction protects against3, 5-diethoxycarbonyl-1,4-dihydroxychollidine-induced chronic cholestasis by upregulating bile acid metabolic enzymes and efflux transporters. *J. Ethnopharmacol.* 269, 113706. doi:10.1016/j.jep.2020.113706

Yang, X., Zhao, Z., Fan, Q., Li, H., Zhao, L., Liu, C., et al. (2022). Cholesterol metabolism is decreased in patients with diminished ovarian reserve. *Reprod. Biomed. Online* 44 (1), 185–192. doi:10.1016/j.rbmo.2021.09.013

Yao, J., Yan, J., Wu, J., Yu, J., He, B., Chen, X., et al. (2021). Predicting target genes of san-huang-chai-zhu formula in treating ANIT-induced acute intrahepatic cholestasis rat model via bioinformatics analysis combined with experimental validation. *Evid. Based Complement. Altern. Med.* 2021, 5320445. doi:10.1155/2021/5320445

Ye, D., Yang, K., Zang, S., Lin, Z., Chau, H. T., Wang, Y., et al. (2016). Lipocalin-2 mediates non-alcoholic steatohepatitis by promoting neutrophil-macrophage crosstalk via the induction of CXCR2. *J. Hepatol.* 65 (5), 988–997. doi:10.1016/j.jhep.2016.05.041

Zhang, F., Sun, W., Chen, J., Jiang, L., Yang, P., Huang, Y., et al. (2018). SREBP-2, a new target of metformin? *Drug Des. Devel Ther.* 12, 4163–4170. doi:10.2147/dddt.S190094

Zhang, L., Mccabe, T., Condra, J. H., Ni, Y. G., Peterson, L. B., Wang, W., et al. (2012). An anti-PCSK9 antibody reduces LDL-cholesterol on top of a statin and suppresses hepatocyte SREBP-regulated genes. *Int. J. Biol. Sci.* 8 (3), 310–327. doi:10.7150/ijbs.3524

Zhu, G., and Feng, F. (2019). UPLC-MS-based metabonomic analysis of intervention effects of Da-Huang-Xiao-Shi decoction on ANIT-induced cholestasis. *J. Ethnopharmacol.* 238, 111860. doi:10.1016/j.jep.2019.111860

frontiers | Frontiers in Pharmacology

TYPE Original Research
PUBLISHED 09 May 2023
DOI 10.3389/fphar.2023.1124015

OPEN ACCESS

EDITED BY
Yi Wu,
Nanjing Agricultural University, China

REVIEWED BY
Fatima Rizvi,
Boston University, United States
Xiao Ma,
Chengdu University of Traditional Chinese Medicine, China

*CORRESPONDENCE
Peixin Guo,
806016344@qq.com

†These authors have contributed equally to this work

RECEIVED 14 December 2022
ACCEPTED 24 April 2023
PUBLISHED 09 May 2023

CITATION
Bai Y, Wu H, Zheng L, Xie Y, Liu F, Wan Y, Li Q and Guo P (2023), Mechanisms of Yajieshaba in the treatment of liver fibrosis through the Keap1-Nrf2 signaling pathway.
Front. Pharmacol. 14:1124015.
doi: 10.3389/fphar.2023.1124015

Mechanisms of Yajieshaba in the treatment of liver fibrosis through the Keap1-Nrf2 signaling pathway

Yuanmei Bai[1†], Haimei Wu[2†], Lijie Zheng[1†], Yuhuan Xie[1], Feifan Liu[1], Yan Wan[1], Qiongchao Li[1] and Peixin Guo[1*]

[1]College of Ethnic Medicine, Yunnan University of Chinese Medicine, Kunming, Yunnan, China, [2]The Second Affiliated Hospital of Guangzhou University of Chinese Medicine, Guangzhou, China

Yajieshaba (YJSB), a traditional Dai medicine formula containing botanical drugs, is commonly employed in Yunnan due to its significant therapeutic effects on liver protection. Consequently, to determine the efficacy of YJSB and the mechanism of action of Kelch-like ECH-associated protein 1 (Keap1)-nuclear factor erythroid 2-related factor 2 (Nrf2) pathway against liver fibrosis. We wanted to see if YJSB could treat CCl_4-induced liver fibrosis by regulating the Keap1-Nrf2 signaling pathway. YJSB significantly improved liver function biochemical indices, liver fibrosis quadruple, hydroxyproline (Hyp), and transforming growth factor-β1 (TGF-β1) levels. The staining results demonstrated that the degree of liver fibrosis was significantly reduced. YJSB reduced the content of malondialdehyde (MDA) and elevated the content of superoxide dismutase (SOD) in the liver, exhibiting antioxidant effects; meanwhile, it regulated the expression of Keap1-Nrf2 pathway protein, increased the expression of NAD(P)H: Quinone oxidoreductase (NQO1), Heme Oxygenase 1 (HO-1), Glutamate cysteine ligase modifier subunit (GCLM), and Glutamate cysteine ligase catalytic subunit (GCLC) expression in the liver decreased while Nrf2 expression increased. Fluorescence immunoassay studies demonstrated that YJSB promoted the trans-nuclearization of Nrf2. YJSB possesses anti-liver fibrosis pharmacological effects that improve liver function and effectively counteract CCl_4-induced liver fibrosis damage. The mechanism of action might be related to the regulation of protein expression of the Keap1-Nrf2 pathway, increasing the ability of the body to resist oxidative stress and reduce oxidative stress injury.

KEYWORDS

Yajieshaba, liver fibrosis, Keap1-Nrf2 oxidative stress pathway, pharmacodynamics, mechanism

Abbreviations: CBRT, Compound Biejia-Ruangan tablet; COL, Colchicine; Col Ⅳ, Collage Type-Ⅳ; CCL4, Carbon tetrachloride; ECM, extracellular matrix; GCLC, Glutamate cysteine ligase catalytic subunit; GCLM, Glutamate cysteine ligase modifier subunit; HA, Hyaluronic acid; HO-1, Heme Oxygenase 1; H&E, Hematoxylin and Eosin; Hyp, hydroxyproline; Keap1, Kelch-like 1; LN, Laminin; MDA, Malondialdehyde; NQO1, NAD(P)H: Quinone oxidoreductase; Nrf2, nuclear factor erythroid-2 related factor; PCIII, procollagen type-III; SOD, Superoxide dismutase; TGF-β1, Transforming growth factor-β1; WB, Western Blotting; YJSB, Yajieshaba.

1 Introduction

Liver fibrosis is a pathological process of "damage-repair" of the liver stimulated by a chronic viral infection, alcohol abuse, drugs, toxic substances, autoimmunity, gallbladder disease, and other factors (Lutz et al., 2020). During this process, hepatic stellate cells proliferate and stimulate the deposition of collagen-based extracellular matrix (ECM), causing abnormal liver function, inducing liver fibrosis, and promoting the formation of cirrhosis, which is estimated to affect 1%–2% of the global population and cause over 1 million deaths annually, severely affecting people's quality of life (Higashi et al., 2017). Currently, the primary treatment for liver fibrosis is antifibrotic therapy and treatment for the underlying cause. For instance, colchicine is employed to prevent the secretion of pro-collagen molecules (Tingting et al., 2020). However, these medications have significant adverse effects, and colchicine could lead to renal damage that results in hematuria and oliguria (Du et al., 2021). In contrast, ethnomedicines possess multi-target, multi-pathway, and multi-level neuroprotective effects and have become popular in recent years in the treatment of liver fibrosis (Rong et al., 2021).

According to Dai medicine, liver fibrosis is classified as liver disease, which is a clinical symptom of toxicity that causes the organism to malfunction (Bai et al., 2022). YJSB is a common medication employed by the indigenous Chinese Dai people to treat liver disease. It has been employed in Dai medicine clinics for over 2,000 years to cure hepatitis and cirrhosis induced by alcohol, drugs, or toxic substances (Xiaohua et al., 2015; Yang et al., 2022). In this composition, *Arundina graminifolia* (D. Don) Hochr, *Dregea sinensis* Hemsl, *Fibraurea recisa* Pierre, *Pueraria montana* var. *lobata* (Willd.) Maesen & S.M.Almeida ex Sanjappa & Predeep, and *Mappianthus iodoides* Hand.-Mazz are the principal botanical drugs (Table 1); *Anodendron nervosum* Kerr, *Clerodendrum chinense* (Osbeck) Mabb, and *Glycyrrhiza uralensis* Fisch. ex DC are the supplementary botanical drugs (Table 1). The entire composition is applied in the ratio 14: 5: 7: 5: 6: 18: 15: 20. While jatrorrhizine ($C_{20}H_{20}NO_4$) and berberine ($C_{20}H_{18}NO_4^+$) are the primary alkaloid components in YJSB (Xiaomei et al., 2022). Some experimental studies discovered that YJSB could reduce the content of enzymes, such as alanine aminotransferase (ALT) and aspartate aminotransferase (AST) in the serum of mice with carbon tetrachloride CCl_4-induced liver injury and exhibit hepatoprotective effects (Xiaohua et al., 2015). Meanwhile, a previous study discovered that in a rat model of liver injury induced by acetaminophen (APAP), YJSB could reduce the serum levels of malondialdehyde (MDA) and lactate dehydrogenase (LDH) and increase the levels of superoxide dismutase (SOD) and plasma glutathione peroxidase (GSH-Px), which would exert an antioxidant effect.

In recent years, oxidative stress has been recognized as a significant contributor to liver fibrosis (Yan et al., 2019). According to Yan et al. (2019), overexpression of antioxidants or antioxidant genes could prevent the activation of hepatic stellate cells and exert antifibrotic effects. The Keap1-Nrf2 signaling pathway is an important mechanism in the oxidative stress response; it regulates the expression of several antioxidants and detoxifying enzymes and plays an important role in maintaining the body's redox homeostasis (Yanshuang et al., 2020). Vincenzo and Laura (2018) discovered that knocking down Nrf2 induces hepatic stellate cells activation, as shown by an increase in α-SMA-positive cells and by gene expression induction of ECM components (collagens and fibronectin). Reduced Nrf2-levels in hepatic stellate cells resulted in increased migration and decreased proliferation. Furthermore, they found that activation of Nrf2-deficient hepatic stellate cells was linked to TGF-β1 activity.

At present, the anti-hepatic fibrosis mechanism of YJSB remains unclear. This study, CCl_4 was administered intraperitoneally to induce a liver injury model in rats, resulting in inflammation, oxidative stress, and fibrosis. It was discussed whether the mechanism of YJSB against liver fibrosis was by regulating proteins in the Keap1-Nrf2 pathway, enhancing the protective effect on liver cells, reducing the production of oxidative stress factors, and thereby inhibiting the process of liver fibrosis.

2 Materials

2.1 Experimental animals

A total of 56 male Sprague–Dawley (SD) rats (200 ± 20 g) were obtained from the Animal Center of Kunming Medical University.

TABLE 1 Contents of YJSB decoction.

Local name	Species name	Family name	Drug name
Weng shang hai	*Arundina graminifolia* (D. Don) Hochr	Orchidaceae	Arundinae herba
Dai bai jie	*Dregea sinensis* Hemsl	Apocynaceae	Dregeae radix
Hei tao han	*Fibraurea recisa* Pierre	Menispermaceae	Fibraureae caulis
Hebie	*Pueraria montana* var. *lobata* (Willd.) Maesen and S. M. Almeida ex Sanjappa & Predeep	Fabaceae	Puerariae lobatae radix
Deng hei han	*Mappianthus iodoides* Hand.-Mazz	Icacinaceae	Mappianthuse caulis
Jie long meng la	*Anodendron nervosum* Kerr	Apocynaceae	Anodendrone caulis
Bai hua chou mu dan gen	*Clerodendrum chinense* (Osbeck) Mabb	Lamiaceae	Clerodendrume radix
Sha yin	*Glycyrrhiza uralensis* Fisch. ex DC	Fabaceae	Glycyrrhizae radix et rhizoma

All botanical drugs were obtained from Xishuangbanna Dai Nationality Hospital in Yunnan Province, China.

The animal certificate number was (Yunnan) K2015–0002. The Yunnan University of Chinese Medicine's Ethics Committee reviewed and approved the animal study (Ethical number: R-06202012). The rats were fed, watered without restriction, and maintained in a favorable environment (23°C ± 2°C, 45%–55% humidity) with a 12:12 light–dark (LD) cycle.

2.2 Drugs

All the botanical drugs of YJSB were procured from Dai Hospital in Xishuangbanna, Yunnan Province, China, and authenticated as genuine by Professor Yanfang Lin, the chief expert in Dai medicine (Table 1). Shanghai Yuanye Biotechnology Co., Ltd. Provided the positive controls for the study, namely, compound Biejia-Ruangan tablet (CBRT) and colchicine (Col) (China, Batch No.: 20200402, S18047). Tianjin Wind Ship Reagent Technology Co., Ltd. Supplied the CCl_4 (China, Batch No.: 20180301). Olive oil was obtained from Meilunbio (United States, Batch No.: MB13084). Jatrorrhizine and berberine were acquired from Shanghai Yuanye Biotechnology Co., Ltd. (China, Batch No.: Z11M8S35796, Y18N8S49558).

2.3 Reagents

Nanjing Jiancheng Biological Engineering Research Institute Co., Ltd. Provided serum glutamic pyruvic transaminase (GPT), serum glutamic oxaloacetic transaminase (GOT), SOD, and MDA kits (China, Batch No.: C009–2–1, C010–2–1, A001–3, and A003–1–2). PIIINP, ColIV, LN, and HA kits were purchased from Jiangsu Enzyme Standard Biotechnology Co., Ltd. (China, Batch No.: MB-1580A, MB-7163A, MB-1837A, and MB-2052A). GCLC, GCLM, NQO1, and HO-1 were obtained from Shanghai Jining Biotechnology Co., Ltd. (Batch No.: 202005). Goat anti-rabbit IgG-488 and goat anti-mouse IgG-594 were purchased from Proteintech (United States, Batch No.: SA00013–2, SA00013–3).

2.4 Instruments

Thermo Scientific Inc. Provided the enzyme marker (Varioskan Flash) and the low temperature high speed centrifuge (Primo R) (United States). Shanghai Hengke Instruments Co., Ltd. Provided a constant temperature drying oven (China). Agilent Technologies Inc. Provided an analytical liquid chromatograph (Agilent 1,200) column C18 (250 mm × 4.6 mm, 5 μm) (United States). An automatic digital pathology section scanner (KF-PRO-005-EX) was obtained from Ningbo Jiangfeng Bioinformatics Co., Ltd. (China). Besides, a nitrogen purge instrument (NDK200–2) was obtained from Mio Instruments (China).

3 Methods

3.1 Drug preparation

Preparation of Yajieshaba (YJSB) low-dose, middle-dose, and high-dose solutions: Prescription botanical drugs were extracted 12 times with water, twice for 20 min each time, and then mixed with YJSB aqueous extract and filtered through gauze. Double-distilled water was added to prepare a solution of 0.44 g botanical drug/mL as the YJSB high-dose solution, and the middle-dose and low-dose were obtained by dilution in equal proportions to 0.22 g raw drug/mL and 0.11 g raw drug/mL as the YJSB middle and low dose solutions with double-distilled water. Colchicine (COL), as an inhibitor of cellular microtubule polymerization, can inhibit cell division and proliferation, as well as the synthesis and secretion of the extracellular matrix, such as collagen, in connective tissue cells. It inhibits the inflammatory response, improving the degree of CCL_4-induced liver fibrosis and patient survival with few serious side effects (Xia et al., 2006; Zesong et al., 2006; Jian-Chang et al., 2009). COL solution preparation: COL powder is weighed with a precision electronic balance, dissolved in double-distilled water, prepared into 0.027 mg/mL colchicine solution, and stored at 4°C. The compound Biejia-Ruangan tablet (CBRT) may prevent liver fibrosis by regulating the expression of inflammatory factors in the body, primarily by down-regulating pro-inflammatory factors and up-regulating anti-inflammatory factors, increasing matrix metalloproteinase inhibitory factor activity and promoting the activation and proliferation of hepatic stellate cells. This can effectively prevent hepatocyte damage and the pro-fibrotic effects of inflammatory factors in the body (Zesong et al., 2006; Yonghong and Chuan, 2022). To make the CBRT solution, a soft liver tablet of turtle shell was dissolved in double-distilled water to make a 0.054 g/mL solution, which was stored at 4°C. The solution of 40% CCl_4 was made by mixing olive oil and CCl_4 solution in a 6:4 volume ratio.

3.2 Analysis of the phytochemical components in blood from YJSB-treated rats by high-performance liquid chromatography (HPLC)

The liver injury model was replicated in male healthy SD rats and randomly divided into a normal group and a drug group of 6 rats each, with the normal group gavaged with an equal volume of double-distilled water and the drug group gavaged with YJSB 2.2 g/kg (Yang et al., 2022), both in a volume of 10 mL/kg. At 1 h after the gavage, blood was taken from the abdominal aorta and centrifuged. The supernatant was taken in a centrifuge tube; five times the amount of methanol was added, vortexed for 10 min, then centrifuged at 6,000 r/min for 15 min. The supernatant was taken, the solvent was evaporated under nitrogen at room temperature, 400 μL of methanol was added to dissolve, and the sample was filtered through a 0.22 μm filter tip and analyzed. The drug-containing serum, normal serum, and control received similar treatments. On a ZORBAX Eclipse Plus-C18 column (250 mm × 4.6 mm, 5 μm), the chromatographic separation was performed using a mobile phase of acetonitrile and 0.1% phosphoric acid solution (22:78) and 50 μL of triethylamine per 1,000 mL of 0.1% phosphoric acid solution at a flow rate of 1 mL/min and a detection wavelength of 346 nm. The injection volume was 80 μL.

3.3 Animal modeling and treatment

Healthy male SD rats were acclimatized and fed for 1 week before the test and randomly divided into seven groups of eight rats each, namely,

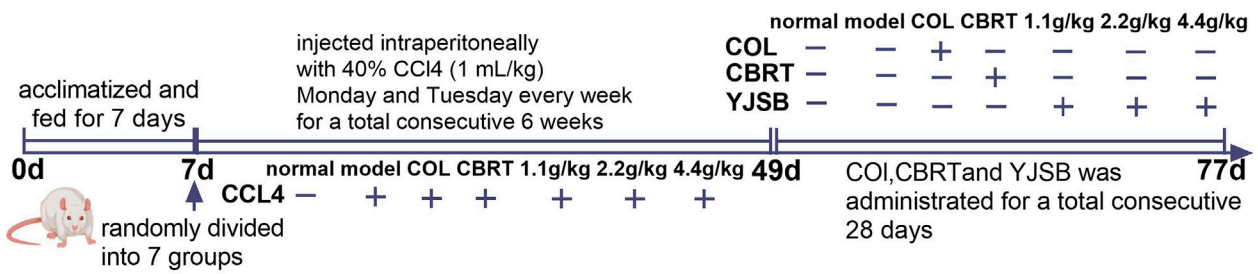

FIGURE 1
Timeline in the experimental intervention.

the normal group, the model group, the Col group, the CBRT group, and the YJSB low, middle, and high dose groups. Except for the normal group that was not intervened, the remaining groups were injected intraperitoneally with 40% CCl_4 olive oil solution at a rate of 1 mL/kg each for model replication. The injections were scheduled for Monday and Tuesday every week for two consecutive days: 1 time/day for 6 weeks (Figure 1). After the model was finished, the normal and model groups were gavaged with double-distilled water. The YJSB group gavage doses were 1.1 g/kg, 2.2 g/kg, and 4.4 g/kg for the YJSB low, middle, and high dose groups, respectively (earlier studies revealed that the maximum single dose of YJSB mice was 88 g raw drug/kg. Therefore, 1/80, 1/40, and 1/20 of the maximum dose were selected as the low, middle, and high doses of YJSB, respectively). In addition, 0.54 g/kg for the CBRT group and 0.27 mg/kg for the Col group were administered 1 time/day and continued for 4 weeks (Figure 1). The medication dose was determined following the conversion formula and the clinical daily dose.

3.4 Determination of liver function and biochemical parameters

After the last administration, the 12-h fasted rats were weighed and anesthetized with pentobarbital (150 mg/mL), followed by blood sampling from the abdominal aorta. The sample was coagulated at room temperature for 30 min and subjected to centrifugation at 4°C, 4,000 rpm for 10 min. The serum was extracted from the sample following centrifugation and was employed to detect AST, ALT, ALP, TBIL, PIIINP, ColIV, LN, HA, Hyp, and TGF-β1.

For pathological examination, the right lobe of the liver was removed and fixed in 4% neutral formaldehyde. The remaining liver tissues were stored in the refrigerator at −80°C for subsequent usage.

3.5 H&E, Masson, Ag staining

The liver tissues were fixed in 4% paraformaldehyde solution for 24 h, following which paraffin sectioning, dewaxing, and dehydration were performed, and H&E, Ag, and Masson's trichrome staining were performed, respectively. The histopathological observation of the liver was performed using an automatic digital pathological biopsy scanner, and the changes in hepatic inflammatory infiltration, collagen fiber, and reticular fiber in each group were assessed.

3.6 Determination of oxidative stress factors

In the liver tissue homogenates, the contents of SOD and MDA were measured following the instructions of the kit.

3.7 Elisa method to determine GCLC, GCLM, NQO1, HO-1 protein content

The protein concentration of liver homogenates was determined using a bicinchoninic acid (BCA) kit, and the expression of GCLC, GCLM, NQO1, and HO-1 was determined using an ELISA kit.

3.8 Western blot method to determine Keap1, Nrf2 protein expression

Total protein was extracted from liver tissue, followed by the following steps: gel preparation (10% isolate, 5% concentrate); constant pressure electrophoresis (70 V, 30 min followed by 110 V, 2 h); constant pressure membrane transfer (110 V, 1 h); milk closure at room temperature for 2 h; Keap1 (1:500), Nrf2 (1:1,000), GAPDH (1:15,000), and primary antibodies were closed overnight at 4°C in the refrigerator; rabbit anti-rat secondary antibodies (1:20,000) closure at room temperature for 1 h and developed. The expression of the target protein was assumed to be represented by the ratio of the target protein bands to the optical density of the internal reference protein bands.

3.9 Fluorescence immunoassay to determine Nrf2 protein in the nucleus

The liver tissue was fixed with 4% paraformaldehyde overnight, dehydrated by an automatic dehydrator, embedded in paraffin, sliced, dewaxed and hydrated, then stained by conventional HE, sealed with neutral gum, observed, antigen repaired, painting circle and serum closure (Wang, 2017), where the antibodies Keap1 and Nrf2 were incubated at a concentration of 1:500 and 1:200, respectively. Keap1 and Nrf2 protein expression and the entry of

TABLE 2 Quality standards of the YJSB.

Drug name	Active ingredients	Control standard
Arundinae herba	water extract	10% minimum
Dregeae radix	95% ethanol extract	10% minimum
Fibraureae caulis	Palmatine chloride	2% minimum
Puerariae lobatae radix	puerarin	2.4% minimum
Mappianthuse caulis	water extract	7% minimum
Anodendrone caulis	95% ethanol extract	16% minimum
Clerodendrume radix	95% ethanol extract	5% minimum
Glycyrrhizae radix et rhizoma	Liquiritin, glycyrrhizic acid	0.5%, 2% minimum

Nrf2 into the nucleus were observed under the fluorescence microscope.

3.10 Statistical methods

For statistical analysis, SPSS 21.0 software was used, and the data of each group were expressed as "mean ± standard deviation" (x ± s), and the one-way ANOVA was used for the two-way comparison between multiple groups. The difference was statistically significant with a *p*-value of <0.05.

4 Results

4.1 Quality control and major chemical composition of YJSB

First, YJSB is a hospital preparation developed by Xishuangbanna Dai Nationality Hospital in Yunnan Province, China. It has been made into capsules (also known as Baijie capsules) and was approved by Yunnan Food and Drug Administration in 2008 (approval number: Yunnan Pharmaceutical Production (Z) 20082252K). There are corresponding quality standards and specifications for hospital preparations to ensure the stability of their components (Table 2). All the medicinal materials were purchased from Xishuangbanna Dai Nationality Hospital of Yunnan Province, and the content of active ingredients met the requirements of Chinese pharmacopoeia and local laws and regulations. For example, the content of Palmatine hydrochloride ($C_{21}H_{21}NO_4$-HCl) in the active ingredients of *Fibraurea recisa* Pierre was not less than 2.0%. The active component of *Pueraria montana* var. *lobata* (Willd.) Maesen and S.M.Almeida ex Sanjappa & Predeep ($C_{21}H_{20}O_9$) is at least 2.4%. In addition, the extraction process of medicinal materials is fixed, which ensures the stability and repeatability of pharmacological action of compounds to a certain extent (Table 2). Secondly, we have studied the main chemical composition of the individual botanicals in the YJSB (Table 3).

4.2 Determination of the content of jatrorrhizine and berberine in the blood of YJSB

The following are the results of the YJSB jatrorrhizine and berberine content determinations: 3 batches of SD rats were collected, treated according to method 2.1, and fed into the sample for analysis. Jatrorrhizine and berberine had retention times of 12.6 and 23.5 min, respectively. The separation degree R was greater than 1.5, and the number of trays was not less than 10000. The control and test products of jatrorrhizine and berberine exhibited good separation effects, and there was no interference in the corresponding position compared to normal serum. These results indicated that the chromatographic conditions could be employed to determine jatrorrhizine and berberine (Figure 2). The relative standard deviation (RSD) values of jatrorrhizine and berberine were 0.249% and 0.383%, respectively (n = 6). The levels of jatrorrhizine and berberine in the three batches of samples were determined (Table 4).

4.3 YJSB improved the general condition of hepatic fibrosis in rats

During the experiment, the rats in the normal exhibited normal hair color and quality and normal food intake and activity. On the other hand, the rats in the model had rough fur, bulging on both sides of the abdomen, and behaviors such as shrugging, loose disarray, and reduced food intake and activity, such as mental depression and huddling. All of the symptoms above improved in the rats receiving treatment. In the model, the surface of liver tissue was uneven and hard, with noticeable white nodule-like alterations, indicating severe liver injury. Following treatment, the CCl_4-induced liver fibrosis was significantly inhibited, the surface of the liver was flattened and softer, and the area covered by white nodules was reduced.

4.4 YJSB improved the inflammatory infiltration of liver tissue in rats with hepatic fibrosis

H&E staining could be employed to observe liver inflammation and changes in liver cell structure. In the normal, the structure of hepatic lobules was complete, and the cords of hepatic cells were mostly arranged in a radial pattern around the central vein (Figure 3). There was no expansion, occlusion, or distortion of hepatic sinuses and no obvious proliferation of hepatocytes, inflammation, and necrosis (Figure 3). In comparison to the normal, the model showed varying degrees of inflammatory cell infiltration in the portal area (Figure 3). Some of the normal liver structures were damaged, with severe disintegration and necrosis, moderate or severe fibrous tissue hyperplasia, and some obvious false lobules (Figure 3). The liver of rats in the treatment exhibited mild inflammatory cell invasion, edema, and necrosis of the liver cells, as well as the reduced proliferation of hepatic lobules and fibrous tissue and improved liver structure compared to the model

TABLE 3 Profile of main chemical composition.

Species name	Compound	References
Arundina graminifolia (D.Don) Hochr	lusianthridin	Liu et al. (2017), Xingyu et al. (2021)
	rhapontigen	Liu et al. (2017), Xingyu et al. (2021)
	p-hydroxytoluene ethyl ether	Liu et al. (2017), Xingyu et al. (2021)
	cucapitoside	Liu et al. (2017), Xingyu et al. (2021)
	dengibsin	Liu et al. (2017), Xingyu et al. (2021)
	1-(4-hydroxy-3,5-dimethoxyphenyl) propan-1-one	Liu et al. (2017), Xingyu et al. (2021)
Dregea sinensis Hemsl	n-carboxyl-2-hydroxy-4-pyrrole	Liao et al. (2016)
	Butanedioic aci,2-hydroxy-1,4-dibutylester	Liao et al. (2016)
	Propanoic acid,3-propoxy-butyl ester	Liao et al. (2016)
	propanoic acid,3-ethoxy-butyl ester	Liao et al. (2016)
	methyl shikimate	Liao et al. (2016)
	n-carboxyl-2-hydroxy-4-pyrrole	Liao et al. (2016)
Fibraurea recisa Pierre	stephanine	Bartley et al. (1994)
	roemarine	Rao et al. (2009)
	jatrorrhizine	Hussain et al. (1989)
	palmatine	Hussain et al. (1989)
	groenlandicine	Rao et al. (2009)
	berberine	Lenka et al. (2007)
Pueraria montana var. *lobata* (Willd.) Maesen and S.M.Almeida ex Sanjappa & Predeep	3′-hydroxypuerarin	Tungmunnithum et al. (2020), Hua and Chang (2022)
	puerarin	Tungmunnithum et al. (2020), Hua and Chang (2022)
	paidzin	Tungmunnithum et al. (2020), Hua and Chang (2022)
	formononetin	Tungmunnithum et al. (2020), Hua and Chang (2022)
	coumestrol	Tungmunnithum et al. (2020), Hua and Chang (2022)
	soyasapogenol A	Tungmunnithum et al. (2020), Hua and Chang (2022)
Mappianthus iodoides Hand. -Mazz	9-hydroxy-4,6-megastigmadien-3-one	Jiang et al. (2018)
	blumenol A	Jiang et al. (2018)
	9,10-dihydroxy-4,7-megastigmadi	Jiang et al. (2018)
	3,3-didemethoxyverrucosin	Jiang et al. (2018)
	mappine A	Xiao et al. (2011)
	mapposidic acid	Xiao et al. (2011)
*Anodendron nervosum*Kerr	3,4-dihydroxybenzaldehyde	Li et al. (2014)
	3,4-dihydroxybenzoic acid	Li et al. (2014)
	oleanolic acid	Li et al. (2014)
	iboluteine	Liu et al. (2019)
	venoter	Liu et al. (2019)
	lirofolines A	Liu et al. (2019)
Clerodendrum chinense (Osbeck) Mabb	octacosanoate taraxerol	Yue (2013)
	taraxerol	Yue (2013)

(Continued on following page)

TABLE 3 (*Continued*) Profile of main chemical composition.

Species name	Compound	References
	myricadiol	Yue (2013)
	friedelin	Yue (2013)
	tetracosanoic acid	Yue (2013)
	indolyl-3-carboxylic acid	Yue (2013)
	elerodenoside A	Yue (2013)
Glycyrrhiza uralensis Fisch. ex DC	glycyrrhizic acid	Tan et al. (2022)
	diisobutyl phthalate	Tan et al. (2022)
	rutinum	Tan et al. (2022)
	liquiritin	Tan et al. (2022)
	phthalate	Tan et al. (2022)
	liquiritigenin	Tan et al. (2022)
	isoglycyrrhizol	Tan et al. (2022)
	scopoletin	Tan et al. (2022)

(Figure 3). These results suggested that YJSB could protect the liver by reducing inflammatory invasion and enhancing liver structure.

4.5 YJSB reduced the deposition of collagen fibers in the liver tissue of rats with hepatic fibrosis

The expression of collagen fibers could be observed using Masson's trachoma staining. In the normal, the structure of hepatic lobules was clear, and only a minor amount of collagen fiber hyperplasia was observed in the portal region (tube wall) (Figure 4). Besides, there was no evident inflammatory cell invasion, edema, and hyperemia (Figure 4). The structure of hepatic lobules in the model was disorganized, and many inflammatory cells invaded the central vein and the portal area compared to the normal (Figure 4). There was significant collagen fiber proliferation with increased collagen fiber expression on the surface of liver tissue (Figure 4); the portal region was visible with some false lobules formed and some significant large areas exhibited in blue (Figure 4). The liver inflammatory cell invasion, collagen fiber expression, and false lobule formation were decreased in the treatment compared to the model (Figure 4). These results suggested that YJSB could protect the liver by reducing the deposition of collagen fibers.

4.6 YJSB reduced the deposition of reticular fibers in the liver tissue of rats with hepatic fibrosis

Ag staining could be employed to observe the deposition of reticular fibers. The structure of the hepatic lobules was clear, and the reticular scaffolds were intact in the normal. There was no evidence of inflammatory cell invasion or reticular fibrosis (Figure 5). Compared to the normal, the model's hepatic lobule structure was disorganized. The reticular scaffolds were damaged, particularly in the collagenous hyperplasia region of the portal and bridge-like necrosis areas (Figure 5). The hepatic reticular fibrous tissue proliferation was reduced in the treatment in comparison to the model (Figure 5); the fibrous tissue was dispersed around the liver cells, and the formation of false lobules was reduced (Figure 5). According to the results, YJSB protects the liver by reducing the deposition of reticular fibers.

4.7 YJSB improved the liver function in rats with hepatic fibrosis

We measured serum ALT, AST, AST/ALT, ALP, and TBIL levels to investigate CCl_4-induced hepatocyte damage. As shown in Figure 5, a significantly enhanced level of ALT, AST, AST/ALT, ALP, and TBIL in the blood was observed in rats treated with CCl_4 (50.87%, 13.66%, 51.03%, 78.75%, and 92.00%, respectively) as compared to normal ($p < 0.01$, $p < 0.05$; Figures 6A–E). When compared to the model, COL therapy resulted in significantly lower ($p < 0.01$, $p < 0.05$; Figures 6A–E) AST (13.26%), AST/ALT (45.06%), ALP (26.39%), and TBIL (28.90%) values in the blood. When compared to the model, CBRT therapy resulted in significantly lower ($p < 0.01$, $p < 0.05$; Figures 6A–E) ALT (35.37%), AST/ALT (29.61%), ALP (24.63%), and TBIL (27.57%) values in the blood. In rats, treatment with YJSB at low, medium, and high doses resulted in significantly lower ($p < 0.01$, $p < 0.05$; Figures 6A–E) ALT (31.01%, 33.21%, and 21.13%, respectively), AST (18.45%, 15.83%, and 13.31%, respectively), AST/ALT (30.41%, 24.61%, and 26.21%, respectively), ALP (24.76%, 28.92%, and 29.50%, respectively) and TBIL (27.58%, 32.09% and 32.01%, respectively) values in the blood as compared to the model. The results showed that YJSB had a protective effect on liver function.

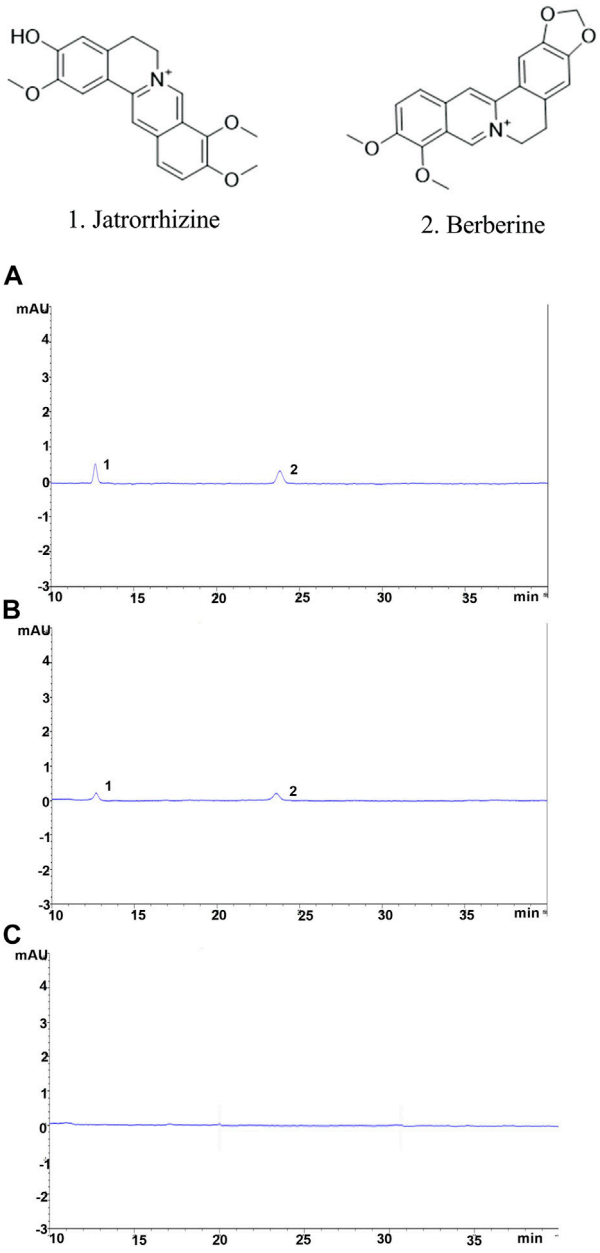

FIGURE 2
Chromatographic conditions and system suitability examination. **(A)** Jatrorrhizine and berberine mixed reference substance, **(B)** spectrum of the test substance, **(C)** spectrum of the normal serum; 1. Jatrorrhizine 2. Berberine.

4.8 YJSB reduced the contents of HA, PIIINP, ColIV, and LN in the serum of rats with hepatic fibrosis

When compared to the control, continuous exposure to CCl_4 caused a significant increase ($p < 0.01$, $p < 0.05$; Figures 7A–D) in HA (1.13-fold), PIIINP (1.25-fold), ColIV (1.36-fold), and LN (1.35-fold). The contents of HA (8.43% and 7.96%, respectively), ColIV (23.31% and 24.31%, respectively), and LN (18.96% and 34.32%, respectively) in the Col and CBRT were significantly decreased ($p < 0.01$, $p < 0.05$; Figures 7A, C, D). The contents of HA (12.17%, 5.79%, and 12.65%, respectively), PIIINP (28.77%, 27.39%, and 21.16%, respectively), and ColIV (20.95%, 31.95%, and 44.16%, respectively) were significantly decreased ($p < 0.01$, $p < 0.05$; Figures 7A–C) in the YJSB low-dose, middle-dose and high-dose, and the content of LN (34.55% and 27.26%, respectively) were significantly lower ($p < 0.01$; Figure 7D) in the YJSB low-dose and high-dose than that in the model. According to the findings, YJSB could significantly improve serum hepatic fibrosis indicators such as HA, PIIINP, ColIV, and LN.

4.9 YJSB reduced the contents of Hyp and TGF-β1 in the serum of model rats

We measured serum Hyp and TGF-β1 levels because TGF-β1 is an essential pro-fibrotic mediator, and Hyp is a recognized marker of collagen accumulation in the liver (Lu et al., 2019). The results indicated that the contents of Hyp (21.98%) and TGF-β1 (40.82%) had significantly increased ($p < 0.01$, $p < 0.05$; Figures 8A, B) in the model when compared to normal. In contrast, therapy with COL, YJSB low-dose, middle-dose, and high-dose in rats caused a significant decrease ($p < 0.01$; Figures 8A, B) in Hyp (10.14%, 15.70%, 13.85%, and 10.51%, respectively) and TGF-β1 (21.96%, 16.19%, 21.66% and 21.23%, respectively) values in the liver homogenate as compared to the model. According to the results, YJSB could significantly improve the serum indicators of hepatic fibrosis, such as Hyp and TGF-β1.

4.10 YJSB affected the release of oxidative stress factors (SOD and MDA)

MDA may indirectly reflect the degree of oxidative stress injury to cells, whereas SOD may protect cells from oxidative stress and

TABLE 4 Sample content measurement results.

Groups	Jatrorrhizine content (ng/mL)	Berberine content (ng/mL)
1	15.3	18.6
2	14.8	18.4
3	15.6	18.5

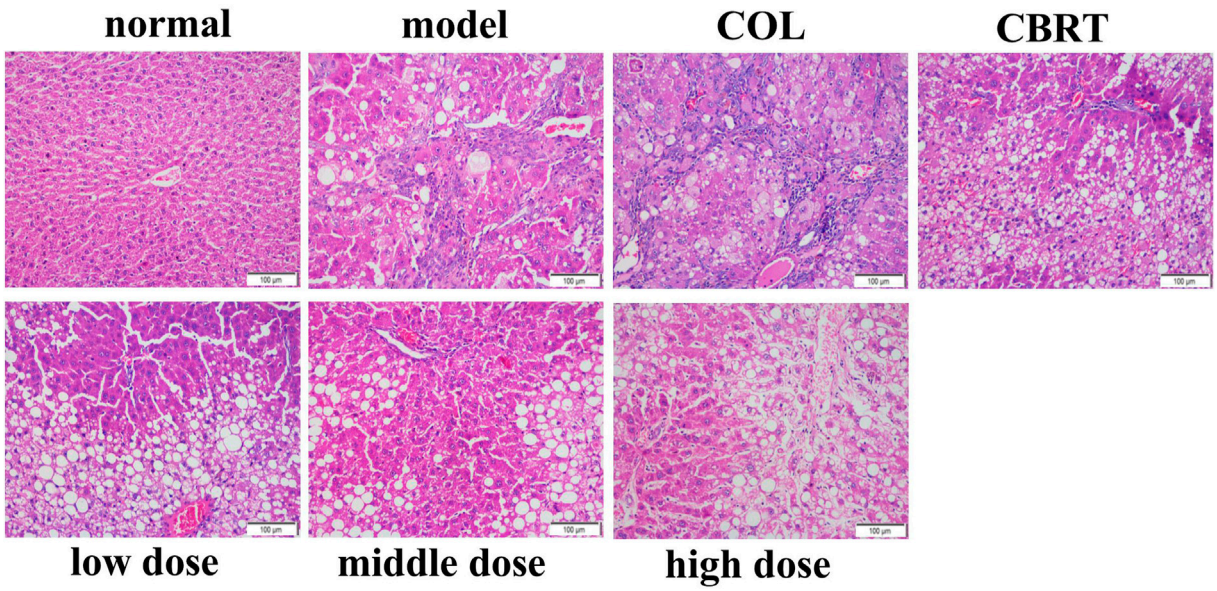

FIGURE 3
YJSB improved the inflammatory infiltration of liver tissue in rats with hepatic fibrosis. H&E staining of the rat liver (200×) (n = 3).

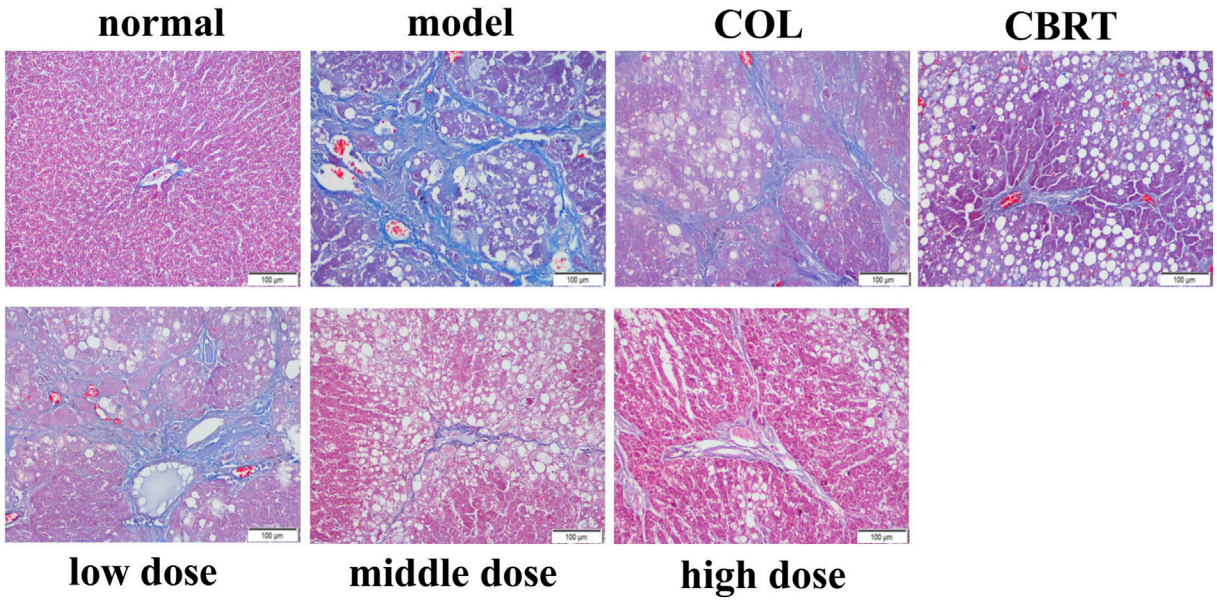

FIGURE 4
YJSB reduced the deposition of collagen fibers in the liver tissue of rats with hepatic fibrosis. Masson's trachoma staining of the rat liver (200×) (n = 3).

rapidly improve and restore the condition of damaged cells (Sha et al., 2016; Margherita et al., 2021), SOD and MDA levels in liver homogenate were measured. The experimental results revealed that, when compared to normal, the model's liver homogenate contained significantly less SOD (14.79%) and significantly more MDA (34.45%) ($p < 0.01$, $p < 0.05$; Figures 9A, B). In the liver homogenates of the Col, CBRT, YJSB low-dose, middle-dose, and high-dose, the content of SOD (18.40%, 16.09%, 20.49%, 17.27%, and 22.49%, respectively) increased significantly ($p < 0.01$, $p < 0.05$; Figure 9A), while the content of MDA (16.44%, 47.31%, 31.00%, and 21.71%, respectively) in the liver homogenate of the Col, CBRT, YJSB low-dose and middle-dose decreased significantly ($p < 0.01$, $p < 0.05$; Figure 9B). According to the findings, YJSB may stimulate the release of oxidative stress factors.

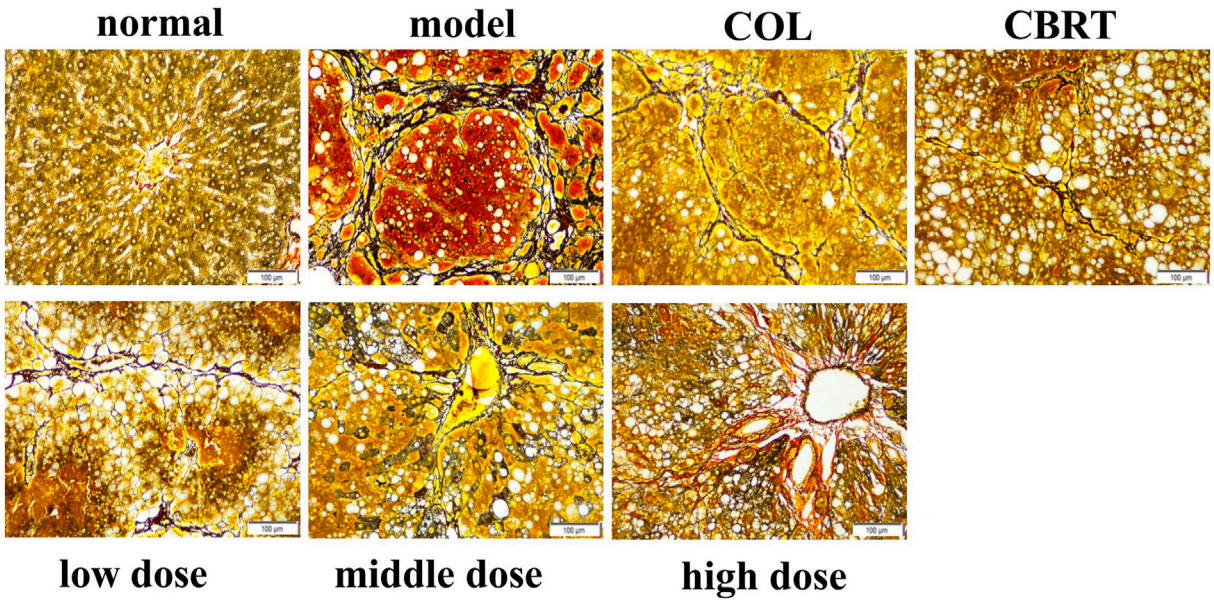

FIGURE 5
YJSB reduced the deposition of reticular fibers in the liver tissue of rats with hepatic fibrosis. Ag staining of the rat liver (200×) (n = 3).

4.11 YJSB promoted the expression of GCLC, GCLM, NQO1, and HO-1 in the Keap1-Nrf2 pathway

To investigate the relationship between GCLC, GCLM, NQO 1, and HO-1 and Keap 1-Nrf 2, we measured GCLC, GCLM, NQO 1, and HO-1 in liver homogenate. The results demonstrated that the contents of GCLC (56.13%), GCLM (45.53%), NQO1 (38.63%), and HO-1 (34.69%) in the liver homogenates were significantly low ($p < 0.01$, $p < 0.05$; Figures 10A–D) in the model when compared to normal. GCLC (1.92-fold, 1.39-fold, 1.52-fold, 1.50-fold, and 1.80-fold, respectively), GCLM (1.52-fold, 1.19-fold, 1.40-fold, 1.54-fold and 1.40-fold, respectively), NQO1 (1.51-fold, 1.07-fold, 1.31-fold, 1.32-fold and 1.44-fold, respectively), HO-1 (1.44-fold, 1.13-fold, 1.25-fold, 1.32-fold and 1.38-fold, respectively) content in the liver homogenate of the COL, CBRT, YJSB low-does, middle-does, and high-dose were significantly increased ($p < 0.01$; Figures 10A–D) in compared to the model. According to the results, YJSB could promote the expression of GCLC, GCLM, NQO1, and HO-1 in the Keap1-Nrf2 pathway.

4.12 YJSB regulated the expression of Keap1 and Nrf2 proteins in the Keap1-Nrf2 pathway

We performed experimental validation of the Keap1 and Nrf2 proteins to investigate the underlying mechanisms of YJSB against mechanisms that cause CCl_4-induced liver fibrosis. When compared to normal, the experimental results showed that Nrf2 (25.75%; $p < 0.01$; Figures 11A, B) protein expression had significantly slowed, and Keap1 (2.21-fold; $p < 0.01$; Figures 11A, C) protein expression had significantly increased. When compared to the model, Nrf2 (1.49-fold, 1.35-fold, 1.33-fold, 1.63-fold, and 1.55-fold, respectively) protein expression in the COL, CBRT, YJSB low-does, middle-does, and high-dose was significantly increased ($p < 0.01$, $p < 0.05$; Figures 11A, B), while Keap1 (62.54%, 41.69%, 37.12%, 38.92%, and 35.53%, respectively) protein expression was significantly decreased ($p < 0.01$, $p < 0.05$; Figures 11A, C). The findings suggest that YJSB can regulate the expression of Keap1 and Nrf2 proteins in the Keap1-Nrf2 pathway.

4.13 YJSB promotes Nrf2 protein to enter the nucleus

Given the importance of Nrf 2 in the liver, we used fluorescence immunohistochemistry to examine Nrf 2 expression in liver tissue.

Fluorescence immunohistochemistry revealed that the nuclei were blue and irregularly shaped. In the cytoplasm, the positive expression of Keap1 was green, and that of Nrf2 was red (Figure 12). When Nrf2 entered the nucleus, it overlapped red and blue, and there was a shadow in the irregular blue circle of the nucleus (Figure 12). The Nrf2 expression and Nrf2 protein entry into the nucleus decreased in the model, while the Keap1 expression signal was stronger than normal (Figure 12). When compared to model, Keap1 expression was decreased, and the signal was weaker in the treatment group (Figure 12). In the treatment group, both the expression of Nrf2 and the number of nuclei entered increased (Figure 12). According to the findings, YJSB may promote the entry of the Nrf2 protein into the nucleus.

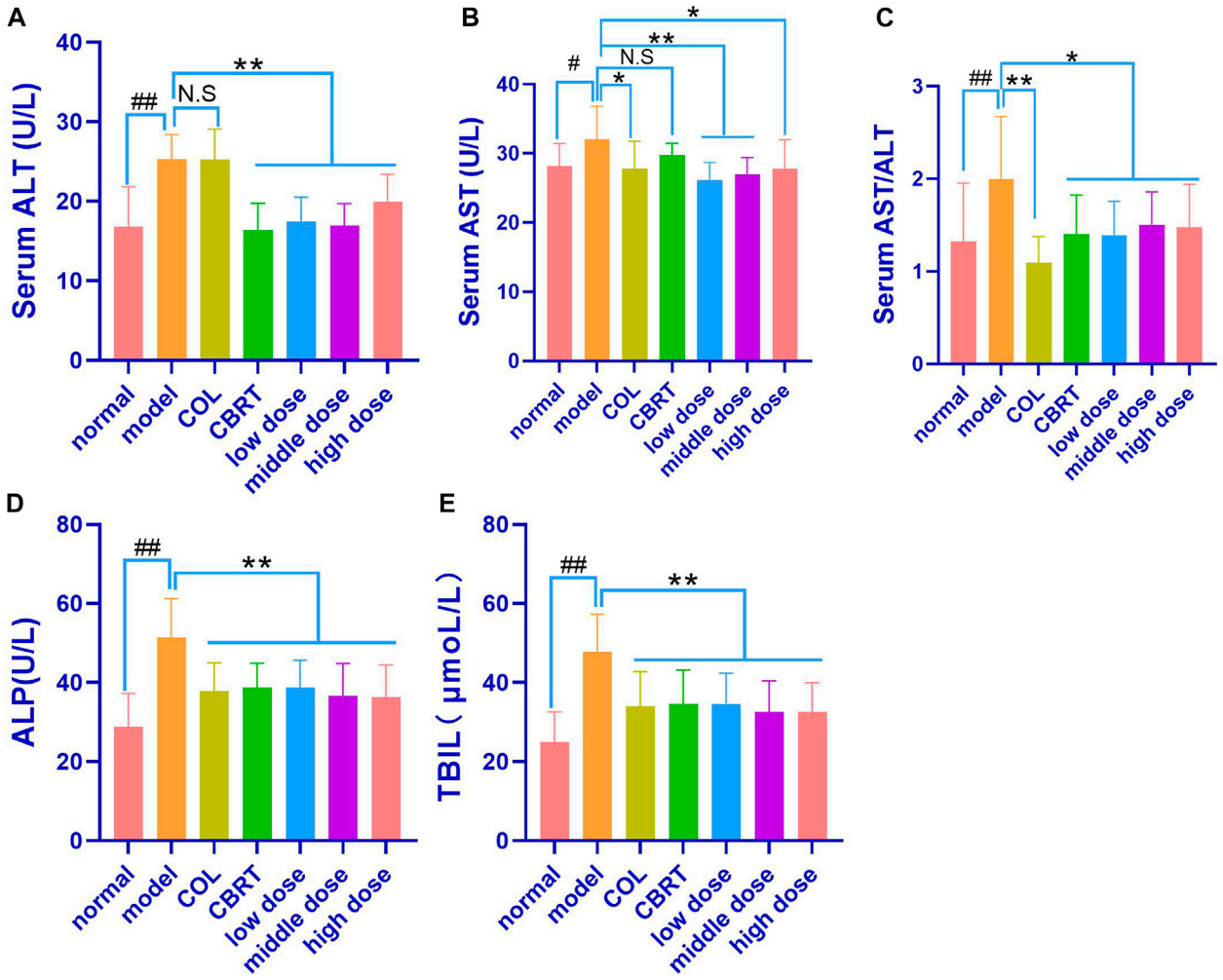

FIGURE 6
YJSB improved liver function in rats with hepatic fibrosis. **(A–E)** The levels of serum ALT, AST, AST/ALT, ALP, and TBIL after the 4-week drug intervention. (n = 8). #$p < 0.05$, ##$p < 0.01$ vs. normal; *$p < 0.05$, **$p < 0.01$, No statistical significance (NS): $p > 0.05$ vs. model.

5 Discussion

The continuous accumulation of experience of the Dai people in the fight against diseases might be summed up as Dai medicine. It has absorbed the experience of ancient Indian and traditional Chinese medicine and possesses distinctive national and local characteristics (Zhen et al., 2013). The Yunnan Dai people of China are rich in medical resources with a wide range of clinical applications, featuring good curative effects and a few adverse effects. Dai medical compound YJSB is an effective substance in treating various liver diseases (Yang et al., 2022). Hepatic fibrosis is a progressive disease with a long course (sometimes decades), which could lead to cirrhosis and liver cancer (Ge et al., 2021). The prevention and treatment of hepatic fibrosis is a common challenge faced by hundreds of millions of patients with the chronic liver disease worldwide. The role of YJSB has a therapeutic effect. We first gave CCl_4 for 6 weeks to replicate the liver fibrosis animal model, and then we gave YJSB for 4 weeks to treat liver fibrosis rats.

YJSB is a hospital preparation developed by Xishuangbanna Dai Hospital in Yunnan, China, made into capsules (also known as Baijie Capsules) and used in hospitals for many years (Xiaohua et al., 2015; Yang et al., 2022). In a previous study, mice were given 88 g/kg in a single gavage and were found to be in good general condition 14 days later with no mortality. The findings above indicate that the toxicity of YJSB is low (Wang, 2013). The doses of YJSB in our present study were 1.1 g/kg, 2.2 g/kg, and 4.4 g/kg, of which 2.2 g/kg was close to the dose of YJSB commonly used clinically converted to rats. No behavioral changes of toxicity were found in the animals during the course of the experiment. After the experiment, the animals were executed, the organs were examined, and no abnormal changes were found in the organs, indicating that the doses in this study were safe.

Although the liver has a significant capacity for regeneration, excessive regeneration might result in fibrosis (Hernandez-Gea and Friedman, 2011). All chronic liver diseases exhibit abnormal regeneration as a common pathological change, and possible sources of myofibroblasts following a chronic liver injury include

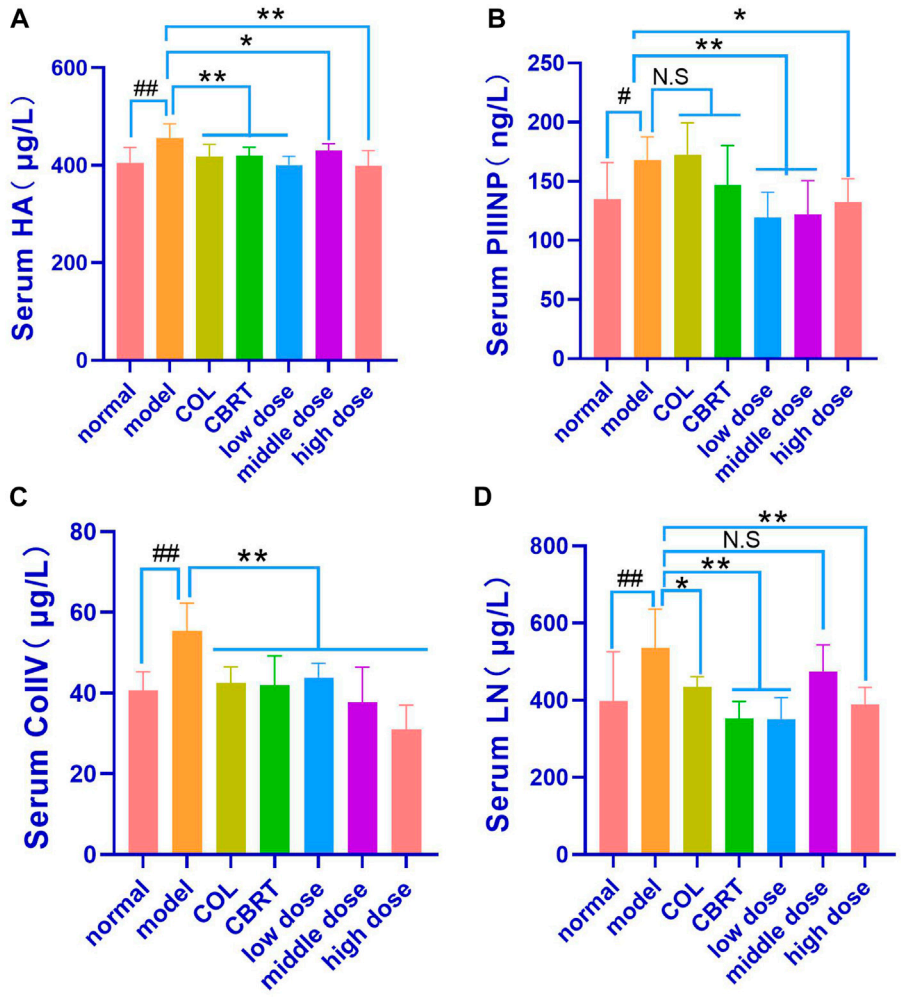

FIGURE 7
YJSB reduced the levels of HA, PIIINP, CollV, and LN in the serum of rats with hepatic fibrosis. **(A–D)** The levels of serum HA, PIIINP, CollV, and LN after the 4-week drug intervention. (HA, PIIINP, and CollV: n = 8; LN: n = 6). $^{\#}p < 0.05$, $^{\#\#}p < 0.01$ vs. normal; $^{*}p < 0.05$, $^{**}p < 0.01$, N.S: $p > 0.05$ vs. model.

portal vein fibroblasts, mesenchymal cells, and fibroblasts (Hernandez-Gea and Friedman, 2011). Hepatic stellate cells are unique mesenchymal cells of the liver (Blaner et al., 2008) that normally exist in a static state and accumulate vitamin A. When oxidative stress damages occur in the body, hepatic stellate cells could be activated to mediate various signaling pathways and lead to cell morphologies similar to myoblast fiber changes. This could result in excessive deposition of collagen-dominated ECM and promote the occurrence and development of hepatic fibrosis (Özlem, 2014; Young et al., 2020).

Increasing evidence reveals that the Keap1-Nrf2 pathway is the most important endogenous antioxidant pathway thus far (Yang et al., 2014). When at rest, Nrf2 conjugates with its molecular partner Keap1 to form a stable dimer that resides in the cytoplasm in an inactive state. When a cell is stimulated by oxidative stress or other stimuli, Nrf2 is activated, dissociates from the dimer after separating from Keap1, and undergoes nuclear transfer; it then enters the nucleus and binds with the antioxidant reaction element (ARE) to induce and regulate target genes. Protein expressions of GCLC, GCLM, NQO1, and HO-1 were increased, thus, enhancing the antioxidant capacity of cells, increasing the concentration of antioxidant stress factor SOD, and reducing the release of oxidative stress factor MDA (Faju et al., 2021). According to an earlier study (Truong et al., 2014), activation of the Keap1-Nrf2 pathway could inhibit the activation of hepatic stellate cells and their production of a large amount of collagen, thus, inhibiting the occurrence and development of liver fibrosis.

In our study, we first established a model of a rat with hepatic fibrosis; CCl_4-induced animal hepatic fibrosis was similar to human hepatic fibrosis in most aspects of morphology and pathophysiology (Shaban et al., 2021). Pathological slides are the gold standard of disease. Our results confirmed the successful replication of the hepatic fibrosis model and the drug's effect on liver tissue at the cellular level. H&E, Ag, and Masson's trichrome staining revealed a trend of liver inflammation, structural changes in liver cells, increased collagen fiber accumulation, and excessive reticular fiber deposition in the model group. YJSB treatment, on the

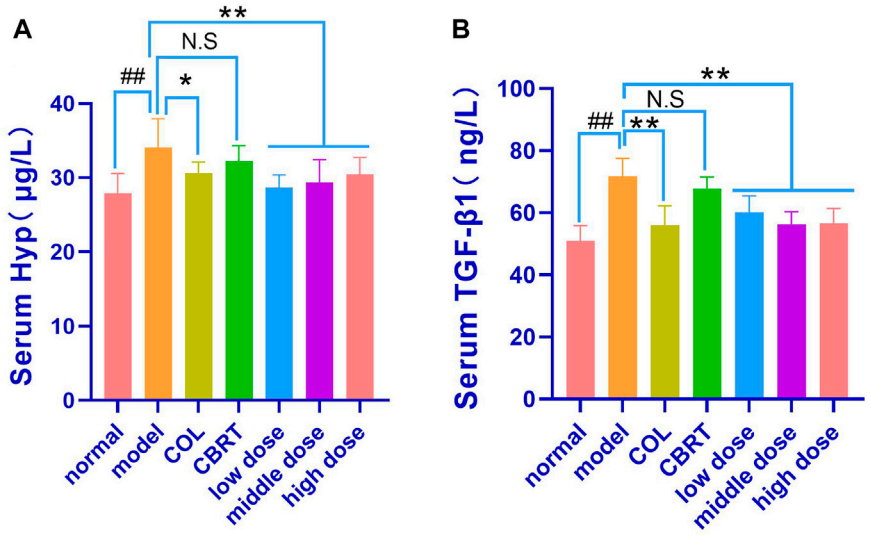

FIGURE 8
YJSB reduced the contents of Hyp and TGF-β1 in the serum of model rats. **(A,B)** The levels of serum Hyp and TGF-β1 after the 4-week drug intervention. (n = 8). $^{\#}p < 0.05$, $^{\#\#}p < 0.01$ vs. Normal; $^{*}p < 0.05$, $^{**}p < 0.01$, NS: $p > 0.05$ vs. model.

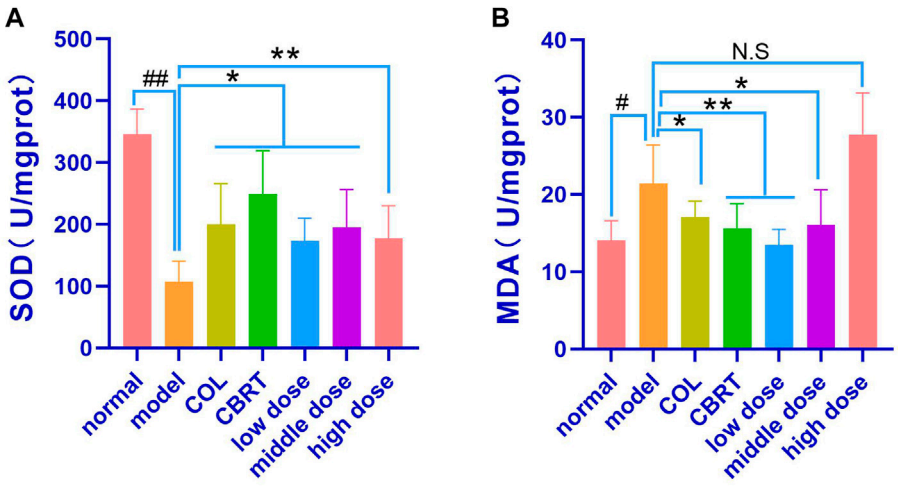

FIGURE 9
YJSB affected the release of oxidative stress factors. **(A,B)** The levels of liver homogenate SOD and MDA after the 4-week drug intervention. (SOD: n = 6; MDA: n = 6). $\#p < 0.05$, $\#\#p < 0.01$ vs. normal; $^{*}p < 0.05$, $^{**}p < 0.01$, NS: $p > 0.05$ vs. model.

other hand, significantly reduced hepatic inflammatory response, improved hepatic cell structural changes, and reduced collagen fiber and reticular fiber deposition, possibly due to its ability to inhibit hepatic stellate cell activation.

We also demonstrated the efficacy of YJSB in the protection of the liver. ALT and AST as liver-specific biomarkers could be employed to evaluate the degree of liver injury, and their activity is positively correlated with liver injury (Behnaz et al., 2021). CCl_4-induced rat hepatic fibrosis model could cause acute liver cell injury, increase cell membrane permeability, and release a significant quantity of ALT, AST, ALP, and TBIL into the blood (Tohru et al., 2005). Clinically, the increase in AST activity is believed to be greater than ALT, indicating the onset of chronic and advanced stages of liver disease (Karim et al., 2015). The ALT, AST, ALP, and TBIL results indicated that the CCl_4-induced hepatic fibrosis model had progressed to a chronic and progressive state at the end of this experiment, consistent with the characteristics of hepatic fibrosis progression. Meanwhile, studies (Behnaz et al., 2021) have demonstrated that HA is one of the matrix components synthesized by mesenchymal cells. HA could accurately and sensitively represent the amount of generated fibers in the liver and the liver cells' damage status compared to other liver detection indexes. LN is a unique non-collagenous structural protein in

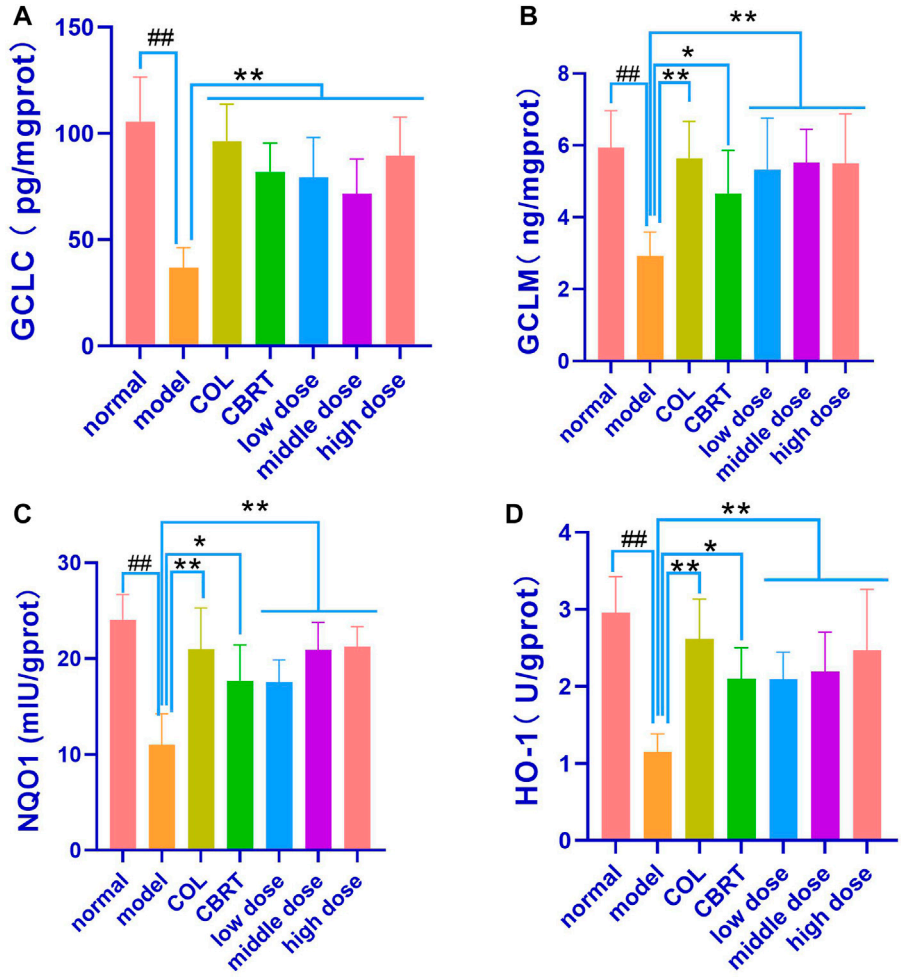

FIGURE 10
YJSB promoted the expression of GCLC, GCLM, NQO1, and HO-1 in Keap1-Nrf2 pathway. **(A–D)** The levels of liver homogenate GCLC, GCLM, NQO1, and HO-1 after the 4-week drug intervention. (n = 8). $^{\#}p < 0.05$, $^{\#\#}p < 0.01$ vs. Normal; $^{*}p < 0.05$, $^{**}p < 0.01$, NS: $p > 0.05$ vs. model.

the basement membrane, predominantly derived from hepatic stellate cells, which could reflect the degree of hepatic fibrosis activity and portal vein pressure. The synthesis status of hepatic fiber and inflammatory activity could be reflected by PCIIINP. ColIV, as the principal component of the basement membrane, represents the collagen renewal rate of the basement membrane and could sensitively reflect the process of liver fibrosis, which is one of the earliest symptoms of liver fibrosis. The levels of HA, LN, PCIIINP, and ColIV in the model group were found to be proportional to the levels of ALT, AST, ALP, and TBIL. YJSB reduced HA, LN, PCIIINP, ColIV, ALT, and AST levels in rat serum, indicating that YJSB had a protective effect on injured liver cells and could improve liver fibrosis. It is likely that CCl_4 causes ECM molecules to form and accumulate, increasing fiber volume, whereas medications could effectively reduce HA, LN, PCIIINP, and ColIV concentrations in serum, preventing the development of hepatic fibrosis.

Second, the activation of hepatic stellate cells by cytokines and other mediators is considered to be an important event in the pathophysiology of liver fibrosis and activated hepatic stellate cells or myofibroblasts are the primary sources of ECM molecules, including collagen, non-collagen glycoprotein, proteoglycan, and glycosaminoglycan (Chhimwal et al., 2020). TGF-β1 has been shown to be an important pro-fibrotic mediator. Hyp has been shown to be a recognized marker of collagen accumulation in the liver (Lu et al., 2019), playing an important role in the activation of hepatic stellate cells, as well as restricting hepatocyte proliferative response and increasing extracellular matrix protein production during hepatic repair (Piotrowska-Kempisty et al., 2020). Our results suggest that the levels of TGF-β1 and Hyp in the model group were significantly increased, promoting the occurrence of liver fibrosis. At the same time, YJSB could effectively reduce the levels of both and prevent hepatic fibrosis.

In addition, reduced fibrosis might be involved in oxidative stress factors and the Keap1-Nrf2 pathway (Alkhalifah et al., 2022). The content of MDA, an end product of lipid oxidation, could indirectly reflect the degree of oxidative stress injury of

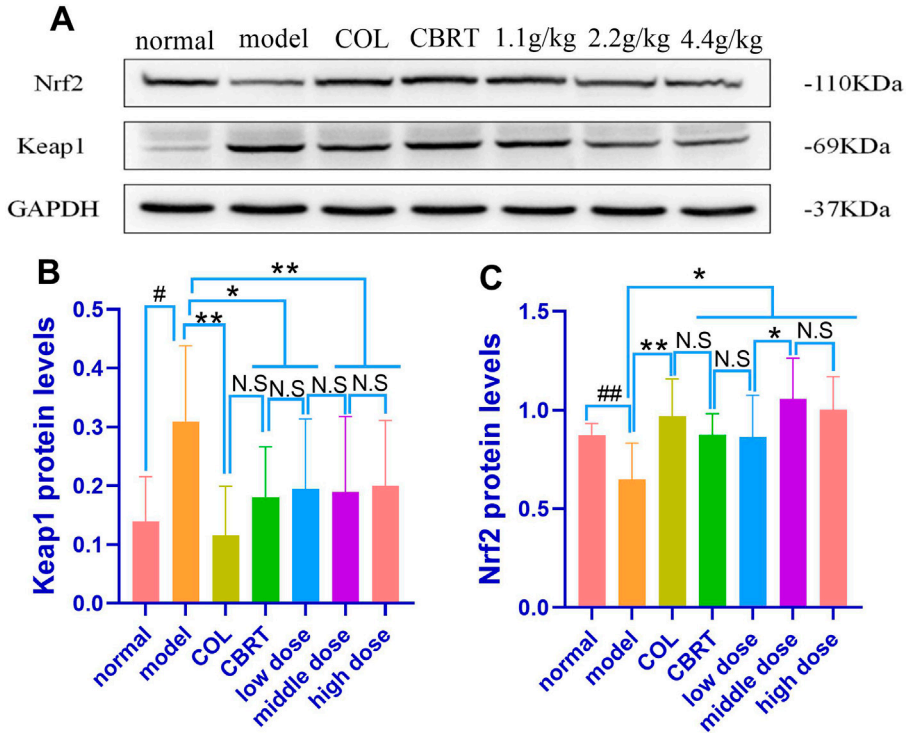

FIGURE 11
The protein expression of Nrf2 and Keap1. **(A–C)** Relative protein levels of Nrf2 and Keap1 in the liver of hepatic fibrosis rats. (n = 8). #$p < 0.05$, ##$p < 0.01$ vs. normal; *$p < 0.05$, **$p < 0.01$ vs. model.

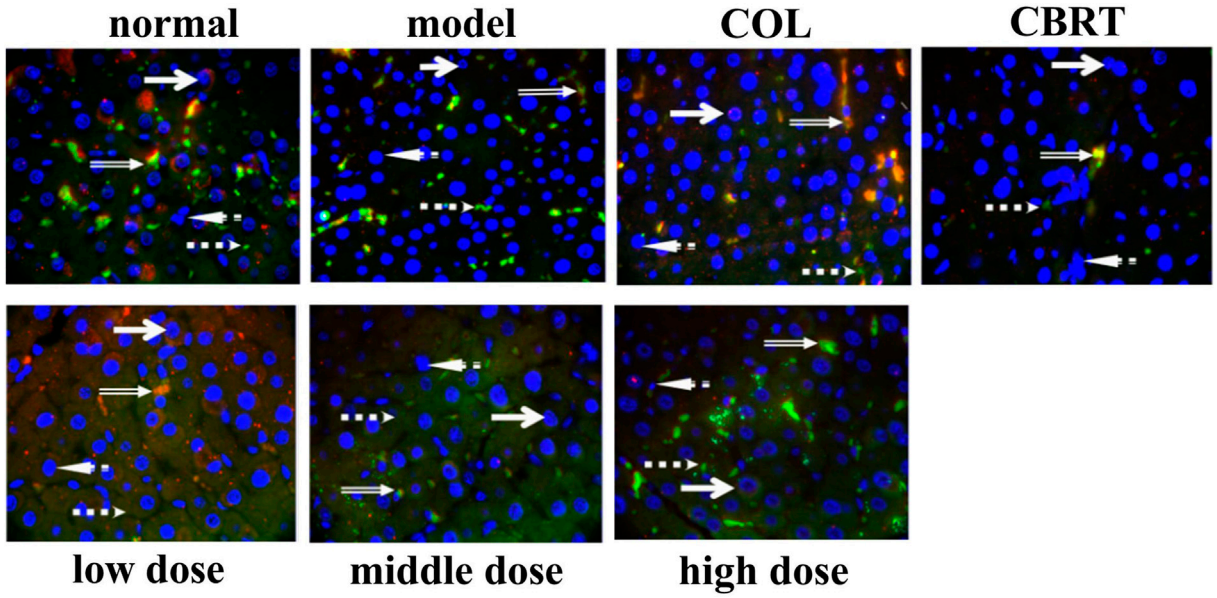

FIGURE 12
Results of fluorescence immunoassay of Keap1 and Nrf2 proteins in liver tissue (1,000×). Red: Nrf2 protein; Green: Keap1 protein; Blue: 4′, 6-diamidino-2-phenylindole (DAPI); Orange: The binding state of Keap1-Nrf2 (n = 3).

cells. SOD, an important antioxidant enzyme, could protect cells from oxidative stress and rapidly improve and restore the condition of damaged cells (Sha et al., 2016; Margherita et al., 2021). The Keap1-Nrf2 signaling pathway plays an important role and regulates GCLC, GCLM, NQO1, and HO-1 at various levels, which is approximately related to oxidative stress (Wenge and Ah-Ng, 2009). Our findings show that YJSB can lower MDA levels while increasing SOD levels in liver homogenates, implying that YJSB can act as an antioxidant stress factor, reducing the degree of liver damage caused by oxidative stress and protecting the liver. Simultaneously, the expressions of GCLC, GCLM, NQO1, and HO-1 in the liver of the model group were significantly decreased. In contrast, the expressions of GCLC, GCLM, NQO1, and HO-1 in the liver of the model group were significantly increased by YJSB, suggesting that YJSB might improve the antioxidant capacity of the redox system in rats, reduce oxidative stress, and interfere with the development of hepatic fibrosis.

Finally, in the CCL_4-induced rat hepatic fibrosis model, the YJSB drug group activated the Keap1-Nrf2 signaling pathway, resulting in Keap1 release in the cytoplasm and Nrf2 entry into the nucleus to initiate a series of antioxidant reactions and promote the generation of antioxidant proteins. In the results of WB, the expression of Nrf2 in the administration group was higher in comparison to the normal group, which might be because the modification of Keap1 cysteine residues in the administration group was improved, which further promoted the dissociation of Keap1-Nrf2 and increased the amount of Nrf2 that entered the nucleus to combat oxidative stress.

In summary, our study suggests that YJSB could significantly protect rats against CCL_4-induced hepatic fibrosis by alleviating liver injury and inhibiting the activation of hepatic stellate cells. The mechanism might be related to its ability to activate the Keap1-Nrf2 signaling pathway, regulate oxidative stress response, and play an anti-hepatic fibrosis role. Because YJSB protects the liver, it could have significant clinical implications. However, none of these studies have directly demonstrated that YJSB inhibits the activity of hepatic stellate cells, and its molecular basis is complex, necessitating further investigation.

Data availability statement

The original contributions presented in the study are included in the article/Supplementary Material, further inquiries can be directed to the corresponding author.

Ethics statement

The animal study was reviewed and approved by Ethics Committee of Yunnan University of Chinese medicine (permit NO. R-06202012).

Author contributions

PG, HW, and YB designed the experiment. YB, HW, FL, and YW did most of the experiments. YB, LZ, YX, and QL analyzed the data and discussed the results. YB and HW wrote the manuscript. All authors read and approved the final manuscript.

Funding

The research was funded by the Regional Fund of the National Natural Science Foundation of China (82160867) to PG, Scientific Research Fund of Yunnan Provincial Department of Education (2019J066) to QL, Joint Special Project on Traditional Chinese Medicine of the Basic Research Program of Yunnan Provincial Department of Science and Technology (202001AZ070001-088) to QL, Yunnan Key Laboratory of Formulated Granules (202105AG070014) to YX, Yunnan Provincial Key Laboratory of Molecular Biology for Sinomedicine (2019DG016) to LZ, Scientific Research Fund of Yunnan Provincial Department of Education (2023Y0446) to YB, The Dai medicine Key Discipline of Pharmacy State Administration of Traditional Chinese Medicine. It is a discipline, with no item No.

Acknowledgments

We thank all the members of our group for their joint efforts to complete this paper.

Conflict of interest

The authors declare that the research was conducted in the absence of any commercial or financial relationships that could be construed as a potential conflict of interest.

Publisher's note

Supplementary material

The Supplementary Material for this article can be found online at: https://www.frontiersin.org/articles/10.3389/fphar.2023.1124015/full#supplementary-material

References

Alkhalifah, E. A. R., Alobaid, A., Almajed, M. A., Alomair, M. K., Alabduladheem, L. S., Al-Subaie, S. F., et al. (2022). Cardamom extract alleviates the oxidative stress, inflammation and apoptosis induced during acetaminophen-induced hepatic toxicity via modulating Nrf2/HO-1/NQO-1 pathway. *Curr. Issues Mol. Biol.* 44 (11), 5390–5404. doi:10.3390/cimb44110365

Bai, Y., Zheng, L., Wu, H., and Guo, P. (2022). Advances in studies on treatment of hepatic fibrosis with Dai and western medicine. *Med. Plant* 13 (04), 81–84. doi:10.19600/j.cnki.issn2152-3924.2022.04.019

Bartley, J. P., Baker, L. T., and Carvalho, C. F. (1994). Alkaloids of stephania bancroftii. *Phytochemistry* 36 (5), 1327–1331. doi:10.1016/s0031-9422(00)89661-2

Behnaz, A., Hamid, M. S., Fatemeh, B., and Ghazal, Z. (2021). FIB-4, APRI, and AST/ALT ratio compared to FibroScan for the assessment of hepatic fibrosis in patients with non-alcoholic fatty liver disease in Bandar Abbas, Iran. *BMC Gastroenterol.* 21 (1), 453. doi:10.1186/s12876-021-02038-3

Blaner, W. S., O'Byrne, S. M., Wongsiriroj, N., Kluwe, J., D'Ambrosio, D. M., Jiang, H., et al. (2008). Hepatic stellate cell lipid droplets: A specialized lipid droplet for retinoid storage. *Biochim. Biophys. Acta.* 1791 (6), 467–473. doi:10.1016/j.bbalip.2008.11.001

Chhimwal, J., Sharma, S., Kulurkar, P., and Patial, V. (2020). Crocin attenuates CCl4-induced liver fibrosis via PPAR-γ mediated modulation of inflammation and fibrogenesis in rats. *Hum. Exp. Toxicol.* 39 (12), 1639–1649. doi:10.1177/0960327120937048

Du, Y. J., Liu, W. C., Chen, X., and Cheng, Y. J. (2021). A case report of colchicine-induced myopathy in a patient with chronic kidney disease. *Beijing Da Xue Xue Bao Yi Xue Ban.* 53 (6), 1188–1190. doi:10.19723/j.issn.1671-167X.2021.06.030

Faju, C., Liangqun, L., Mei, P., Yanfang, Y., Li, W., Lilang, L., et al. (2021). Identification of triterpenoids and hepatoprotective property of Fructus Rosa roxburghii against alcohol-induced liver injury by regulating keap1- Nrf2 signaling. *Phytomedicine Plus* 1 (4), 100102. doi:10.1016/j.phyplu.2021.100102

Ge, H., Wang, A., Su, Y., Yu, C., Gao, L., and Li, Y. (2021). Ameliorative effects of Qingganjiuwei powder, a traditional Mongolian medicine, against CCl 4 -induced liver fibrosis in rats. *J. Ethnopharmacol.* 264, 113226. doi:10.1016/j.jep.2020.113226

Hernandez-Gea, V., and Friedman, S. L. (2011). Pathogenesis of liver fibrosis. *Annu. Rev. Pathology Mech. Dis.* 6 (1), 425–456. doi:10.1146/annurev-pathol-011110-130246

Higashi, T., Friedman, S. L., and Hoshida, Y. (2017). Hepatic stellate cells as key target in liver fibrosis. *Adv. Drug Deliv. Rev.* 121, 27–42. doi:10.1016/j.addr.2017.05.007

Hua, C., and Chang, L. (2022). Research progress on chemical constituents, biological activities and processing and utilization of puerariae lobatae radix. *China Fruit Veg.* 42 (10), 36–40+84. doi:10.19590/j.cnki.1008-1038.2022.10.007

Hussain, R. A., Jinwoong, K., and Christpher, W. W. B. (1989). Unambiguous carbon-13 NMR assignments of some biologically active protoberberine alkaloids. *Heterocycles* 29 (12), 2257. doi:10.3987/com-89-5168

Jian-Chang, S., Ya-Jun, H., Xia, L., Guo-Rong, Y., and Le-Xin, W. (2009). Curcumin prevents liver fibrosis by inducing apoptosis and suppressing activation of hepatic stellate cells. *J. Nat. Med.* 63 (4), 415–420. doi:10.1007/s11418-009-0347-3

Jiang, Z., Feng, X., Guo, W., Wang, Y., Wang, T., Cai, L., et al. (2018). Chemical constituents from stems and leaves of Mappianthus iodoides. *Chin. Traditional Herb. Drugs* 49 (02), 282–287.

Karim, S. M. F., Rahman, M. R., Shermin, S., and Sultana, R. (2015). Correlation between aminotransferase ratio (AST/ALT) and other biochemical parameters in chronic liver disease of viral origin. *Delta Med. Coll. J.* 3 (1), 13–17. doi:10.3329/dmcj.v3i1.22234

Lenka, G., Jirí, D., and Radek, M. (2007). Quaternary protoberberine alkaloids. *Phytochemistry* 68 (2), 150–175. doi:10.1016/j.phytochem.2006.10.004

Li, S., Yang, C., zen, X., Jiang, Z., Tiao, K., Sun, J., et al. (2014). Study on the chemical constituents in the stems of Bousigonia mekongensis. *J. Yunnan Minzu Univ. Sci. Ed.* 23 (04), 235–238.

Liao, M., Zhang, Y., Chen, F., and Yao, Y. (2016). Study on chemical constituents of Marsdenia tenacissima. *J. South-central Minzu Univ. Sci. Ed.* 35 (03), 39–41.

Liu, L., Ma, X., Yang, Z., Tan, W., Zhou, Z., Wen, Y. F., et al. (2019). Optimal cumulative cisplatin dose in nasopharyngeal carcinoma patients based on induction chemotherapy response Root of Bousigonia mekongensis. *J. Chin. Med. Mater.* 42 (01), 83–94. doi:10.1016/j.radonc.2019.04.020

Liu, Q., Dai, R., Lyu, F., and Lin, F. (2017). Research progress in chemical constituents and pharmacological activities of baiyangjie. *Chin. J. Mod. Appl. Pharm.* 34 (04), 618–624. doi:10.13748/j.cnki.issn1007-7693.2017.04.032

Lu, J., Zhang, J., Wang, Y., and Sun, Q. (2019). Caveolin-1 scaffolding domain peptides alleviate liver fibrosis by inhibiting TGF-β1/smad signaling in mice. *Int. J. Mol. Sci.* 19 (6), 1729. doi:10.3390/ijms19061729

Lutz, W., Dieudonnée, T., and Bernhard, R. (2020). Effects of nintedanib in an animal model of liver fibrosis. *BioMed Res. Int.* 2020, 3867198. doi:10.1155/2020/3867198

Margherita, S., Domenico, R., and Sabrina, L. (2021). SMADS-mediate molecular mechanisms in sjögren's syndrome. *Int. J. Mol. Sci.* 22 (6), 3203. doi:10.3390/ijms22063203

Özlem, E. G. (2014). Cellular and molecular mechanisms in the pathogenesis of liver fibrosis: An update. *World J. gastroenterology* 20 (23), 7260–7276. doi:10.3748/wjg.v20.i23.7260

Piotrowska-Kempisty, H., Nowicki, M., Jodynis-Liebert, J., Kurpik, M., Ewertowska, M., Adamska, T., et al. (2020). Assessment of hepatoprotective effect of chokeberry juice in rats treated chronically with carbon tetrachloride. *Molecules* 25 (6), 1268. doi:10.3390/molecules25061268

Rao, G.-X., Zhang, S., Wang, H.-M., Li, Z.-M., Gao, S., and Xu, G.-L. (2009). Antifungal alkaloids from the fresh rattan stem of Fibraurea recisa Pierre. *J. Ethnopharmacol.* 123 (1), 1–5. doi:10.1016/j.jep.2009.02.046

Rong, Y., Jie, X., Yanfeng, T., Chuantao, F., Chunchun, H., Qian, Y., et al. (2021). The positive role and mechanism of herbal medicine in Parkinson's disease. *Oxidative Med. Cell. Longev.* 2021, 9923331. doi:10.1155/2021/9923331

Sha, L., Ming, H., Hor-Yue, T., Ning, W., and Yibin, F. (2016). Insights into the role and interdependence of oxidative stress and inflammation in liver diseases. *Oxidative Med. Cell. Longev.* 2016, 4234061. doi:10.1155/2016/4234061

Shaban, N. Z., El-Kot, S. M., Awad, O. M., Hafez, A. M., and Fouad, G. M. (2021). The antioxidant and anti-inflammatory effects of Carica Papaya Linn. seeds extract on CCl4-induced liver injury in male rats. *BMC complementary Med. Ther.* 21 (1), 302. doi:10.1186/s12906-021-03479-9

Tan, W., Fang, D., Lu, J., and Liu, Y. (2022). Research progress on chemical constituents and biological activities of Glycyrrhiza uralensis Fisch*. *Chem. Eng.* 36 (02), 56–58+67. doi:10.16247/j.cnki.23-1171/tq.20220256

Tingting, C., Yuan, L., Minwei, Z., Jiafei, C., Bai, Y., Nanyuan, F., et al. (2020). Effects of Salvia miltiorrhiza and Radix astragali on the TGF-β/Smad/Wnt pathway and the pathological process of liver fibrosis in rats. *Cell. Mol. Biol. (Noisy-le-Grand, France)* 66 (6), 46–51. doi:10.14715/cmb/2020.66.6.9

Tohru, A., Hitoshi, T., Akihiko, S., Shigenobu, K., Junitsu, I., Kazuhiko, S., et al. (2005). NAD(P)H oxidase plays a crucial role in PDGF-induced proliferation of hepatic stellate cells. *Hepatology* 41 (6), 1272–1281. (Baltimore, Md). doi:10.1002/hep.20719

Truong, H. N., Nguyen, H. N., Nguyen, T. K. N., Le, M. H., Tran, H. G., Huynh, N., et al. (2014). Establishment of a standardized mouse model of hepatic fibrosis for biomedical research. *Biomed. Res. Ther.* 1 (2).

Tungmunnithum, D., Intharuksa, A., and Sasaki, Y. (2020). A promising view of kudzu plant, Pueraria Montana var. lobata (willd) Sanjappa and pradeep: Flavonoid phytochemical compounds, taxonomic data, traditional uses and potential biological activities for future cosmetic application. *Cosmetics* 7 (1), 12. doi:10.3390/cosmetics7010012

Vincenzo, P., and Laura, S.-D. (2018). Nrf2 protects stellate cells from Smad-dependent cell activation. *PloS one* 13 (7), e0201044. doi:10.1371/journal.pone.0201044

Wang, F. (2017). The incidence of Gastrointestinal Stromal Tumors in Yunnan Tumor Hospital. Master thesis. Kunming Medical University.

Wang, H. (2013). Mechanism study on enhance liver detoxification of YaJieShaBa. Master thesis. Yunnan College of Traditional Chinese Medicine.

Wenge, L., and Ah-Ng, K. (2009). Molecular mechanisms of Nrf2-mediated antioxidant response. *Mol. Carcinog.* 48 (2), 91–104. doi:10.1002/mc.20465

Xia, L., Jianchang, S., Yajun, H., and Li, F. (2006). Colchicine inhibition of hepatic stellate cell activation and the effect of anti fibrosis. *Guangdong Med.* (12), 1796–1798.

Xiao, X.-B., Lin, Y.-X., Xu, G.-B., Gong, X. B., Gu, Y., Tong, J. F., et al. (2011). Two new cytotoxic alkaloids from Mappianthus iodoides Hand.-Mazz. *Helvetica Chim. acta* 94 (9), 1594–1599. doi:10.1002/hlca.201100187

Xiaohua, D., Jin, Z., Hui, W., Haifeng, C., Chao, Z., and Zepu, Y. (2015). Effect of Yajieshaba, a preparation of Dai indigenous medicine, on enhanced liver detoxification. *J. Traditional Chin. Med.* 35 (2), 197–205. doi:10.1016/s0254-6272(15)30028-5

Xiaomei, L., Wenfang, L., Han, Z., Xiaoming, W., Yuhong, H., Yuhong, L., et al. (2022). Biodistribution and pharmacokinetic profile of berberine and its metabolites in hepatocytes. *Phytomedicine Int. J. phytotherapy Phytopharm.* 104, 154288. doi:10.1016/j.phymed.2022.154288

Xingyu, Z., Weichi, C., Yimei, D., Pengwen, S., Yourou, Q., Jie, N., et al. (2021). Phytochemistry and pharmacological activities of Arundina graminifolia (D.Don) Hochr. And other common Orchidaceae medicinal plants. *J. Ethnopharmacol.* 276, 114143. doi:10.1016/j.jep.2021.114143

Yan, Z., Zhecheng, W., Dongcheng, F., Huanyu, Z., Musen, L., Yan, H., et al. (2019). p66Shc contributes to liver fibrosis through the regulation of mitochondrial reactive oxygen species. *Theranostics* 9 (5), 1510–1522. doi:10.7150/thno.29620

Yang, J.-J., Tao, H., Hu, W., Liu, L.-P., Shi, K.-H., Deng, Z.-Y., et al. (2014). MicroRNA-200a controls Nrf2 activation by target Keap1 in hepatic stellate cell proliferation and fibrosis. *Cell. Signal.* 26 (11), 2381–2389. doi:10.1016/j.cellsig.2014.07.016

Yang, L., U, X. Y., Zhang, C., Chen, P., and Duan, X. (2022). Yajieshaba prevents lipopolysaccharide-induced intestinal barrier injuryanti-inflammatory and anti-apoptosis. *J. traditional Chin. Med.* 42 (5), 707–714. *tsa chih ying wen pan* 42. doi:10.19852/j.cnki.jtcm.2022.05.005

Yanshuang, L., Yingran, L., Bin, Z., Li, C., Donglai, M., Hongfang, W., et al. (2020). Protective effects of crocetin on arsenic trioxide-induced hepatic injury: Involvement of suppression in oxidative stress and inflammation through activation of Nrf2 signaling pathway in rats. *Drug Des. Dev. Ther.* 14, 1921–1931. doi:10.2147/DDDT.S247947

Yonghong, X., and Chuan, X. (2022). Compound biejia-ruangan tablet as an adjunctive therapy to entecavir for chronic Hepatitis B complicated with hepatic fibrosis: A systematic review and meta-analysis of randomized controlled trials. *Medicine* 101 (32), e30020. doi:10.1097/MD.0000000000030020

Young, C. Y., Jin-I, S., Jong-Ik, H., and Dong-Sik, K. (2020). Co-administration of everolimus and N-acetylcysteine attenuates hepatic stellate cell activation and hepatic fibrosis. *Am. J. Transl. Res.* 12 (6), 2627–2639.

Yue, J. (2013). Study on Chemical constituents of Dai medicine bin hao and Voacanga africana Stapf. *Master*. Kunming: Yunnan University of Traditional Chinese Medicine.

Zesong, L., Shaoxi, C., Yuan, J., RuiJun, G., and Wen, Z. (2006). Colchicine inhibited the expression of tissue inhibitor of metalloprotenase-1 and interleukin-6 in cultured activated hepatic stellate cells. *Wuhan Univ. J. Nat. Sci.* 11 (3), 720–724. doi:10.1007/bf02836697

Zhen, T., Yifan, C., Jie, L., Xiao, C., and Yan, Z. (2013). Ethnomedicine: Fading or flowering? ——heritage and development of Dai medicine. *J. Med. Coll. PLA* 28 (01), 54–59. doi:10.1016/s1000-1948(13)60017-9

frontiers | Frontiers in Pharmacology

TYPE Original Research
PUBLISHED 13 June 2023
DOI 10.3389/fphar.2023.1101703

OPEN ACCESS

EDITED BY
Chunfeng Lu,
Nantong University, China

REVIEWED BY
Murali Ganesan,
University of Nebraska Medical Center, United States
Liang Shan,
Anhui Medical University, China

*CORRESPONDENCE
Junying Huang,
hjunying@gzhu.edu.cn
Ruoting Zhan,
zhanrt@gzucm.edu.cn
Guifang Zhang,
zhanggf@gzucm.edu.cn

RECEIVED 18 November 2022
ACCEPTED 30 May 2023
PUBLISHED 13 June 2023

CITATION
Li J, Wu B, Zeng L, Lin Y, Chen Q, Wang H, An L, Zhang J, Chen S, Huang J, Zhan R and Zhang G (2023), Aqueous extract of *Amydrium sinense (Engl.) H. Li* alleviates hepatic fibrosis by suppressing hepatic stellate cell activation through inhibiting Stat3 signaling.
Front. Pharmacol. 14:1101703.
doi: 10.3389/fphar.2023.1101703

Aqueous extract of *Amydrium sinense (Engl.) H. Li* alleviates hepatic fibrosis by suppressing hepatic stellate cell activation through inhibiting Stat3 signaling

Jingyan Li[1], Bingmin Wu[1], Lishan Zeng[1], Ying Lin[1], Qiuhe Chen[1], Haixia Wang[1], Lin An[1], Jiajun Zhang[1], Siyan Chen[1], Junying Huang[2]*, Ruoting Zhan[1,3]* and Guifang Zhang[1,3]*

[1]Guangdong Key Laboratory for Translational Cancer Research of Chinese Medicine, Joint Laboratory for Translational Cancer Research of Chinese Medicine of the Ministry of Education of the People's Republic of China, International Institute for Translational Chinese Medicine, School of Pharmaceutical Sciences, Guangzhou University of Chinese Medicine, Guangzhou, Guangdong, China, [2]College of Life Sciences, Guangzhou University, Guangzhou, Guangdong, China, [3]Key Laboratory of Chinese Medicinal Resource from Lingnan, Ministry of Education, Guangzhou University of Chinese Medicine, Guangzhou, China

Background: The present study aimed to investigate the protective effect of the water extract of *Amydrium sinense* (Engl.) H. Li (ASWE) against hepatic fibrosis (HF) and clarify the underlying mechanism.

Methods: The chemical components of ASWE were analysed by a Q-Orbitrap high-resolution mass spectrometer. In our study, an *in vivo* hepatic fibrosis mouse model was established via an intraperitoneal injection of olive oil containing 20% CCl_4. *In vitro* experiments were conducted using a hepatic stellate cell line (HSC-T6) and RAW 264.7 cell line. A CCK-8 assay was performed to assess the cell viability of HSC-T6 and RAW264.7 cells treated with ASWE. Immunofluorescence staining was used to examine the intracellular localization of signal transducer and activator of transcription 3 (Stat3). Stat3 was overexpressed to analyse the role of Stat3 in the effect of ASWE on HF.

Results: Gene Ontology (GO) and Kyoto Encyclopedia of Genes and Genomes (KEGG) analyses showed that candidate targets of ASWE, associated with protective effects against hepatic fibrosis, were related to inflammation response. ASWE ameliorated CCl_4-induced liver pathological damage and reduced the liver index and alanine transaminase (ALT) and aspartate transaminase (AST) levels. ASWE also decreased the serum levels of collagen I (Col I) and hydroxyproline (Hyp) in CCl_4-treated mice. In addition, the expression of fibrosis markers, including α-SMA protein and *Acta2*, *Col1a1*, and *Col3a1* mRNA, was downregulated by ASWE treatment *in vivo*. The expression of these fibrosis markers was also decreased by treatment with ASWE in HSC-T6 cells. Moreover,

Abbreviations: Acta2, Actin alpha 2; AS, *Amydrium sinense (Engl.) H. Li*; ASWE, water extract of *Amydrium sinense (Engl.) H. Li*; ALT, Alanine transaminase; AST, Aspartate transaminase; CCl_4, carbon tetrachloride; Col I, Collagen 1; Col III, Collagen 3; Col1a1, Collagen 1a1; Col3a1, Collagen 3a1; ECM, extracellular matrix; GAPDH, Glyceraldehyde-3-phosphate dehydrogenase; H&E, Hematoxylin and eosin; HF, Hepatic fibrosis; HSCs, Hepatic stellate cells; LPS, lipopolysaccharide; Il1β, Interleukin-1 beta; Il6, Interleukin-6; Stat3, Signal transducers and activators of transcription 3; Tnf-α, Tumor necrosis factor-α; TGF-β, Transforming growth factor beta; α-SMA, alpha smooth muscle actin.

ASWE decreased the expression of inflammatory markers, including the *Tnf-α*, *Il6* and *Il1β*, in RAW264.7 cells. ASWE decreased the phosphorylation of Stat3 and total Stat3 expression and reduced the mRNA expression of the *Stat3* gene *in vivo* and *in vitro*. ASWE also inhibited the nuclear shuttling of Stat3. Overexpression of Stat3 weakened the therapeutic effect of ASWE and accelerated the progression of HF.

Conclusion: The results show that ASWE protects against CCl_4-induced liver injury by suppressing fibrosis, inflammation, HSC activation and the Stat3 signaling pathway, which might lead to a new approach for preventing HF.

KEYWORDS

***Amydrium sinense*, hepatic fibrosis, carbon tetrachloride, α-SMA, Stat3**

1 Introduction

Hepatic fibrosis (HF) is a challenging clinical disease and a reversible wound-healing response during liver injury repair. HF is observed in patients with chronic viral hepatitis, nonalcoholic fatty liver disease, alcoholic liver disease, obesity and cholestatic and autoimmune liver diseases (Mederacke et al., 2013; Zheng et al., 2013). Without effective treatment, the continued development of HF results in the development of cirrhosis and hepatoma, leading to increased mortality due to liver disease worldwide (Hernandez-Gea and Friedman, 2011; Roeb, 2018). It is generally recognized that hepatic stellate cells (HSCs) are critical in the occurrence and development of HF. In response to various complex adverse factors, quiescent HSCs are activated and transdifferentiate into myofibroblast-like cells, leading to the excessive deposition of extracellular matrix (ECM), the formation of fibrotic nodules, and ultimately the acceleration of HF. Numerous experimental and clinical studies have also confirmed that inhibiting HSC activation is a potentially effective strategy for the treatment of HF (Lee et al., 2015; Tsuchida and Friedman, 2017).

Inflammation, which is one of the most prominent characteristic features of HF, is thought to accelerate the further development of HF due to the critical role of inflammation in the underlying pathogenesis of HF (Seki and Schwabe, 2015). Recent studies have noted that genes that regulate the inflammatory response to injury determine the fibrotic response to injury. For example, tumor necrosis factor-α (Tnf-α), interleukin 1β (Il1β), and interleukin 6 (Il6) may trigger the accumulation of associated cells (e.g., neutrophils) that drive the early stages of disease progression and maintain ongoing inflammation in the liver (Duffield et al., 2005; Mitchell et al., 2009). Typically, HF patients have elevated serum levels of inflammatory cytokines (Liaskou et al., 2013). HSCs are the main source of ECM, and can be activated by inflammation or mechanical stimulation, thus promoting the development of HF and the reconstruction of the intrahepatic structure (Kisseleva and Brenner, 2007; Lu et al., 2015). HSCs are highly sensitive to proinflammatory cytokines, leading to the activation of proinflammatory signaling pathways such as signal transducer and activator of transcription 3 (Stat3) and the subsequent production of chemokines and cytokines (Seki and Schwabe, 2015). Stat3 has been highlighted as a regulator of many biological processes, including cell survival, apoptosis, inflammation and angiogenesis (Zou et al., 2020; Xiao et al., 2022). Stat3 is essential for transducing fibrotic signaling in HF. Several studies have demonstrated that sustained activation of Stat3 promotes inflammation, leading to various pathological manifestations of HF, such as increased the expression of the fibrosis markers alpha smooth muscle actin (α-SMA), collagen 1 (Col I) and collagen 3 (Col III) (Deng et al., 2013; Xiang et al., 2018). Blockade of the Stat3 signaling pathway inhibits the morphological transdifferentiation of HSCs and reduces the mRNA expression of profibrotic genes (Wang et al., 2018).

To date, the pathogenesis of HF has been widely examined. However, precise and efficient drugs for treating HF have not been successfully identified (Schuppan et al., 2018). The ethnic medicine *Amydrium sinense (Engl.) H. Li* (AS) is the dried whole herb of the genus *Amydrium* in the family *Araceae*. This Chinese vine has long been used to treat diseases. According to the literature and related books, AS is mainly used in folk medicine to treat common diseases related to acute and chronic tissue inflammation, such as rheumatism, angina pectoris, fractures, bruises, and sprains. In our preliminary studies, we found that the water extract of AS (ASWE) could markedly inhibit the activation of HSCs. Therefore, we hypothesized that ASWE might protect against HF. Therefore, the present study was designed to analyse the chemical composition of ASWE, investigate the antihepatic fibrosis effect of ASWE in combination with *in vitro* and *in vivo* experiments, and clarify the underlying mechanism.

2 Materials and methods

2.1 Chemicals and antibodies

Carbon tetrachloride, methanol, acetonitrile, chloroform, isopropanol, anhydrous ethanol, and formic acid were purchased from Macklin (Shanghai, China). Transforming growth factor-β1 (TGF-β1) and lipopolysaccharide (LPS) were purchased from Aladdin (Shanghai, China). Fetal bovine serum (FBS), penicillin/streptomycin solution and Trizol reagent were obtained from Thermo Fisher Scientific. Dimethyl sulfoxide was purchased from Sigma-Aldrich Corporation (St. Louis, MO, United States). Trypsin was obtained from Invitrogen (Carlsbad, CA, United States). The enhanced BCA protein assay kit (P0010), Alexa Fluor 488-conjugated anti-mouse IgG (H + L) secondary antibody, and DAPI staining solution were purchased from Beyotime Biotechnology (Shanghai, China).

Antibodies against α-SMA (14395-1-AP), Stat3 (10253-2-AP), and GAPDH (6,004-1-lg) were obtained from Proteintech (Chicago, United States). Antibody against phospho-Stat3 (p-Stat3) (Tyr705) was purchased from Cell Signaling Technology (Boston, MA,

United States). Goat anti-rabbit IgG (H + L) secondary antibody (BS13278), and Goat anti-mouse IgG (H + L) secondary antibody (BS12478) were procured from Bioworld Technology (St. Paul, MN, United States).

2.2 Herb collection and extraction

The herbs used in the experiment were collected from Yangshan County, Qingyuan City, Guangdong Province, and were identified as the whole plant of *Amydrium sinense (Engl.) H. Li* by Zhang Guifang, Associate Professor, Guangzhou University of Traditional Chinese Medicine. The dried whole herb of *Amydrium sinense (Engl.) H. Li* was soaked for 1 h in advance and then decocted thrice with 20-fold volumes of distilled water for 1 h each. The drug solutions were combined and filtered. Afterwards, those drug solutions were concentrated under reduced pressure and freeze-dried to obtain the water extract of *Amydrium sinense (Engl.) H. Li* (ASWE).

2.3 Analysis of ASWE by Q-Orbitrap high-resolution mass

In this study, the chemical components of ASWE were analyzed by the Q-Orbitrap high-resolution mass spectrometer, which was used for the rapid identification of complex components in herbal medicines. The system was equipped with an ESI source and operated in the Full MS scan/dd-MS2 (Top N) scan mode to accurately determine the mass number of the samples and the acquisition of fragment ions. The detection instruments included Thermo Scientific™, Ultimate™3000RS, Thermo Scientific™, Q Exactive™ and RP-C18 column (150 mm × 2.1 mm, 1.8 μm). Mass spectrometry conditions were as follows: scan range, 150–2,000 m/z; aux gas heater temperature, 350°C; capillary temperature, 300°C; spray voltage, 3.8 kV; and sheath gas pressure, 40 Arb. High purity nitrogen gas (purity ≥99:999%) was used as both aux gas and sheath gas. High purity argon gas (purity ≥99: 999%) was used as the collision gas. Full-mass and dd-MS2 data in positive and negative modes were obtained at 70,000 and 17,500 FWHM (full width, half maximum), respectively. Chromatography conditions were as follows: column temperature, 35°C; water phase (A), 0.1% aqueous solution of formic acid; organic phase (B), acetonitrile solution containing 0.1% formic acid. The gradient elution sequence [A:B (v/v) at time (Villesen et al.)] was set as follows: (98:2) at 0 min; (98:2) at 1 min; (80:20) at 5 min; (50:50) at 10 min; (20:80) at 15 min; (5:95) at 20 min; (5:95) at 25 min; (98:2) at 26 min; and (98:2) at 30 min. The injected sample volume was 5.00 μL, and the sample flow rate was 0.30 mL/min. All data were acquired and processed using the CD2.1 software (Thermo Fisher), and then retrieved and compared in the mzCloud, mzVault, and ChemSpider databases.

2.4 Prediction of targets for ASWE chemicals and identification of HF-related targets

Potential targets of main chemical compounds of ASWE were obtained from the Encyclopedia of Traditional Chinese Medicine (ETCM) Database (http://www.tcmip.cn/ETCM/index.php/Home/Index/) (Xu et al., 2019). The HF-related targets were obtained from the following databases: DisGeNET (https://www.disgenet.org/) (Piñero et al., 2020), GeneCards (https://www.genecards.org/) (Stelzer et al., 2016), Comparative Toxicogenomics Database (CTD) (https://ctdbase.org/) (Zhao et al., 2022b)). We used "hepatic fibrosis" as the search term, and the organism was restricted to *Homo sapiens*.

2.5 Construction of network and functional enrichment analysis

After the screening and mapping of the active compounds and active targets for ASWE were completed, Cytoscape 3.7.1. was used to construct a protein-protein interaction (PPI) network of ASWE potential targets together with HF-related targets (Martin et al., 2010). To explore the biological processes of core targets, Gene Ontology (GO) biological function and KEGG pathway enrichment analyses were performed with the online tool DAVID Bioinformatics Resources 6.8 (Chen et al., 2017). The screening criteria were set as $p < 0.05$, and the species was limited to *H. sapiens*.

2.6 Experimental animals and treatments

Male C57BL/6J mice (age, 8 weeks), body weight 20 ± 2 g, were procured from the Experimental Animal Center of Guangzhou University of Chinese Medicine [SCXK (Guangdong) 2019–0202]. The experimental procedures and animal care were approved by the Laboratory Animal Ethics Committee of Guangzhou University of Chinese Medicine (No. ZYD-2020–135). Mice were fed and watered *ad libitum* and maintained in a suitable environment (22°C–24°C, 45%–50% relative humidity) with a 12 h light/dark cycle. After 1 week of acclimatization, mice were randomly divided into 5 groups ($n = 6$): the control group, the CCl_4 group, the ASWE drug-treatment groups (40, 80, 160 mg/kg/day respectively). In addition to the control group, hepatic fibrosis was induced in mice via intraperitoneally injecting (i.p.) of 20% CCl_4-olive oil (1:4 v/v, 5 mL/kg) twice a week for 4 weeks (Liu et al., 2021a; Song et al., 2023). The control group was given the same dose of olive oil. At the beginning of modeling, all treatment groups received an intragastric administration of ASWE (dissolved in PBS) at the doses of 40, 80, and 160 mg/kg once each day for 4 weeks. On the same day, mice in the control and CCl4 groups received equal volumes of PBS using a gastric gavage. At the end of treatment, blood samples were collected from orbital sinus by rapidly removing the eyeball after the mice were anesthetized with 0.2% sodium pentobarbital (0.2 mg/kg, i.p.). Approximately 1 mL blood was collected in an EP tube for each mouse. Following blood sample collection, the mice were sacrificed by cervical dislocation. Liver tissues were obtained by a midline laparotomy.

2.7 Calculation of the live index

The liver tissues were washed with pre-cooled saline and blotted with filter paper. The liver weights were weighed and recorded. The liver index was expressed as (liver weight, mg)/(body weight, g) × 100%.

2.8 Liver histology

The morphology of liver lobes was photographed for retention. Liver tissues were fixed in 4% paraformaldehyde (Solarbio, China), sequentially dehydrated and then embedded in paraffin. The paraffin-embedded tissue samples were then sectioned into 5 μm slices and finally routinely stained with hematoxylin and eosin (H&E) and Masson's trichrome (Solarbio, China). The images were captured under a light microscope (E100, Nikon Corporation).

2.9 Immunohistochemistry assay

The paraffin-embedded liver tissues were subjected to immunohistochemical staining with Stat3 antibody. Then, microscopic areas in all liver sections were randomly selected for examination, and photographed in a blinded manner using a section digital scanner (E100, Nikon Corporation).

2.10 Serum biochemical assay

Briefly, blood samples were kept at room temperature for 2 h and then centrifuged at 4°C (3,500 rpm, 10 min). After that, mice serum samples were collected for analysis. The serum levels of alanine transaminase (ALT) and aspartate aminotransferase (AST), which are normally used to assess liver function (Li et al., 2022b), were determined according to the instructions of the ALT (C009-2–1) and AST (C010-2–1) kits (Nanjing Jiancheng Institute of Biological Engineering, Nanjing, China). To observe collagen deposition in the liver tissues, the level of hydroxyproline (Hyp) in serum was determined using hydroxyproline assay kit. The level of Col Ⅰ in serum was detected by a standard sandwich ELISA method (E-EL-M0325c, Elabscience, Wuhan, China).

2.11 Cell culture and treatments

The leukemia cells in mouse macrophage (RAW264.7) and the rat hepatic stellate cells (HSC-T6) were purchased from the Cell Bank of Academy of Sciences (Shanghai, China). The cells were cultured in Dulbecco's modified Eagle's medium (DMEM) containing 10% FBS and penicillin/streptomycin (1:100) at 37°C in a humidified atmosphere containing 5% CO_2.

The cells were inculated on 6-well culture plates in a serum-free conditioned medium for 12 h. Then HSC-T6 cells were stimulated with 10 ng/mL TGF-β1 for 1 h, and then ASWE (0.25 mg/mL, 0.5 mg/mL, 1.0 mg/mL) was dissolved in the DMEM supernatant containing TGF-β1 for 24 h (Dewidar et al., 2019; Zhao et al., 2022a). RAW264.7 cells were treated with 1 μg/mL LPS for 1 h. Afterwards, the cells were cultured in the DMEM supernatant containing ASWE (0.25 mg/mL, 0.5 mg/mL, 1.0 mg/mL) and LPS for 24 h (Lee et al., 2019; Zhou et al., 2021). Thereafter, total protein and RNA were extracted for subsequent experiments.

2.12 Cell viability assay

Cell viability was tested by a Cell Counting Kit-8 (CCK-8) assay (Dojindo Laboratories, Kyushu island, Japan). Cells, seeded in 96-well plates at equal densities for 24 h, were treated with ASWE at the concentration ranging from 0.05 to 2.50 mg/mL for 24 h. Then, CCK-8 solution (10 μL) was added to each well and incubated for 2 h at 37°C. Afterwards, the absorbance value at 450 nm was measured with a microplate reader (Thermo Varioskan LUX, MA, United States).

2.13 Immunofluorescent assay

To observe Stat3 nucleus shuttling, cultured cells were fixed with 4% paraformaldehyde for 10 min. Afterwards, the cells were permeabilized with 0.1% Triton X-100 for 10 min, followed by incubation with 10% goat serum for blocking the non-specific staining and incubation with Stat3 antibody overnight at 4°C. Thereafter, Alexa Fluor 488-conjugated anti-mouse IgG (H + L) secondary antibody was used to incubate in the dark for 1 h at room temperature. The nuclei were stained with DAPI solution for 10 min in the dark at room temperature. Finally, the cells were examined with a confocal microscope (LSM 710, Carl Zeiss, Germany).

2.14 Plasmid transfection

For overexpression studies, the Stat3 plasmid was constructed with pcDNA3.1. The plasmid was confirmed by DNA sequencing, which was performed at Sangon Biotech Co. Ltd (Shanghai, China). HSC-T6 and RAW264.7 cells were transiently transfected with the Stat3 plasmid or empty vector using Lipofectamine 2,000 reagent (Invitrogen, Carlsbad, CA, United States) according to the manufacturer's instructions and then incubated for 48 h before harvesting.

2.15 Western blot analysis

Radioimmunoprecipitation assay (RIPA) buffer (Beyotime, Nantong, Jiangsu, China) supplemented with 1% protease inhibitor cocktail (Beyotime, Nantong, Jiangsu, China) was used for protein extraction from tissues and cells. The concentrations of total protein samples were determined based on the instructions of bicinchoninic acid (BCA) protein assay kit (Thermo Fisher Scientific, MA, United States). The procedure for Western blot was in the light of our previously described procedure (Li et al., 2019; Li et al., 2022a). Image-Pro Plus 6.0 software (Rockville, MD, United States) was utilized to calculate the intensity of immunoreactive bands in different lanes. The results were expressed as density values normalized to GAPDH.

2.16 Total RNA extraction and quantitative real-time PCR

Total RNA was extracted from the liver tissues or cells with Trizol reagent (Accurate Biotechnology, Human, China) in

TABLE 1 Primer sequences used for quantitative PCR.

Species	Primers	Sequences
Mus	*Gapdh*-forward	GCCTCGTCCCGTAGACAAAA
	Gapdh-reverse	TACGGCCAAATCCGTTCACA
	Acta2-forward	GAAGCTCGTTATAGAAAGAGTGG
	Acta2-reverse	TCAGGGAGTAATGGTTGGAAT
	Col1a1-forward	TTCTCCTGGCAAAGACGGAC
	Col1a1-reverse	CGGCCACCATCTTGAGACTT
	Col3a1-forward	ACGTAAGCACTGGTGGACAG
	Col3a1-reverse	CAGGAGGGCCATAGCTGAAC
	Tnf-α-forward	ATGGCCTCCCTCTCATCAGT
	Tnf-α-reverse	TTTGCTACGACGTGGGCTAC
	*Il1*β-forward	TGCCACCTTTTGACAGTGATG
	*Il1*β-reverse	TGATGTGCTGCTGCGAGATT
	Il6-forward	GTCCTTCCTACCCCAATTCCA
	Il6-reverse	CGCACTAGGTTTGCCGAGTA
	Stat3-forward	TGTCAGATCACATGGGCTAAAT
	Stat3-reverse	GGTCGATGATATTGTCTAGCCA
Rat	*Gapdh*-Forward	AGTGCCAGCCTCGTCTCATA
	Gapdh-Reverse	GATGGTGATGGGTTTCCCGT
	Acta2-forward	CATCCGACCTTGCTAACGGA
	Acta2-reverse	GTCCAGAGCGACATAGCACA
	Col1a1-forward	GTGCGATGGCGTGCTATG
	Col1a1-reverse	ACTTCTGCGTCTGGTGATACA
	Col3a1-forward	AGATGCTGGTGCTGAGAAGAAAC
	Col3a1-reverse	GCTGGAAAGAAGTCTGAGGAAGG

accordance with specific instructions. RNA concentrations and purity were assessed by the measurement of optical density at 260 and 280 nm. The mRNA levels of the target genes were determined using the SYBR Green Quantitative PCR kit (TOYOBO, Japan) as previously described (Li et al., 2016). The semi-quantitative RT-qPCR data of every target gene were expressed as $2^{-\Delta\Delta CT}$ relative expression compared with endogenous GAPDH. Results were presented as fold change to control group. The primers used in the real-time PCR analysis were designed by Sangon Biotech Co (Shanghai, China). Primer sequences are listed in Table 1.

2.17 Statistical analysis

Data were expressed as the mean ± standard deviation (SD) from at least three independent experiments. Statistical analysis was performed using GraphPad Prism version 7.0 (San Diego, CA, United States). Statistical analyses between two groups were performed by Student's t-test and multiple groups were performed by one-way analysis of variance (ANOVA). In all cases, a value of $p < 0.05$ was regarded to be statistically significant.

3 Results

3.1 Components in ASWE

Generally, the composition of aqueous extract of herbs is complex, therefore, we used the Q-Orbitrap method, which has a series of advantages (Feng et al., 2021) for the detection of main chemical components in ASWE. The total ion chromatogram of ASWE was obtained as shown in Figure 1, while a total of 45 compounds were successfully characterized as shown in Table 2, including syringic acid, neochlorogenic acid, 4-(2-Hydroxyethyl)-2-methoxyphenyl *ß*-D-glucopyranoside, coniferin, catechin, asperulosidic acid, chlorogenic acid, fraxin, fraxetin, 2-anisic acid, ageratriol, ferulic acid, suberic acid, 1,2,3,4-tetramethyl-1,3-cyclopentadiene, naringeninchalcone and other active ingredients.

3.2 Compound-target network analysis and functional analysis of ASWE targets for treating HF

A total of 250 putative targets of ASWE were predicted by the, ETCM database. Based on the DisGeNET, GeneCards and CTD Databases, 998 HF-related genes were collected. Screening showed that of the 250 ASWE targets, 44 were also known therapeutic targets for treating HF (Supplementary Figure S1A). To reflect the relationship between targets and compounds, we have used Cytoscape 3.7.1 to map out the compound-target relation network diagram. As shown in Supplementary Figure S1B, the compound-target diagram consisted of 52 nodes (8 core active compound nodes and 44 active target nodes). Then, to identify the biological function of the core targets, GO and KEGG enrichment analyses of the 44 core targets were performed using the DAVID online tool. As shown in Supplementary Figure S1C, 8 vital biological processes were obtained by mapping targets. The majority of these targets were closely related to the mechanism of HF. The KEGG enrichment analysis showed that the targets were notably related to the non-alcoholic fatty liver disease, alcoholic liver disease, hepatitis C, hepatitis B (Supplementary Figure S1D). These analytical results suggested that inflammatory response might be involved in the anti-antifibrotic process of ASWE against HF.

3.3 ASWE alleviated hepatic injury in CCl4-induced mice

To determine the effect of ASWE on the occurrence and development of hepatic injury and fibrosis in CCl_4-induced mice, we firstly examined the morphological changes of liver tissues, as shown in Figure 2A, the livers of the control group were smooth, soft and dark red. However, the livers of the model group had a rough, lusterless surface with speckled and granular lesions and a hard texture, indicating that the liver was severely damaged. In contrast, after treatment with

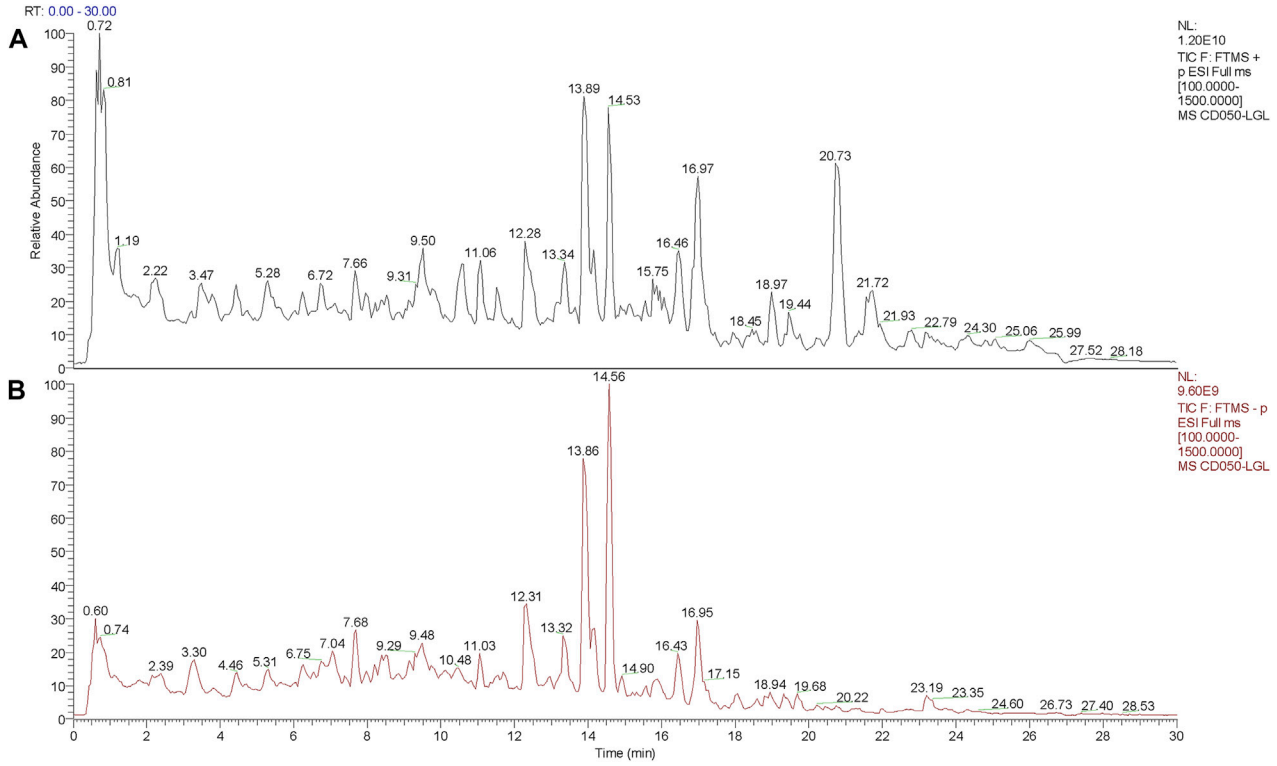

FIGURE 1
Components in ASWE. **(A)** Positive mode. **(B)** Negative mode.

ASWE, the livers were smooth with relatively rosy color and soft texture, and the number of grain was obviously reduced. In addition, H&E staining of liver tissue samples from the model group revealed severe inflammatory infiltration and hepatocyte necrosis in portal areas. However, ASWE treatment significantly reduced the abnormal histological changes listed above (Figure 2B).

Similarly, CCl_4 occasioned a considerable increase in liver weight and reduce in body weight, which led to an increase in liver index values. However, ASWE clearly dose-dependently ameliorated the symptoms listed above (Figures 2C–E). Moreover, to further explore the protective effects of ASWE on HF, we measured the transaminase activity including ALT and AST in the serum, which were the key hallmarks of liver function (Suciu et al., 2020). Compared to the control group, the serum levels of ALT and AST were significantly increased in the model group. Interestingly, the serum levels of ALT and AST were markedly dose-dependently reduced by ASWE treatment as compared with the model group (Figures 2F, G). Taken together, these results imply that ASWE treatment protects mice from liver damage induced by CCl_4 treatment *in vivo*.

3.4 ASWE ameliorated collagen deposition and the expression of fibrotic markers in CCl_4-induced HF mice

Considering that collagen deposition is one of the important features of HF (Zhang et al., 2022). We examined the degree of collagen deposition in CCl_4-induced HF mice. Masson staining results showed severe collagen deposition in the CCl_4 group. However, ASWE treatment clearly dose-dependently alleviated collagen deposition as compared with CCl_4 treatment (Figure 3A). Meanwhile, the biomarkers of fibrogenesis, including Hyp and Col Ⅰ, were further examined by corresponding kits. As shown in Figures 3B, C, the levels of Hyp and Col Ⅰ in serum in the CCl_4 group were significantly higher than that in the control group, and ASWE treatment significantly reduced the levels of Hyp and Col Ⅰ.

HF is always accompanied with activation of HSCs which are the primary source of activated myofibroblasts that produce ECM in the liver (Seki and Schwabe, 2015; Tsuchida and Friedman, 2017; Baghaei et al., 2022). Therefore, the expression levels of liver fibrosis marker α-SMA, which is closely related to activation of HSCs, was detected by Western blot and RT-qPCR. The results showed that the protein and mRNA expression of α-SMA was markedly enhanced in the CCl_4 group. Whereas, ASWE treatment significantly inhibited the expression of this important fibrosis marker (Figures 3D, E). Moreover, the RT-qPCR results also showed that CCl_4 treatment cause an excessive mRNA expression of *Col1a1* and *Col3a1*. And these abnormal expressions induced by CCl_4 treatment were dose-dependently reversed by ASWE treatment (Figure 3F). Collectively, these results demonstrate that ASWE can inhibit collagen accumulation and the activation of HSCs in CCl_4-induced HF mice, thereby alleviating liver fibrogenesis.

TABLE 2 Identification of the chemical constituents obtained for ASWE.

NO.	t_R/min	Formula	m/z	Area	Identification
1	3.15	$C_9H_{10}O_5$	198.05	5,736,783	Syringic acid
2	3.25	$C_{16}H_{18}O_9$	354.09	427,680	Neochlorogenic acid
3	3.50	$C_{15}H_{22}O_8$	347.16	5,965,580	4-(2-Hydroxyethyl)-2-methoxyphenyl *ß*-D-glucopyranoside
4	4.72	$C_{16}H_{22}O_8$	359.16	3,845,334	Coniferin
5	4.78	$C_{15}H_{14}O_6$	290.08	147,186	Catechin
6	4.97	$C_{18}H_{24}O_{12}$	449.15	12,057,938	Asperulosidic acid
7	5.16	$C_{16}H_{18}O_9$	354.09	206,555	Chlorogenic acid
8	5.91	$C_{16}H_{18}O_{10}$	370.09	17,855,131	Fraxin
9	5.91	$C_{10}H_8O_5$	208.04	329,023	Fraxetin
10	7.06	$C_8H_8O_3$	134.04	314,471	2-Anisic acid
11	7.10	$C_{15}H_{24}O_3$	234.16	1,446,924	Ageratriol
12	7.89	$C_{10}H_{10}O_4$	194.06	2,110,227	Ferulic acid
13	7.97	$C_8H_{14}O_4$	174.09	1,482,813	Suberic acid
14	8.19	C_9H_{14}	122.11	2,598,184	1,2,3,4-Tetramethyl-1,3-cyclopentadiene
15	8.29	$C_{15}H_{12}O_5$	272.07	40,728	Naringeninchalcone
16	8.56	$C_{26}H_{34}O_{11}$	539.24	3,498,548	Lariciresinol 4-O-glucoside
17	8.84	$C_{10}H_{18}O$	136.13	10,407,830	Eucalyptol
18	9.39	$C_{21}H_{20}O_{12}$	464.10	405,504	Quercetin-3β-D-glucoside
19	9.68	$C_{15}H_{10}O_7$	302.04	61,506	Quercetin
20	10.00	$C_9H_{16}O_4$	188.10	17,678,287	Azelaic acid
21	10.14	$C_{17}H_{17}NO_3$	283.12	1,611,911	(2E)-3-(4-Hydroxyphenyl)-N-[2-(4-hydroxyphenyl)ethyl]acrylamide
22	10.15	$C_{11}H_{12}O_5$	206.06	2,707,861	Sinapinic acid
23	11.08	$C_{21}H_{20}O_{10}$	432.11	349,693	Afzelin
24	11.08	$C_{15}H_{10}O_6$	286.05	137,921	Kaempferol
25	11.45	$C_{15}H_{22}O$	218.17	4,531,989	Nootkatone
26	11.53	$C_{18}H_{28}O_3$	292.20	5,454,425	8-{3-Oxo-2-[(2E)-2-penten-1-yl]-1-cyclopenten-1-yl}octanoic acid
27	12.07	$C_{18}H_{28}O_3$	292.20	11,601,814	9S,13R-12-Oxophytodienoic acid
28	12.88	$C_{15}H_{24}O$	220.18	16,534,693	(−)-Caryophyllene oxide
29	13.02	$C_{24}H_{30}O_8$	446.19	6,336,847	1,4-Bis(3,4,5-trimethoxyphenyl)-hexahydrofuro[3,4-c]furan
30	13.20	$C_{13}H_{24}N_2O$	224.19	1,205,424	N,N′-Dicyclohexylurea
31	13.36	$C_{18}H_{32}O_5$	328.22	301,864,820	Corchorifatty acid F
32	13.97	$C_{18}H_{34}O_4$	314.25	1,439,020	(+/−)12(13)-DiHOME
33	15.52	$C_{18}H_{30}O_3$	294.22	65,271,268	9-Oxo-ODE
34	16.29	$C_{12}H_{26}O_4S$	266.16	6,561,369	Dodecyl sulfate
35	16.43	$C_{18}H_{39}O_7P$	398.24	1,004,724	Tris(2-butoxyethyl) phosphate
36	16.81	$C_{16}H_{30}O_2$	254.22	1,358,160	Palmitoleic acid
37	16.99	$C_{18}H_{30}O_2$	278.22	607,385,742	α-Eleostearic acid
38	17.96	$C_{21}H_{38}O_4$	354.28	1,211,259	1-Linoleoyl glycerol

(Continued on following page)

TABLE 2 (*Continued*) Identification of the chemical constituents obtained for ASWE.

NO.	t_R/min	Formula	m/z	Area	Identification
39	18.00	$C_{30}H_{48}O_4$	489.38	182,542	Maslinic acid
40	18.52	$C_{10}H_{10}O_3$	160.05	1,083,312	4-Methoxycinnamic acid
41	19.29	$C_{20}H_{39}NO_2$	325.30	6,981,250	Oleoyl ethanolamide
42	19.38	$C_{30}H_{48}O_3$	438.35	1,528,445	Oleanolic acid
43	20.63	$C_{19}H_{39}NO$	297.30	1,238,856	Tridemorph
44	22.50	$C_{22}H_{45}NO$	339.35	2,599,655	Docosanamide
45	22.74	$C_{10}H_{12}O_2$	164.08	353,952	4-Phenylbutyric acid

3.5 ASWE inhibited the activation of HSCs and suppressed inflammation *in vitro*

To further investigate the antifibrotic effect of ASWE and its underlying mechanism, we used HSC-T6 cells and RAW264.7 cells for *in vitro* experiments. we first performed a CCK8 assay to assess whether ASWE had cellular toxicity on HSC-T6 cells and RAW264.7 cells. The results indicated that the viabilities of HSC-T6 and RAW264.7 cells were higher than 80% when the cells were treated with 0.05–2.0 mg/mL ASWE, while ASWE at 2.5 mg/mL exhibited significant inhibition to both cell types (Figure 4A). This results indicated that ASWE had no remarkable toxicity for HSC-T6 and RAW264.7 cells when the concentration of ASWE is lower than 2.0 mg/mL. This prompts us to select the appropriate doses of ASWE (0.25, 0.5, and 1 mg/mL) in the further experiments. After that, we further observed the expression of α-SMA protein in TGF-β-stimulated HSC-T6 cells. As shown in Figure 4B, the expression of α-SMA, which was promoted by the TGF-β1 stimulation, was inhibited by ASWE treatment in a dose-dependent manner. In addition, consistent with the *in vivo* results, ASWE downregulated the expressions of the genes that were related to collagen deposition in HSC-T6 cells, including *Acta2*, *Col1a1*, and *Col3a1* (Figure 4C). Inflammatory response is closely associated with HF, and the development of fibrosis usually leads to an increase in inflammatory factors (Parola and Pinzani, 2019). Therefore, the mRNA expression of *Tnf-α*, *Il1β*, and *Il6* was investigated by RT-qPCR analysis and the results showed that their expression was significantly augmented by the LPS stimulus and observably diminished by ASWE treatment in a dose-dependent manner in LPS-stimulated RAW 264.7 cells, and the high dose group (ASWE-high group) had the best effect. (Figure 4D). Overall, these results provide evidence that ASWE can inhibit HSCs activation and attenuate the inflammatory response.

3.6 Stat3 signaling pathway could be involved in the regulation of the anti-fibrotic process of ASWE

In the above experiments, we found that ASWE had anti-inflammatory effects. Currently, domestic and international studies have confirmed that the Stat3 signaling pathway is closely linked to the secretion of pro-inflammatory factors and this pathway also plays a crucial role in the fibrosis process of liver (Guan et al., 2021) (Ma et al., 2022). Therefore, we speculated that ASWE is likely to have a regulatory role on the transcriptional activity of Stat3. To investigate the effect of ASWE on Stat3 signaling pathway, we examined the expression of Stat3 and the phosphorylation level of Stat3 at tyrosine 705 (p-Stat3), which is responsible for the activation of Stat3 (Wen et al., 1995) as well as the mRNA expression of *Stat3* gene. Apparently, the expressions of p-Stat3 and total Stat3 were both elevated and the expression of *Stat3* gene was upregulated in LPS-stimulated RAW 264.7 cells. Notably, ASWE treatment reversed LPS-induced upregulation of phosphorylated Stat3, total Stat3, and *Stat3* gene (Figures 5A, B). These observations suggest that ASWE treatment can reverse LPS-induced activation of Stat3.

After activation, Stat3 transported from the cytoplasm to the nucleus to regulate the transcription of its target genes (Kurdi and Booz, 2010). Thus, the nuclear translocation of Stat3 was investigated by detecting the subcellular distribution of Stat3 under confocal microscope. As shown in Figure 5C, the immunofluorescence staining results showed that Stat3 fluorescence was assembled in the nucleus of the TGF-β1-treated cells, whereas it was retained in the cytoplasm in the control cells. Administration of different doses of ASWE inhibited the nuclear shuttling of Stat3. Summarily, these results demonstrated that ASWE had an inhibitory effect on Stat3 activation and nuclear translocation. This suggests that ASWE is likely to alleviate the inflammatory response by inhibiting the activity of Stat3 signaling pathway, and thus exhibiting the antifibrotic effect.

3.7 ASWE restrained HSCs activation through suppression of the Stat3 signaling pathway

The aforementioned experiments results prompted us to further clarify the significance of the Stat3 signaling pathway in inhibiting fibrosis and inflammation of ASWE. Therefore, we used the Stat3 plasmid to overexpress Stat3 for the next experiments. As shown in Figures 6A, B, Stat3 was successfully overexpressed in HSC-T6 cells and RAW 264.7 cells. Furthermore, as shown in Figure 6C, ASWE inhibited the elevated expression of α-SMA protein induced by TGF-β1 in HSC-T6 cells, but this effect was reversed by

10.3389/fphar.2023.1101703

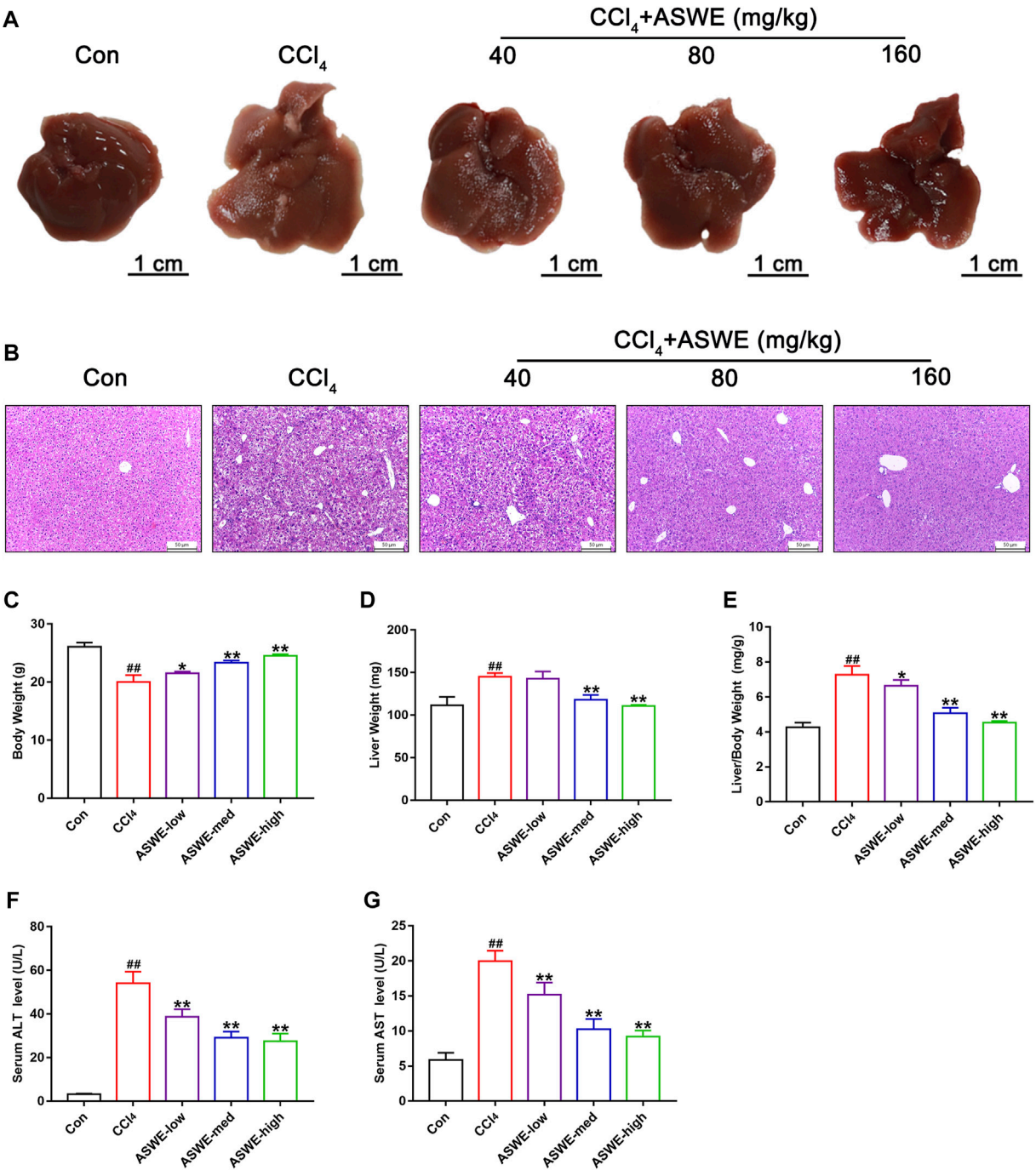

FIGURE 2
ASWE alleviated hepatic injury in CCl_4-induced mice. **(A)** Representative liver photographs from control, model, and drug-treated groups (scale bar: 1 cm); **(B)** H&E staining (scale bar: 50 μm); **(C–E)** Body weight, liver weight and liver/body weight index (%) in mice; **(F,G)** The levels of ALT and AST in the serum. Data are presented as mean ± SD ($n = 6$). $^{\#}p < 0.05$, $^{\#\#}p < 0.01$, compared with control group; $^{*}p < 0.05$, $^{**}p < 0.01$, compared with CCl_4 group.

Stat3 overexpression. Meanwhile, Stat3 overexpression enhanced the mRNA expression levels of the fibrosis markers *Acta2*, *Col1a1*, and *Col3a1* and the inflammation markers *Tnf-α*, *Il1β* and *Il6*, which weakened the inhibitory effect of ASWE (Figures 6D, E). These results provide evidence that ASWE inhibits the activation of HSCs by suppressing the Stat3 signaling pathway.

3.8 ASWE inhibited the activation of Stat3 in CCl4-induced HF mice

In order to verify that ASWE indeed exerts an antifibrotic effect by inhibiting the activation of HSCs through suppression of the Stat3 signaling pathway. Immunohistochemistry assay was performed to observe the expression of Stat3 in CCl_4-induced HF

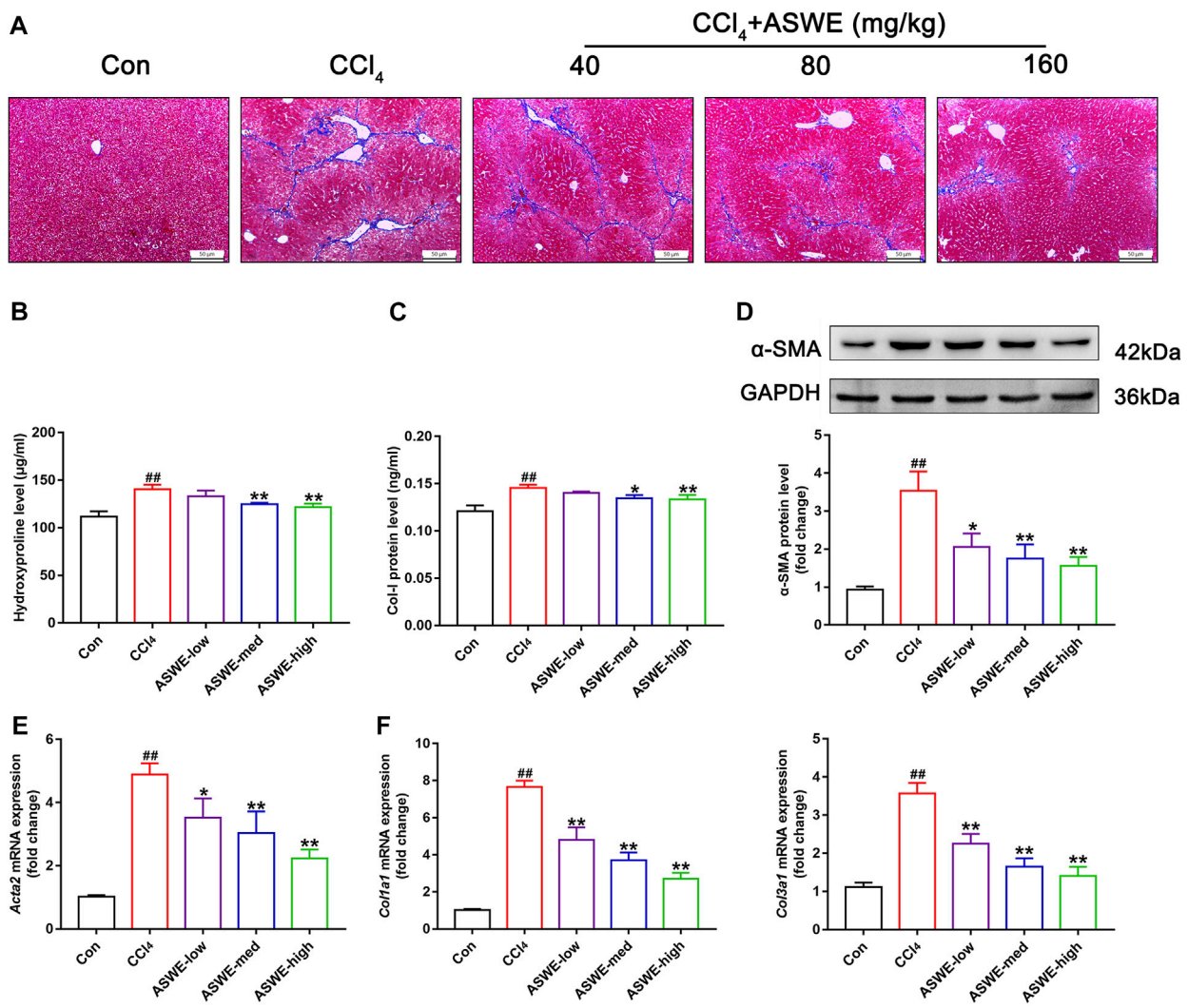

FIGURE 3
ASWE ameliorated collagen deposition and the expression of fibrotic markers in CCl_4-induced HF mice. **(A)** Masson staining (scale bar: 50 μm); **(B,C)** The levels of Hyp and Col I in the serum ($n = 6$); **(D)** The protein expression of α-SMA ($n = 3$); **(E,F)** The mRNA expressions of fibrotic markers (*Acta2*, *Col1a1*, and *Col3a1*). Data are presented as mean ± SD ($n = 4$). $^{\#}p < 0.05$, $^{\#\#}p < 0.01$, compared with control group; $^{*}p < 0.05$, $^{**}p < 0.01$, compared with CCl_4 group.

mice. As the results showed, significantly higher Stat3 expression in mouse livers with CCl_4 treatment was found as compared with the control group (Figure 7A). Thus, it can be seen that CCl_4 significantly promoted the expression of Stat3, while ASWE treatment reduced the expression of Stat3 in a dose-dependent manner. Thereafter, we further observed the protein expression of p-Stat3 and Stat3 in liver tissues by Western blot. Meanwhile, we also performed RT-qPCR analysis to examine the expression level of *Stat3* gene. The results showed that ASWE significantly reduced the elevation of the phosphorylation level of Stat3 at tyrosine 705 (p-Stat3), the increase of Stat3 protein expression and the upregulation of *Stat3* gene induced by CCl_4 stimulation in a dose-dependent manner (Figures 7B, C). The anti-inflammatory effect of ASWE in the livers of HF mice was also confirmed by RT-qPCR analysis. As shown in Figure 7D, ASWE inhibited the expression of inflammation-related genes, including *Tnf-α*, *Il1β*, and *Il6*, which was elevated by CCl_4 treatment. The above *in vitro* and *in vivo* results consistently demonstrated that ASWE could inhibit the activation of HSCs by inhibiting the Stat3 signaling pathway, and ultimately alleviate HF.

4 Discussion

HF is a reversible wound-healing response during liver injury that is characterized by excessive deposition of ECM. Long-term persistent development of HF will lead to cirrhosis and even liver cancer, threatening public health. Currently, clinically effective and safe drugs and treatments for HF are lacking. Therefore, exploring and developing new drugs and therapies to treat HF is a research challenge (Bataller and Brenner, 2005; Tsochatzis et al., 2014). Traditional Chinese medicine (TCM) has unique advantages and development prospects in the treatment of chronic inflammation-related diseases

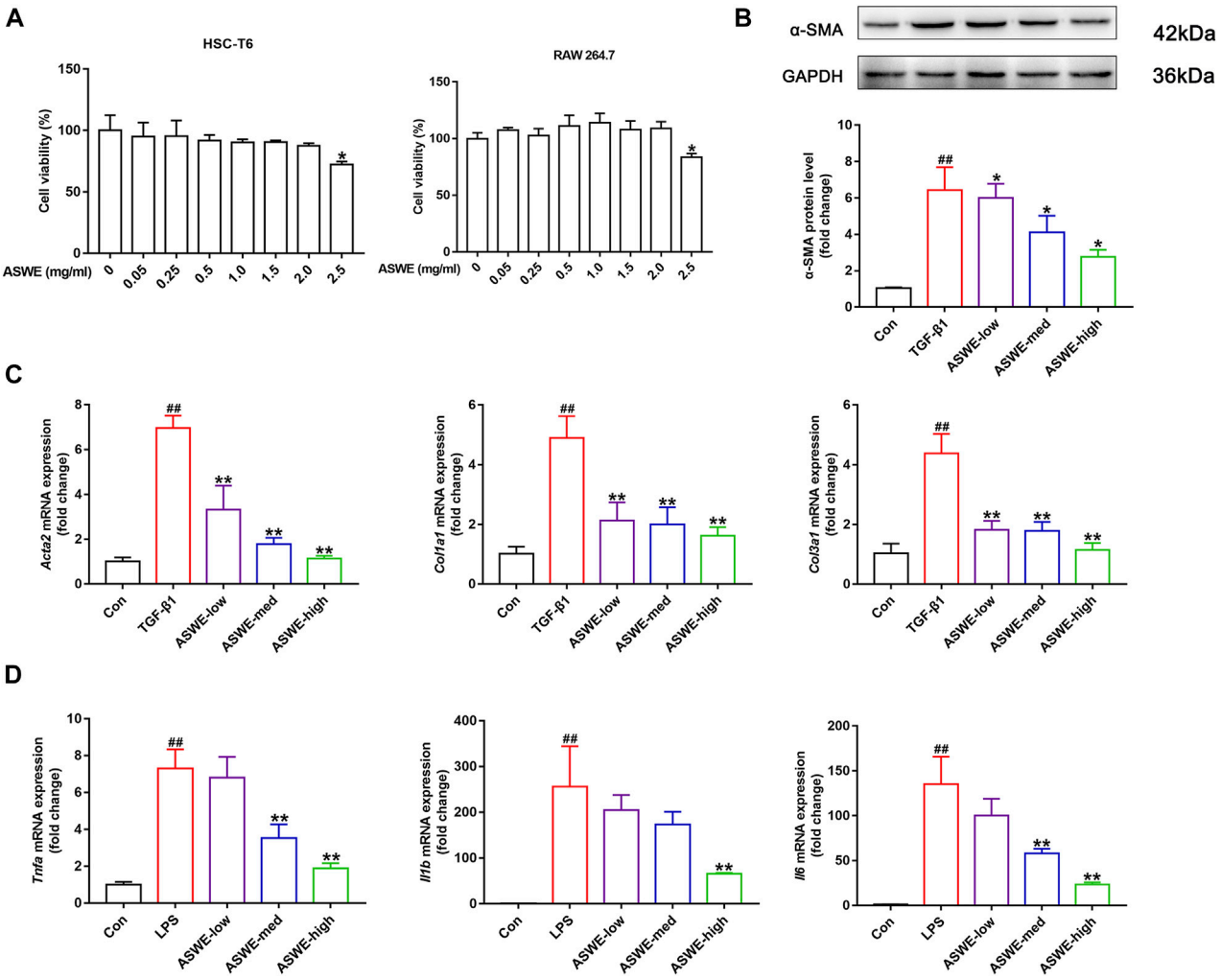

FIGURE 4
ASWE inhibited the activation of HSCs and suppressed Inflammation *in vitro*. **(A)** The viabilities of HSC-T6 and RAW264.7 cells; Data are presented as mean ± SD (n = 3). *p < 0.05, compared with control group; **(B)** The protein expression of α-SMA (n = 3); **(C)** The mRNA expressions of fibrotic markers (*Acta2*, *Col1a1*, and *Col3a1*). **(D)** The mRNA expressions of inflammatory factors (*Tnf-α*, *Il1β*, and *Il6*). Data are presented as mean ± SD (n = 4). #p < 0.05, ##p < 0.01, compared with control group; *p < 0.05, **p < 0.01, compared with model group (TGF-β1 or LPS group).

such as HF (Cheng et al., 2017; Liu et al., 2021b; Ran et al., 2021). TCM has been used for centuries as a complementary and alternative treatment to prevent liver fibrosis. At present, some compounds in TCM inhibit liver fibrosis, such as paeoniflorin (Chen et al., 2012), salvianolic acid B (Li et al., 2012), quercetin (Wu et al., 2011), puerarin (Li et al., 2013), tetrandrine (Ezhilarasan et al., 2012), matrine (Zhang et al., 2001), silybin (Zhang et al., 2001), and oxymatrine (Chai et al., 2012). *Amydrium sinense* (Engl.) H. Li is a unique herbal that is used to treat a variety of common diseases. In the current study, we demonstrated the potential antifibrotic effect of the water extract of *Amydrium sinense* (Engl.) H. Li in a CCl_4-induced chronic liver fibrosis mouse model for the first time. Mechanistically, we revealed that ASWE protected the liver by inhibiting HSC activation by suppressing Stat3 signaling pathway.

First, the chemical components of ASWE were analysed by a Q-Orbitrap high-resolution mass spectrometer (Figure 1; Table 2) and the main targets of compounds in ASWE were predicted using the, ETCM database. A total of 250 putative targets of ASWE were predicted and 998 HF-related genes were collected. Screening showed that of the 250 ASWE targets, 44 were also known therapeutic targets for treating HF. To reflect the relationship between targets and compounds, we have used Cytoscape 3.7.1 to map out the compound-target relation network diagram, the compound-target diagram consisted of 52 nodes (8 core active compound nodes and 44 active target nodes). Then, to identify the biological function of the core targets, GO and KEGG enrichment analyses of the 44 core targets were performed using the DAVID online tool, 8 vital biological processes were obtained by mapping targets. The majority of these targets were closely related to intracellular receptor signaling pathway, cellular response to external stimulus, regulation of lipid metabolic process, regulation of inflammatory response and fatty acid metabolic process. These biological processes are partially associated with the mechanism of HF. Cellular component analysis revealed that these targets are distributed in the transcription regulator complex, extrinsic

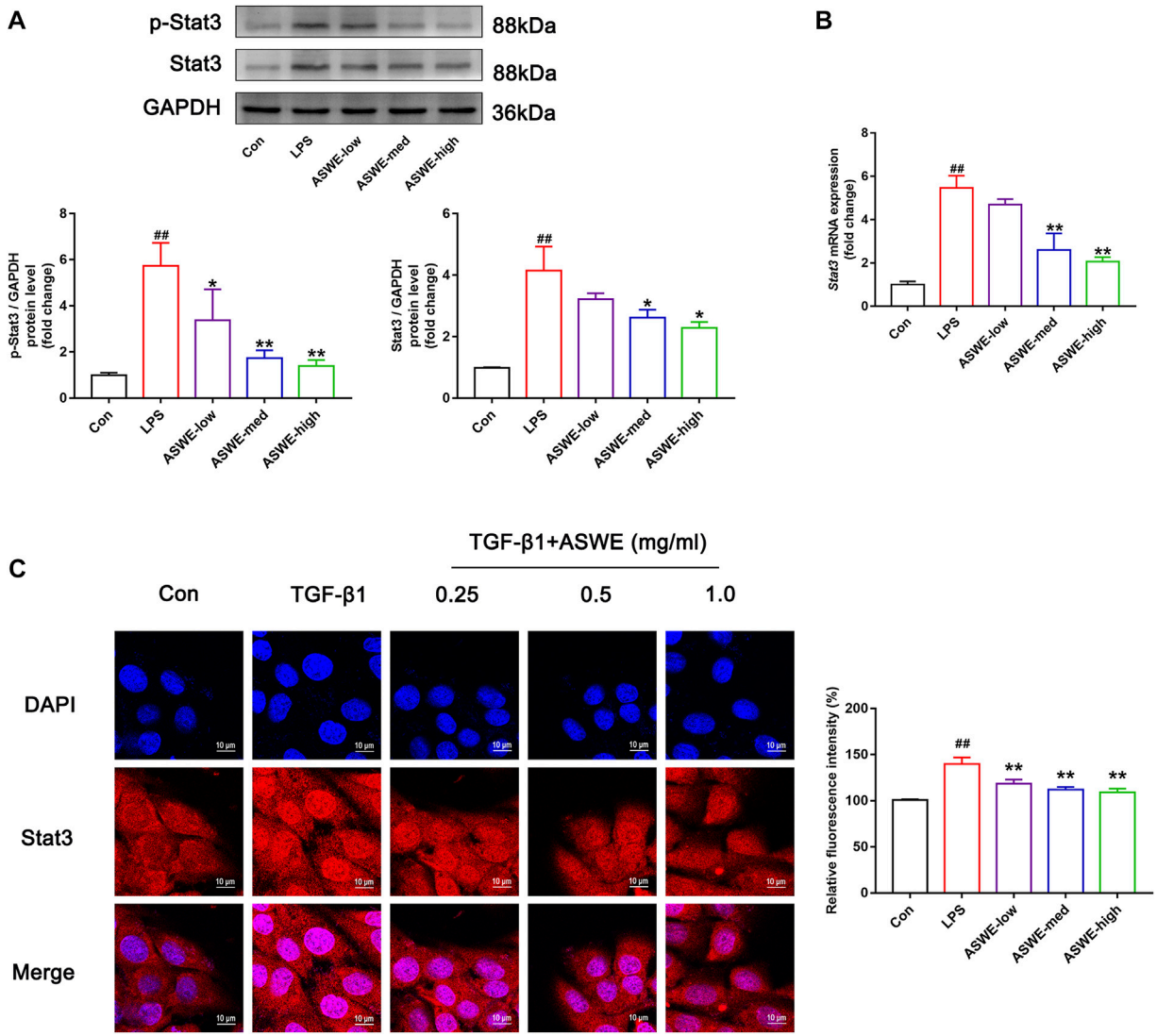

FIGURE 5
Stat3 signaling pathway could be involved in the regulation of the anti-fibrotic process of ASWE. **(A)** The protein expressions of p-Stat3 and total Stat3 ($n = 3$); **(B)** The mRNA expression of Stat3. Data are presented as mean ± SD ($n = 4$). $^{\#}p < 0.05$, $^{\#\#}p < 0.01$, compared with control group; $^{*}p < 0.05$, $^{**}p < 0.01$, compared with LPS group. **(C)** The subcellular location of STAT3 in HSC-T6 cells by immunofluorescent staining (scale bar: 10 μm).

component of cytoplasmic side of plasma membrane, cytoplasmic side of plasma membrane, extrinsic component of plasma membrane, cytoplasmic side of membrane. Molecular function analysis showed that these targets are related to nuclear receptor activity, ligand-activated transcription factor activity, RNA polymerase Il-specific DNA-binding transcription factor binding and DNA-binding transcription factor binding. These analytical results suggested that inflammatory response might be involved in the anti-antifibrotic process of ASWE against HF. The biological functions and pathways involving 44 targets in the treatment of HF were evaluated via KEGG enrichment analysis. Overall, the targets were notably related to the non-alcoholic fatty liver disease, alcoholic liver disease, hepatitis C, hepatitis B (Supplementary Figure S1). These results strongly suggested that ASWE might play an important role in protecting liver.

Intraperitoneal injection of CCl_4 has been widely used to establish a stable fibrotic model that partially resembles liver fibrosis in humans. CCl_4 is metabolized by cytochrome P450 enzyme (CYP2E1) to generate free radicals in the liver, destroying the integrity of the cell membrane and resulting in lipid peroxidation and hepatic injury (Slater et al., 1985; El-Agroudy et al., 2016). Repeated exposure to CCl_4 eventually enhances liver fibrogenesis (Tsukamoto et al., 1990). In the present study, we established a mouse model of CCl_4-induced hepatic fibrosis and evaluated the protective effect of ASWE against fibrosis. We used three different doses (40 mg/kg, 80 mg/k and 160 mg/kg) of ASWE to assess its effects. The results showed that after continuous intraperitoneal injection of the CCl_4-olive oil solution for 4 weeks, the mice in the HF model group showed deterioration of liver morphology, increased liver volume, less weight gain, and an elevated liver index, indicating severe liver injury, which was consistent with the clinical manifestations of HF (Ekser et al., 2012). In contrast, treatment with ASWE ameliorated

10.3389/fphar.2023.1101703

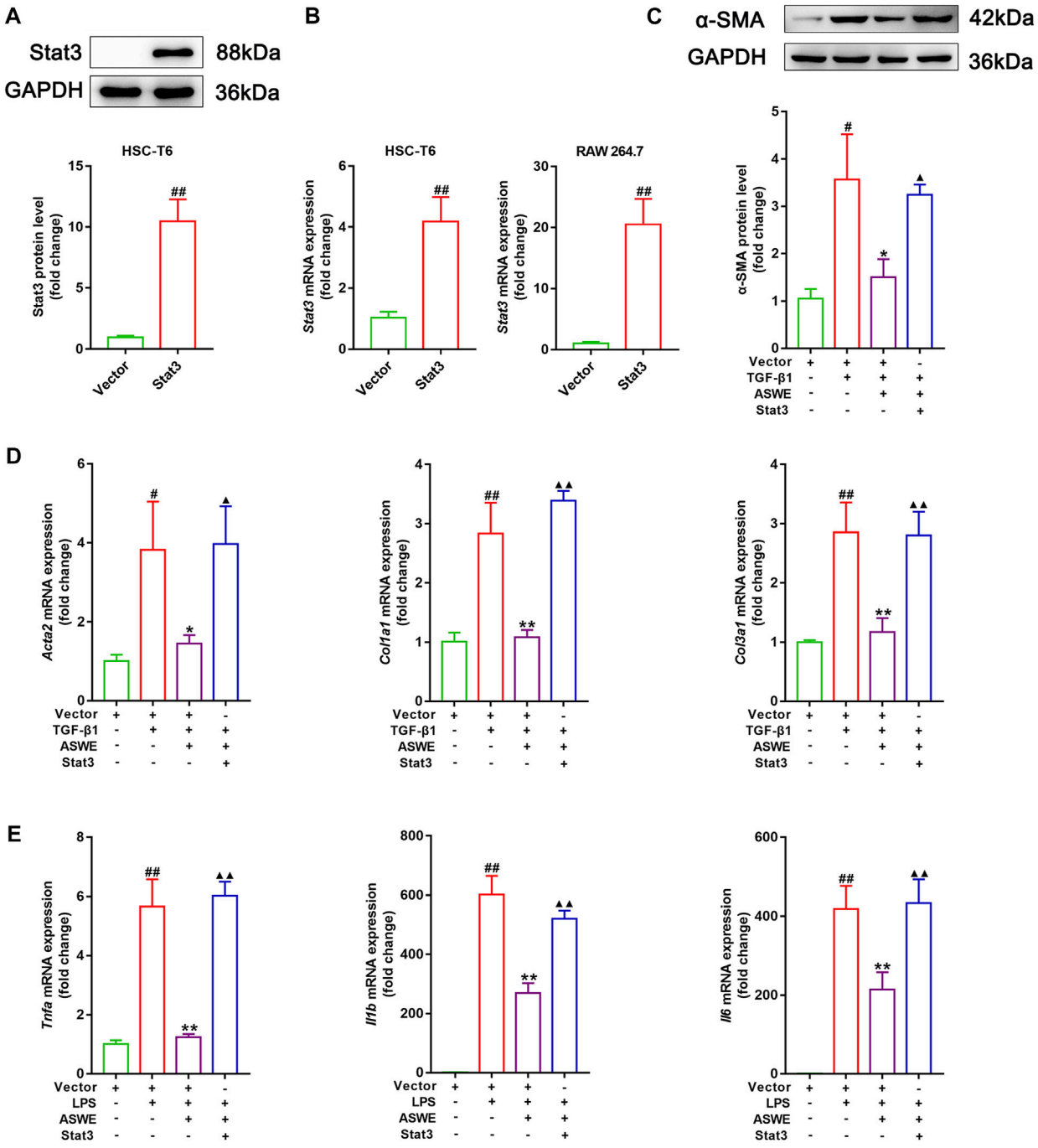

FIGURE 6
ASWE restrained HSCs activation through suppression of the Stat3 signaling pathway. **(A)** The protein expression of Stat3; **(B)** The mRNA expression of *Stat3*. **(C)** The protein expression of α-SMA (n = 3); **(D,E)** The mRNA expressions of *Acta2*, *Col1a1*, *Col3a1*, *Tnf-α*, *Il1β*, and *Il6*. Data are expressed as mean ± SD (n = 4). $^{\#}p < 0.05$ and $^{\#\#}p < 0.01$ vs. control group; $^{*}p < 0.05$ and $^{**}p < 0.01$ vs. model group (TGF-β1 or LPS group); $^{\blacktriangle}p < 0.05$ and $^{\blacktriangle\blacktriangle}p < 0.01$ vs. AHWE group.

these changes. In addition, H&E staining showed obvious pathological changes in the liver tissue of HF mice, such as inflammatory cell infiltration, massive adipose tissue vacuolization and hepatocyte necrosis. However, ASWE significantly attenuated these abnormal changes in liver fibrosis (Figures 2A–E). ALT and AST are two validated liver enzymes that are commonly used to assess liver function. Elevated serum levels of ALT and AST often reflect the degree of hepatocyte injury (Giannini et al., 2005). The results showed that ASWE treatment abrogated the increased levels of ALT and AST in the model group (Figures 2F, G), which provided conclusive evidence that ASWE protected hepatocytes from chronic injury.

In the normal liver, HSCs are in a quiescent and nonproliferating state, and HSC activation is crucial in liver

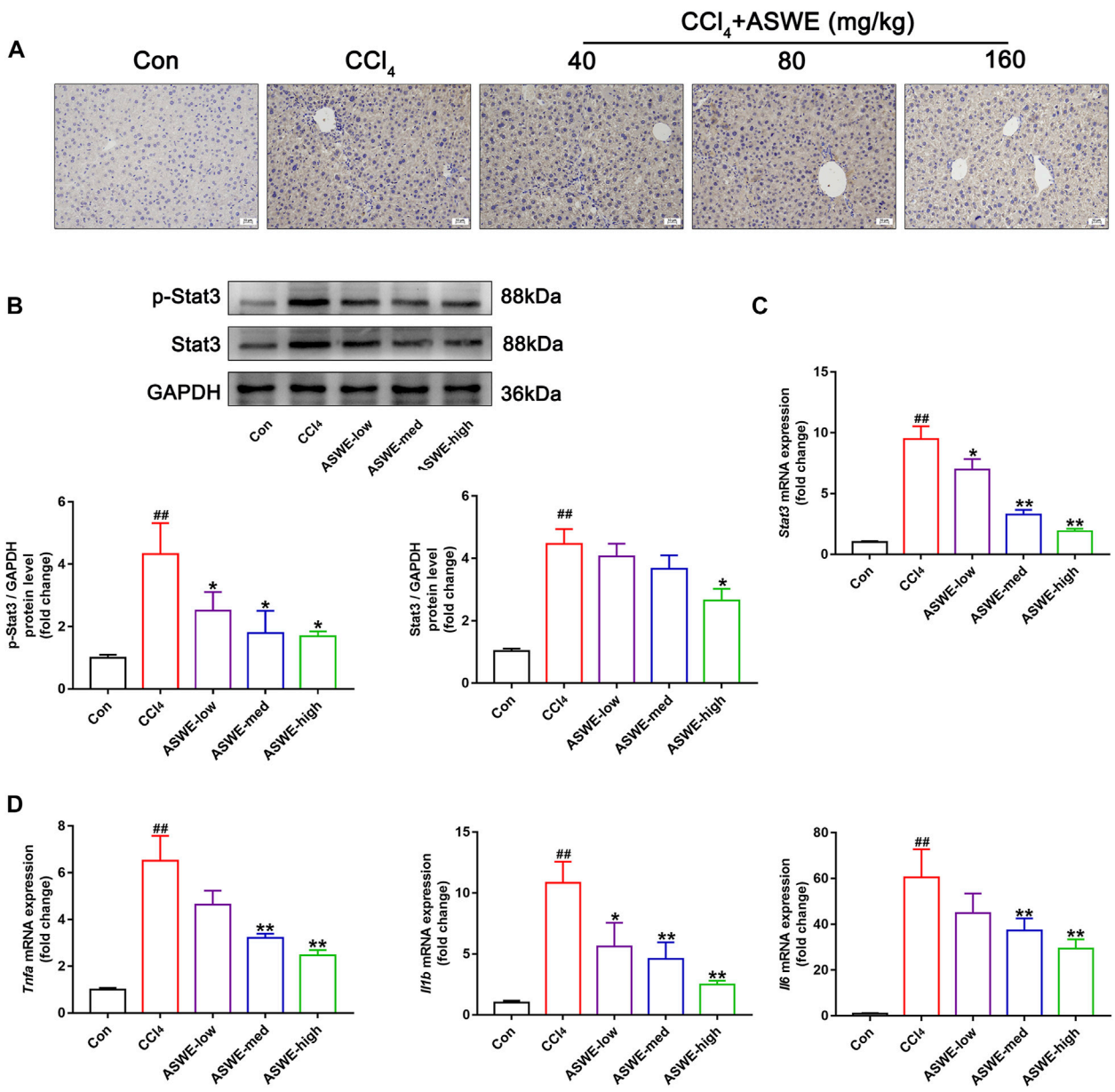

FIGURE 7
ASWE inhibited the activation of Stat3 pathway in CCl_4-induced HF mice. **(A)** The protein expression of Stat3 in the livers of C57BL/6J mice was detected by immunohistochemistry (scale bar: 10 μm). **(B)** The protein expressions of p-Stat3 and total Stat3 in mice (n = 3); **(C)** The mRNA expression of Stat3 in mice. **(D)** The mRNA expressions of inflammatory factors (*Tnf-α*, *Il1β*, and *Il6*) in mice. Data are presented as mean ± SD (n = 4). $^{\#}p < 0.05$, $^{\#\#}p < 0.01$, compared with control group; $^{*}p < 0.05$, $^{**}p < 0.01$, compared with CCl_4 group.

fibrogenesis. During liver fibrosis, α-SMA is typically known as a biomarker of HSC activation and fibrogenesis and represents the primary pathophysiological event (Friedman, 2008). Activated HSCs play a crucial role in the excessive synthesis and deposition of ECM by secreting collagen and insoluble fibrin, which is one of the main components of the ECM (Higashi et al., 2017). Evidence has indicated that the excessive deposition of ECM can be reduced by inhibiting the activation of HSCs (Tsochatzis et al., 2014; Magdaleno et al., 2018). Therefore, inhibiting HSC activation has been recognized as an effective strategy for the prevention and treatment of liver fibrosis (Tomita et al., 2014; Pawlak et al., 2015). In this study, the Masson staining results showed that a large number of collagen fibers were formed in the liver tissue of the model group. However, different doses of ASWE reduced the accumulation of collagen fibers. Furthermore, we measured serum levels of Col-I and HYP, which are characteristic of collagen fibers and reflect the degree of liver fibrosis (Lee et al., 2005), and showed that ASWE could reduce collagen accumulation in mouse livers induced by CCl_4 stimulation. The Western blot results showed that the high expression of α-SMA protein in the model group was reduced by ASWE treatment. The RT-qPCR results further showed that ASWE could reverse the high

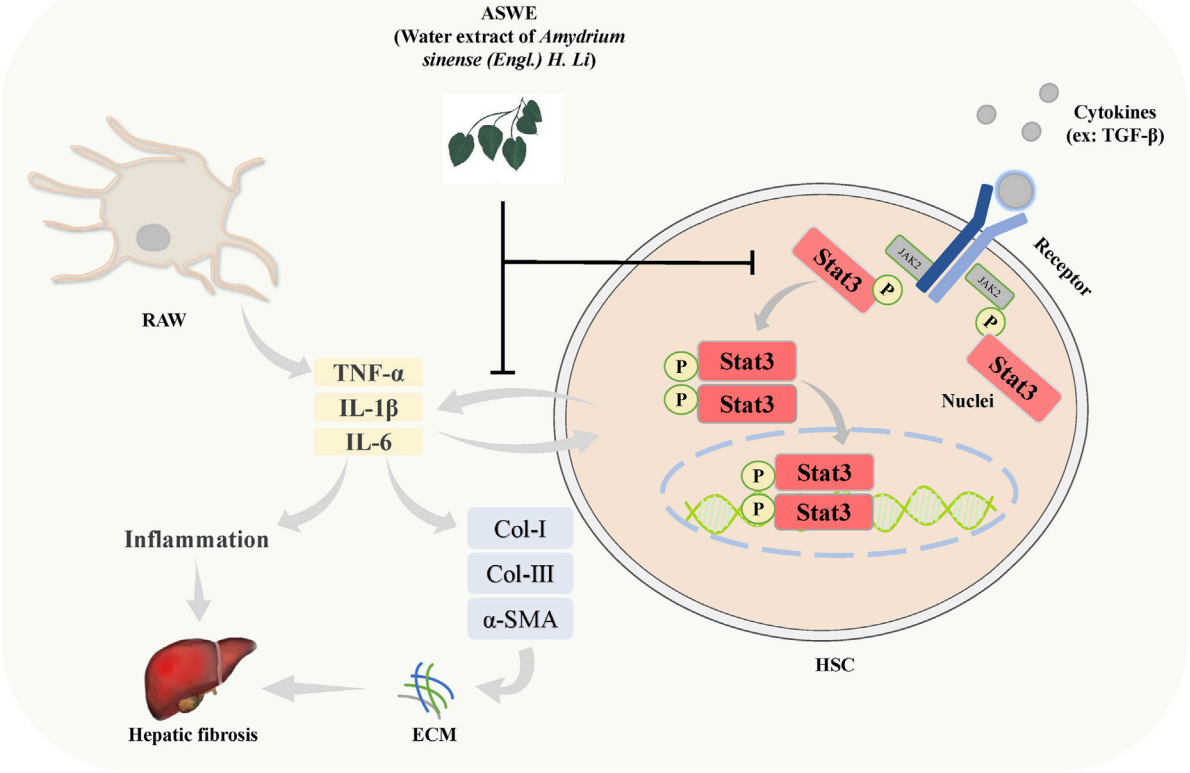

FIGURE 8
Schematic diagram of the protective role of ASWE in HF via suppressing hepatic stellate cell activation through inhibiting Stat3 signaling. AHWE inhibited the expression and distribution of Stat3 in liver tissues, and decreased the expression levels of p-Stat3 and Stat3 protein and *Stat3* mRNA induced by CCl_4. CCl_4 upregulated the inflammatory genes such as *Tnf-α*, *Il6*, and *Il1β*, leading to the formation of a hepatic inflammatory microenvironment and promoting HF. In contrast, ASWE significantly reversed these detrimental changes.

expression of fibrosis-related genes in the model group, including *Acta2*, *Col3a1*, and *Col1a1* (Figure 3). These results suggested that ASWE could inhibit the activation of HSCs and the excessive deposition of ECM induced by CCl_4, thereby suppressing HF, suggesting that ASWE was an effective and potent agent for treating liver fibrosis.

Moreover, we established an *in vitro* model of HSC activation by stimulating HSC-T6 cells with TGF-β1, a crucial profibrogenic factor. In accordance with the *in vivo* results, ASWE significantly reduced the elevated protein expression of α-SMA in TGF-β1-treated HSC-T6 cells. In addition, ASWE reversed the high expression of fibrosis-related genes (*Acta2, Col3a1, Col1a1*) induced by TGF-β1, suggesting that ASWE could inhibit HSC activation and promote ECM degradation. Inflammation leads to the activation of effector cells, which causes the deposition of ECM. Cytokines released from inflammatory cells play a key role in the underlying pathogenesis of liver fibrosis (Lieber, 2004). Proinflammatory cytokines, including Tnf-α, Il1β, and Il6, are released from innate immune cells and promote fibrogenesis by active HSCs (Wu et al., 2020). Thus, we established an *in vitro* model of cellular inflammation by stimulating RAW 264.7 cells with LPS. As the results showed, ASWE significantly abrogated the increased expression of inflammation-related genes (*Tnf-α, Il1β, and Il6*) induced by LPS stimulation (Figure 4). Therefore, we showed that ASWE could inhibit HSC activation and the inflammatory response *in vitro*. Thus, we speculate that ASWE may protect against liver fibrosis injury through anti-inflammatory effects.

It has been well documented that JAK2/Stat3 signaling is constantly activated during the progression of HSC activation, leading to various pathological manifestations of HF (Zhao et al., 2021). Blockade of the Stat3 signaling pathway impairs the morphological transdifferentiation of HSCs and reduces the expression of profibrotic genes (Wang et al., 2018; Choi et al., 2019). In unstimulated cells, Stat3 is inactive and located in the cytoplasm. The binding of Stat3-related cytokines to their receptors activates the receptor-associated Janus tyrosine kinases (JAK), which phosphorylates Stat3. Stat3 dimerizes in response to tyrosine phosphorylation at site 705, which results in its nuclear translocation, and Stat3 functions as a transcriptional factors for downstream genes, such as inflammation-related genes (*Tnf-α, Il1β, and Il6*). Inhibition of Stat3 phosphorylation could inhibit Stat3 nuclear localization (Xiang et al., 2018). We hypothesized that the Stat3 signaling pathway might be involved in the regulation of the antifibrotic effect of ASWE. In subsequent studies, we further found that the antifibrotic activity of ASWE was closely related to the Stat3 signaling pathway *in vitro* and *in vivo*. ASWE could inhibit the phosphorylation and activation of Stat3 and inhibit its nuclear translocation

(Figure 5). In addition, the overexpression of Stat3 elevated the expression levels of α-SMA protein and *Acta2*, *Col1a1*, *Col3a1*, *Tnf-α*, *Il6*, and *Il1β* mRNA (Figure 6). These results indicated that ASWE could weaken the effects of ASWE on suppressing HSC activation and attenuating inflammation, and ultimately aggravate the progression of HF.

Based on these *in vitro* experiments, we confirmed that ASWE exerted its antifibrotic effects by mediating the Stat3 signaling pathway to inhibit the activation of HSCs. Notably, we verified the consistent regulatory mechanism in CCl_4-induced mice. ASWE inhibited the expression and distribution of Stat3 in liver tissues, and decreased the expression levels of p-Stat3 and Stat3 protein and *Stat3* mRNA induced by CCl_4. CCl_4 upregulated inflammatory genes such as *Tnf-α*, *Il6*, and *Il1β* (Figure 7), leading to the formation of a hepatic inflammatory microenvironment and promoting HF. In contrast, ASWE significantly reversed these detrimental changes. These results provided evidence that the regulation of the Stat3 signaling pathway was involved in the *in vivo* suppression of HF by ASWE treatment, which was consistent with the *in vitro* findings.

5 Conclusion

The present study demonstrated that ASWE effectively improved CCl_4-induced hepatic fibrosis induced in mice. The underlying molecular mechanism may involve ASWE-mediated inhibition of HSC activation and the inflammatory response by suppressing the Stat3 signaling pathway (Figure 8). Therefore, our data provide further support for the antifibrotic mechanism of ASWE. ASWE is expected to become an effective drug for the treatment of liver fibrosis and provide an effective reference and new ideas for clinical treatments.

Data availability statement

The original contributions presented in the study are included in the article/Supplementary Material, further inquiries can be directed to the corresponding authors.

Ethics statement

The animal study was reviewed and approved by the Laboratory Animal Ethics Committee of Guangzhou University of Chinese Medicine.

Author contributions

JL, BW, and GZ designed the experiments and wrote the manuscript. JL, BW, LZ, YL, QC, HW, LA, JZ, and SC carried out the experiments and analyzed the data. JH, RZ, and GZ supervised and corrected the manuscript. All authors contributed to the article and approved the submitted version.

Funding

This work was supported by grants from the National Natural Science Foundation of China (Nos 82104163 and 82003826), Guangdong Basic and Applied Basic Research Foundation (Nos 2019A1515110607 and 2021A1515011016), Guangdong Science and Technology Project "Overseas Master" Project (No. 2020A141401022), Guangzhou Basic Research Program (No. 202102010376), Project of Traditional Chinese Medicine Bureau of Guangdong Province (No. 20221117), Project of south medicine innovation team in modern agricultural industry technology system of Guangdong Province (No. 2022KJ148) and the Special Funds in Key Areas of "Serving Rural Revitalization Plan" for Higher Education Institutions of Guangdong Province (2019KZDZX 2017).

Acknowledgments

We thank the International Institute for Translational Chinese Medicine of Guangzhou University of Chinese Medicine for technical assistance.

Conflict of interest

The authors declare that the research was conducted in the absence of any commercial or financial relationships that could be construed as a potential conflict of interest.

Publisher's note

Supplementary material

The Supplementary Material for this article can be found online at: https://www.frontiersin.org/articles/10.3389/fphar.2023.1101703/full#supplementary-material

SUPPLEMENTARY FIGURE S1
Network of compound and disease targets and enrichment of GO and KEGG analysis. **(A)** The common targets of compound targets and HF targets. **(B)** Compound-HF target network. **(C)** The GO biological process (BP), cellular component (CC) and molecular function (MF) analysis diagram. **(D)** Enriched KEGG pathways of potential key targets.

References

Baghaei, K., Mazhari, S., Tokhanbigli, S., Parsamanesh, G., Alavifard, H., Schaafsma, D., et al. (2022). Therapeutic potential of targeting regulatory mechanisms of hepatic stellate cell activation in liver fibrosis. *Drug Discov. Today* 27, 1044–1061. doi:10.1016/j.drudis.2021.12.012

Bataller, R., and Brenner, D. A. (2005). Liver fibrosis. *J. Clin. Invest.* 115, 209–218. doi:10.1172/JCI24282

Chai, N. L., Fu, Q., Shi, H., Cai, C. H., Wan, J., Xu, S. P., et al. (2012). Oxymatrine liposome attenuates hepatic fibrosis via targeting hepatic stellate cells. *World J. Gastroenterol.* 18, 4199–4206. doi:10.3748/wjg.v18.i31.4199

Chen, L., Zhang, Y. H., Wang, S., Zhang, Y., Huang, T., and Cai, Y. D. (2017). Prediction and analysis of essential genes using the enrichments of gene ontology and KEGG pathways. *PLoS One* 12, e0184129. doi:10.1371/journal.pone.0184129

Chen, X., Liu, C., Lu, Y., Yang, Z., Lv, Z., Xu, Q., et al. (2012). Paeoniflorin regulates macrophage activation in dimethylnitrosamine-induced liver fibrosis in rats. *BMC Complement. Altern. Med.* 12, 254. doi:10.1186/1472-6882-12-254

Cheng, L., Ren, Y., Lin, D., Peng, S., Zhong, B., and Ma, Z. (2017). The anti-inflammatory properties of citrus wilsonii tanaka extract in LPS-induced RAW 264.7 and primary mouse bone marrow-derived dendritic cells. *Molecules* 22, 1213. doi:10.3390/molecules22071213

Choi, S., Jung, H. J., Kim, M. W., Kang, J. H., Shin, D., Jang, Y. S., et al. (2019). A novel STAT3 inhibitor, STX-0119, attenuates liver fibrosis by inactivating hepatic stellate cells in mice. *Biochem. Biophys. Res. Commun.* 513, 49–55. doi:10.1016/j.bbrc.2019.03.156

Deng, Y. R., Ma, H. D., Tsuneyama, K., Yang, W., Wang, Y. H., Lu, F. T., et al. (2013). STAT3-mediated attenuation of CCl4-induced mouse liver fibrosis by the protein kinase inhibitor sorafenib. *J. Autoimmun.* 46, 25–34. doi:10.1016/j.jaut.2013.07.008

Dewidar, B., Meyer, C., Dooley, S., and Meindl-Beinker, A. N. (2019). TGF-B in hepatic stellate cell activation and liver fibrogenesis-updated 2019. Cells, 8, 1419. doi:10.3390/cells8111419

Duffield, J. S., Forbes, S. J., Constandinou, C. M., Clay, S., Partolina, M., Vuthoori, S., et al. (2005). Selective depletion of macrophages reveals distinct, opposing roles during liver injury and repair. *J. Clin. Invest.* 115, 56–65. doi:10.1172/JCI22675

Ekser, B., Gridelli, B., and Cooper, D. K. (2012). Porcine alanine transaminase after liver allo-and xenotransplantation. *Xenotransplantation* 19, 52–55. doi:10.1111/j.1399-3089.2011.00686.x

El-Agroudy, N. N., El-Naga, R. N., El-Razeq, R. A., and El-Demerdash, E. (2016). Forskolin, a hedgehog signalling inhibitor, attenuates carbon tetrachloride-induced liver fibrosis in rats. *Br. J. Pharmacol.* 173, 3248–3260. doi:10.1111/bph.13611

Ezhilarasan, D., Karthikeyan, S., and Vivekanandan, P. (2012). Ameliorative effect of silibinin against N-nitrosodimethylamine-induced hepatic fibrosis in rats. *Environ. Toxicol. Pharmacol.* 34, 1004–1013. doi:10.1016/j.etap.2012.07.004

Feng, K., Wang, S., Han, L., Qian, Y., Li, H., Li, X., et al. (2021). Configuration of the ion exchange chromatography, hydrophilic interaction chromatography, and reversed-phase chromatography as off-line three-dimensional chromatography coupled with high-resolution quadrupole-Orbitrap mass spectrometry for the multicomponent characterization of Uncaria sessilifructus. *J. Chromatogr. A* 1649, 462237. doi:10.1016/j.chroma.2021.462237

Friedman, S. L. (2008). Hepatic stellate cells: Protean, multifunctional, and enigmatic cells of the liver. *Physiol. Rev.* 88, 125–172. doi:10.1152/physrev.00013.2007

Giannini, E. G., Testa, R., and Savarino, V. (2005). Liver enzyme alteration: A guide for clinicians. *Cmaj* 172, 367–379. doi:10.1503/cmaj.1040752

Guan, Y., Enejder, A., Wang, M., Fang, Z., Cui, L., Chen, S. Y., et al. (2021). A human multi-lineage hepatic organoid model for liver fibrosis. *Nat. Commun.* 12, 6138. doi:10.1038/s41467-021-26410-9

Hernandez-Gea, V., and Friedman, S. L. (2011). Pathogenesis of liver fibrosis. *Annu. Rev. Pathol.* 6, 425–456. doi:10.1146/annurev-pathol-011110-130246

Higashi, T., Friedman, S. L., and Hoshida, Y. (2017). Hepatic stellate cells as key target in liver fibrosis. *Adv. Drug Deliv. Rev.* 121, 27–42. doi:10.1016/j.addr.2017.05.007

Kisseleva, T., and Brenner, D. A. (2007). Role of hepatic stellate cells in fibrogenesis and the reversal of fibrosis. *J. Gastroenterol. Hepatol.* 22 (Suppl. 1), S73–S78. doi:10.1111/j.1440-1746.2006.04658.x

Kurdi, M., and Booz, G. W. (2010). Deciphering STAT3 signaling in the heart: Plasticity and vascular inflammation. *Congest. Heart Fail* 16, 234–238. doi:10.1111/j.1751-7133.2010.00175.x

Lee, H. S., Shun, C. T., Chiou, L. L., Chen, C. H., Huang, G. T., and Sheu, J. C. (2005). Hydroxyproline content of needle biopsies as an objective measure of liver fibrosis: Emphasis on sampling variability. *J. Gastroenterol. Hepatol.* 20, 1109–1114. doi:10.1111/j.1440-1746.2005.03901.x

Lee, S. J., Kim, S. J., Lee, H. S., and Kwon, O. S. (2019). PKCδ mediates NF-κB inflammatory response and downregulates SIRT1 expression in liver fibrosis. *Int. J. Mol. Sci.* 20, 4607. doi:10.3390/ijms20184607

Lee, Y. A., Wallace, M. C., and Friedman, S. L. (2015). Pathobiology of liver fibrosis: A translational success story. *Gut* 64, 830–841. doi:10.1136/gutjnl-2014-306842

Li, J., Gao, H., Huang, J., Wang, P., Huang, Y., Luo, W., et al. (2016). PKCζ interacts with STAT3 and promotes its activation in cardiomyocyte hypertrophy. *J. Pharmacol. Sci.* 132, 15–23. doi:10.1016/j.jphs.2016.03.010

Li, J., Huang, J., Lu, J., Guo, Z., Li, Z., Gao, H., et al. (2019). Sirtuin 1 represses PKC-ζ activity through regulating interplay of acetylation and phosphorylation in cardiac hypertrophy. *Br. J. Pharmacol.* 176, 416–435. doi:10.1111/bph.14538

Li, J., Wu, J., Huang, J., Cheng, Y., Wang, D., and Liu, Z. (2022a). Uncovering the effect and mechanism of rhizoma corydalis on myocardial infarction through an integrated network pharmacology approach and experimental verification. *Front. Pharmacol.* 13, 927488. doi:10.3389/fphar.2022.927488

Li, R., Xu, L., Liang, T., Li, Y., Zhang, S., and Duan, X. (2013). Puerarin mediates hepatoprotection against CCl4-induced hepatic fibrosis rats through attenuation of inflammation response and amelioration of metabolic function. *Food Chem. Toxicol.* 52, 69–75. doi:10.1016/j.fct.2012.10.059

Li, S., Wang, L., Yan, X., Wang, Q., Tao, Y., Li, J., et al. (2012). Salvianolic acid B attenuates rat hepatic fibrosis via downregulating angiotensin II signaling. *Evid. Based Complement. Altern. Med.* 2012, 160726. doi:10.1155/2012/160726

Li, W., Xiao, H., Wu, H., Xu, X., and Zhang, Y. (2022b). Organophosphate pesticide exposure and biomarkers of liver injury/liver function. *Liver Int.* 42, 2713–2723. doi:10.1111/liv.15461

Liaskou, E., Zimmermann, H. W., Li, K. K., Oo, Y. H., Suresh, S., Stamataki, Z., et al. (2013). Monocyte subsets in human liver disease show distinct phenotypic and functional characteristics. *Hepatology* 57, 385–398. doi:10.1002/hep.26016

Lieber, C. S. (2004). Alcoholic fatty liver: Its pathogenesis and mechanism of progression to inflammation and fibrosis. *Alcohol* 34, 9–19. doi:10.1016/j.alcohol.2004.07.008

Liu, Y., Li, J., Liao, L., Huang, H., Fan, S., Fu, R., et al. (2021a). Cyclin-dependent kinase inhibitor roscovitine attenuates liver inflammation and fibrosis by influencing initiating steps of liver injury. *Clin. Sci. (Lond)* 135, 925–941. doi:10.1042/CS20201111

Liu, Y. T., Qi, S. L., and Sun, K. W. (2021b). Traditional Chinese medicine, liver fibrosis, intestinal flora: Is there any connection?-a narrative review. *Ann. Palliat. Med.* 10, 4846–4857. doi:10.21037/apm-20-2129

Lu, D. H., Guo, X. Y., Qin, S. Y., Luo, W., Huang, X. L., Chen, M., et al. (2015). Interleukin-22 ameliorates liver fibrogenesis by attenuating hepatic stellate cell activation and downregulating the levels of inflammatory cytokines. *World J. Gastroenterol.* 21, 1531–1545. doi:10.3748/wjg.v21.i5.1531

Ma, Y., Lu, L., Tan, K., Li, Z., Guo, T., Wu, Y., et al. (2022). Reduced peroxisome proliferator-activated receptor-α and bile acid nuclear receptor NR1H4/FXR may affect the hepatic immune microenvironment of biliary atresia. *Front. Immunol.* 13, 875593. doi:10.3389/fimmu.2022.875593

Magdaleno, F., Schierwagen, R., Uschner, F. E., and Trebicka, J. (2018). Tipping" extracellular matrix remodeling towards regression of liver fibrosis: Novel concepts. *Minerva Gastroenterol. Dietol.* 64, 51–61. doi:10.23736/S1121-421X.17.02442-4

Martin, A., Ochagavia, M. E., Rabasa, L. C., Miranda, J., Fernandez-De-Cossio, J., and Bringas, R. (2010). BisoGenet: A new tool for gene network building, visualization and analysis. *BMC Bioinforma.* 11, 91. doi:10.1186/1471-2105-11-91

Mederacke, I., Hsu, C. C., Troeger, J. S., Huebener, P., Mu, X., Dapito, D. H., et al. (2013). Fate tracing reveals hepatic stellate cells as dominant contributors to liver fibrosis independent of its aetiology. *Nat. Commun.* 4, 2823. doi:10.1038/ncomms3823

Mitchell, C., Couton, D., Couty, J. P., Anson, M., Crain, A. M., Bizet, V., et al. (2009). Dual role of CCR2 in the constitution and the resolution of liver fibrosis in mice. *Am. J. Pathol.* 174, 1766–1775. doi:10.2353/ajpath.2009.080632

Parola, M., and Pinzani, M. (2019). Liver fibrosis: Pathophysiology, pathogenetic targets and clinical issues. *Mol. Asp. Med.* 65, 37–55. doi:10.1016/j.mam.2018.09.002

Pawlak, M., Lefebvre, P., and Staels, B. (2015). Molecular mechanism of PPARα action and its impact on lipid metabolism, inflammation and fibrosis in non-alcoholic fatty liver disease. *J. Hepatol.* 62, 720–733. doi:10.1016/j.jhep.2014.10.039

PiñERO, J., RamíREZ-Anguita, J. M., SaüCH-Pitarch, J., Ronzano, F., Centeno, E., Sanz, F., et al. (2020). The DisGeNET knowledge platform for disease genomics: 2019 update. *Nucleic Acids Res.* 48, D845–d855. doi:10.1093/nar/gkz1021

Ran, D., Hong, W., Yan, W., and Mengdie, W. (2021). Properties and molecular mechanisms underlying geniposide-mediated therapeutic effects in chronic inflammatory diseases. *J. Ethnopharmacol.* 273, 113958. doi:10.1016/j.jep.2021.113958

Roeb, E. (2018). Matrix metalloproteinases and liver fibrosis (translational aspects). *Matrix Biol.* 68-69, 463–473. doi:10.1016/j.matbio.2017.12.012

Schuppan, D., Ashfaq-Khan, M., Yang, A. T., and Kim, Y. O. (2018). Liver fibrosis: Direct antifibrotic agents and targeted therapies. *Matrix Biol.* 68-69, 435–451. doi:10.1016/j.matbio.2018.04.006

Seki, E., and Schwabe, R. F. (2015). Hepatic inflammation and fibrosis: Functional links and key pathways. *Hepatology* 61, 1066–1079. doi:10.1002/hep.27332

Slater, T. F., Cheeseman, K. H., and Ingold, K. U. (1985). Carbon tetrachloride toxicity as a model for studying free-radical mediated liver injury. *Philos. Trans. R. Soc. Lond B Biol. Sci.* 311, 633–645. doi:10.1098/rstb.1985.0169

Song, Y., Wei, J., Li, R., Fu, R., Han, P., Wang, H., et al. (2023). Tyrosine kinase receptor B attenuates liver fibrosis by inhibiting TGF-β/SMAD signaling. *Hepatology Publ. Ahead Print*. doi:10.1097/HEP.0000000000000319

Stelzer, G., Rosen, N., Plaschkes, I., Zimmerman, S., Twik, M., Fishilevich, S., et al. 2016. The GeneCards suite: From gene data mining to disease genome sequence analyses. *Curr. Protoc. Bioinforma.*, 54, 1–30. doi:10.1002/cpbi.5.1-1.30.33

Suciu, A., Abenavoli, L., Pellicano, R., Luzza, F., and Dumitrascu, D. L. (2020). Transaminases: Oldies but goldies. A narrative review. *Minerva Gastroenterol. Dietol.* 66, 246–251. doi:10.23736/S1121-421X.20.02660-4

Tomita, K., Teratani, T., Suzuki, T., Shimizu, M., Sato, H., Narimatsu, K., et al. (2014). Free cholesterol accumulation in hepatic stellate cells: Mechanism of liver fibrosis aggravation in nonalcoholic steatohepatitis in mice. *Hepatology* 59, 154–169. doi:10.1002/hep.26604

Tsochatzis, E. A., Bosch, J., and Burroughs, A. K. (2014). Liver cirrhosis. *Lancet* 383, 1749–1761. doi:10.1016/S0140-6736(14)60121-5

Tsuchida, T., and Friedman, S. L. (2017). Mechanisms of hepatic stellate cell activation. *Nat. Rev. Gastroenterol. Hepatol.* 14, 397–411. doi:10.1038/nrgastro.2017.38

Tsukamoto, H., Matsuoka, M., and French, S. W. (1990). Experimental models of hepatic fibrosis: A review. *Semin. Liver Dis.* 10, 56–65. doi:10.1055/s-2008-1040457

Wang, Z., Li, J., Xiao, W., Long, J., and Zhang, H. (2018). The STAT3 inhibitor S3I-201 suppresses fibrogenesis and angiogenesis in liver fibrosis. *Lab. Invest.* 98, 1600–1613. doi:10.1038/s41374-018-0127-3

Wen, Z., Zhong, Z., and Darnell, J. E., JR. (1995). Maximal activation of transcription by Stat1 and Stat3 requires both tyrosine and serine phosphorylation. *Cell* 82, 241–250. doi:10.1016/0092-8674(95)90311-9

Wu, B. M., Liu, J. D., Li, Y. H., and Li, J. (2020). Margatoxin mitigates CCl4-induced hepatic fibrosis in mice via macrophage polarization, cytokine secretion and STAT signaling. *Int. J. Mol. Med.* 45, 103–114. doi:10.3892/ijmm.2019.4395

Wu, L. C., Lu, I. W., Chung, C. F., Wu, H. Y., and Liu, Y. T. (2011). Antiproliferative mechanisms of quercetin in rat activated hepatic stellate cells. *Food Funct.* 2, 204–212. doi:10.1039/c0fo00158a

Xiang, D. M., Sun, W., Ning, B. F., Zhou, T. F., Li, X. F., Zhong, W., et al. (2018). The HLF/IL-6/STAT3 feedforward circuit drives hepatic stellate cell activation to promote liver fibrosis. *Gut* 67, 1704–1715. doi:10.1136/gutjnl-2016-313392

Xiao, L., Ma, X., Ye, L., Su, P., Xiong, W., Bi, E., et al. (2022). IL-9/STAT3/fatty acid oxidation-mediated lipid peroxidation contributes to Tc9 cell longevity and enhanced antitumor activity. *J. Clin. Invest.* 132, e153247. doi:10.1172/JCI153247

Xu, H. Y., Zhang, Y. Q., Liu, Z. M., Chen, T., Lv, C. Y., Tang, S. H., et al. (2019). Etcm: An encyclopaedia of traditional Chinese medicine. *Nucleic Acids Res.* 47, D976–d982. doi:10.1093/nar/gky987

Zhang, D., Zhang, Y., and Sun, B. (2022). The molecular mechanisms of liver fibrosis and its potential therapy in application. *Int. J. Mol. Sci.* 23, 12572. doi:10.3390/ijms232012572

Zhang, J. P., Zhang, M., Zhou, J. P., Liu, F. T., Zhou, B., Xie, W. F., et al. (2001). Antifibrotic effects of matrine on *in vitro* and *in vivo* models of liver fibrosis in rats. *Acta Pharmacol. Sin.* 22, 183–186.

Zhao, J., Bai, D., Qi, L., Cao, W., Du, J., Gu, C., et al. (2022a). The flavonoid GL-V9 alleviates liver fibrosis by triggering senescence by regulating the transcription factor GATA4 in activated hepatic stellate cells. *Br. J. Pharmacol.* 180, 1072–1089. doi:10.1111/bph.15997

Zhao, J., Liu, X., Chen, Y., Zhang, L. S., Zhang, Y. R., Ji, D. R., et al. (2021). STAT3 promotes schistosome-induced liver injury by inflammation, oxidative stress, proliferation, and apoptosis signal pathway. *Infect. Immun.* 89, e00309-e00320. doi:10.1128/IAI.00309-20

Zhao, Q., Pan, W., Shi, H., Qi, F., Liu, Y., Yang, T., et al. (2022b). Network pharmacology and molecular docking analysis on the mechanism of Baihe Zhimu decoction in the treatment of postpartum depression. *Med. Baltim.* 101, e29323. doi:10.1097/MD.0000000000029323

Zheng, Z., Xu, X., Zhang, X., Wang, A., Zhang, C., HüTTEMANN, M., et al. (2013). Exposure to ambient particulate matter induces a NASH-like phenotype and impairs hepatic glucose metabolism in an animal model. *J. Hepatol.* 58, 148–154. doi:10.1016/j.jhep.2012.08.009

Zhou, M., Tang, Y., Liao, L., Liu, M., Deng, Y., Zhao, X., et al. (2021). Phillygenin inhibited LPS-induced RAW 264.7 cell inflammation by NF-κB pathway. *Eur. J. Pharmacol.* 899, 174043. doi:10.1016/j.ejphar.2021.174043

Zou, S., Tong, Q., Liu, B., Huang, W., Tian, Y., and Fu, X. (2020). Targeting STAT3 in cancer immunotherapy. *Mol. Cancer* 19, 145. doi:10.1186/s12943-020-01258-7

Frontiers in Pharmacology

Explores the interactions between chemicals and living beings

The most cited journal in its field, which advances access to pharmacological discoveries to prevent and treat human disease.

Discover the latest Research Topics

See more →

Frontiers

Avenue du Tribunal-Fédéral 34
1005 Lausanne, Switzerland
frontiersin.org

Contact us

+41 (0)21 510 17 00
frontiersin.org/about/contact